STRUCTURAL GEOLOGY, METAMORPHISM AND ORIGIN OF THE KANMANTOO COPPER DEPOSIT, SOUTH AUSTRALIA

by

Jeffrey Christopher Schiller, B.Sc. (Hons)

A thesis submitted to the Department of Geology and Geophysics at the University of Adelaide for the degree of Doctor of Philosophy

October 2000

ABSTRACT

The Kanmantoo copper mineralisation is located 40 km southeast of Adelaide in South Australia. Disseminated and vein style chalcopyrite-pyrrhotite-magnetite mineralisation occurs in amphibolite facies metasediments within the Adelaide Fold Belt. Open cut mining of the deposits ceased in 1976 following the production of over 4 million tonnes of 0.87% Cu. The mine is presently abandoned. The purpose of this thesis is to document the geological setting of the mineralisation with a broader view to establishing the origin of the mineralisation.

The origin of the Kanmantoo mineralisation is contentious, especially with regard to it's timing relative to metamorphism and tectonism. Previous theories have argued for either metamorphosed or metamorphogenic mineralisation. The recent recognition of convincing meta-exhalites near the Kanmantoo deposits has added support to the pre-metamorphic theories, which suggest that the Kanmantoo deposit represents a sub-seafloor feeder system to meta-exhalite deposits. The metamorphogenic theories argue for structurally controlled emplacement during metamorphism.

The Kanmantoo copper mineralisation occurs in the Cambrian Kanmantoo Group, a thick sequence of rapidly deposited psammitic and lesser pelitic sediments. The mineralisation is stratabound within a relatively Fe rich meta-pelitic unit, a garnet-andalusite-biotite schist (GAB schist), that extends along strike for approximately 6km. Surrounding rocks are predominantly quartz-feldspar-mica schists (meta-psammites) and quartz-mica schists (meta-pelites). No igneous rocks occur close to the deposits. Mineralisation is associated with a variety of lode schists that are characterised by high contents of Fe-Mg rich minerals, such as chlorite, biotite, almandine rich garnet, staurolite and magnetite. The most common lode schist is quartz-chlorite-garnet±andalusite. Andalusite occurs in the lode schists in approximate inverse proportion to chlorite. The lode schists and the sulphide mineralisation comprising the Main Lode occur in a series of lenses that, in gross outline, define a pipe-like structure that plunges steeply towards the northeast.

Relict bedding in the Kanmantoo Mine is generally well preserved. The dominant structure defined by bedding in the mine is the Mine Synform that plunges approximately 15˚S and occupies approximately two thirds of the pit. On a mesoscopic scale the dominant structure is a schistosity (S_2) with an erratically developed mineral lineation, both very regular in orientation. The schistosity strikes north-south and dips 73ºE. It is axial planar to the Mine Synform and all other mesoscopic and macroscopic folds. The mineral lineation plunges steeply to the southeast and most fold axes plunge shallowly to the south. Thus, the pipe-like Main Lode is discordant to both the fold axes in bedding and the mineral lineation. In keeping with regional studies the dominant schistosity in the mine area is assigned to the D_2 deformation. Occurrences of post D_2 structures are limited to rare crenulations, kinks and joints, all indicating increasingly brittle styles of deformation. Veins in the mine are quartz, quartz-sulphide, sulphide or coarse-grained silicates and are either parallel to S_2 or are slightly oblique, folded and boudinaged. Veins in the immediate mine surrounds are mostly quartz, are oblique to S_2 and are folded and boudinaged. Many minor shear zones occur in the mine, principally in the western limb of the Mine Synform. Some shear zones were important in controlling the copper distribution.

Most sulphide minerals in the mine occur as disseminated, microscopic grains and in mesoscopic veins, both parallel to the S_2 schistosity, or as irregular veins and patches. Copper

distribution in the mine was studied using the detailed assay database developed for grade control. In plan view, that is perpendicular to the plunge of the lodes and of the gross pipe, the copper distribution pattern is somewhat irregular, but consistent patterns are seen in both the high and low grade areas that are inferred to represent primary controls on distribution. Viewed in vertical section, the copper distribution is very regular, forming steep shoots, some parallel to the schistosity and others slightly oblique. The mineralisation occurs in two styles – East Limb and West Limb styles. All East Limb style lodes occur on the eastern limb of the Mine Synform and are characterised by a NNE trend and an association with host rocks that have fabrics inferred to represent metamorphic crystallisation during high fluid pressures. West Limb style lodes occur on the western limb of the Mine Synform, are north-south trending in general, and are not associated with the fabrics associated with the East limb style.

An extensive microstructural study of all lithologies in the mine was undertaken. Sulphide minerals were involved in all stages of the metamorphic and structural history. An early fabric, S_1, is preserved in andalusite, garnet, staurolite and biotite porphyroblasts. In the mine area there is little evidence of crenulation of S_1 and it is concluded that S_2 developed from S_1 generally not by a crenulation cleavage mechanism, but by rotation and recrystallisation of S_1 during flattening. Not all porphyroblasts developed at the same stage, a series of porphyroblast producing reactions is indicated in most rock types. Some sulphide minerals and chlorite (or the assemblage needed for the subsequent formation of chlorite) were introduced to the metasediments together by a hydrothermal event during or before D_1. The proportion of total sulphide that can be attributed to this stage is low. Many microfabric differences amongst the metasediment and the lode schists (e.g. biotite shape and size) are attributed to high fluid contents near the sulphide deposit during metamorphic mineral growth. In particular, the fluid possibly caused significant local reductions in the differential stress during deformation.

Metamorphic mineral assemblages and mineral chemistries are documented. A close approach to chemical equilibrium is indicated by the relatively close agreement between rim compositions of given minerals in most rocks, plus the regular X_{Fe} plots and the relative X_{Fe} values for different minerals. The peak metamorphic temperature and pressure are similar for both lode schists and surrounding metasediments. Pressure is estimated at 3-4 kb and temperature estimates differ depending on whether experimental phase equilibria studies or mineralogical geothermometers are used for estimates. The former provide a temperature range of 530-565ºC, the latter 480-510ºC, but with a few higher values overlapping the former range.

Geochemically, the schists surrounding the mine are comparable with typical psammites and pelites, but the host unit to the Kanmantoo mineralisation has anomalously high Fe and Mn and low Ca and Na. It is unclear whether this represents unusual original sedimentary composition or post-sedimentary metasomatic alteration. Most lode schists appear to be derived by chemical alteration of the surrounding GAB schists. Composition-volume estimates of this process indicate that the most common rocks associated with copper mineralisation appear to have undergone volume increases during alteration. In contrast, coarse-grained silicate zones (with low silica contents) mostly appear to have undergone a volume decrease. For all lithologies where an alteration trend can be deduced Fe and S were added during alteration. The most common variety of lode schist generally appears to have experienced addition of Si, Mn, Mg and Cu, but a depletion of the alkalis Na and K. Alteration style is similar to chloritisation associated with other deposits such as the footwall zones of volcanogenic massive sulphide deposits.

Despite the growing weight of evidence over the last decade in favour of exhalative mineralisation in the Kanmantoo-Strathalbyn region, detailed mapping in the mine does not

support its circumstantial link to the Kanmantoo copper deposit. On the basis of the present study it is concluded that there is no firm evidence that the bulk of the mineralisation is pre-metamorphic, although the possibility has not been excluded. A strong structural control is imposed on the distribution of copper and on certain lithologies associated with copper mineralisation. The dominant control is the Mine Synform. Sulphide mineralisation was associated with several phases of hydrothermal activity during metamorphism, of which the earliest that can be established is syn-D_1. The most important metasomatic event or events appear to pre-date D_2. Ore fluids were probably derived from either metamorphic or magmatic fluids, or some combination of both. Both felsic and mafic intrusions in the region have appropriate timing to supply heat, metals and, for the felsic intrusions, fluids.

DECLARATION

OF

ORIGINALITY

I declare that this thesis does not incorporate without acknowledgement, any material previously submitted for a degree in any university to my knowledge. Also, to the best of my knowledge, it does not contain any materials previously published or written by another person, except where due reference is made in the text.

Signed,

J. C. Schiller

ACKNOWLEDGEMENTS

Over the many years it has taken me to complete this study many generous people have helped me. I am sure each is aware of my gratitude, but I thank them all again. I would like particularly to acknowledge the assistance of the following people and organisations.

Kanmantoo Mines Limited, and in particular Mr. John Treloar, the former Mine Manager at the Kanmantoo Mine, are thanked for permission to do the study and for access to the mine and any company data that I required. Jack Ballinger is thanked for cheerful assistance, especially with surveying. Chief Geologist, Dave O'Connor was supportive of the study concept, and provided useful comments on the proposed work. Mr Keith Rogers, former Exploration Manager of Mines Exploration Pty. Ltd. provided access to company reports and thin sections.

The University of Adelaide provided a Post Graduate Research Scholarship and research facilities.

Dr. Ross Both and Dr. Pat James, who supervised the study, provided guidance and support. Valuable discussions were held with my colleagues at the Department of Geology and Mineralogy, especially Dr. Robin Oliver, Rosemary Allen, Steve Hancock, Neil Mancktelow, Alan Purvis, Paul Spry, Graham Teale, Dick Glen and Bill Laing.

Dr. Keith Turnbull and Phil McDuie provided help with chemical analyses and John Stanley was responsible for painstaking XRF analyses of major and trace elements. Geoff Trevallyan and Wayne Mussared prepared high quality thin and polished sections.

Dr. Ron Vernon of Macquarie University is thanked for stimulating discussions, accommodation in Sydney and access to his department's electron microprobe. Dr. Dave Sewell, at Melbourne University, gave instruction in the use of microprobes. Thanks to Dr. Rod Holcombe for use of his stereographic plotting program, GEOrient.

Stimulating and useful discussions were held with Vic Bogacz, Jakob Rebek, Tony Belperio, Justin Gum and Steve Toteff.

For patient typing of the text I thank Pauline Booth, Trish Kastropil, Pam I'Anson, Sharon Yap, Rhonda MacGuire and Lynne Morton. Drafting was done by Wayne Groenveld, Bill Stach and Kerry Steel. Mike Tuite is thanked for providing services from CRA Exploration Pty Ltd whilst I was an employee.

Finally, I thank my wife, Karen. During the various periods over the years when I made yet another attempt to complete the thesis, Karen supported and encouraged me, sacrificed holidays, typed draft copies and prodded me to work during tough periods caused by the pressures of work and family. Without her help all the work done for this study would still be a large pile of papers and data, stored in boxes under my bed.

CONTENTS

Page Number

ABSTRACT

DECLARATION OF ORIGINALITY

ACKNOWLEDGEMENTS

LIST OF TABLES

LIST OF FIGURES

1. INTRODUCTION 1

1.1 Location 1
1.2 Background 1
1.3 Objects and scope 2
1.4 Previous work 3
1.5 Refereed publications from this study 3
1.6 Discovery and copper production from the Kanmantoo Mine 4
1.7 Grids 4

2. REGIONAL GEOLOGY 7

3. LITHOLOGIES 11l

3.1 Introduction 11
3.2 Classification 11
3.3 Methods of study 13
3.3.1 Kanmantoo Mine 13
3.3.2 Mine area 15
3.3.3 Kanmantoo district 15
3.4 Metasediments 15
3.4.1 Quartz-mica-feldspar schist 18
3.4.2 Quartz-mica-andalusite schist 20
3.4.3 Garnet-biotite schist 21
3.4.4 Garnet-andalusite-biotite schist 22
GAB(1) schist 24
GAB(2) schist 27
GAB(3) schist 28
3.4.5 Pyritic schist 29
3.4.6 Calc-silicate rocks 30
3.4.7 Quartzites and related rocks 31

3.5 Lode schists 32
3.5.1 Varieties 32
3.5.2 Group 1 lode schists 34
Andalusite-bearing lode schists 36
GBCl group – chlorite rich variety 36
GBCl group – biotite rich variety 37
3.5.3 Group 2 lode schists 37
3.5.4 Group 3 lode schists 38
3.5.5 Group 4 lode schists 39
3.5.6 Geometry of the lode schists 39
3.6 Laterite 41

4 COPPER MINERALISATION 43

4.1 Introduction 43
4.2 Form of sulphide occurrence 43
4.3 Sulphide mineralogy 46
4.4 The spatial distribution of copper in the Kanmantoo Mine 46
4.4.1 Data sources and methods of study 46
4.4.2 Statistical description of copper assays at 520 and 600 levels 49
4.4.3 Contouring of copper grades 50
4.4.4 Image processing of copper grades 52
4.5 Spatial relationship between copper and lode schists 59
4.6 Types of copper mineralisation 62
4.7 Other copper deposits in the Kanmantoo Mine area 63
4.8 Other copper deposits in the Kanmantoo district 65

5. MACRO-STRUCTURE AND MESO-STRUCTURE 66

5.1 Introduction 66
5.2 Structural notation 67
5.3 Regional setting of the Kanmantoo deposits 68
5.4 The Kanmantoo Mine Area 72
5.4.1 Introduction 72
5.4.2 Bedding 73
5.4.3 Schistosity and mineral lineation 78
5.4.4 Fold axes and bedding-schistosity intersections 79
5.4.5 Veins 82
5.4.6 Shear zones 87
5.4.7 Crenulations and kinks 88
5.4.8 Faults and joints 90
5.5 Structure and copper mineralisation 92

6 MICRO-STRUCTURE 95

6.1 Introduction 95
6.2 QMF schist 95
6.3 QMA schist 98

6.4 GAB(1) schist 101
6.4.1 Description of Q and M domains 101
6.4.2 Description of internal fabrics in porphyroblasts 105
6.4.3 The origin of internal fabrics 108
6.4.4 The orientation of andalusite grains 109
6.4.5 The sequence of mineral growth 113
6.5 GAB(2) schist 116
6.6 GAB(3) schist 119
6.6.1 Description of S_1 and S_2 119
6.6.2 Andalusite and biotite 122
6.6.3 Garnet 126
6.6.4 Staurolite 126
6.6.5 Sulphide and oxide minerals 127
6.7 The shape of biotite grains in GAB schist 128
6.7.1 Description of biotite grains 128
6.7.2 Discussion 129
6.8 Lode schists 132
6.8.1 Group 1 (quartz rich) lode schists 132
6.8.2 Group 2 (quartz poor) lode schists 135
Foliations 135
Garnet 136
Amphibole 141
Sulphide minerals 142
6.9 The Microstructure of chlorite 144
6.9.1 Fe-poor chlorite 144
Chlorite associated with biotite 144
Chlorite associated with andalusite 146
Group 2 lode schists 147
6.9.2 Fe-rich chlorite 147
6.10 Discussion and conclusions 149
6.10.1 The genetical relationship between S_1 and S_2 149
6.10.2 Growth relationships between andalusite and staurolite 152
6.10.3 Chlorite and sulphide minerals 152
6.10.4 Conclusions 154

7. METAMORPHISM 156

7.1 Introduction 156
7.2 Mineral assemblages 156
7.3 Mineral chemistry 162
7.3.1 Andalusite 162
7.3.2 Staurolite 162
7.3.3 Garnet 166
7.3.4 Cordierite 171
7.3.5 Amphiboles 172
7.3.6 Chlorite 173
7.3.7 Biotite 174
7.3.8 Muscovite 175
7.3.9 Plagioclase 175
7.3.10 Oxide minerals 175

7.4 Evidence of chemical equilibrium 175
7.5 Physical conditions of metamorphism 178
7.5.1 Comparison with experimental data 178
7.5.2 Garnet-biotite geothermometry 181
7.5.3 Garnet-cordierite geothermometry 184
7.5.4 Garnet-cordierite-andalusite-quartz equilibrium 185
7.5.5 Magnetite-ilmenite equilibrium 186
7.5.6 Conclusions 187

8. GEOCHEMISTRY 188

8.1 Introduction 188
8.2 Geochemistry of the metasediments 190
8.2.1 Introduction 190
8.2.2 QMF schists 193
8.2.3 GAB(1) schist 193
8.2.4 QMA schist 196
8.2.5 GB schist 196
8.2.6 Pyritic schist 196
8.2.7 Pre-metamorphic mineralogies of the metasediments 197
8.3 Geochemistry of the rocks closely associated with mineralisation 200
8.3.1 Chemical composition 200
8.3.2 Composition-volume relationships 202
8.3.3 Discussion 206

9. ORIGIN OF COPPER MINERALISATION 208

9.1 Introduction 208
9.2 Previous theories 208
9.3 Some constraints on the origin 212
9.4 Discussion 213
9.4.1 Evidence for hydrothermal activity 213
9.4.2 Timing of mineralisation 214
9.4.3 Structural controls on mineralisation 216
9.4.4 Evidence for a syn-sedimentary origin 219
9.4.5 Regional controls 221
9.4.6 Origin of the mineralising fluids 222
9.5 Similar deposits 225
9.5.1 Cobar 226
9.5.2 Ducktown 227
9.6 Conclusions 229

REFERENCES 230

APPENDIX 1 Lithological coding system
APPENDIX 2 Surveying and grids
APPENDIX 3 Sample locations
APPENDIX 4 Composition-volume estimations
APPENDIX 5 Rock geochemical analyses *[on computer disk]*
APPENDIX 6 Mineral microprobe analyses *[on computer disk]*
APPENDIX 7 Publications resulting from this study

LIST OF FIGURES

1 Photograph of the Kanmantoo Mine area
2 Photograph of the south wall of the Kanmantoo Mine
3 Location plan and regional geology
4 Stratigraphic column and geochronological framework for Fleurieu Peninsular and Kangaroo Island
5 Plan showing all pit face mapping traverses on 440 bench
6 Pit face mapping traverses for the northern portion of the 440 bench
7 Local geology [*in map pocket*]
8 Geology of the Kanmantoo district
9 Transitional relationships between metasediments
10 Approximate mineralogical proportions of the three most common rock types from the immediate Kanmantoo Mine area
11 Westerly view of a QM schist exposure with excellent relict bedding
12 Photograph of QF schist showing an antiform in profile
13 Folded relict bedding in QMA schist
14 Photograph of GAB(1) schist from the eastern side of the Kanmantoo Mine
15 Close up of the appearance of relict bedding and S_2 schistosity in typical GAB(1) schist
16 Schistosity surface in typical GAB(1) schist
17 Photograph of GAB(2) schist
18 Photograph of GAB(2) schist
19 Distribution of all GAB(2) and GAB(3) schists mapped in the Kanmantoo Mine
20 Photograph of GAB(3) schist
21 Photograph of banded garnet quartzite
22 Schematic diagram showing relationship between quartz rich lode schists
23 Photograph of G(A)BCl schist with discrete shear zone
24 Cross section through the Main Lode on 12,000N
25 Longitudinal projection of the main lodes of the Kanmantoo Mine vicinity

looking west
26 Photograph of anastomosing sulphide veins in high grade ore
27 Sheeted sulphide veins from high grade ore at the southern end of the West Limb
28 Photograph of sulphide rich specimen
29 Examples of sulphide veinlets in lode schist
30 Plan for the 520 level showing assay control sample locations
31 Cumulative frequency plot of log transformed assay data from the 520 and 600 levels
32 Copper distribution - 600 level (contours) [*in map pocket*]
33 Copper distribution - 640 level (contours) [*in map pocket*]
34 Copper distribution - 680 level (contours) [*in map pocket*]
35 Copper distribution >0.5%- contours for 520 level and cross-section 12000 N
36 Image of copper assays for 520 level
37 Image of copper assays for 600 level
38 Grey-scale image of copper for 520 level
39 Interpreted main features of copper distribution for the 520 level
40 Image of copper assays for cross-sections 11700N, 12000N and12300N
41 (a). Interpreted lithological units used to estimate mean Cu grades, 520 level. (b) Comparison of lode schist and grade contour, 520 level.
42 View to the ENE from the ruins of the Paringa Mine
43 Structural domains in the Kanmantoo region
44 Diagram showing the stratigraphic implications of the regional structural interpretation
45 The Kanmantoo Mine –Plan of S_0 [*in map pocket*]
46 Stereographic projection of poles to S_0
47 The Kanmantoo Mine - fold limb relationships [*in map pocket*]
48 The Kanmantoo Mine area - fold limb relationships [*in map pocket*]
49 The Kanmantoo Mine area - alternative structural interpretations
50 The Kanmantoo Mine area - structural interpretation
51 The Kanmantoo Mine - stereographic projections of S_2 and $L_{2/2}$
52 The Kanmantoo Mine area - stereographic projections of S_2 and $L_{2/2}$
53 The Kanmantoo Mine - plan showing $L_{2/0}$, $F_{2/0}$ [*in map pocket*]
54 Stereographic projections of fold axes and bedding-schistosity lineations ($F_{2/0}$, $L_{2/0}$)
55 The Kanmantoo Mine area - plan showing $F_{2/0}$, $L_{2/0}$ [*in map pocket*]
56 The Kanmantoo Mine - plan showing angle between $L_{2/2}$ and $F_{2/0}$ [*in map pocket*]
57 The Kanmantoo Mine area - plan showing angle between $L_{2/2}$ and $F_{2/0}$ [*in map pocket*]

58 Photograph of relatively well preserved bedding in GAB(2) schist
59 The Kanmantoo Mine - stereographic plots, veins
60 The Kanmantoo Mine area - stereographic plot, quartz veins
61 Photograph of QMA schist with low andalusite content
62 Photomontages of an exposure of the 4100 Shear Zone on the 520 level
63 Photograph of low silicified ridge in QM schist with EW fractures
64 Photograph of part of Figure 63
65 The Kanmantoo Mine, stereographic plot, summary
66 The Kanmantoo Mine, stereographic plot, lode schists and copper zones
72 Photomicrographs of QF schist with gentle fold in bedding
73 Photomicrographs of typical QM schist with strong S_2 schistosity
74 Scatter diagram of aspect ratios of micas in QM schist
75 Photomicrographs of QM schist with augen-like bodies
76 Photomicrographs of bedded QM schist and QMA schist
77 Photomicrographs of andalusite porphyroblast from the QMA schist band shown in Figure 76
78 Photomicrographs of andalusite porphyroblast from the QM schist band shown in Figure 76
79 Photomicrograph of GAB(1) schist with andalusite poor beds
80 Photomicrograph of detail of andalusite grain marked A in Figure 79
81 Graphs of aspect ratios of biotite in GAB(1) schist
82 Graph of aspect ratios of sulphides in Q and M domains of GAB(1) schist
83 Graph of aspect ratios vs. divergence from mean S_2 for biotite in Q and M domains of a GAB(1) schist sample.
84 Photomicrograph of composite andalusite crystals with a weak S_1
85 Photomicrograph of andalusite crystal with a strong S_1 fabric
86 Line drawing of GAB schist
87 Rare example of curved S_1 in andalusite
88 Photograph showing disposition of andalusite grains in outcrop (top view)
89 Photograph showing disposition of andalusite grains in outcrop (side view)
90 Rose diagrams of andalusite long axes in outcrop
91 Sketch showing the effect of 50% flattening on the external and internal fabrics of a foliation
92 Photomicrograph of GAB(1) schist with staurolite
93 Diagram showing the inferred sequence of mineral growth for various lithologies
94 Photomicrographs of GAB schist varieties
95 GAB(2) schist with typical andalusite porphyroblast containing a high proportion of quartz inclusions
96 Two garnet inclusions within an andalusite poikiloblast

97 Graph of aspect ratios of biotite in GAB(2) schist
98 Drawings of thin sections of GAB(3) schist
99 Microstructures of GAB(3) schist, (a)-(h)
100 Histograms of relationship between (001) of biotite and mean S_2 trace in GAB(3) schist
101 Photomicrographs of GAB(3) schist, (a)-(d)
102 Comparison of biotite shapes and orientations in GAB schist varieties
103 Photomicrograph of garnet layer in quartz rich lode schist
104 Photomicrograph of folded garnet layer in quartz rich lode schist
105 Photomicrograph of quartz rich lode schist with folded quartz vein and garnet rich zones
106 Photomicrograph of quartz rich lode schist with staurolite
107 Photomicrographs of quartz poor lode schists, (a)-(d)
108 Photomicrographs of garnets in quartz poor lode schists, (a)-(h)
109 Photomicrographs of relationships between silicate and sulphide minerals, (a)-(e)
110 Photomicrograph of coarse biotite incompletely replaced by Fe-poor chlorite
111 Photomicrograph of andalusite with chlorite corona
112 Photomicrographs of iron rich chlorite microstructures
113 A'FK diagram
114 A'FM diagram (Thompson projection)
115 AFM diagram
116 SiO_2-Al_2O_3-FeO-MgO diagram
117 SiO_2-FeO-MgO-Al_2O_3 enlargement
118 SiO_2-FeO-MgO-Al_2O_3 tetrahedron-enlargement
119 Graphs of staurolite composition
120 Staurolite grain study
121 Garnet composition ternary diagram
122 Graphs of garnet composition
123 Graphs of garnet composition
124 Garnet grain study
125 Graphs of cummingtonite composition
126 Graphs of chlorite composition
127 Graphs of biotite composition
128 Graphs of X_{Fe} comparisons
129 Experimental phase equilibria
130 Comparison of the iron free chemistry of some Kanmantoo Group metasediments
131 Ternary plot of Niggli ratios of some Kanmantoo Group sediments
132 MgO vs FeO in some Kanmantoo Group metasediments

133 FeO vs K_2O in some Kanmantoo Group metasediments
134 Ternary plot of Niggli ratios of rocks from the Kanmantoo Mine
135 Apparent volume change (fv) estimates for major elements
136 Comparison of geochemical trends in several copper deposits
137 Geological interpretations of the 640, 600, 560, 520 and 400 levels [*in map pocket*]
138 Geological interpretations of the 480 and 350 levels [*in map pocket*]
139 Geological interpretations of the 440 and 300 levels [*in map pocket*]

LIST OF TABLES

1 Lithological classification used in this study
2 Mineral compositions of common lithologies
3 Proportions of Kanmantoo Group metasediments exposed in road cuts of the South-Eastern Freeway (based on data reported by Drexel, 1978)
4 Lode schists sorted according to general quartz content and correlation with Lindqvist (1969) categories
5 Mineral variations in quartz rich lode schists
6 Estimates of relative abundance of Group 1 (quartz rich) lode schists based on pit mapping data Estimates of relative abundance of Group 1 (quartz rich) lode schists based on pit mapping data
7 Examples of sulphur and copper contents for different types of amphibole bearing lode schist
8 Iron contents of four samples of Group 3 lode schists
9 Overall orientation of lode schist bodies associated with East and West Limbs
10 Estimate of the mineralogy of an ore sample
11 Summary of levels and cross-sections for which the copper distribution was studied
12 Statistical parameters for assay data from the 520 and 600 levels
13 Mean copper grades for all lithological groups for the 520 level
14 Average copper contents of GBCl group lode schists for the 520 level
15 Comparison of the orientations of GBCl group lode schists and copper zones for East and West Limbs
16 Structural elements and notation of the Kanmantoo Mine area
17 A correlation of S surfaces described in the Kanmantoo Mine area
18 Proportions of the main mineral groups for 327 veins from the Kanmantoo Mine
19 Mineral assemblages of the Kanmantoo Mine area
20 Observed types of chemical zoning in Kanmantoo Mine garnets

21 X_{Fe} ratios of grain edges for various minerals
22 Al and Si ratios of biotite and chlorite grain edges
23 Cation ratios of garnet and biotite rims
24 Garnet-biotite thermometry
25 Garnet-cordierite thermometry
26 P-T estimates from gar-crd-qtz-and bearing assemblages
27 Fe-Ti oxide thermometry
28 Examples of Niggli *al-alk* ratios for common aluminous minerals in sediments
29 Chemical compositions and Niggli ratios of some common sedimentary rock types
30 Chemical compositions and Niggli ratios for some common Kanmantoo Group metasediments
31 Metal contents of Kanmantoo Group metasediments from road cuts along the South-Eastern Freeway
32 FeO contents of GAB(1) schist and QMF schist in drill hole KS 31
33 Niggli ratios for GAB(1) schist samples
34 Base metal and trace element contents of GAB(1) schist and pyritic schist
35 Mean chemical composition of GAB schist varieties occurring in the Kanmantoo Mine area
36 Mean chemical compositions of lode schists from the Kanmantoo Mine
37 Summary of indicated changes in element abundance and volume by alteration

1. INTRODUCTION

1.1 Location

The Kanmantoo Mine is located 40 km east southeast of Adelaide in South Australia on the Barker 1:250,000 map sheet (SH 54-13), at approximately 35º 06'S, 139º 00'E. It is in low hills on the eastern flank of the Mount Lofty Ranges and is close to both the South Eastern Freeway and the Princes Highway, which passes through the township of Kanmantoo, 2.5 km north of the mine. The township of Callington is 10km to the southeast of the mine, and the Adelaide-Murray Bridge railway line passes 4km south of the mine. The mine occurs on the eastern side of a low, north-south trending hill flanked by ploughed fields and some poorly timbered grazing land. Figure 1 is a view of the immediate mine area and Figure 2 shows the pit viewed from the northeast.

1.2 Background to this study

The Kanmantoo copper lodes are hosted by folded and regionally metamorphosed rocks. Like many base metal and precious metal deposits in regional metamorphic terranes (Marshall and Gilligan, 1993; Vokes, 2000; Marshall and Spry, 2000), the origin of the Kanmantoo lodes is not well understood and remains contentious despite many studies. The core of the contention is whether the lodes represent *metamorphosed* or *metamorphogenic* mineralisation, as these terms are defined by Marshall and Spry (2000). Some studies have advocated a pre-metamorphic origin (Verwoerd and Cleghorn, 1975; Seccombe et al., 1985; Both, 1990; Both et al., 1995; Toteff, 1999; and Marshall and Spry, 2000), perhaps involving substantial local metamorphic remobilisation of sedimentary sulphides (Lindqvist, 1969). Others have advocated a syn-metamorphic origin (Oliver et al., 1998).

Arguments in favour of a metamorphosed origin for the Kanmantoo lodes have gained much credibility in recent years with the recognition of convincing exhalative deposits in the Kanmantoo district, some of them close to the Kanmantoo Mine (Toteff, 1999). The recognition of these rocks has provided strong support for the theory that the Kanmantoo lodes represent a palaeo-feeder system for the exhalative deposits (Seccombe et al., 1985; Toteff, 1999). Marshall and Spry (2000) expressed an opinion that the “exhalites in the near vicinity of the Kanmantoo deposit have particular importance; either they are genetically significant, or one must invoke the remarkably fortuitous circumstance whereby a metamorphogenic deposit is spatially associated but genetically unrelated to exhalative units”. Whilst the author is sympathetic with this opinion, a sizeable dilemma has been created by key information gathered during this study that requires a syn-tectonic, and a metamorphogenic, origin for the bulk of the Kanmantoo deposit. This thesis presents the data supporting this conclusion.

Prior to the start of open cut mining in 1970, the relationship of the mineralisation to the host rocks, and hence the origin of mineralisation, was unclear, despite several geological studies including a doctorate thesis completed in 1969 (Lindqvist, 1969). At the stage prior to mining the favoured origin of mineralisation involved metamorphic modification and remobilisation of a disseminated sulphide body conformable with relict bedding in the host metasediments (Lindqvist, 1969; Verwoerd and Cleghorn, 1975).

The author was the last geologist to work at the mine before it closed in 1976. As an employee of Mines Exploration Pty. Limited. (a subsidiary of BH South Limited), the author

was involved in mining geology and exploration geology in the Kanmantoo Mine area. Twelve months were spent during 1974 carrying out regional geological mapping to the north and east of the mine. The following fifteen months, during 1975 and early 1976 (just before the mine closed), were spent as the mine geologist. By the end of this period, the open cut mine had reached the RL 300' bench, 128m below the original hill top, and underground development of several lodes beside the open cut were nearing completion. The author was responsible for all routine mapping of the exposures provided by mining operations and developed the opinion that the structural relationship between the copper lodes and their host rocks was inconsistent with the then current genetical model. Much of the field data presented in this study was derived from this period of employment.

1.3 Objects and Scope

The primary aim of this study has been to investigate the origin of the Kanmantoo copper mineralisation by studying certain aspects of its geological setting. Specific aims were:

(a) To document the variety and spatial distribution of lithologies associated with copper mineralisation.

(b) To determine the structural geological setting of the mineralisation, in particular the relationship of lode geometry to folded bedding in the surrounding schists.

(c) To document the spatial distribution of copper within the Kanmantoo Mine and compare it to the structure of the host rocks.

(d) To study the microstructure of the lode schists and their enclosing rocks, particularly the sulphide minerals and any hydrothermal alteration products.

(e) To study the petrology of the rocks associated with mineralisation.

(f) To determine the major and minor element geochemistry of the lode schists and their host metasediments, firstly to examine how the host metasediments differ from surrounding metasediments and secondly, to evaluate the chemical effects of possible hydrothermal alteration.

Most of the work completed for this study was done in the immediate Kanmantoo Mine area, however, the semi-regional setting was studied using 1:5,000 scale geological mapping of a 90km^2 area done by Mines Exploration Pty. Ltd. geologists, including the author who mapped 30 km^2 (described in detail later).

For the Kanmantoo Mine area, work completed was mainly geological mapping, petrological studies and the collection and chemical analysis of samples. An area of 230ha surrounding the mine was mapped at 1:2,400 scale. In the open cut mine, over 18,000m of bench faces were mapped at the mine scale of 1:480. Structural measurements were taken and plotted onto maps and stereographic projections. Selected samples were collected and examined under transmitted and reflected light, and 374 mineral compositions were determined by electron microprobe. Rock samples were analysed for up to 26 elements including all major elements. Further details of this work are discussed in the various sections in which the results are presented.

1.4 Previous Work

Most detailed regional geological studies of the southern Mount Lofty Ranges have concentrated on stratigraphy, structure and metamorphism rather than metallogeny. Included are the studies of Sprigg and Campana (1953), Kleeman and Skinner (1959), Mirams (1962), Thomson (1965, 1969), Offler and Fleming (1968), Fleming (1971), Daily and Milnes (1971, 1972, 1973) and Mancktelow (1979, 1989), Dimoke and Sandiford (1992), Flottmann et al. (1994, 1998), Sandiford et al. (1995) and Oliver and Zakowski (1995). Studies dealing with sulphide mineralisation were reported by Dickinson (1942, principally dealing with copper), Askins (1968, principally lead-zinc), George (1969a.b, on the Nairne syn-sedimentary pyrite deposit), Thomson (1975), Spry (1976, principally lead-zinc-copper), Seccombe et al (1985, sulphur isotopes), Spry et al. (1988), Both (1990), Toteff (1994, 1999, syn-sedimentary copper, lead and zinc), Both et al. (1995, principally lead-zinc), Gum et al. (1995), Gum (1998), Oliver et al. (1998), and Smith (1998). Several of these referred to aspects of the geology of the Kanmantoo copper deposit, and they will be discussed elsewhere in this thesis. Regional review papers were published by Parker (1986), Both (1990), Belperio et al. (1997), and Marshall and Spry (2000).

Previous studies, specifically of the Kanmantoo copper deposit, were carried out by Lindqvist (1969), Verwoerd and Cleghorn (1975), Schiller (1978, and various company reports), Nero (1993), Oliver et al. (1998) and several unpublished documents by the staff of the Kanmantoo Mines Ltd. and Mines Exploration Pty. Ltd. Of these, the major work is the Ph.D. thesis of Lindqvist (1969), who studied the Kanmantoo deposit when it was being evaluated prior to mining. Although Lindqvist's study produced much valuable information, its scope was restricted to surface outcrop and diamond drill core. The drill core was especially valuable at that time because the deposit was covered by laterite and its geological setting was unclear.

Verwoerd and Cleghorn's (1975) reference paper was written by two of the senior mining geologists and was based on data available at the initial stages of mining. The authors presented a summary of the discovery of the Kanmantoo deposit and the results of much of the evaluation diamond drilling. However, little is mentioned about the geology as revealed by the preliminary mining operations. Their conclusions closely follow those of Lindqvist, echoing the prevailing theories at the time. Prior to, and during mining, many unpublished reports were written for company purposes by staff of Kanmantoo Mines Ltd. and Mines Exploration Pty. Ltd., and the data from several of these is used in this thesis. Nero (1993) completed an Honours thesis on the mine and its surrounds seventeen years after the mine ceased operations, but she had only limited access to the mine.

A more detailed account of previous work on the Kanmantoo copper mineralisation is presented in Chapter 9.

1.5 Refereed publications resulting from this study

Contributions to three publications have resulted from the work presented here. Copies are included in Appendix 7. The publications are:

1. Seccombe et al. (1985)

2. Spry et al., (1988)

3. Oliver et al. (1998)

1.6 Discovery and copper production from the Kanmantoo Mine

Copper mineralisation was first discovered in the Kanmantoo district in 1846 (Dickinson, 1942). The lodes that were subsequently mined consisted of numerous, small, lenticular and pipe-like bodies occurring on the eastern side of the ridge now containing the Kanmantoo open cut mine. The lodes were mined continuously until 1875 for a total production of 24,000 tonnes of ore at an approximate average grade of 8.5% copper. The mining history of this area is documented by Chilman (1982), who reported that the word Kanmantoo is a corruption of the aboriginal expression *Kungna tuko* meaning different tongue, related to the use of the area as a meeting place.

A period of little activity followed the first phase of mining until 1961, when Mines Exploration Pty. Ltd., in conjunction with McPhar Geophysics, began exploration in the Kanmantoo district. The exploration concentrated on the use of ground geophysical methods. In January 1962, an induced polarisation programme commenced and strong anomalies were obtained over the laterite covered hill containing the old Kanmantoo workings on its edge. Subsequent magnetic investigations and drilling located the Kanmantoo deposit beneath the laterite, which did not have geochemically anomalous copper contents. Further details of the discovery story can be found in Verwoerd and Cleghorn (1975).

The Kanmantoo Mine was operated by Kanmantoo Mines Limited, a subsidiary of BH South Limited, between 1970 and 1976. Production from the mine during this period is listed below (Treloar, 1980):

Sulphide ore	4,051,000 tonnes
Oxidized ore	507,000 tonnes

The mean grade of sulphide ore, as deduced from data published in annual reports by Kanmantoo Mines Ltd., was 0.87% Cu.

1.7 Grids

During production at the Kanmantoo Mine the grid used on the mine was a local, imperial grid. All mine-based data was recorded with respect to this grid, including mapping, surveying, drill logs etc. For simplicity and accuracy this grid has been retained in this study for much of the presentation. In the district surrounding the mine, data has been recorded with respect to the Australian Metric Grid, Zone 54 (Australian Geodetic Datum, 1966). This metric grid was used for all regional mapping.

The relationship between the local mine grid and the Australian Metric Grid is explained in Appendix 2.



Figure 1. View of the mine and infrastructure, looking west (left edge) to NNW (right edge). The open cut mine, in the upper centre, occurs on a ridge extending across the page. The mine is flanked to the left by the surface workings of the South Eastern Mineralisation that occur below the flat lying laterite surface. On the skyline above the mine is the top of the waste dump. To the right of the mine is the haul road and, further right, the pipeline and track to the tailings dam, and then the sealed public road to Kanmantoo. In the foreground is the recycling dam and associated tanks, and to the right can be seen the run-of-mine pad, the crusher shed from which the conveyor belt extends towards the top of the fine ore bins, where the photograph was taken.

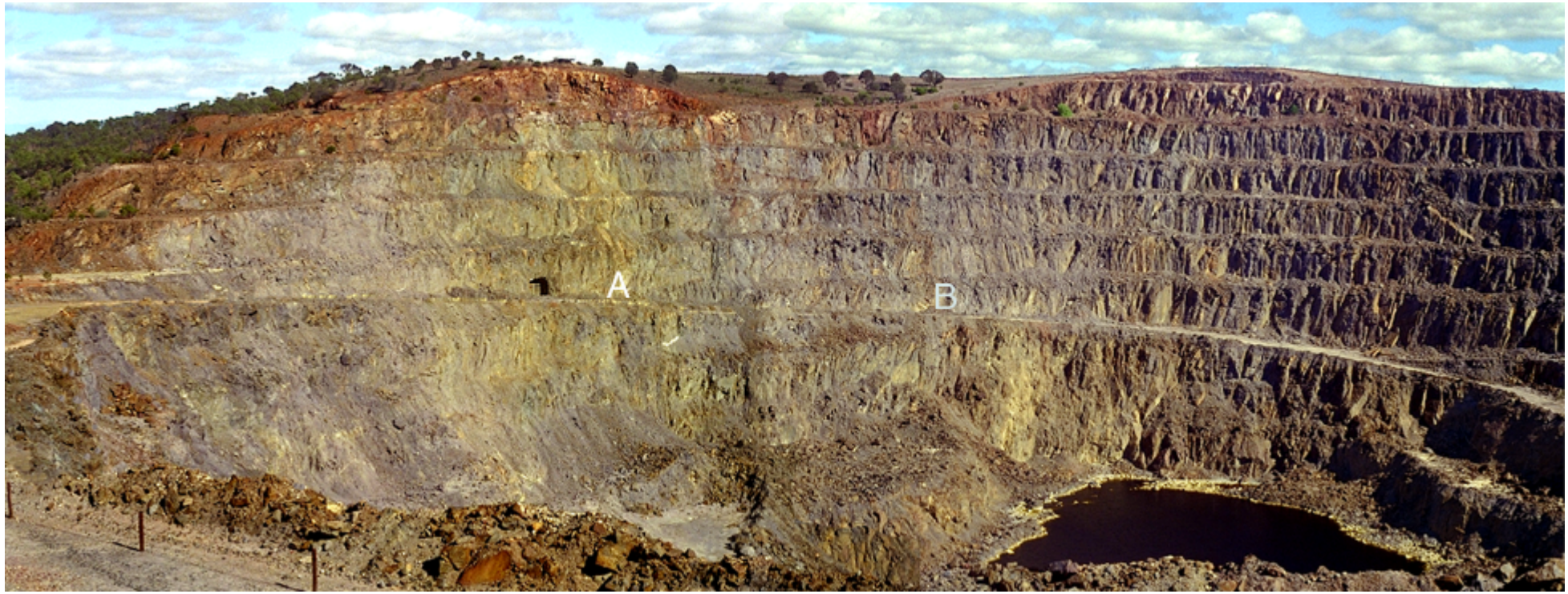


Figure 2. South wall of the Kanmantoo open cut mine. The original land surface is visible at the top with some laterite visible on the left side. The old surface workings of the South Eastern Mineralisation are hidden in the trees at the very left side. The main access to and from the pit was the haul road that can be seen curving from the pit entry at the centre of the left edge, down to lower right. The northern limit of the South Eastern Mineralisation is exposed in the pit above and below the letter A on the haul road and shows as a yellowish stained zone. The portal to the left of the letter A is the only entry to the underground workings and its elevation is approximately the same as the 520 bench level. The letter B marks the position where the extension of the Main Lode crosses the haul road, but the mineralisation is very weak there.

2. REGIONAL GEOLOGY

The Kanmantoo copper deposit occurs in the southern part of the Adelaide Fold Belt, part of an orogenic belt that extends from its well exposed areas in the Mount Lofty Ranges, Fleurieu Peninsula and Kangaroo Island (Figure 3), eastwards below the Murray Basin as far as western Victoria. The oldest rocks in the fold belt are Precambrian basement inliers exposed along the core of the Mount Lofty Ranges in several areas. They comprise the late Palaeoproterozoic to early Mesoproterozoic Barossa Complex metasediments and granites, deformed and metamorphosed during the Olarian Orogeny (ca 1600-1550 Ma) (Belperio et al., 1998). The next group of rocks belong to the Adelaide Geosyncline and in the Adelaide region they date back to ca 770 Ma when deposition of thick clastics and minor carbonates of the Burra Group commenced. They were followed by the glacigene rich Sturtian-Marinoan Umberatana Group and finally the post-glacial Wilpena Group. Belperio et al. (1998) point out that data by Dalziel (1991) and Powell et al. (1994) suggest that the eastern margin of Australia separated from the rest of Rodinia during sag phase sedimentation of the Umberatana and Wilpena groups. However, the present position of the continental margin remains uncertain.

In the Early Cambrian sedimentation resumed in the Adelaide region with deposition of shallow marine shelf and carbonate sediments of the Normanville Group. The uppermost units in the Normanville Group are the Heatherdale Shale and the Truro Volcanics. U-Pb dating of a tuff unit within the Heatherdale Shale reported an age of 526 ± 4 Ma (Cooper et al., 1992). The Truro Volcanics are altered basic to intermediate submarine lavas (Forbes et al., 1972; Rankin et al., 1991, Gatehouse et al 1992) representing renewed crustal extension in this region. Geochemically, the volcanic rocks indicate within-plate affinities (Gravestock and Gatehouse, 1995). Further extension resulted in the development of the Kanmantoo Trough and the thick clastic sediment package within it, known as the Kanmantoo Group. The most common rocks throughout the Kanmantoo Group are meta-sandstones, meta-arkoses and meta-pelites (Thomson, 1969a; Daily and Milnes, 1973). Minor meta-sedimentary lithologies include pyritic schists, meta-conglomerates, calc-silicates and marbles.

Deposition of the Kanmantoo Group commenced in the Early Cambrian. The type of sediment and isotopic dates indicate that deposition was rapid. Isotopic dating constrains sedimentation, burial and heating of the Kanmantoo Group to a period of less than 12 Ma (between 526-514 Ma, Foden et al., 1999). The large scale tectonic controls responsible for deposition of the Kanmantoo Group remain conjectural despite considerable recent work. Von der Borch (1980) argued that the Kanmantoo Group was deposited on a continental slope and an abyssal plain on oceanic crust, following Early Cambrian rifting. Support for a passive continental margin setting was obtained by subsequent work on basic rocks occurring within the Mount Lofty Ranges (Liu and Fleming, 1989) and beneath the Murray Basin (Gatehouse et al, 1992), which show that the basic rocks have MORB chemical affinities. According to Belperio et al. (1998) the types of sediments within the Kanmantoo Group indicate a continental shelf to slope environment rather than an oceanic setting.

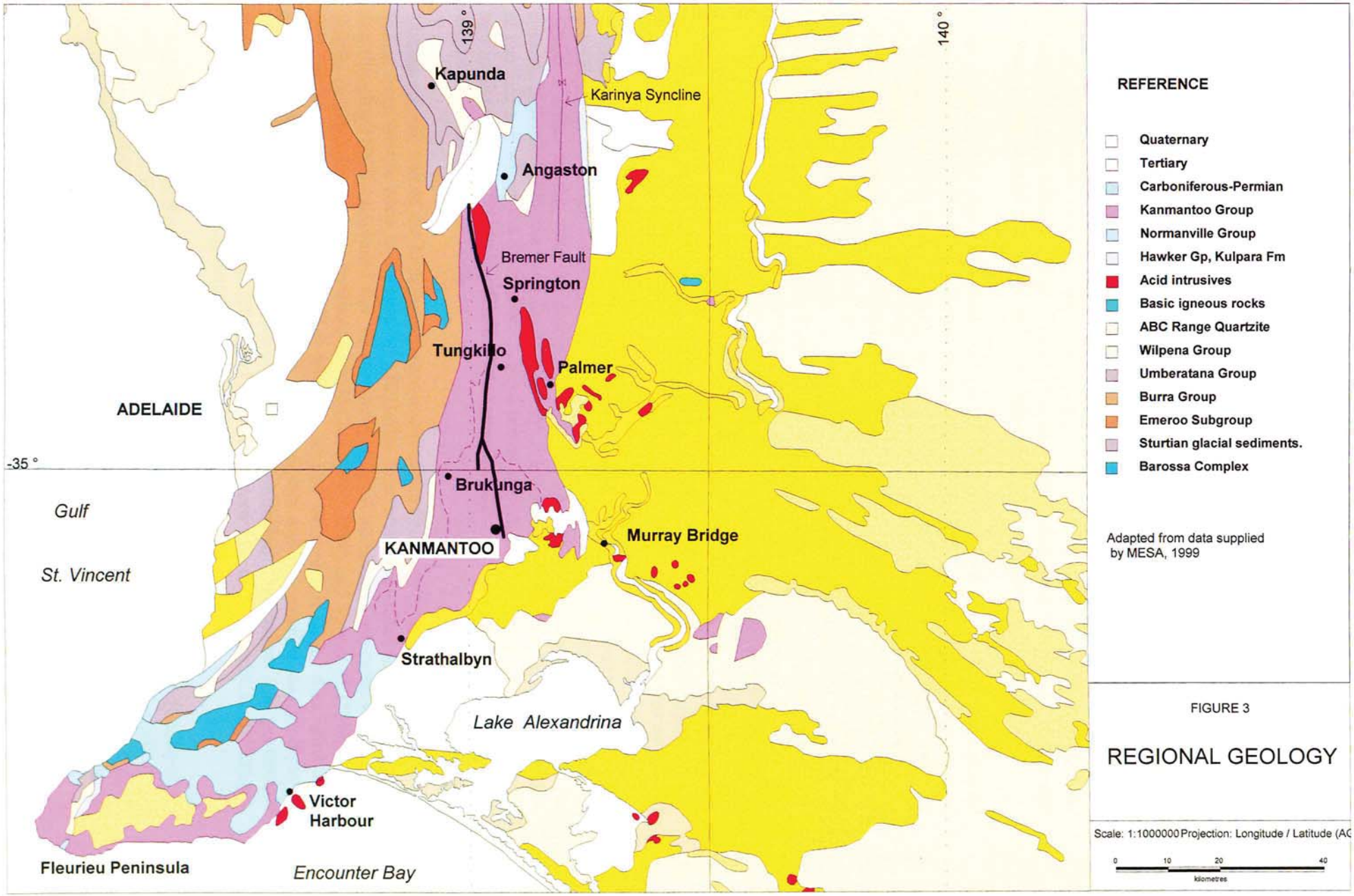
Two stratigraphic subdivisions of the Kanmantoo Group have been proposed. An early and now out-dated subdivision by Forbes (1957) and Thomson and Horwitz (1962), was based principally on rocks exposed in the Nairne-Kanmantoo district. This subdivision was superseded by the currently accepted subdivision, proposed by Daily and Milnes (1971, 1972,

1973) and shown in Figure 4. It was based on the excellent exposure along the southern coast of Fleurieu Peninsula, which has long been recognised as a type locality for the Kanmantoo Group (Sprigg and Campana, 1953). Mancktelow (1979) attempted to link the stratigraphy of the Nairne-Kanmantoo district with the type area, but experienced some difficulty because many of the characteristic lithologies of the well exposed type area are poorly outcropping meta-pelites and could not be recognised further north. Recent work by the South Australian Department of Mines and Energy has successfully adapted the type section stratigraphy to the Karinya Syncline area in the northernmost exposed Kanmantoo Group rocks.

The Kanmantoo copper deposits occur within the upper part of the Tapanappa Formation (Mancktelow, 1979; Spry et al., 1988; Both, 1990, Gum, 1998). The Tapanappa Formation is a thick sequence of silty sands conformably overlying the Talisker Calc-siltstone, a transgressive unit containing sulphidic sediments including the Nairne Pyrite Member (Dyson et al., 1994). The Tapanappa Formation represents the onset of a period of rapid sedimentation of submarine shelf sediments. Thin siltstone and mudstone units occur which may be rich in pyrite and pyrrhotite and anomalous in base metals (Gum et al., 1994). The Kanmantoo copper mineralisation is hosted by the Paringa Andalusite Member (Kleeman and Skinner, 1959, an informal name) within the upper part of the Tapanappa Formation.

Most sedimentation was terminated at about 510 Ma (Belperio et al., 1998) by a period of compressional tectonism known as the Delamerian Orogeny (Thomson 1975), which resulted in the folding, faulting and metamorphism of the rocks of the Mount Lofty Ranges. Isotopic dating indicates that the earliest deformation (D_1) pre-dates 514±5 Ma (Foden et al., 1999) and the D_2 deformation was estimated at 510±2 Ma by Chen and Liu (1996). The Delamerian Orogeny is generally considered to result from plate convergence (Powell et al., 1994; Belperio et al., 1998), but details of the plate locations are open to debate. Haines and Flottmann (1998) proposed that thick foreland basin deposition continued during the Delamerian Orogeny and the sediments now lie below Gulf St. Vincent. The regional structure of the southern Adelaide Fold Belt has been described by Offler and Fleming (1968), Mancktelow (1979,1990), Jenkins (1990), Steinhardt (1991), Jenkins and Sandiford (1992), Flottman et al. (1994), Preiss (1995), and Haines and Flottmann (1998). The structure of the fold belt as exposed in the Mount Lofty Ranges, differs on the eastern and western sides, more or less separated by the Meadows-Williamstown Fault. The structure of the western part of the fold belt is dominated by fold and thrust belt tectonics. In contrast, the eastern side is characterised by steeper faults and upright folds. On the western side Flottman et al. (1994) interpreted an imbricate set of thrusts verging towards and over the Gawler Craton foreland region. Further to the west are essentially undeformed Cambrian cover sediments on the cratonic basement (Flottman and Cockshell, 1995; Flottmann et al., 1998). On the eastern side of the fold belt (where the Kanmantoo mineralisation occurs), the steep faults were interpreted by Flottman et al. (1994) to involve the Adelaidean and Barossa Complex rocks, in contrast to the western side of the fold belt.

Metamorphism was of the high temperature-low pressure (Buchan) type. Metamorphic grade varied from biotite zone in the west to sillimanite zone with migmatites in the east. Offler and Fleming (1968) concluded that the metamorphic peak coincided temporally with the first ductile deformation (D_1). In contrast, Mancktelow (1979, 1990) and Spry et al. (1988) argued that the metamorphic peak coincided with the second deformation (D_2). Sandiford et al. (1995) proposed that the timing of peak metamorphism and deformation was diachronous


139 °
140 °
-35 °
Kapunda
Karinya Syncline
Angaston
Bremer Fault
Springton
Tungkillo
Palmer
ADELAIDE
Brukunga
KANMANTOO
Murray Bridge
Gulf
St. Vincent
Strathalbyn
Lake Alexandrina
Victor
Harbour
Fleurieu Peninsula
Encounter Bay
REFERENCE
Quaternary
Tertiary
Carboniferous-Permian
Kanmantoo Group
Normanville Group
Hawker Gp, Kulpara Fm
Acid intrusives
Basic igneous rocks
ABC Range Quartzite
Wilpena Group
Umberatana Group
Burra Group
Emeroo Subgroup
Sturtian glacial sediments.
Barossa Complex
Adapted from data supplied
by MESA, 1999
FIGURE 3
REGIONAL GEOLOGY
Scale: 1:1000000 Projection: Longitude / Latitude (AC
0
10
20
40
kilometres

across the belt and was related to mid-crustal granite intrusion. The various fold generations are best exposed in the higher grade rocks on the eastern side of the Mount Lofty Ranges, where the structural and metamorphic history appears to be more complex.

Granite intrusions in the fold belt define distinct chemical and temporal groups (Foden et al., 1990; Turner and Foden, 1990; Sandiford et al., 1992; Foden et al., 1999). The oldest and most strongly deformed granite in the Adelaide Fold Belt, the Rathjen Gneiss, has been dated at 514±5 Ma for the age of igneous crystallization (Foden et al., 1999). The Rathjen Gneiss has geochemical affiliations with anorogenic or intra-plate granites (Foden et al., 1999). Field relations indicate that the Rathjen Gneiss pre-dates the earliest fabric (a sub-horizontal foliation) attributed to S_1 (Oliver and Zakowski, 1995). The next oldest group of granites are syn-tectonic. They have variably developed deformation fabrics and appear to contain no evidence of D_1 deformation (Mancktelow, 1979; Sandiford et al., 1992). Zircon ages indicate post-514 Ma to 490 Ma. This group is predominantly I-type but includes some S-types (Milnes et al, 1977, Sandiford et al., 1992). The third and youngest group consists of undeformed A-type granites that are associated with mafic magmatism (Turner et al., 1992). They are 490-480 Ma and occur mostly as isolated exposures within the Murray Basin.

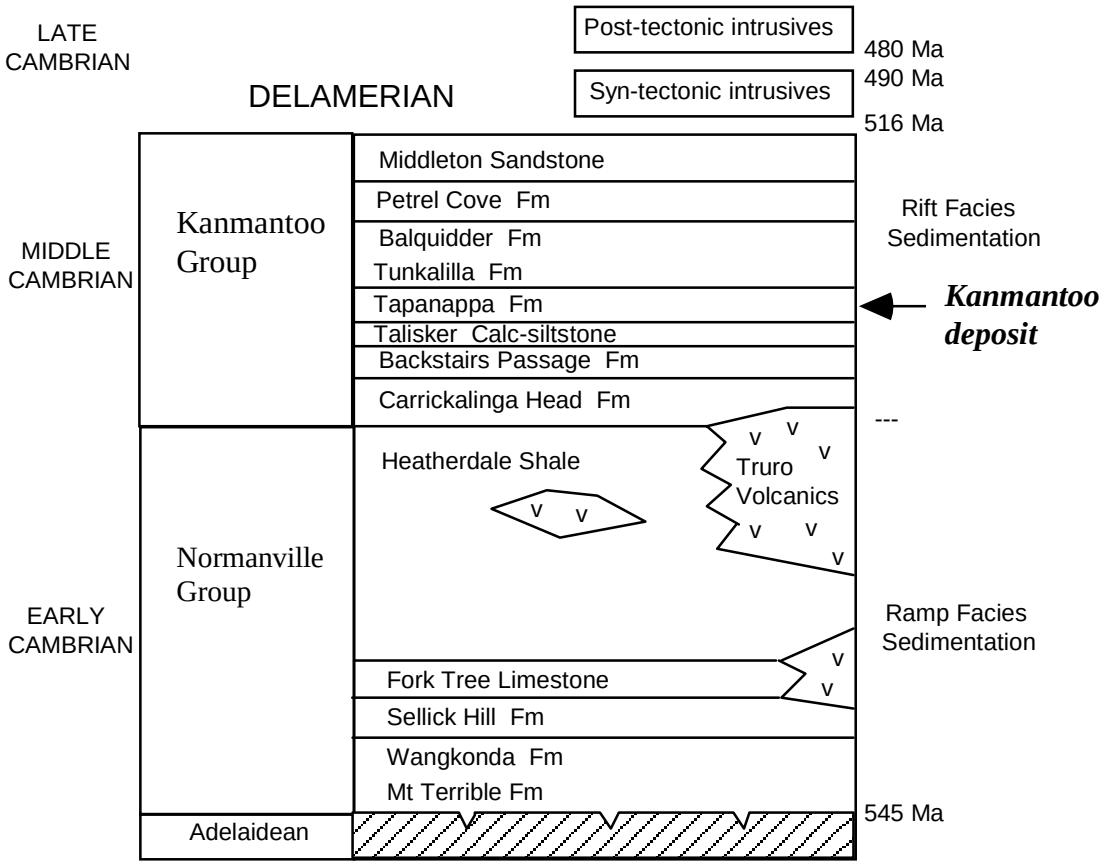


Figure 4. Stratigraphic column and geochronological framework for Fleurieu Peninsular and Kangaroo Island (based on Belperio et al., 1998).

3. LITHOLOGIES

3.1 Introduction

This chapter describes both the copper mineralised rocks associated with the Kanmantoo copper deposit and also the unmineralised rocks in the surrounding district. Many of the rocks described in this chapter have been described previously in considerable detail. In particular, Lindqvist (1969) described the mineralised rocks and the metasediments of the Kanmantoo Mine area, and Fleming (1973) described the metasediments of the Kanmantoo-Dawesley district. The lithological classification used here is derived from the scheme used by Mines Exploration Pty. Limited. for its regional and mine mapping programs, and is similar to that of most other workers in the area.

In the Kanmantoo district, the degree of exposure is good enough to be able to locate major features. The percentage of outcrop, as it was defined by the 1:5,000 scale mapping program of the Kanmantoo district by Mines Exploration Pty. Ltd., can be estimated. On average for a mapped area of 60 sq km area in which the mine is located in the NW quadrant, the overall proportion of outcrop was 30%. The best exposures occur in the quartz rich schists where the outcrop proportion is approximately 50%. Schists with abundant, coarse andalusite, such as the ridge hosting the Kanmantoo Mine, also tend to outcrop well. In contrast, the common micaceous schists exhibit the poorest exposure. In the Kanmantoo Mine, exposure is complete because the rocks are unweathered from close to the surface, but the exposures are subject to being obscured by dust, or are not easy to examine closely for safety reasons.

3.2 Classification

For this study the lithologies of the Kanmantoo district and the mine have been subdivided as shown in Table 1. Also shown are the abbreviations used for some of the lithologies and these will be used henceforth rather than the full description.

Table 1. Lithological classification used in this study.

Kanmantoo district		Kanmantoo Mine*	
Lithology	Abbreviation	Lithology	Abbreviation
Metasediments		*Lode schists*	
Garnet-andalusite-biotite schist*	GAB schist	Garnet-andalusite-biotite-chlorite schist	GAB(Cl) schist
Quartz-mica-feldspar schists	QMF schist	Garnet-andalusite-biotite-chlorite schist	GABCl schist
Quartz-mica schist	QM schist	Garnet-andalusite-biotite-chlorite schist	G(A)BCl schist
Quartz-feldspar schist	QF schist	Garnet-biotite-chlorite-andalusite schist	GBCl(A) schist
Quartz-mica-andalusite schist	QMA schist	Garnet-biotite-chlorite schist	GBCl schist
Garnet-biotite schist	GB schist	Garnet-chlorite-biotite schist	GClB schist
Pyritic schist		Garnet-chlorite schist	GCl schist
Calc-silicate rocks		Garnet-biotite schist	GB schist
Meta-chert and related rocks		Biotite-staurolite rock	
		Muscovite-chlorite rock	
Laterite		Chlorite-magnetite rock	
		Amphibole-bearing schist	
		Muscovite-bearing schist	

* GAB schist also occurs in the Kanmantoo Mine

All lithologies listed for the district are interpreted to be metasediments, of amphibolite facies metamorphic grade. These lithologies are inferred to be derived from sediments because they

commonly have sedimentary structures, especially bedding, and their bulk compositions. No igneous rocks have been recognised in the Kanmantoo district. The nearest occurrences of igneous rocks are the meta-dolerite dykes located 13km to the northwest of the mine, pegmatites located 10km to the east (Gum, 1998) and the Monarto Granite outcrops located 15km to the east.

The mineral compositions of the lithologies are summarised in Table 2. Each of the lithologies listed above will be described in this chapter, and their mineralogies, including any subdivisions (which are described later), are shown in Table 2. Some of lithologies listed in Table 1 are transitional with one another, however each is distinctive enough to pose no significant problems of classification.

Table 2. Mineral compositions of common lithologies.

	Qtz	And	Gar	Sta	Bio	Mus	Cht	Amp	Fel	Crd	Sul	Ilm	Mt
District													
QM schist	M	-	m	-	M,m	M	t	-	M	-	t	t	t
QF schist	M	-	t	t	m	m	t	-	M	-	t	t	t
QMA schist	M	m,t	m	t	M,m	M	t	-	M	-,t	t	t	t
GAB schist	M	m,t	m	m,t	M	t	t	-	t	-,t	t	t	t
Pyritic schist	M,m	-,m	m,t	t	t	t	t	t	t	t	M,m	t,m	t
Calc-silicate schist	t	-	m,t	-	-,t	-	-	M	M	-	-	t	t
Quartzite	M	-	-	-	-	-	-	-	-	-	t	-	-
Mine													
GAB(1) schist	M	m,t	m	m,t	M	t	-	-	t	-,t	t	t	t
GAB(2) schist	M	m,t	m	m,t	M	t	t	-	t	-	t	t	t
GAB(3) schist	M	M,m	m	m,t	M,m	t,m	m,t	-	t	-,t	t,m	t	t
GAB(Cl) schist	M	m	m	m,t	M	t	m	-	t	-	t	t	t
GABCl schist	M	m	m	m,t	M	t	m,M	-	t	-	t	t	t
G(A)BCl schist	M	m	m	m,t	M	-	m,M	-	-	-	t,m	t	t
GBCl(A) schist	M	m,t	m	m,t	M,m	-	M,m	-	-	-	t,m	t	t
GBCl schist	M	-	m	m,t	M	-	M,m	-	-	-	t,m	t	t
GClB schist	M	-	m	m,t	m	-	M	-	-	-	t,m	t	t
GCl schist	M	-	m	m,t	m,t	-	M	-	-	-	t,m	t	t
GB schist	M	-	m	m,t	M	-	m,t	-,t	-	-	t,m	t	t
Biotite-staurolite rock	-	-	m,M	M	M	-	M	-	-	-	m	t	t
Muscovite-chlorite rock	-	-	m	m	m	M	M	-	-	-	m	m	t
Chlorite-magnetite rock	m	-	m	m	-	-	M	-	-	-	-	-	M
Amphibole-bearing schist	m,t	-	m	-	t,m	-	M,m	m	-	-	m	t	t
Muscovite-bearing schist	M	-	m	t	M	M	-	-	t	m,t	m,t	t	t

Notes.
M = major constituent (more than 20%) m = minor (1-20%)
t = trace (less than 1%) - = not observed

Qtz = Quartz Mus = Muscovite Crd = Cordierite
And = Andalusite Cht = Chlorite Sul = Sulphide
Gar = Garnet Amp = Amphibole Ilm = Ilmenite
Sta = Staurolite Fel = Feldspar Mt = Magnetite
Bio = Biotite

3.3 Methods of Study

3.3.1 Kanmantoo Mine

During mining, most of the new faces exposed by successive blasts were geologically mapped at the standard mine scale of 1:480 (40 feet to an inch). The pit face mapping technique used was established at the start of mining in the Kanmantoo pit. Measuring tapes were stretched along the base of faces and geological features were recorded against the tape position. The mine surveyor surveyed selected control points along the mapped faces so that the mapping could be coordinated with the mine grid. The results were then plotted manually onto a series of master plans, one for each bench (level). Most benches are 12.1m (40 feet) apart vertically. Plans showing the geology of each bench evolved progressively with time, as each bench grew larger. Features that were mapped included rock types, structural measurements and copper mineralisation.

Only three mine geologists, including the author who was the last, carried out routine pit mapping when the mine operated, and the style of mapping varied a little between each geologist. This study presents the results only of the author's mapping, except where noted otherwise. In total, the author mapped an aggregate face length of 18,014m and 1,954 individual lithological changes were recorded. The author was the sole mapper for the 250 ramp and the 300 bench, mapped nearly all of the 350 and 400 benches, and approximately 70% (by area) of the 440' bench, 35% of the 480' bench, and 20% of the 520' bench. On the 560 bench and above only the perimeters were mapped for this study.

Although the quality of the pit face mapping was generally good, it suffered at times because of the following factors.

- Poor exposure as a result of dirty faces.
- Haste due to mine scheduling pressures.
- Lack of survey control, again this was usually due to mine scheduling pressures.
- Inexperience with the lithologies in the early stages. Unfortunately only one pass was generally available because the faces, except for the final perimeters, were destroyed by blasting and can never be re-mapped.
- Difficulty in recognising certain lithologies, for example the andalusite in dark, hard varieties of GAB(3) schist can be difficult to see.

To present and analyse the mapping data for this study a lithological database was created from the 1,954 mapping records mentioned above, and the positions of all mapped faces were digitised. To create the database a four character coding system was devised which recorded any comments made for the following four features of a lithological unit: the mineral constituents, the fabric, the appearance of the main porphyroblast (usually andalusite) and the hardness of the rock. Details of the coding system are documented in Appendix 1. The major mineral constituents were always referred to because they are fundamental to the standard nomenclature used at the mine, but comments regarding the other features were not always noted. Once coded, all pit mapping data was compiled into a database using Microsoft Excel software. The spatial attributes of the lithological units were digitised from the original map sheets into a database using MapInfo software. Initially, the mapping was digitised with respect to the local mine grid and then the data was converted to other, common coordinate systems.

An example of the faces mapped for one level, the 440 bench, is shown in Figure 5, in this case representing 3,370m of combined traverses and 426 lithological segments. An example of the lithological code mentioned in the previous paragraph is shown in Figure 6, for the northern-most part of the 440 level. The compilations were then used to produce geological interpretations for each bench and they are presented in Figures 137 to 139 (located in the map pocket). In order to be able to get a better understanding of the geology of some benches, consideration was also given to some of the mapping done by other geologists for parts of the some levels. This additional interpretation allows a cross section to be constructed on 12,000'N so that correlation between benches is possible.

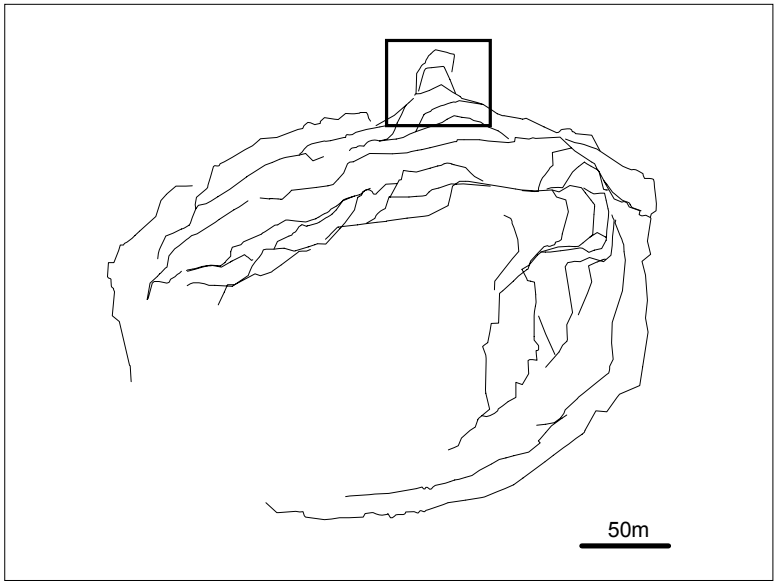


Figure 5. Plan showing all pit face mapping traverses on 440 bench. The rectangle in the northern part of the diagram shows the area covered in Figure 6.

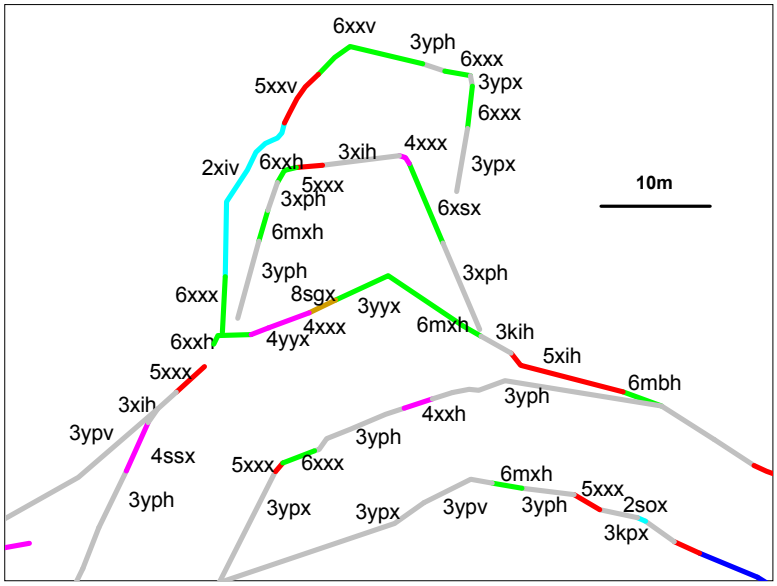


Figure 6. Pit face mapping traverses for the northern portion of the 440 bench. Individual lithological segments are coloured according to the major lithology mapped within the segment. The codes, shown as labels, are explained in Appendix 1.

3.3.2 The immediate mine surrounds

Outcrops within an area of 230ha surrounding the Kanmantoo pit were geologically mapped for this study on aerial photographs at a scale of 1:2,400. The mapping was compiled onto local base plans and is presented as Figure 7 (in map pocket) at a scale of 1:5,000.

3.3.3 The Kanmantoo district

The geological setting of the district beyond the immediate mine area was compiled principally from outcrop mapping at 1: 5,000 scale completed by Mines Exploration Pty Ltd during 1973-1975 when the mine was operating. Six map sheets covering an area of 90km^2 were used to derive the regional geological interpretation shown in Figure 8. The author mapped two of the map sheets. Copies of the original mapping are available on open file at MESA. Other information was obtained from Drexel (1978), S. Toteff (pers. comm., 1996) and from aeromagnetic data flown by CRA Exploration Pty Ltd in 1979. Most of the metasediments shown on Figure 8 belong to the Tapanappa Formation, which was described by Gum (1998) as consisting predominantly of grey, massive to laminated, fine- to coarse-grained meta-greywackes, that grade into thin, very fine-grained, laminated meta-siltstones.

3.4 Metasediments

Throughout the Kanmantoo district certain metasediments tend to occur together as interbeds and define district scale units of consistent lithological mixes or associations. Three of the associations are:

- micaceous versus quartzofeldopathic units
- andalusite bearing versus non-andalusite bearing units
- ferromagnesian rich versus ferromagnesian poor units.

The broad lithological distribution in the Kanmantoo district is shown in Figure 8. Figure 7 shows the outcrop geology for the Kanmantoo Mine area. Both maps will be discussed in subsequent sections. The sedimentary setting of many of these metasediments was described by Gum (1998).

The first association of lithologies occurs within the QMF schist classification and comprises a range of interbedded lithologies varying between micaceous (QM schist end member) and quartzo-feldspathic (QF schist end member). This association corresponds to the transitional lithologies of metamorphosed pelite-psammopelite-psammite, as adopted by Fleming (1973). Variations between micaceous and quartzo-feldopathic compositions can be observed at scales ranging from adjacent beds (in Bouma type sequences for example) to district scale where it is taken into account in the definition of Formations. As an extension of the transitions within QMF schists, QMA schist can be regarded as an andalusite bearing variety of QM schist, with which it is usually interbedded. The relationships between these lithologies are represented in Figure 9.

The last association is manifest by the tendency for ferromagnesian rich and ferromagnesian poor lithologies to form mutually exclusive units at a district scale. The difference between rocks belonging to the ferromagnesian rich and ferromagnesian poor groups is that the former have a greater relative abundance of biotite, garnet and staurolite compared to muscovite. Rocks from the ferromagnesian rich group usually have little or no muscovite. Interbedded QMF schist and QMA schist are the key components of the ferromagnesian poor association and the abundance of QMF schists in the district means that this is the dominant association.

3.3.2 The immediate mine surrounds

Outcrops within an area of 230ha surrounding the Kanmantoo pit were geologically mapped for this study on aerial photographs at a scale of 1:2,400. The mapping was compiled onto local base plans and is presented as Figure 7 (in map pocket) at a scale of 1:52,500.

3.3.3 The Kanmantoo district

The geological setting of the district beyond the immediate mine area was compiled principally from outcrop mapping at 1: 5,000 scale completed by Mines Exploration Pty Ltd during 1973-1975 when the mine was operating. Six map sheets covering an area of 90km^2 were used to derive the regional geological interpretation shown in Figure 8. The author mapped two of the map sheets. Copies of the original mapping are available on open file at MESA. Other information was obtained from Drexel (1978), S. Toteff (pers. comm., 1996) and from aeromagnetic data flown by CRA Exploration Pty Ltd in 1979. Most of the metasediments shown on Figure 8 belong to the Tapanappa Formation, which was described by Gum (1998) as consisting predominantly of grey, massive to laminated, fine- to coarse-grained meta-greywackes, that grade into thin, very fine-grained, laminated meta-siltstones.

3.4 Metasediments

Throughout the Kanmantoo district certain metasediments tend to occur together as interbeds and define district scale units of consistent lithological mixes or associations. Three of the associations are:

- micaceous versus quartzofeldopathic units
- andalusite bearing versus non-andalusite bearing units
- ferromagnesian rich versus ferromagnesian poor units.

The broad lithological distribution in the Kanmantoo district is shown in Figure 8. Figure 7 shows the outcrop geology for the Kanmantoo Mine area. Both maps will be discussed in subsequent sections. The sedimentary setting of many of these metasediments was described by Gum (1998).

The first association of lithologies occurs within the QMF schist classification and comprises a range of interbedded lithologies varying between micaceous (QM schist end member) and quartzo-feldspathic (QF schist end member). This association corresponds to the transitional lithologies of metamorphosed pelite-psammopelite-psammite, as adopted by Fleming (1973). Variations between micaceous and quartzo-feldopathic compositions can be observed at scales ranging from adjacent beds (in Bouma type sequences for example) to district scale where it is taken into account in the definition of Formations. As an extension of the transitions within QMF schists, QMA schist can be regarded as an andalusite bearing variety of QM schist, with which it is usually interbedded. The relationships between these lithologies are represented in Figure 9.

The last association is manifest by the tendency for ferromagnesian rich and ferromagnesian poor lithologies to form mutually exclusive units at a district scale. The difference between rocks belonging to the ferromagnesian rich and ferromagnesian poor groups is that the former have a greater relative abundance of biotite, garnet and staurolite compared to muscovite. Rocks from the ferromagnesian rich group usually have little or no muscovite. Interbedded QMF schist and QMA schist are the key components of the ferromagnesian poor association and the abundance of QMF schists in the district means that this is the dominant association.

GAB schist and GB schist also tend to occur together and they are the main components of the ferromagnesian rich association. Although less abundant, there are several, large ferromagnesian rich units, including the unit that hosts the Kanmantoo copper mineralisation, a fact that is considered important and will be discussed in detail later in subsequent sections.

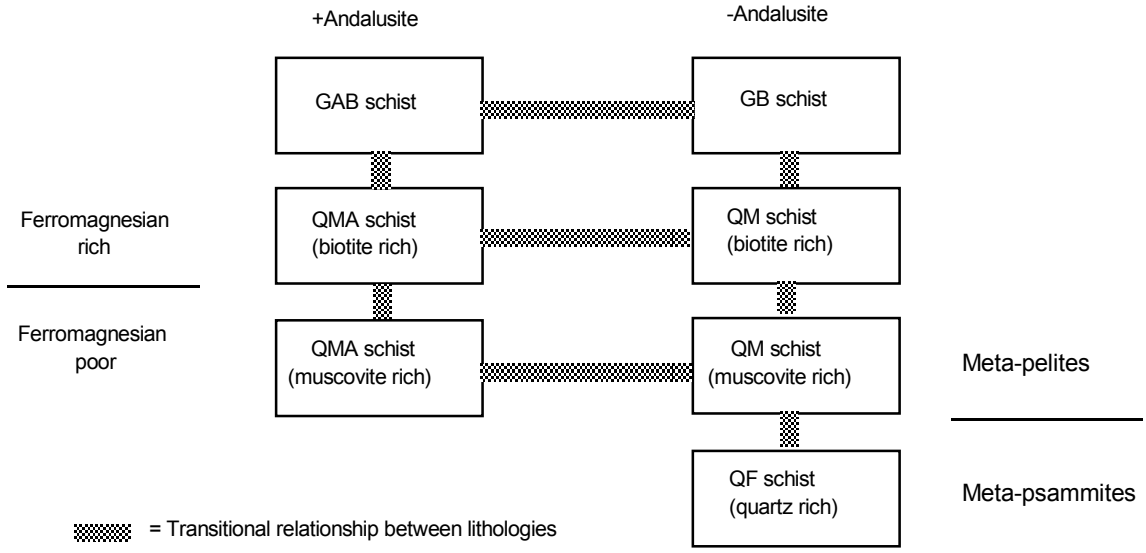


Figure 9. Transitional relationships between metasediments

Useful data on the regional abundances of various metasediments was collected by Drexel (1978) from road cuttings exposed during the construction of the South-Eastern Freeway. Many of the exposures were rehabilitated soon afterwards and are not accessible now. Drexel's survey extends from its western end in the upper portion of the Backstairs Passage Formation eastwards through the entire Talisker Calc-silicate and Tapanappa Formations into the Brown Hill Subgroup. (Because the formation boundaries were not known in this district at the time of his study, Drexel used the earlier stratigraphic nomenclature of Thomson and Horwitz (1962), to classify his samples.) The results from the 544 surface or near surface composite samples are summarised in Table 3 and show that psammo-pelitic metasediments, with 10 to 25% mica contents, are overwhelmingly the most common rock type exposed in the road cuttings.

Table 3. Proportions of Kanmantoo Group metasediments exposed in road cuts of the South-Eastern Freeway (based on data reported by Drexel, 1978).

Lithological description Drexel (1978)	This study	Precursor sediment type	% Total
Metasandstone	QF schist	Psammite	3.3
Laminated metasandstone	QF schist	Psammite	2.5
Micaceous metasandstone (<10% mica)	QF schist	Psammite	2.9
Mica-feldspar-quartz schist (10-25% mica)	QMF schist	Psammo-pelite	70.3
Biotite schist (>25% mica)	QM schist	Pelite	7.0
Andalusite-mica-feldspar-quartz schist	QMA schist	Pelite	6.2
Andalusite-garnet-mica-quartz schist	QMA schist or GAB schist	Pelite	1.8
Laminated pyrite-andalusite-muscovite-quartz schist	Pyritic schist	Pyritic pelite	2.7
Muscovite schist	Pyritic schist	Pyritic pelite	2.5
Feldspathic metasandstone	Pyritic schist	Pyritic psammite	0.6
		Total	99.8

With regard to Drexel's data, it should be noted that the exposures in the road cuttings are not representative of the entire section because the road cuttings were blasted only through the hills and so the data is strongly biased in favour of the more resistant units. Drexel notes that of the of the total 11,490m length of freeway studied 6,420m (or 56%) was available as road cuttings and that the remainder of the section will contain softer lithologies. If the proportion of pelites in the unsampled portions of the section was 50%, for example, then the overall proportion of pelite throughout the entire section calculates as 34%.

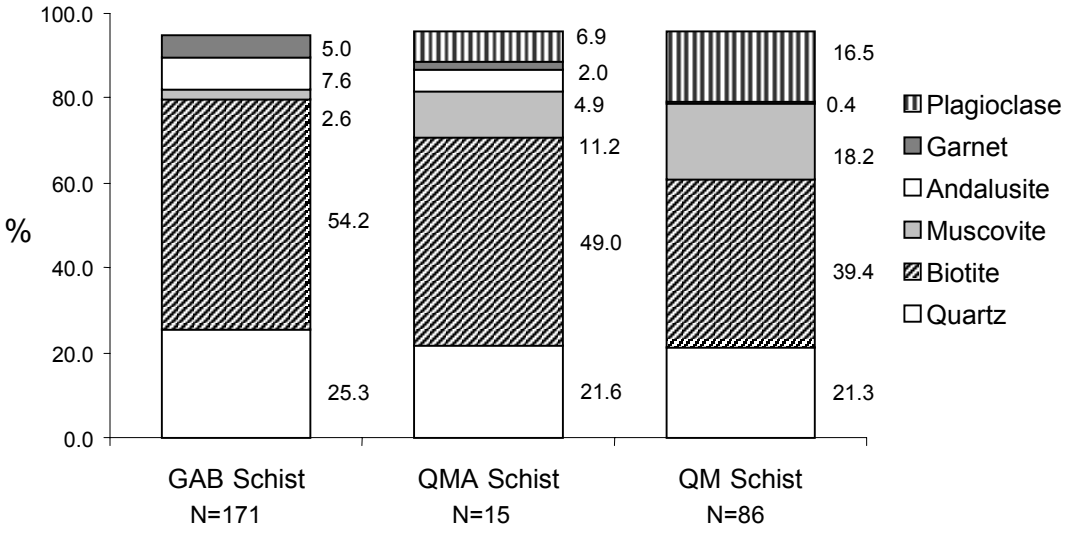


Figure 10. Approximate mineralogical proportions of the three most common lithologies in the Kanmantoo Mine area. (Semi-quantitative estimates based on XRD data from hole KSD 31.)

In the immediate Kanmantoo Mine area, mapping and drilling have shown that the most common metasediments are GAB schist, QM schist and QMA schist. The best available survey of the modal composition of lithologies close to the mine was completed by M.E.P.L. in 1972 on samples from diamond drill hole KS31. This hole of 1161m in length was drilled below the present base of the mine from the hanging wall sequence to the foot wall sequence (that is east to west) and intersected the Main Lode at approximately 360m vertical depth. Estimates of the mineralogical proportions of the three most common metasediments mentioned above are shown in Figure 10. This histogram was prepared by the author from 272 semi-quantitative estimates of modal contents reported by Trueman (1972). The modal estimates were made from X-ray diffraction analyses of samples that were collected every 3m or 6m down-hole. Classification of lithologies used in the figure is as reported in the drill logs and is expected to be similar to the classification used in this study, with some possible discrepancies between GAB schist and QMA schist. In the drill logs many of the GAB schists that were analysed were described as "lody" and had higher chlorite and sulphide contents.

3.4.1 Quartz-mica-feldspar schist

Rocks of this group are, by far, the most common in the Kanmantoo Group in the Strathalbyn-Kanmantoo district. They consist principally of quartz, plagioclase, K feldspar, muscovite and biotite, with minor garnet. The proportions of the constituent minerals vary such that a range between quartzo-feldspathic schists and micaceous schists occurs which is interpreted to represent original psammites and pelites, respectively (Lindqvist, 1969; Fleming, 1973). The quartzo-feldspathic schists outcrop better than the micaceous schists and

so give an exaggerated impression of their abundance in the district. In the immediate area around the Kanmantoo Mine, the micaceous varieties (QM schist) are more common (Figure 11) and form the low lying areas east and west of the ridge containing the mine. Many of these are relatively fine-grained and resemble phyllites. More quartzo-feldspathic varieties (QF schist) outcrop immediately southeast of the mine and also a kilometre to the east-northeast of the mine.



Figure 11. North-westerly view of a QM schist exposure with excellent relict bedding. The traces of bedding and schistosity on a steep joint surface are shown. Two schistosity parallel fractures reveal the bedding-schistosity intersection lineation plunging shallowly to the south (indicated by the line). Also well exposed are several partly anastomosing late stage kinks (for example below the hammer) with typical sub-horizontal axial planes.

Relict bedding is common in all varieties of QMF schist and, together with many other sedimentary structures, confirms a sedimentary origin for this lithological group. Other sedimentary structures include cross bedding, scour structures, graded bedding, climbing ripples, flame structures and concretions. Coarse bedding (one metre wide or greater) is defined by alternating units of quartzofeldspathic and micaceous schists and commonly can be traced continuously for many hundreds of metres. Within quartzofeldspathic schist units, internal bedding is typically uncommon, whereas many micaceous schists preserve bedding as fine as 2mm thick. Facing directions are uncommon near the mine, but the few examples present indicate a lack of overturning.

A penetrative schistosity can be recognised in most varieties of QMF schist. It is most apparent in the micaceous varieties, which generally have a prominent schistosity and mineral lineation. Crenulations are uncommon near the Kanmantoo Mine. The quartzo-feldspathic varieties display a moderate to poorly developed, but penetrative, schistosity depending on the mica content, and typically no mineral lineation is apparent. The extreme quartzofeldspathic types are granofelsic with no apparent oriented fabric. Mesoscopic folds occur throughout the Kanmantoo district but are not as evident in the poorly exposed QMF schists near the

Kanmantoo Mine. An example is shown in Figure 12 and it displays the typical parallelism of schistosity to the fold axial plane.

QMF schist is an important host to copper mineralisation in the Kanmantoo district, and this is described in section 3.6.



Figure 12. Example of QF schist showing an antiform in profile. Note the silicified joints, mostly shallow dipping. The coin at bottom is 3cm in diameter.

3.4.2 Quartz-mica-andalusite schist

Most examples of this widespread lithology can be regarded as an andalusite bearing variety of QM schist. It consists principally of quartz, plagioclase, muscovite, biotite and andalusite, with minor amounts of garnet and staurolite. Because of its coarse grain-size, andalusite usually is the most prominent mineral present. It varies in size from less than 1mm to 10mm and may be rounded or euhedral. In abundance, andalusite varies from a few grains, in what is essentially QM schist, to about 10%. Where abundant, andalusite grains tend to be euhedral. As in QM schist, muscovite is usually more abundant than biotite. Garnet and staurolite are most common in the biotite rich varieties, in particular a variety that is transitional with GAB schist and occurs near the Paringa shaft southwest of the Kanmantoo Mine (labelled QMA(G) schist in Figure 7).

Figure 8 shows that QMA schist is common in the Kanmantoo district, especially to the west of the Paringa Andalusite Member where several north-south trending units of QMA schist occur and are interpreted as part of the limbs of a single, folded QMA schist unit. QMA schist is invariably interbedded with micaceous varieties of QMF schist.

Bedding is usually obvious. Andalusite is either concentrated in bands parallel to bedding, or is randomly distributed. Just south of the Kanmantoo Mine, QMA schist contains ellipsoidal bodies, possibly of diagenetic origin, which Lindqvist (1969, pp 50-52) described as stretched inclusions and used as strain markers.



Figure 13. Folded relict bedding in QMA schist showing typical variations in andalusite content and strong schistosity axial planar to the fold. The coin is 3cm in diameter.

Like QMF schist and GAB schist, QMA schist has a well developed axial planar schistosity which is prominent in all examples except the very porphyroblastic rocks in which the schistosity wraps around so many andalusite crystals that it becomes less obvious. Figure 13 shows an excellent example of folds in interbedded QMA schist and micaceous QMF schist. Elongate andalusite and its pressure shadow material form lineations in the schistosity in many outcrops and commonly steeply plunging crenulations extend away from andalusite grains. QMA schist does not contain significant sulphide mineralisation, neither in the Kanmantoo Mine vicinity nor in the surrounding district.

3.4.3 Garnet-biotite schist

This is a dark rock consisting principally of quartz and biotite with lesser garnet and staurolite. Compared to most metasediments in the Kanmantoo Mine area, it is garnet rich, generally containing up to 10% modal garnet. These rocks are closely associated with GAB schist. Individual units of GB schist contain little internal relict bedding although the units themselves are parallel to bedding in the enclosing GAB schists. Schistosity and mineral lineations tend to be less prominent than in many nearby rocks.

North of the mine thick units rich in GB schist were mapped on the western margin of the Paringa Andalusite Member and to the north of it (refer Figure 8). North of the Kanmantoo Mine Toteff (1999) also reported occurrences of similar rocks associated with the footwall of meta-exhalite horizons. In the Kanmantoo Mine area GB schist is common, especially 300m northeast of the mine in a well-exposed, interbedded unit with GAB schist. Rocks, referred to as coticles, with up to 40% garnet were described from this unit by Smith (1998). The unit can be followed in outcrop from the road to Kanmantoo southwards through the mine infrastructure where it can be seen to change along strike, ultimately to typical QM schist and QF schist south of the public road. From north to south the intermediate section has progressively less GAB schist, more biotite rich QM schist (rather than GB schist), less garnet and more muscovite. The overall transition from north to south may represent a sedimentary

facies change or a trend imposed by chemical alteration; this is considered further in a subsequent chapter. GB schist has also been observed near the O'Neil workings and west of the Paringa workings, again associated with GAB schist.

GB schist associated with metasediments is similar to one of the varieties of lode schist, which has similar mineralogy and fabric and a related origin is possible. Some of the differences between the lode and stratiform varieties are listed below:

(a) Form
The stratiform variety forms units of regular width that are traceable along strike for up to fifty metres. By contrast, the lode variety forms less regular bodies, generally of limited lateral extent, or elongated lenses parallel to the schistosity rather than nearby bedding.

(b) Mineralogy
The lode variety commonly has, in addition to sulphide minerals, abundant chlorite and minor cummingtonite. In contrast, chlorite is rare in the stratiform variety and cummingtonite has not been observed. Trace amounts of andalusite occur in the stratiform variety but not in the lode variety.

(c) Variability
The stratiform variety is more homogeneous with respect to appearance, mineralogy and fabric, especially grain size.

(d) Copper mineralisation
The lode variety is closely associated with copper lodes whereas the stratiform variety has little copper and two samples analysed in this study reported only trace copper.

3.4.4 Garnet-andalusite-biotite schist

GAB schist is a conspicuous rock consisting of coarse andalusite crystals in a dark matrix of biotite and quartz principally, but with lesser staurolite, garnet and muscovite. Muscovite in GAB schists is rare in the immediate Kanmantoo Mine area, but occurs on the margins of the open cut mine and is common to the north of the mine. Although it has not been quantified, mapping suggests that the muscovite:biotite ratio increases away from the mine and may be an index of zoning. This rock type was called andalusite-staurolite schist by Lindqvist (1969). Its distribution in the Kanmantoo district is shown in Figure 8. Outside the Kanmantoo district GAB schist appears to be uncommon, but it is known to occur in association with copper mineralisation at South Hill and at Wheal Ellen (Spry et al., 1988). Three different types of GAB schist are recognised in this study on the basis of fabrics, and are termed GAB(1) schist, GAB(2) schist and GAB(3) schist. The former variety is by far the most common; the latter two varieties have been recognised only in the Kanmantoo Mine vicinity.

The principal differences between the three varieties are microstructural, for they have similar mineralogies. However, one mineralogical difference is that GAB(2) schist and especially GAB(3) schist contain sulphide minerals and chlorite, in some cases in sufficient quantities that they were an important source of low to medium grade ore. GAB(2) schist, on the other hand, rarely contains as much as 0.1% Cu, but may have a substantial pyrrhotite content (up to 2% approximately). In both varieties the chlorite content is roughly proportional to the sulphide content.

GAB(1) schist is the typical variety occurring throughout the district. In the mine area, typically it is separated from bodies of copper mineralisation by GAB(2) schist and/or GAB(3) schist, and the relative scarcity of the latter two varieties in the district appears to be due to their close spatial association with copper mineralisation. The Kanmantoo deposit and other adjacent deposits are enclosed in a unit rich in GAB(2) schist. Also enclosed are several bodies of GAB(3) schist that have a more intimate association with mineralisation. For example, in the Kanmantoo Mine, the gross geometry of GAB(3) schist follows that of the lode schists and copper mineralisation, as discussed in more detail in subsequent sections.

The boundaries between the three varieties of GAB schist are gradational when considered on a large scale, for example the scale of the Kanmantoo Mine, and in particular, it is difficult to place a general contact between GAB(1) and GAB(2) schists. On a smaller scale, say of a metre or so, both sharp and gradational contacts between all GAB schist varieties occur. In many cases, the transition from one variety to another is an interbanded zone of both varieties with individual bands varying in width and definition. These bands are commonly difficult to trace laterally, even from one blast face to the next, which may be only 15m away. The classification for GAB schist used here was recognised too late in the study to allow sufficiently detailed mapping of the spatial relationship between the varieties. More detailed knowledge may well provide valuable information on the setting of the copper mineralisation.

In the Kanmantoo district most GAB schist occurs in lens shaped bodies (Figure 2) which have minor contents of other lithologies, principally GB schist. The long dimensions of the lenses are typically aligned north-south. Of the many GAB schist lenses that have been recognised, most occur in a belt extending north from the Kanmantoo Mine and most of the few lenses outside this belt occur to the west of it. The largest single GAB schist unit occurs in the southern part of this belt and contains the Kanmantoo Mine; it is called the Paringa Andalusite Member in this study, following Kleeman and Skinner (1959). The boundaries of the Paringa Andalusite Member are unexposed normally and available information suggests that they are complex in shape. Information from mapping and drilling confirms this complexity in the Kanmantoo Mine vicinity, and is discussed in detail later. The reasons for the complexity seem to result from a combination of folding, faulting and perhaps even pre-deformational irregularities. There are few exposed contacts between the Paringa Andalusite Member and its adjacent lithologies. The best exposures of its eastern contact with the micaceous QMF schists is near the O'Neil workings south of the pit, where it appears to be unsheared, and in the portal to the Spitfire Adit, where it is sheared (Figure 7). There the contact is sharp, but immediately adjacent to the contact over several metres width the QMF schist contains bands of QMA schist and several shear zones approximately parallel to the schistosity.

The Paringa Andalusite Member is widest immediately north of the Kanmantoo Mine and so there is a coincidence between the widest portion of the largest GAB schist body and the largest known copper lode. This coincidence is considered to be significant in terms of the genesis of the deposit and will be discussed in Chapter 9. As the Paringa Andalusite Member decreases in width north of the Kanmantoo Mine a contiguous lithological unit, rich in GB schist and about 200-300m wide, occurs on its western margin. This unit appears to terminate to the north at approximately the same position as does the Paringa Andalusite Member, that is just north of the Princes Highway (see Figure 8).

North of the Paringa Andalusite Member are several GAB schist lenses that are separate from it but approximately along strike. It is possible that all these GAB schist lenses, including the Paringa Andalusite Member, are parts of a continuous, single body of GAB schist, if this northern section is assumed to have a rather complex shape in three dimensions. That is, a section other than the present land surface may show that the northerly GAB schist lenses are

part of the Paringa Andalusite Member. It is interesting to note the occurrence of minor chalcopyrite mineralisation in one of the northerly lenses, at Black Hill (D O'Connor, pers. comm.)

A further three lenses of GAB schist occur in the Kanmantoo district. The first is located 300m east of the Kanmantoo Mine and was mentioned in Section 3.2.3 because it contains a relatively high proportion of GB schist interbeds. It appears to be unmineralised. A second lens of GAB schist occurs 2.5km northwest of the Kanmantoo township and 2.5km west of the Paringa Andalusite Member (Figure 8). This lens, too, appears to be unmineralised and is contained within a QMA schist unit that is an interpreted extension of the general stratigraphic position of the Kanmantoo deposit, as described in Chapter 4. The varieties of GAB schist in this lens are transitional with QMA schist. The third lens occurs at South Hill, 3.5km southwest of the Kanmantoo Mine. Like the two lenses described above, the South Hill lens is relatively small, but unlike them it is not contained within QMA schist, nor does it appear to be in the stratigraphic position of the Kanmantoo deposit. Furthermore, the South Hill lens contains copper mineralisation similar to the Kanmantoo deposit in most respects, but is a smaller body. The South Hill lens, described by Spry (1976), contains chalcopyrite mineralisation and was drilled as a copper prospect by Mines Exploration without success from an economic point of view.

In his survey of the South-Eastern Freeway road cut exposures, Drexel (1978) described a rock type that he correlated stratigraphically with GAB schists at the Kanmantoo Mine and this conclusion is supported here (and is discussed in Chapter 4). Although the freeway rocks have a similar mineral assemblage to GAB schist, they lack the diagnostic textural features and so are not equivalent.

An important feature of GAB schist is that it hosts copper mineralisation at several localities, some were mentioned in preceding paragraphs. The southern half of the Paringa Andalusite Member, in particular, contains many dozens of chalcopyrite rich bodies in addition to the Kanmantoo deposit. These bodies range in maximum dimension from less than a metre to hundreds of metres. Many of these smaller deposits have been mined and others have been intersected by drilling. However, in the Kanmantoo district the association between copper and GAB schist is not exclusive, for example several GAB schist lenses contain no known copper and, conversely, there are copper deposits in the Kanmantoo district such as the Bremer deposit, that occur in other rock types.

All three varieties of GAB schist are described in the following paragraphs to keep them together, even though two of the varieties are closely associated with the lode schists described in the next section.

GAB(1) schist

A mesoscopic banding, not usually parallel to the schistosity, is common in GAB(1) schist and is inferred to be relict bedding. The banding is of two types; the most widespread and obvious type is manifested by variations in the proportion of quartz, resulting in interbeds richer in quartz within predominantly mica rich schist. An excellent example of this type of bedding is shown in Figure 14.

The quartz rich beds typically contain little or no andalusite and, where present, andalusite is small and irregular in shape, unlike the coarse, well formed crystals in the micaceous beds. Another difference is that the prominent schistosity of the micaceous beds is more weakly developed in the quartz rich beds and in many examples is not apparent. In parts of the Kanmantoo Mine where relict bedding is well exposed, individual beds have been traced for

at least 13m, without significant change in thickness. In general, the widths of beds vary between 1cm and 10cm. Internal laminations within beds have not been observed, perhaps they never existed or were destroyed during metamorphic recrystallisation.

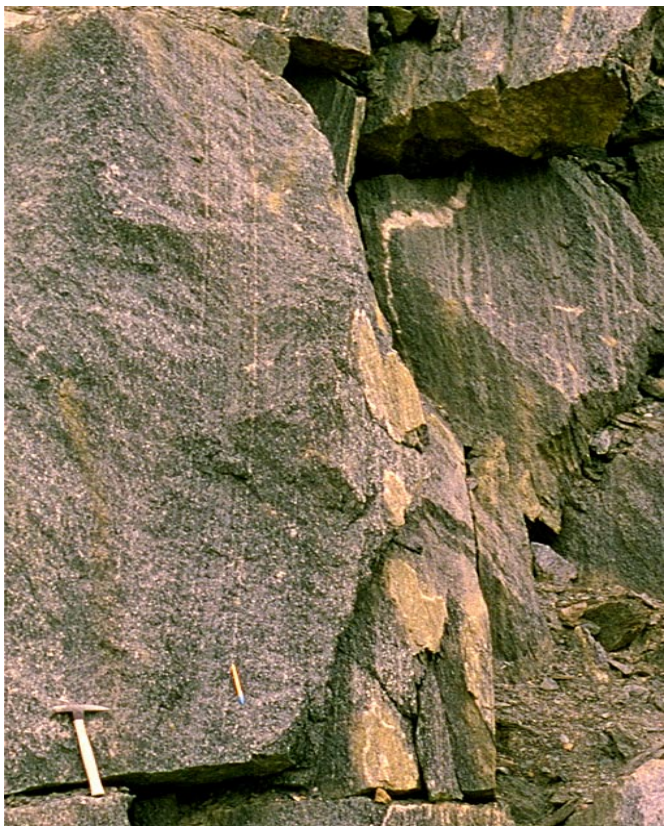


Figure 14. Example of GAB(1) schist from the eastern side of the Kanmantoo Mine. The photograph shows very regular relict bedding that can be traced for many metres. Bedding dips steeply west. The pen shown at the bottom is approximately parallel to the trace of east dipping S_2 schistosity. Figure 15 is a detail of the area near the pen and Figure 16 is of the schistosity parallel surface immediately to the right of the pen and parallel to the line of view. Looking north.

Another type of layering which is also inferred to represent bedding, is defined by concentrations of andalusite crystals in subparallel planar zones. In many cases, the andalusite concentrations are as few as one andalusite crystal every two or three centimetres, but the planar effect is visible because these crystals are either coarser than those in the adjacent schist or contain darker cores approximately parallel to their long dimensions. Thin sections show the cores to be narrow zones of relatively abundant quartz and/or ilmenite inclusions. Where different types of relict bedding occur together, they are parallel.

At Petrel Cove near Victor Harbor (60km southwest of Kanmantoo Mine) Kanmantoo Group metasediments have andalusite rich bands which are discordant to bedding and similar to those at the Kanmantoo Mine (Bowes, 1953; Talbot and Hobbs, 1968; Offler and Fleming, 1968; Lindqvist, 1969; Daily and Milnes, 1973; Mancktelow, 1979; Dymoke and Sandiford, 1992). Although the exact history of these bands is uncertain, the general consensus favours a metasomatic origin, associated with a nearby granite body. The andalusite rich bands superficially resemble the layering in GAB schist, but the latter are considered to be bedding for the following reasons:

(a) In the Kanmantoo district, the layering in GAB schist is parallel to layering in adjacent QMF schist, where sedimentary structures confirm it as relict bedding.

(b) At Victor Harbor the andalusite layering is developed locally (around a granite stock) whereas in the Kanmantoo district layering in GAB schist is widespread and regular, seemingly more consistent with a sedimentary origin. Furthermore, no granite is known to occur in the Kanmantoo district.

(c) Andalusite rich layering, similar to that in GAB schist, is a feature also of QMA schist, in which it can clearly be identified as bedding by its association with (other) sedimentary structures. The concentration of andalusite as a result of the recrystallisation of certain beds with suitable bulk chemistry is compelling.

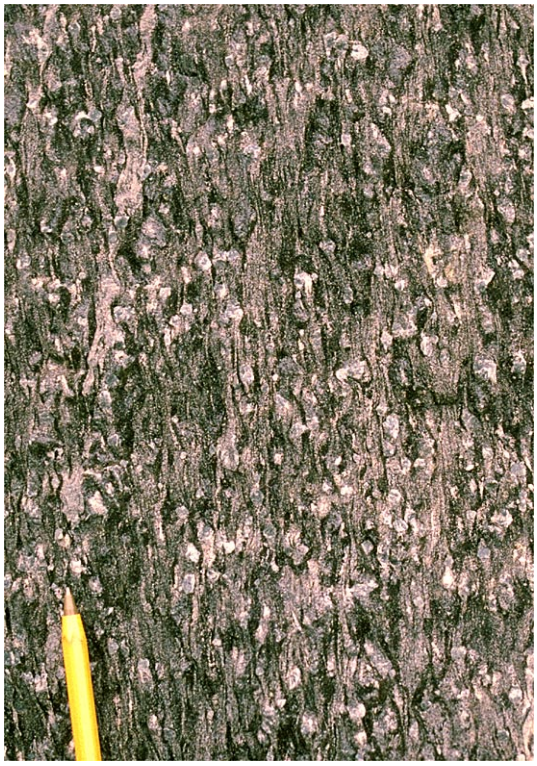


Figure 15. Close up of the appearance of relict bedding and S_2 schistosity in typical GAB(1) schist. Detail of Figure 14. At this scale the bedding is usually less obvious than from a distance. The schistosity is domainal and its trace is parallel to the pen. Looking north.



Figure 16. Schistosity surface showing typical lumpy appearance due to biotite rich foliae wrapping around the andalusite grains. The mica lineation (L_2) pitches steeply south, parallel to the line marked. The yellow biro in background is same as in Figure 15. Looking west.

No sedimentary structures other than bedding have been identified with confidence in GAB schist. Possible load casts and flame structures occur but they could be argued as deformation products. If real, they indicate that the bedding is facing upwards. In addition, a possible scour channel was observed high up a face in the eastern section of the Kanmantoo Mine, which also indicated that the bedding is upright.

Apart from the prominent andalusite crystals, one of the notable features of GAB(1) schist is a coarse, well developed segregation schistosity. Thin micaceous bands parallel to the schistosity wrap around the andalusite crystals producing a wavy, undulatory foliation that is described further in Chapter 6. Like QMF schist and QMA schist, the schistosity contains a mica lineation and is parallel to the axial planes of folds in bedding. The schistosity and mica lineation are illustrated in Figure 16.

GAB(2) schist

GAB(2) schist differs from GAB(1) schist principally in the following features: it has a homogeneous, predominantly undifferentiated matrix; the schistosity is less prominent; andalusite porphyroblasts are typically round or avoid, rather than prismatic and some are yellowish (apparently due to iron staining of the abundant inclusion grain boundaries within the porphyroblast). Compared to GAB(1) schist the biotite grains tend to be more evenly distributed and more equant, consequently GAB(2) schist commonly has a speckled appearance rather than a strongly schistose appearance. In addition, GAB(2) schist tends to have less well preserved bedding than either GAB(1) schist or GAB(3) schist. Figures 17 and 18 show two examples of preserved bedding in GAB(2) schist.

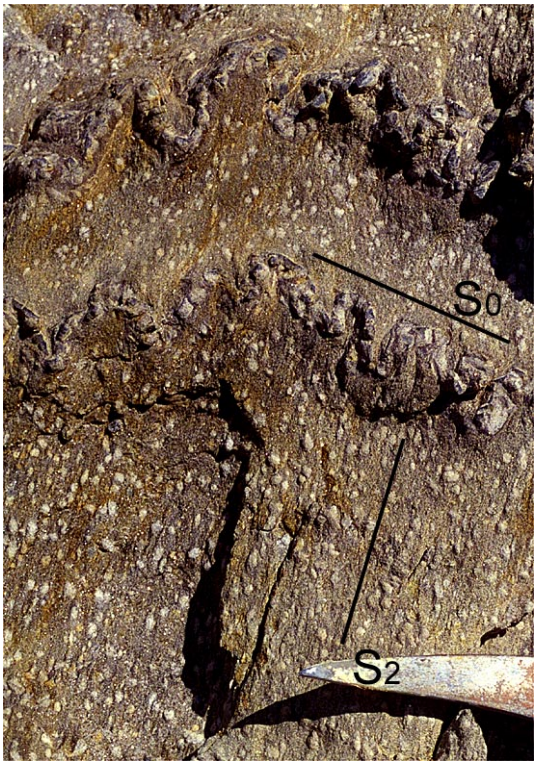


Figure 17. GAB(2) schist. Typical example with weak schistosity (S_2) and round to oval shaped, scattered andalusite grains. This example shows thin contorted layers composed almost entirely of andalusite. Such layering appears to reflect bedding.



Figure 18. GAB(2) schist. This example shows typical weak schistosity but has less typical preserved bedding and strongly aligned andalusite grains. The coin is 24mm in diameter.

The distribution of GAB(2) schist is clearly related to the distribution of GAB(3) schist and to copper mineralisation. It is spatially associated with the Main Lode, the South Eastern Mineralisation, the O'Neil Lode and minor lodes further south. Mapping in the pit indicated that its distribution in detail is scattered, but mostly it is either mixed with GAB(3) schist or, particularly near the East Limb, it appears to be marginal to GAB(3) schist and transitional with GAB(1) schist.

GAB(3) schist

When fresh this lithology tends to be a hard, massive-appearing rock, commonly with no easily visible schistosity in hand specimen. Some varieties, and also slightly weathered samples, have a more obvious fabric and mineralogy. Coarse, ragged, andalusite and biotite grains impart to GAB(3) schist a distinctive, clotty texture that earned it the name of "pudding stone" at the mine. Despite its unusual texture many fresh samples are difficult to recognise except on close inspection, because the andalusite crystals are dark and not obvious, and so the rocks appear to be homogeneous. Hence, some GAB(3) schist was mistakenly mapped as quartz-chlorite-garnet rock, one of the hard, massive lode schists with which it is associated.

Bedding is commonly well preserved in GAB(3) schist and the schistosity, though vague in hand specimen, is usually obvious when viewed in thin section. GAB(3) schist contains many quartz and sulphide veinlets and hosts much of the lower grade chalcopyrite mineralisation in the Kanmantoo Mine.

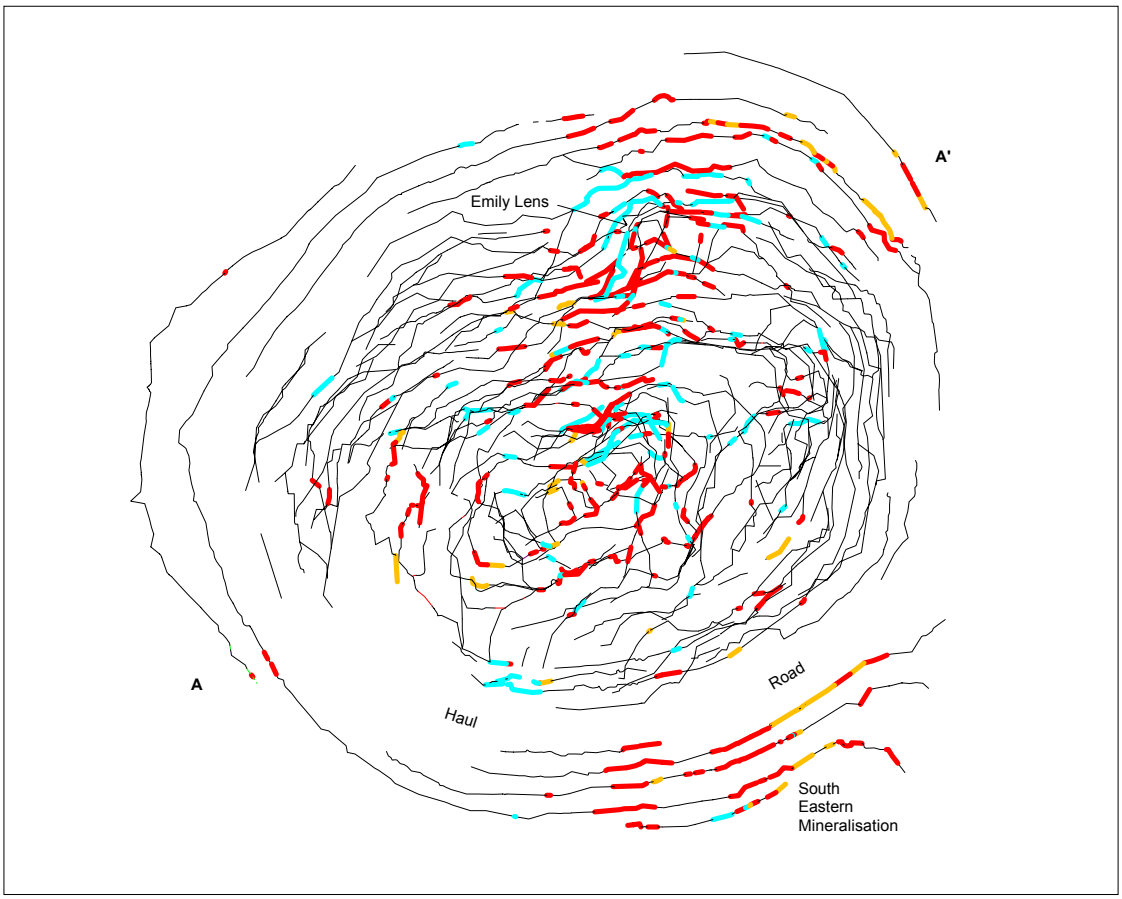


Figure 19. Distribution of GAB(2) and GAB(3) schists as mapped in the Kanmantoo Mine. Red is GAB(3) schist, orange is GAB(2) schist and blue is rocks mapped as massive or with weak schistosity.

GAB(3) schist has a limited distribution - all known examples occur in the Kanmantoo Mine area. Minor exceptions are a narrow (0.5m wide) band occurring just east of the Paringa shaft and small occurrences 200m south of the O'Neill workings. Within the Kanmantoo pit, GAB(3) schist is associated with GAB(2) schist and other rocks that were mapped as *massive* (a relative description) or as *weak schistosity*, and these categories are shown for all mapping in the pit in Figure 19. This figure shows that most of these rocks occur in a general north-south trending zone through the centre of the pit. There is a concentration along the eastern

limb of the Main Lode that tends to diverge northwards over Emily Zone and then widen at the northern limit of the pit. To the south the zone, like the copper mineralisation, does not persist with any strength south of the haul road. There is another concentration of this group of lithologies on the south-eastern part of the pit where the northern end of the South-Eastern Mineralisation occurs. This zone does not extend northwards past the haul road except as occasional occurrences. A third trend may be represented by a vague north-easterly pattern of occurrences (between the points marked A and A' on Figure 19) that extends completely across the pit through its centre.



Figure 20. GAB(3) schist. Shows characteristic ragged andalusite porphyroblasts, set in a matrix with clotty biotite grains and finer grained quartz and chlorite. Note the typical poor schistosity and the random orientation of the andalusite grains. The coin is 24mm in diameter.

3.4.5 Pyritic schist

Compared to typical Kanmantoo Group schists, these rocks have abnormally high pyrite contents and are enriched also in several other sulphides (particularly pyrrhotite, galena and sphalerite) and carbonaceous material. There is considerable evidence suggesting that they were derived by the metamorphism of sulphidic black shales (Skinner, 1958; George, 1967; Jenson and Whittle, 1969; Spry, 1976). These rocks have well preserved bedding, defined by variations in the proportions of sulphide and silicate minerals. Calc-silicate interbeds are present at the Brukunga Mine near Nairne and may represent metamorphosed marls.

Narrow pyritic schist bands occur within most QMF schist units between Brukunga and Callington, and Figure 2 shows many of these. Pyritic schist units are known to persist along strike for tens of kilometres and the Nairne Pyrite Member of the Talisker Calc-siltstone is an excellent example of this. However, in the Kanmantoo district exposures are not good enough to trace most units for more than a few tens of metres. Normally, they outcrop as gossanous units one to two metres wide and tend to have evidence of strong ductile deformation and in some cases, brecciation. In road cuttings the weathered pyritic schists usually occur as pale, crumbly units with scattered ferruginous zones and form interbeds 1m to 3m thick in feldspathic schists. Pyritic schist bands have not been observed interbedded in QMA schist or GAB schist units nor have they been observed in the QMF schist units immediately west of the Paringa Andalusite Member. Nor have they been observed in the sequence due east of the Kanmantoo Mine, but they do occur several kilometres to the east,

on the eastern side of the Bremer Fault. Hence, the nearest known outcrop of pyritic schist to the Kanmantoo deposit is approximately one kilometre away. In Chapter 8 the geochemistry of pyritic schists is compared with that of GAB schist, but it is interesting to note at this stage that both of these rock types have anomalously high iron contents with respect to other Kanmantoo Group metasediments. In pyritic schist the iron is bound in sulphide minerals, whereas in GAB schist it is bound in silicate minerals.

In his survey of the South-Eastern Freeway road-cuts, Drexel (1978) distinguished three separate pyritic lithologies (see Table 3), all interbedded, ranging from meta-pelites to meta-psammites. One of the varieties, the laminated pyrite-andalusite-muscovite-quartz schist, occurs only in the 90m thick Talisker Calc-Siltstone where it is the dominant lithology and contains abundant carbonaceous material. It is noteworthy that Drexel recorded pyritic units within biotite schists only a few metres below the garnet-andalusite rich unit that is thought to be the lateral equivalent of the mine sequence. Although this may have important implications with respect to the Kanmantoo deposit, as mentioned above no similar rocks have been observed close to the deposit.

3.4.6 Calc-silicate rocks

These rocks consist principally of amphibole (mainly hornblende), plagioclase and quartz. Two varieties occur in the Kanmantoo-Brukunga district, one is inferred to be a metasediment; the other is associated with several copper deposits and is probably of metasomatic origin.

The calc-silicate rocks of presumed sedimentary origin typically have regular banding parallel to their contacts and to bedding in adjacent rocks, and this banding too is interpreted to be relict bedding. These rocks were probably derived from marls (George, 1967). The calc-silicates of the Brukunga-Callington district occur in three general areas: west of Callington, about three kilometres west-northwest of Kanmantoo, and within the Nairne pyrite deposit. The first group is represented by a series of outcrops (Figure 8) that appear to be part of a continuous horizon parallel to bedding in the surrounding QMF schists.

A narrow band of calc-silicate rock in drill core from east of the Kanmantoo Mine, reported by Lindqvist (1969), may also be part of this first group. Unfortunately, there is no sample remaining now so the author could not examine it, but the adjacent drill core indicates that the band must have been less than 15cm wide. Although narrow, its occurrence is important for it is possibly a lateral continuation of the horizon near Callington and is the closest known occurrence to the Kanmantoo deposit.

The calc-silicate rocks west of Kanmantoo were described by Fleming (1971). Several separate horizons were mapped (Figure 8) and it has been assumed that they represent separate beds, however, an alternative is that they represent portions of one or two isoclinally folded beds. Supporting this latter interpretation is the recognition of a macroscopic isoclinal fold in this area (Figure 2) by the author and smaller isoclinal folds are also outlined by some of the pyritic schists further south. Fleming (1971) also interpreted the presence of tight and isoclinal folds in this area. The interpretation of the structure shown in Figure 8, and described in more detail in Chapter 3, indicates that these calc-silicate rocks occur in a similar stratigraphic position to those near Callington and possibly the narrow band east of the Kanmantoo Mine also. Note that calc-silicate rocks seem to occur only in QMF schist units that also contain pyritic schist and that in the Callington area the calc-silicate rocks occur at the top of the pyritic sequence. A close relationship between calc-silicate rocks and pyritic schist is also demonstrated by their mutual occurrences at the Brukunga Mine, where many of the sulphide rich beds are calc-silicates rather than the more common meta-pelites.

The second variety of calc-silicate rocks in the Kanmantoo-Brukunga district is associated with the copper deposits around Callington, including the Bremer deposit and the smaller deposits north of it, such as the Wheal Friendship near Strathalbyn (Figure 3). Hornblende or actinolite accumulations are common near the sulphide veins and are interpreted to result from carbonate-quartz reactions during metamorphism. Rare carbonate has been observed by the author in thin sections of rocks from the Bremer deposit, but not in contact with quartz.

3.4.7 Quartzites and related rocks

At the Aclare Mine, located 9.3km south-southwest of the Kanmantoo Mine, well layered quartz rich rocks containing Pb-Zn-As sulphide mineralisation were concluded by Askins (1968) to be metamorphosed sulphidic sediments. Similar rocks occur 5.7km north at the old Wheal Margaret workings (also known as Scotts Creek Mine) and numerous workers speculated that both were parts of one base metal rich sedimentary horizon (Seccombe et al., 1985). Recently, similar rocks were found to be associated with the Angas Pb-Zn deposit near Strathalbyn; they include spessartine-almandine rich quartzites that have been compared by Both et al (1995) to the coticules described by Spry (1990). Coticules (spessartine-quartz rocks) are commonly associated with massive sulphide deposits in metamorphic terranes. Believing the garnet quartzites to represent exhalite cherts, Aberfoyle Ltd embarked on a search for others in the Aclare-Kanmantoo region and located several new outcrops (Toteff, 1994, 1999). Toteff believes that the quartzite outcrops define two stratigraphically distinct meta-exhalite horizons, referred to here as the Kanmantoo and Aclare horizons.

The Kanmantoo horizon comprises ferruginous or siliceous rocks and can be followed erratically for approximately 7km, from 5km north to 2km south of the Kanmantoo Mine. Surface exposures are rarely good enough to see the full width but the unit seems to be from 0.5-1.0m wide. Lithologies include well layered garnet quartzite, some with magnetite (Figure 21), banded and massive ironstones, gossanous layers, banded iron formation and ferruginous schist. The outcrops occur within the Paringa Andalusite Member, approximately 50-100m west of its contact with QMF schist, and seem to be associated with GB schist and garnet rich sections of the GAB schist. Unfortunately, the unit cannot be located close to the Kanmantoo Mine and its relationship to the copper deposits remains an intriguing mystery. Toteff (1999) concluded that the Kanmantoo copper deposits represent a feeder to overlying exhalative mineralisation and, on the basis his geological mapping, also concluded that the known deposits probably came to within 200m of the sea floor.

The Aclare horizon comprises siliceous and calc-silicate rocks and can be followed, erratically again, over approximately 6km around an arc extending from the Wheal Margaret Mine, south to the Aclare Mine, and eastwards to Callington. Most of the outcrops are of layered calc-silicate rocks. Fine-grained, laminated to banded garnet quartzites occur at the two mines where they are associated with stratiform Pb-Zn mineralisation. Spessartine rich garnets are common. Unlike the Kanmantoo horizon, this horizon has little ironstone and no anomalous developments of almandine-rich garnets in the enclosing metasediments.

The Aclare horizon comprises siliceous and calc-silicate rocks and can be followed, erratically again, over approximately 6km around an arc extending from the Wheal Margaret Mine, south to the Aclare Mine, and eastwards to Callington. Most of the outcrops are of layered calc-silicate rocks. Fine-grained, laminated to banded garnet quartzites occur at the two mines where they are associated with stratiform Pb-Zn mineralisation. Spessartine rich garnets are common. Unlike the Kanmantoo horizon, this horizon has little ironstone and no anomalous developments of almandine-rich garnets in the enclosing metasediments.



Figure 21. Banded garnet quartzite float from beside small pit surrounded by GAB schist. Located 1.8km north of the Kanmantoo Mine.

The discovery of these rocks is important, firstly because they represent rare marker units that will assist with structural and stratigraphic mapping in this district. Secondly, if the reasonable premise is accepted that these rocks have an exhalative origin, important implications follow for regional metallogenesis. Both of these points are discussed in Chapters 5 and 9 respectively.

Gum (1998) included the garnet rich rocks of the Kanmantoo-Aclare district within his Angas Garnet Member, which he stated could be traced along strike almost continuously for 50km.

Mapping completed for this study located garnet rich quartzites in two localities near the Kanmantoo Mine, but apart from their general similarity to some of the quartzites discussed above there is no compelling evidence that they represent exhalite horizons. One occurrence is in an area of poor outcrop immediately north of the waste dump and west of the explosive magazine, where a few blocks of loosened, iron-stained, medium to coarse-grained garnet quartzite were noted. Nearby exposures were GAB schist and vein quartz. A second locality is 150m south of the site of the treatment plant where 1cm wide pods of medium-grained garnet quartzite occur within QF schist. The pods appear to be detached portions of a narrow competent bed of garnet quartzite and are associated with folded laminations within the host lithology. They do not appear to be sulphidic.

3.5 Lode schists

3.5.1 Varieties

In the Kanmantoo Mine, lithological groups that are spatially associated with copper mineralisation are GAB(2) schist, GAB(3) schist and a complex group of transitional lithologies referred to as the lode schists. The lode schists comprise many different, but related lithologies. Compared to the enclosing GAB(1) schist, the most obvious differences are the abundance of chlorite and sulphide minerals, and the paucity or absence of andalusite.

Other common minerals in the lode schists are almandine garnet, biotite, staurolite, Fe-Ti oxides and, in some cases, cummingtonite or muscovite. The abundance of chlorite in the mine area is unusual in the amphibolite facies rocks of the Kanmantoo district. The only other known occurrence, but with much lesser quantities, is at South Hill.

A schistosity with an associated lineation is present in most lode schists, but not in most of the coarser grained varieties (Group 2 below) that have only weakly developed or non-existent foliations. Contacts between the different varieties of lode schist are both sharp and diffuse and tend to be subparallel to the schistosity. Lensoidal bodies are common, as is sulphide and quartz veining. Contacts with GAB schist tend to be sharp but some are transitional over distances up to several metres and may be either concordant or discordant to bedding in GAB schist.

Table 4. Lode schists sorted according to general quartz content and correlation with Lindqvist (1969) categories.

Quartz abundance	Group	Lithology	Lindqvist correlation
Quartz rich (with chlorite)	1a	GAB(Cl) schist	Lode schist
	1a	GABCl schist	
	1a	G(A)BCl schist	
	1a	GBCl(A) schist	
	1b	GBCl schist	
	1b	GClB schist	
	1b	GCl schist	
	1c	GB schist	
Quartz rich (with muscovite)	4	Muscovite-bearing schist	
Variable quartz	3	Amphibole-bearing schist	Alteration zones
Quartz absent or rare	2a	Biotite-staurolite rock	
	2b	Muscovite-chlorite rock	
	2c	Chlorite-magnetite rock	

The lode schist varieties as shown in Table 1 have been subdivided into the following four groups, based on their mineralogies. Of the 4 groups, the quartz rich rocks of Group 1 are by far the most common. The other groups are listed in approximate order of importance as hosts of sulphide mineralisation.

Group 1	Quartz rich lode schists	(abbrev.: lode schist 1)
Group 2	Quartz poor / absent lode schists	(abbrev.: lode schist 2)
Group 3	Amphibole bearing lode schists	(abbrev.: lode schist 3)
Group 4	Muscovite rich lode schists	(abbrev.: lode schist 4)

Groups 1 to 3 contain no muscovite and are low K_2O assemblages. Some of the four groups have been further subdivided resulting in the classification presented in Table 4, such that a total of 13 varieties of lode schist are recognised in this study. The transitional nature of the mineralogical changes between the lode schist varieties has made classification difficult and this has led to much of the inconsistency in mapping by mine geologists. The classification of lode schists in Table 4 was finalised by the author as a result of petrological studies after the mine closed and it differs to the classification used during most routine mine mapping and by Lindqvist (1969).

The simple classification of mineralised rocks used by Lindqvist (1969) is compared in Table 4 with the scheme used in this study. Lindqvist described two major rock types associated

with the Kanmantoo mineralisation: (his) *lode schists* and *alteration zone* rocks. Both are contained within (his) andalusite-staurolite schist (called GAB schist here). Lindqvist's *alteration zones* form discrete bodies within the larger bodies of *lode schists*, and the *alteration zones* are characterised by the coarse grainsize of their constituent minerals, principally biotite, muscovite, garnet, staurolite and minor grunerite. The *alteration zones* vary in width from one centimetre to one metre approximately. Lindqvist's *lode schists* correspond to the dominant quartz rich group recognised in this study, and his alteration zones correspond to the rocks with no or little quartz.

3.5.2 Group 1 lode schists

A well defined schistosity is usually present in all rocks of this group and, in most cases, a weak mineral lineation is visible on the schistosity plane. The transitions between the varieties of lode schist, referred to previously, are most notable in and a characteristic of Group 1 rocks. A summarised description of the mineral variations between members of this group is shown in Table 5 and is also represented in Figure 22. The proportions used in Figure 22 are estimated only and the purpose of the figure is only to show the mineralogical relationships between the various lode schists.

Table 5. Mineral variations in Group1 lode schists.

	Lithology	Mineral variation
andalusite bearing Lode Schists	GAB(Cl) schist	GAB Schist but with minor chlorite
	GABCl schist	Similar to above but with more chlorite
	G(A)BCl schist	Similar to above but with less andalusite
	GBCl(A) schist	Similar to above but with minor andalusite
GBCl group (no andalusite)	GBCl schist	Similar to above but no andalusite and biotite > chlorite
	GClB schist	Similar to above but chlorite > biotite
	GCl schist	Similar to above but with little-no biotite
	GB schist	Garnet-biotite schist, little-no chlorite

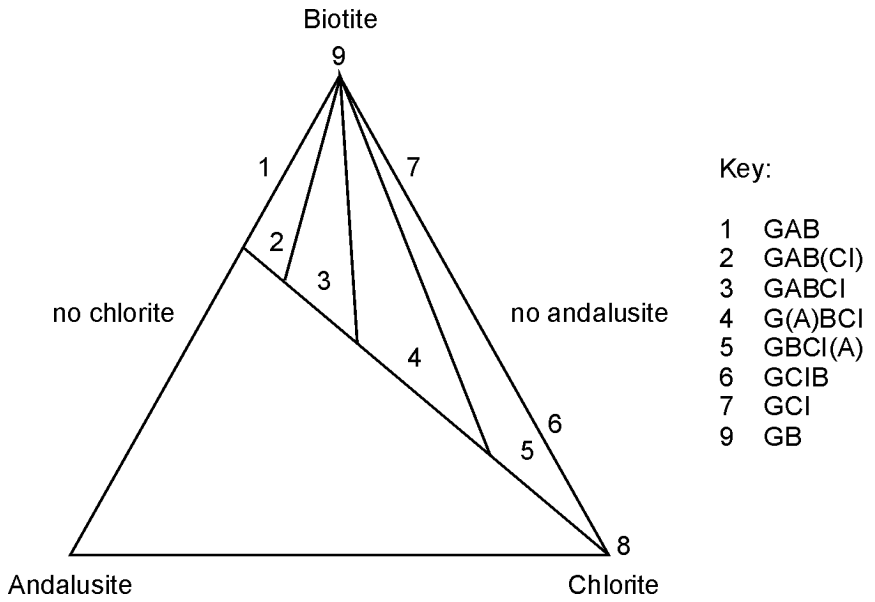


Figure 22. Schematic diagram showing relationship between Group 1 lode schists.

An idea of the relative abundances of each of the varieties of Group 1 lode schist can be derived from the pit face mapping data. This has been compiled in Table 6. Firstly, the aggregate number of segments, or individual lithological units mapped, for each variety is shown, as the total and as a percentage of the total. Secondly, the aggregate length of

segments mapped is shown, also as the total and as a percentage. The last column shows the mean length of segments for each variety, derived simply by dividing the total length by the total number of segments for each variety. The second set of results is considered to be the best estimate available of abundance, because they represent averages that are weighted for measured length along the pit faces and are therefore a better estimate of volume. However, the trends of the segments are at all angles relative to the strike of the units and so it is an inconsistent data set that does not represent true widths. Furthermore, the data are likely to be affected by bias during mapping because certain categories were favoured, especially when time for mapping was short or faces were partially obscure. For example GABCl schist tended to be used as a general classification for chlorite and andalusite bearing lode schists, and GBCl schist tended to be used for andalusite free lode schists. This would explain the apparent abundance indicated for GABCl schist and GBCl schist in Table 6. It is considered likely that the trend of decreasing andalusite from GAB schist to GBCl(A) schist is more regular than the data in indicates.



Figure 23. G(A)BCl schist. This example is from within the western part of the Main Lode and displays a thin shear (arrowed) with apparent normal displacement. The shear is parallel to the east dipping schistosity and appears to have drag folded the tip of a tension vein. The exposure surface is rust coloured from weathered sulphide minerals dispersed through the schist.

Table 6. Estimates of relative abundance of Group 1 (quartz rich) lode schists based on pit mapping data.

Lithology	Aggregate number of segments	%	Aggregate length of segments	%	Average length of segments
GAB(Cl) schist	147	11	1,942m	18.5	13.2m
GABCl schist	456	33	3,572m	34.0	7.8m
G(A)BCl schist	122	9	788m	7.5	6.5m
GBCl(A) schist	161	12	1,005m	9.6	6.2m
GBCl schist	345	25	2,061m	19.6	6.0m
GClB schist	25	2	174m	1.7	7.0m
GCl schist	70	5	675m	6.4	9.6m
GB schist	68	5	281m	2.7	4.1m

The relative abundance of the lode schists not included in Table 6 is estimated to be less than 1% or 2% each. Most of these excluded lithologies occur as veins or irregular masses within other lithologies, especially those without andalusite, and because of their small size they were generally not mapped as separate units but were included as part of the host during mapping.

Andalusite bearing lode schists of Group 1
[GAB(Cl) schist, GABCl schist, G(A)BCl schist and GBCl(A) schist]

A useful distinction among the quartz rich lode schists is between those that contain andalusite and those that do not (see Table 5). This distinction was probably well recognised during pit face mapping, except in the case of a type of hard, siliceous, dark lode schist (a variety of GAB3 schist) that was sometimes mapped as GBCl. Subsequent petrological studies showed the presence of andalusite grains that were difficult to see on pit walls, especially when they were poorly exposed or inaccessible. Hence, an unknown portion of the rocks recorded in the database as GBCl is likely to contain andalusite. A characteristic feature of Lode Schists that are chlorite and andalusite rich is that the andalusite commonly is rimmed by chlorite and presumably has been partly replaced by it. Though it can be discerned in hand specimen, this texture is not obvious. Rarely is andalusite completely replaced by chlorite except in what seem to have been small andalusite grains originally. Biotite, unlike adjacent andalusite grains, does not seem to be replaced by chlorite even though both layer silicates are intimately mixed. To understand the important question of how chlorite occurs in the lode schists petrological study is required and this is discussed in Chapter 6.

Chlorite poor examples of Group 1 lode schists are transitional with all varieties of GAB schist, that is GAB(1), GAB(2) or GAB(3) schists, the transition being an increase in the proportion of chlorite at the expense of biotite and andalusite. By comparison, the chlorite rich examples are transitional only with GAB3 schist.

GBCl group of lode schists – chlorite rich varieties
[GBCl schist, GClB schist and GCl schist]

The principal minerals present in the rocks belonging to the GBCl group, that is the Group 1 lode schists without andalusite, are quartz and chlorite and biotite. This lithology is very similar to andalusite bearing lode schists except that does not contain andalusite, or any chlorite clumps that would suggest its earlier presence prior to replacement. It is characteristically a homogeneous rock consisting predominantly of chlorite and quartz, with minor sulphide minerals occurring as both disseminated grains and in veins, each parallel to a weak to well developed schistosity. A common feature is a distinct garnet layering, usually observed as one or two subparallel bands contorted into irregular or elasticas folds (this is described more fully in Chapter 6). In some cases the folds seem to have the schistosity approximately parallel to their axial planes. The garnet layering usually is not clearly related to other planar features, such as bedding, and its origin is not clear. Individual garnet layers are 1mm to 3mm in width, well defined and consist predominantly of garnet with small inclusions of ilmenite and quartz. The layers commonly have a medial quartz zone separating two garnet bands or have quartz rich selvedges.

GBCl group lode schists – biotite rich variety
[GB schist]

Principal minerals present are quartz and biotite. These rocks differ from the Group 1 lode schists described above, in that they are biotite rich rather than chlorite rich. Chlorite is usually a minor constituent (less than 20%) or is not present. Two subvarieties can be distinguished; those with minor amphibole and those without. Those with amphibole tend to host zones of amphibole bearing lode schist. The amphibole minerals (grunerite-cummingtonite) are commonly concentrated in thin planar zones that are parallel to the schistosity and to the axial plane of folds in (inferred) relict bedding. In addition, the long axes of the amphibole needles define a mineral lineation on these planes, parallel to the mica lineation in surrounding schists. Amphibole bearing GB schist typically contains much less copper and sulphur than adjacent Group 3 lode schist, as shown for two examples in Table 7.

Table 7. Examples of sulphur and copper contents for different types of amphibole bearing lode schist.

Rock Type	Sample No.	S	Cu
GB schist with amphibole	517-060 (nam)	460 ppm	145 ppm
Group 3 lode schist	517-060(am)	5.83%	4.62%
GB schist with amphibole	517-077 (lay)	227 ppm	7 ppm
Group 3 lode schist	517-077 (v)	6,360 ppm	349 ppm

The more common variety of GB schist without amphibole tends to be gradational with GAB(2) schist to which it is similar, lacking only andalusite, and in some cases it appears to occur in zones of more intense deformation within GAB(2) schist. For example, sample number 517-140 was collected from a 40cm wide zone of GB schist containing tightly folded quartz veins in greater abundance than the adjacent GAB(2) schist.

3.5.3 Group 2 lode schists

Although these 3 lithologies are grouped with the other lode schists because they are spatially associated with them, they are not true schists. Usually no foliation is apparent and, at best, a weak foliation is developed in some specimens. For staurolite-biotite rock the principal minerals present are biotite, chlorite and staurolite. These rocks are characterised by an abundance of coarse-grained hydrous silicate minerals and only a weak foliation, or more commonly, none at all. They represent most of the rocks within Lindqvist's "alteration zones". Most examples appear to be undeformed or weakly deformed. Considerable variation exists in the modal proportions of the major minerals, particularly staurolite which varies from less than 10% to over 50%. In the staurolite rich rocks, staurolite forms prisms up to 15mm long and occurs principally with biotite. However, in the staurolite poor rocks, staurolite tends to be more equant and occurs with garnet in a chlorite and biotite matrix. In all varieties quartz is a minor mineral. Unlike most other lode schists there is no interstitial quartz and the little quartz that is present occurs as inclusions in staurolite and garnet. Staurolite-biotite rock tends to form veins and less regular bodies that are subparallel to the schistosity in the surrounding rocks and that vary in width from a few millimetres to one metre approximately. For example, several veins can be observed in one thin section of

Group 1 lode schist. The contacts tend to be sharp, especially in the case of chlorite-biotite rich varieties. Layering within these rocks is extremely rare.

Chlorite-muscovite rock consists of coarse, decussate chlorite and muscovite with minor staurolite, garnet and abnormally large ilmenite laths (up to 3cm). Apart from the presence of muscovite this uncommon lithology is similar to the phyllosilicate rich varieties of staurolite-biotite rock described above. Again, interstitial quartz is absent, no foliation has been observed, the rocks occur as vein-like masses and, apart from minor undulose extinction of the phyllosilicate minerals, these rocks appear to be undeformed. No layering has been observed.

In chlorite-magnetite rock the principal minerals present are chlorite and magnetite. Typically, chlorite exceeds magnetite, but rare samples with magnetite contents up to 70% occur. Minor minerals include garnet, staurolite and sulphides. Quartz is rare within the chlorite-magnetite mass, but does occur as veins that are the only easily recognisable planar surface. However, a weak preferred orientation of chlorite can be seen in some thin sections. The chlorite rich varieties are similar to the chlorite rich varieties of chlorite-muscovite rock, both in composition and microfabric.

3.5.4 Group 3 lode schists

The principal minerals present are chlorite, biotite and quartz, but the characteristic feature of this group is the presence of amphibole (cummingtonite-grunerite), although it seldom constitutes more than 10% of the rocks. The only other lode schist containing amphibole is GB schist that invariably occurs adjacent to Group 3 schist.

Apart from the common presence of amphibole, there is quite a lot of variation in the appearance and composition of rocks within this group. Garnet, chlorite and sulphide minerals are usually present; biotite occurs in some cases but, viewed in thin section, has a greenish and corroded appearance suggesting that it may not be stable. The quartz content varies from nil to 40% approximately and, where abundant, quartz may contain many fine amphibole needles arranged in asbestiform sheaths around clear quartz lenses (described in Chapter 6). These rocks are among the most iron rich occurring in the Kanmantoo deposit, exceeded only by massive sulphide rocks or the magnetite rich versions of chlorite-magnetite rocks, and most of this iron is bonded in silicate minerals. For example, the Fe0 (total) contents of four samples of Group 3 lode schists are shown in Table 8. For comparison, the measured iron contents of two massive sulphide-magnetite rocks from the Kanmantoo deposit is (as Fe0): 46.5% and 44.9%.

Table 8. Iron contents of four samples of Group 3 lode schists.

Sample Number	FeO (total) %
517-060am	34.42
517-061A	31.15
517-061B	39.49
517-077v	41.25

3.5.5 Group 4 lode schists

The principal minerals present are quartz, biotite and muscovite. Muscovite rich lode schists are uncommon in the Kanmantoo Mine; most occur in certain parts of the South Eastern Mineralisation, and the north-eastern section of the Kanmantoo open cut mine, where they are associated with muscovite bearing GAB(3) schist. Both Group 4 lode schists and associated GAB(3) schist contain biotite and muscovite bearing assemblages rather than the more common biotite and chlorite. Some of the very schistose types of Group 4 lode schists occur in well defined planar zones parallel to the schistosity, whereas other types have a weak schistosity and gradational boundaries.

3.5.6 Geometry of the lode schists

Pit face mapping completed by the author and others was used to interpret the positions of the main bodies of lode schist on each bench, as described in section 3.2.1**.** Plans showing the interpretations are in Figures 137 to 139 (located in the map pocket). Generally, the interpreted boundaries represent zones where one lithology is dominant but the zone may contain minor amounts of other lithologies as well. In the interpretations only the largest lenses of lode schist are shown and there are many smaller bodies between. As seen in plan view, the lode schists within the pit form many bodies which can be divided into two groups on the basis of their trends and location, an eastern group and a western group, which are referred to in this study by the terms *East Limb* and *West Limb* respectively. The East Limb lode schists trend north-north-easterly and those comprising the West Limb trend north-south. These terms were used during mining, specifically for the East and West Limbs of the Main Lode, and are local names that relate to copper distribution, and are not used in the structural sense of a fold limb. The boundary between both zones is transitional over several tens of metres, and appears to have a north-south or north-northeast trend and an easterly dip. On the eastern side of the East limb the trends are north-south again.

Lode schists within the East Limb principally form a single, large lens of lode schist, with a few smaller lenses adjacent to it, all trending north-north-easterly and dipping steeply to the east. The main lens is the biggest individual lens of lode schist known in the Kanmantoo Mine. In the upper levels of the mine, it had a strike extent of at least 300m and a maximum width of approximately 40m.

In the West Limb area, lode schist lenses are more numerous than in the East Limb, but they seem to have a smaller total volume. Viewed in plan, the lenses have a marked north-south trend and large length:width ratios, typically greater than 10:1. They have an observed maximum width of 10m and maximum length of approximately 70m, but many persist beyond this as very narrow zones. The mined portion of the West Limb was largest in the upper levels of the mine (above the 560 level approximately), where the individual lenses of lode schist comprising the West Limb were larger and more closely spaced.

When the Main Lode is viewed in cross section similar differences to those seen in plan can be distinguished for the lode schist lenses comprising the East and West Limbs, with regard to their shapes and orientations. These features are demonstrated well in the cross section constructed for 12,000N shown in Figure 24, in which the East Limb is represented by the two easternmost lode schist lenses (on the right hand side), and the West Limb is represented by the rest of the lenses. In the West Limb the lenses are more numerous and more regular in shape and dip, and have higher aspect ratios. In contrast, the East Limb comprises a few larger bodies with less regular shape, less regular dip and less vertical persistence. Of

particular interest is the rather abrupt termination with depth of the main lens of the East Limb between the 350 and 300 levels.

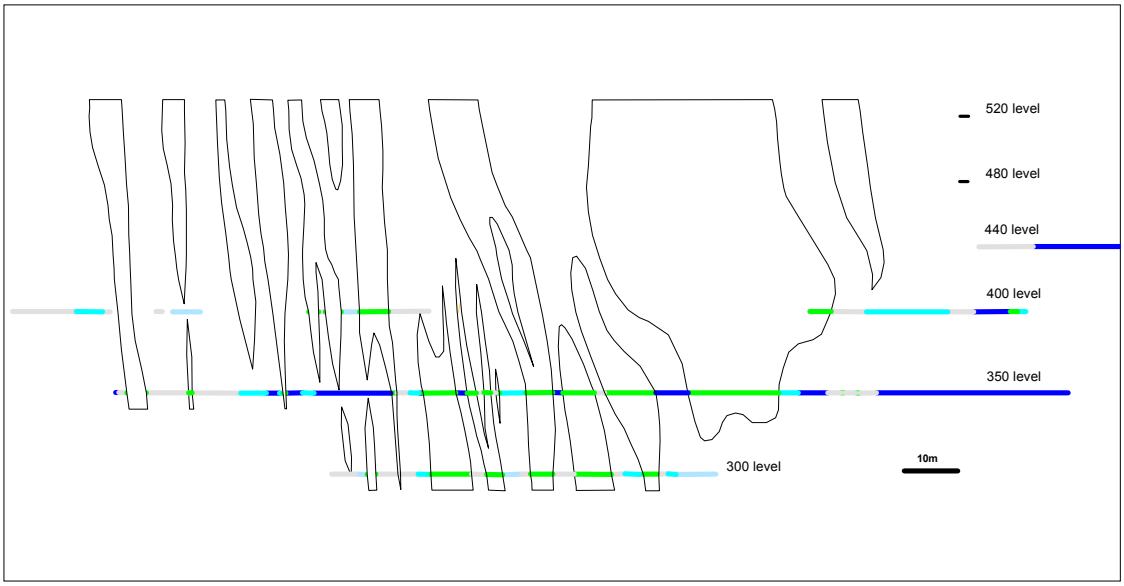


Figure 24. Cross-section through the Main Lode on 12,000'N, looking north. The interpreted outlines of GBCl group lode schist are shown, superimposed on coloured traverses for benches in this area that were mapped by the author. The traverses were derived from the level interpretations shown in Figures 137 to 139. GAB schist is shown as dark blue, GAB(Cl) and GABCl as grey, G(A)BCl and GBCl(A) as light blue, and GBCl group lode schists as green. On the upper benches interpretations were made from mapping done by other mine geologists.

Using the plans and the cross section in Figure 24, estimates were made (to the nearest 5º) of the overall orientation of the GBCl group lode schists of the East Limb and the West Limb, and they are shown in Table 9. These figures are significant when compared with patterns of copper distribution and with structural features, as discussed in Chapters 4 and 5 respectively.

Table 9. Overall orientation of lode schist bodies associated with East and West Limbs

	Strike	Dip
East Limb	020	70-85ºE
West Limb	000	84-89ºE

Viewed in longitudinal section (Figure 25), an envelope enclosing high grade copper and the collective lenses of both the East and West Limbs defines a zone plunging steeply to the north.

Thus, in three dimensions, the enveloping surface to the numerous lenses comprising the Main Lode (both East and West Limbs) is pipe-like in shape with a steep northerly plunge. The pipe-like body has cross sectional dimensions of approximately 300m (north-south) and 150m (east-west). Its maximum vertical dimension has not been discovered despite drilling

to vertical depths of approximately 600m. The axis of the pipe lies within, or very close to, the mean schistosity plane, and pitches to the north at 70 degrees approximately. Because an unknown portion of the Main Lode was removed by erosion, and because it is still open at depth, its current and original vertical extent is not known.

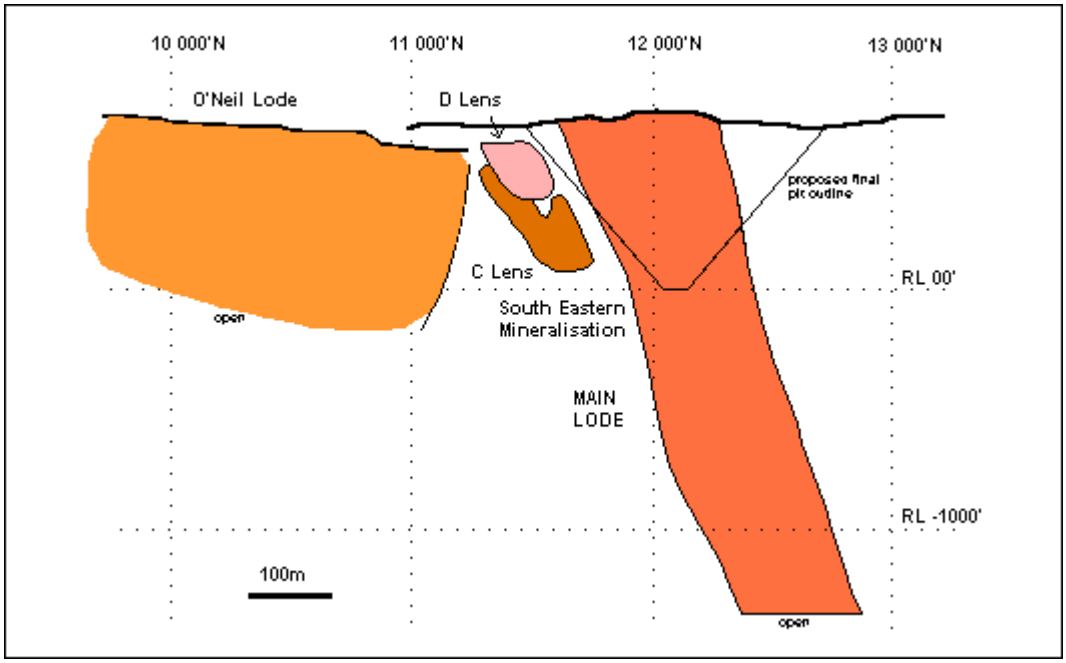


Figure 25. Longitudinal projection looking west of the main lodes of the Kanmantoo Mine vicinity. Note that the main Lode and O'Neil Lode are open at depth. C Lens and D Lens are the two largest lenses of the South Eastern Mineralisation. This figure is base on diamond drilling information and was derived from a drawing prepared by Kanmantoo Mines Limited.

Viewed in longitudinal section (Figure 25), an envelope enclosing high grade copper and the collective lenses of both the East and West Limbs defines a zone plunging steeply to the north.

Thus, in three dimensions, the enveloping surface to the numerous lenses comprising the Main Lode (both East and West Limbs) is pipe-like in shape with a steep northerly plunge. The pipe-like body has cross sectional dimensions of approximately 300m (north-south) and 150m (east-west). Its maximum vertical dimension has not been discovered despite drilling to vertical depths of approximately 600m. The axis of the pipe lies within, or very close to, the mean schistosity plane, and pitches to the north at 70 degrees approximately. Because an unknown portion of the Main Lode was removed by erosion, and because it is still open at depth, its current and original vertical extent is not known.

3.6 Laterite

Prior to the start of mining in 1970 the Main Lode was hidden below a capping of strongly oxidised rock which extends to the south of the present open cut mine for 360m along the top of MacFarlane Hill (Figure 7). A reasonably well exposed section through this regolith occurs on the southern parts of the uppermost benches of the mine but was not examined in any detail in this study. Although mine workers have traditionally referred to the ferruginous crust on the top of MacFarlane Hill as *laterite,* it is not a true laterite nor are there the other

elements of a true laterite profile. Rather, the crust is more correctly termed a ferricrete. Similar ferricretes occur throughout the Mount Lofty Ranges and Kangaroo Island and commonly were misrepresented as laterites (Milnes et al, 1985). Over GAB schist the zone of strongly oxidized rock is only a few metres thick, but over the sulphide deposit it extended to seven metres. Verwoerd and Cleghorn (1975) state that below the base of the ferricrete the copper minerals were malachite and azurite to a vertical depth of 25m. Below this was a transitional zone to sulphide minerals that contained the primary sulphide minerals plus chalcocite, covellite and minor bornite, cuprite and native copper. Although not referred to specifically by Verwoerd and Cleghorn, it seems that the lodes did not form a true gossan because these authors comment that the lodes had no surface expression.

The coincidence of the Kanmantoo deposit and ferricrete may not be accidental, for the only other ferricrete capping known to the author in the Kanmantoo district also occurs on GAB schist, at Black Hill, 6 km north of the Kanmantoo Mine. There, weak copper mineralisation has been intersected in diamond drill core from Black Hill (D. O'Connor, pers. comm.). Thus, there may be a relationship between ferricrete, GAB schist and copper mineralisation. However, the South Hill copper prospect, also in GAB schist (Figure 2), does not have a ferricrete capping, but one may have been developed and subsequently removed by erosion.

Kanmantoo-style copper mineralisation and its surrounding GAB schist contain iron rich minerals and the known copper mineralisation seems to occur in the more iron rich parts of the Paringa Andalusite Member, where biotite is much more abundant than muscovite, for example. Similarly, of the other small GAB schist bodies in the Kanmantoo district, most appear to have higher muscovite proportions than the South Hill body which contains copper mineralisation. Perhaps the lode schists and the most iron rich GAB schist promoted more intense weathering compared to surrounding rocks, producing a resistant capping which tended to be preserved during later erosion. Ferricrete may be a guide to copper mineralisation.

4 COPPER MINERALISATION

4.1 Introduction

The dispersed nature of sulphide mineralisation in the Kanmantoo Mine and its common occurrence as veins indicates that it is most appropriately classified as a *disseminated vein style* of mineralisation. The irregular and diffuse character of most of the mineralisation has compounded the problem of understanding its relationships to the associated lithologies and the structural framework. These relationships are key diagnostic factors in understanding the origin of the copper mineralisation, especially with respect to the question of whether the copper deposit formed during sedimentation or deformation.

The primary aim of this chapter is to describe the mode of occurrence and the spatial distribution of copper within the Kanmantoo Mine. Comparisons of the copper distribution will then be made with the lithological distribution (in this chapter) and structural elements (in the next chapter). Copper mineralisation in the Kanmantoo Mine is considered at scales ranging from veins to the mine scale in this chapter, whereas copper occurrence at the microscopic scale is described later in Chapter 6. At the vein scale considerable detail, especially on mineralogy, has been reported by Lindqvist (1969) and Spry (1976) and is not repeated here. At the mine scale there has been little analysis of copper distribution other than that required for grade control during mining, and it is fortunate that a substantial database of assay results from the mine is available for analysis. Although most of this chapter is focused on the Kanmantoo Mine, minor descriptions of other copper occurrences in the district are presented at the end of the chapter.

4.2 Forms of sulphide occurrence

Most sulphide minerals in the Kanmantoo deposit occur in one of two forms:
- within veins and veinlets, or
- as disseminated grains and composite grains.

Generally both types of sulphide occur together and their abundances tend to increase or decrease together. This applies to all varieties of the sulphide bearing lithologies, including GAB(3) schist and GAB(2) schist. Sulphide minerals are most common in the various types of lode schist, especially the andalusite free varieties. A general discussion of all vein types forms part of the next chapter, but some aspects of the sulphide rich veins will be described here because it helps understand copper distribution.

In the zones with higher copper grades, sulphide rich veins are numerous, of various sizes, and anastomosing to subparallel in form. In width, the veins are normally 2-10mm and rarely exceed 15cm. Laterally, individual veins extend for variable lengths, usually between a few centimetres and a metre approximately, but they have been observed to persist for at least 10m. An example of anastomosing vein sets from the Emily Lens on the 440 Bench is shown in Figure 26. Commonly, the anastomosing veins form two dominant sets, one is subparallel to the schistosity and the other tends to form a consistently oriented linking set, generally shallower in dip. Another common style of vein occurrence is sheeted, subparallel veins, generally oriented subparallel to the schistosity. An example of this style from the southern limit of the West Limb is shown in Figure 27.

Although most sulphide veins occur as subparallel or anastomosing sets, some mineralisation also occurs in other vein types. Firstly, there are less regular shaped veins and sulphide-rich masses, especially in the East Limb of the Main Lode. The larger masses provide the only

samples that could be termed massive sulphide (for example see Figure 28). Secondly, significant sulphide contents also occur in sulphide-quartz and quartz-sulphide veins throughout the mine.

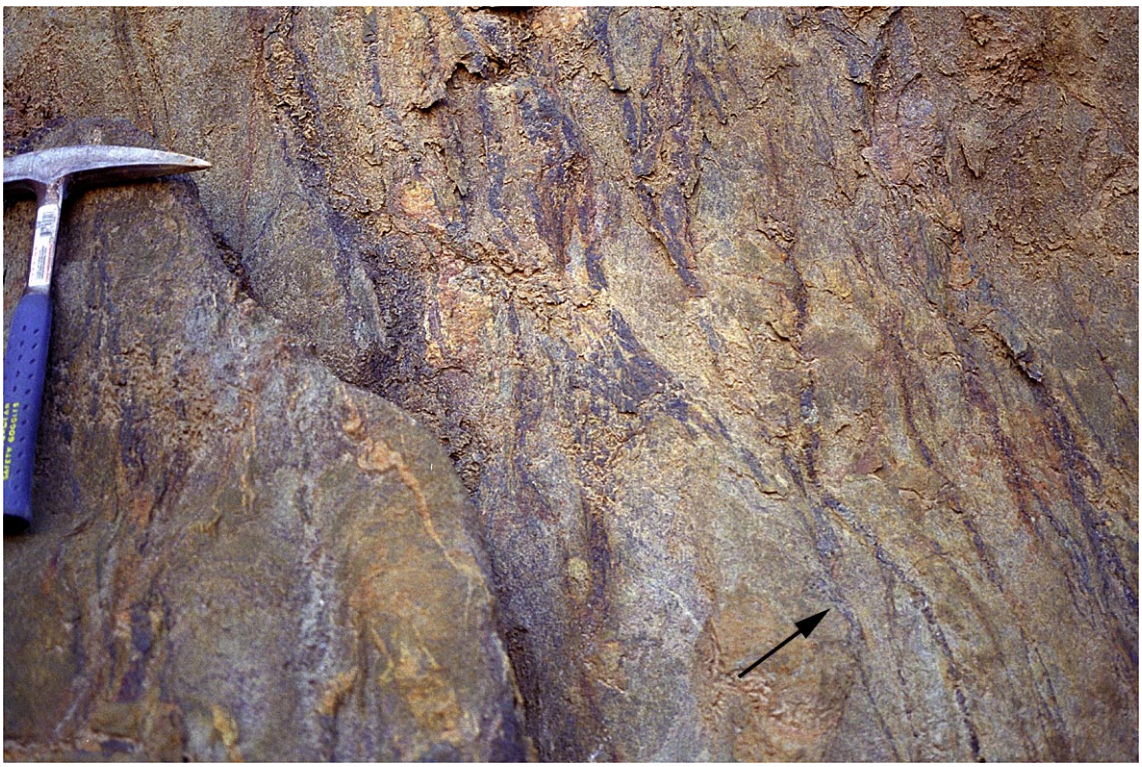


Figure 26. Anastomosing sulphide (chalcopyrite-pyrrhotite) veins in high grade ore. This example is from Emily Lens but is typical of other high grade zones. The exposure is tarnished by the products of weathered sulphide minerals that have stained the surface and made the veins dark (arrowed).



Figure 27. Sheeted sulphide veins (white) from high grade ore at the southern end of the West Limb (viewed looking south). The veins are approximately parallel to schistosity. Note the hammer at lower left for scale.



Figure 28. Sulphide rich specimen. The palest material is chalcopyrite, the medium grey is pyrrhotite, and the dark grey/black is magnetite. Not distinguishable from the magnetite is black biotite. The sample also has isolated garnet euhedra within sulphide mineralsd or with biotite. Note the foliated character of the sample, defined by crude layers and by elongate biotite aggregates. The bar at the base of the photograph is 1cm long.

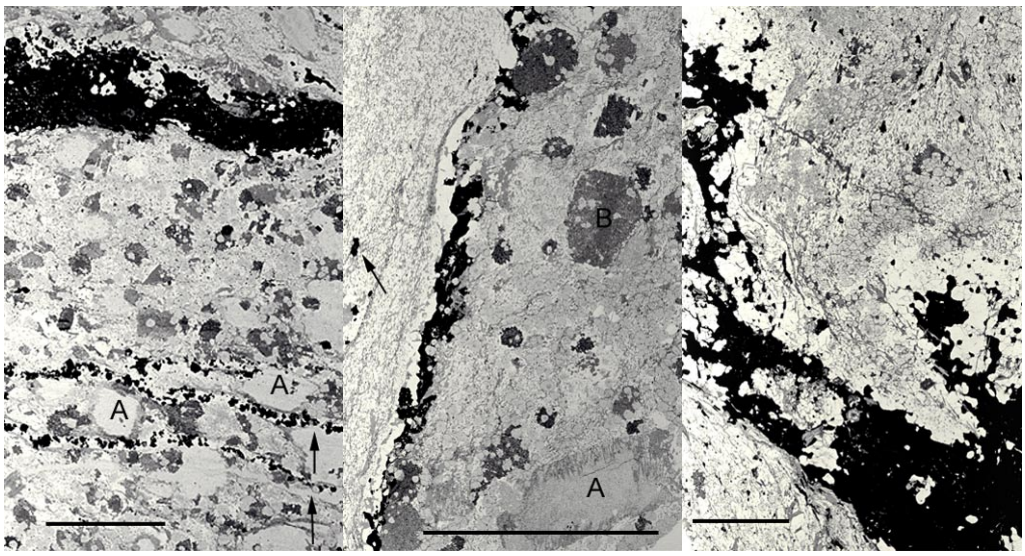


Figure 29. Examples of sulphide veinlets in lode schist. Photographs of large thin sections under plane polarised transmitted light, the bar at the base of each photograph is 1cm long. (a). Centimetre scale vein at top with two millimetre scale veinlets (arrowed) at base. The host rock is GABCl schist with andalusites (A) surrounded by chlorite coronas. [Sample No. 517-070]. (b). Sulphide veinlet separating two lithologies, GCl schist on left and G(A)BCl schist on right. Again the andalusite (A) has a chlorite corona. The ragged, dark shapes are biotite grains, the largest is labelled B. [Sample No. 517-004]. (c). Irregular sulphide-quartz vein. The host rock is G(A)BCl schist. [Sample No. 517-010].

Many of the sulphide veins and quartz-sulphide veins are within discrete fault structures and within broader shear zones. This feature is evident at various scales. An example within a thin section is shown in Figure 29b in which a sulphide vein separates two different lode schist varieties. Most disseminated sulphide grains occur in the quartz rich mineralised

lithologies, in particular GAB(3) schist and quartz rich lode schists. A similar style of disseminated sulphide grains also occurs in veins or zones characterised by very coarse grained hydrous silicate minerals (such as veins of quartz poor lode schist), where the sulphide minerals tend to be interstitial to the silicate minerals.

4.3 Sulphide mineralogy

The most copper rich portions of the Kanmantoo deposit principally consist of chalcopyrite, pyrrhotite, magnetite, pyrite and variable amounts of silicate minerals, particularly quartz, chlorite, garnet and biotite.
Many minor sulphide minerals accompany chalcopyrite and pyrrhotite, including cubanite, galena, pentlandite, mackinawhite and bismuthinite (for more detailed lists refer to Lindqvist, 1969 and Spry, 1976). Minor amounts of ilmenite are associated with magnetite.

Cubanite occurs as exsolution lamellae in chalcopyrite and rarely constitutes more than 20% of the composite grains. Primary pyrite is less common than pyrrhotite and much of the pyrite occurs as secondary melnikovite pyrite (after pyrrhotite). Melnikovite pyrite is most abundant in the near surface mineralisation and in certain lenses in the lower levels of the present mine. For example, it was common in ore mined from a group of lenses in the eastern part of the mine, known as M Lens, to the east of the East Limb. It was reported also from the O'Neil Lode.

The estimated mineralogical proportions of an ore parcel with a head grade of approximately 1.5% copper are shown in Table 10. These proportions were calculated by the author from micrometric grain counts of both ore concentrate and tailings sub-samples derived from the trial ore parcel during metallurgical testwork (Patterson, 1969). The mineralogy of the original, unprocessed ore parcel was not counted and was estimated here by assuming a typical ratio of 1:29.4 for concentrate:tailings. The data in Table 10 demonstrate the characteristically high content of silicate minerals in the ore. Compared to typical unoxidised ore observed by the author, the pyrite content in this sample seems abnormally high and the pyrrhotite content low. Although it is not stated in the above report whether the pyrite is secondary, it seems likely to be melnikovite pyrite after pyrrhotite, especially as the sample was obtained from the upper parts of the Kanmantoo deposit.

Table 10. Estimate of the mineralogy of an ore sample.

Mineral	% proportion by weight of whole sample	% proportion by weight of non-silicate component
silicate minerals	92.0	-
chalcopyrite	4.3	54
pyrite	1.5	19
pyrrhotite	0.4	5
magnetite	1.4	17
ilmenite	0.4	5
Total	*100.0*	*100*

4.4 Copper distribution in the Kanmantoo Mine

4.4.1 Data sources and methods of study

The main source of information on copper distribution within the Kanmantoo open cut mine is the record of assays from drill-holes used for blasting. As open cut mining proceeded, cuttings from blast holes were routinely sampled and assayed for copper in order to control

the grade of ore delivered to the mill. Tens of thousands of assay results were accumulated from all rock units throughout the mine, and these have been used in this study to document the distribution of copper within the Kanmantoo Mine.

The grade control procedure used during mining required that as each blast hole was drilled it be sampled at its base (that is, close to the bench below the drill hole collar) and at a point approximately halfway along the hole. The driller normally collected the samples and they were simple grab samples of 100-200g from the conical pile of drill cuttings surrounding the drill collar. The sample representing the bottom of the hole was taken from the top of the pile and so was reasonably representative of the bottom hole position. The sample meant to represent the halfway point, that is 20 feet below the collar, was grabbed roughly from the middle of the pile and is less representative of the intended position. The samples were placed in paper sample bags and assayed by the AAS method at the company's laboratory located at the mine. The assaying was carried out under the supervision of a chemist and assay standards were used for quality control. The lower detection limit was 0.005% Cu.

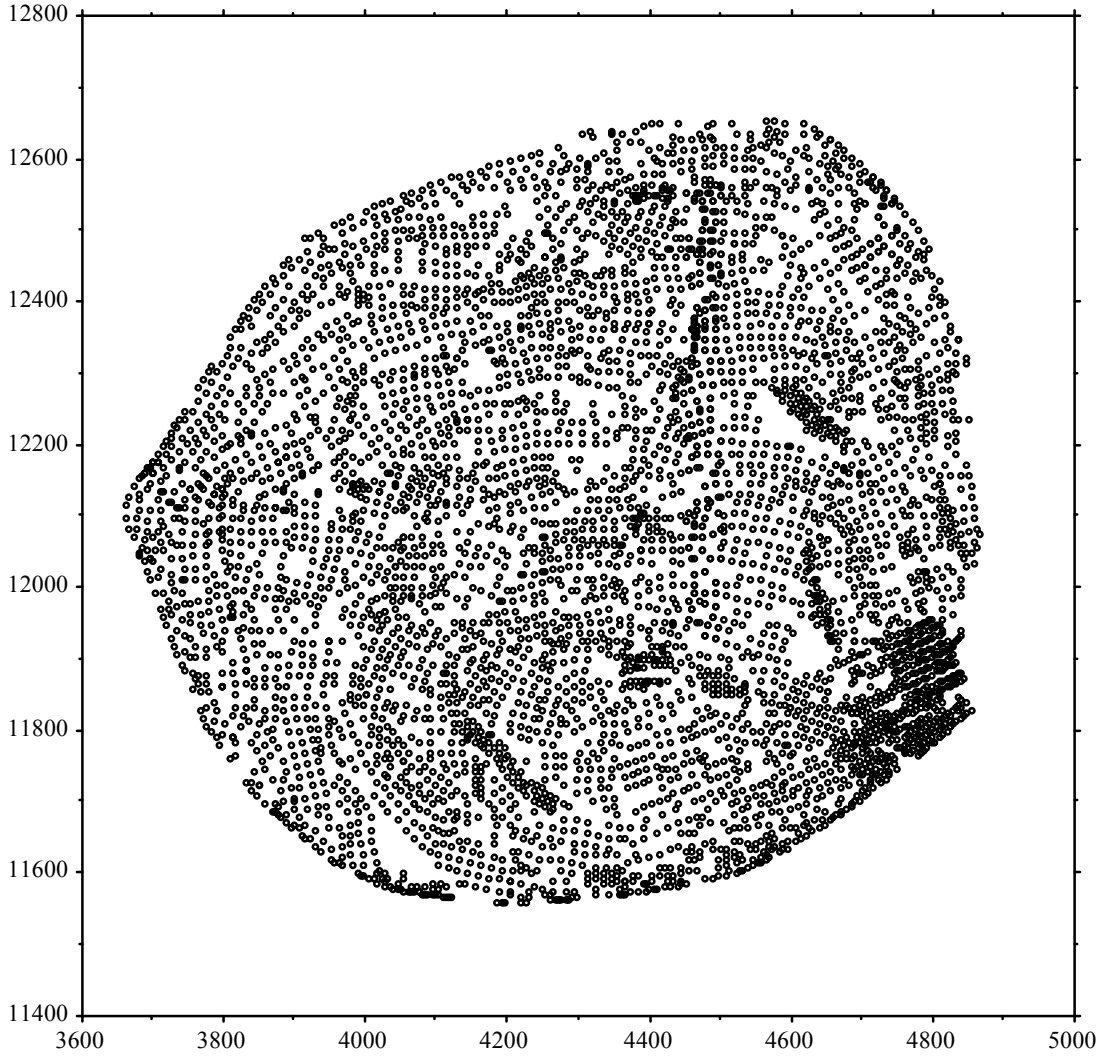


Figure 30. Plan for the 520 level showing assay control sample locations. The plotted position represents the base of the hole. Areas of increased density of data are due to more closely spaced holes using smaller drill rigs to control blasting in key areas like final pit perimeters, ramps and some ore zones.

During the time the mine operated all data were recorded manually. Surveying controlled the location of the drill holes and the surveyor plotted manually onto bench plans the projected position of the bottom of each drill-hole. One master plan was prepared for each bench. Two assay results were written beside the plotted position of the base of each hole, one figure representing the level of the bench shown and the other figure representing a position above.

The density of assay data from drill-holes depended on the spacing between holes and that depended upon several factors including whether the holes were in waste rock or ore. For waste rock the spacing was usually 4.3m and for ore it was usually 4.0m. Another factor was the type of drill rig used - smaller rigs had more closely spaced holes. For each of the upper benches, say above the 480 bench, over 5,000 assays results were recorded (or over 10,000 including the mid-point samples). Figure 30 displays the data points for the 520 bench and is representative of all the benches. On the 520 bench 5,144 data points cover an area of approximately 9.5 ha and so there is one sample per 18 square metres on average. Note the variations in data density shown on Figure 30; for example there are areas with little data shown, mostly because the assays were not recorded. Also, there are areas of high data density, particularly where the smaller rigs were used for carefully controlled blasting on new ramps and perimeter walls.

For this study assay results were available for the following seven benches, all separated by 12.2m (40 feet): the 480, 520, 560, 600, 640, 680 and 720 benches. The data used was on ammonia paper prints made from the original master plans and was used in this study to produce two types of data presentation:

- manual contouring of grades, and
- image processing of grades.

Both methods were applied to plan views and vertical east-west sections. The particular levels and cross-sections that were contoured and imaged are shown in Table 11. Note that because the mineralisation plunges steeply, plan views represent approximate orthogonal sections of the deposit. Plan views of the uppermost benches are also informative because data is available over approximately 360m width, or 70% of the horizontal width of the Paringa Andalusite Member. Vertical cross sections can only be constructed for the 73m (240 feet) vertical extent provided by the available data. This is only half of the full vertical extent of the mine, but it is the best half of all the data because the benches above had poor records and the primary grade distribution was affected to an unknown degree by supergene processes. The benches below have less data because they are not as wide and are increasingly focused on the high grade mineralisation with increasing depth.

Table 11. Summary of levels and cross-sections for which copper distribution was studied.

	Contours		Images
	<0.5% Cu	>0.5% Cu	
Levels	600,640,680	520	520,600
Cross-sections	-	12,000N	11,700N, 12,000N, 12,300N

4.4.2 Statistical description of copper assays at the 520 and 600 levels

As part of this study a database of copper values for the 520 bench and the 600 bench was created, as is explained in section 4.4.4. While a detailed statistical analysis (as opposed to spatial analysis) of this data is beyond the scope of this study, a simple statistical analysis is included because it provides additional understanding of the mineralisation. Basic statistical parameters are presented in Table 12 for data-sets from each of the 520 and 600 levels, and also for the combined data-set.

Despite a data population of over 10,000 data points it is probably not representative of the blast hole samples from the whole mine because the ore bearing areas in the mine tended to be more closely sampled and it is likely that the sample population is somewhat biased in favour of the higher grade zones from the central portion of the mine.

Table 12. Statistical parameters for assay data from the 520 and 600 levels.

Parameter	520 level	600 level	Both levels	Both levels with 0.3% cut
No. of samples	5143	5353	10496	2709
Minimum Cu %	0.005	0.005	0.005	0.30
Maximum Cu %	14.7	17.0	17.0	17.0
Mean Cu %	0.30	0.50	0.40	1.36
Std. deviation	0.74	1.23	1.03	1.68
Coeff. variation	249.32	246.54	256.10	123.36
Mode	0.005	0.005	0.005	0.30
Geometric mean	0.05	0.08	0.07	0.90
Kurtosis	71.33	41.94	55.85	18.42
Skewness	6.67	5.53	6.24	3.64

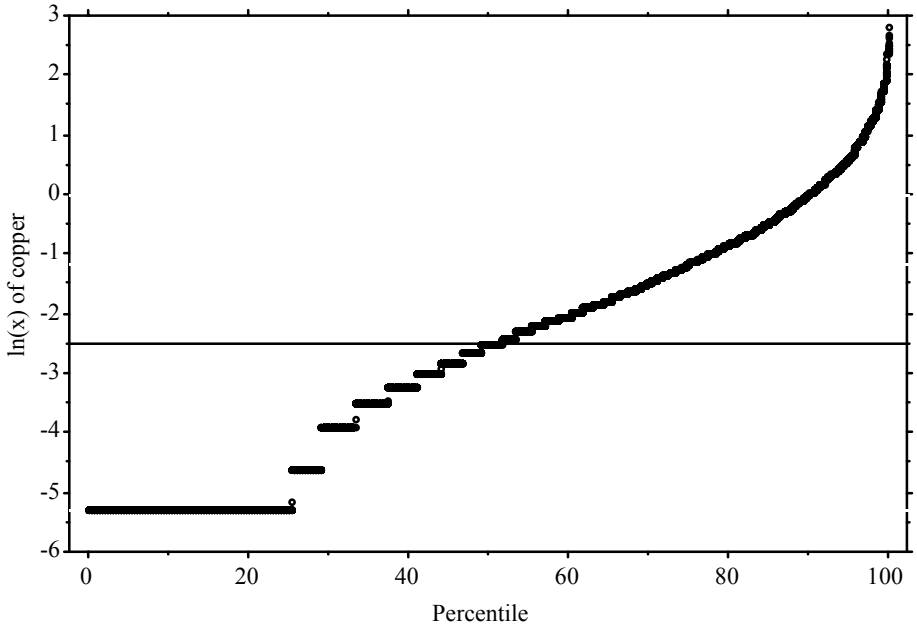


Figure 31. Cumulative frequency plot of transformed assay data from the 520 and 600 levels. Horizontal lines represent the 25th, 50th, 75th and 90th percentile values.

4.4.3 Contouring of copper grades

Some manual contouring of the assay data was completed using the original data, and the contouring took into account the assay result recorded for the particular bench, the second assay result in the blast hole (that is the sample mid way down the hole) and any mineralisation recorded during mapping.

Separate sets of manual contours were prepared to highlight details within the higher and lower grade portions of the deposit, using an arbitrary threshold grade of 0.5% copper. To put this figure of 0.5% Cu in context, the lower cut off grade used during mining was 0.3% Cu and the mean head grade was 0.85% Cu. For the mineralisation below 0.5% Cu, three of the upper benches in the mine were contoured using three arbitrarily chosen contour intervals of 0.5%, 0.1% and 0.01% copper. A total of over 30,000 sample results were contoured and the results for the 600, 640 and 680 levels are shown on Figures 32 to 34. Because the sampling on the 680 level was less dense than the other two benches the contours there are less detailed. For the mineralisation above 0.5% Cu, only one level was contoured, the 520 level (Figure 35), and in addition, manual contours were prepared for a cross-section on 12,000N. No cross-section was prepared for the lower grade mineralisation below 0.5% Cu.

The first impression of the copper distribution as shown in Figures 32 to 34 is of a rather irregular pattern, but closer study reveals consistent, regular features in the patterns on each level. These features will be outlined by discussing the number, sizes and trends of the lenses defined by the contour pattern. Many lenses with copper contents greater than 0.5% are apparent on the figures, but most are relatively small. The largest lens or body, which occurs southwest of the centre of each bench, is the Main Lode, and was the principal ore source during mining. It is irregular in shape and consists of two parts or lobes, called the East and West Limbs during mining. These are most distinctive in Figure 32. The West Limb is the larger of the two (at these levels of the mine) and has a general northerly trend, in contrast to the north-northeasterly trend of the East Limb. The actual and relative sizes of the East and West Limbs change from level to level, for example on these levels the length of the West Limb increases from 145m on the 680 level, to 175m on the 600 level. Variations in the sizes of the two Limbs is known to occur on other levels as well. Similar features to those seen in copper contours are described in Chapter 3 for the lode schists and it will be shown later that there is a close relationship between the distributions of copper and the lode schists.

Two dominant trends are highlighted by the contours - northerly and north-north-easterly. A strong northerly trend throughout the mine is defined by all copper contours (but especially by the 0.5% contour) at all scales. The north-northeasterly trend, which is less prominent than the northerly trend, is highlighted on Figure 32 as three zones. The trends can be traced across much of the mine as lines connecting pods of higher grade mineralisation, usually greater than 0.5% copper. Many of the pods have northerly trends, and so are oblique to the lines on which they lie. Note that the central of the three north-north-easterly trending lines corresponds to the East Limb described above.

The spatial arrangement of the two dominant trends defines several domains bounded by approximately north-south trending lines. The westernmost and easternmost thirds of the levels shown in Figures 32 to 34 are dominated by northerly trends, whereas the north-north-easterly trends are best developed in the central area. The boundaries between the domains appear to be abrupt in places, for example on the western side of the central domain on the 600 level (labelled *A* in Figure 32). The eastern boundary of the central domain is less pronounced but is close to 4600E. Each of the domains host both trends, for example in the central domain the northerly trend is imposed on zones with an overall north-north-easterly trend, where it is manifest as northerly trending corrugations on the overall trend of the

contours. Another feature of the central domain is the northerly trending zone labelled *B* in Figure 32**.** Evidence of the north-north-easterly trend in the two outside domains is weak in these contours, but is apparent in the images described in the next section.

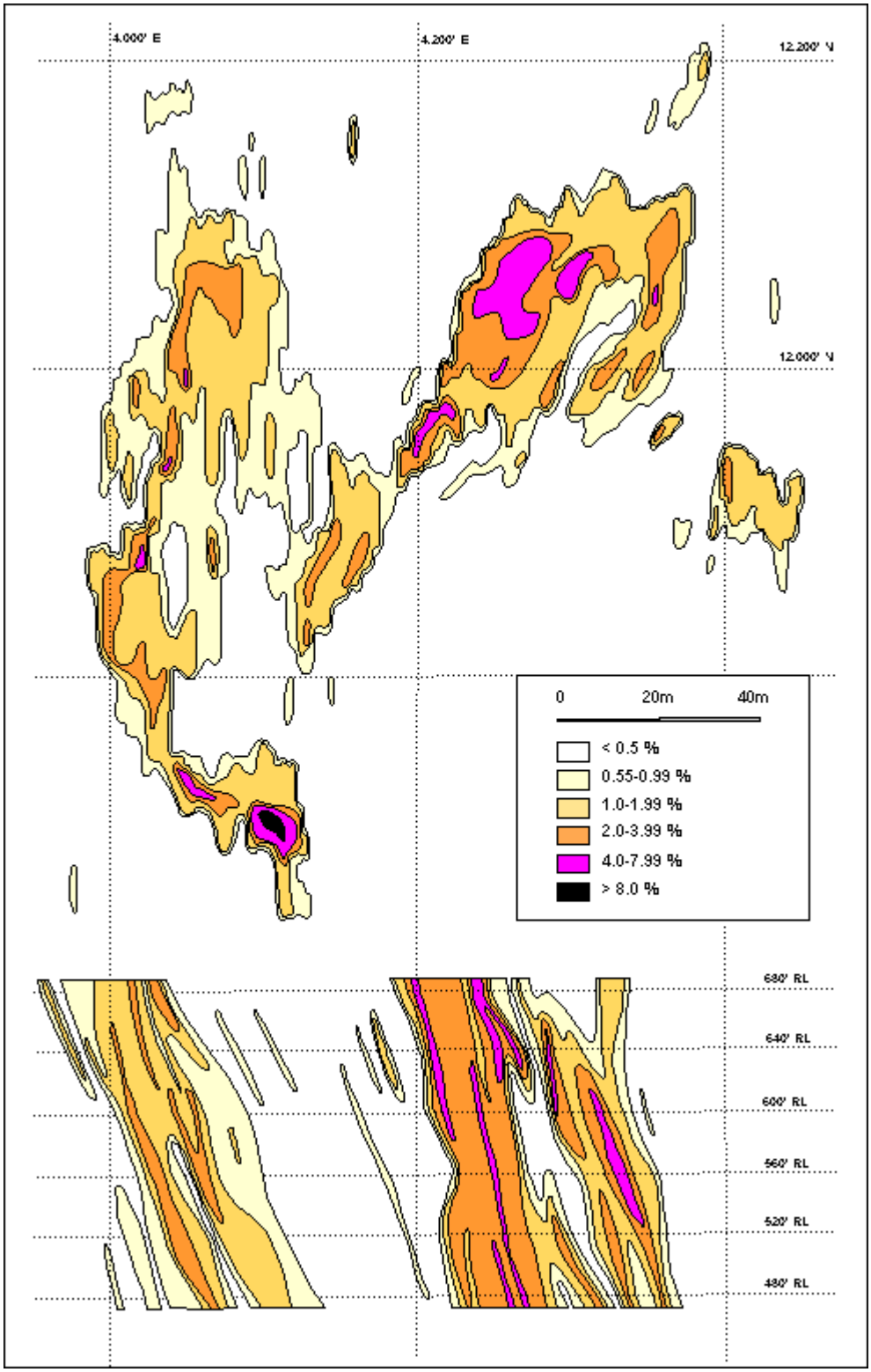


Figure 35. Copper distribution >0.5%. Contours for the 520 level and cross-section for 12,000N.

Contours of copper greater than 0.5% are shown in Figure 35 for the central, high grade part of the 520 level and for cross-section 12000N between the 680 bench and the 480 levels. The mineralisation represented for the 520 level is predominantly the East and West Limbs of the Main Lode and the domain boundaries mentioned above are located at approximately 4125E and 4400E. The two trends that can be recognised in the lower grade mineralisation, that is northerly and north-north-easterly, can also be recognised in the higher grade mineralisation at the 520 level and seem to be a little more prominent. The north-north-easterly trend is represented by the East Limb. The West Limb is on the left hand side of the plan view in Figure 35 and has the characteristic northerly trend, which can be followed for almost the full extent of the figure. Of interest is the sinistral, sigmoidally shaped zone at the southern end of the West Limb. This curve is apparent in Figures 32 to 34, and in Figure 32 its southernmost tip is labelled *A*. Figure 32 shows that this zone has two high grade centres and the north-western one lies on the projection of the East Limb line and the south-eastern one may be on a parallel line linking it with the large, north-north-easterly trending protuberance 120m to the north-northeast.

In cross-section, the pattern of contours for higher grade mineralisation shown in Figure 35 is markedly different from that seen in plan view. The pattern is very regular and comprises steeply dipping, sub-parallel contours. It displays a persistence of individual shoots not seen in plan view. For example, a zone only one to two metres wide (containing 4.0 to 7.99% copper), can be traced for at least 50m down dip, but note that on the 520 level this zone has a strike extent of only a few metres. Other, lower grade zones can be traced over even greater distances down dip. Another feature illustrated by this cross section is the strong alignment of the contours, indicating a common steep easterly dip in both the East and West Limbs. Despite the strong alignment of contours they are not all parallel. In the West Limb, the contours dip between 65-72º east. On the western half of the East Limb, which is the most persistent laterally and the highest grade portion, the contours have a steeper dip of approximately 79-85º east. Further east, in the eastern half of the East Limb, the contours are a little shallower at 72-78º east. This variation in dip is discussed further in the next section and in the next chapter where it will be shown that the 70-75º east dips of the West Limb are parallel to the mean schistosity trace and that the dips in the East Limb are steeper than the schistosity trace.

4.4.4 Imaging of copper grades

To use image processing programs for spatial display of the copper assays it was necessary beforehand to convert the manually recorded assay results to a digital version. This was done from the mine assay plans using a digitiser and Interdex v.5.0 software to create a database of easting, northing, RL and copper grade for each sample point. Grade control assay data from two benches were digitised, the 520 bench (5,144 points) and the 600 bench (5,354points). In addition, data from three cross-sections, 11700N, 12000N and 12300N were digitised. Images prepared in two ways are presented here, most were made using Interdex and are presented as colour representations of the original assay results in Figures 36, 37 and 39 (plans) and Figure 40 (cross sections). In addition, a grey scale image, Figure 38, was prepared for the 520 level using ER Mapper software.

Interdex creates images by dividing the complete sampled area into a grid of squares (called pixels) each of which is then assigned a grade based on its surrounding assay values. Grades assigned to each pixel are derived from all points within a defined search radius from the centre of the pixel, using an inverse distance weighting method. The pixel width and the search radius are selected by the user and in this case were 5 feet and 50 feet respectively. The pixels are then coloured on a spectrum according to their grades, and in this case the lower grades are shown in cool, dark colours (black, purple, blue) and the higher grades are

Contours of copper greater than 0.5% are shown in Figure 35 for the central, high grade part of the 520 level and for cross-section 12000N between the 680 bench and the 480 levels. The mineralisation represented for the 520 level is predominantly the East and West Limbs of the Main Lode and the domain boundaries mentioned above are located at approximately 4125E and 4400E. The two trends that can be recognised in the lower grade mineralisation, that is northerly and north-north-easterly, can also be recognised in the higher grade mineralisation at the 520 level and seem to be a little more prominent. The north-north-easterly trend is represented by the East Limb. The West Limb is on the left hand side of the plan view in Figure 35 and has the characteristic northerly trend, which can be followed for almost the full extent of the figure. Of interest is the sinistral, sigmoidally shaped zone at the southern end of the West Limb. This curve is apparent in Figures 32 to 34, and in Figure 32 its southernmost tip is labelled *A*. Figure 32 shows that this zone has two high grade centres and the north-western one lies on the projection of the East Limb line and the south-eastern one may be on a parallel line linking it with the large, north-north-easterly trending protuberance 120m to the north-northeast.

In cross-section, the pattern of contours for higher grade mineralisation shown in Figure 35 is markedly different from that seen in plan view. The pattern is very regular and comprises steeply dipping, sub-parallel contours. It displays a persistence of individual shoots not seen in plan view. For example, a zone only one to two metres wide (containing 4.0 to 7.99% copper), can be traced for at least 50m down dip, but note that on the 520 level this zone has a strike extent of only a few metres. Other, lower grade zones can be traced over even greater distances down dip. Another feature illustrated by this cross section is the strong alignment of the contours, indicating a common steep easterly dip in both the East and West Limbs. Despite the strong alignment of contours they are not all parallel. In the West Limb, the contours dip between 65-72° east. On the western half of the East Limb, which is the most persistent laterally and the highest grade portion, the contours have a steeper dip of approximately 79-85° east. Further east, in the eastern half of the East Limb, the contours are a little shallower at 72-78° east. This variation in dip is discussed further in the next section and in the next chapter where it will be shown that the 70-75° east dips of the West Limb are parallel to the mean schistosity trace and that the dips in the East Limb are steeper than the schistosity trace.

4.4.4 Imaging of copper grades

To use image processing programs for spatial display of the copper assays it was necessary beforehand to convert the manually recorded assay results to a digital version. This was done from the mine assay plans using a digitiser and Interdex v.5.0 software to create a database of easting, northing, RL and copper grade for each sample point. Grade control assay data from two benches were digitised, the 520 bench (5,144 points) and the 600 bench (5,354points). In addition, data from three cross-sections, 11700N, 12000N and 12300N were digitised. Images prepared in two ways are presented here, most were made using Interdex and are presented as colour representations of the original assay results in Figures 36, 37 and 39 (plans) and Figure 40 (cross sections). In addition, a grey scale image, Figure 38, was prepared for the 520 level using ER Mapper software.

Interdex creates images by dividing the complete sampled area into a grid of squares (called pixels) each of which is then assigned a grade based on its surrounding assay values. Grades assigned to each pixel are derived from all points within a defined search radius from the centre of the pixel, using an inverse distance weighting method. The pixel width and the search radius are selected by the user and in this case were 5 feet and 50 feet respectively. The pixels are then coloured on a spectrum according to their grades, and in this case the lower grades are shown in cool, dark colours (black, purple, blue) and the higher grades are

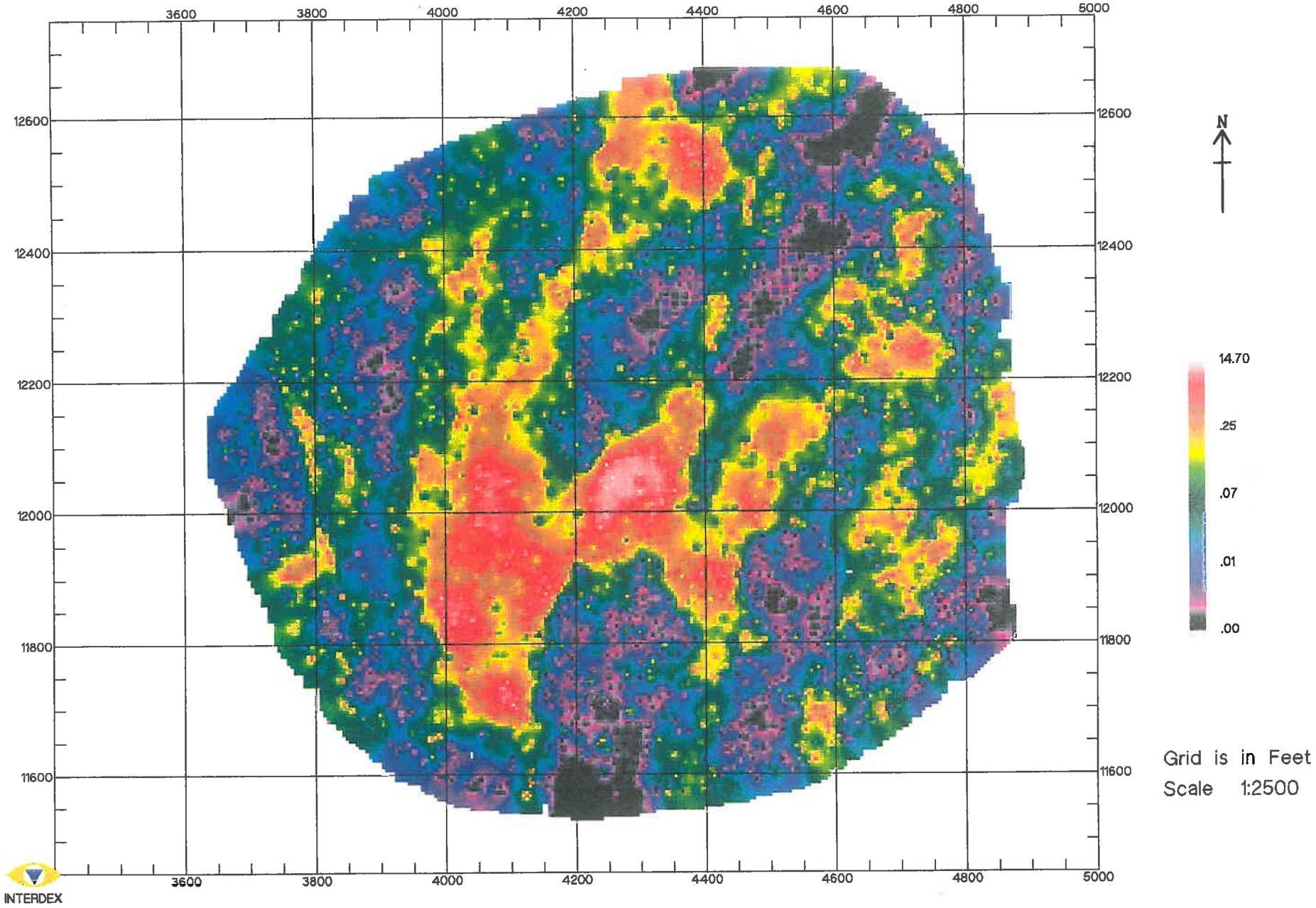


Figure 36. Image of copper assays for 520 level

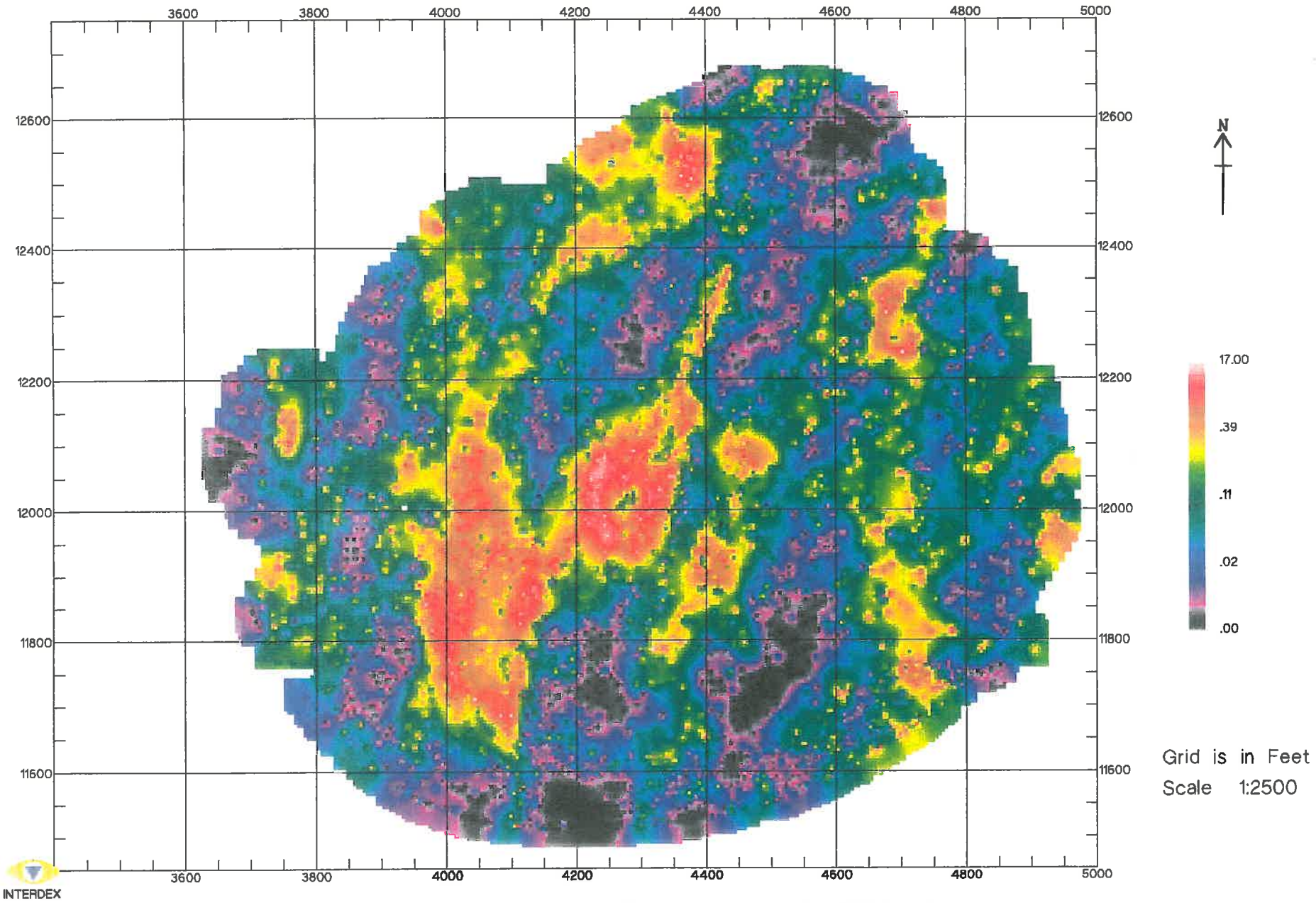
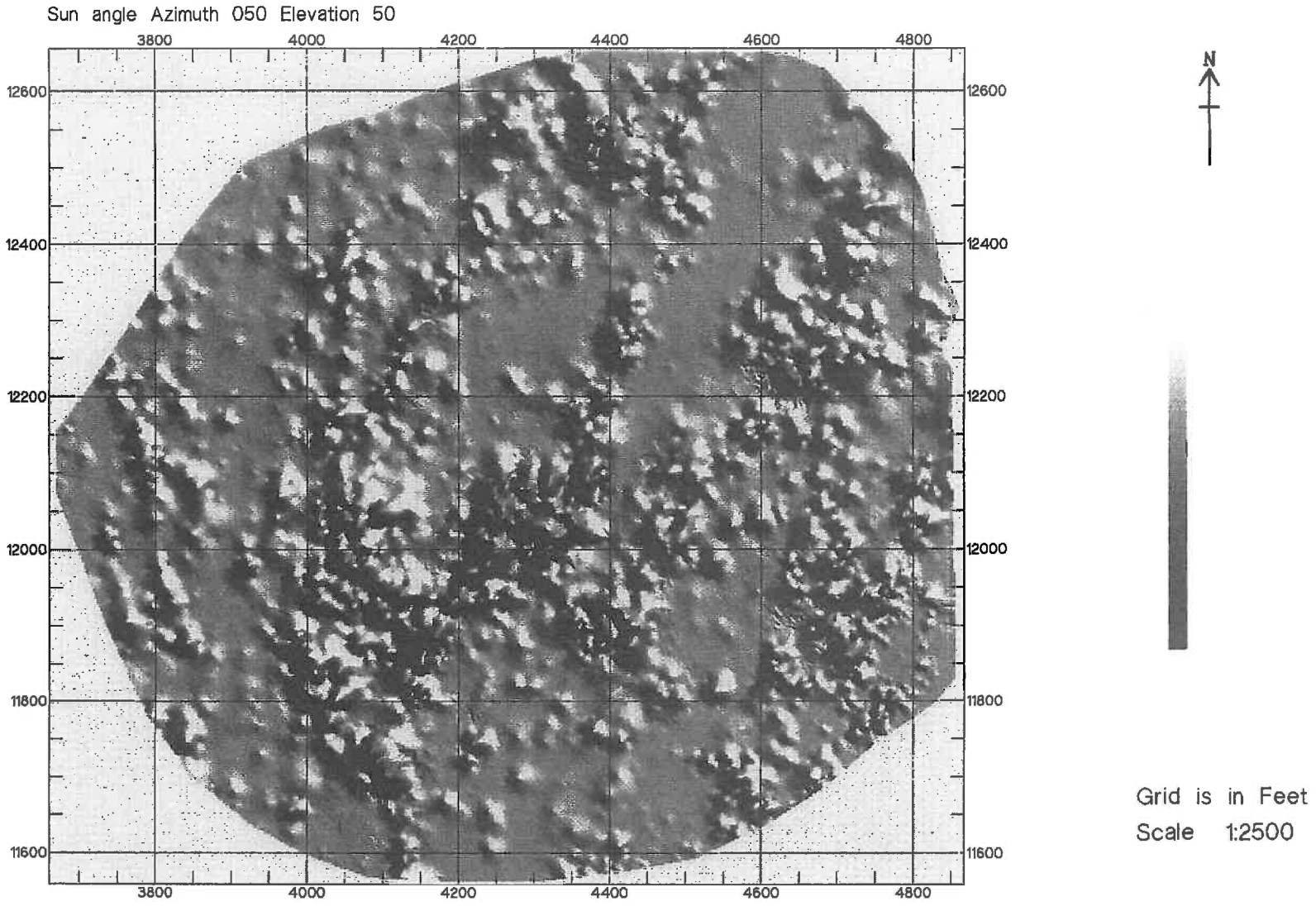


Figure 37. Image of copper assays for 600 level



INTERDEX

Figure 38. Grey-scale image of copper for 520 level

shown in warm, bright colours (red, white). The values assigned to the colours are shown in a bar on each figure. Note that the scale used to assign colours is not linear. A linear conversion is inappropriate because the data are negatively skewed and important patterns will be obscured by the many low values that would dominate the image. Modifying or stretching the data prior to assigning a colour scheme produces more informative images. With Interdex a non-linear process is applied known as cumulative weighting (as defined in the Interdex manual) or histogram equalising. Using Interdex's colour scheme, this process has the effect of producing an image containing more detail about the higher values in the grade distribution.

The patterns of copper distribution defined for the 520 and 600 levels in Figures 36 and 37 are similar to those described from contoured data in the previous section. Again the three domains referred to in the previous section (western, central and eastern) are apparent. An interpretation of the main features of the 520 level image is shown in Figure 39.

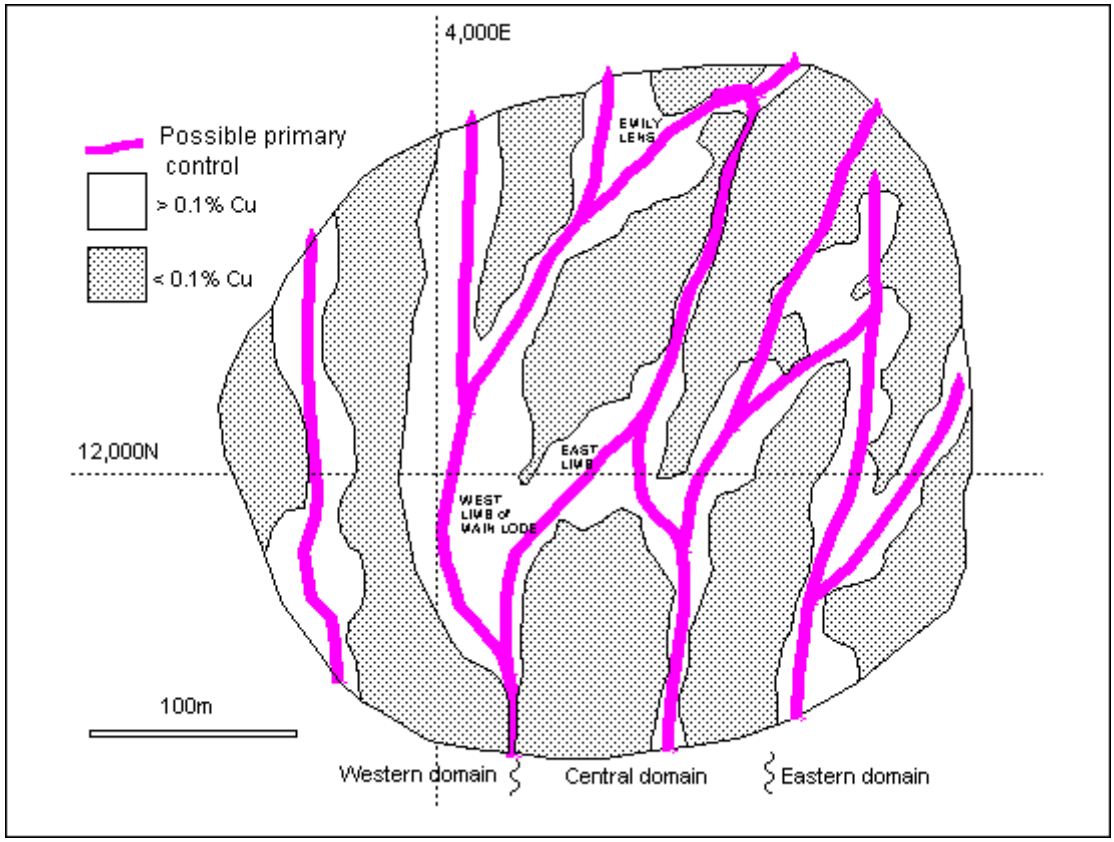


Figure 39. Interpreted main features of copper distribution on the 520 level. This figure should be compared with Figure 36. The areas shown as greater than and less than 0.1% Cu are approximate only and in places include some lower grade material to maintain continuity of the zone. The traces of inferred planar features that may represent primary controls on copper distribution are shown. In some cases they correspond with discrete structures, for example the boundary between the western and central domains at the southern margin is the sinuous 4100 Shear Zone. In other cases the lines probably do not represent discrete structures, for example the most western line represents what appears to be a wider zone of relatively abundant shears and sulphide veins. The pattern of inferred controls shown for this level is similar for all levels.

The western domain, west of 4150E approximately, has two higher grade zones trending north-south, the eastern one being the West Limb. The West Limb persists to the northern limit of the data where it is a relatively broad zone (about 80m wide) with only patchy high grade pockets. At its southern end the West Limb narrows abruptly and is represented only by a narrow zone near 4100E. The second and weaker zone in the western domain is centred on 3750E approximately and is about 30m wide. It has an oblique, north-north-westerly grain within it, particularly apparent on the 600 level. The low grade zone separating these two northerly trending zones persists for the full 250m-300m extent of the available data and appears to be cut by several north-easterly trending structures.
The central domain displays clearly the three north-north-easterly trending high grade linear zones marked on Figure 32. The central linear zone corresponds to the East Limb. On both levels the East Limb can be followed northwards as a narrow unit of 5-8m width beyond the main bulk of the East Limb to the limits of the data. This northern section of the East Limb is slightly more northerly in trend than the main part, changing in azimuth from approximately 035º to 020º towards the north. The northern linear grade zone in the central domain arcs away from the West Limb and merges to the northeast with the blocky, high grade Emily Lens area. There is a suggestion that a structure continues through to link up with the extension of the East Limb near 12600N. The southern linear zone in the central domain has its strongest grades opposite the East Limb where it has a north-north-easterly trend. It continues to the southern limit of data but is weaker and changes trend to almost north-south.

The eastern domain contains a broad, relatively diffuse, high grade zone that is best defined on the 600 level. Beyond the southern limits of the pit this zone hosts the C and D Lenses of the South Eastern Mineralisation. Within the pit it seems to weaken to the north of 12450N approximately where it intersects a northeast trending structure. A suggestion of another north-south trending zone is apparent at the eastern margin of Figure 37 that probably corresponds to the northern extension of the zone hosting the F and G Lenses of the South Eastern Mineralisation. Between these two zones is a linking, strongly mineralised north-north-easterly trending structure.

A grey scale, pseudo-topographic image of copper assays from the 520 level is shown in Figure 38. To make this, the data was gridded with Surfer 6 software using kriging, the grid was blanked using a Surfer digitised blanking file and then converted to ER Mapper format using a private program developed for Southern Geoscience Consultants in Western Australia. ER Mapper created the image using a shading effect with the "sun" positioned in the northeast. This image displays the features described above and also highlights several subtle northwest, northeast and east-northeast trending structures. The latter trend will be referred to again in the next chapter.

Cross-sectional images are shown in Figure 40. The central section is of 12000N and corresponds to Figure 35b, discussed in the previous section. Again, it is clear that grade distribution is much more regular viewed in cross-section compared to plan. All figures define zones that tend to persist for the full extent of the levels represented, however on the western side of the uppermost level (that is RL 720 ft) the images suggest loss of copper, perhaps by supergene processes. By referring to both the plans and the sections the three dimensional character of the various high grade zones can be studied (but note that the colour schemes are not directly comparable).

An important feature that is revealed by the cross-sections is changes in dip of some of the mineralised zones. Dip variations indicated by the contours were discussed in the previous section, but only for grades above 0.5% Cu in the central portion of the 520 level, where only slight changes in dip were noted. In contrast, most of the effects seen in cross section (Figure 40) are due to lower grade mineralisation. In the images the variation in dip is much more

marked and is seen across the full width of the pit. The principal feature is a fanning of dip from approximately 70ºE on the western side of the mine to 70ºW on the eastern side.

Most of the mine has easterly dipping zones of copper mineralisation but to the east of 4400-4500E, depending on the section, vertical and westerly dips prevail. Even some individual lodes change dip as they traverse across the mine. For example, the East Limb has a well defined overall dip of 80ºE on section 12000N (centred on 4250E) but on section 12300N (where it is centred at 4400E) it is subvertical. It was noted above from the plan views that there is also a change of trend from 035º to 020º between these segments. The westerly dips that prevail on the eastern side of the mine are apparent on each section but are best defined by the high grade zone centred on 4650E on 12300N. Finally, the cross-sections have subtle features suggestive of flat to moderately east dipping and moderately west dipping faults that influence copper distribution.

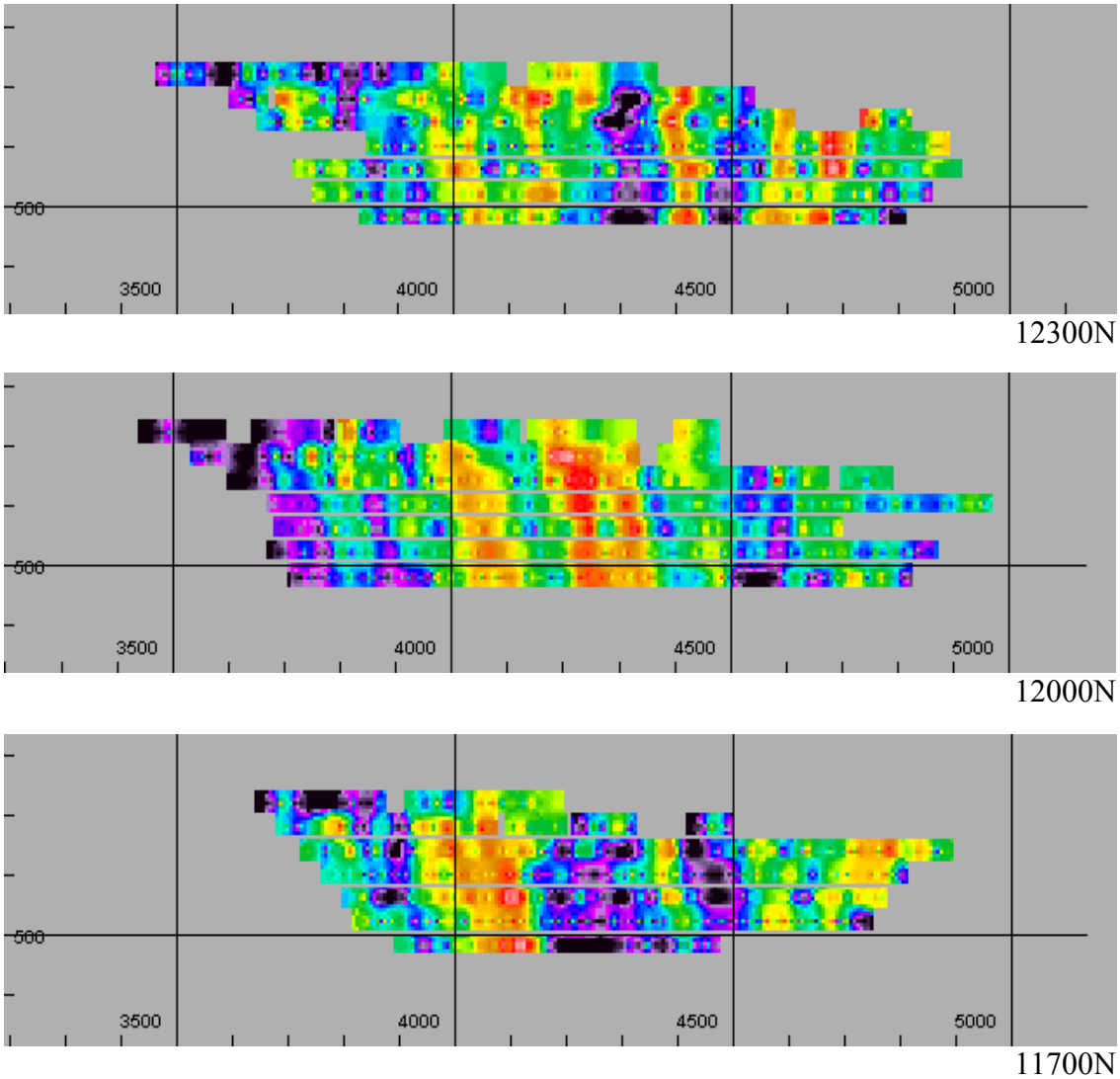


Figure 40. Cross-sectional images of copper grades along sections 12,300N, 12,000N and 17,000N. Note that the colour schemes do not correspond exactly to the same grade ranges in each image.

4.5 Spatial relationship between lode schist and copper

It is clear from mapping that sulphide abundance is greater in certain lithologies, namely the lode schists. Of the various lode schists, those that have no andalusite and are chlorite rich host the highest grade mineralisation. Thus, the best hosts are GClB schist, GBCl schist and GCl schist. A comparison of copper contents for various lithologies can be studied quantitatively for the 520 level, where both assay data and interpreted lithological blocks are available. Figure 41a shows the geological interpretation based on the author's mapping and also an interpreted outline of the largest lenses of andalusite-free lode schist, as interpreted from earlier mapping by others.

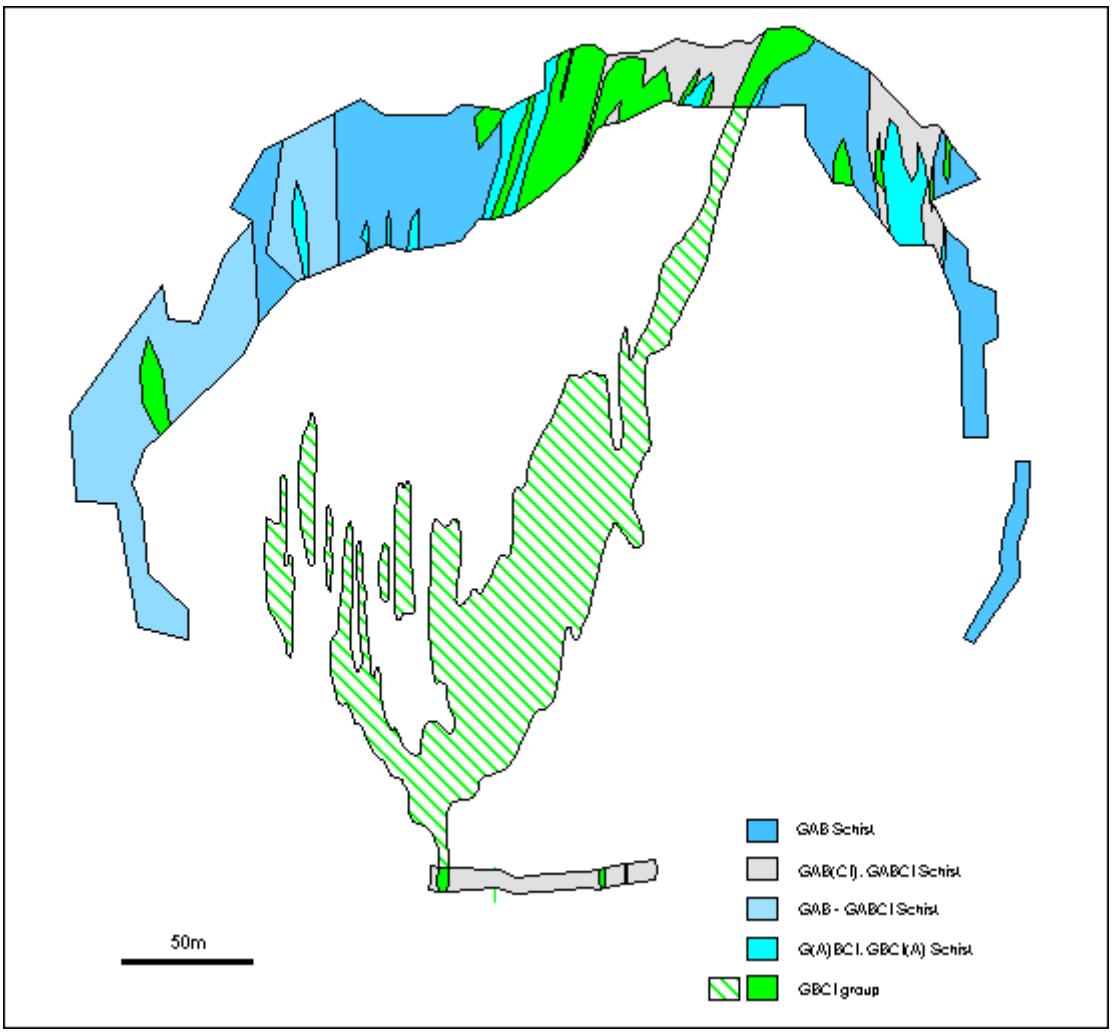


Figure 41a. Interpreted lithological units on the 520 level used to estimate mean Cu grades for each lithological group in Table 13 (the solid-coloured units) and Table 14 (the striped units). The stippled area was interpreted from the mapping of other geologists.

The average copper grades for the various lithologies shown in Figure 41a are presented in Tables 13 and 14. The results confirm the field observation that those rocks with little or no andalusite and abundant chlorite have higher mean copper contents. Table 13 indicates a steady increase in mean copper content from a relatively low level of 0.08% in the GAB schist country rock, to 0.15% in its chloritic versions, GAB(Cl) schist and GABCl schist. The intermediate level of 0.09% in the GAB - GABCl schist group is also consistent, because this is a broad group where the lithologies of the first two groups were mapped as mixed. In the

lithologies with weak andalusite the mean grade increases again to 0.38%, only just below the mean of 0.39% for the andalusite free GBCl group. This value of 0.39% seems a little low as an average for this group, but that is probably because the units sampled are on the margins of the main copper bearing zones, which were in the centre of the pit. The striped zone of GBCl group rocks shown in Figure 41a was derived from records of mapping done by other mine geologists and includes the central, higher grade part of the level. Average copper grades for GBCl group schists from these lenses are shown in Table 14. As expected, the mean grade for this central portion of the Main Lode is much higher at 0.98% Cu. Similar higher grades were derived for the GBCl group rocks belonging to isolated lenses in West Limb and for Emily Lens.

Table 13. Mean copper grades for all lithological groups for the 520 level.

Lithology	No. samples	Total area (m2)	Mean grade (% Cu)
GAB schist	286	6,580	0.08
GAB(Cl) schist & GABCl schist	121	2,138	0.15
GAB-GABCl schist	222	4,980	0.09
G(A)BCl schist & GBCl(A) schist	55	1,074	0.38
GBCl group	128	2,570	0.39

Table 14. Average copper contents (% Cu) of GBCl group lode schists for the 520 level. Based on lithological interpretations using mapping by other mine geologists.

Location	Area (m2)	No. samples	Mean	Min.	Max.
Main Lode	105,454	529	0.98	0.005	14.7
West Limb lenses	1,142	50	0.50	0.005	2.5
Emily Lens	883	50	0.89	0.005	5.9

A comparison of copper distribution and andalusite free lode schist is shown in Figure 41b. This figure shows that most of the mineralisation greater than 0.5% is within lode schist, but the correspondence is not perfect. The mean grade of some of the lode schist shown is less than 0.5% and, conversely, some of the mineralisation above 0.5% is shown as not being hosted by lode schist. Explanations for this latter observation are that the mineralisation is hosted by other lithologies, especially GAB(3) schist, or that the mineralisation is hosted by many small lode schist lenses that were not represented in the figure. Note that in Figure 41b the East Limb the mineralisation has a different trend (approximately 035˚) compared to the enclosing lode schist unit (approximately 025˚).

A comparison between the East and West Limbs of the gross orientations of copper zones and lode schist (andalusite free variety) is shown in Table 15, where the figures represent strike/dip. The estimates for the lithologies are derived from Table 9 in the previous chapter. The estimates for the copper zones are obtained from Figure 35 for the higher grade mineralisation, and from Figures 36 and 37 for lower grade mineralisation. The results suggest that the copper lodes and lode schists do not correspond, an unexpected and interesting result given the common association at a mesoscopic scale that was observed when mapping. Table 15 shows that in the West Limb the andalusite free lode schists and copper contours have the same strike, but the former have steeper dips than the latter. It will be shown in the next chapter that the copper lodes in the West Limb tend to be parallel to or very slightly steeper than the schistosity, which is very regular. Therefore, the lode schist lenses of

the West Limb are steeper than the schistosity. In the East Limb, lode schists and copper appear to be approximately parallel in strike, despite some local divergences as shown in Figure 41b, but the copper zones are slightly steeper. The apparent divergence between copper zones and lode schists requires more work to confirm and to understand.

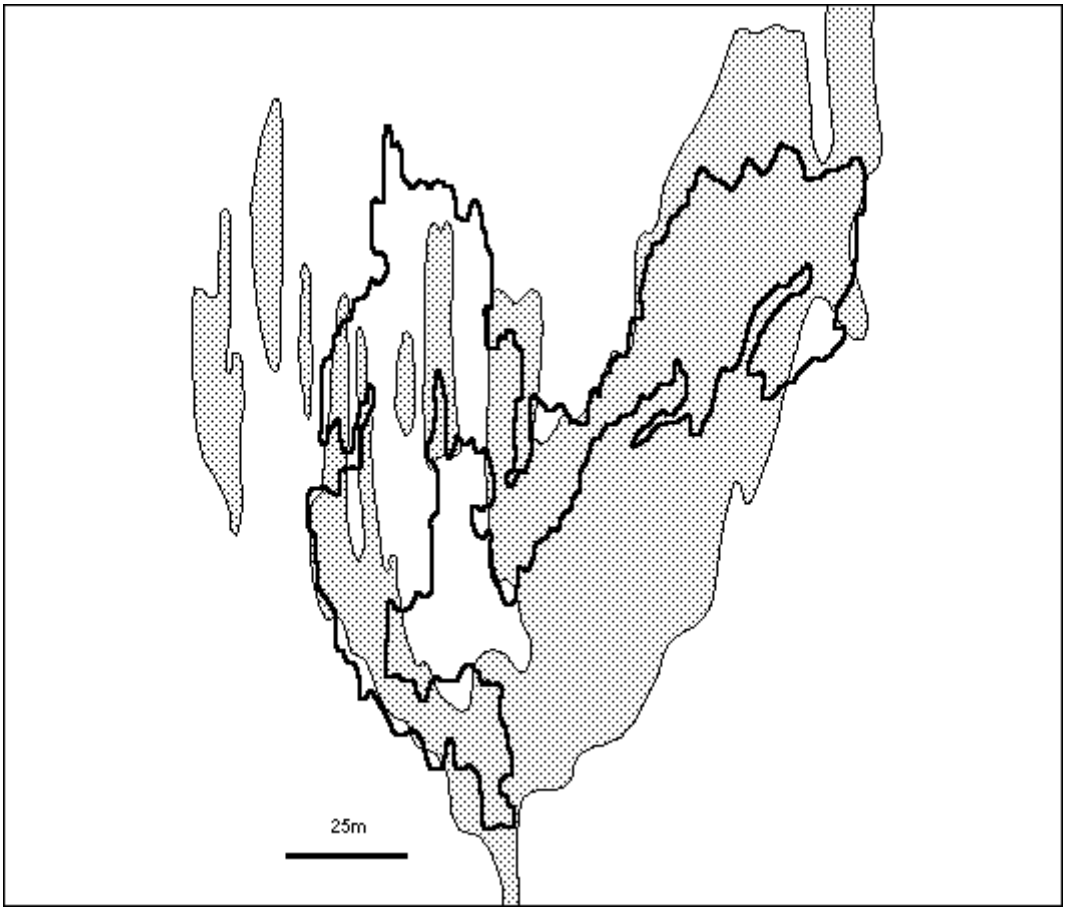


Figure 41b. Comparison of lode schist and grade contour, 520 level. The stippled area is the lode schist outline shown in the central portion of Figure 41a. Overlain as a bold line is the 0.5% Cu contour shown in Figure 35.

Table 15. Comparison of the general orientations of GBCl group lode schists and copper zones for East and West Limbs. Orientations are shown as strike/dip angle and dip direction.

Feature	West Limb	East Limb
Lode schist (andalusite free)	000/84-89E	020/70-85E
Copper zones	000/70-75E	020/90E and 035/80E

4.6 Types of copper mineralisation

Some of the lithological differences between the East Limb and West Limb of the Main Lode have been discussed in previous sections. Two slightly different types of mineralisation can be recognised in the Kanmantoo deposit, one is associated with the West Limb, the other with the East Limb and here they will be called West Limb type and East Limb type mineralisation. (Previously these two types were referred to as Emily style and West Limb style; Schiller, 1978). Other, smaller lenses in and out of the pit can be allotted to one of these two classifications. For example, the numerous lodes comprising the South Eastern Mineralisation are of the East Limb type, whereas the Paringa and Otto workings are of the West Limb type.

The principal differences between the two types are listed below; some of these are based only on observation during mapping and have not been quantified.

(a) Association with GAB(3) schist

One of the most characteristic features of East Limb style mineralisation is its association with GAB(3) schist, a lithology absent from West Limb style. The largest volumes of this lithology have been observed in the open cut and in the underground workings within the South Eastern Mineralisation. GAB(3) schist is associated also with small, old workings located 300m to 400m south of the pit perimeter. To the author's knowledge, GAB(3) schist has not been reported in association with the O'Neil Lode nor with other copper deposits in the Kanmantoo region.

(b) Strike

East Limb style lodes generally trend north-north-easterly, or they may form zones of multiple lodes with this trend. In contrast, West Limb type lodes trend northerly and occur in zones which also trend northerly.

(c) Shape of the lodes

In general, West Limb type mineralisation occurs in groups of parallel lenses with large length: width ratios, whereas East Limb type tends to be less elongated, although there are exceptions.

(d) Form of the veins within lodes

West Limb type lodes usually contain long sulphide veins parallel to the schistosity and the veining tends to be extremely regular. East Limb type lodes also contain such veins but also many anastomosing veins and irregular veins, and sulphide or quartz-sulphide masses.

(e) Associated lode schist varieties

Although both types of mineralisation have a variety of lode schists present, East Limb type lodes have more variety than West Limb type. For example, the quartz poor-absent lode schists and the amphibole bearing varieties are most common in East Limb type lodes.

(f) Copper content

The average grade of East Limb type lodes is higher than West Limb type. Mining in the West Limb area generally required more attention to grade control because it is not only the greater proportion of high grade sections in the East Limb that is responsible for higher overall grades, but also the lower proportion of weakly mineralised rock separating veins or high grade sections.

(g) Mineralogy

Although chalcopyrite, pyrrhotite and magnetite, occur in both types of lodes they occur in different proportions. West Limb type lodes contain little magnetite and generally pyrrhotite and/or pyrite exceeds chalcopyrite. In East Limb type lodes, magnetite is common and increases with increasing copper content. Magnetite constitutes up to 40% of fist sized hand specimens, and is especially abundant in parts of the south-western tip of the East Limb, that is the zone common to both the East and the West Limbs. High magnetite contents are also common in parts of the South Eastern Mineralisation.

4.7 Other copper deposits in the Kanmantoo Mine area

The largest deposits in the area surrounding the Kanmantoo deposit are, in descending order, the South Eastern Mineralisation, the O'Neil Lode, the Paringa Lode and the West Kanmantoo Lodes. Little work has been done on these for this study except as follows. Firstly, the surface mine workings were examined. Secondly, underground mapping was done during mining development in the South Eastern Mineralisation but the details were not available for this study.

The South Eastern Mineralisation comprises six known lenses behind the south-eastern wall of the Kanmantoo open cut mine. The lenses were accessed by a decline from the haul road in the open cut mine and underground development was near completion when the mine closed in 1976. The two largest lenses are C Lens and D Lens but both have weak to no surface expression. Several copper mineralised lenses of lode schist are shown exposed on the south-eastern wall of the open cut mine in Figure 7. Of these, the westerly cluster corresponds to the extensions of C Lens and the single easterly lens appears to correspond to D Lens. The surface workings further east (the Spitfire Workings) represent the more easterly F and G Lenses. Information about much of the South Eastern Mineralisation is restricted to diamond drilling and, for C and D Lenses, some underground development exposure. According to O'Connor (1974), both C and D Lenses have well defined footwalls and hanging walls and their lateral margins appear to terminate abruptly rather than taper off over a considerable distance like many of the lenses of the West Limb, so that when viewed in cross-section, C and D Lenses appear well rounded at their ends. O'Connor's diagrams indicate that the overall bearings of the lenses are approximately 020-025 for C Lens, 010-020 for D Lens and 000 for F and G lenses.

In longitudinal section a steep northerly plunge to the lenses of the South East Mineralisation is apparent, like the Main Lode, but they are not as persistent down dip (Figure 25**)**. Surface and underground mapping by the author showed that C and D Lenses are discordant to bedding and they also appear to be slightly oblique to the schistosity. The associated lithologies and mineralisation are similar to the Main Lodes and, in particular, are of the East Limb type because of their association with GAB(3) schist. A difference however, is that many of the GAB(3) schists associated with the South East Mineralisation are muscovite bearing.

The O'Neil Lode differs from nearby deposits in that it is a single, tabular body of marked strike persistence. Information about it comes from diamond drilling and limited surface exposure. It has a minimum length of 440m, an average width of between one and two metres and is discordant to both bedding and schistosity. The sulphide mineralogy is similar to other local deposits although abnormally high in cubanite that was found to have a detrimental effect on metallurgical recovery (Trueman, 1974). O'Connor (1974) noted that, although the typical garnet and chlorite rich rocks are associated with the lode (Figure 3), they are seldom strongly developed. Instead, the lode material resembles altered andalusite schist. The lode contains abundant quartz and on the surface it can be followed, in part, as a ferruginous quartz vein. Its northern limit is at or near the contact between GAB schist and QMF schist, and its southern limit is unknown. The O'Neil Lode appears to have formed in a major fracture.

The group of lodes extending from the mine to south of the O'Neil Lode are similar in style. In particular, they have predominantly north-northeast trends and an association with GAB(3) schist. Their disposition is suggestive of a zone of en echelon veins. This idea is considered further in Section 5.5.

The Paringa Lode occurs southwest of the Kanmantoo deposit, near the contact between GAB schist and QMA schist/QMF schist. Little is known about it. Although it is a copper lode, Dickinson (1942) reported that a silver-lead lode was discovered in the Paringa Mine in 1847, with specimens assaying up to 24% lead and 760 ppm silver.



Figure 42. View to the WNW of the ruins of the Paringa Mine chimney and flue, built by Cornish miners around 1848. The chimney rests on GAB schist on the western edge of MacFarlane Hill. Immediately below (and to the left in the photograph) can be seen some of the Paringa Mine's surface workings. Behind that in the middle distance is the curved line of old pits following a relatively narrow GAB schist unit within QMF schist. Behind and to the right is the southern edge of the waste dump. In the distance are typical rounded hills of the Kanmantoo Group and on the horizon, Mount Barker.

The West Kanmantoo workings, which produced only 4,000 tonnes of ore (Dickinson, 1942), occur in a geologically complex area where several narrow bands of GAB schist occur in QMF schist (Figure 7). The copper mineralisation is confined to the GAB schist horizons and, like them persists over a minimum strike length of 280m, although only a metre or so wide. The lodes contain abundant quartz and are associated with intense local deformation of the adjacent GAB schist. In the field, they give the impression of having been concentrated in shears, which were confined to the GAB schist (or its precursor).

4.8 Other copper deposits of the Kanmantoo district.

Copper mineralistion within QMF schist is insignificant close to the Kanmantoo Mine, but in the surrounding district this group of lithologies hosts all of the numerous, small base metal occurrences. The biggest of these occurred at the old Bremer Mine, 3.8km southeast of the Kanmantoo Mine and adjacent to the small township of Callington (Figure 8). The mineralisation was described by Dickinson (1942), Duncan (1973), Spry (1976), Seccombe et al. (1985) and Both (1990). Copper is hosted by two tabular quartz lodes, the Bremer and Boundy Lodes, that have dimensions of 100m x 100m x 1.1m (average width) in the old workings and a northerly plunge of about 45º (Dickinson (1942). The lodes strike 140º and dip 70º-90º to the west (Duncan, 1973). They are discordant to both relict bedding and schistosity. Host rocks are biotite-rich schists (Spry, 1976).

A group of old copper workings located about 2km north of the Bremer Mine appears to have a similar style of mineralisation. This group of workings was described in brief by Schiller (1974c). All occur in well bedded, gently folded, QF schist in which bedding trends east-west in general and dips to the south at 40º-50º. At Wheal Friendship the old workings exploited a 0.5-1.0m wide zone of shattered, ferruginous vein quartz striking 160º and dipping 80º-85ºE. The Bremer No.4 workings trend 140 and expose copper mineralised quartz veins a few centimetres wide that dip 85ºE. The Wonga Wonga workings trend approximately 050º, are inclined moderately to steeply north-westerly and expose complex, thin stockwork style quartz veinlets. These deposits and the Bremer deposits have several features in common. Firstly, they occur as tabular bodies associated with vein quartz and are discordant to both bedding and schistosity. Secondly, all have amphibole rich gangue minerals that are inferred to represent metamorphosed silicate-carbonate alteration assemblages.

The Wheal Maria workings, east of Wheal Friendship, comprise a few low dumps in a ploughed field, so little can be deduced about lode geometry. The dumps contain malachite and azurite bearing reef quartz, hematite-quartz rock and massive, medium grained QF schist.

Several isolated occurrences of malachite stained quartz veins occur in the district around Wheal Friendship; the veins are usually 10-20cm wide, of limited strike extent, trend 110-140 and dip 70º-90ºN.

QMF schists to the southwest of Kanmantoo Mine host several small occurrences of lead-zinc mineralisation. Unlike the small copper deposits described above, these appear to be conformable with relict bedding. The largest lead-zinc deposit in this area occurs at the Aclare Mine and was described by Askins (1968), Spry (1976), Chilman (1982) and Both (1990). The deposit is tabular, parallel to the schistosity and is hosted by a 0.5m to 4.0m thick quartzite. The quartzite is inferred to be metamorphosed exhalite sediment, as discussed in the preceding chapter. Previous mining concentrated on an isoclinally folded and thickened pod plunging approximately 30 degrees to the south. Sphalerite, galena, pyrite and pyrrhotite occur in folded layers parallel to inferred relict bedding in the enclosing QMF schists.

5. MACRO-STRUCTURE AND MESO-STRUCTURE

5.1 Introduction

The metamorphic rocks of the Kanmantoo region display evidence of several phases of deformation associated with the Delamerian Orogeny. The phases of deformation have been described in numerous structural studies, of which the most significant are considered to be the field based, regional studies of Offler and Fleming (1968) and Mancktelow (1979, 1990). Other important work has been reported by Talbot (1962), Mills (1964), Lindqvist (1969), Fleming (1971), Daily and Milnes (1971, 1973), Marlow (1975), Spry (1976), Toteff (1977), Flint (1978), Fleming and White (1984), Jenkins (1990), Steinhardt (1991), Jenkins and Sandiford (1992), Flottmann et al. (1994, 1995), Oliver and Zakowski (1995) and Haines and Flottmann (1998). Recent reviews of the effects of the Delamerian Orogeny have been presented by Preiss (1995) and Belperio et al. (1998).

In the Kanmantoo region the major structure affecting the Kanmantoo Group is a complex syncline that occupies the eastern portion of the ranges. This structure was called the Kanmantoo Syncline by Mancktelow (1979), who ascribed it to his first deformation phase, D_1. Preiss (1995) however has assigned it to the second major fold phase, his ***D***D_2 (the ***D*** in Preiss' notation indicates the Delamerian Orogeny). The Kanmantoo Mine lies either on or near the axial trace of the Kanmantoo Syncline, but because of the complexity of the structural setting near Kanmantoo and the lack of critical exposures the exact relationship is unclear.

The first comprehensive regional structural and metamorphic synthesis of the Mount Lofty Ranges was that of Offler and Fleming (1968) who recognised at least three phases of folding. Their first phase involved the formation of inclined folds principally, with a well developed cleavage. Structures of the second and third phases are best developed on the eastern side of the ranges where they commonly overprint the first phase. Both phases produced folds and crenulation cleavage. Many subsequent authors supported these observations, for example Daily and Milnes (1973) and Flint (1978), although the former authors recognised only two deformations in the type section of the Kanmantoo Group.

Mancktelow (1979, 1990) recognised two major schistosity forming events (D_1, D_2), followed by minor deformations that produced crenulations and kinks. The effects of Mancktelow's first event occur throughout the ranges as a penetrative schistosity associated with folds of all scales, including the Kanmantoo Syncline. The effects of the second event were only developed in limited areas, generally in the medium to high metamorphic grade region where new foliations were produced by crenulation of S_1. Mancktelow correlated the peak of metamorphism with the onset of the D_2 event. A third deformation event (D_3) was recognised, but this produced only minor crenulations and kinks and was not of regional significance. The relationships between D_1, D_2 and D_3 in the schemes of Offler and Fleming and that of Mancktelow appear to have been largely reconciled as additional field work has modified previous interpretations. The structural history of the eastern Mount Lofty Ranges, including the Kanmantoo district, remains controversial. An interesting recent development is the proposal by Oliver and Zakowski (1995) of an early extensional phase of deformation prior to all compressional deformation that has been described so far.

5.2 Structural notation

Standard abbreviations are used in this study to denote planar and linear structural elements. Thus, planar elements are denoted S_1, S_2 etc, the fold axes F_1, F_2 etc, and other linear elements like mineral lineations or the intersection of planar elements, are denoted L_1, L_2 etc. In keeping with common practice, the subscripts correspond to the inferred chronological order of formation of the element, as indicated by overprinting relationships. However, in this study the overprinting relationships do not indicate necessarily formation during separate deformation episodes. Instead they may represent separately preserved stages of one continuous event, as will be discussed later. Further information on linear elements is included by the use of a subsequent number to indicate the phase of the structure that was deformed. This scheme is similar to that of Bell and Duncan (1978) but does not use superscripts or subscripts. For example, $F_{2/0}$denotes a second phase fold axis produced by folding bedding (S_0), and $F_{2/1}$ is a second phase fold axis produced by folding S_1 surfaces. Similarly, $L_{2/0}$ is a lineation produced by the intersection of S_0 and S_2, and L_2 is a lineation on S_2, usually a mineral lineation. Table 16 lists the structural notation used in this study.

Table 16. Structural elements and notation of the Kanmantoo Mine area

Planar Element	Description	Linear Element	Description
S_0	Bedding	-	
S_1	Inclusion trails in porphyroblasts	-	
S_2	External schistosity to porphyroblasts	$L_{2/2}$	Mineral lineations in S_2
		$L_{2/0}$	S_0-S_2 intersection
		$F_{2/0}$	Fold axes in bedding
S_3	Axial plane to crenulations *	$F_{3/2}$	Fold axes of crenulations
S_4	Axial plane to kinks	$F_{4/2}$	Fold axes to kinks

*Note: The products of more than one crenulation forming and kink forming event may be present.

Table 17 compares the various structural notations used in the Kanmantoo area. The notation used here follows that of Mancktelow (1979), and so differs from other relevant studies of Offler and Fleming (1968), Fleming (1971) and Lindqvist (1969), because each attributed certain structural effects to different structural events. For example, although both Fleming and Mancktelow agreed that the slaty cleavage on the western side of the Mt Lofty Ranges represented the first recognisable event (F_1 and D_1 respectively), they disagreed on the relative timing of the dominant schistosity in the Kanmantoo area. Mancktelow attributed this schistosity to D_1 whereas Fleming attributed it to F_1 (initially at least). Lindqvist (1969) recognised two foliations in the Kanmantoo Mine area but considered both to be separate stages of a continuous event. Lindqvist's conclusion differs from the general practice of assigning each recognised planar fabric, especially those within porphyroblasts, to separate deformation events. In the most recent publication on the Kanmantoo Mine, Oliver et al. attributed the major schistosity there to S_3 and the inclusion trails in andalusite porphyroblasts to S_2. These correlations have a strong impact on the interpretation of the timing of mineralisation and will be discussed more fully elsewhere.

Table 17. A correlation of S surfaces described in the Kanmantoo Mine area

This Study	Mancktelow (1979)	Lindqvist (1969)	Offler and Fleming (1968)	Oliver et al. (1998)
S_1	S_1	S_1a	-	$?S_2$
S_2	S_2	S_1b	S_1	S_3

Structural measurements are abbreviated here such that measurements of planes are written as strike/dip and dip direction (for example 005/73E) whereas lines are written as plunge-plunge direction (for example 73-005).

5.3 Regional structural setting of the Kanmantoo copper mineralisation

This section presents an interpretation of the structural setting of the Kanmantoo district based on the most detailed geological mapping available, principally that carried out by Mines Exploration Pty. Limited. The aim is to describe the broader setting of the Kanmantoo mineralisation and in particular to identify any structures, especially major structures like regional faults or fold hinges, that may have played a part in the origin of the mineralisation. The area considered in this section is shown in Figure 8. Different structural interpretations of all or part of this area were proposed by Dickinson (1942), Kleeman and Skinner (1959), Lindqvist (1969), Poole (1969), Fleming (1971), Mancktelow (1979), Gum (1998) and Toteff (1999).

One of the most prominent regional fold structures recognised on the eastern Mount Lofty Ranges is the Kanmantoo Syncline. This structure is well defined by many pyritic schist marker units, especially those of the Talisker Calc-siltstone that are exposed 15-30km north of Kanmantoo, between Harrogate and a few kilometres west of Tungkillo. In this area the apparent isoclinal hinge of the Kanmantoo Syncline occurs just west of, and parallel to, the trace of the Bremer Fault (for example, refer to the Adelaide 1:250,000 geological map). To the south of these exposures the Kanmantoo Syncline is difficult to define as an individual structure, but its axial trace would project just east of the Kanmantoo Mine. In the Kanmantoo district several authors have presented maps with a fold named as, or equivalent to, the Kanmantoo Syncline (Thomson and Horwitz, 1962; Kleeman and Skinner, 1959; Mancktelow, 1979; Preiss, 1995; Toteff, 1999) but they do not agree in position exactly. For example, Kleeman and Skinner's Figure 1 indicated that the axial trace of the Kanmantoo Syncline passes a few hundred metres to the east of the Kanmantoo Mine whereas Toteff placed it approximately 1.5km to the east. The reasons why the axial trace is difficult to define include insufficient outcrop in some key areas, a lack of marker horizons and complex structural geology including probable north-south faulting near the inferred axial trace.

In contrast to the region further north, the structure of the Kanmantoo district does not appear to be dominated by a simple syncline. Rather, the district has at least three north-south trending structural and lithological domains that are separated by known or inferred faults - the Kanmantoo Fault and the Bremer Fault, located 2.0km and 5.5km east of Kanmantoo Mine respectively (Figure 43). The sub-vertical Bremer Fault is one of the major faults within the eastern Mt Lofty Ranges (Preiss, 1987, figure 109). The domain in which the Kanmantoo Mine occurs is the most westerly domain and it is bounded to the east by a north to north-northwesterly trending linear feature called here the Kanmantoo Fault. This structure was first proposed by Schiller (1974b) on the basis of geological mapping, and was subsequently supported by an aeromagnetic survey that indicates that it extends over at least 17km southwards from its northernmost recognisable limit, located approximately 10km north of Kanmantoo township. From there it can be traced southwards close to Kanmantoo, through or close to the Bremer Mine and is lost 2-3km south of Callington where it runs parallel to a fold limb. The Kanmantoo Fault appears to converge with the Bremer Fault south of Callington. The magnetic data indicate another parallel linear feature located approximately 2.5km to the east of the Kanmantoo Fault, and the data also supports the inferred fault shown at the northern limit of Figure 8 (also proposed by Fleming, 1973). It is likely that the Kanmantoo region contains many unrecognised meridionally trending faults and they may be an important aspect of the structural and metallogenic history.

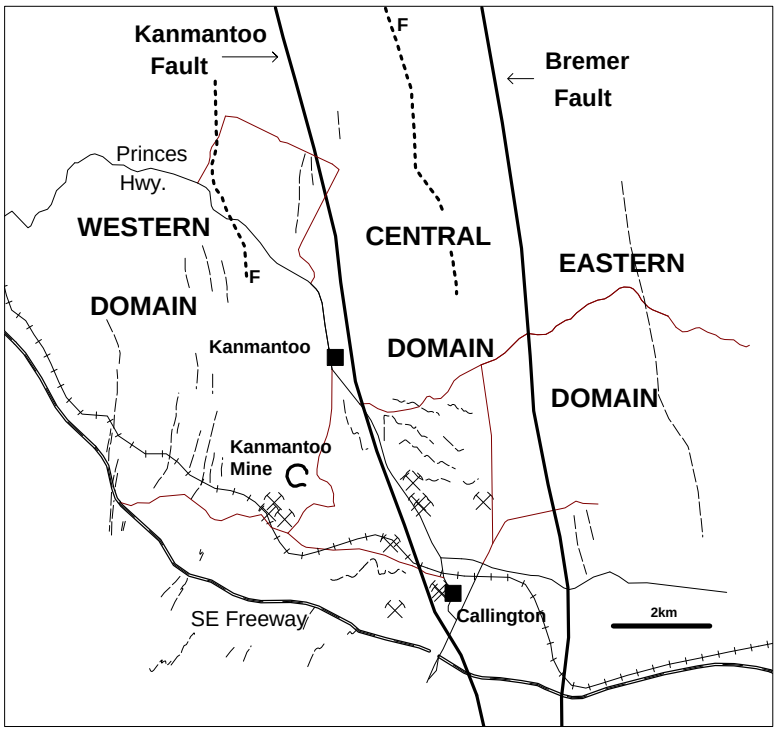


Figure 43. Structural domains in the Kanmantoo district. The three domains are separated by north-south trending faults. The main roads, the railway, principal mines and bedding trends (thin dashed lines) are shown.

Each of the three domains has distinguishing lithologies and bedding trends. West of the Kanmantoo Fault, that is in the domain containing the Kanmantoo Mine, bedding trends and geological contacts are predominantly north-south, although just to the west of Callington the dominant bedding trends are close to east-west. Another characteristic of the western domain is that it contains lithologies that tend to be rich in andalusite, staurolite and biotite. East of the Kanmantoo Fault, in the central domain, bedding trends are predominantly east-west and the lithologies comprise a monotonous sequence of QMF schist with abundant quartzofeldspathic beds. East of the Bremer Fault, in the eastern domain, lithologies also are dominated by QMF schist but there they have abundant interbeds of pyritic schist, north-west trending bedding and abundant isoclinal folds.

The Paringa Andalusite Member lies close to the eastern limit of the western domain described above. West of the Paringa Andalusite Member are two QMA schist units (the Dawesley Andalusite Member of Gum, 1999), both north-south trending. Of these two units, the most westerly is well exposed on the Princes Highway (the northwest corner of Figure 8) where it is thickest, contains coarse andalusite and resembles GAB schist. Nine kilometres south of the highway this unit thins and disappears, apparently by sedimentary facies changes. Immediately south of Princes Highway the unit appears to be bifurcated, suggesting further sedimentary facies lensing. There are few rock types present in this lens apart from QMA schist and QM schist. However, the other QMA schist unit to the east, between the unit just discussed and the Paringa Andalusite Member, contains minor lenses of GAB schist and GB schist. These latter rock types are typical of the Paringa Andalusite Member and so the trend in their regional abundance within QMA schist seems to be an increase from west to east towards the Kanmantoo Mine.

Because the rock units west of Kanmantoo have predominantly north-south trends for many kilometres this whole area was interpreted by many as a single limb of the Kanmantoo Syncline, without significant minor folds (for example Kleeman and Skinner, 1959; Mancktelow, 1979). However, in this study it is proposed that this area has large F2 folds, that are outlined by the andalusite bearing lithologies, as shown in Figure 8.

The hinge area of a proposed, large F_2 fold is shown in the topmost part of Figure 8. Just north of Princes Highway the two QMA schist units discussed above converge around what is suggested here to be a disrupted F_2 fold hinge. This key area containing the proposed F_2 (or perhaps even F_1) hinge is structurally complex and unfortunately the detail needed to fully resolve the structural setting cannot be obtained by mapping because of poor outcrop. The evidence for the F_2 hinge is largely the converging QMA schist units and is supported by magnetic patterns, but it is conceded that support for this interpretation is not compelling. This area is complicated by the occurrence of both F_2 and F_3 folds, and probable faulting (Fleming, 1971; Schiller, 1974a). In particular the structural setting is complicated by the existence of a F_3 syncline on the immediate western side of the proposed F_2 hinge. Parts of the F_3 fold are well exposed (for example in cuttings along the Princes Highway) where clearly the domainal S_2 crenulation cleavage is folded in a broad open structure with a NW-SE trending axial plane. This and similar structures were originally assigned as second generation (F_2) folds by Offler and Fleming (1968) and also by Mancktelow (1979), but have since been assigned as F_3 by Preiss (1995) and Fleming (as reported in Preiss, 1995).

F_2 folds are interpreted to occur immediately south of Princes Highway where an isoclinal fold pair has been inferred from mapping by Schiller (1974). The fold pair has the right asymmetry (dextral) to be a parasitic couple on the western limb of the larger F_2 fold proposed above. In this area F_2 folds are smaller and occur as many minor isoclinal folds with rarely exposed hinges that are best defined by some of the thin meta-sedimentary units within the QMF schist sequence, especially pyritic schist. Aeromagnetic patterns associated with this area are dominated by the responses of several very magnetic minor units (calc-silicate rocks and pyrrhotite bearing schists) but do not seem to provide much convincing information on structure.

Therefore, it is concluded that the two mapped QMA schist horizons represent the two limbs of a south plunging F_2 synform with the QMA schist lensing out to the south along the western limb. This interpretation is supported by Gum (1998, Plan III) whose mapping along the Adelaide-Melbourne railway indicates an anticlinal hinge in the expected position. Gum noted a reversal of his stratigraphic units Wistow Slate Member and Dawesley Andalusite Member. The southern extension of the eastern limb of the fold can be followed to another key area, again with poor outcrop, north of the Aclare Mine. A south closing, antiformal hinge is proposed in this area, as shown on Figure 8, for the following reasons.

(a) The QMA schist unit does not continue through the area of poor outcrop, according to the available information. The exposure south of the Aclare Mine is much better and no QMA schist has been recognised.

(b) QMA schist is sporadically exposed to the northeast of Aclare Mine in a belt trending towards the Kanmantoo Mine. This belt is very slightly divergent to the western belt and so is consistent with another limb.

(c) The rather broad area of poor outcrop at the inferred hinge position is itself unusual, especially as it is surrounded to the east, south and west by better outcropping QMF schist. This is consistent with a south closing hinge in a relatively soft rock (like QMA schist).

(d) Figure 8 shows that the QMF schist unit between the Paringa Andalusite Member and the QMA schist unit to the west has no pyritic schist, unlike the QMF schist unit to the west and this too is consistent with a closure. The unit with pyritic schist is folded around the hinge and occurs further to the northeast. However, if the closure were not present then the QMF schist unit without pyritic schist should continue through. The abundance of pyritic schist in the rocks south of the Aclare Mine indicate that this is not the case.

(e) The abundance of folded pyritic schists in the area south of the Aclare Mine is consistent with a hinge area.

(f) Key support has been provided recently by mapping by Toteff (1999). This mapping identified a calc-silicate marker unit that defines a complex synformal structure north of the Aclare Mine, disturbed by many north to north-northeasterly trending faults.

The interpretation shown in Figure 8 has the QMA schist belt continuing northwards from the Aclare Mine area to the Kanmantoo Mine area but lensing out in between. More detailed mapping may establish better continuity, but this stratigraphic position appears to be represented to the north by another aluminous horizon, the Paringa Andalusite Member.

East of the Kanmantoo Mine another north-south trending QMA schist unit has been mapped (Rose, 1973; Schiller, 1974a,b) which converges at a low angle with the Paringa Andalusite Member several kilometres north of the mine. In this case the abrupt change in lithologies and the low angle between the two units (only 5-10) suggest a faulted contact rather than a fold hinge. Immediately to the east of the mine this QMA schist unit swings around another antiformal hinge and passes east into a zone of predominantly east-west trending bedding where it appears to lens out about one kilometre east of the Wheal Friendship Mine. The unit narrows markedly across a zone of no outcrop where the Kanmantoo Fault is proposed to occur. The area of east-west bedding trends is where Mancktelow (1979) placed the axial trace of the Kanmantoo Syncline.

With an antiform inferred in the Aclare Mine region and another known to occur east of the Kanmantoo Mine, there should be a synform between, located close to the mine. Previous workers who have mapped the Kanmantoo Mine area in some detail have inferred a syncline to occur between the Paringa Andalusite Member and the narrow GAB schist unit east of the mine (Dickinson, 1942; Lindqvist, 1969). This position seems the most likely because the narrow tongue of QMF schist shown on Figure 8 can be interpreted as an isoclinal fold closure and the narrow GAB schist unit as a part of the Paringa Andalusite Member repeated on an eastern limb. However, such a synform was not revealed by the detailed mapping carried out in this study as discussed later in this chapter.

Wherever the axial plane of the Kanmantoo Syncline occurs in the Kanmantoo area, it is different in character to the major fold to the north near Tungkillo. There, the syncline is well defined by pyritic schist units as a tight to isoclinal fold truncated axially by the Bremer Fault. To the south the projection of its axial trace continues away from the Bremer Fault and towards the Kanmantoo Mine area, and aeromagnetic data suggests that it may intersect the Kanmantoo Fault north of Kanmantoo township. Any continuation south of the fault is unclear. Possible continuations include the Mine Synform and a major fold southwest of Callington (shown on the Barker 1:250 000 sheet). East of the Kanmantoo Fault a wide zone of east-west to southeast trending bedding (refer Figure 8) represents the largest hinge zone in the Kanmantoo district, but does not appear to correspond to the southern extension of the Kanmantoo Syncline. An en echelon relationship is possible whereby the Kanmantoo Syncline dies out southwards but the overall regional synclinal structure resumes to the east

via a sinistral en echelon pattern. Sinistral en echelon patterns were recognised by Mancktelow (1979) in the Kanmantoo Group rocks of the Palmer district. Also, dextral en echelon patterns have been recognised in the Adelaidean rocks of the Mt Lofty Ranges (Thomson, 1969a,b).

If the structural interpretation described above is correct the following conclusions can be made with respect to the regional setting of the Kanmantoo mineralisation.

(a) The regional fold pattern may be more complex than previously supposed. What was thought to be a multiple layer sequence of different units within the Tapanappa Formation in this region may be the same sequence repeated by folding and with facies changes revealed in repeated limbs.

(b) The Paringa Andalusite Member is inferred to be laterally equivalent to a much larger QMA schist lens (the Dawesley Andalusite Member proposed by Gum, 1998) which has been tightly folded and faulted. The QMF schists above this lens are quartzo-feldspathic and have many pyritic schist and minor calc-silicate interbeds. In contrast, the QMF schists immediately below it have few or none and are micaceous. However, there are other pyritic schists further below it including the extensive beds within the Talisker Calc-siltstone. The stratigraphic implications of this interpretation are shown diagramatically in Figure 44.

(c) The lead-zinc mineralisation of Aclare and Wheal Margaret deposits occurs in a similar but slightly higher stratigraphic position, to that of the Kanmantoo deposit. Together with other factors this is an important conclusion that allows a theory linking the genesis of lead-zinc and copper deposits, discussed in Chapter 9.

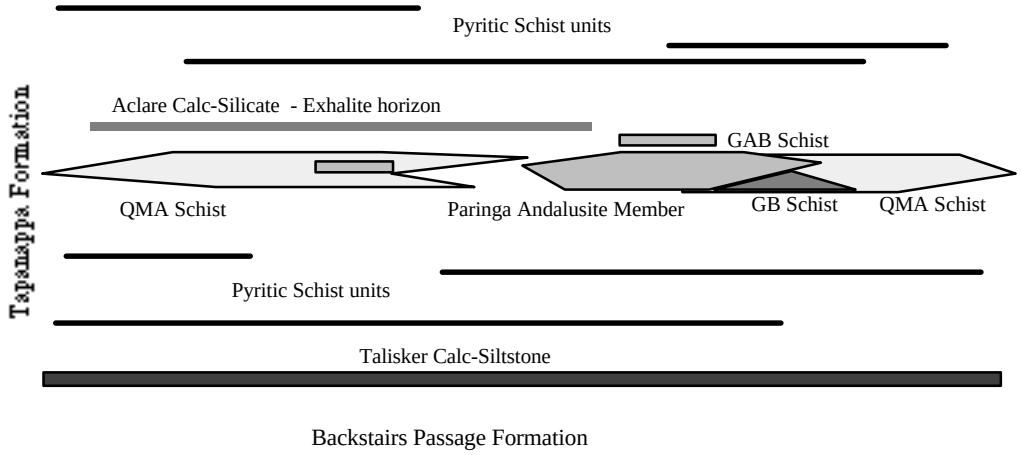


Figure 44. Diagram showing stratigraphic implications of the regional structural interpretation.

5.4 The Kanmantoo Mine Area

5.4.1 Introduction

This section deals with the area shown in Figure 7, comprising 230 ha surrounding the Kanmantoo deposit. Mapping and structural data collection were done in two stages: firstly, on a detailed scale (1:480) in the open cut mine and secondly on a larger scale (1:2,400) in the

surrounding area. Further details of the methods used were discussed in chapter 3.2. The data for these two scales are presented separately.

The detailed structural setting of the Kanmantoo deposit has not been established previously because of poor exposure prior to mining. The excellent exposure provided by the Kanmantoo open cut mine has made possible the detailed mapping described here. On a mesoscopic scale the structure of the Kanmantoo Mine area appears to be relatively straight forward, for only a single schistosity can be seen which is approximately constant in orientation over the whole mine area and is parallel to the axial planes of folds. No mesoscopic evidence of a foliation predating the schistosity was observed and the schistosity has not been extensively folded, although a small number of crenulations and kinks are present.

5.4.2 Bedding

Relict bedding in the Kanmantoo Mine area can be recognised in all rock types except some lode schists. In width, the beds range from fine laminations (in QM schist) to lithological layering a few centimetres thick (especially in GAB schist) up to massive beds a metre or so thick (in QF schist). More detailed descriptions of bedding can be found in Sections 3.2.1 and 3.2.4. Individual beds can rarely be followed along strike for more than a few metres due to outcrop limitations. Typically planar bedding is exposed and fold hinges are uncommon. Other sedimentary structures, like way up structures, are rare.

The few mesoscale folds that have been observed occur in the following limited areas: the open cut mine, especially the south-eastern portion; in QMF schist southeast of the mine; in GAB schist immediately northeast of the mine and in the QMA(G) schist exposed near the railway line south-southwest of the open cut mine. The areas between these are folded too, as indicated by changing vergences, but mesoscale folds are either not developed or are not exposed. Photographs of folded bedding for various rock types are shown in Figures 11 and 12.

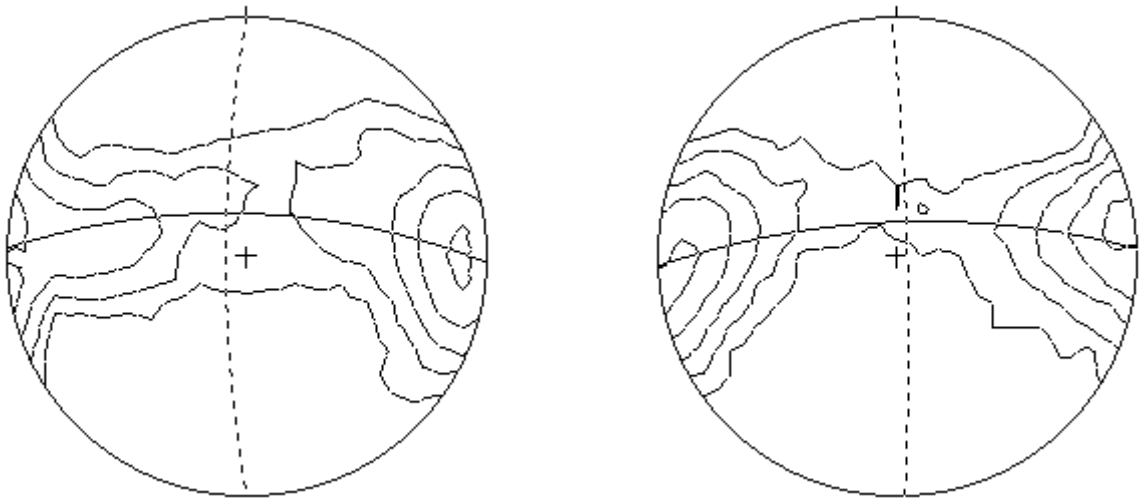
In tightness, folds in bedding vary from gentle to isoclinal (using the terminology of Fleuty, 1964), but most are midway between these two extremes. Fold styles and sizes are controlled by bedding thickness and competency as described throughout Fleurieu Peninsular by Mancktelow (1979). Generally, folds in GAB schist are more open than those in QMF schist or QMA schist. In sections of GAB schist with thicker bedding, open folds of concentric style are common. By contrast, laminated QM schists which are more homogeneous and have lesser competency contrasts on the scale of the folds, tend to develop similar styles. Most tight and isoclinal folds occur in the south-western part of Figure 7.

The Kanmantoo Mine

Many of the measurements of bedding taken in the Kanmantoo Mine are shown in Figure 45, which represents a mine plan approximately as it is at present but with some modifications added to maximise the display of data. Only layering in GAB schist is shown because this is most likely to be relict bedding, and although layering is present in some of the GBCl group lode schists it is not plotted on Figure 45 because its origin is uncertain. Some layering in GBCl group lode schists is regular and approximately continuous with bedding in adjacent GAB schist and appears to be altered bedding, but some of the layering is diffuse, irregular and parallel to the schistosity, perhaps suggesting tectonic or metasomatic origins.

The density of bedding measurements in Figure 45 reflects the relative degree of preservation of bedding in the different parts of the mine. Typically, bedding is common and well

preserved on the eastern side of the mine, even close to high grade mineralisation. In contrast, poorly preserved bedding occurs throughout the western half of the mine where scattered, vague layering is commonly parallel or slightly steeper than the schistosity, and in many cases one cannot be certain whether it is bedding or a metamorphic layering. Only discrete lithological layers which are of similar appearance to the bedding elsewhere were plotted, especially those oblique to the schistosity. Thus the data shown on Figure 45 are a little biased against examples of bedding subparallel to schistosity.



(a) The Kanmantoo Mine
Total S_o poles

(b) Area surrounding the Kanmantoo Mine
Total S_o poles

Figure 46. Stereographic projection (equal area) of poles to bedding. (a) The Kanmantoo Mine. N = 951, contours at 1%, 2%, 4%, 8% and 16% per 1% area. Preferred orientation (dashed line) is 000/83W, calculated girdle (solid line) is 092/76N, calculated beta axis is 14-182. (b) The area surrounding the Kanmantoo Mine. N = 502, contours at 1%, 2%, 4%, 8% and 16% per 1% area, maximum 22.3%. Preferred orientation (dashed line) is 177/88E, calculated girdle (solid line) is 088/78N, calculated beta axis is 12-178.

Most bedding measurements have strikes only slightly east or west of north and so they are subparallel to the gross trend of the Paringa Andalusite Member. Note that the area shown in Figure 45 represents about 70% of the total width of the Paringa Andalusite Member at the mine site. Bedding dips both to the east and west. A contoured stereographic plot of the bedding measurements, shown in Figure 46, contains a girdle indicating shallowly south plunging folds. The maximum of the plot, or the preferred orientation, represents bedding with north-south strikes and subvertical or steep westerly dips. The plot is influenced by the erratic preservation of bedding throughout the mine and so emphasises the eastern half of the mine.

The bedding distribution in the mine is dominated by a major synform, called the Mine Synform in this study, and the other folds in the mine appear to be minor folds on its limbs. The hinge of the Mine Synform is well exposed in the south of most benches and has an easting of approximately 4200’. In Figure 45 it can be traced northwards from the southern limit of the mine close to the GBCl group lode schists on the RL300' level. North of the GBCl group lode schists bedding is not so well preserved but the general position of the axial plane trace of the Mine Synform can be detected even though its exact position is not clear.
Bedding measurements in the hinge of the Mine Synform show that it has an average plunge of approximately 25 towards the south. The bedding trends (as viewed in plan) also suggest

that the fold is tight but because of the shallow fold axis a plan represents a section at a high angle to the fold profile and so in plan view the fold's tightness will be considerably exaggerated. Although the full extent of the limbs are not exposed in the mine, the Mine Synform appears to have an interlimb angle of approximately 40 in profile, and so would be classified as "close" according to Fleuty (1964).

In order to recognise fold limbs in the mine, relationships between bedding and the axial plane schistosity have been plotted in Figure 47. The axial plane traces of many folds are shown on this figure, of which most have been observed during mapping. Four relationships between bedding and schistosity are represented on Figure 47: the two opposing limbs (full and open circles), hinge areas (triangles) and sites where bedding and schistosity are parallel or close to parallel (squares). In addition, plunge directions are shown by the triangles and some of the circles and these are discussed later.

Several minor folds occur in the eastern domain. Immediately east of the GBCl group lode schists belonging to the East Limb is a wide zone of northwest trending bedding which passes eastwards into a series of minor folds, dominated by a large antiform. This antiform is part of a minor fold pair on the eastern limb of the Mine Synform and is typical of the minor folds exposed in the eastern side of the mine. The folds are particularly well exposed in the southeastern part of the mine, where they are clearly sinistral (as viewed in plan) fold pairs. A few dextral (as viewed in plan) fold pairs occur on the western limb of the Mine Synform, but because of the lack of preserved bedding they are seen only in the upper benches in the south of the mine and in the area to the west of the present limits of the RL350' and RL400' benches. In the extreme western portion of the mine where bedding is commonly subparallel to the schistosity, much tighter folding occurs.

The area surrounding the Kanmantoo Mine

Bedding measurements in the area surrounding the Kanmantoo Mine are shown on Figure 7 and the relationships between bedding and schistosity are shown on Figure 48. A stereographic plot of the bedding measurements for the whole area shown in Figure 7 is shown in Figure 46b. Note that the pattern is very similar to that shown by the mine measurements and the preferred orientations and girdles are within 5 of one another. Because the area surrounding the Kanmantoo Mine is not nearly as well exposed as the mine, the structure is more difficult to determine. In general, the vergence plots in the eastern half of the area shown in Figure 48 are closed circles and those in the western half are open circles, indicating again that two major limbs occur in this area. However, the exact position of the boundary between these two limbs is not revealed by available exposure.

The few measurements taken to the north of the mine are consistent with the axial trace of the Mine Synform continuing to the north and an area of probable parasitic folding occurs immediately northeast of the mine. Structural measurements south of the mine are not consistent with a through-going synform and, instead, all measurements indicate that only the east limb is present within the GAB schist as far west as a north-south line through the Paringa Shaft. Without knowing that the synform exists in the mine, the data would most simply be interpreted as a synformal axial plane passing just to the east of the Paringa Shaft. Unfortunately the critical area that may explain the measurements, immediately south of the mine, is covered by ferricrete.

South of the mine, the eastern contact between GAB schist and QMF schist presents an additional obstacle to interpreting a simple south plunging synform because it trends north-north-easterly rather than north-north-westerly. This can be explained by inferring either a faulted contact or a plunge change with its consequent change of bedding trend. The contact

between GAB schist and QM schist exposed at the Spitfire Adit has evidence of strong shearing, a good exposure the same contact near the O' Neil workings is sharp and appears to be unaffected by shearing.

The north-south trending boundary close to the Paringa Shaft, separating zones of different vergence and lithology, may represent a fault rather than an axial plane. It may be significant that some persistent shear zones are exposed in old copper workings in this area, located close to the boundary between both zones of differing vergence.

Three explanations of the structure of the area south of the mine are discussed below and are shown in Figure 49.

(a) The Mine Synform may simply continue southwards beyond the mine without deviation or plunge reversal, as shown in Figure 49a. The problem here is that to continue southwards, somewhere it must cross the contact between GAB schist and QMF schist and where it does a hinge should be evident. No convincing hinge has been recognised, but an apparent dextral offsetting of the contact ESE of the Paringa Shaft could represent a flexure. In addition, there is a photogeological feature within GAB schist resembling a north-closing fold in the correct position to represent the Mine Synform. The weakness of this explanation is that it does not explain the lack of vergence changes on the western side of the GAB schist without invoking an intermediate antiform for which there is no evidence, neither south of the mine nor to the north within the mine.

(b) The Mine Synform may continue southwards beyond the mine, but is offset to the west via a dextral en echelon fold pattern (Figure 49b). This implies that the Mine Synform dies out south of the mine and an intervening antiform is hidden beneath the laterite and soil. Although this theory is generally consistent with the available information, as in (a) there is no evidence of the proposed antiform in the mine as one would expect. Therefore, to fit the spatial constraints, such an en echelon pattern requires that the trend of the intervening antiform's axial plane is located beyond the southwest edge of the mine. Two possibilities are shown on Figure 49b, one a small antiform with an axial plane more oblique than any observed in this area. The second possibility involves a larger antiform, extending beyond the GAB schist and QMF schist contact to explain the irregularity mentioned in (a). Again, there is no evidence of an antiform in this area, or of the required plunge reversal along the inferred synformal axial plane.

(c) A third possibility is that the Mine Synform is dextrally faulted. As no fault has been observed in the exposed rocks, if present, its most likely position is considered to be the north-northwest trending structure shown in Figure 49c, concealed beneath soil and laterite. Apart from explaining the apparent displacement of the Mine Synform, such a fault also explains several other features. Firstly, it would account for the termination of the GAB(3) schist unit south of the O'Neil Lode and possibly the O'Neil Lode too. Secondly, it could explain the apparent irregularity in the GAB schist/QMF schist contact mentioned previously. Furthermore, this fault is approximately parallel to other interpreted faults north of the mine that also dextrally displace the contact. A third point in favour of this fault is that it would tend to align zones of $S_0//S_2$ observed in the mine and in outcrops southwest of the mine. The fault could also account for the widening of the Paringa Andalusite Member immediately to the north. Therefore, circumstantial evidence exists to support a fault here and of the three explanations discussed, this seems the most plausible, although none are satisfactory and more data is required to resolve the structural setting of this area.

Another area of geological complexity is shown in the south-western corner of Figure 7. It is difficult to interpret this area as a continuous structure because it contains blocks with apparently straightforward geology internally, but which have obscure relationships to adjacent blocks. For this reason several faults have been interpreted to separate the blocks although, again, there is little direct evidence of them except near the Otto Shaft where a fault is exposed that is associated with copper mineralisation. The inferred faults are shown on Figure 50.

A relatively large body of GAB schist to the west of the Paringa Shaft appears to be linked to the main GAB schist body hosting the Kanmantoo deposit by a series of narrow GAB schist bands separated by QMF schist. If all the GAB schist bodies are continuous, the intervening narrow bands suggest an unusual zone of sedimentary inter-fingering as shown in the geological interpretation in Figure 50. The narrow GAB schist units contain evidence of shearing, malachite stained quartz veins and small mine workings. Bedding measurements are continuous at the northern end of the narrow bands, but at the southern end, there is a slight angular discordance. This can be explained by a fault that, in addition, would explain the problematical relationship between the hinge zone in the QMF schist further north and the through-going, northerly trending GAB schist body west of it.

A feature of the area west of the Paringa Shaft is the relative abundance of mesoscale folds in bedding exposed in the GAB schist north of the railway line. Also, several tight to isoclinal folds are exposed in the railway cutting and to a lesser extent in the outcrops to the north. Commonly changing vergences indicate the presence of many other folds, but their hinges are not exposed. These vergence changes extend northwards to some small workings, but do not appear to persist further north than this, nor does the occurrence of QMA(G) schist which is abundant near the Paringa Shaft Hence a fault has been interpreted near the small workings. Despite the complex geology, this area is dominated by one vergence type (the open circles on Figure 48), the same as that dominating the rest of the schists to the west of McFarlane Hill.

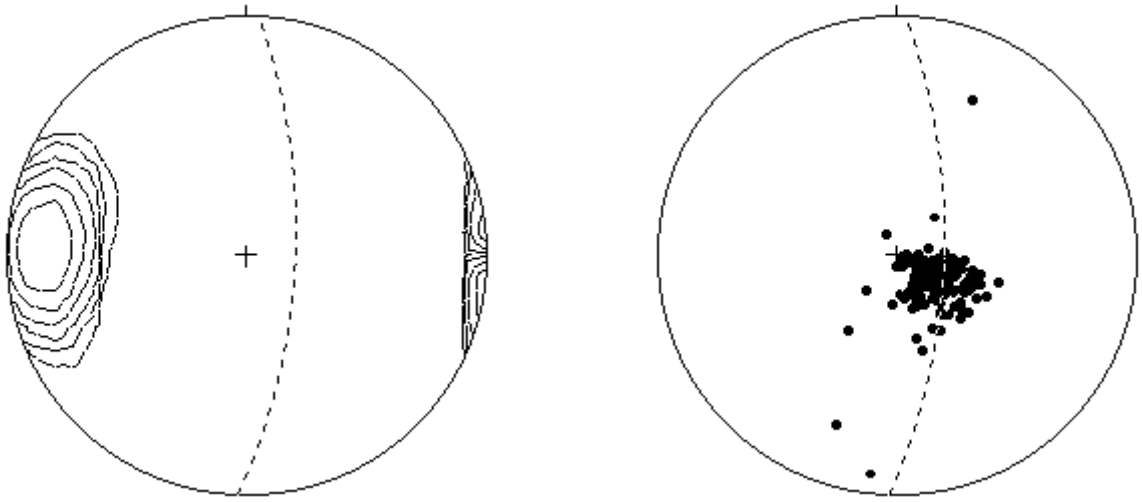
In section 5.3.2 it was noted that the southern extension of the axial plane trace of the Kanmantoo Syncline may lie close to the Kanmantoo Mine. The possibility of a major synform occurring between the Kanmantoo Mine and the south closing anticline east of it (shown on Figure 8) will now be considered. In this area the orientation of bedding (Figure 7) and its relationship to the schistosity (Figure 48) are not consistent with a hinge because there is no change in vergence. Instead, this area appears to be part of a single limb and is consistent with the eastern limb of the Mine Synform continuing right across to the anticlinal hinge 2km to the east. The only area where easterly dips are common is immediately east of the mine, but only in a narrow zone, with westerly dips resuming further east. In addition, further south near the oxidised ore stockpile, bedding dips to the west. Hence, the data indicates that this zone has limited width and limited extent parallel to its axial plane, and therefore it seems most likely to be a local zone of minor folding.

It is concluded that no major synform occurs immediately east of the Kanmantoo Mine and that the Mine Synform is the largest fold in the immediate mine area. Whether it is equivalent to the Kanmantoo Syncline is unclear.

5.4.3 Schistosity and mineral lineation

Throughout the Kanmantoo Mine area, a well developed schistosity (S_2) is present. It occurs in all major rock types and typically has a steeply plunging mineral lineation ($L_{2/2}$), usually defined by mica. Therefore, the schists have an LS fabric (Flinn, 1965) which, in the terminology of Schwertner (1970), would more specifically be termed an L<S fabric because the schistosity is more pronounced than the lineation.

Both the schistosity and the lineation are characterised by relatively constant orientation over the whole mine area, and beyond for many kilometres. Mesoscale irregularities of orientation are caused by cleavage refraction and rare post-schistosity folds, crenulations, kinks or warps. Figure 51a shows a contoured stereographic projection of 997 measurements of poles to schistosity from the mine. The data define a strong point maximum with minor dispersion representing strikes wavering about a north-south trend. The preferred orientation of the schistosity is 002/74E. Also plotting as a point maximum, $L_{2/2}$ has an average pitch on S_2 of 81ºS and has an preferred orientation of 74-123 (Figure 51b).

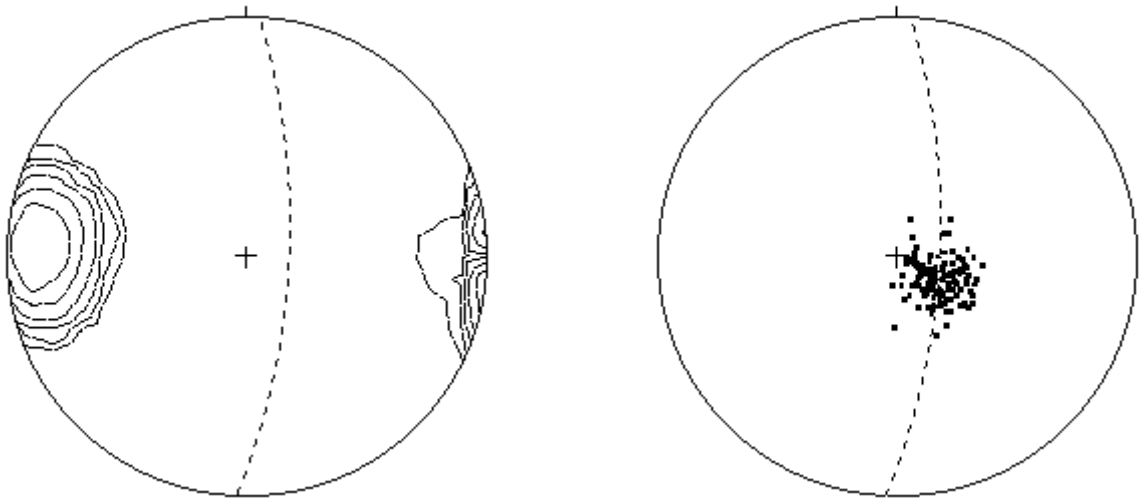


(a) Kanmantoo Mine - S_2 (b) Kanmantoo Mine - $L_{2/2}$

Figure 51. Stereographic projections (equal area) of measurements from the Kanmantoo Mine. (a) Poles to schistosity. N = 997, contours at 1%, 2%, 4%, 8%, 16% and 32% per 1% area. Preferred orientation (dashed line) is 002/74E. (b) Mineral lineations $L_{2/2}$. N = 149, preferred orientation is 74-123. Dashed line is same as in (a).

The schistosity is parallel to the axial plane of mesoscale folds and also macroscale folds where it can be established. For example, this can be demonstrated for the Mine Synform, by referring to Figure 47. Like the schistosity the strike of the axial plane is close to north-south. From the RL680' level to the RL350' level (that is 100.6m vertically) the axial plane is displaced horizontally by 30m approximately due to its easterly dip. Therefore, its estimated average dip over this distance is 73º, close to the average of 71º determined from the contoured stereographic plot.

Data for the area surrounding the mine are shown in Figure 52 and are almost identical to the data obtained from the mine.



(a) S_2 Area surrounding the mine (b) $L_{2/2}$ Area surrounding the mine

Figure 52. Stereographic projections (equal area) of S_2 and $L_{2/2}$ from the area surrounding the Kanmantoo Mine. (a) Poles to schistosity S_2. N = 428, contours at 1%, 2%, 4%, 8%, 16% and 32% per 1% area. Preferred orientation (dashed line) is 003/76E. (b) Mineral lineation $L_{2/2}$. N = 133, preferred orientation is 74-119. Dashed line is same as in (a).

Two lines of evidence indicate that the mineral lineation is probably parallel to the direction of maximum extension during D_2. Firstly, the lineation is parallel to the longest axes of stretched inclusions in QMF schist occurring near the railway, south of the mine (Lindqvist, 1969). Secondly, the lineation is consistently perpendicular, or nearly so, to the long axes of boudinaged quartz veins in the mine. The schistosity wraps around the boudins and the lineation tends to be abnormally prominent immediately adjacent to many of the boudins. It is deflected with the schistosity around the boudins.

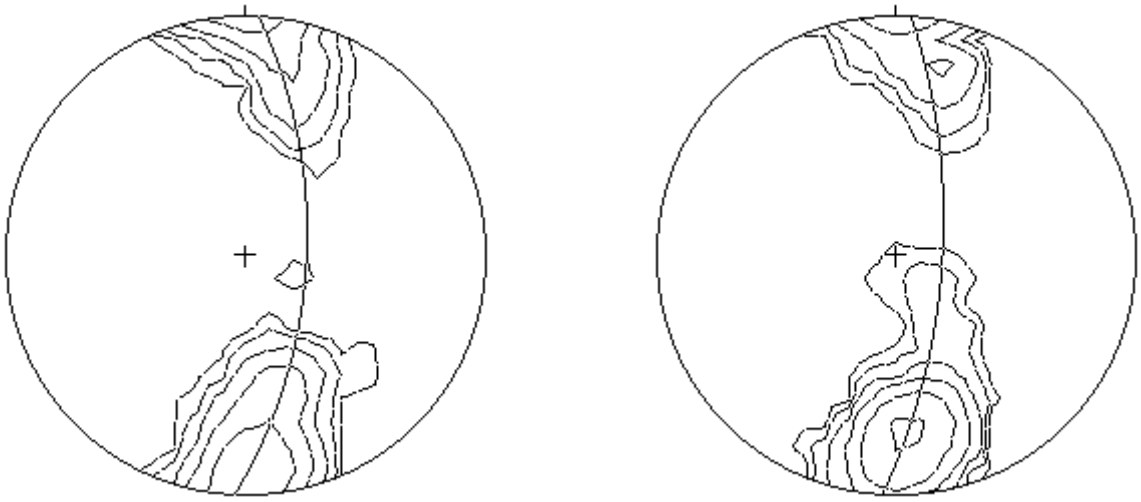
5.4.4 Fold axes and bedding-schistosity intersections

In the Kanmantoo Mine area, mesoscopic folds in bedding are not common and so fold axes ($F_{2/0}$) can rarely be measured directly. Instead, information about the orientation of fold axes must be obtained from the geometrically equivalent layering-schistosity intersections ($L_{2/0}$). Together with bedding, $L_{2/0}$ and $F_{2/0}$ are the most variably orientated structural elements in the mine area.

In general $L_{2/0}$ plunges shallowly south, but some plunge shallowly north. Measurements of $L_{2/0}$ in the Kanmantoo Mine are shown in plan form in Figure 53, and as a stereographic projection in Figure 54a. The few $F_{2/0}$ measurements made were found to be parallel to $L_{2/0}$ and so they are not plotted separately. Note that three types of measurements are plotted: firstly measured $L_{2/0}$, that is measured directly as a pitch on the schistosity or bedding plane; secondly $L_{2/0}$ calculated from measurements of S_0 and S_2 ; and finally observed $L_{2/0}$ where the plunge direction of $L_{2/0}$ could be seen but not accurately measured.

The predominance of shallow southerly plunges is shown clearly in Figure 54a. An examination of Figure 53 shows that southerly plunges predominate in the southern half of the mine, whereas the northern part of the mine contains mainly northerly plunges but with a significant number of southerly plunges as well. The data indicate that for most of the mine the boundary between the northerly and southerly plunging zones is regular in shape and

clearly defined; it is shown on Figure 53 as a dashed line. This boundary has an east-north-easterly strike and its position on successive benches indicates that generally it dips towards the south. However, in the upper levels of the mine (particularly the eastern part of the RL520' and RL560' levels) the bounding surface appears to have a sub-vertical or steep northerly dip, suggesting that it may be a curved surface, concave towards the south.



(a) $L_{2/0}$ The Kanmantoo Mine (b) $L_{2/0}$ Area surrounding the mine

Figure 54. Stereographic projections (equal area) of fold axes and bedding-schistosity lineations ($L_{2/0}$). Contours at 1%, 2%, 4%, 8%, 16% and 32% per 1% area. (a) The Kanmantoo Mine. N = 219, maximum 33.8%. Preferred orientation is 12-178, calculated girdle (solid line) is 003/69E. (b) Area surrounding the Kanmantoo Mine. N = 144, maximum 34.7%. Preferred orientation is 19-178, calculated girdle (solid line) is 003/74E.

The dips of the boundary between the north and south plunging zones can be estimated using the horizontal displacements between benches. For example, between the RL300' bench and the RL480' bench (54.9m vertically) the boundary is displaced approximately 104m horizontally, giving an average dip of approximately 30º south-southeast. A similar calculation for the interval between the RL480' and RL560' benches gives an average of approximately 70º north-north-west. Within the northern zone several bands of alternating north and south plunges can be recognised and in some cases followed from one bench to another. By contrast, most of the few northerly plunges in the southern zone seem to occur in a northerly trending band located a few metres to the east of the axial plane trace of the Mine Synform.

Although there is quite a range of plunge angles, they do not seem to vary regularly, neither across the schistosity nor parallel to it. Even in areas where many measurements could be obtained, sudden changes in plunge angle are common. This has been observed even on the scale of a metre or so, mainly in the western part of the RL400' and RL350' benches. In one case the pitch of the layering intersection on a schistosity plane varied from 2ºN to 53ºS over only one metre. However, in most areas where $L_{2/0}$ can be observed for more than a few metres, the variations were much more gradual. For example the southeastern corner of the RL440' bench has a gradual change from 16ºS to 29ºS over a distance of 50m parallel to the schistosity. Possible reasons for the changes in $L_{2/0}$ attitude will be considered later.

The measurements of $L_{2/0}$ and $F_{2/0}$ for the area surrounding the Kanmantoo Mine are shown in Figures 54b and 55. The data represented on the stereographic projection (Figure 57b) are similar to the measurements from the mine, but the preferred orientation is 5 steeper. Both figures show that shallow southerly plunges predominate, but there are also many shallow

northerly plunges. The boundary that was recognised in the mine, between the zones of south plunges and both south and north plunges is also evident in the rocks immediately to the east of the mine and corresponds closely in position. This suggests, that if a fault occurs in this area, as shown on Figure 50, then it must have only a minor displacement here, or alternatively the boundary was imposed after faulting. It is interesting that there is a small lode (Boundary Lode) in this area that also has an east-northeast trend; this is an unusual trend for lodes in the Kanmantoo Mine area and so both may be related. The boundary does not seem to continue further eastwards, however, for it cannot be recognised in the well exposed and well bedded rocks in the ridge east of the mine. There, all L_2 plunges are southerly, as they are further south along the ridge and in the rocks on the eastern side of McFarlane Hill.

On the western side of the McFarlane Hill and west of the Paringa Shaft, $L_{2/0}$ has a large range of orientations further testifying to this area being more structurally complex than many surrounding areas. Some of the northerly plunges are very steep, for example 78º was measured directly west of the Paringa Shaft. Another area of steep dips, but in this case towards the south, occurs further north in a hinge area exposed in feldspathic QMF schist. Here $L_{2/0}$, and in many cases S_0, dip from 40ºS to 79ºS and they are considerably steeper than in most of the surrounding rocks. It was mainly for this reason, and the occurrence of the feldspathic rock type, that the block was interpreted to be separated from adjacent areas by faults, as shown on Figure 50.

Possible causes of the variation in the orientation of $L_{2/0}$ will now be considered. There are three general possibilities - the causes could have been pre-S_2, syn-S_2, or post-S_2 or perhaps a combination of these. Pre-S_2 causes would be due to the bedding being non-planar prior to F_2 folding as a result of either soft sediment or tectonic deformation. Clearly, the D_1 deformation could have caused the non-planarity of bedding but no direct mesoscopic evidence of earlier folds has been observed in this study. Another problem is that regional studies (Mancktelow, 1979) showed that the orientation of S_1 is typically similar to S_2, that is it strikes north-south and dips steeply east, and so F_1 folds would have north-south trends rather than the observed trend in the mine which is east-northeast. A third problem is that F_1 folds presumably would have regular axial planes and one would expect superimposed effects to reflect this regularity. However, the boundary surface recognised in the mine appears to be curved. With the exception of possible slump folds on the northern limit of the mine, no evidence for soft sediment deformation is known. Nevertheless, it cannot be discounted and would explain the apparently irregular nature of the plunge over short distances.

The second possibility explaining the observed $F_{2/0}$ plunge changes is that they were produced when S_2 was formed (syn-S_2). Curved fold axes may develop during inhomogeneous strain as a result of differential flattening perpendicular to the axial plane of folds (Ramsay, 1962). Many folds are thought to begin with their fold axes perpendicular to the long axis of the finite strain ellipsoid and, as the folds are subsequently flattened, they become progressively tighter and the fold axes rotate towards the long axis of the ellipsoid (Bryant and Reed, 1969; Sanderson, 1972, 1973). If the long axis of the strain ellipsoid is parallel to a mineral lineation, then the fold axes will rotate towards the mineral lineation. This has been demonstrated by many people (for example, Roberts and Sanderson, 1973; Mancktelow, 1979). However, the final attitude of the hinge depends not only on the magnitude and nature of the strain, but also on the initial orientation of the folded surface relative to the axes of the strain ellipsoid. Hence, a problem in studying fold rotations is that assumptions must be made regarding the initial variability of bedding. A figure of 15º to 25º is commonly used (Sanderson, 1973).

Because $L_{2/0}$ has a relatively constant orientation in the Kanmantoo Mine area an impression of the angle between $L_{2/0}$ and $L_{2/2}$ can be obtained directly from the plots of $L_{2/0}$. In order to

remove the small errors produced by variations in $L_{2/0}$ the angles have been calculated only for sites where both $L_{2/0}$ and $L_{2/2}$ were measured. They are plotted on Figure 56 (the mine) and Figure 57 (the surrounding area). These figures show that high angles, between 50º and 70º, are most common, as one would expect from shallow $L_{2/0}$ and steep $L_{2/2}$ but, like $L_{2/0}$ orientations, rather abrupt changes are common which do not seem to define any obvious pattern.

The third possibility that could account for the variations observed in $L_{2/0}$ is post-S_2 folding or faulting. Faulting can be eliminated because suitable faults have not been observed in the well-exposed rocks in the mine. Folding also is considered unlikely because the boundary surface described previously is irregular and also because the associated folds should be evident in areas where extreme changes in $L_{2/2}$ occur. Such folds have not been observed and therefore post-S_2 effects are considered unlikely to account for the $L_{2/0}$ variability.

Summarising, it is considered equally likely that the observed irregularities in $L_{2/0}$ are due to either soft sediment deformation or to subsequent passive rotation of fold hinges during inhomogeneous strain. Both may have occurred, but the relative importance of either effect is unknown. If both occurred the initial deviations produced by soft sediment deformation would be exaggerated by flattening.

5.4.5 Veins

Many veins occur within the mine and the surrounding area, in all rock types. In the mine most veins consist of quartz, quartz-sulphide or sulphide, and some aspects of the sulphide rich varieties were described in Chapter 4. Mineralogically, the veins can be considered to be combinations of three mineral groups – quartz, other silicate minerals and sulphide minerals. The relative abundance of veins with different broad mineral assemblages is shown in Table 18. The data for the table represent 321 veins in the pit that were measured and described briefly. They are divided into the five broad mineralogical groups shown in the table, though considerable variation occurs within most groups. The vein mineralogies used in this table are as noted during mapping, and do not represent detailed mineralogical work, for example by thin section study. It is considered likely that in many of the veins in the two most common groups, pure quartz veins and pure sulphide veins, small quantities of other minerals would be detected by more detailed observation.

Table 18. Proportions of the main mineral groups for 327 veins from the Kanmantoo Mine.

Minerals in veins	Proportion
Sulphide only	29%
Sulphide-quartz / quartz-sulphide	21%
Quartz only	39%
Quartz-silicate	7%
Quartz-silicate-sulphide	4%

Quartz rich veins typically consist of only quartz, but many also contain minor quantities of other silicates, especially biotite, chlorite, staurolite, muscovite, garnet, cummingtonite and andalusite. Although most of these accessory minerals occur in quartz veins hosted by all local rock types, there is a strong tendency for the accessory mineral assemblage to reflect the host rock. Thus, in Fe-Mg rich host rocks like GAB schist and the lode schists the most common accessory minerals in quartz veins are similarly rich in Fe and Mg, like biotite, garnet, staurolite, grunerite and chlorite. Conversely, within Fe-Mg poor host rocks like QMF

Schist the most common accessory minerals in quartz veins are muscovite and biotite. Biotite is a common accessory in quartz veins of all host rock types. Andalusite is very uncommon as a vein mineral – it was noted in quartz veins as the only accessory mineral, and also with muscovite and chalcopyrite.

Within the mine, quartz veins occur throughout the whole extent of the mine and in all lithologies. Internally, most veins are unzoned and show no obvious sign of deformation. However, many do show signs of deformation in the form of cleavage, boudinage (Figure 58), folding and recrystallisation. The recrystallisation shows as a granular texture of the quartz in many veins. This texture can be subtle and seems to be harder to recognise in fresh rocks compared to weathered, surface equivalents. Therefore, recrystallised veins may be common in the pit.

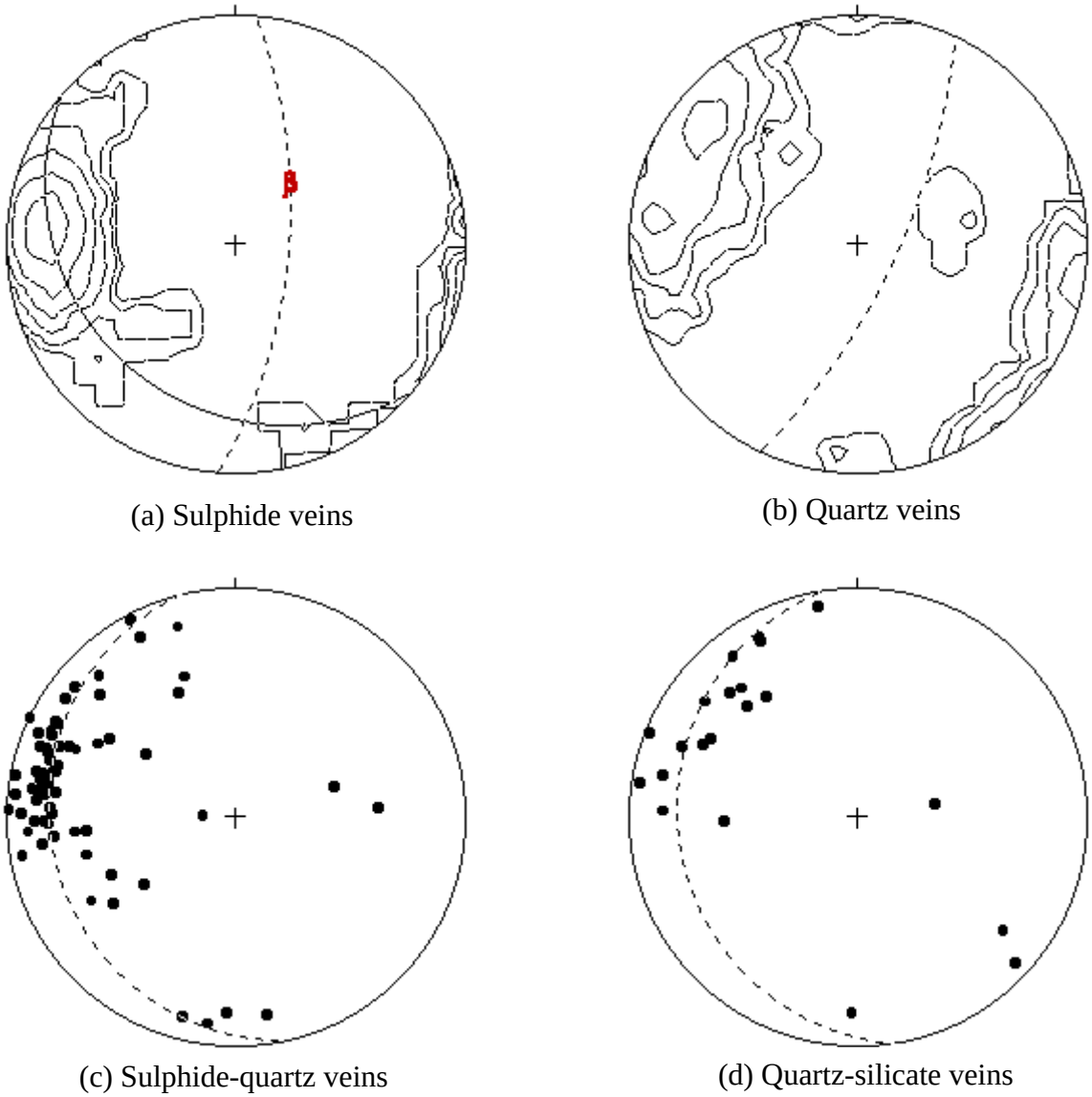
The external appearance of quartz veins differs throughout the mine. On the eastern limb of the Mine Synform most veins are regular and planar, and some have been observed to extend for in excess of 10m. On the western limb, planar veins occur also but there is much more evidence of deformed veins, in particular ductilely boudinaged quartz veins are common.



Figure 58. Relatively well preserved bedding in GAB(2) schist in the western part of the pit. The sub-vertical bedding is slightly oblique to the schistosity indicating that the site represents a limb of a subsidiary fold on the western limb of the Mine Synform. Note the boudinaged quartz vein with detached boudins on the right hand side. Looking south.

Many quartz veins have selvages consisting of Fe-Mg rich minerals and with little or no interstitial quartz. The most common selvage minerals are coarse grained biotite and staurolite, with or without garnet. Selvages seem to occur most commonly beside quartz veins that contain the less common accessory minerals like muscovite and andalusite. The central vein may also contain some sulphide minerals, mainly chalcopyrite and pyrite. Nero (1993) described the petrology of some selvages from veins in the Kanmantoo Mine.

Vein orientations within the mine are plotted as stereographic projections in Figure 59 for the first four vein types shown in Table 18.



(a) Sulphide veins

(b) Quartz veins

(c) Sulphide-quartz veins

(d) Quartz-silicate veins

Figure 59. Stereographic projections (equal area) of poles to veins of various compositions from the Kanmantoo Mine. (a) Sulphide veins. N = 93, contours at 1%, 2%, 4%, 8%, 16% and 32% per 1% area, maximum 47.3%. Preferred orientation (dashed line) is 005/71E. Calculated girdle is 131/30SW and beta axis (â) is 60-041. (b) Quartz veins. N = 125, contours at 1%, 2%, 4%, 8%, and 16% per 1% area, maximum 21.6%. Preferred orientation (dashed line) is 025/76E. (c) Sulphide-quartz and quartz-sulphide veins. N = 68, preferred orientation is 014/72E. Calculated girdle (dashed line) is 167/21W and beta axis (â) is 69-077. (d) Quartz-silicate veins. N = 22, preferred orientation is 037/74E. Calculated girdle (dashed line) is 190/23W and beta axis (â) is 67-080.

These plots show that all vein types have a spread of orientations. The sulphide veins define a strong peak and a girdle with that has a â axis of 60-041, close to the overall plunge of the main lode. In comparison, the quartz veins exhibit more variation in their orientation, no convincing girdle and a weaker, bipolar peak. One of the two maxima in the peak corresponds to the peak defined by sulphide veins and is within a few degrees only of the preferred orientation of the schistosity. The second maximum is centred at 037/74SE and is

similar to the general orientation of the East Limb of the Main Lode, and to many recrystallised and folded quartz veins in the surrounding area.

In the area surrounding the mine most outcropping veins consist of quartz with some biotite, muscovite and iron oxide/hydroxide. Many veins have a granular appearance indicating probable recrystallisation. This feature may be visible in natural outcrop only because weathering has enhanced the appearance of grain boundaries. Many veins are either folded symmetrically about S_2 or are boudinaged. Folded veins commonly have a fanning cleavage and in samples where both folded and boudinaged veins occur, the former have a greater degree of discordance to S_2. The degree of boudinage varies from weak necking to pronounced detachment forming isolated quartz lenses. The long axes of the boudins are consistently sub-perpendicular to the mineral lineation. Many of the small copper workings expose boudinaged quartz-azurite veins, for example the West Kanmantoo workings.

A stereographic plot of the orientations of the quartz veins in the area surrounding the mine is shown in Figure 60. The data includes measurements of the common folded and recrystallised veins (Figure 61). The range in orientation is similar to that shown by quartz veins within the mine. Figure 60 shows that folded and boudinaged veins have a variety of similar orientations. Also shown are a few measurements of the plunges of boudin long axes, which are typically shallow. Axes of folds in quartz veins plunge steeply towards the north-east and south-east. They lie on the schistosity plane and vary in orientation according to the gross orientation of the vein. The steeply north-east plunging axes are the only feature observed that corresponds to the overall plunge of the Main Lode.



Figure 61. QMA schist with low andalusite content. Looking east. Note the well preserved bedding and the dextrally folded quartz vein with steep northerly plunge (visible on the right hand side). The strike of S_2 is not visible but it lies between the vein and bedding.

common accessory minerals in quartz veins are similarly rich in Fe and Mg, like biotite, garnet, staurolite, grunerite and chlorite. Conversely, within Fe-Mg poor host rocks like QMF Schist the most common accessory minerals in quartz veins are muscovite and biotite. Biotite is a common accessory in quartz veins of all host rock types. Andalusite is very uncommon as a vein mineral – it was noted in quartz veins as the only accessory mineral, and also with muscovite and chalcopyrite.

Within the mine, quartz veins occur throughout the whole extent of the mine and in all lithologies. Internally, most veins are unzoned and show no obvious sign of deformation. However, many do show signs of deformation in the form of cleavage, boudinage (Figure 58), folding and recrystallisation. The recrystallisation shows as a granular texture of the quartz in many veins. This texture can be subtle and seems to be harder to recognise in fresh rocks compared to weathered, surface equivalents. Therefore, recrystallised veins may be common in the pit.

The external appearance of quartz veins differs throughout the mine. On the eastern limb of the Mine Synform most veins are regular and planar, and some have been observed to extend in excess of 10m. On the western limb, planar veins occur also but there is much more evidence of deformed veins, in particular ductilely boudinaged quartz veins are common.

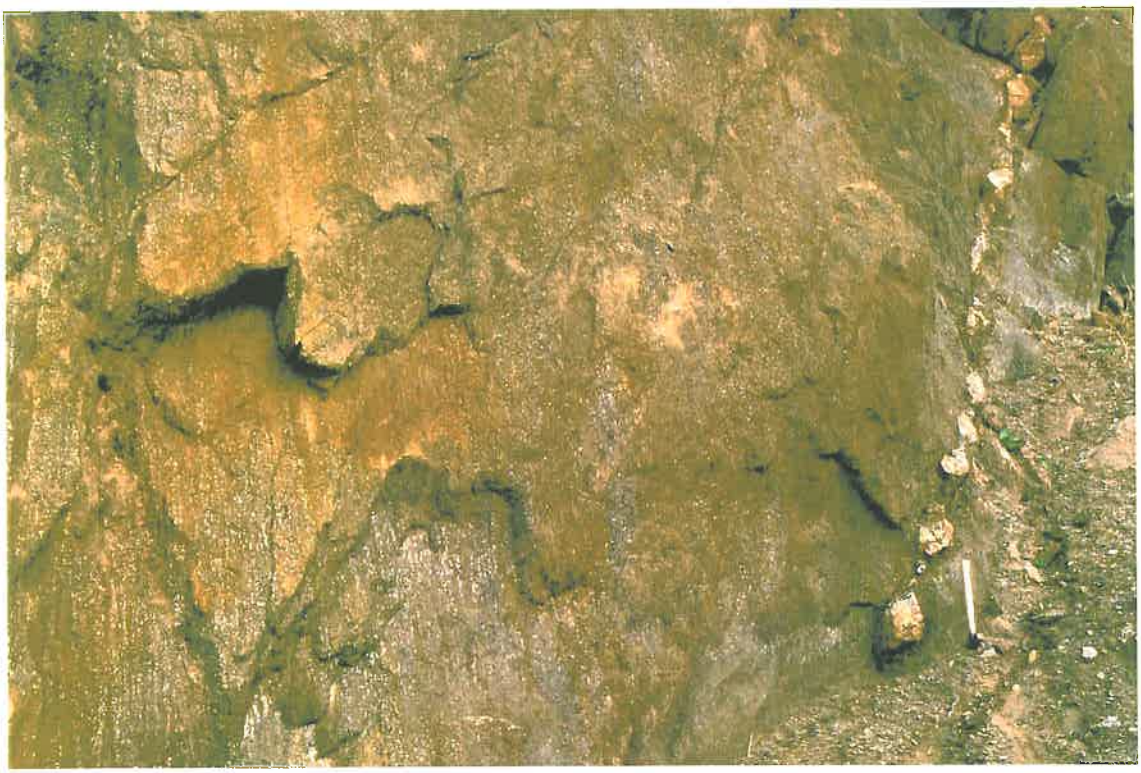


Figure 58. Relatively well preserved bedding in GAB(2) schist in the western part of the pit. The sub-vertical bedding is slightly oblique to the schistosity indicating that the site represents a limb of a subsidiary fold on the western limb of the Mine Synform. Note the boudinaged quartz vein with detached boudins on the right hand side. Looking south.

Many quartz veins have selvages consisting of Fe-Mg rich minerals and with little or no interstitial quartz. The most common selvage minerals are coarse grained biotite and staurolite, with or without garnet. Selvages seem to occur most commonly beside quartz veins that contain the less common accessory minerals like muscovite and andalusite. The

Field relationships constrain the timing of formation of most quartz veins. Evidence of folding, extension and recrystallisation indicates that many of the veins were affected by D_2 deformation. There is some evidence suggesting that quartz veins formed during D_2. Firstly, in some outcrops containing both folded bedding and folded quartz veins the intensity of folding is less in the veins, indicating vein formation after folding of bedding had begun. Secondly, rare examples of small saddle reef type structures suggest that some vein formation was contemporaneous with folding.

Thus, in the Kanmantoo Mine and surrounding area most quartz veins are not parallel to S_2. Rather, with their typical north-northeast to northeast strikes they have a consistent dextral relationship with S_2. The range of orientations defines a great circle whose pole is close to $L_{2/2}$, indicating that the veins may have formed in response to the same forces responsible for foliation development. It is notable that the quartz veins have a similar trend to the east limb of the Main Lode and to several other lodes. These are the only two features that have this trend direction.

5.4.6 Shear zones

Features that were mapped in the mine as shear zones tend to be discrete, fairly sharply bounded tabular zones up to several metres in width with pronounced foliation exhibited by veins and schistosity. The zones are usually subparallel to the surrounding schistosity and many are discordant to bedding. Internal lithologies are predominantly medium-grained quartz rich lode schists without andalusite, particularly quartz-biotite-garnet schist, quartz-chlorite-garnet schist or a variety with both biotite and chlorite. Within shear zones and parallel or subparallel to the shear zone boundaries is a pervasive schistosity and varying quantity of quartz and sulphide veins. Typically the sulphide veins are persistent, subparallel or anastomosing stringers (see also Section 4.2) whereas the quartz and quartz-sulphide veins tend to be lensoidal and thicker.

One of the main shear zones of this type is called the 4100 Shear Zone which is exposed in the southern wall of the mine and occurs at the southern end of the West Limb. It corresponds to the copper rich feature labelled as A on Figure 32 and is shown in its local setting in Figure 62. The 4100 Shear Zone has a north-south strike and an average dip of 70E and so it is parallel to the axial plane of the Mine Synform that is only 13m to the east. To the south the 4100 Shear Zone can be followed to the edge of the mine and to the north it merges with the lode schists of the West Limb. Mapping information suggests that at this point it splits into several shears, one continues northwards and another major split, called the Sigmoid Shear Zone, swings north-westerly for approximately 80m then swings back to a north to north-north-easterly trend. The Sigmoid Shear Zone was documented clearly by mapping on the 600 Level where it is shown with widths varying from approximately 0.5m to 2.2m and with dips varying from 55º-80º towards the east or north-northeast. On other levels the Sigmoid Shear Zone was not recognised or was not exposed for mapping because the whole shear (with its attendant high grade mineralisation) was removed within ore blasts. This shear is an important control on copper distribution in the West Limb and corresponds to the high grade sigmoidal feature shown clearly on Figure 35.

During mining insufficient attention was paid to the shear zones and this is unfortunate because most shears are mineralised and it is likely that they are of fundamental importance in the origin of the deposits. Many of the shears that were identified are difficult to follow in the mapping records along strike from blast-face to blast-face. During mapping it was principally the abundance of veins that led such structures to be identified as shear zones. Where the extensions of shear zones can be inferred along strike many were mapped only as lode schist,

perhaps due to inadequate mapping, but more likely it reflects the lateral variability of the zones, especially with respect to changing width and vein content.

Another expression of shearing in the mine is suites of narrow shears that usually occur in GAB schist and are especially abundant in the West Limb of the Main Lode. The shear system comprises two sets of anastomosing shears - the dominant set is subparallel to the schistosity and the other is shallower. This style is also mineralised and a typical example is shown in Figure 23. In this figure note that two types of quartz vein occur, the most abundant is quartz- chalcopyrite veins (weathered) occurring mainly in the dominant shear set, and the other is the extensional style vein with the folded upper tip. The attitude and deflection of the extensional vein and the general lack of vein material in the shallower shear set suggest normal movement on the dominant set, but there is insufficient information on the kinematics of the shear systems to know if this conclusion can be applied widely.

The kinematic parameters of the various shear sets are unknown. All have a steeply south plunging mineral lineation (but it is weak usually) suggesting oblique slip with a dominant vertical component, but whether the shears are normal or reverse is not clear. No convincing shear sense indicators or displaced markers were seen and the internal foliation is parallel to the shears. As mentioned above the veins shown in Figure 23 and in several other examples suggest normal movement. The extensional quartz veins in the immediate hanging wall of the 4100 Shear Zone shown in Figure 62 may be consistent with normal displacement also if they are extensional, at least at the time that the veins formed. However, the curvature of the veins (unfortunately obscured by scree) as they approach to the shear zone suggests drag that would indicate reverse movement on the shear zone.

Shear zones of various scales occur in other areas of the mine, for example several intense shear zones are exposed on the southern wall of the pit between 4400E and 4800E, corresponding to the positions of the South Eastern mineralisation. Shears were also mapped at 3800E corresponding to the mineralised zone there and in the area around Emily Lens. Significantly, few shears have been reported from the central part of the pit occupied by the East Limb style of mineralisation.

The characteristic anastomosing pattern of the shear zones is seen at various scales and it is proposed here that the interaction of the shear sets created the large dilational zones needed to form large bodies of mineralisation. With respect to the West Limb the important shear sets are north-south (represented by the 4100 Shear Zone) and north-northwest trending (represented by the Sigmoid Shear Zone) and most of the mineralisation is in the former.

5.4.7 Crenulations and kinks

In the Kanmantoo Mine area crenulations and kinks are uncommon and little attention has been paid to them in this study. The most common crenulations are very fine and tend to be parallel to $L_{2/2}$. In some cases, it is difficult to decide in hand specimen which of the two is present. Coarser crenulations, with an amplitude of one centimetre or so have only been observed at a few sites. They have either northerly or easterly striking axial planes. No axial plane foliations have developed. Larger scale $F_{3/2}$ folds (or $F_{3/0}$ folds) have not been observed near the Kanmantoo Mine.


S1
S0

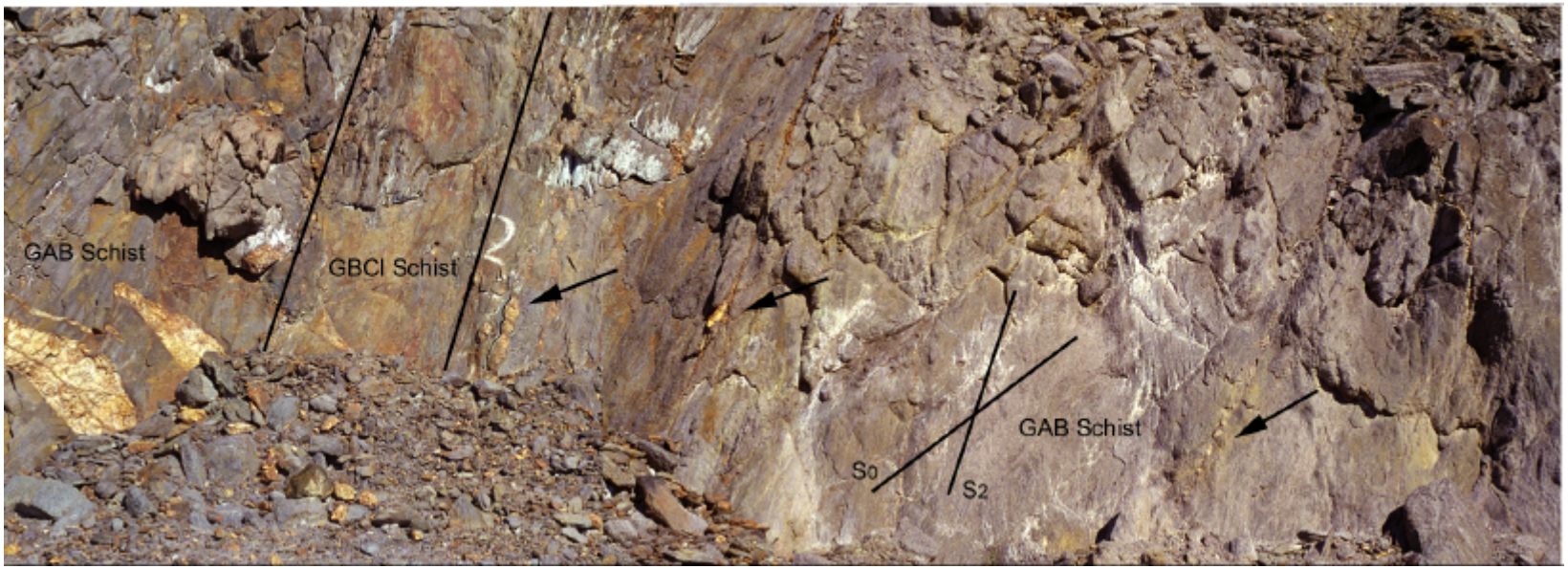

GAB Schist
GBCI Schist
GAB Schist
S0
S2

Figure 62. (previous page) Photomontages of an exposure of the 4100 Shear Zone on the 520 level.

The two strips represent a continuous panorama view. GAB schist shown near the left hand edge of the top strip is located only several metres west of the hinge area of the Mine Synform, and the easterly dipping bedding (S_0) of its west limb is well preserved and regular in dip across to the left edge of the strip. Bedding is emphasised by numerous andalusite rich beds. The schistosity (S_2) is slightly steeper in dip than the bedding. On the left side of the lower strip a one metre wide band of GBCl schist is marked and it marks the 4100 Shear Zone position. The band of GBCl schist is approximately parallel to schistosity and discordant to bedding on both sides. Internal schistosity in the band is parallel to the external schistosity. No convincing signs of the movement direction on the shear were seen in the band or in adjacent rocks. In the strongly deformed rocks most structures are parallel to the schistosity. The quality of bedding preservation is excellent to the east of the band, but degrades within a metre or so of it. On the immediate western side of the band bedding is barely recognisable within a 2m wide zone characterised by shearing and boudinage of quartz veins (arrowed). West of the third boudinaged vein that is marked the bedding is again recognisable, but is less well preserved than to the east of the shear zone. Note the discordant quartz veins in the hanging wall of the shear zone. Though well developed here, such veins are not typical. The yellow patches are surface oxidation stains on the wall.

Kinks ($F_{4/2}$) are present in the mine and surrounding area. They have irregular, subhorizontal axial planes and both angular and slightly rounded hinges. They are most easily observed in the fine grained QMF schists as shown in Figure 12. In many cases, a fracture occurs at the axial plane. Kinks are rarely observed in outcrops. The best examples occur in freshly exposed, micaceous varieties of QMF schist, such as the cuttings where the treatment mill was located. Kinks also occur in GAB schist in the mine, but are only observed from the right position with a suitable lighting direction. Another kink-like structure is associated with jointing, as described in the next section.

5.4.8 Faults and joints

In the mine small faults with minor displacement have been observed. However, in the surrounding area few have been observed although many have been interpreted to exist. Where faults can be observed, for example near the Otto Shaft (Figure 7), they are strongly foliated and veined zones. No breccias have been observed.

The reasons for many of the interpreted faults shown on Figure 50 have already been discussed. Only those north of the Kanmantoo Mine have not. The contact between GAB schist and QMF schist to the east and north of the mine is known from a few key exposures and drilling to be irregular in shape. For example, a well exposed contact at the Spitfire Mine adit (Figure 7) lies to the west of where the contact might otherwise be inferred from exposures on the north-eastern edge of the pit. Other irregularities were indicated by drilling, and also by outcrop pattern. Topographic changes at the edge of GAB schist outcrops have been found from drilling and mapping to closely reflect the position of the contact with QM schist. This contact is inferred to have several dextral offsets, the two most prominent being immediately northeast of the mine and also near the northern limit of Figure 7. These offsets can be explained by faulting or folding, or perhaps both, but folding alone is not sufficient. Northwest trending faults, as shown on Figure 50, have been inferred because they fit the

outcrop pattern best (including the lack of evidence of faulting in those outcrops) and because a copper mineralised fault with this trend occurs nearby.

Joints, up to several tens of metres in length, are numerous, but have no influence on the distribution of rock types. Several prominent joints have been recognised between the Kanmantoo and Aclare Mines. These joints are characterised by marked strike persistence, slight topographic rises (such that they resemble low, linear welts, one to two metres wide) and they contain quartz fill usually but some also have albite and tourmaline. The welts are possibly due to silicification from solutions migrating within the joints and the joints may have been important as a means of admitting metasomatic fluids to the region after metamorphism. The effects of this can be observed in the Kanmantoo deposit, as discussed in Chapter 6.



Figure 63. Low silicified ridge in QM schist with EW fractures (arrowed at right) separated by kinking of the S_2 schistosity.



Figure 64. Close up of part of Figure 63, showing detail of the kink bands bounded by sub-vertical fractures.

Approximately 300m east-southeast of the oxidised ore stockpile (Figure 7) an east-west trending joint is exposed. It is not a single fracture, but a sheeted zone of closely spaced (5cm apart), parallel fractures over a width of approximately one metre. The fractures strike east-west and dip steeply north. Associated with many of them are kink-like folds of the schistosity and each limb is separated by one of the fractures (Figure 64). Because minor differential movement occurred on the fractures they are minor faults. The fracture zone cannot be followed to the east or west due to lack of outcrop or very poor outcrop. However, 220m north of the Paringa Shaft, structures identical to those described above occur. As they also have an east-west trend and are aligned with those to the west, they may be part of a single structure with a minimum strike extent of 800m.

A second major joint or joint zone of regional extent has been recognised (Schiller, 1974b) which passes just south of the Kanmantoo Mine. It is exposed just south of the railway line (Figure 7) and can be followed discontinuously to the northeast as far as the Bremer Fault scarp, 6 km east of the Kanmantoo Mine. All its individual exposures are collinear. While it is clearly a large fracture, detailed mapping has shown that there is little or no displacement across it. As shown on Figure 8, the joint can be traced for at least seven kilometres. However, many kilometres further to the east-northeast, the projected joint position corresponds to some topographic features, especially in the drainage pattern.

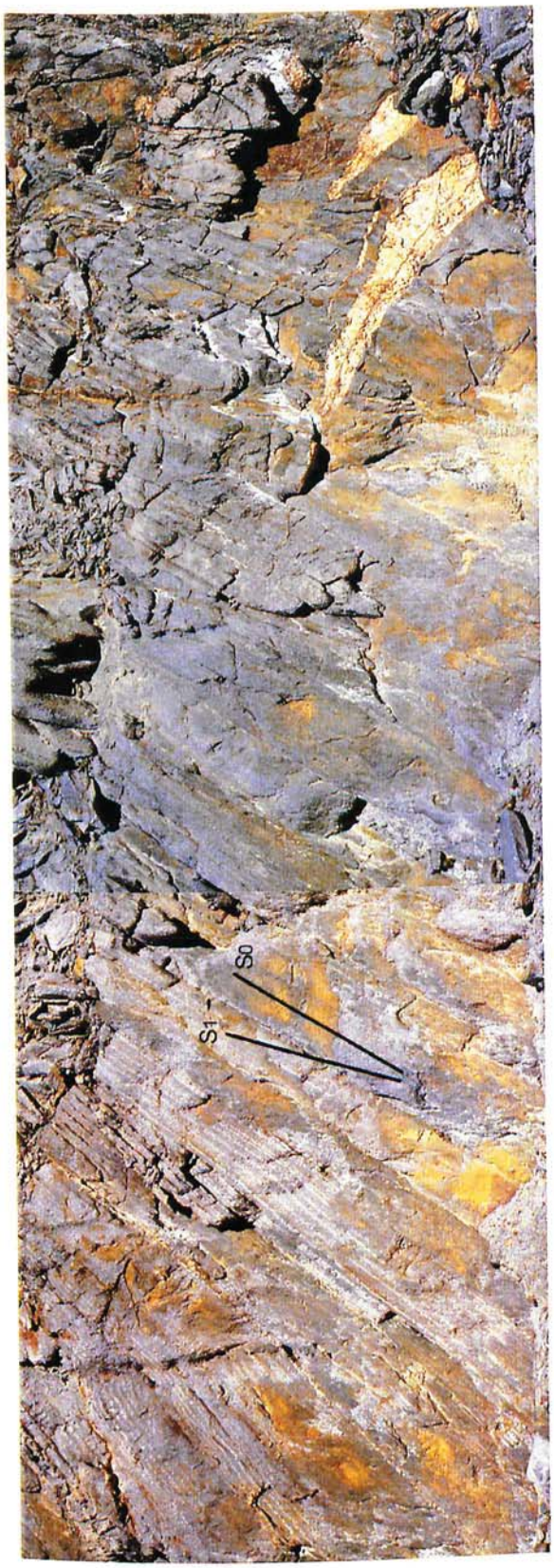
5.5 Structure and copper mineralisation

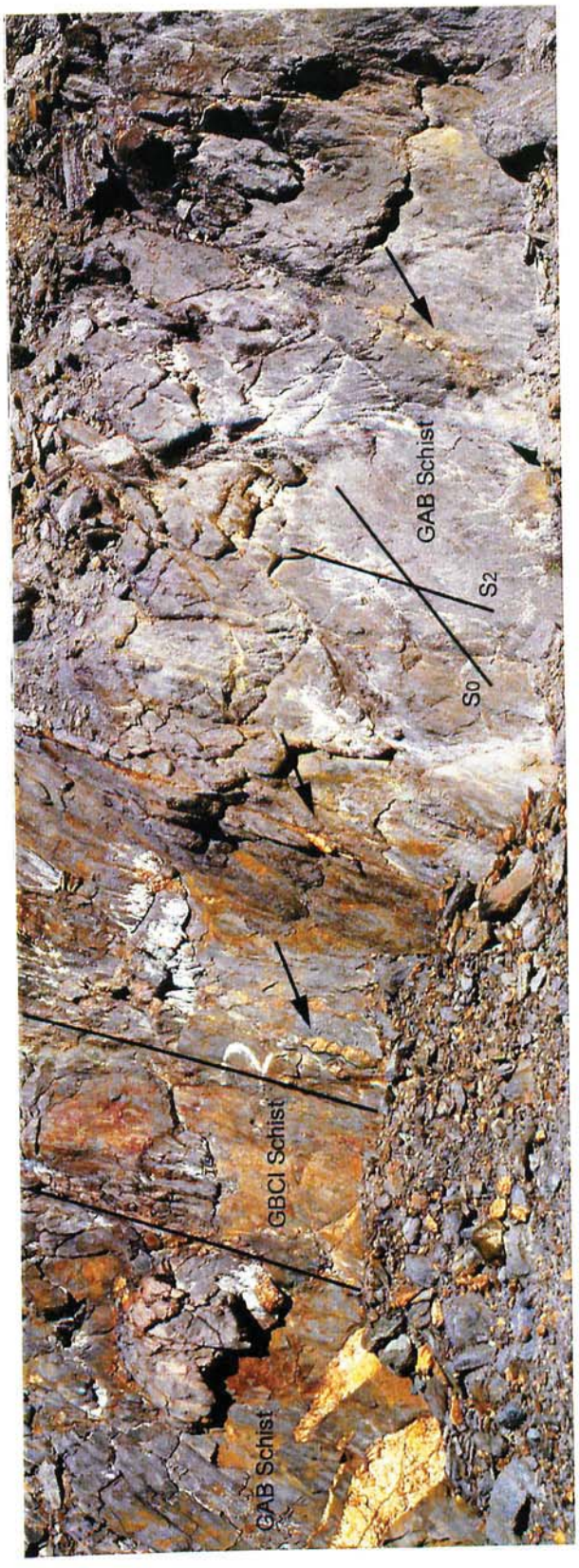
The shape and disposition of GBCl group lode schists and copper mineralisation was described in Chapters 3 and 4 and summarised in Table 15. Of interest was the conclusion that the interpreted copper zones and the interpreted lode schist bodies do not coincide in both the West Limb and the East Limb of the Main Lode. In this section the main features of the structural setting and the mineralised rocks will be summarised, and their relationship to one another considered. This relationship provides critical constraints on the origin of mineralisation. Stereographic projections summarising many of the structural features of the mine are shown in Figures 65 and 66.

Relict bedding in the Kanmantoo Mine defines a single, major synform (the Mine Synform); its axial plane occurs in the centre of the mine and passes through the Main Lode. The fold has a southerly plunge of approximately 15º and other minor folds have similar plunges, but vary from slightly steeper south to shallowly north (Figure 65). Parallel to the axial plane of all folds is a prominent schistosity (S_2) that has only minor variation in attitude; it has a steeply south pitching mineral lineation ($L_{2/2}$) that appears to be parallel to the direction of maximum extension. The two limbs of the Mine Synform differ in deformation style. In the eastern limb bedding tends to be easily recognisable and regular and shears are uncommon. In the western limb bedding typically is vague, shears parallel or subparallel to schistosity are common, and many veins are boudinaged. The two limbs are not equally disposed about the axial plane. The eastern limb is 30º-40º divergent from the axial plane, whereas the western limb diverges by only 0º–10º. It is considered that that some of the bulk strain of the western limb was partitioned in shearing along schistosity surfaces and on slightly oblique discrete shear planes.

The mineralised rocks and their relationship to structure vary, depending on the scale considered. At the meso-scale a pronounced control on much of the mineralisation is seen in the common parallelism between sulphide bearing veins and the S_2 schistosity. The control by S_2 becomes less evident as the scale increases. At the larger scale of individual lodes (that is mineralised bodies with many sulphide lenses) the control by S_2 is also apparent in some lodes (especially the West Limb mineralisation), but others are oblique to S_2. (especially the West Limb mineralisation). At the even larger scale of the Main Lode overall, the control by S_2 is less apparent and a relationship with the Mine Synform is seen. The Main Lode is approximately centrally positioned on the axial plane of the Mine Synform and extends across both fold limbs. The enveloping surface to the complex of the Main Lode and its associated lode schists is pipe-like in shape with dimensions of approximately 300m x 150m x +600m. The long axis of this pipe plunges steeply to the north-east and lies in, or close to, the average S_2 plane, an apparent coincidence that puzzled mine geologists.

The Main Lode is grossly discordant to bedding and, although it lies in the overall schistosity plane, its plunge is neither parallel to the plunge of folds in bedding nor to the mineral lineation (Figure 65).


S1
S0


GAB Schist
S2
S0
GBCl Schist
GAB Schist

The Main Lode consists of two styles of mineralisation that have different lode orientations. West Limb style mineralisation includes numerous lodes and lenses of GBCl group lode schist that strike parallel to the schistosity but are slightly steeper in dip. In the East Limb style lode schist occurs mostly in a single large lens that strikes north-north-easterly and dips steeply to the east. At a more detailed scale, the individual sulphide veins are mostly subparallel to schistosity, especially in the West Limb style. In the East Limb style of mineralisation such veins occur also, but are subordinate to less regular sulphide veins, masses and disseminations.

The occurrence of different styles of mineralisation on each limb of the Mine Synform indicates that the Mine Synform was probably a primary control during the formation of the lodes. As will be discussed in a subsequent section, the alternative to control on the location of lodes by folding is that the lodes controlled the position of the fold limbs. While the latter proposal is possible, it seems much less likely. If it were true then the extent of the Mine Synform would probably be restricted to the extent of the Mine Synform. Unfortunately, it is not possible to check this with any certainty because of insufficient information on the extent of the Mine Synform north and south of the pit.

The gross orientations of GBCl group lode schists and copper zones for the East Limb shown in Figure 66 show that both features intersect the average schistosity plane close to the gross plunge of the Main Lode. Similar plunges were observed for fold axes of quartz veins. The coincidence demonstrated on Figure 66 supports the conclusion that the overall control of the Main Lode is the relationship between the East Limb lode and the schistosity.

Some of the other copper lodes in the Kanmantoo Mine area have similar structural settings to the East Limb of the Main Lode as well as similar associated lithologies. The various lodes of the South Eastern Mineralisation trend north north easterly whereas the O'Neil Lode trends more north-easterly. Apart from having a slightly different attitude, the O'Neil Lode is markedly more tabular than either the South Eastern Mineralisation or the East Limb. However, on the scale of the overall lodes, all of these are oblique to both bedding and schistosity. Their en echelon pattern suggests that they may represent a suite of large dilational zones. Their steep dip argues against their formation by pure shear if $L_{2/2}$ was the extension direction. Rather, flat lying dilational veins would have been produced. Another possibility for their formation is that pre-existing fractures were placed under tension during the D_2 event. However, the apparent lack of folding of the lode schist unit comprising the East Limb argues against this. Thus, the origin of the dilational zones is unexplained at present.

The numerous small copper lodes in the Paringa-Otto area, southwest of the Main Lode differ from the others in having various orientations. They are all confined to GAB schist, and some appear to be associated with faults or shears. The associated retrogression of andalusite to muscovite indicates that the shears post-date D1, for part of their history at least.

6. MICRO-STRUCTURE

6.1 Introduction

The main purpose of this chapter is to draw conclusions on the structural history of the schists in the Kanmantoo Mine area and on the copper mineralisation hosted by them. It has been shown in previous chapters that copper mineralisation in the Kanmantoo Mine is strongly dependent on certain geological structures, especially at a mesoscopic scale. Schists in the Kanmantoo Mine area, like many others in the wider region, have a single, prominent schistosity and appear, from a mesoscopic point of view, to have suffered only one deformation. Regional studies have shown that this schistosity (S_2) has developed from an earlier schistosity or slaty cleavage (S_1) that is preserved as inclusion trails in porphyroblasts (Spry, 1976; Mancktelow, 1979; Spry et al., 1988). S_1 in the Kanmantoo region, and the whole eastern side of the Mount Lofty Ranges, has been correlated with the only foliation recognised on the western side of Mount Lofty Ranges (Mancktelow, 1979; Preiss, 1995). In the Kanmantoo Mine area, two planar fabrics can be recognised in porphyroblastic rocks. S_1 is preserved as inclusion trails in porphyroblasts and S_2 is the domainal schistosity in the matrix. Correlations of S_1 and S_2 for the mine area with other workers in the Kanmantoo region, especially with the important early work of Offler and Fleming (1968) and Fleming (1971), were discussed in Chapter 5. An alternative conclusion of the S_1 and S_2 fabrics was proposed by Lindqvist (1969) in his study of the Kanmantoo copper mineralisation. He assigned both fabrics (his S_1a and S_1b) to different stages of a single deformation event (his B_1). In this study S_1 and S_2 could alternatively be referred to by the non-genetic terms of S_i and S_e, for internal and external fabrics respectively, and this has been done in some cases. However, the current understanding of S_1 and S_2 for the Kanmantoo region is well accepted, so the prevailing system has been followed here.

Although Lindqvist (1969) described the microstructures of both silicate and sulphide minerals from the Kanmantoo Mine area, he concentrated on the sulphide minerals. He concluded that the sulphide minerals had been metamorphosed together with their host rocks, and that they were present in the rocks when the earliest recognisable fabric (his S_1a) was produced. This chapter deals with some of the subject matter covered by Lindqvist (1969) but describes the silicate microstructures in considerably more detail and proposes different origins.

Several terms that are frequently used in this chapter will be defined here, all follow the terminology of Hobbs et al., (1976, pp. 73, 74). *Fabric* includes the complete spatial and geometrical configuration of all those components that make up a rock. Features that contribute to a fabric are said to be *penetrative* and are known as *fabric elements*. Fabric elements that can be observed with a microscope constitute the *microfabric* and this includes the more specific term of *microstructure* that refers to grain shapes, arrangement of grains and the internal substructure of grains.

6.2 QMF schist

In the Kanmantoo Mine area QMF schists have a pervasive S_2 schistosity in which a mineral lineation can be observed commonly, especially in the more micaceous varieties. These rocks lack porphyroblasts, other than small garnets perhaps, and so there is no evidence of S_1. Nor, in the Kanmantoo Mine area, is there is much evidence of crenulations of S_2. Recognition of crenulations is made harder by the tendency for crenulations to be finely developed in micaceous QM schist only, and it is in this rock also that the mica mineral lineation develops best and both tend to be sub-parallel. Therefore most of these rocks present an apparently simple story of a single foliation forming deformation. The S_2 schistosity is parallel to the axial planes of folds in bedding (Figure 72) and is defined principally by the preferred

orientation of the (001) crystallographic planes of biotite and muscovite (Figure 73). Unlike the micas, quartz and feldspar are commonly equidimensional or only moderately elongated, its grain size depends partly on the size and spacing of micas, as also observed in many other regions (Voll, 1960; Vernon, 1976). Garnet is a common accessory (Figure 73) and tends to be more common in the micaceous interbeds, but within these shows no preferred pattern. Garnet usually forms idioblastic grains that are approximately 0.05mm in diameter and contain few inclusions. The schistosity is truncated at the garnet margins. It can be seen in Figure 73 that muscovite tends to be narrower than biotite. This is confirmed by the data shown in Figure 74, where measurements of the aspect ratios and lengths of mica grains in a typical QM schist. The data show that muscovite grains tend to have higher aspect ratios than associated biotite grains although both minerals have similar lengths.

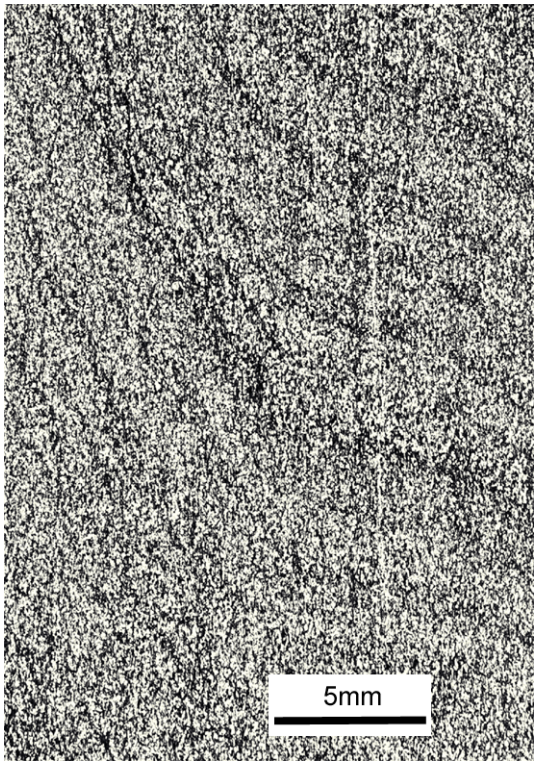


Figure 72. Well bedded example of QF schist with gentle fold in bedding and well developed axial planar S_2 schistosity (lengthwise in the photo). Plane polarised light (PPL). [Sample No. 517-181]



Figure 73. Typical QM schist with strong S_2 schistosity (lengthwise in the photo) defined by biotite and muscovite laths. Bedding (S_0, marked), almost at right angles to S_2 is defined by variations in mica vs. quartz + feldspar. PPL. [Sample No. 517-2870, from hole KS31 at 875m depth.]

In Chapter 3 it was noted that QM schist is transitional with QMA schist and that both lithologies are interbedded. These lithologies are mineralogically similar, differing principally in the presence or absence of andalusite. Some QM schists that are associated with QMA schist contain small, augen-like bodies. They vary from 2 to 4mm in length and, like the surrounding rock, consist of quartz, muscovite and biotite. Many are shown in Figure 75 where they are the pale ellipses, some with darker centres. The schistosity encloses these bodies but does not pass through them. The micas within the augen-like structures appear to be randomly disposed, unlike the well-aligned micas in the surrounding rock. The author observed no internal fabric within the centres of the augen-like structures, however Lindqvist (1969) described similar augen with sigmoidal fabrics, continuous with the surrounding schistosity.

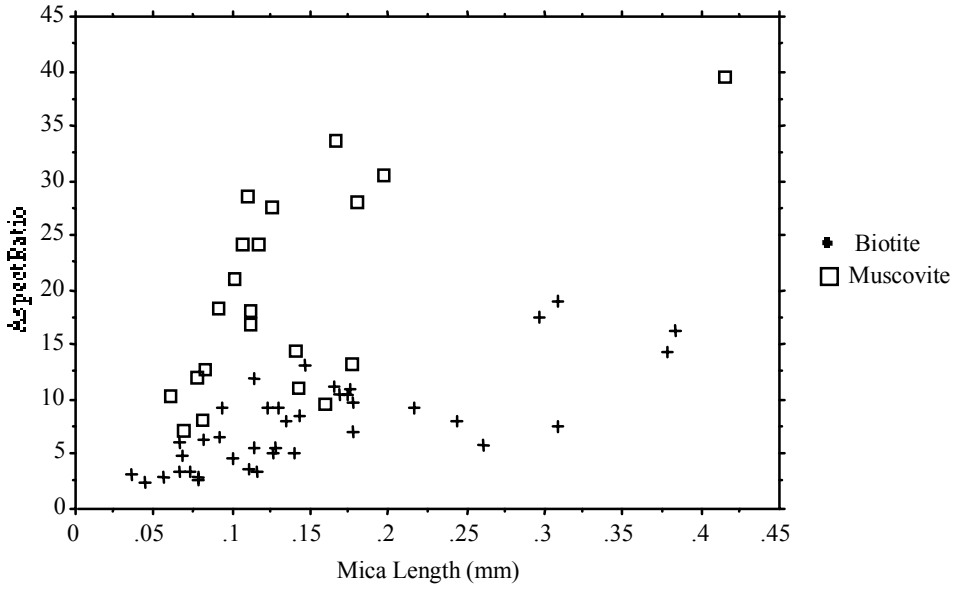


Figure 74. Scatter diagram of aspect ratios of micas in QM schist

The common elongation of the augen-like structures appears to be due to the presence of structures similar to strain shadows and the elongation is emphasised by the adjacent strain caps (Passchier and Trouw, 1996). Quartz grains in the strain shadows are equidimensional and are coarser than quartz grains in either the augen-structures or the surrounding rock. The boundaries between the strain shadows and both the augen-like structures and the surrounding rock are typically gradational.

Thin micaceous zones, which are parallel to the matrix schistosity form symmetrical *strain caps* (Passchier and Trouw, 1996) that help define S_2. They occur on both sides of each augen-like structure and dissipate at some distance from the structure. This is illustrated in Figure 75 (but note that in this figure the micaceous zones are enhanced by weathering). In addition, similar but longer and more persistent discrete cleavages occur in the rock that also define S_2. The longer micaceous zones described above are similar to *discrete cleavages*, as described by many authors, including Durney (1972), Gray (1978, 1979), and Mancktelow (1979). Passchier and Trouw (1996, Fig.4.6) refer to it as *spaced schistosity* with *discrete cleavage domains*. The origin of discrete cleavages has been attributed by most of these authors to pressure solution during deformation, that is the cleavages are thought to have formed by the preferential removal, in solution, of minerals like quartz and feldspar from zones which then become progressively narrower and enriched in minerals like mica and opaques. In some cases the pressure solution process is thought to be dependent on the presence of a strain resistant particle or object (Durney, 1972) and this could explain why this type of cleavage is not observed in the schists without augen-structures. The association with augen and the lack of evidence for crenulation argues against crenulation cleavage mechanisms.

Thus there are three features that define S_2: the matrix schistosity, the strain caps and the discrete cleavages. The discrete cleavages are commonly zones of discontinuity as shown in Figure 75, where thin quartz veins terminate, and in some cases appear to be offset, at the zones. Some of the quartz veins show a sinistral curvature as they approach the discrete cleavage, suggesting that the cleavages may be micro-shears, or that the cleavages result from wide spaced crenulation cleavage. There is no evidence of such a crenulation cleavage in the matrix but this can be accounted for by assuming its destruction by the progressive crenulation process, as described by Bell and Rubenach (1983). In these authors' scheme the

cleavage would be Stage 5. Mechanisms of cleavage and schistosity formation will be discussed further at the end of this chapter.



Figure 75. QM schist with augen-like bodies. The schistose matrix has thin, dark discrete cleavages at which several quartz veinlets terminate. The two white patches with X marked are holes in the thin section. PPL.
[Sample No. 517-212]

The origin of the augen-like structures is uncertain. Because they are commonly more concentrated in zones parallel to bedding and also because the schistosity wraps around them, it is concluded that they are either of sedimentary origin or are replacement products of pre- to syn- D_2 porphyroblasts, perhaps cordierite. So far, augen-structures that are not closely associated with andalusite have been described. However, some augen-structures contain andalusite, and in these the andalusite appears to have replaced many of the minerals of the augen-structure. In some cases the andalusite also appears to have replaced micas surrounding the augen-structure. This is considered in the following section. In these cases the quartz inclusions within the central part of the andalusite, which presumably are inherited from the augen-structure, are equidimensional whereas those inherited from the matrix are elongated and wrap around the augen parallel to S_2. Thus, it seems that andalusite grew after the matrix schistosity had been deflected around the augen. As there is no apparent discordance between S_1 and S_2 at the andalusite margins it seems that there has been little deformation of the QM schist after andalusite growth. This conclusion contrasts with those obtained from GAB(1) schist, as will be shown in a later section.

6.3 QMA schist

Andalusite grains in QMA schist characteristically contain a large number of inclusions that commonly define a planar fabric throughout the grain. Also many andalusite grains contain a core with randomly oriented inclusions and a planar fabric at the rim, as described in the preceding section. In addition, many examples of interbedded QM schist and QMA schist contain andalusite bearing augen-structures in the QM schist interbeds. Figure 36b illustrates such a case; here the left hand side is the augen bearing QMF schist and the right hand side has a QMA schist bed (the medium grey grains are the andalusite porphyroblasts). This figure also clearly illustrates some points mentioned previously. For example, note that the distribution of augen-structures reflects the bedding, which is also visible within QMF schist interbed in the top left hand corner of the figure. In addition, the discrete cleavage zones

augmenting the schistosity are clearly visible and in several places discontinuities at these zones can be seen. Although there are no augen-structures in the QMA schist bed shown in this figure (nor in many other similar ones in other rocks) perhaps it was augen-rich and the augen were completely consumed by the growth of andalusite. Rocks such as that shown in Figure 36b demonstrate the transitional relationship between micaceous varieties of QMF schist and QMA schist.

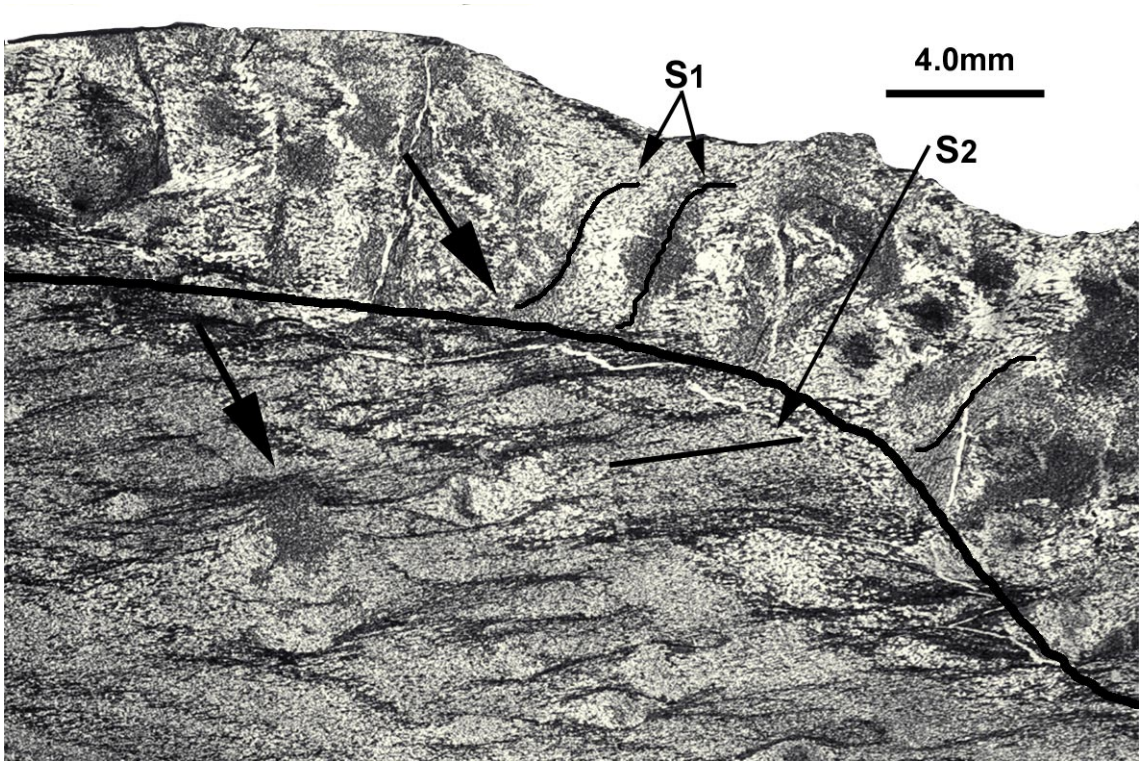


Figure 76. Bedded QM schist and QMA schist. In the QMA schist (at top and separated by black line) the andalusite are the irregular, medium grey shapes. The QM schist contains augen structures and a prominent S_2 fabric defined by matrix schistosity, strain caps and discrete cleavage. Internal fabric (labelled S_1) in andalusite is mostly at a high angle to S_2 but is continuos with it in part. The upper and lower arrows point to the sites shown in Figures 77 and 78 respectively. PPL. [Sample No. 517-212.]

The relationship between S_1 and S_2 in QMA schist interbeds within QM schist will now be discussed. Figure 76 illustrates features that are common to many rocks. In the QM schist portion of the section shown in this figure, the schistosity S_2 is parallel to the length of the photograph throughout. However, in the QMA schist bed two schistosity directions can be recognised corresponding to S_1 and S_2. S_2 in QMA schist is approximately parallel to S_2 in QMF schist and S_1 is almost at right angles to it, as shown in Figure 77. It can be seen though, that S_1 is partly continuous with S_2 and it curves smoothly into the QMA schist band. The andalusite grains are optically continuous and so are not strongly deformed and, therefore, the sigmoidal S_1 within them is inferred to have formed before the andalusite grew.

Figure 78 illustrates a single andalusite grain in the QM schist that appears to have replaced both the augen (with its random inclusion pattern) and the adjacent micaceous zone (with its strongly aligned quartz grains). The inclusion shape and degree of preferred orientation vary towards the upper margin of the andalusite grain. Note that there is only a small wrapping effect of the S_2 schistosity around the andalusite, indicating only minor flattening after the growth of andalusite.

Two interpretations of the relationships between the structures labelled as S_1 and S_2 in Figure

76, 77 and 78 follow. The first involves a single, refracted schistosity and the second a crenulation cleavage. Firstly, the smooth curvature between S_1 and S_2 may represent a schistosity refraction that was present in a bedded metasediment with sufficient competency differences to develop cleavage refraction. One of the beds contained many augen-structures and the schistosity wrapped around them forming strain caps and discrete cleavages at their margins. Next, andalusite grew relatively quickly by replacing the augen-structures and part of the micaceous rock adjacent to the structures. Thus, the sigmoidal schistosity refraction pattern was preserved. Subsequent rotation during folding may have increased the initial angle of the refraction, but the continuity remained. That subsequent deformation occurred is indicated by the orientation of S_2 in the QMA schist band. The micas defining S_2 are unlikely to be rotated original micas because the andalusite grains would have rotated too, particularly as the micas occur so close the andalusite margin (Figure 78). Therefore, it appears that they are new micas, possibly a product of the andalusite forming reaction.

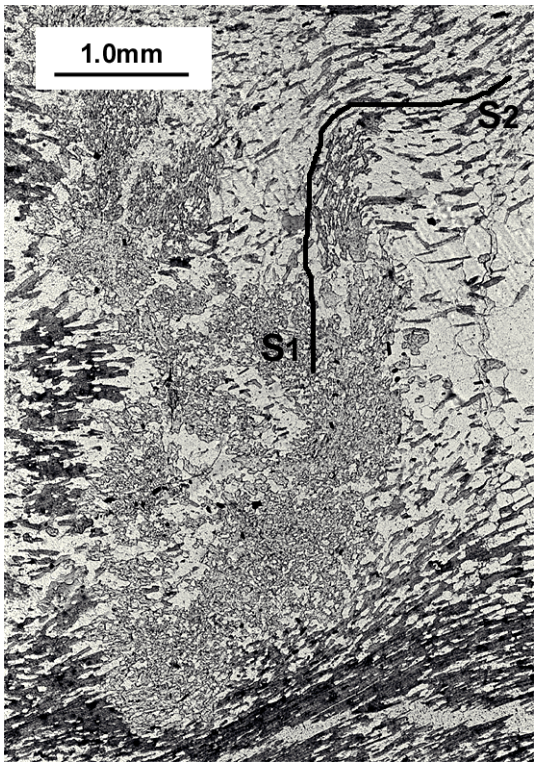


Figure 77. Andalusite porphyroblast from the QMA schist band shown in Figure 76. Many of the inclusions are irregular in shape, but some define a strong S_i (S_1) that is at a high angle to surrounding S_e (S_2) at the bottom and sides but is continuous at top as marked. PPL.



Figure 78. Andalusite porphyroblast from the QM schist band shown in Figure 76. The andalusite straddles a biotite rich discrete cleavage zone (top half) and a quartz rich zone (bottom half). The crystal shape of the andalusite is better developed in the biotite rich zone where its inclusions tend to be more elongate and aligned parallel to the surrounding S_2 schistosity. Crossed polars.

The second proposed origin involves formation of S_1, followed by growth of andalusite in the early stages of a D_2 crenulation that progressed to completion with the formation of the S_2 schistosity and the destruction of S_1 except in the andalusite porphyroblasts. These considerations apply also to GAB schist and will be dealt with further on.

6.4 GAB(1) schist

The characteristic features of GAB(1) schist are coarse andalusite porphyroblasts and a strongly schistose, domainal matrix. GAB(1) schist is microstructurally similar to some varieties of QMA schist, especially those with abundant, coarse andalusite. The main difference between these two rock types is mineralogical. The constituent minerals of GAB(1) schist are andalusite, biotite and quartz with minor garnet and staurolite and, compared to QMA schist, garnet, biotite and staurolite are much more abundant. Muscovite is common in some samples of GAB(1) schist but is not always present. Feldspar is usually absent near the Kanmantoo Mine.

Andalusite porphyroblasts have many quartz inclusions that typically define an internal fabric (S_1) and, less commonly, garnet also has a weaker internal fabric. Other minerals, like staurolite and biotite do not have internal fabrics in rocks near the Kanmantoo Mine, but some samples to the north have strong internal fabrics similar to coexisting andalusite. The matrix has a prominent continuous schistosity (S_2) that is emphasised by domains parallel to it comprising two planar alternating mineralogical zones that will be called Q domains (quartz rich) and M domains (mica rich). In the terminology of Passchier and Trouw (1996) these fabrics represent a *continuous schistosity* and a *disjunctive, spaced schistosity* respectively. The Q and M domains are morphologically similar to the micaceous bands in QMA schist described in the previous section. They are illustrated at mesoscopic scale in Figure 15 and in microscopic scale in Figures 79 and 81.

6.4.1 Description of Q and M domains

Both Q and M domains have identical mineral compositions, but the proportions of these minerals differ greatly. Andalusite is almost entirely confined to the Q domains with only some of the margins projecting slightly into M domains. In comparison with Q domains, M domains have more garnet, biotite and staurolite, but less quartz. Similar mineralogical compositions of domains in Kanmantoo Group metasediments have been described by Fleming (1971), Marlow and Etheridge (1977), Spry (1976), Mancktelow (1979) and others.

Some of the minerals within the domains have preferred orientations parallel to the domains. In both Q and M domains biotite has a preferred dimensional orientation and a preferred crystallographic orientation of (001) planes parallel to the domains. However, the degree of preferred orientation is visibly weaker in the Q domains than it is in the M domains. A similar difference in the apparent degree of preferred dimensional orientation within each domain can also be recognised for quartz grains. For example, in Q domains quartz forms polygonal aggregates of equidimensional or slightly elongated grains but in M domains quartz grains have a marked preferred dimensional orientation parallel to the domains. The crystallographic orientations of quartz grains were not investigated.

Thus, it is a combination of both the parallel domains and the preferred orientation of some of their constituent minerals that defines the schistosity (S_2) that is so prominent in hand specimens of GAB(1) schist. Garnet and staurolite have no apparent preferred dimensional orientation but the long axes of andalusite porphyroblasts may have a preferred alignment, as discussed later.

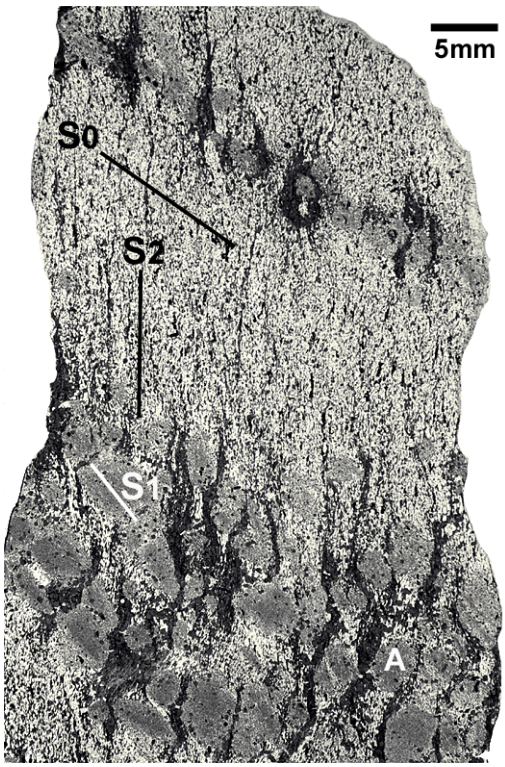


Figure 79. GAB(1) schist with andalusite poor beds. Bedding (S_0) is at a high angle to S_2 schistosity, which is enhanced by domains in andalusite rich beds. Internal fabric S_1 within andalusite is consistently sub-parallel to bedding. PPL. [Sample No. 517-040]

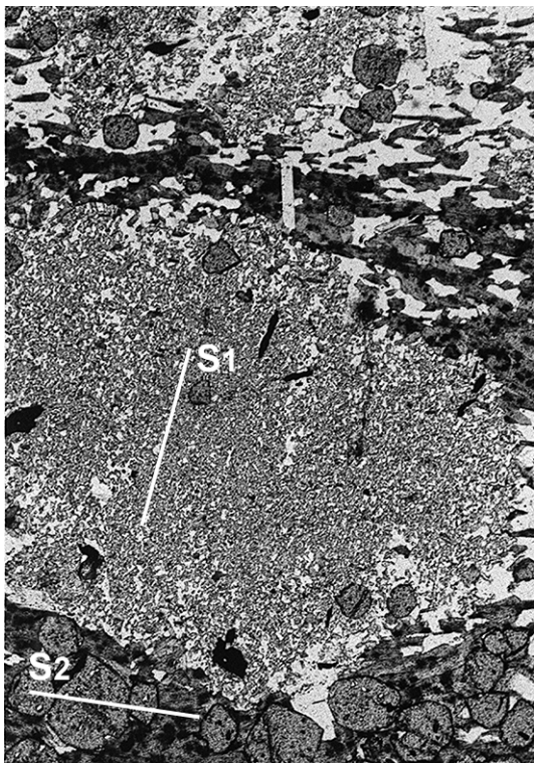


Figure 80. Detail of andalusite grain marked A in Figure 79 (rotated 90 CCW). S_1 is well defined by quartz and opaque inclusions. Note the biotite and garnet rich strain cap composition. The pale lath replacing biotite at the top of the andalusite is chlorite. PPL.

The occurrence and position of domains in GAB(1) schist is strongly influenced by the location of andalusite porphyroblasts, for example the domains rarely occur in quartzose interbeds with no andalusite. This is illustrated by the bedded GAB(1) schist shown in Figure 79 that also shows that the M domains dissipate with distance from the andalusite porphyroblasts. In this example they are *strain caps* according to the classification scheme of Passchier and Trouw (1996).

The widths of both Q and M domains vary. Q domains are widest near andalusite margins and so the width of any Q domain depends on the size of andalusite porphyroblasts. Where more than one porphyroblast occurs in a Q domain it is thinnest between them. In some cases the widest portions of Q domains contain a combination of both an andalusite porphyroblast and quartz, which appears to have the same effect as single andalusite crystals in other parts of the same rock (see Figure 38a, lower left hand corner). M domains are typically much narrower than Q domains except in very biotite rich and andalusite poor varieties of GAB(1) schist. In most cases the widths of M domains are about a third to a fifth the width of the andalusite porphyroblasts. An effect of the varying widths of individual Q domains is to produce an undulatory S_2 that is especially obvious in hand specimen size samples which typically break along M domains, revealing mica covered domes on the schistosity surface (illustrated in Figure 16). Each of the domes corresponds to an andalusite grain below the micaceous surface. In detail, the domes are ellipsoidal with the long axes parallel to the mineral lineation usually visible in the surrounding micas of the M domain.

By observing thin sections of many samples of GAB(1) schist, relationships between the size, shape and orientation of biotite and sulphide grains within each domain are apparent. In particular, biotite and sulphide grains within M domains tend to be longer and more elongated than those in adjacent Q domains. Furthermore, biotite grains within M domains have a stronger preferred orientation than those within Q domains. These features are typical of all specimens of GAB(1) schist observed in this study and in order to demonstrate the features, measurements of the dimensions and orientation of biotite and sulphide grains were made and are described in following paragraphs.

Firstly, measurements of the shape and size of biotite grains will be discussed. Measurements of the shapes of biotite grains in the Q and M domains of an apparently typical specimen of GAB(1) schist are presented in Figure 81. Data in the first graph were measured from a section cut perpendicular to both S_2 and the L_2 mica lineation, whereas the second graph represents a section cut perpendicular to S_2 and parallel to L_2. The latter graph demonstrates a pronounced overall linear relationship between the aspect ratios and lengths of biotite grains; however, this linear relationship is not indicated in the data from the section perpendicular to L_2.

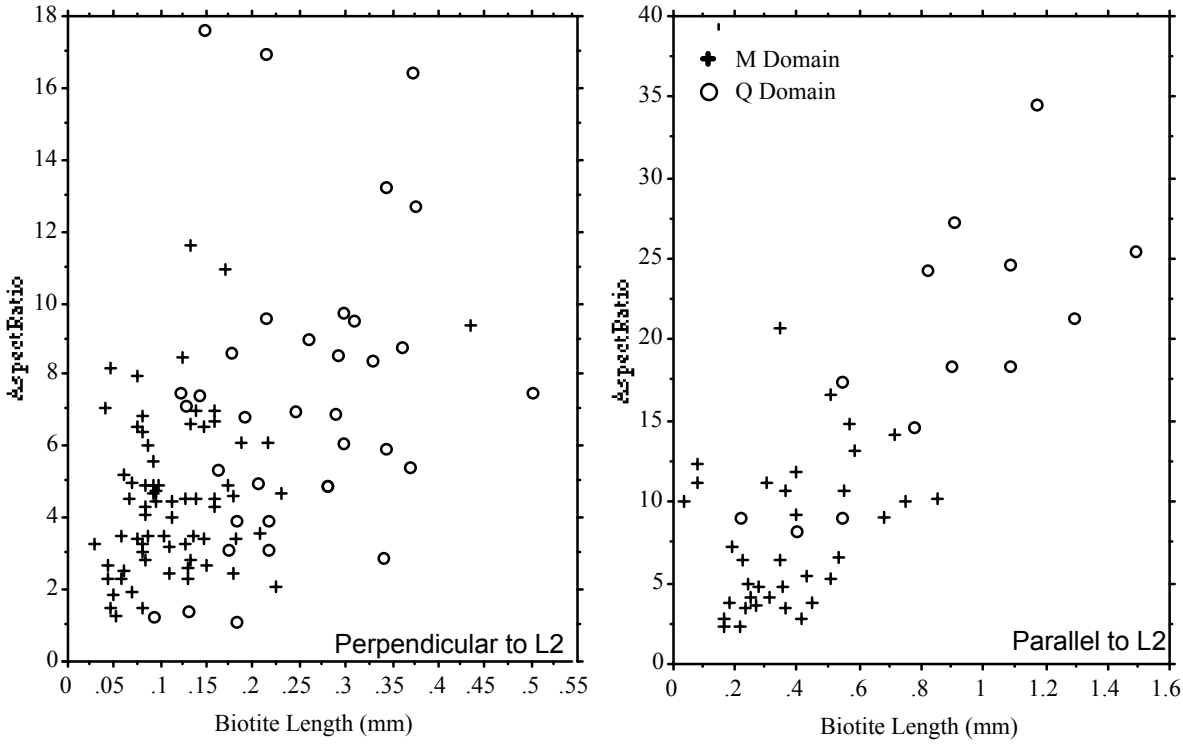


Figure 81. Graphs of aspect ratios of biotite in GAB(1) schist.

In both sections the biotite in the M domains tends to be longer and to have higher aspect ratios than biotite in Q domains, although there is some overlap in the plots. Furthermore, the biotite measured in the section parallel to L_2 tend to be larger than those measured in the section perpendicular to it (note that the scales are different on the graphs). Similar relationships between the size and shape of mica minerals have been described for crenulation cleavage domains in a Kanmantoo Group metasediment by Marlow and Etheridge (1977). It can be calculated from the data presented in Figure 81 that the mean relative proportions of biotite grains in the Q domains of this rock are approximately 11:3:1, whereas they are 23:7:1 in the M domains.

Sulphide grain shapes in GAB(1) schist are similar to biotite in that they tend to be longer and

to have higher aspect ratios in M domains compared to Q domains (Figure 82).

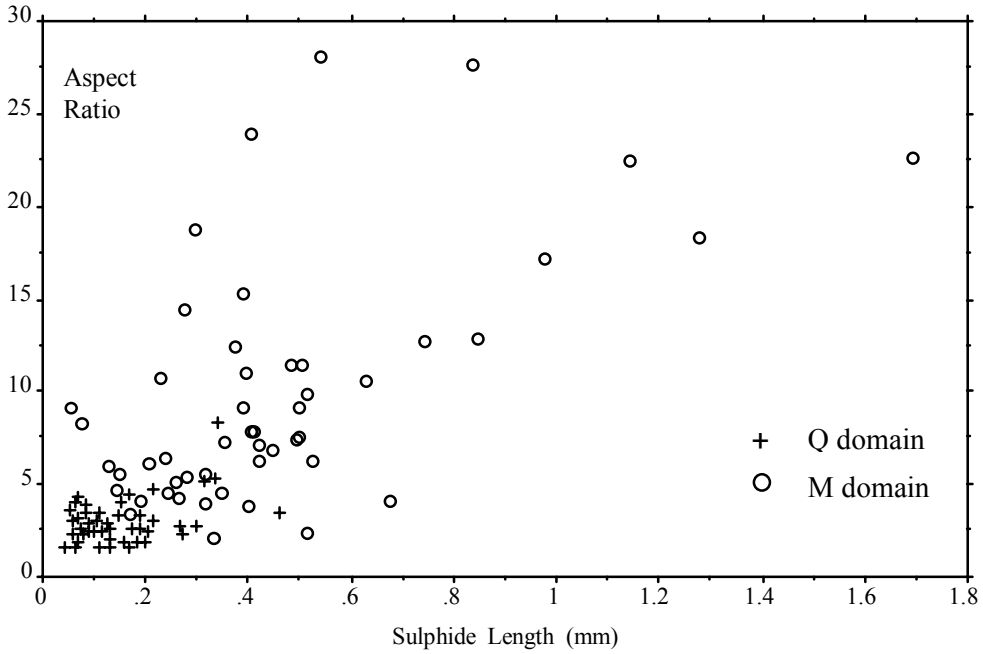


Figure 82. Graph of aspect ratios of sulphide minerals in Q and M domains of GAB(1) schist. The section is parallel to L_2.

Measurements of the orientation of micas within Q and M domains will now be considered. The degree of crystallographic preferred orientation of biotite can be estimated by measuring the orientation of the trace of (001) planes in sections cut perpendicular to S_2. Measurements taken from the same rock discussed above are shown in Figure 83. In each case measurements of the traces of the (001) planes were taken relative to a reference line set as close to the average trend of S_2 in the thin section as could be visually estimated. The difference in trend between this reference line and the trace of the (001) plane for any given biotite grain is plotted as the abscissa in Figure 83. Aspect ratios are plotted as the ordinate. Both graphs show measurements from a section cut perpendicular to the lineation and, unlike Figure 81, the Q domain and the M domain are shown on separate graphs.

In Figure 83 the data for the Q domain (first graph) show no apparent relationship between the trends of the (001) planes and aspect ratio. Furthermore, the extreme variability of the (001) plane trends indicates a poor preferred orientation. It should be noted, however, that many samples of GAB(1) schist have strong preferred orientations of biotite in Q domains, especially the more quartz rich varieties. Orientation data from the M domains is shown in the second graph of Figure 83 and it demonstrates a weak relationship between the (001) plane trends and aspect ratios. That is, within M domains of this rock, biotite grains that are subparallel to the schistosity tend to be more elongated than those at a high angle to it. The measurements taken from this rock confirm observations that biotite grains within M domains tend to be longer, more elongated and more strongly aligned than those in adjacent Q domains. An interesting aspect of the measurements is the unexpectedly poor relationship shown in the data for the M domain. Although a general trend is apparent it is weaker than anticipated from observation of the thin section, possibly because the eye is influenced by the strong linearity of the whole M domain. The line shown the second graph of Figure 83 will be discussed later.

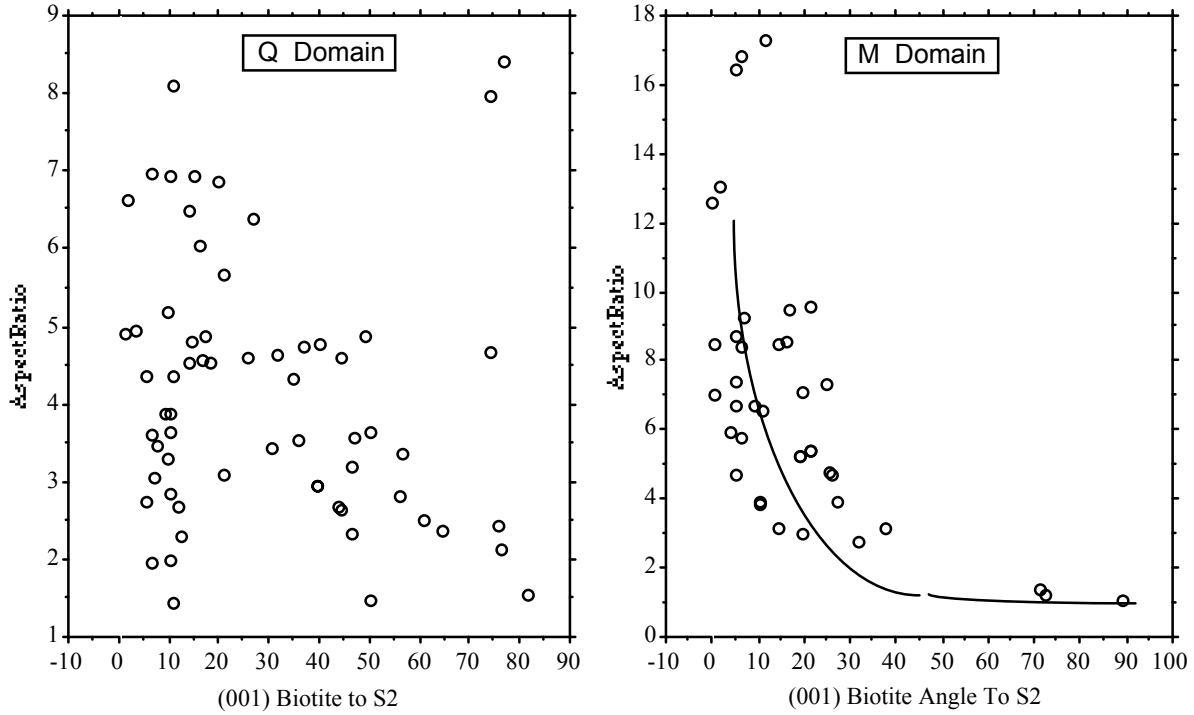


Figure 83. Graph of aspect ratios vs. divergence from mean S_2 for biotite in Q and M domains of a GAB(1) schist sample. Refer to text for explanation.

6.4.2 Description of internal fabrics in porphyroblasts

The following descriptions apply to GAB schist samples occurring within or near the Kanmantoo Mine. Similar rocks from elsewhere in the Kanmantoo district were described by Fleming (1971) and Spry (1976). In all samples of GAB(1) schist that were examined the andalusite crystals contain many inclusions that comprise from (an estimated) 10% to over 50% of porphyroblast volumes. By far the most common mineral inclusion is quartz, others are ilmenite, garnet, biotite, muscovite and, rarely, chalcopyrite or pyrrhotite.

The inclusions typically define linear patterns within the andalusite porphyroblast, when viewed in thin section. The pattern is defined in two ways. Firstly, and most commonly, the individual inclusions are elongated and aligned, as shown in Figures 84, 85 and 86, all from the same sample. Secondly, the density of quartz inclusions may define vague bands in which the quartz inclusions are typically irregular in shape and more coarse grained than adjacent elongated quartz inclusions. Figure 80 shows an example of this; the porphyroblast has diffuse, relatively wide bands of coarser inclusions trending slightly obliquely to the length of the photograph. Where both types of inclusion patterns occur in the same porphyroblast they are parallel.

The inclusion trails when observed in section are typically rectilinear across the entire andalusite grain and rarely curved. It is assumed that they represent planar fabrics. The trace of S_1 tends to be parallel to the long axes of andalusite crystals in GAB(1) schist, and GAB(3) schist too, and this feature is most obvious in those samples in which the prismatic form is well developed. An explanation for this feature may be that the planar anisotropy present in the rock prior to andalusite growth (and now represented by S_1) influenced the crystallographic orientation of the andalusite crystals as they grew. This is discussed further in Section 5.3.5.

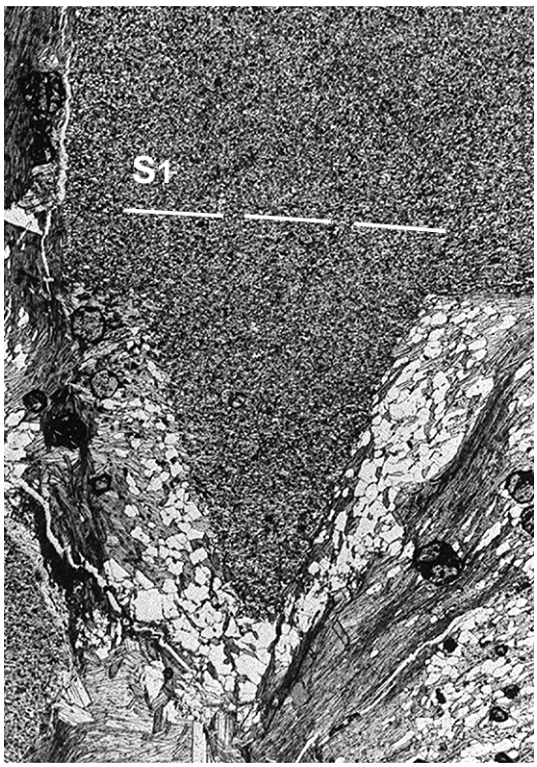


Figure 84. Composite andalusite crystals in the top part of the photograph sharing a weakly developed S_1 fabric as marked. S_2 wraps around the andalusite and a well defined strain shadow. PPL. [Sample No. 517-185. Width of photograph is 6.4mm.]

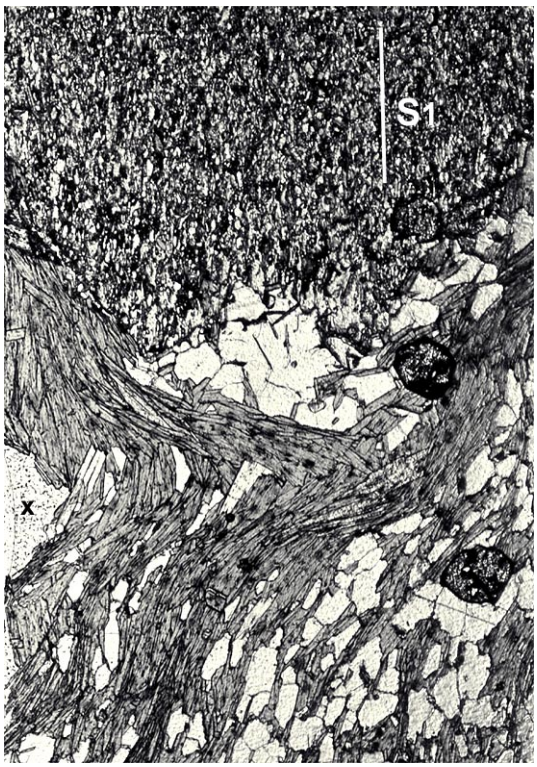


Figure 85. Andalusite crystal in top part of photograph with a strong S_1 fabric parallel to its length. Note the drag like structure in S_2 at the base of the andalusite. PPL. [Sample No. 517-185. Width of photograph is 3.1mm.]

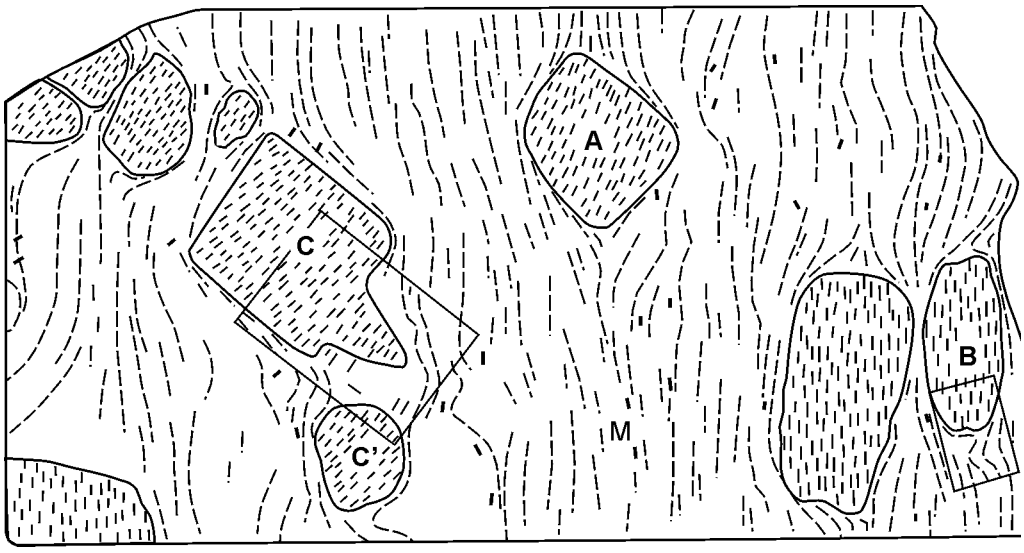


Figure 86. Line drawing of a thin section of GAB(1) schist. Andalusite grains are shown with S_1 internal fabric marked as short lines. In the matrix, the trend of S_2 is shown by thick long lines and S_1 in garnets by short thick lines. The letters A, B, C and M are discussed in the text. The left and right insets are illustrated in Figures 84 and 85 respectively. [Sample No. 517-185. Section perpendicular to $L_{2/2}$. Length is 49mm.]

Some andalusite porphyroblasts do not display S_1 when viewed in section and this can be explained in the following ways. Firstly the section may be parallel to S_1 and if the fabric has no linear element then it will appear dimensionally random. This is more likely to be the case where S_1 is visible in surrounding porphyroblasts. A second explanation is that no S_1 is present in the porphyroblast and this is more likely where surrounding porphyroblasts are the same, although a rock with S_1 parallel in all porphyroblasts could be fortuitously sectioned parallel to S_1 and so not reveal it. Thirdly, a fabric may have existed prior to andalusite growth but was destroyed before or during porphyroblast development. If this occurred it appears to have been erratic, for it did not destroy all fabrics and it could also be argued that the porphyroblasts preserve different degrees of fabric development, that is, the degree of fabric development itself was erratic rather than the quality of its preservation. It seems most likely that S_1 is common within andalusite but is not always visible, depending on the whether the section was cut appropriately.

Generally, quartz inclusions are evenly distributed throughout andalusite porphyroblasts. S_1 also is more or less equally defined throughout the porphyroblasts and extends right to the porphyroblast margin. Usually S_1 and S_2 are not parallel and the change from S_1 to S_2 is not continuous, but occurs abruptly at the porphyroblast margin.

So far, examples of fabrics in typical GAB(1) schist have been described. An unusual variety occurs in a zone a few metres wide containing muscovite rich rocks at the western side of the 640 level of the mine. This zone is anomalous in the area for several reasons. Firstly, the field relations indicate locally greater deformation, and it is probably a substantial shear zone. Secondly, andalusites from this zone contain strongly curved S_1. Figure 87 shows an example in which S_1 is markedly curved and is continuous with S_2. Another unusual feature shown in Figure 87 is the occurrence of fibrolite in the strain shadow of the andalusite and in apparent equilibrium with andalusite. The fibrolite is strongly aligned with S_2. More work is required on this zone, but it appears to have been a high D_2 strain zone in which S_1 was more intensely folded prior to andalusite nucleation, compared to surrounding rocks. The higher strain may also have facilitated the local development of fibrolite and muscovite.

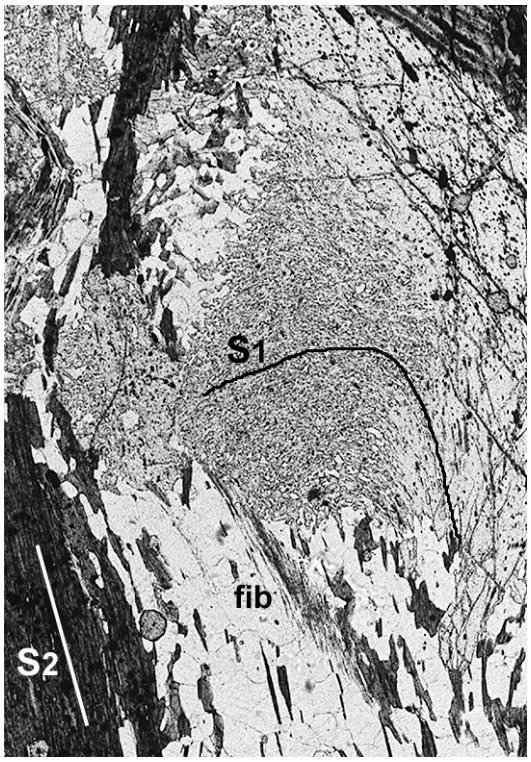


Figure 87. Rare example of curved S_1 in andalusite. In the centre, abundant quartz inclusions define a former crenulation hinge zone of the S_1 foliation. To the right, the andalusite contains many opaque inclusions, but no quartz, in the former limb zone that was presumably mica rich and quartz poor. Note the fibrolite needle cluster in the quartz below the andalusite, labelled "fib", and its parallelism to S_2. PPL. [Sample No. 517-072. Width of photograph is 3.1mm.]

The pattern of quartz inclusions in andalusite crystals of GAB(1) schist differs in many respects to those in QMA schist. For example, in GAB(1) schist the cores of andalusite porphyroblasts usually do not contain randomly oriented inclusions with an enveloping S_1 close to the porphyroblast margin, such as was described earlier for QMA schist. Nor is there any evidence of augen-like structures. In contrast, Spry (1976) described a typical sample of GAB(1) schist from South Hill, 3.5 km southeast of the Kanmantoo Mine, with unusually rich history preserved. Within the andalusite porphyroblasts are augen shaped bodies which have no S_1 and the andalusite surrounding the augen structures contains fewer but larger inclusions, including biotite grains which wrap around the augen structures. S_2 wraps around the entire porphyroblast. The porphyroblast is similar to those occurring in QMA schist near the Kanmantoo Mine but quite different to those in GAB(1) schist there. Clearly, andalusite development is not identical in the Kanmantoo district, even in the same rock type from different areas.

Garnet is a common inclusion in andalusite porphyroblasts and has quartz inclusions of its own that typically are aligned, defining S_1. However, the quartz inclusions are restricted to the cores of the crystals, the garnet rims being inclusion free, and so there is a lack of continuity of S_1 within each porphyroblast even though the traces of S_1 in each may be parallel. A further difference between garnet and andalusite porphyroblasts is that quartz inclusions in garnet tend to be smaller than those in the surrounding andalusite. Similarly, garnet inclusions in andalusite tend to be slightly smaller than garnets located in the matrix. These features also apply to garnets within GAB(2) schist, GAB(3) schist and some varieties of GBCl group lode schists, and possible explanations will be discussed in subsequent sections. In all cases S_1 within andalusite abuts the garnet rim where it stops abruptly and without apparent deviation. Commonly S_1 within garnet is parallel, or nearly so, to S_1 within andalusite.

6.4.3 The origin of internal fabrics

Three possible origins for S_1 are:

(a) a relict bedding fabric;
(b) exsolution (Ferguson and Harte (1974, page 474) or replacement of the host crystal along certain crystal planes (Vernon, 1978, page 290);
(c) a relict tectonic fabric.

Hobbs et al., (1976, page 153) state that many sediments have strong preferred orientations of layer silicates which may be mistaken for deformational microfabrics. For example, Nickelsen (1979) and Stringer and Lajtai (1979, p.2170) have described areas where the first generation tectonic foliation is a crenulation cleavage, formed from a preferred orientation of clay minerals and detrital micas, with or without recrystallisation. The best way to demonstrate that S_1 in schists from the Kanmantoo Mine area is of sedimentary origin is to compare its orientation to the orientation of sedimentary structures, such as bedding. In Figure 80, S_1 is approximately parallel to bedding, however, in many similar rocks it is not. One of the problems is that even if the fabric was originally sedimentary subsequent rotation during deformation of the andalusite grains relative to bedding would obscure its origin. It may be pertinent that Mancktelow (1979) did not report any bedding fabrics in the lower grade biotite bearing slates on the western side of the Mt Lofty Ranges.

The second alternative for the formation of S_1, that is by exsolution or preferred replacement, requires that the inclusions are oriented along certain crystallographic directions in the host mineral. This is rejected for the following reasons:

(a) S_1 has a variety of orientations with respect to the crystallographic orientation of the

host crystals and continue without deviating across the contact between differently oriented crystals of the same mineral.

(b) where garnet and staurolite occur within andalusite, S_1 continues from one mineral to the next without deviating.

(c) some inclusion trails are smoothly curved.

The third alternative involves a tectonic origin, that is S_1 represents a relict schistosity. S_1 inclusion trails in GAB(1) schists are similar to others in the Mt Lofty Ranges, and these have been ascribed by many authors to tectonic origins (eg Offler and Fleming, 1968; Daily and Milnes, 1973; Mancktelow, 1979, 1990).

Hence, the origin of S_1 is attributed to either a sedimentary or tectonic fabric. Because sedimentary fabrics are less widely known, especially in metamorphic rocks where tectonic fabrics are common, S_1 is considered more likely to be a relict schistosity.

6.4.4 The orientation of andalusite

In outcropping GAB(1) schist, in which the orientation of many andalusite crystals can be compared, a weak to moderate tendency for their long axes to be at low angles to the schistosity is apparent (Figure 88). Viewed on the schistosity plane however, the long dimensions of andalusite crystals appear to be randomly disposed (Figure 89).



Figure 88. Disposition of andalusite grains in outcrop, looking down the steep mineral lineation L_2. The pen is 145 mm long.



Figure 89. Same outcrop as Figure 88 but showing a surface approximately parallel to the mean schistosity plane. Looking east.

The traces of the long axes of the andalusite grains shown in Figure 88 are represented by the top left hand rose diagram in Figure 90. This is a plot of measurements of the angular difference between the long dimensions of andalusite crystals and a reference line which is north-south and parallel to the strike of the schistosity. Although this data does not represent the third dimension, a close relationship between andalusite orientation and the schistosity is

demonstrated. The remaining rose diagrams represent the angular differences between the long axes of andalusite prisms and a horizontal line, but measured on the schistosity plane. In particular, the top right hand rose diagram represents the rock shown in Figure 89 and the broad maximum of the plot reveals that the andalusite grains have a preferred orientation despite their random appearance. In this rock most andalusite grains plunge towards the north. Reference back to Figure 89 shows that this preferred orientation is an overall effect and not due to local zones of strongly aligned crystals.

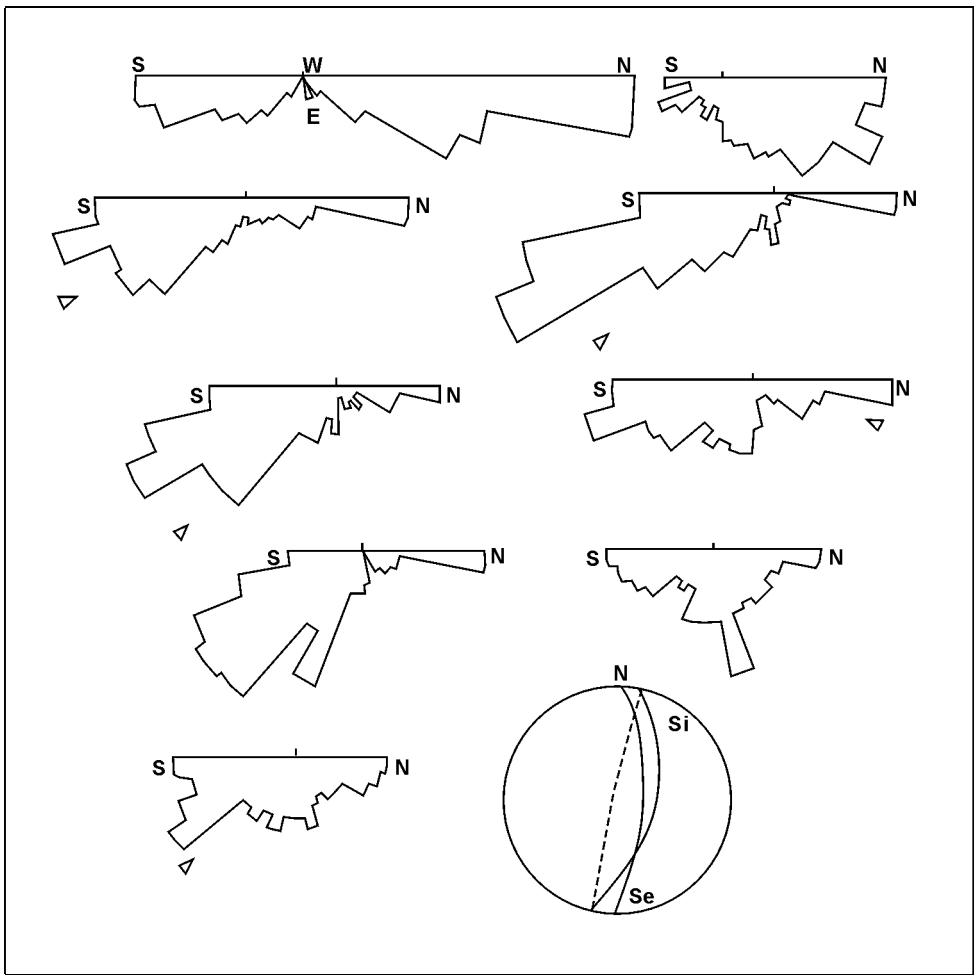


Figure 90. Rose diagrams of andalusite long axes in outcrop. Outcrops of GAB schist with large surfaces parallel to the S_2 were photographed with horizontal lines marked and the pitches of all elongate andalusite grains were measured. The north-south line N-S is horizontal. The triangle indicates the pitch of the bedding intersection where observed.

Similar rose diagrams for sections parallel to the schistosity planes of seven other rocks are also shown in Figure 90. In some cases the intersection of bedding ($L_{2/0}$) could be measured on the schistosity plane and this is represented by a small triangle beside the rose diagram. In all cases the mineral lineation ($L_{2/2}$) pitches at approximately 80 to the south. Not all of the samples have a preferred orientation of andalusite but most do. Where present, the preferred orientation is broadly defined and plunges shallowly towards the south and, although close in orientation to $L_{2/0}$ in most examples, it does not correspond exactly. In one case $L_{2/0}$ pitches towards the north whereas most andalusite long axes in the same rock pitch towards the south. Hence no clear relationship between $L_{2/0}$ and the preferred pitch of andalusite long axes is apparent, suggesting that bedding had little or no influence on the orientation of andalusite

crystals. Nor do the andalusite crystals show any relationship to $L_{2/2}$.

In the likely absence of a control by bedding, two possible explanations for the weak preferred dimensional orientation of andalusite are considered, they are:

(a) randomly oriented andalusite prisms were rotated towards the S_2 schistosity plane; or

(b) the andalusite grains grew with a preferred orientation.

It was suggested in Section 6.4.3 that, because S_1 is commonly parallel to the long axis of its host andalusite grain, the orientation of the grain at nucleation and growth was influenced by the orientation of S_1. Such a control would provide a means whereby andalusite could obtain a preferred orientation given the reasonable assumption that the precursor to the current expression of S_1 was regular in orientation at least on the scale of an andalusite crystal (up to 2cm). Assuming that the attitude of andalusite crystals was influenced by S_1, and having measured the attitude of S_2, one could estimate the line of intersection between S_1 and S_2 if the attitude of S_1 was known. Unfortunately, it is not, but Mancktelow's (1979) regional observations may be useful here. He noted that his first schistosity had a strike of 10 to 30 more east of north than his second schistosity. Furthermore, the dips of the first schistosity are 10 to 30 shallower than the second.

This situation is represented by the stereoscopic diagram at the base of Figure 89, where an assumed average orientation for S_1 of 010/70E has been used, and for S_2 the known average of 000/70E. The interesting result indicated by this figure is that the line of intersection of the two planes plunges shallowly towards the south, similar to the maxima in the rose diagrams discussed previously. Hence it may explain these weak preferred orientations. They may be weak because the long axes of the andalusite prisms may be randomly arranged in S_1 and also many may be discordant to S_1. The few northerly plunging preferred orientations of andalusite may have been caused by non-parallelism of the precursor version of S_1, for example by fanning of cleavage, which resulted in some steep S_1 planes, as shown in the stereographic diagram (dashed line).

Therefore, of the two possible explanations that were proposed above for the observed preferred orientation of andalusite crystals in GAB(1) schist, the latter is favoured, that is that andalusite grew with a preferred orientation, specifically within the plane of S_1 which was close in attitude to S_2. But there is evidence also that the crystals rotated after growth. An example is shown in Figure 86 which is a sketch of a thin section of GAB(1) schist with many prismatic andalusite porphyroblasts. This figure shows lengthwise sections (e.g. at the point labelled B) and basal sections (e.g. at the point labelled A) of the andalusite grains. Grains labelled C and C' in the figure are connected by a quartz rich zone and appear to have behaved effectively as a single, elongated grain. All grains have well preserved S_1 which is constant in trend within each grain but varies between them. S_1 in the basal section (at A) is intermediate in trend between that in grains B and C + C', which have their longest dimension slightly oblique to the average trend of S_2 in the section (e.g. at point M). Although S_2 wraps around the porphyroblasts, it also abuts them. Furthermore, along the lower left hand margin of the composite andalusite grain shown in Figure 84 S_1 is locally continuous with S_2. At the ends of some crystals are asymmetrical, drag-type structures in the matrix and on the margin of the strain shadows. This is well developed beside grain B in Figure 86 and shown in detail in Figure 85.

The observations described above are consistent with the flattening of S_2 about rigid andalusite porphyroblasts, accompanied by mechanical rotation of the porphyroblasts, in the manner described by Ramsay (1962, page 323). It is proposed that andalusite grew in a schistose matrix of probable tectonic origin during D_1. Figure 91a represents this stage, with

one basal and two longitudinal sections of andalusite shown. Progressive flattening followed, with the axis of compressive stress at a high angle to the initial foliation, but not strictly perpendicular. The flattening event could have been either a separate event to that which produced S_1, in which case the deformation could have resulted from bulk pure shear. Or the flattening could have been part of a continuous deformation, providing that porphyroblast growth was relatively rapid compared to the strain rate (Fyfe, 1976). The latter process requires a rotational component to the progressive strain and so general non-coaxial shear is necessary (Hanmer and Passchier, 1991). Figure 91b represents the plane normal to the extension direction after 50% flattening and with an initial angle between the traces of the schistosity and the plane of flattening of 30 . The crystals with elongated sections (together with their S_1) are rotated towards the flattening plane, the sense of rotation depending of their original disposition. Figure 91b is directly comparable with Figure 86, and the processes described above may explain the microstructure of this rock and others like it. Presumably, grain A did not rotate much but grains C + C' rotated clockwise and grain B rotated anticlockwise.

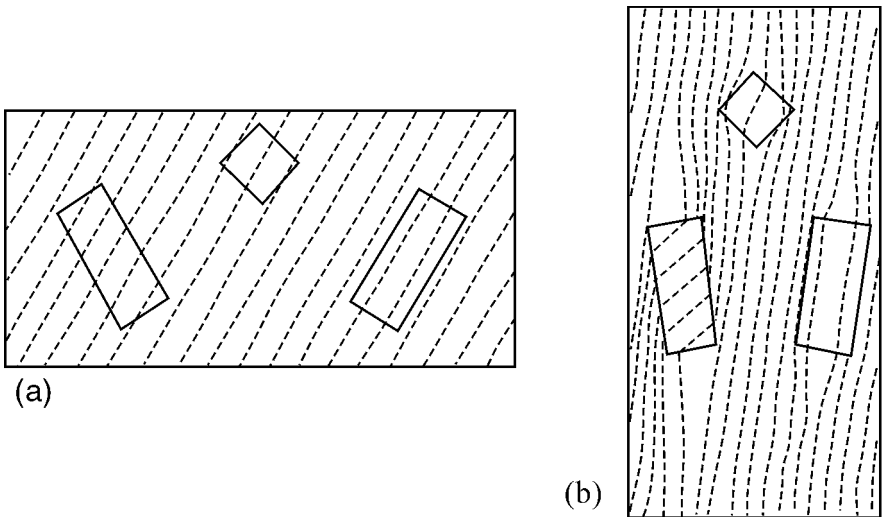


Figure 91. Sketch showing the effect of 50% flattening (pure shear, plane strain) on the external (Se) and internal (Si) fabrics of a foliation. Se developed by syn-deformational recrystallisation of Si. Porphyroblasts have rotated with the matrix. The long axes of two andalusite crystals are parallel to the page and a third is at right angles. The initial foliation in (a) is at 70º to the axis of flattening. Compare this drawing with Figures 84, 85 and 86.

If the features in this example are due to passive rotation of porphyroblasts and matrix during flattening, then it is possible to estimate, from the variations in trend of S_1 shown in Figure 86, that the apparent rotations of both B and C + C' were about 25º and that the apparent angle between S_1 originally and S_2 presently was about 30º. It appears that not all andalusites rotated passively with the matrix. Some porphyroblasts rotated, in the same overall sense, relative to the matrix, producing the drag-like structures referred to above. An important conclusion is that S_2 could have been derived from S_1 simply by rotation during bulk flattening and recrystallisation to produce a coarser matrix without involving crenulation cleavage. This subject is considered further at the end of the chapter.

In summary, the long axes of andalusite prisms are not randomly orientated. Their tendency for parallelism to S_2 as observed in many outcrops of GAB(1) schist, is considered to be due to their preferred growth within S_1 and an initial low angle between S_1 and S_2. Rotation of andalusite and S_1 during the development of S_2 is indicated and the relative amounts of strain associated with S_1 and S_2 are unknown. Because the andalusite porphyroblasts were probably

not randomly orientated initially they cannot be used as a strain gauge without further information and the uncertain amounts of non-passive rotation of andalusite would also complicate any strain calculations.

6.4.5 The sequence of mineral growth

Several techniques can be used to deduce the relative ages of co-existing minerals from observations of thin sections. These include overgrowth of one mineral by another, relationships of minerals to tectonic fabrics and, to some extent, grain size of inclusions. Each of these methods must be applied with care and it should be remembered that each (apparent) phase of porphyroblast growth will involve many other minerals and perhaps the whole rock, in the chemical reaction producing it (Vernon, 1976). In this section the possible changes in the matrix of GAB(1) schist will be discussed first, followed by porphyroblast development.

Although there are many complicating factors, it is a common observation that the grain size of meta-pelites, in both regional (e.g. Binns, 1964, Kretz, 1994) and contact (e.g. French, 1968) metamorphic settings, tends to increase with increasing metamorphic grade. The common occurrence of inclusions in porphyroblasts that are smaller than the same minerals in the matrix has usually been interpreted as recording a trend of increasing matrix grain size within single rocks, (Rast, 1958; Harte and Johnson, 1969). This also seems to be the case for the rocks of the Kanmantoo Mine area where for example, quartz grains within andalusite are smaller than matrix quartz grains. As a rule, there does not appear to be a significant zoning in the grain size of quartz inclusions and this may indicate that the prophyroblast grew much faster than the rate of change of the matrix quartz grain size.

However, in some cases, both for GAB(1) schist and GAB(3) schist, the quartz inclusions appear to increase in grain size towards the porphyroblast margin, apparently recording growth of andalusite during a period of increasing matrix grain size. This is illustrated, to some extent, for GAB(1) schist in Figure 5.4b and much better in Figure 5.11c, for GAB(3) schist, in which it seems to be more common. The quartz inclusions are not optically continuous and so do not represent replacement of one or more larger grains (Vernon, 1978, page 293).

Because the quartz inclusions in andalusite are approximately the same size (about 0.05mm) in all samples of GAB(1) schist and furthermore, are also approximately the same size in andalusites in QMA schist and GAB(3) schist it seems likely that, in all these rocks, andalusite grew at the same stage during matrix grain size increase. In addition, they appear to have grown rapidly compared to the grain size change.

Garnets are included in andalusite and so presumably pre-date andalusite growth. Many garnet inclusions contain a few quartz inclusions in their cores, but typically the rims are inclusion free. The inclusion of one mineral (A) in another (B) occurs when mineral B grows at a faster rate than mineral A can diffuse away from the site of growth (Vernon, 1976, page 145). Given slower growth rates of B it may not contain inclusions. Thus evidence of different growth rates in one mineral may be revealed by its inclusion pattern. Therefore, in the garnets from GAB(1) schist of the Kanmantoo Mine area, the garnet cores are inferred to have grown more rapidly than the rims and so did not allow the included minerals to diffuse from the growth site until the presumed slower growth during rim formation.

The following growth sequence is proposed for garnet and andalusite. Prior to porphyroblast growth a fine grained schist, phyllite or slate formed. Subsequently, garnet grew, initially rapidly so that quartz inclusions were trapped but later more slowly. Then andalusite grew, relatively rapidly throughout for it contains many inclusions of approximately the same size.

Because garnet crystals in the matrix tend to be slightly coarser than the included garnets they possibly continued to grow, perhaps as part of the andalusite-producing reaction. Vernon (1976) noted that an included mineral may have nucleated at the same time as its host but because the host grew more rapidly, it covered the included mineral and so prevented its further development. Although this is possible for garnet and andalusite in GAB(1) schist it seems unlikely because, unlike andalusite, garnet has evidence inferring different rates of growth and it is the initial growth phase that was more rapid.

In GAB(1) schist, staurolite and sillimanite (as fibrolite) occur in the matrix and neither has been observed as an inclusion in andalusite or garnet. Staurolite tends to form inclusion-free, idioblastic crystals within biotite of M domains, features that are consistent with its growth after the formation of the domains. This deduction is based mainly on the observation that porphyroblasts of the Kanmantoo Mine area occurring within a quartz free matrix also have no quartz inclusions. Similarly, those porphyroblasts in a quartzose matrix have quartz inclusions and the grain size of the inclusions is typically similar to the size of the matrix quartz grains. The exact stage of staurolite growth, however, is difficult to deduce in most examples of GAB(1) schist. A possible exception is shown in Figure 92.



Figure 92. GAB(1) schist with staurolite. Porphyroblasts of garnet (g), staurolite (s), and part of a quartz rich andalusite poikiloblast (a, lower left corner) occur in a matrix with Q and M domains. Note that the staurolite is idioblastic against biotite but terminates abruptly against the quartz in the Q domain. Refer to text for a discussion. PPL. [M.E.P.L. Sample No. 5796, from hole KS31, 493.8m depth. Width of photograph is 1.9mm.]

The important features shown in Figure 92 are as follows:

1. The twinned staurolite crystal is almost completely confined to the M domain except for a small extension that appears to follow a narrow biotite zone in the Q domain.

2. The staurolite margin is idioblastic within the M domain but irregular against the quartz grains in the Q domain.

3. The staurolite has no quartz inclusions similar to the surrounding M domain,.

There are two possible explanations for this microstructure. Firstly, that staurolite grew after the domains formed by replacing biotite and secondly, that staurolite growth predated domain formation and was partly removed from the Q domain during its formation. The second possibility seems less likely because the staurolite appears to be related to the biotite zone in

the Q domain and also no "undigested remants" of staurolite in Q domains have been observed in other GAB(1) schists. Therefore, staurolite in GAB(1) schist is inferred to postdate domain formation, unlike andalusite. Relatively late formation of some (not all) staurolite has occurred in other rock types too. This is discussed later and is in agreement with Lindqvist's (1969, page 72) interpretation of the time of staurolite growth in lode rocks.

Sillimanite is uncommon in the Kanmantoo Mine area. It occurs as fibrolite needles parallel to S_2 within quartz of Q domains or, less commonly, within quartz and biotite of M domains. Figures 87 illustrates the first case. The second case is very common in GAB(1) schist from the Wheal Ellen Mine and South Hill (Spry, 1976) but not near the Kanmantoo Mine. Sillimanite is not parallel to S_1. Its parallelism with S_2 indicates that it most likely formed during the development of S_2 and this stage appears to correspond to the peak metamorphic temperature (Schiller, 1978; Mancktelow, 1979).

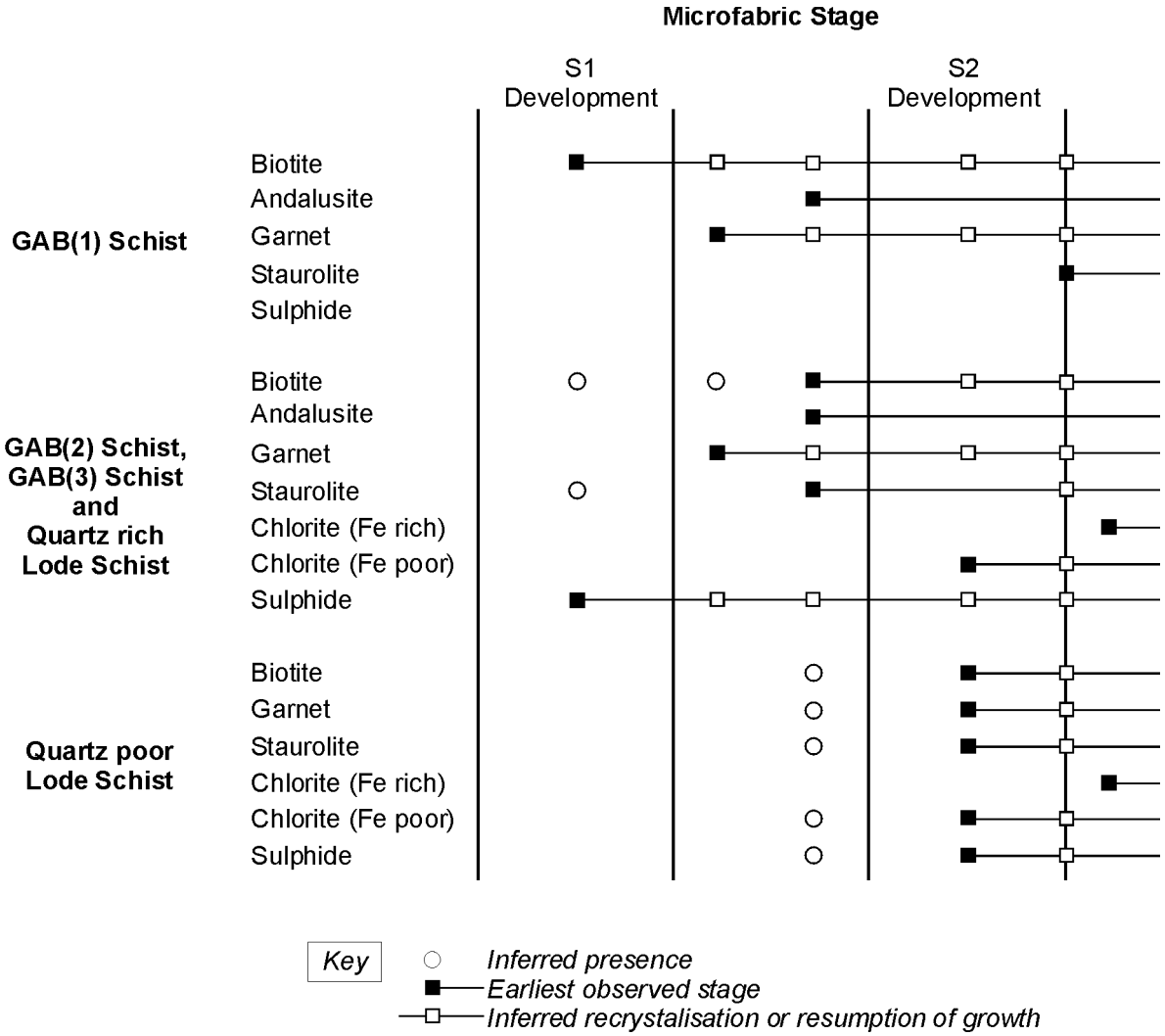


Figure 93. Diagram showing the inferred sequence of mineral growth for various lithologies.

The overall interpretation of grain growth in GAB(1) schist will now be summarised (see Figure 93). The earliest preserved feature, apart from bedding, is S_1 in garnet. It probably represents a relict schistosity but may be a sedimentary fabric instead. Next, a garnet producing reaction or reactions occurred, such that garnets grew rapidly initially but then more slowly. Next, an andalusite producing reaction occurred. While andalusite and garnet were forming the deformation responsible for the formation of S_1 may have been continuing, however, it produced few crenulations in S_1. Once andalusite was present, domains began to develop accompanied by rotation of the matrix schistosity and then a staurolite producing

reaction occurred. Because garnets in the matrix are coarser than those included in andalusite, continuous or resumed garnet growth subsequent to or during andalusite growth seems likely and it may be part of the reactions that produced andalusite and staurolite.

Staurolite formation seems to have involved biotite as a reactant and it is likely that biotite participated also in many or all of the other reactions forming porphyroblasts. Like quartz, biotite probably increased in grain size from the S_1 stage to the present S_2 stage in the same manner that mica grain size tends to increase with metamorphic grade. A history of continual or episodic recrystallisation seems likely for biotite.

6.5 GAB(2) schist

GAB(1) schist and GAB(2) schist are mineralogically very similar, it is primarily microstructural differences which distinguish them. The microstructural changes are easily visible in hand specimens. GAB(2) schists are transitional with GAB(1) schists and encompass a range of lithologies from rocks similar to GAB(1) schist to a rock which might be considered to be the ideal, typical GAB(2) schist. This in turn is transitional with GAB(3) schist. The transition from GAB(1) schist to the typical GAB(2) schist is illustrated in Figure 94b,c. Note especially the diminished domainal development and the change in biotite shape to less elongate. Figure 94d shows GAB(3) schist and here the biotite grains are even more equant. Thus, there is a microstructural transition from GAB(1) schist to GAB(3) schist, with GAB(2) schist intermediate between the two.

Figure 94 (following page). Micrographs of GAB schist varieties.

(a). GAB(1) schist with strongly schistose matrix and well developed domains and strain caps adjacent to andalusite poikiloblasts (labelled A) and quartz rich pods between andalusite (labelled Q). A weak S_1 within andalusite is parallel to S_2. [Sample No. 517-149. Photo width is 16.1mm]

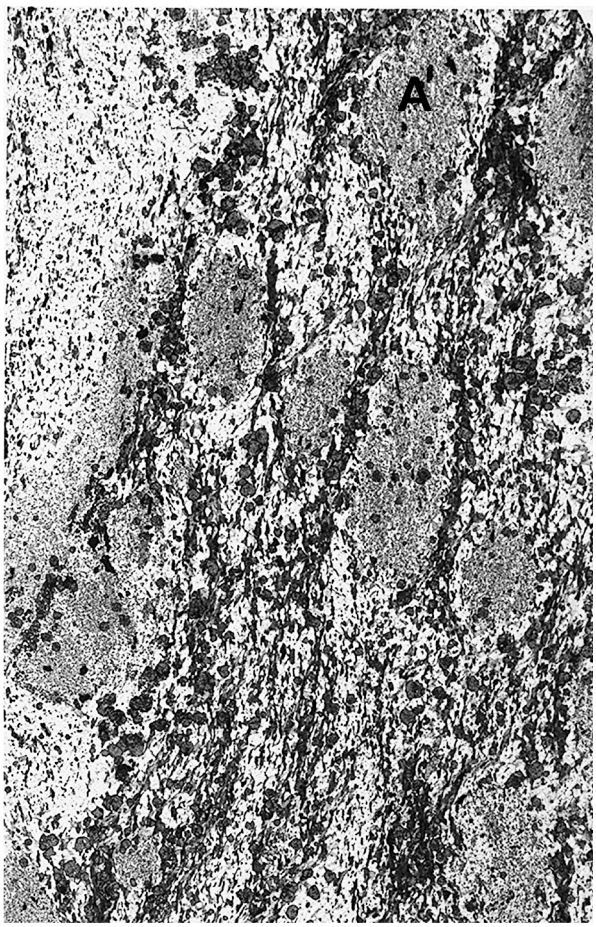
(b). Transitional example between GAB(1) and GAB(2) schists. It has a weaker, speckled, matrix schistosity, and strain caps but no domains. Andalusite (A) has relatively low inclusion content like GAB (1) schist. A weak S_1 is parallel to S_2. [Sample No. 517-148. Photo width is 16.1mm]

(c). GAB(2) schist showing typical weak matrix schistosity. However, unlike a typical GAB(2) schist, this example has some M domainal development and, like (b), the andalusite has relatively low inclusion content. A weak S_1 is parallel to S_2. [Sample No. 517-147. Photo width is 16.3mm].

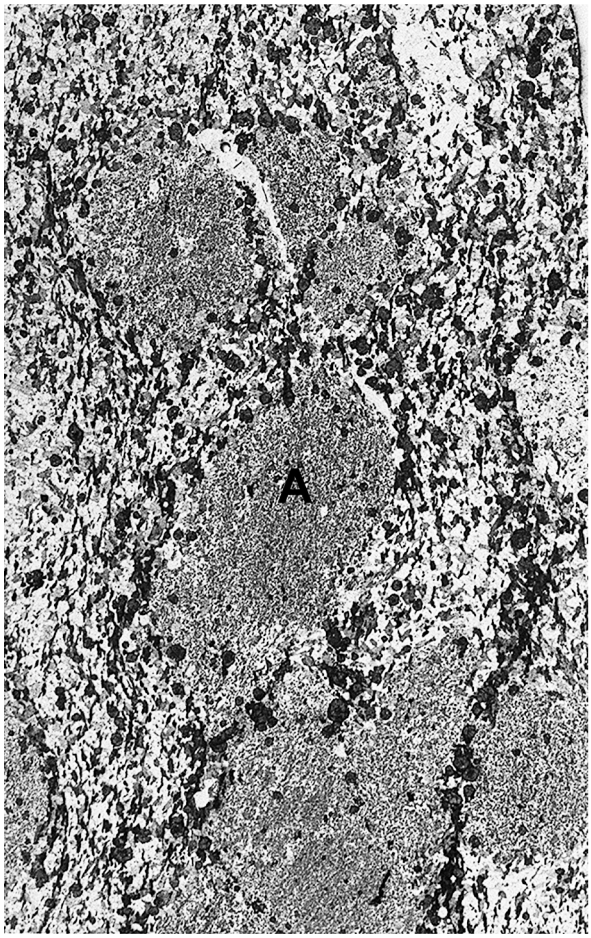
(d). GAB(3) schist with typical clotty texture resulting from the equant biotites. There is no domain development or matrix schistosity. Note the folded quartz vein (Qv) in the upper left corner. [Sample No. 517- 143. Photo width is 7.1mm]



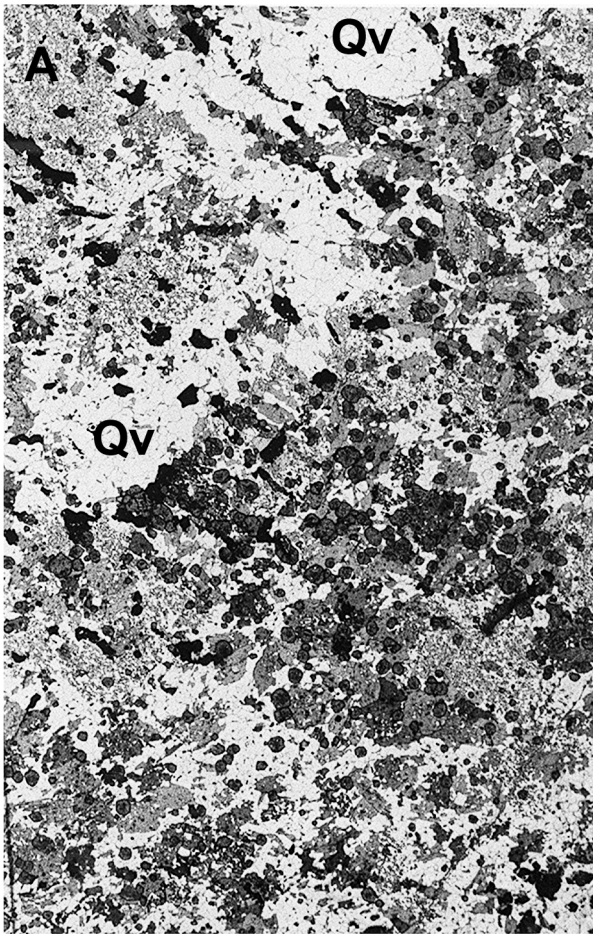
a



b



c



d

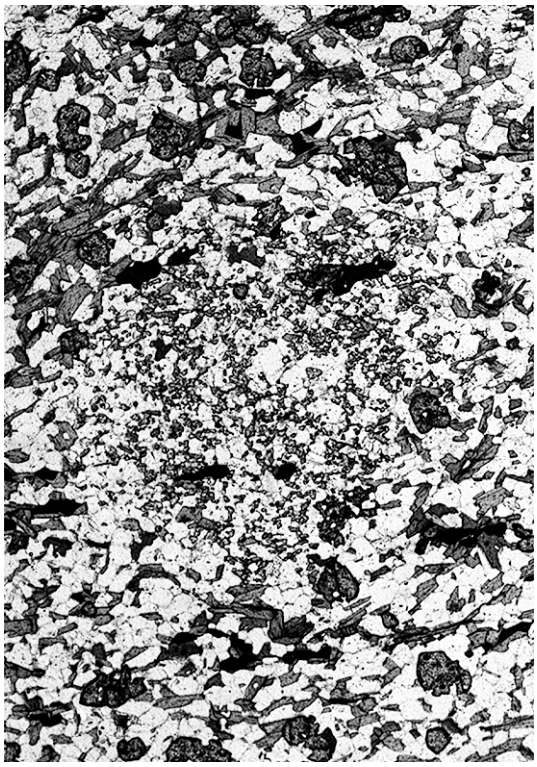


Figure 95. GAB(2) schist with typical andalusite porphyroblast containing a high proportion of quartz inclusions that do not define an internal fabric. Opaque inclusions however, define an internal fabric parallel to the weakly developed S_2 schistosity in the matrix, trending left to right. [Sample No. 517-141. Photo width is 4.2mm].



Figure 96. Two garnet inclusions within an andalusite poikiloblast. Quartz and coarser opaques (chalcopyrite-pyrrhotite) define S_1 common to both garnet and andalusite. [Sample No. 517-141. Photo width is 0.35mm].

In comparison with GAB(1) schist the typical GAB(2) schist has the following differences:

(a) The matrix has no, or weak, domainal development, even near andalusite (Figure 94c).

(b) Andalusite porphyroblasts in GAB(2) schist are typically round or elliptical, rarely are they idioblastic, and most have a much higher quartz:andalusite ratio than those in GAB(1) schist (Figure 95). S_1 is usually indistinct or not present.

(c) Sulphide minerals are much more common in GAB(2) schist than GAB(1) schist. They occur both within the matrix and the porphyroblasts (Figure 96).

(d) Although GAB(2) schist contains a schistosity and mineral lineation, both tend to be weakly developed. This is due to the shape and low degree of preferred orientation of biotite. When mapped in the mine these rocks were often described as weakly schistose, or speckled, rather than the schistose description typical of GAB(1) schist. Figures 97a, b show measurements for biotite grain shape and orientation for a typical GAB(2) schist specimen, viewed in a section cut perpendicular to the mineral lineation. Figure 97a demonstrates a wide range of both lengths and aspect ratios, with no apparent relationship between the two. The average of the 98 aspect ratio measurements is 3.7 (standard deviation =2.4) whereas the measurements for the typical GAB(1) schist specimen, shown in Figure 81, have a mean of 5.3 (standard

deviation = 3.2, 100 measurements from both domains). This confirms that biotite grains in GAB(2) schist tend to be less elongated than those in GAB(1) schist, a feature obvious in hand specimens and thin section.

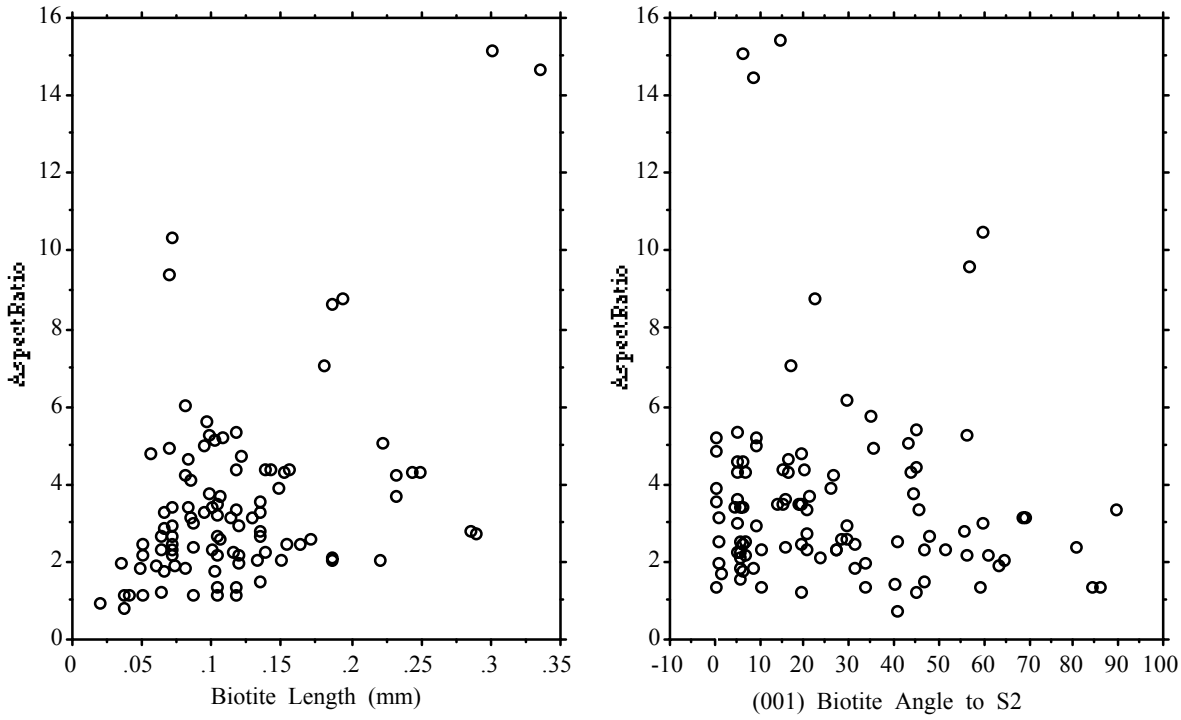


Figure 97. Graphs of aspect ratios of biotite in GAB(2) schist.

Figure 97b shows that the traces of (001) planes of biotite in a GAB(2) schist sample are extremely variable, but have a weak tendency to occur at a low angle to the visually estimated average trend, used as a reference line. Comparison with similar measurements but in GAB(1) schist, shown in Figure 83 reveals that biotite grains in GAB(2) schist have similar indicated preferred orientations to those in Q domains but seem to be much weaker than M domains. Therefore, biotite grains in GAB(2) schist tend to be less elongated and less aligned than biotite grains in GAB(1) schist.

6.6 GAB(3) Schist

6.6.1 Description of S_1 and S_2

The microfabric of GAB(3) schist is characterised by coarse, equant and apparently random biotite and andalusite grains. Superficially, the microstructure resembles those formed by thermal metamorphism of pelites and the matrix is typically not domainal and in many cases does not contain S_1. Where present, S_2 is defined by relatively fine-grained (0.3mm) chlorite and sulphide minerals, or less commonly by either muscovite or a weak preferred orientation of biotite, especially the finer grained biotites. In many samples, S_2 is defined by a combination of biotite and chlorite (but not muscovite and chlorite) and commonly is deflected around porphyroblasts. S_1 is prominent in most porphyroblastic minerals including andalusite, garnet, staurolite, and, unlike any other local rock, biotite. However, in andalusite with a high proportion of quartz inclusions (greater than 50% say), S_1 is weak or absent. Quartz and sulphide minerals are the most common inclusions in all porphyroblasts. Although the grain size of the inclusions is similar in most porphyroblasts there is a tendency for the grain size to decrease in the following order: biotite > andalusite=staurolite > garnet. This trend possibly records a corresponding change in matrix grain size during porphyroblast growth, so may reflect the order in which the portions of the

porphyroblasts containing inclusions grew.

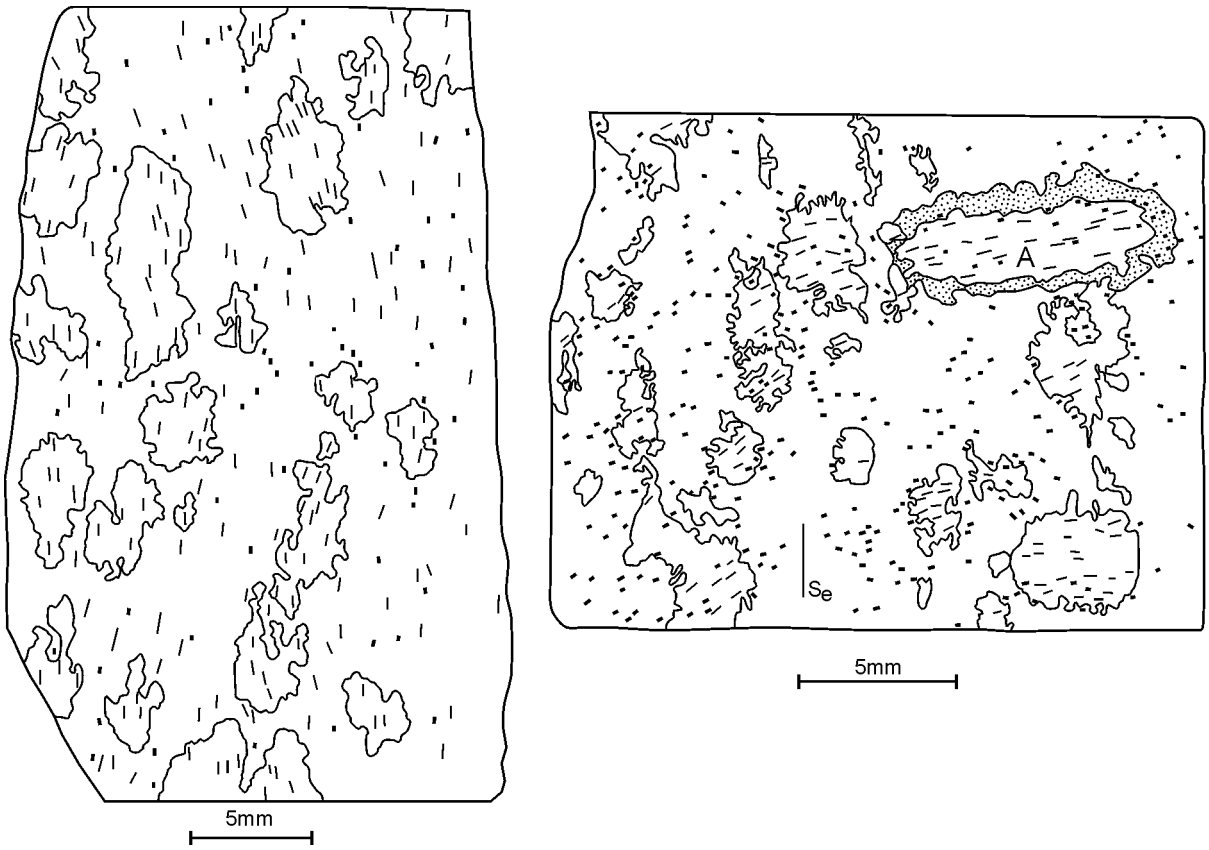
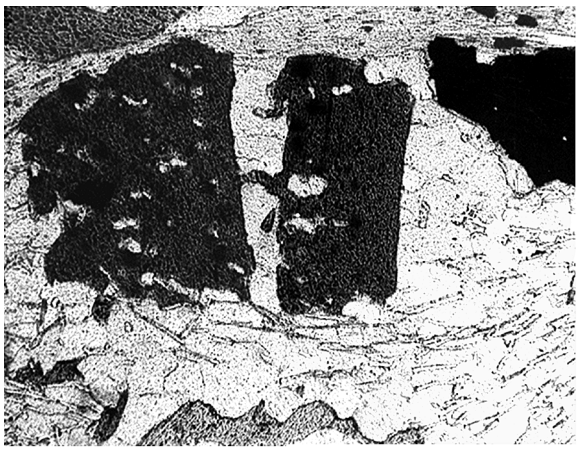
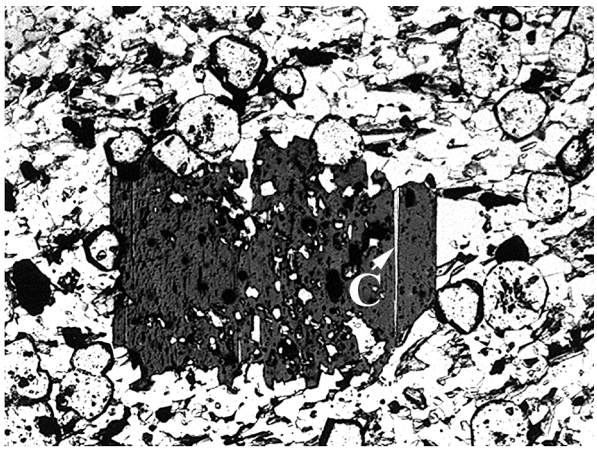


Figure 98. Drawings of thin sections of GAB(3) schist. (a). Example with S_1 parallel to S_2 in andalusite and garnet. S_2 is poorly developed in the quartz-chlorite-(garnet) matrix. The long dashes indicate S_1 in andalusite and S_2 in the matrix. [Sample No. 517- 044. Perpendicular to S_2 and $L_{2/2}$.] (b). Another example with S_1 highly discordant to S_2. All porphyroblasts shown are biotite except that labelled A, which is andalusite with a chlorite corona (stippled). The trend of S_2 is constant across the thin section and is shown. The dashed lines represent S_1 in biotite and the thick short lines represent S_1 in garnet. [Sample No. 517- 049. Perpendicular to S_2.]

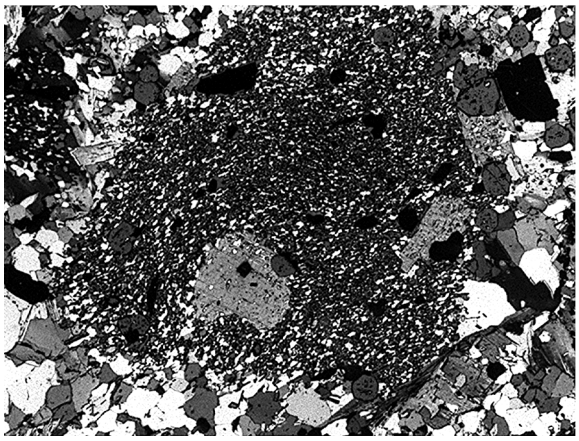
In general, relationships between S_1 and S_2 in GAB(3) schist are similar to those in GAB(1) schist. One important difference, however, is that in GAB(3) schist, S_1 in many porphyroblasts is commonly constant in trend throughout a whole thin-section, irrespective of the angle between S_1 and S_2. Furthermore, the parallel trend in S_1 applies to co-existing andalusite, biotite and garnet. Figure 98a shows a slightly wavy S_1 in andalusite and garnet parallel to one another and to S_2. Figure 98b, however, shows S_2 (trending from top to bottom in the diagram) at a high angle to S_1. Throughout the thin section S_1 defines a regular gentle curve in andalusite, garnet and biotite. S_2 is constant in trend across the thin section, perhaps axial planar to a fold in S_1. Note that S_1 is parallel to the long axes of andalusite porphyroblasts in both Figures 98a, b. Any theory to account for the origin of this feature must allow S_2 to develop such that the porphyroblasts are not significantly rotated relative to one another. In the case where S_1 is parallel to S_2 a continuous development of S_2 from S_1 could explain it. If the deformation was non-coaxial then the andalusite grains presumably rotated passively with the developing S_2 fabric. It is a little harder to explain the case where S_1 is consistently highly discordant to S_2. This is discussed further later.



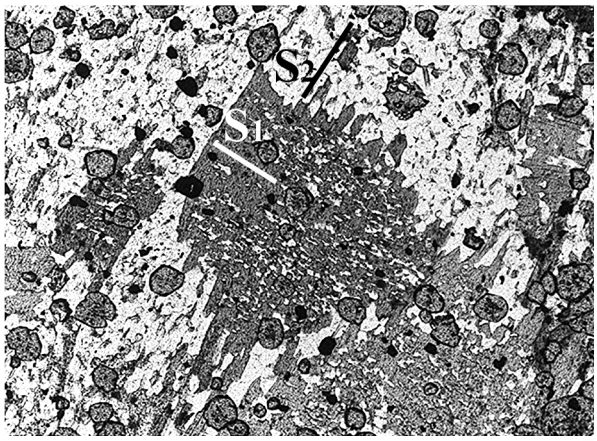
a



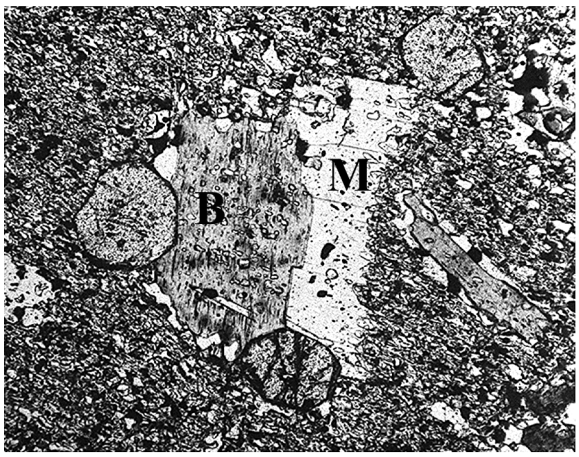
b



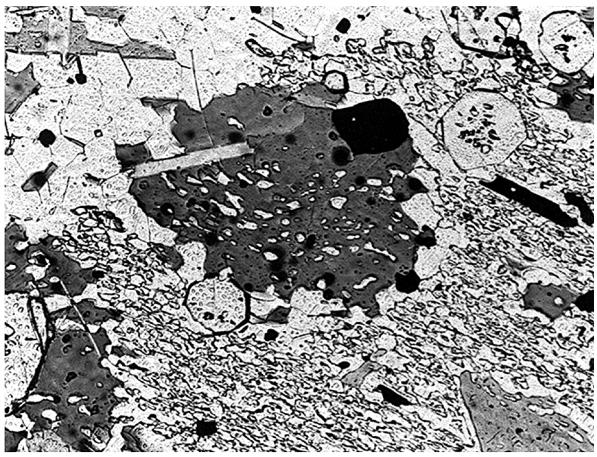
c



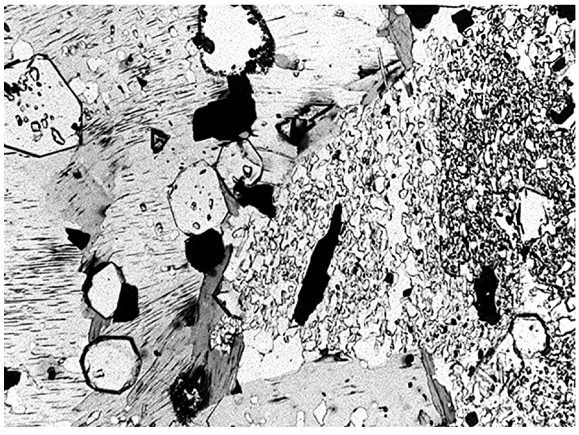
d



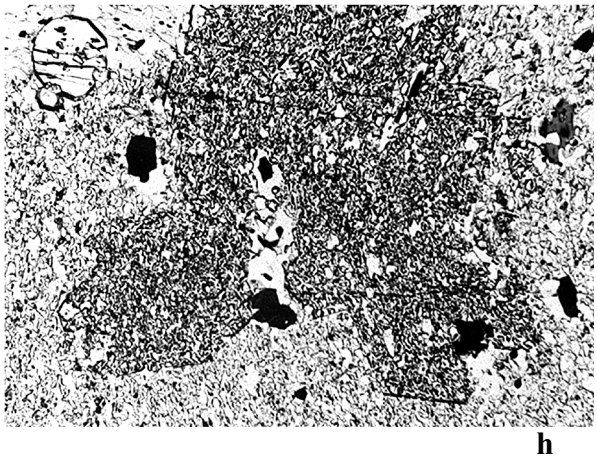
e



f



g



h

Figure 99. Microstructures of GAB(3) schist (previous page).
(a) Biotite grain separated on its (001) plane with quartz and biotite fill and enclosed by S_2 defined by a quartz-muscovite assemblage. [PPL. Sample No. 517-129. Photo length is 1.7mm.]
(b) Biotite grain separated on its (001) plane with chlorite (C) wedge. [PPL. Sample No. 517-049. Photo length is 4.9mm.]
(c) Andalusite grain with inclusions of quartz, biotite, garnet and opaques and S_1 suggestive of wrapping around the biotite inclusion. [XPL. Sample No. 517-130. Photo length is 2.8mm.]
(d) Biotite porphyroblast with ragged extensions parallel to the (001) plane and to S_2. S_1 in biotite is perpendicular to S_2. [Cross polars. Sample No. 517-049. Photo length is 5.1mm.]
(e) Composite biotite(B)-muscovite(M) grain with apparent equilibrium grain boundaries, within andalusite. [PPL. Sample No. 517-130. Photo length is 2.3mm.]
(f) Biotite grain with sinuous S_1 trail. The cross-cutting grain on the left is chlorite. Biotite is surrounded on right by andalusite poikilioblast. [PPL. Sample No. 517-067. Photo length is 2.5mm.]
(g) Biotite grain at left with kinks. Andalusite and staurolite poikiloblasts at right with S_1 defined by quartz grains, aggregates and by coarse sulphides. [PPL. Sample No. 517-067. Photo length is 2.1mm.]
(h) Staurolite (darker, central) surrounded by andalusite (lighter), both with numerous quartz inclusions defining a continuous S_1. [PPL. Sample No. 517-130. Photo length is 2.4mm.]

6.6.2 Andalusite and biotite

Andalusite is usually irregular in shape, perhaps elongate, with irregular margins. Quartz inclusions in most andalusite porphyroblasts are elongate and evenly distributed, as in GAB(1) schist, suggesting again that andalusite grew in a fine grained, schistose rock. In some cases there is a suggestion of slight increase in inclusion grain size from core to rim.

Amongst rocks of the Kanmantoo Mine area the microstructure of biotite is one of the unique features of GAB(3) schists. The equant shapes of biotite contrast strongly with the elongate biotite of GAB(1) schist, and many GAB(2) schists too. In addition, there are exposures in the Kanmantoo Mine where the transition from GAB(2) schist to GAB(3) schist can be studied. The most obvious change is a transition from the "speckled" appearance of GAB(2) schist, with smaller biotite grains, to a "clotty" appearance in GAB(3) schist, with much coarser biotite. Corresponding to this change is a noticeable decrease in the strength of the schistosity defined by biotite. These features are illustrated in Figure 94c, d. Biotite shapes in GAB(3) schist are similar to those formed during metamorphism in a static environment (for example, Plate XIV(a) in Spry, 1969; Yardley et al.,1990).

The relative time of growth of the biotite porphyroblasts is not clear. Some relevant observations are that the biotite porphyroblasts contain S_1 and that S_2 wraps around them (Figure 99a). These features apply to andalusite too, and so its relative age appears to be similar to andalusite. However, Lindqvist (1969, page 71) has interpreted these biotites to be "post-tectonic", replacing poikiloblastic andalusites and inheriting part of their quartz inclusion patterns. No doubt he was influenced in this interpretation by a common lack of apparent association of the biotite porphyroblasts with deformation and by the fact that some biotite porphyroblasts occur within or beside andalusite (Figures 99c, f).

An alternative interpretation for the origin of biotite porphyroblasts and one considered more plausible is that biotite, like andalusite, grew in the period between the tectonic stages represented by S_1 and S_2. Several reasons are given below and while none of them are proof they are consistent with pre-S_2 growth of biotite.

(a) No obvious replacement microstructures by biotite have been observed. Biotite grains

do not rim andalusite (unlike chlorite), nor are they preferentially associated with it.

b) Replacement of andalusite by biotite has not been observed in other rocks in the Kanmantoo Mine area.

(c) Some biotite porphyroblasts exhibit apparent micro-boudinage structures with the gap filled by quartz (Figure 99a) or chlorite (Figure 99b). The separation plane is (001) of biotite and S_2 wraps around the porphyroblast. This microstructure has not been observed in any other local rocks, including those where S_2 wraps andalusite porphyroblasts. Microstructures similar to these were described by Vernon and Flood (1979) for phyllites and metasandstones from the Hill End Trough. There, biotite porphyroblasts were concluded to be syn-deformational and grew after a slaty cleavage formed but were deformed by the late stages of the same event. Vernon and Flood suggest that the biotite porphyroblasts started to grow during a period of only mild strain. Prior (1987) also described phyllites with syntectonic biotite porphyroblasts flanked by discrete cleavages that had dissolved some of the biotite grains. This has not been observed in GAB schist.

(d) No independent evidence, such as other reaction products, of a late stage biotite producing reaction has been observed.

It is concluded that the biotite porphyroblasts in GAB(3) schist pre-date S_2 and post-date S_1. Some evidence suggests that biotite growth continued during S_2 formation, and a good example is shown in Figure 99d. In this rock, those biotite porphyroblasts with (001) planes subparallel to S_2 have extensions parallel to S_2 on their margins. Biotite grains in the same rock, and others, with (001) planes oblique to S_2 do not have these extensions (Figure 99b).

Despite the apparent growth of biotite prior to S_2 development, and perhaps during it, there is little evidence of severe intra-crystalline deformation, although undulose extinction is common and some kinking occurs (Figure 99g). It is possible that the biotite clots deformed by slip on the (001) plane, without leaving any apparent intracrystalline evidence of having done so. Where this has been described by other authors (e.g. Mancktelow, 1979) two changes occur: (a) rhomb-like or lens-like biotite shapes are commonly produced and (b) the (001) plane rotates towards a plane normal to the maximum principal stress.

Rhomb-like biotite shapes are rare. Some effort was directed to seeking evidence of the second effect mentioned above by comparing the traces of (001) planes of biotite porphyroblasts with S_2. Angles between (001) planes and a reference line, set approximately parallel to S_2 were measured in thin sections. Presumably, S_2 was almost perpendicular to the maximum principal stress and it will be assumed that the mineral lineation in S_2 represents the direction of maximum elongation during S_2 formation. Two samples were chosen with distinct S_2 and mineral lineation and, in addition, contained many biotite porphyroblasts. In both samples S_1 traces in garnet, andalusite and biotite vary little throughout the thin sections used; in the first sample (517-047) the mean S_1 trend is only slightly oblique to S_2 but in the second sample (517-049) it is at a high angle.

The angles between (001) traces of biotite and the trace of S_2, as measured from a section cut parallel to the mineral lineation and perpendicular to S_2 of the first sample, are shown in histogram form in Figure 100b. This reveals a large range of values but with a broad peak corresponding approximately to the trace of S_2. If the mineral lineation is the direction of maximum extension this section should reveal any tendency for the (001) planes to be distributed about S_2. As a check, similar measurements from a section perpendicular to the mineral lineation were taken and Figure 100c shows that they have an apparently irregular distribution. Therefore, this rock appears to have either no relationship, or a very weak

relationship, between the (001) planes of biotite and S_2. A similar relationship in the second sample is shown in Figure 100d for measurements from a section parallel to the lineation and perpendicular to S_2. However, this distribution has a broad peak between 0º and –90º.

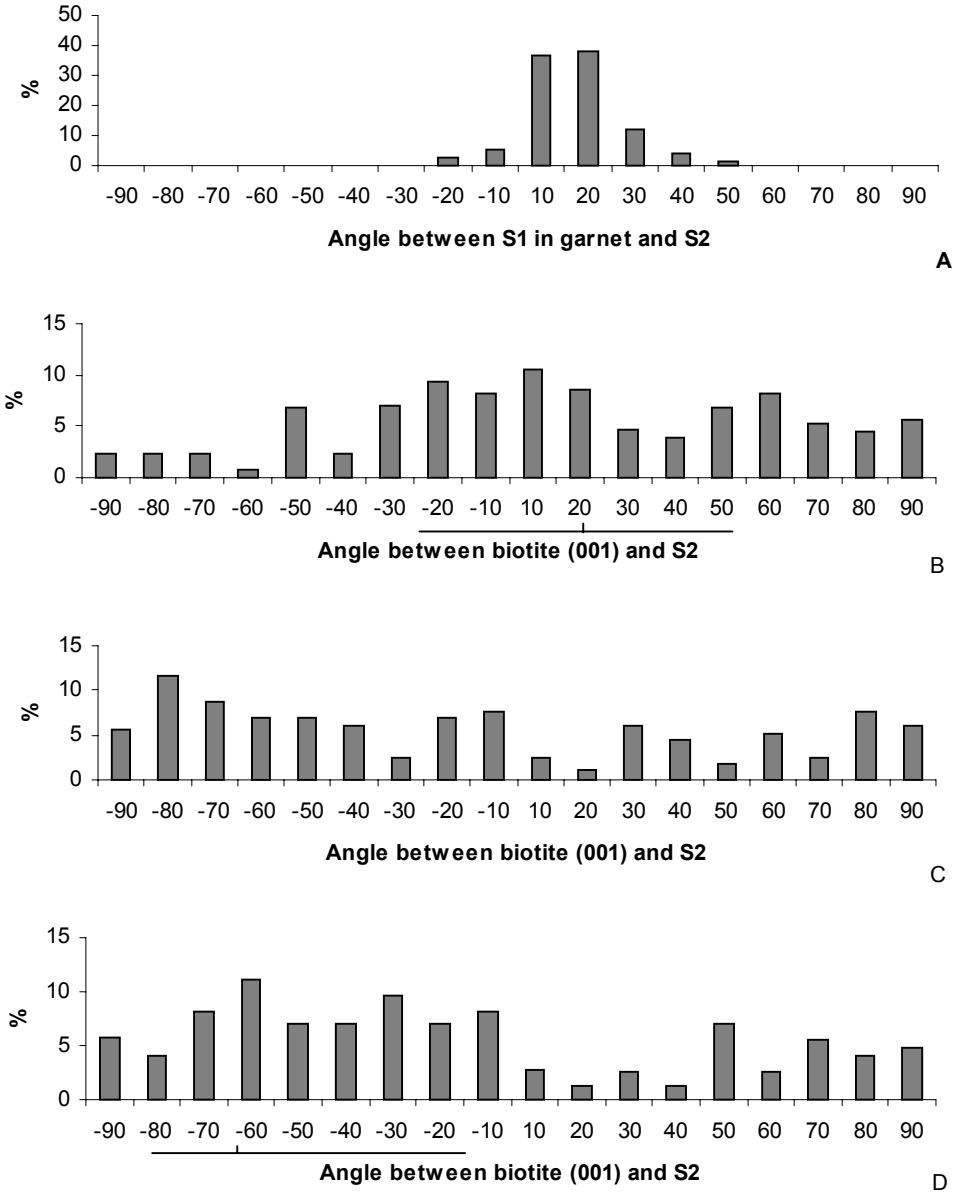
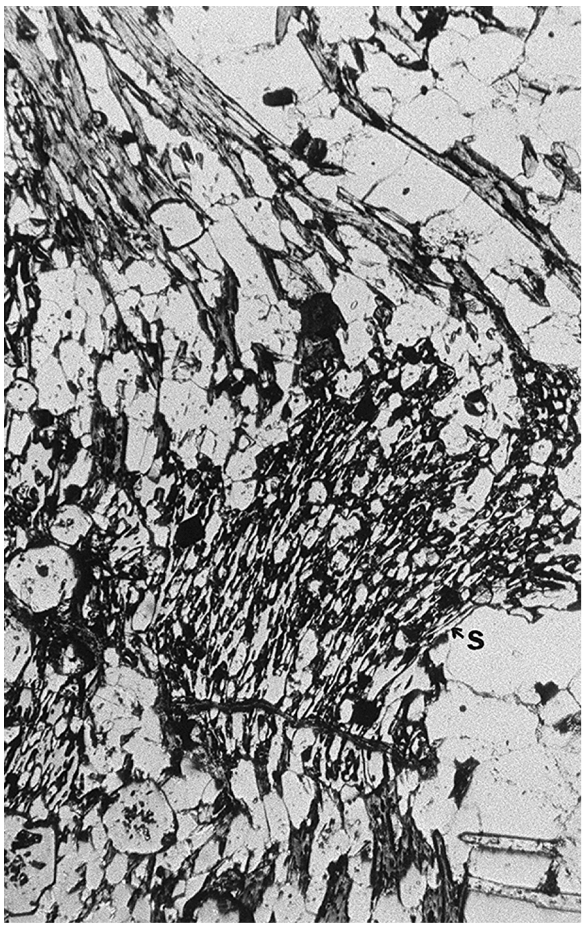
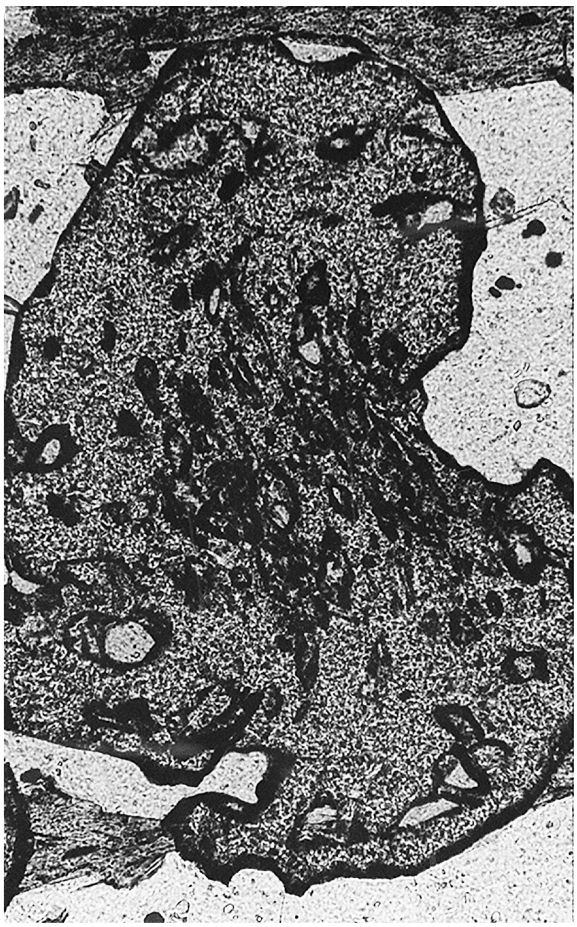


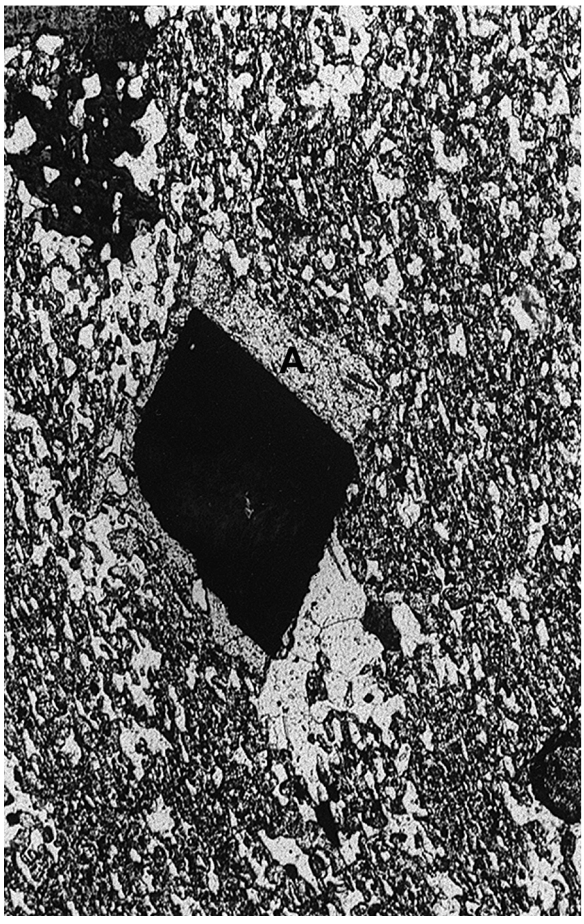
Figure 100. Histograms of measurements of the angular difference between the estimated mean trend of S_2 in a thin section (set at 0˚) and individual examples of either S_1 in garnet, or (001) planes of biotite grains. A, B. Sample No. 517-047, section cut // $L_{2/2}$. C. Sample No. 517-047, 90˚ to $L_{2/2}$. D. Sample No. 517-049, // $L_{2/2}$. The lines at the base of histograms B and D represent the range of S_1 in biotite and the tick is the mean of the range.



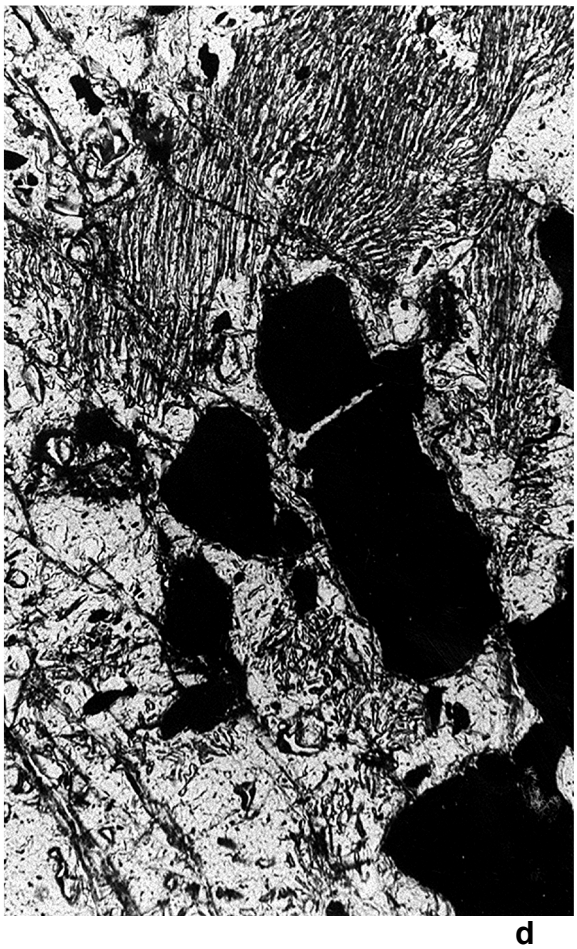
a



b



c



d

Figure 101 (previous page). Photomicrographs of GAB(3) schist.

(a) Staurolite (labelled *s*) with sinuous S_1 that is continuous with S_2 in the quartz-chlorite matrix. [PPL. Sample No. 517-024. Photo width is 2.1mm.]
(b) Garnet with a sinuous S_1 continuous with S_2 in the matrix. [PPL. Sample No. 517-045. Photo width is 0.53mm.]
(c) Magnetite inclusion in a single andalusite grain. S_1 in andalusite abuts a sharply bounded inclusion free zone on the NE/SW sides of the magnetite that resembles a replaced pressure fringe. On the NNW/SSE sides there is a quartz rich zone resembling a strain shadow parallel to S_1. [PPL. Sample No. 517-067. Photo width is 0.61mm.]
(d) Staurolite with simplectic quartz intergrowths. The opaque grains are magnetite. [PPL. Sample No. 517-112. Photo width is 0.5mm.]

In order to explain the broad peaks of S_2 in Figure 100, they were compared to the traces of S_1 in the same thin sections. The measured ranges of S_1 traces for both samples are shown on Figures 100b, d as broad lines at the base of the histograms (the mean value is also shown at the base) and a correspondence between the peaks and the ranges of S_1 is apparent, especially for the second sample.

In conclusion, the crystallographic orientation of biotite porphyroblasts in the two samples, shows no consistent relationship to S_2 and so it is considered that the porphyroblasts are unlikely to have undergone significant amounts of slip on the (001) plane during S_2 development. A very weak crystallographic preferred orientation of biotite seems to be present but its origin is more likely to be related to S_1 than S_2, as suggested elsewhere for andalusite. Etheridge et al., (1974) suggested that mica growth is strongly influenced by anisotropies in the supply of its components and so a planar fabric like the precursor to S_1 may explain the apparent relationship between the orientations of biotite and S_1.

6.6.3 Garnet

Most garnet porphyroblasts contain an inclusion free rim and a core with inclusions that typically define a simple, linear trending S_1. Hence, they are similar to garnets in other varieties of GAB schist. Rare examples of garnets with sigmoidal S_1 have been observed in GAB(3) schist (Figure 101b). The cause of the sigmoidal pattern like this is unclear and the rarity of such examples makes its origin hard to resolve. If the inclusion pattern in the garnet is of the "snow-ball garnet" type, then non-coaxial strain is involved and, in this case, a relative rotation angle of approximately 120 is indicated. Alternatively, the microstructure can equally well be due to preservation of a crenulation short limb by garnet overgrowth. Compared to most other garnets in GAB(3) schists, the one shown in Figure 101b is unusual in having inclusions near the rim, but they are coarser grained than those near the core. Furthermore, the garnet is largely enclosed by quartz but has a projection (in the lower left hand corner), continuous with an adjacent chlorite band that has possibly been replaced by the garnet. Garnet growth by a chlorite consuming reaction is possible.

6.6.4 Staurolite

Staurolite is a ubiquitous, but minor constituent of GAB(3) schists. Its two most common habits are as isolated grains in the matrix or as intimate intergrowths with andalusite poikiloblasts. Where staurolite occurs in a quartz free environment, such as chlorite or biotite aggregates, it is typically idiomorphic and has few inclusions. However, where it occurs in a quartz rich environment it normally forms irregularly shaped grains with many quartz inclusions that are typically coarser than those in nearby garnet cores and define S_1 parallel to S_2.

In staurolite-andalusite intergrowths the shape and size of quartz inclusions within both minerals are similar (Figures 99g, h). They both contain parallel S_1 traces that may be either parallel or discordant to S_2, and it seems that in these intergrowths both minerals grew simultaneously. In contrast, staurolite in the matrix, with its coarser inclusions parallel to S_2, seems to have developed later. In staurolite-andalusite intergrowths, staurolite commonly develops its crystal form against andalusite but the reverse case has not been observed.

Simplectic staurolite-quartz intergrowths occur in many samples of GAB(3) schist. The example shown in Figure 101d occurs in a continuous zone of staurolite flanking a chalcopyrite-pyrrhotite-magnetite-(ilmenite) vein. The origin of simplectic structures in silicates is not completely understood, although it is generally agreed that they are eutectoid structures and so both minerals forming them crystallised at the same time (Vernon, 1976; Kretz, 1994). Eutectoid structures have been closely studied in alloys, in which typically it is found that during relatively rapid cooling a single homogeneous solid, A, transforms to a lamellar intergrowth of two different solids, B and C (Ruoff, 1972, p. 446). The spacing between lamellae is related to atomic diffusion rates and so is determined by the temperature at which the eutectoid transformation occurs. The simplectic intergrowth of Figure 101d is very similar to the illustration of the pearlite microstructure in steel shown by Ruoff (1972, p. 460).

A close spatial relationship is observed between simplectic staurolite and sulphide rich veins, as shown in Figure 101d. At relatively high temperatures such veins may have contained sulphide and oxide minerals with abundant aluminium and silicon in solid solution. Upon cooling, a silicon and aluminium rich phase formed along the margin of a sulphide-oxide vein. Upon further cooling the silicon and aluminium rich phase transformed into the simplectic quartz-staurolite intergrowth now present. On the basis of observation, it is considered more likely that the simplectic intergrowth was derived from oxides, rather than sulphides, because:

(a) magnetite is more abundant within the vein near its contact with staurolite; and

(b) as a rule, magnetite and ilmenite tend to have higher silicon and aluminium contents than chalcopyrite or pyrrhotite.

If the argument above is correct, then it supports other evidence (discussed elsewhere), that the sulphide minerals have been metamorphosed. Similar simplectic quartz-staurolite intergrowths occur within the metamorphosed pyrite and pyrrhotite rich rocks at the Brukunga Mine (Vernon, pers. comm., 1979). In this case a euhedral staurolite crystal with an outer inclusion free rim has an optically continuous, hexagonal core consisting of simplectic staurolite and quartz.

6.6.5 Sulphide and Oxide Minerals

By far the most common of these minerals are chalcopyrite, pyrrhotite, pyrite and magnetite. Sulphide minerals occur both in the matrix, where they are typically elongated parallel to S_2 and in andalusite and staurolite porphyroblasts, where they are typically parallel to S_1 (for example Figure 99f,g). Those parallel to S_1 are commonly much larger than associated quartz grains and, in rare cases, they occur with chlorite, parallel to S_1, in andalusite indicating that both sulphide and chlorite were present during the formation of S_1.

Magnetite tends to occur as equant inclusions in biotite or andalusite (Figure 99f,g,h). It is uncommon in the adjacent matrix. Like the sulphide minerals, the formation of at least some magnetite grains appears to predate andalusite growth. For example, Figure 101c shows a

euhedral magnetite grain within andalusite. The magnetite has a pressure fringe-like structure now consisting of andalusite that is optically continuous with the rest of the andalusite poikiloblast. This feature is shaped more like a pressure fringe than a pressure shadow, as defined by Spry (1969), because S_2 is truncated at its boundary; and its shape reflects the straight edges of the magnetite grain. Presumably the original fringe minerals were replaced by andalusite together with much of the matrix surrounding the magnetite grain.

6.7 The shape of biotite grains in GAB schist

Mica grain shapes have a marked spatial relationship to copper mineralisation at the Kanmantoo Mine and provide clues to understanding its origin. Much of the information relevant to this topic was presented in previous sections as each GAB schist variety was described. It has been shown that in the order GAB(1) schist to GAB(2) schist to GAB(3) schist, in general, biotite becomes more equant and less schistose. In this section methods of describing and comparing mica grain shapes are discussed, followed by a discussion of the factors that are considered to influence mica grain shapes and finally, an attempt is made to explain the observed changes of biotite in GAB schist.

6.7.1 Description of the biotite grains

Flinn (1965) classified rocks with tectonic fabrics (L-S fabrics) according to the relative strength of the L and S components and so a rock can be classified as one of the following: L, L>S, L=S, L<S and S, in order of lineation-only to schistosity-only. A mineral lineation can be defined in two ways, firstly as a dimensional preferred orientation of elongated minerals that is typically the case with amphiboles in lineated amphibolites, for example. A second type of lineation is produced when platy minerals are arranged such that they share a common axis, in much the same way that the blades of a paddle wheel share a common axis. Micas can define both types of lineation at the same time, for example the dispersed plates may have a common axis or line and, in addition, the plates may be elongated in this same direction. Therefore, schists can have both types of lineation because the schistosity forming mica flakes can be elongated in a common direction and also the orientation of the flakes can vary within the general schistosity plane about the same direction.

To fully describe an L-S fabric both the shape and the orientation of the aligned minerals must be described. Ideally, the shapes and relative attitudes of the minerals should be measured and both aspects represented on a single diagram. Practically, it is difficult to collect the three-dimensional data for each mineral. As a compromise, inferences can be made from two-dimensional data obtained from sections perpendicular to the mineral lineation. For mica grains, the aspect ratio would be measured instead of the total (triaxial) shape and the traces of (001) planes instead of absolute orientation (this makes the assumption that (001) is parallel to the long dimensions of mica grains).

Therefore, to represent both the shape and orientation of minerals defining an L-S fabric a diagram such as that shown in Figure 102a can be used. For a given rock, or domain within a rock, the mean aspect ratio is plotted against the standard deviation of measurements of the relative trend of the traces of (001) planes. The latter measurements are the angular differences between the trend of (001) planes and a reference line approximately parallel to S_2 (as described previously). Figure 102a clearly reflects the observed changes in biotite shape for the GAB schist varieties, and for the Q and M domains in the GAB(1) schist. It demonstrates a clear negative relationship between the two variables plotted, and quantifies the tendency which is apparent in thin sections for rocks that have the most equant biotites to have the most randomly oriented biotites. Both crystallographic and dimensional preferred orientations are diminished in the transition from GAB (1) schist to GAB(2) schist to GAB(3) schist.

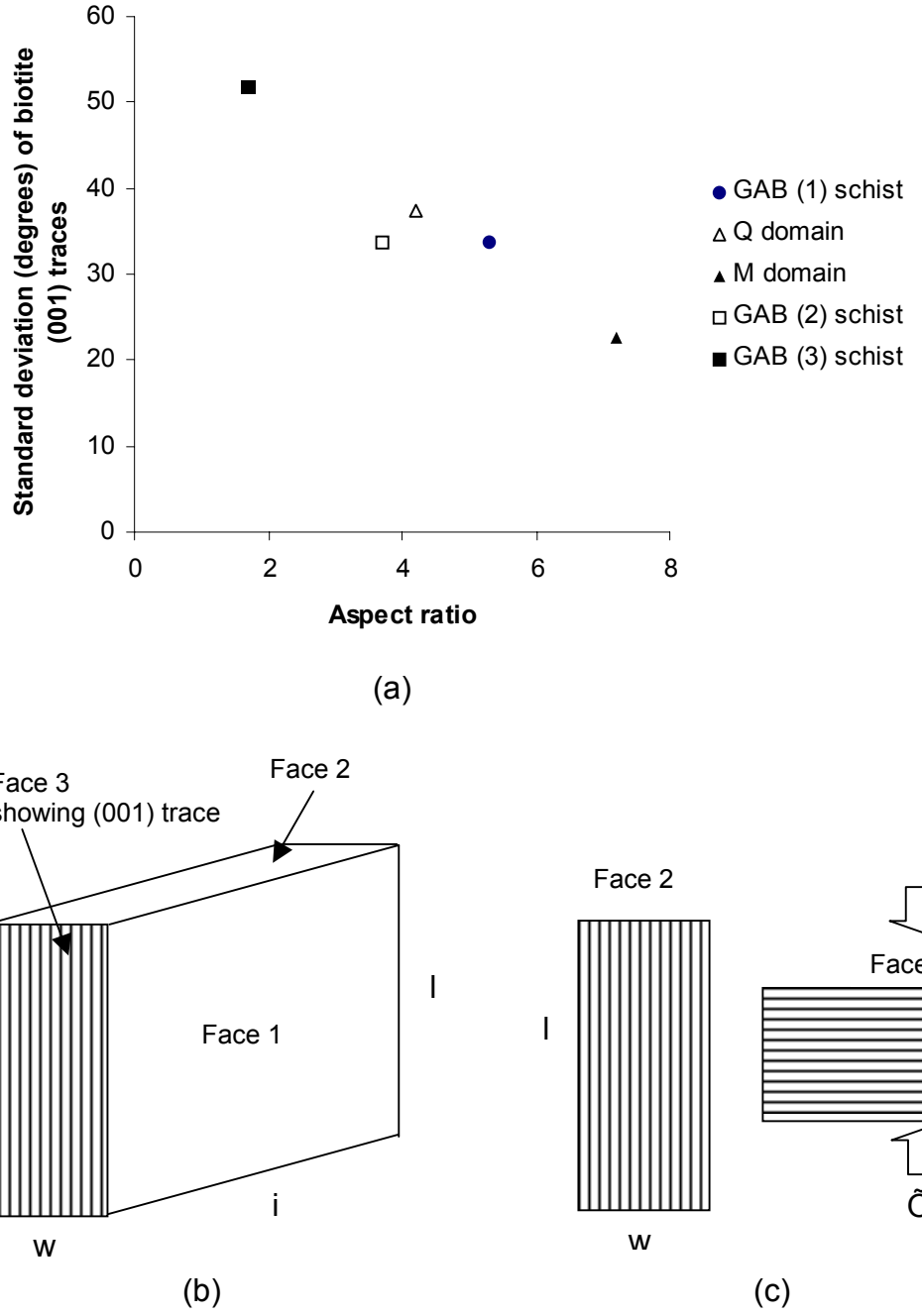


Figure 102. Comparison of biotite shapes and orientations in GAB schist varieties. (a). Measurements for one typical sample each of GAB(1) schist, GAB(2) schist and GAB(3) schist, the graph shows the mean aspect ratio of biotite grains plotted against the standard deviation of all angles measured between the mean S_2 trend and (001) trends in individual grains. (b), (c). Refer to text for explanation.

6.7.2 Discussion

The equilibrium shape of a mica crystal in an isotropic and homogeneous environment is considered to be a hexagonal prism (Kretz, 1966) with the prism axis perpendicular to (001). The ratio of the width of the prismatic grain (measured across the basal section) and its length should be constant at equilibrium, regardless of the grain size. This constant value is influenced by temperature, mineral composition and absorption (Kretz, 1966).

However, equilibrium mica grain shapes are not usually present in metamorphic rocks, for at

least three reasons. Firstly, equilibrium (chemical or microstructural) may not have been attained, and secondly, stress has commonly been present at some stage of mica growth. Thirdly, mica grains are usually not surrounded by a truly isotropic environment, although phlogopite surrounded by calcite seems to closely approach it (Kretz, 1966). Hence mica grains surrounded by quartz and feldspar in metapelites rarely develop as hexagonal prisms. To examine mica shapes in quartz-mica aggregates isolated mica grains should be used, but while this can be done in quartz rich rocks or Q domains it is obviously impractical in very micaceous rocks or M domains where mica-mica contacts are prevalent. Consequently, the data shown for M domains in Figures 102d,e are not directly comparable with that for associated Q domains and the other rocks. Nevertheless the trend is evident.

Within metamorphic rocks, the shapes of mica grains are related to:

(a) their temperature of formation;
(b) the type of mica;
(c) their crystallographic orientations with respect to the strain axes;
(d) their size; and
(e) the presence of stress.

These will now be discussed in turn with particular reference to explaining the diagnostic change in shape of biotite grains in rocks of the Kanmantoo Mine.

The influence of temperature on biotite shape in thermal and regional metamorphic rocks has been demonstrated by Jones and Galway (1972), who found a consistent trend of decreasing aspect ratio of biotite with increasing metamorphic temperature. However, in rocks at the Kanmantoo Mine temperature is essentially the same in all rock types as indicated by mineral thermometry described in Chapter 6. Therefore this is not an explanation for the shape variation.

Regarding the type of mica, the data collected from a sample of QMF schist (Figure 74a) show a clear tendency for muscovite to have higher aspect ratios than co-existing biotite. But this is not relevant to shape variations in biotite only.

Regarding crystallographic orientations with respect to the strain axes, Etheridge (1973) demonstrated a relationship between the aspect ratio of individual mica grains and their orientation with respect to the schistosity. Mica grains with the highest aspect ratio were those that were subparallel to the schistosity (see dashed line of Figure 74h). Figure 74f, h considered together, show a similar relationship to that found by Etheridge (1973) for both Q and M domains of GAB(1) schist sample, although the trend is most obvious in the M domain, where the data conform closely to Etheridge's line. However, in GAB(3) schist the biotite grains have neither crystallographic nor dimensional preferred orientations, and are not part of the S_2 matrix schistosity. Thus, their relationship to any strain axes at the time of crystal growth is not clear. It will be argued later that these grains grew in an environment subject to low or nil deviatoric stress.

Figures 74a,d,e show that, as mica grains become longer, their aspect ratios tend to increase. This tendency is very clear in the QMF schist specimen for both muscovite and biotite, although the data for each mineral appear to define separate lines. In this rock, for a given aspect ratio biotite tends to be longer than muscovite. The same trend is present in the specimen of GAB(1) schist (Figures 74d, e) but is better defined in the section cut parallel to the lineation in which longer grains occur (note that the scales are different on these two figures).

The trend of an increase of aspect ratio with grain length, shown in many rocks observed in

the Kanmantoo Mine area, agrees with that reported by Kretz (1966). In contrast, Jones and Galway (1972) found a tendency for aspect ratio to decrease as biotite grain size increased. Apparently, there is no consistent trend and an explanation may be related to the effects of stress or strain and the history of grain growth relative to these. For example, Gray (1979) has shown that the quartz grains occurring in the limbs of microfolds develop larger aspect ratios as the folds become tighter. The data of Marlow and Etheridge (1977) indicate the same trend, for quartz, feldspar and mica grains. A feature of crenulated cleavages is that mica grains within the mica rich domains have both higher aspect ratios and a more pronounced preferred orientation than those occurring in quartz rich domains.

In GAB(3) schist, two features indicate that the grain size does not control grain shape. Firstly, equant grains of various sizes occur. Secondly, biotite grain sizes are comparable to other rock types with different grain shapes. So while biotite grain size is related to shape in certain rock types in the Kanmantoo Mine, it does not appear to be a controlling influence.

Finally, the effect of stress on biotite grain shape will be considered. Using thermodynamic considerations, Rosenfeld (1955, page 576) derived mathematical expressions relating the dimensions of a crystal to both the pressures (P_n normal) to each of its faces (n = 1, 2, 3) and their interfacial tensions (T_n) with a surrounding isotropic environment, at equilibrium. The expression, as adapted from Rosenfeld's equation 7c and in which the subscripts refer to the faces of the crystal shown on Figure 102b, is:

$$(P_1-P_2) = 2(T_1/w - T_2/l) \qquad (1)$$

Equation 1 can also be expressed by the linear relationship:

$$1/\text{aspect ratio} = w/l = w(P_2 - P_1)/2T_2 + T_1/T_2 \quad (2)$$

Equation (2) relates the aspect ratio of two crystal surfaces to the difference in pressure acting on those surfaces, for a given crystal width. If we consider a mica crystal with its (001) planes perpendicular to w (as observed in many rocks) and if we assume that l=i, we can apply equation (2) to the two mica grains of Figure 5.14c. Both grains have (001) planes perpendicular to one another and both exist in an isotropic environment to which a differential stress is applied such that the maximum stress component is vertical in the diagram. Applying equation (2) to Figure 102c (left diagram) we find that because P_2 is greater than P_1 and T_1 and T_2 are constant, l/w decreases as w increases. On the other hand, in the case shown in Figure 102c (right diagram), P_2 is less than P_1 and so l/w increases as w increases. This may explain the variation of grain shape with respect to the strain axes if the stress and strain axes were approximately parallel and so could account for the variation of mica grain shape in the Q and M domains of GAB(1) schist.

The differential stress associated with deformation of regional metamorphic rocks is thought to be a small proportion of the confining pressure acting upon the rock (Winkler, 1976, page 26). The effect of high fluid pressure (P_f) is to reduce total stress (S) such that the effective stress ö = S - P_f. Therefore, high P_f conditions could lead to hydrostatic conditions during regional metamorphism. This concept is considered to be important in explaining the biotite microstructure in GAB(3) schist. As P_f increases the effective stress decreases and extensional fracturing will occur when P_f exceeds (S_3 + T), where S_3 is the minimum principal stress and T is the tensile strength of the rock (Etheridge et al., 1984). The fracturing produces dilation, deposition from the fluid, repeated fracturing and so on. The fracturing is responsible for higher permeabilities during deformation. The dilatancy generated produces gradients in P_f and possibly can draw fluids into the deforming zone in a type of dilatancy pumping mechanism (Etheridge et al., 1983).

The processes described above have obvious relevance to hydrothermal mineralization in metamorphic terrains. High pore fluid pressures present during folding of slate belt rocks were associated with mass accretion and sulphide mineralisation at the Pb-Zn Elura deposit in New South Wales according to De Roo (1989). Cox and Etheridge (1989) describe similar processes leading to intragranular, syn-deformational mass accretion, also during greenschist metamorphic grade, from rocks near Mt Lyell in Tasmania. Hayward (1992) also concluded that similar processes were associated with gold mineralisation in the Haile Mine of the Carolina Slate Belt.

The discordant nature of the Kanmantoo deposit is consistent with an origin from hydrothermal solutions (and this theory is developed in Chapter 8) and hence large amounts of associated fluids. The rocks with more equant and more randomly oriented biotite are closely associated with the deposit and presumably their origins are closely related to it. It is proposed here that the different microstructures are a result of high fluid contents associated with the copper deposit during the period of biotite producing reactions in GAB(3) schist. It is proposed that the high P_f was responsible for near hydrostatic conditions.

It was shown earlier that some sulphide minerals were present during the formation of S_1 and so some of the interpreted hydrothermal activity pre-dates andalusite formation at least. Hydrothermal fluids are inferred to have remained near the deposit, trapped in fluid inclusions, in hydroxyl rich minerals, and in intergranular films and tubules. During metamorphism and deformation large amounts of this fluid may have been released by metamorphic reactions and recrystallisation of fluid inclusion bearing minerals.

For the Kanmantoo deposits, it is proposed that until the fluids diffused away from the environment surrounding the deposit the differential stress was locally reduced, in proportion to the amount of fluid present. This resulted in the growth of micas near the deposit with shapes more typical of static metamorphism (in GAB(3) schist) and also affected the shape and degree of preferred orientation of mica further away from the deposit, in GAB(2) schist. GAB(1) schist and local QMF schists were not affected by this process and so schistose rocks more typical of the products of regional metamorphism formed. Because equant biotite grains in GAB(3) schist appear to be associated with andalusite growth, it is presumed that most of the fluid was released at this stage and perhaps by the andalusite forming reaction. The abundant fluid may also account for the relatively large size of biotite in GAB(3) schist.

6.8 Lode schists

Lode schists contain most of the high grade sulphide mineralisation, as veins and as disseminated grains. Because the lode schists are discordant to bedding in the surrounding metasediments (Chapter 4) they may be younger and so not record as many events as the metasediments. In Chapter 3 the lode schists were subdivided into several varieties of which the quartz rich and quartz poor varieties are by far the most common and the microfabrics of these two varieties are described here. Apart from the mineralogical differences between these two varieties there are two important differences in microfabric, which are basically that the quartz rich variety is relatively, fine grained and schistose whereas the quartz poor variety is relatively coarse grained and non-schistose.

6.8.1 Group 1 (quartz rich) lode schists

These rocks comprise quartz and chlorite essentially with minor garnet, andalusite, staurolite, biotite, chalcopyrite, pyrrhotite and ilmenite. As described in Section 3.3.1 and Table 3.2 the most common quartz rich lode schists are of two types, those with andalusite and those without.

Most quartz rich lode schists consist of a polygonal aggregate of quartz and chlorite in apparent microstructural equilibrium (discussed further later). The chlorite laths are aligned and define a schistosity (S_2) that, in some rocks, may be augmented by parallel, wispy zones of chlorite or garnet rich bands. S_1 is preserved within garnets and is identical to S_1 in garnets of GAB(3) schist. It is likely that S_1 in garnets of quartz rich lode schists represents an equivalent tectonic stage to the same feature in GAB(3) schist; likewise for S_2 in each rock type. This assumption is supported by the close relationship between both rock types, for example both may occur in a single, thin section where S_1 and S_2 appear to be identical in both rock types and are usually parallel. S_2 is defined principally by chlorite, but if biotite is present it will also tend to be parallel to S_2, or alternatively, forms approximately equant grains. Chlorite will be discussed further in the next section.

Garnet occurs in several habits, mainly as dispersed grains, as irregularly shaped clusters of many grains, and also in layers. All may contain S_1. The layers also vary from moderately defined (Figure 103) to well defined (Figure 104). In the former figure note that the garnet layer occurs in a matrix of chlorite and quartz and that it is parallel to S_2. Some of the well defined garnet layers are continuous for over 30cm without significant change in thickness and adjacent garnet layers are subparallel to one another. They are commonly disharmonically folded with S_2 approximately parallel to the axial planes of the folds. S_1, where present, tends to be parallel to the layers and so is folded around the hinges, indicating that the layers formed prior to S_2 and that the garnets within them post-date S_1.

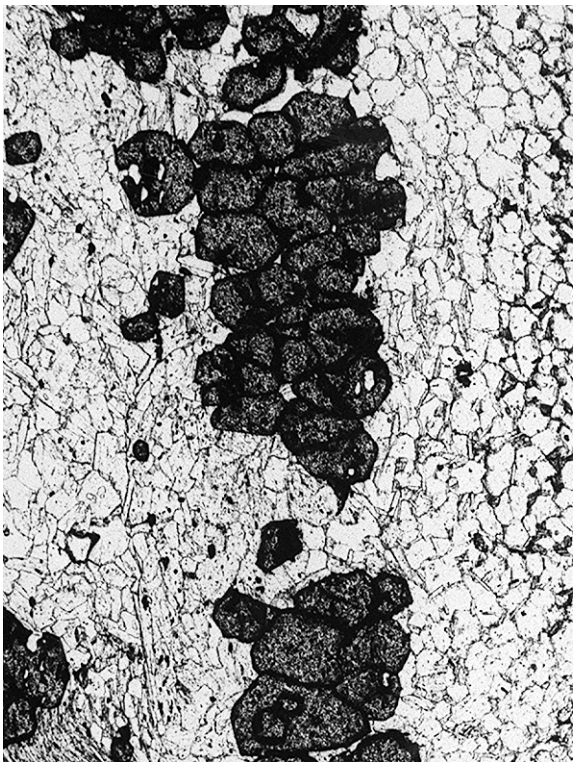


Figure 103. Garnet layer in quartz rich lode schist. The layer consists of garnet (dark) aggregates that form detached blocks parallel to S_2 in the surrounding quartz-chlorite matrix. [PPL. Sample No. 517-114. Photo width is 1.9mm.]

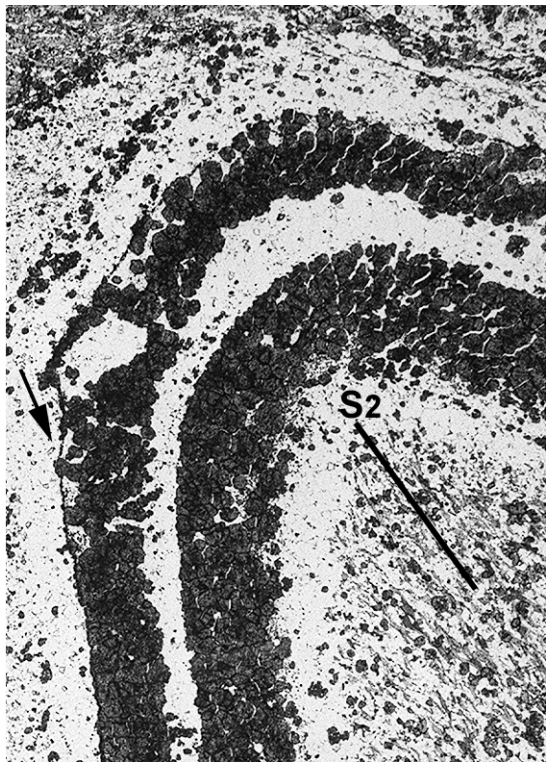


Figure 104. Folded garnet layer in quartz rich lode schist. This is an example of the very regular garnet layering that occurs in quartz-chlorite schist. Like this example it is commonly folded. Note the thin ilmenite band on the top and left side of the upper garnet layer (arrowed) and the axial planar S_2 schistosity. [PPL. Sample No. 517-109. Photo width is 8.5mm.

Figure 104 illustrates many typical features of the garnet layers, firstly, the regularity of the two parallel layers and that they are folded with S_2 (lower right-hand corner) approximately parallel to the axial plane. Secondly, a quartz rich and chlorite poor selvedge zone surrounds the layers. Thirdly, there is a fine and persistent thin string of ilmenite grains along one side of the layers, which is as continuous and regular as the layers. Finally, the fold style appears to be concentric and, with respect to this, note the apparent tensional features in the folded garnet layers on the right hand limb of Figure 104.

The origin of the garnet layers is unclear. They may represent altered bedding but few occur in rocks with recognisable bedding to compare. A possible exception is the rather complex sample shown in Figure 105, however, in this example the garnet layers are poorly defined. The lower half of the photograph displays fairly regular layering for a lode schist that may represent bedding. The dark grains in the layering (staurolite) have a prominent S_1 oblique to the layers. Below that is a garnet layer with S_1 parallel to the layer (although this is not obvious in the photograph). S_1 in garnet is approximately parallel to S_1 in staurolite.

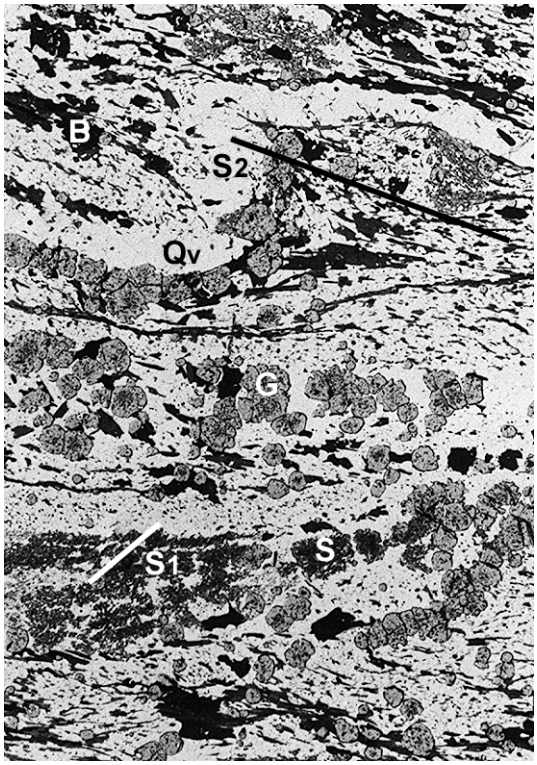


Figure 105. Quartz rich lode schist with folded quartz vein and garnet rich layers. Minerals are mainly quartz and chlorite, with biotite (B), staurolite (S), and garnet (G). The vein (Qv) has garnet along part of its lower margin and is folded with S_2 (as shown) as axial planar schistosity. S_1 is preserved in ragged staurolite grains (shown) that also form layers in the lower part of the figure. [PPL. Sample No. 517-095. Photo width is 7.9mm.]

The top of Figure 105 shows a folded quartz vein with S_2 approximately parallel to the axial plane. Part of the left side of this vein has a contiguous garnet layer that has S_1 parallel to the layer and the folded vein. The folded vein has an opposite vergence to that indicated by the possible S_0/S_1 relationship. The garnet layers (as chemical zones) and the quartz vein can be correlated with S_1 whereas the garnet grains are interpreted to have grown in the period between the tectonic stages represented by S_1 and S_2. The interpretation of this sample is that prior to S_2 development, layers with the S_1 schistosity were tightly folded and that veins with marginal pre-garnet accumulations were parallel to S_1. The layers are very regular and probably represent relict bedding. Growth of staurolite and garnet then preserved the S_1 fabrics. D_2 folding followed producing S_2 and the opposite fold vergence in this sample.

Staurolite in quartz rich lode schists is a minor component that mostly occurs as scattered grains whose relative age is difficult to determine. However, Figure 106 illustrates an informative grain showing a single (optically continuous) staurolite grain spanning the contact between a quartz rich zone and a chlorite rich zone. The contact between the zones is parallel

to S_2 in the quartz rich zone. In the chlorite rich zone the staurolite is regular in shape whereas it is ragged in the quartz rich zone.

In Figure 106 quartz inclusions in staurolite reflect the surrounding zones, those in the ragged side are numerous and tend to be elongated parallel to S_2. By contrast, there are few inclusions in the other part of the staurolite crystal and they are equant, like the surrounding rock. In both sides of the staurolite crystal the quartz inclusions appear to be slightly smaller than those outside the crystal, perhaps due to either grain growth after staurolite formation or consumption of part of the included grains during staurolite formation. Therefore, staurolite is interpreted to have grown after the formation of S_2. The same conclusion was derived for staurolite growth in GAB(1) schist, but in that case the staurolite producing reaction appeared to involve biotite whereas in the lode schists it appears to involve chlorite.

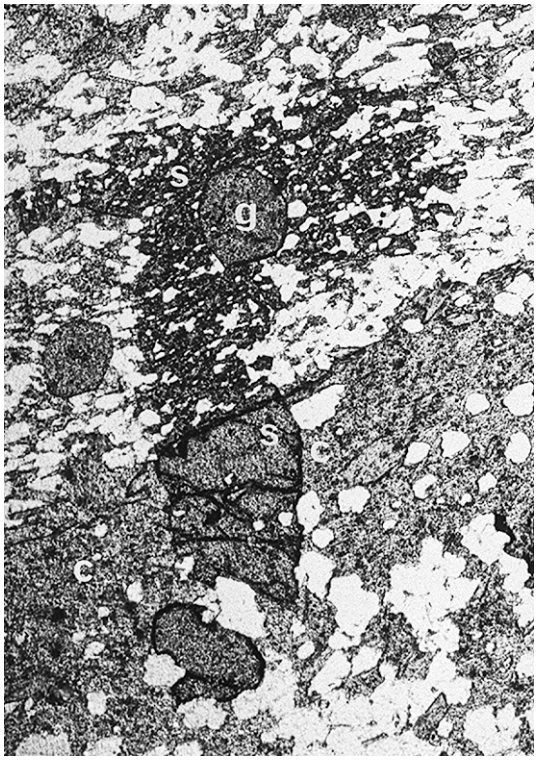


Figure 106. Quartz rich lode schist with staurolite. A single staurolite (s) grain with garnet (g) inclusion straddles the boundary between quartz rich and chlorite (c) rich zones. Note the differences in staurolite grain shape and the number and shape of quartz inclusions on each side of the boundary. [PPL. Sample No. 517-048. Photo width is 2.9mm.]

6.8.2 Group 2 (quartz poor) lode schists

These rocks consist of varying proportions of staurolite, biotite, garnet and chlorite. Muscovite is common in one particular lithology, but is generally rare. Rare too, are quartz and S_1. Quartz poor lode schists differ from most other rocks of the mine area in their relatively coarse grain size and their lack of a strong preferred orientation. In fact, many appear to have random fabrics and this, together with their close association with the sulphide mineralisation led Lindqvist (1969, page 91) to suggest that his "alteration zones", which are characterised by this rock type, postdate the period of maximum tectonic activity. While some of these rocks observed by the author seem to have random fabrics, most have at least a weak preferred orientation, including both a schistosity and a lineation and this is usually much more obvious in hand specimen than in thin section.

Foliations

Some of the types of foliations in quartz poor lode schists are described here. Figure

107a shows an example of the staurolite and biotite rich lode schist (2a) in which the long dimensions of the staurolite crystals are clearly aligned and are parallel to a weakly defined foliation in the surrounding biotite. A more pronounced biotite foliation is shown in Figure 107c; note the apparent "snow-ball" inclusion pattern.

Some staurolite grains show evidence of brittle deformation where two grains appear to have been forced together (Figure 107b). The resulting fractures are usually subparallel to the (001) plane of one, or both, staurolites. The contact between two impinging staurolite grains typically has a bead-like string of clear, high relief grains, possibly garnet, and suggests that the fracturing occurred at sufficiently elevated temperatures for the local formation of a new mineral phase.

In some biotite rich lode schists, the schistosity and lineation, which are easily recognisable in hand specimens, appear to be a modified crenulation cleavage when viewed in thin sections cut perpendicular to the lineation. A good example, shown in Figure 107d, contains alternating subparallel zones containing micas trending parallel to the zones, and micas trending at a high angle to the zones. The boundaries between these zones are irregular in detail and most of the micas display equilibrium microstructures. The lengths of the micas, parallel to their (001) traces, are similar in each zone but the aspect ratios of the grains that are at a high angle to the zone boundaries are approximately double that of the grains parallel to it. These features may have been produced by mimetic recrystallisation and possibly coarsening of a previously crenulated mica rock.

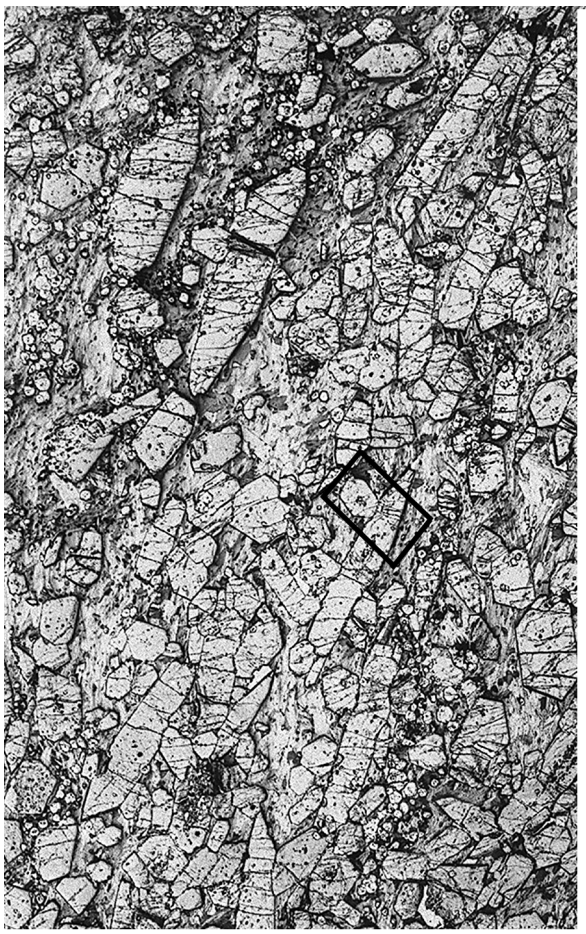
Thus many of the quartz poor lode schists retain the effects of at least one foliation-producing episode. They differ from other local rocks (for example, GAB(1) schist, GAB(3) schist and quartz rich lode schists) mainly in their weaker expression of foliations.

Garnet

Further evidence of the history of the quartz poor lode schists can be found in their garnet microstructures. Garnets enclosed in layer silicates are typically idiomorphic, whereas garnets occurring in a quartz rich matrix may be either idiomorphic or irregular in shape. Furthermore, the type, shape and size of inclusions in garnet are similar to its surrounding matrix. For instance, comparison with other local rocks suggests that the large garnet shown in Figure 108a grew in a quartz poor environment because it has no quartz inclusions. In this case the outer zone of the garnet contains several swarms of subparallel ilmenite inclusions. Many of the ilmenite swarms occur near the garnet margin and are parallel to (001) planes of the adjacent biotite (top left hand corner of Figure 108a) and this feature is common to many garnets in biotite rich lode rocks.

Microprobe data (presented in Chapter 8) shows that biotite contains much more $Ti0_2$ than garnet. It is suggested, therefore, that the inclusions are the product of a garnet producing reaction involving biotite and that the excess $Ti0_2$ remained close to the reaction site, as ilmenite inclusions in garnet. This interpretation was also proposed by Lindqvist (1969, page 72). Ilmenite swarms not parallel to (001) planes of adjacent biotite grains probably formed in a similar manner but from grains with no remnants or with subsequent recrystallisation and reorientation of some of the matrix biotites. Thus another possible product of this reaction is "new" biotite.

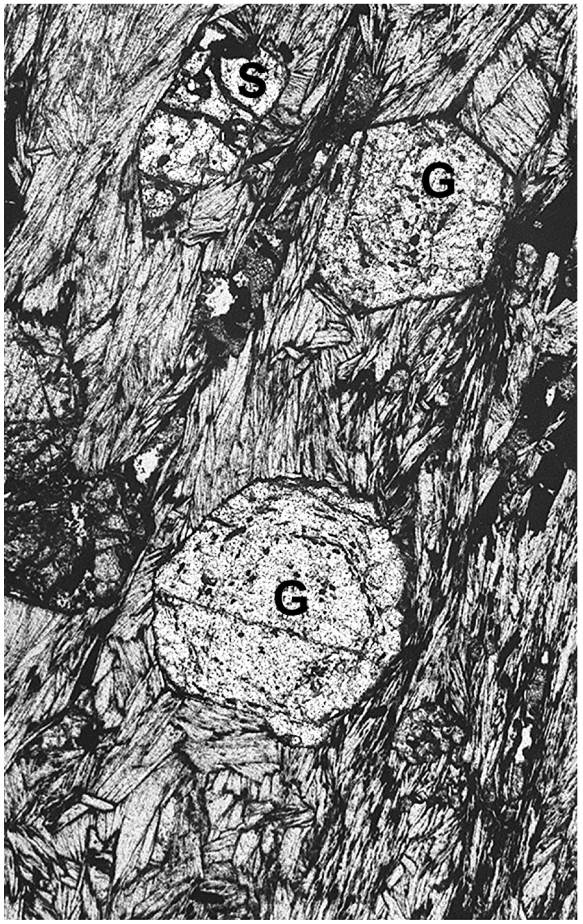
Another example of idiomorphic garnet without quartz inclusions occurring in a quartz free matrix is shown in Figure 108b but in this case the garnet contains relatively coarse grained magnetite inclusions which also occur in the matrix, although less abundantly. Again, the inference is that quartz was not included because little, if any, was present during garnet growth.



a



b



c



d

Figure 107 (previous page). Quartz poor lode schists.

(a) Biotite-staurolite rock. Abundant prismatic staurolite crystals display a dimensional preferred orientation. They occur in a matrix of randomly disposed chlorite, biotite, garnet and ilmenite. [PPL. Sample No. 517-177. Photo width is 15.8mm.]

(b) Detail of (a) located just right of centre (shown in a). This photograph shows fracturing of a staurolite prism, apparently by contact with the staurolite grain in cross-section beside it. Note the general lack of quartz except for some small inclusions at the centre of the cross-sectional staurolite. The black spots in the matrix are pleochroic haloes. [PPL. Sample No. 517-177. Photo width is 2.8mm.]

(c) Garnet-chlorite rock. Idiomorphic garnets (labelled G) occur in a felted chlorite-(staurolite-ilmenite) matrix with no quartz and a weak S_2 fabric. The lower garnet has an apparent spiral inclusion trail of ilmenite. The vague grain at top centre is staurolite (labelled S). [PPL. Sample No. 517-054. Photo width is 2.0mm.]

(d) Biotite-chlorite-magnetite rock. The layer silicates are arranged in rough, alternating lengthwise zones of grains that are oblique or parallel to the zone boundaries. Green biotite is the most common mineral and intergrown dark (brown) chlorite lamellae (arrowed, centre right) are visible in some biotite grains oriented lengthways. [PPL. Sample No. 517-077s. Photo width is 1.5mm.]

Figure 108 (following page). Photomicrographs of garnets in quartz poor (Group 2) lode schists.

(a) Garnet with several swarms of subparallel ilmenite inclusions, some parallel to (001) of adjacent biotite (top left), others not. [PPL. Sample No. 517-061. Photo length is 2.6mm.]

(b) Garnet with magnetite inclusions. A cummingtonite prism is visible in the top right corner. [PPL. Sample No. 517-077. Photo length is 2.0mm.]

(c) Garnets with abundant quartz inclusions in quartz free matrix of biotite, chlorite and amphibole. [PPL. Sample No. 517-059. Photo length is 1.7mm.]

(d) Garnets with inclusion rich cores and apparent pull-apart structures infilled by quartz (arrowed). [PPL. Sample No. 517-061. Photo length is 1.7mm.]

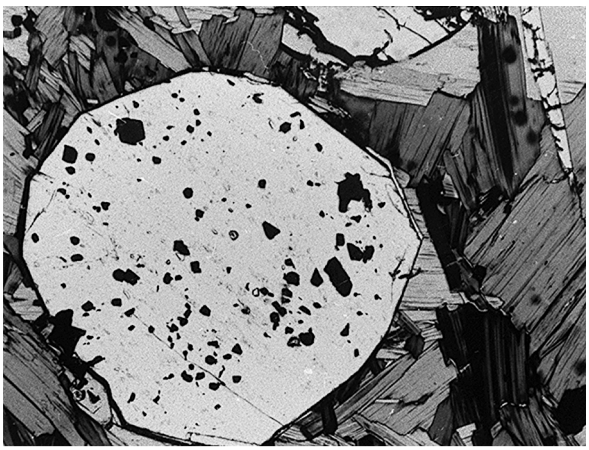
(e) Idiomorphic and broken garnets separated by quartz with and without fine needles of amphibole. [PPL. Sample No. 517-203. Photo length is 3.8mm.]

(f) Garnets in chlorite-(biotite) matrix with apparent pull-apart structures infilled by chlorite and sulphide minerals. [PPL. Sample No. 517-061. Photo length is 5.0mm.]

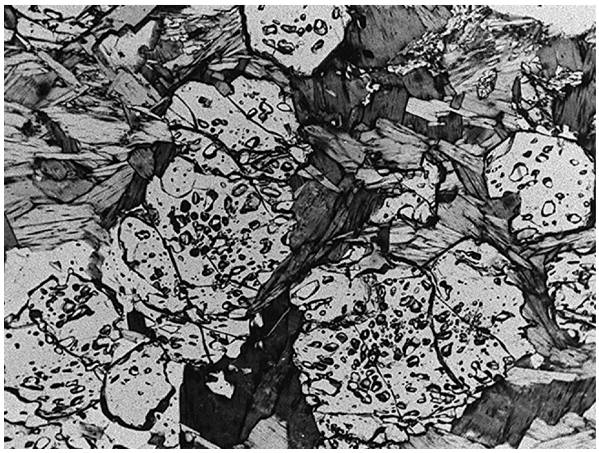
(g) Chlorite and amphibole defining a schistosity (S_2) whereas biotite is equant. [PPL. Sample No. 517-077L. Photo length is 1.8mm.]



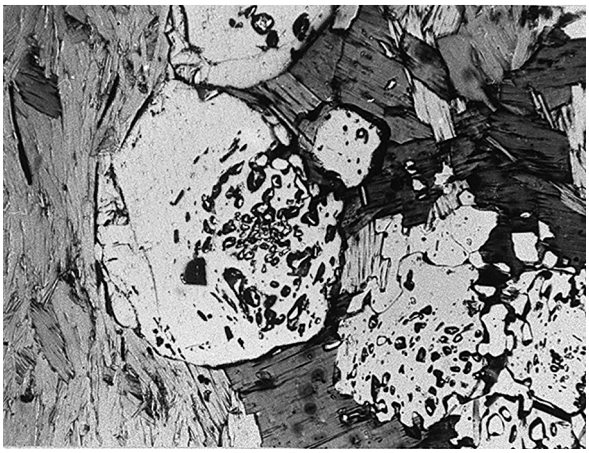
a



b



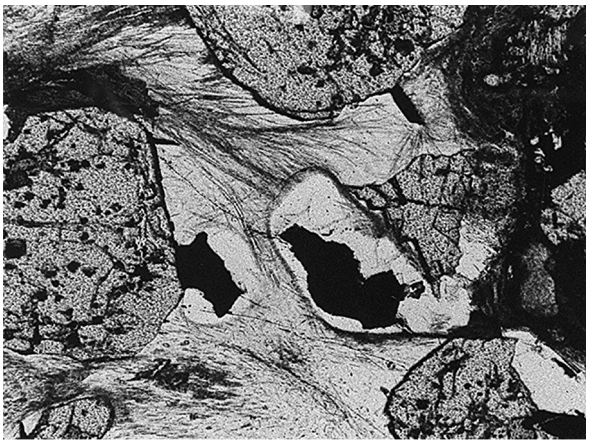
c



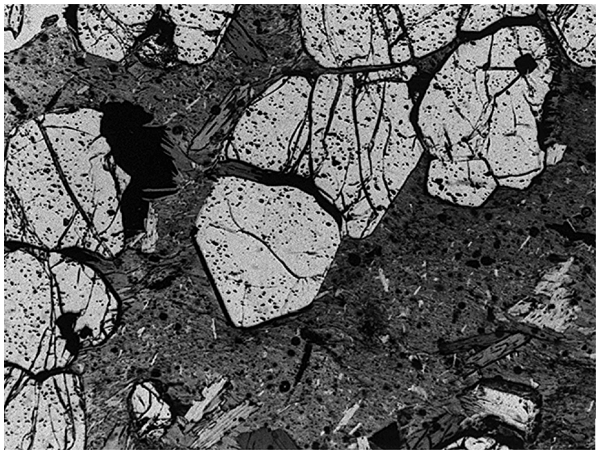
d



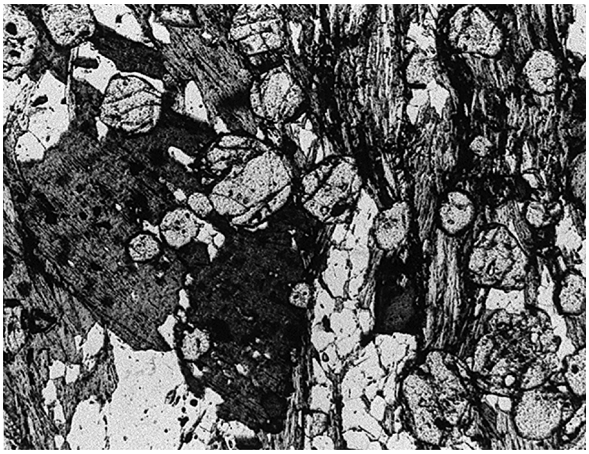
e



f



g



h

Another example of idiomorphic garnet without quartz inclusions occurring in a quartz free matrix is shown in Figure 108b but in this case the garnet contains relatively coarse grained magnetite inclusions which also occur in the matrix, although less abundantly. Again, the inference is that quartz was not included because little, if any, was present during garnet growth.

In contrast, the garnets shown in Figure 108c occur in a quartz free matrix but have many quartz inclusions and also some irregular boundaries. It is suggested that such garnets grew in a quartz rich environment and that the size of the indentations on the garnet rims reflects the size of the quartz grains being enclosed when the garnet ceased growing. This interpretation is supported by a few garnets in other parts of the same rock that are still in contact with quartz (Figure 108d, lower right hand corner). Presumably, nearly all of the matrix quartz subsequently was replaced by biotite, perhaps during a metasomatic event.

Further information on the history of the lithology discussed above is revealed within some garnets occurring near its contact with a chlorite rich zone. Figure 108d shows the contact between two assemblages, with chlorite to the left hand side, biotite and garnet to the right hand side, and a garnet occurring on the contact. Internally, this garnet can be divided into several zones according to the number and type of inclusions present. A small core with many quartz inclusions occurs to the middle right hand side of the grain. The inclusions define a weak S_1, trending from top right to bottom left in the photograph. (Although S_1 is not obvious in the photograph it can be seen in the thin section and other similar garnets nearby). Surrounding the core are more quartz inclusions but they are coarser grained, more elongate and wrap around the core. At the outer limit of this zone, on the side closest to the chlorite, elongated grains also wrap around the core. Finally, the outer portion of the garnet, which projects into the chlorite, is inclusion free.

A complex history for this rock seems likely and indeed, where there is information preserved, similarly complex histories are indicated for many quartz poor lode rocks. The microstructures illustrated in Figure 108c, d can be explained by the following sequence of events, although others are possible:

(a) Formation of a schistosity in a rock consisting of quartz and layer-silicate minerals, perhaps the same as the quartz rich varieties of lode schist.

(b) Initial garnet growth (the cores).

(c) Formation of the chlorite and ilmenite rich zones, but these may have formed earlier.

(d) Deformation of the matrix such that elongated quartz grains were deflected around the pre-existing garnet in the quartz rich zone, but ilmenite was deflected around it in the adjacent chlorite rich zone. To explain the mis-orientation of S_1 in the cores between different garnets, rotation of garnets at this stage or deformation of the schistosity prior to any garnet growth was possible.

(e) Further garnet growth.

(f) Metasomatism caused the replacement of matrix quartz by biotite. It is possible that the chlorite zone post-dates biotite formation, but because the inclusions in the garnet spanning the contact reflect the assemblages on either side, most of the garnet is interpreted to have grown after the two zones had formed.

This interpretation involves the growth of one mineral, garnet, at different stages and probably by different reactions. Other reaction products, no longer apparent, may have been involved

also. An important deduction from this rock, which can probably be applied to many other similar quartz poor lode schists, is their association with a metasomatic event (or events) that resulted in the abundance of hydrated minerals, in this case biotite, and the paucity of quartz.

A dilational state seems to have prevailed in rocks during metasomatism. This is suggested by the "pull-apart" structures shown by several minerals, but especially by garnet. Grains or aggregates of grains, which appear to have formerly been in contact, seem to have moved apart along either grain boundaries or fractures within grains, such that they now resemble jigsaw pieces. In the rock described in the preceding paragraphs, spaces between the "fragments" appear to have been filled by biotite, and in other rocks by quartz, chlorite or sulphide minerals. When viewed in thin section, not all the fragments appear to match but this can be explained by relative movement of the fragments on planes oblique to those of the thin sections.

Rocks with interpreted "pull-apart" or dilational structures typically contain amphibole, a mineral that is rare in other local rocks. Figures 108e, f show dilational structures involving garnet with quartz as the infilling phase. Note in Figure 108f (middle right), the garnet grain (fragment?) with a serrated edge, suggesting rupture along rational faces. In Figure 108g the gaps between garnet are occupied by pyrrhotite, chalcopyrite and chlorite. This chlorite is much coarser than that constituting the rest of the matrix. In this example the garnets contain numerous ilmenite inclusions that are similar in size, shape and distribution to those in the fine grained chlorite matrix. Biotite laths appear to be replaced by matrix chlorite. It seems that this was a biotite bearing rock in which fine grained chlorite rich zones developed, corroding some of the pre-existing biotite in the process. The chlorite and ilmenite defined a schistosity parallel to the zones. Subsequently, garnet grew at the expense of chlorite (but not ilmenite) and these were later ruptured, the gaps being filled by coarser chlorite and sulphide minerals. So again a relatively complex history involving at least one deformational event and a metasomatic event is indicated for this quartz poor lode rock.

Amphiboles

Microprobe analyses of amphiboles occurring in lode schists (presented in Chapter 9) show that they have compositions close to, and on both sides of, the grunerite-cummingtonite boundary, but most are cummingtonite. Some of the microstructures of amphibole were mentioned in the previous section. Amphibole has been observed in two forms, which are:

- fine needles in quartz; and
- coarse, euhedral prisms.

The fine grained variety occurs in rocks showing the dilational features described above. In Figure 108f all the quartz shown is optically continuous and the rounded amphibole free zones, which are common in these rocks, possibly represent quartz rich portions of the rock before dilation and their margins may have been rounded by chemical corrosion. Not all the amphibole fibres are preferentially aligned as shown in Figure 108f, many appear to be random and Figure 108f also shows some radiating amphibole in the top right hand corner.

The coarser, euhedral amphibole prisms are typically associated with quartz poor lode rocks. They occur as scattered, prisms that do not seem to have a preferred orientation. In one sample, however, they define a prominent lineation, parallel to the regional mineral lineation $L_{2/2}$. This rock consists of folded quartz rich and biotite rich layers that possibly represent bedding. The biotite is relatively coarse, with no apparent preferred orientation. Amphibole occurs in thin zones that transgress the layering and are parallel to the axial planes of the folds. Thin sections cut parallel to this lineation reveal that the amphibole is associated with

and parallel to fine schistose biotite and that both minerals appear to be replacing the coarser biotite (Figure 108h). Thus, amphibole seems to occur in zones of solution, parallel to both the axial plane of folds and the contact of the layered rock with the biotite-garnet-amphibole vein.

Sulphide minerals

The microstructures of the sulphide minerals have been described in detail by Lindqvist (1969), who concluded that disseminated sulphide minerals were present during the earliest tectonic phase and were subsequently remobilised into coarser grained concentrations. Here, only microstructural evidence for the involvement of the sulphide minerals in the metamorphism will be described.

Sulphide rich rocks commonly have a coarse layering defined by zones rich in silicates, magnetite, or sulphides and magnetite. The coarse layering, like sulphide veins, appears to be parallel to the overall schistosity. However, the silicates consist predominantly of apparently randomly oriented chlorite with lesser garnet and staurolite (Figure 109a), and where enclosed in chlorite, the latter two minerals tend to be euhedral and have opaques as inclusions that do not define S_1. Against sulphides, staurolite usually develops irregular faces (e.g. against chalcopyrite in Figure 109a) whereas garnet invariably develops its crystal form (Figure 109b). Chlorite also occurs within sulphide minerals, with its (001) plane as a grain boundary (Figures 109c, e). Thus, many local metamorphic silicate minerals occur within sulphides and in apparent equilibrium.

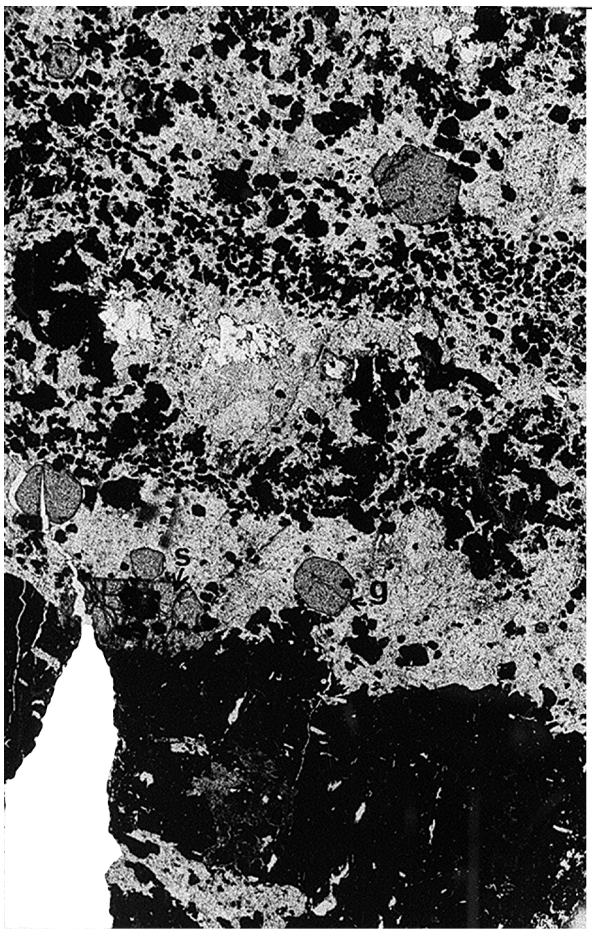
Like many metamorphosed sulphide deposits (Vokes, 1969, 2000; Marshall and Spry, 2000) the Kanmantoo copper deposit does not preserve much detailed evidence of its tectonothermal history in the sulphide minerals themselves. The most convincing evidence that the sulphide minerals were metamorphosed is found in their microstructural relationships and in their intimate association with metamorphic silicate minerals. These microstructural relationships have already been described - the most important observations are the parallelism of sulphide grains to both S_1 and S_2. The associated silicate minerals are the same as those occurring in the surrounding metamorphic rocks. In addition, some important microstructures that are suggestive of (but not diagnostic of) a metamorphic history are listed below:

(a) The sulphide minerals are relatively coarse grained (up to 8mm).

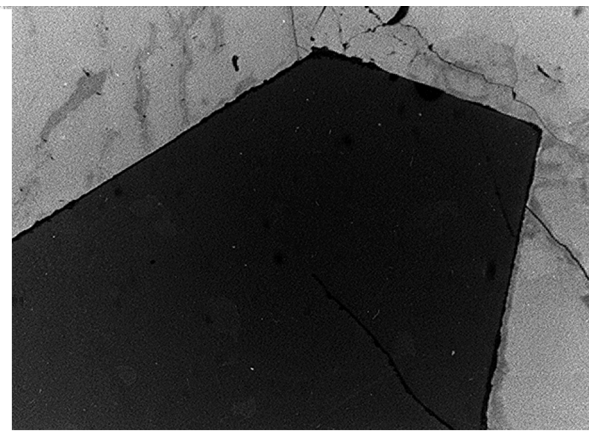
(b) Exsolution is widespread. Figure 109d shows cubanite lamellae in chalcopyrite. Sphalerite exsolution lamellae in pyrrhotite, and ilmenite in magnetite are also common.

(c) Magnetite "porphyroblasts" containing chalcopyrite and pyrrhotite inclusions are themselves surrounded by these minerals (Figure 109d).

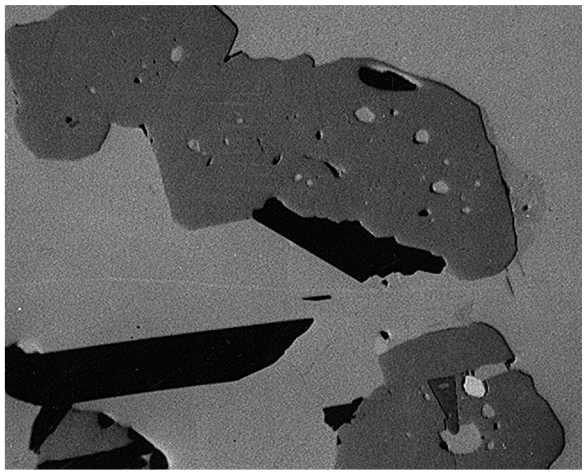
(d) A pronounced gneissosity is present in some sulphide-oxide rocks.



a



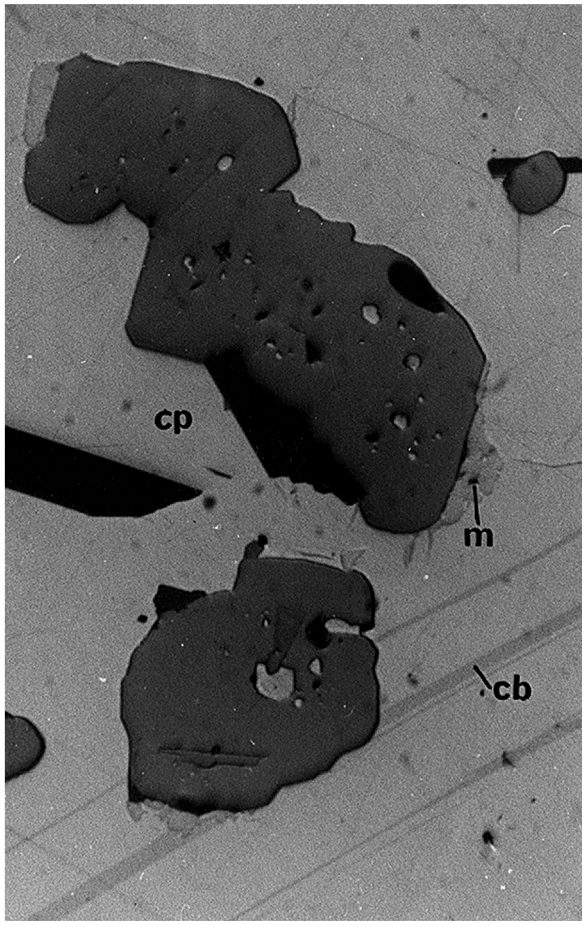
b



c



d



e

Figure 109 (previous page). Relationships between silicate and sulphide minerals.

(a) Chlorite-magnetite rock with minor garnet (g) and staurolite (s). Note the opaque vein (chalcopyrite, pyrrhotite, magnetite) at the base and the diffuse magnetite rich bands parallel to the vein. The chlorite does not define a schistosity. The white patches in the centre are holes in the thin section. [PPL. Sample No. 517-110. Photo width is 7.0mm.]
(b) Idioblastic inclusion free garnet surrounded by pyrrhotite. [Reflected light. Sample No. 517-220. Photo width is 1.0mm.]
(c) Back scattered Xray image. Silicate minerals are black, magnetite is medium grey and includes, and is enclosed by, light grey chalcopyrite. The magnetite grain at lower right has a dark grey triangular ilmenite and white LA-Ce phosphate (?monazite). [Sample No. 517-014. Photo width is 0.30mm.]
(d) Ilmenite (i, medium grey) in chalcopyrite (c) and pyrrhotite (p). A garnet crystal (g) is shown at top right. [Reflected light. Sample No. 517-163. Photo width is 10mm.]
(e) Same as (c) above but taken with reflected light. Cubanite (cb) exsolution lamellae and mackinawhite (m) occur in chalcopyrite (cp). [Reflected light. Sample No. 517-110. Photo width is 0.35mm.]

6.9 The microstructure of chlorite

Chlorite is a minor phase in most rocks of the Kanmantoo Mine area and the Kanmantoo district where it occurs mainly as laths that crosscut the S_2 schistosity (an example is shown in Figure 80). In the Kanmantoo district chlorite is nowhere as common as it is close to, and within, the Kanmantoo copper deposit and in other nearby and similar deposits. Locally, there is a clear and obvious association of chlorite with sulphide mineralisation.

In the Kanmantoo Mine two chlorite varieties have been recognised in this study that can be distinguished by their optical properties, their chemical compositions and their habits. The two varieties will be termed the Fe-rich variety and the Fe-poor variety. These terms are a result of microprobe analyses, discussed in Chapter 7.

6.9.1 Fe-poor chlorite

This is by far the most common variety, probably accounting for more than 95% of all chlorite in the Kanmantoo deposit. Most of it occurs in one of the following habits:

(a) polygonal quartz-chlorite aggregates;

(b) chlorite associated with biotite;

(c) chlorite associated with andalusite;

(d) in quartz poor lode schists.

The first of these has already been discussed in Section 6.7.2, and descriptions of the other three follow. Finally interpretations of chlorite microstructures and their relationships to the origin of the sulphide deposits are discussed at the end of this chapter.

Chlorite associated with biotite

Many GAB(3) schists have chlorite intergrown with both biotite porphyroblasts and the finer grained biotite defining S_2. In the biotite porphyroblasts, chlorite is associated with microstructures that are inferred to result from micro-boudinage of the biotite porphyroblasts.

Chlorite occurs as either straight-sided wedges or as parallel-sided grains, within or at the edge of the porphyroblast, and bounded by the (001) plane of biotite. Lindqvist (1969) regarded this chlorite as post "alteration zone" replacement of biotite. The thin chlorite wedge shown on the right hand side of the biotite porphyroblast in Figure 99b has an apparent angle of 1 to 2 only, which corresponds with the optical misorientation of the host biotite.

In Figure 99b the (001) plane of chlorite is parallel to the (001) plane of biotite only on the right hand biotite fragment and intersects the (001) plane of the left hand biotite fragment at a low angle. Rather than a replacement product of biotite, it appears to be infilling the space in a biotite grain which has separated on a (001) plane and then the two portions rotated slightly. Therefore, an origin similar to that associated with the dilational features described in Section 5.5.4 is proposed. It is possible that similar, but parallel sided, chlorite grains in biotite also formed by extension of the host grains, but without rotation. In some biotite grains both parallel sided and wedge shaped chlorite grains occur, perhaps reflecting different sections through wedge shapes in all grains.

The proposal above that the relationship of chlorite to biotite porphyroblasts is one of space filling rather than replacement is supported by the data shown in Figure 100e, which was measured on a section cut parallel to the mineral lineation of a sample of GAB(3) schist in which the biotite porphyroblasts do not have any apparent severe internal strain. Approximately one quarter to one fifth of the biotite porphyroblasts have associated chlorite. For each of these porphyroblasts the angle between the trace of the (001) plane in biotite and the estimated average trend of S_2 was measured. The measurements plotted in Figure 100e indicate that chlorite occurs in grains with (001) traces at a high angle to S_2. This relationship with S_2 is consistent with the extension occurring during the formation of S_2, possibly parallel to the mineral lineation. Many rocks with these chlorite microstructures also contain quartz between what appear to be two portions of a separated grain (Figure 99a). Extensional microstructures in biotite, similar to those described above have been described by Vernon and Flood (1979).

Not all chlorite-biotite intergrowths appear to be non-replacement relationships as described so far. A rare but convincing replacement microstructure is shown in Figure 110 in which optically continuous remnants of biotite are enclosed in a chlorite mass preserving the shape of the original biotite. Most chlorite-biotite grain boundaries in this example are parallel to the (001) plane of the biotite, and most chlorite is relatively fine grained. The (001) plane of biotite appears to have been exploited preferentially during replacement but replacing chlorite grains that are discordant to biotite (001) can be seen at the base. The replacing chlorite looks similar to the matrix chlorite but is slightly darker, allowing the original shape of the biotite grain to be seen.

Another example of chlorite apparently replacing biotite was observed in some GAB(1) schists located near the Kanmantoo deposit. In these rocks some chlorite was cross cutting biotite and muscovite defining S_2, but others were parallel to S_2 and had a notable preference to replace those biotite grains immediately adjacent to andalusite porphyroblasts.

Summarising, matrix chlorite is typically closely associated with biotite but generally there is little evidence that the biotite has been replaced. Rather the schistose biotite-chlorite intergrowths exhibit relatively stable microfabrics with no sign of replacement. If replacement of biotite did occur it was incomplete and the resultant mixture now defines S_2, perhaps because the replacement was mimetic as proposed by Lindqvist (1969), or because the replacement preceded the formation of S_2 and the initial replacement microfabrics were destroyed during S_2 formation. Equally likely however, is that the schistose biotite-chlorite intergrowths are non-replacement microfabrics. Similarly, the chlorite associated with the coarse grained biotite porphyroblasts appears to have a space-filling role rather than one of

replacement. Only in a few rocks is the iron-poor chlorite clearly replacing biotite and in these cases the replacement appears to post date S_2 formation.

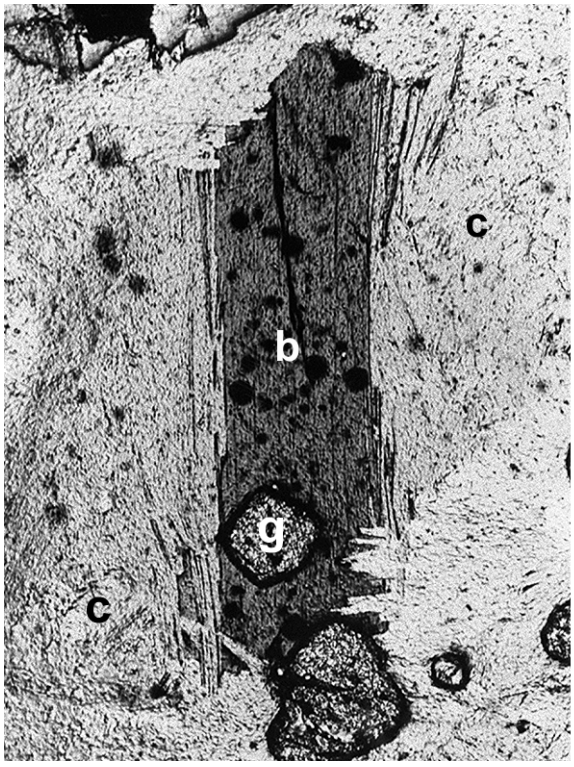


Figure 110. Coarse biotite incompletely replaced by Fe-poor chlorite. The slightly darker shape of the original biotite grain is apparent, leaving an unreplaced rectangular area (b) surrounded by chlorite (c). Garnet (g) is not replaced by chlorite. [PPL. Sample No. 517-010. Photo width is 1.8mm]



Figure 111. Andalusite with chlorite corona. The andalusite grain (a) has a strong S_1 parallel to S_2 defined by biotite (b) and finer grained chlorite in the matrix. Coexisting Fe-Mg rich phases biotite and garnet do not have chlorite rims. [PPL. Sample No. 517-066. Photo width is 5.0mm]

Chlorite associated with andalusite

Andalusite bearing lode schists typically have coronas of chlorite on andalusite (Figure 111). This chlorite is optically similar to adjacent chlorite that defines S_2 and is associated with biotite. The chlorite coronas are interpreted to have formed by rim replacement of andalusite, for the following reasons:

(a) Chlorite generally occurs around the entire perimeter of andalusite in approximately constant thickness.

(b) The chlorite rim commonly reflects the shape of andalusite grains (pseudomorphous replacement).

(c) In some cases the rimming chlorite has quartz inclusions that are similar in shape and size to those in the adjacent andalusite; such inclusions are rare in any other chlorite.

In the coronas surrounding andalusite, chlorite has a variety of orientations. Many chlorite grains are parallel to S_2 and have a more or less continuous microfabric with matrix chlorites as shown in Figure 111. Other chlorite grains are perpendicular to the andalusite boundaries, or are random.

In rocks with chlorite coronas on andalusite, no other coexisting minerals appear to have been replaced by chlorite. This applies to Fe-Mg rich minerals like biotite, as discussed previously, and also garnet and staurolite. (However, the latter two minerals are replaced by Fe-rich chlorite, producing easily distinguishable microfabrics that are restricted to zones adjacent fractures.) The lack of involvement of other phases in the formation of the Fe-poor chlorite coronas is most easily explained by metasomatic reaction, probably during the formation of S_2, when the metasomatic fluids could also have formed the chlorite wedges in the distended biotite porphyroblasts of the same rocks.

Group 2 lode schists

These rocks were discussed in Section 5.7.3. Generally, the microstructure of chlorite is similar to other coexisting minerals in the sense that, if they define a foliation, so does chlorite. Chlorite appears to occur in microstructural equilibrium with biotite and in some rocks defines a schistosity whereas coexisting biotite does not (Figure 108g). Fe-poor chlorite has not been observed replacing garnet or staurolite; hence it appears to be in equilibrium with all other phases in the rocks, except Fe-rich chlorite if present.

6.9.2 Fe-rich Chlorite

This chlorite variety has replaced selectively garnet and staurolite, unlike Fe-poor chlorite, but not biotite, andalusite or Fe-poor chlorite, all of which it post-dates. Garnet is replaced by radial aggregates of fine-grained, green chlorite, and staurolite is replaced by random aggregates of fine-grained, brownish chlorite. Fe-rich chlorite has been observed in the following three associations:

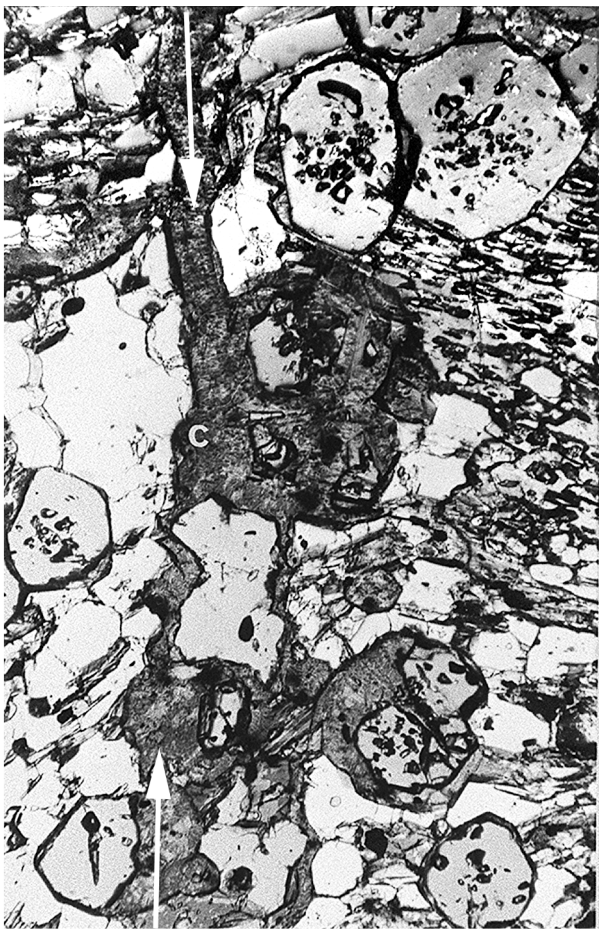
(a) Associated with fractures. These fractures are transgressive to S_2 and are usually emphasised in thin sections by iron staining. Garnet and staurolite adjacent to the fractures are extensively replaced (Figure 112b) but are unaltered in the rest of the rock, except where they are in contact with sulphide minerals, either chalcopyrite or pyrrhotite (Figure 112a). The sulphide minerals adjacent to altered silicate minerals seem to be unaltered and perhaps to have acted as a local catalysing agent for the alteration contiguous minerals. Many altered garnets are surrounded by two, separate chlorite rims (for example Figure 112a), indicating perhaps more than one alteration phase.

(b) Associated with veins. Rocks close to veins that are rich in quartz, siderite, chlorite, tourmaline and albite (for example Figure 112d) also have chloritised garnet and staurolite. These veins are identical to those observed in some of the very large joints in the Kanmantoo area and appear to post-date the ductile deformation phases.

(c) Associated with biotite rich domains. In one rock, intense deformation along biotite rich domains has produced abundant kinking of biotite and shattering of garnet (Figure 112c). Fe-rich chlorite has replaced the garnet fragments, not the biotite. However, this rock occurs near one of the veins described in (b) above and so the two maybe related.



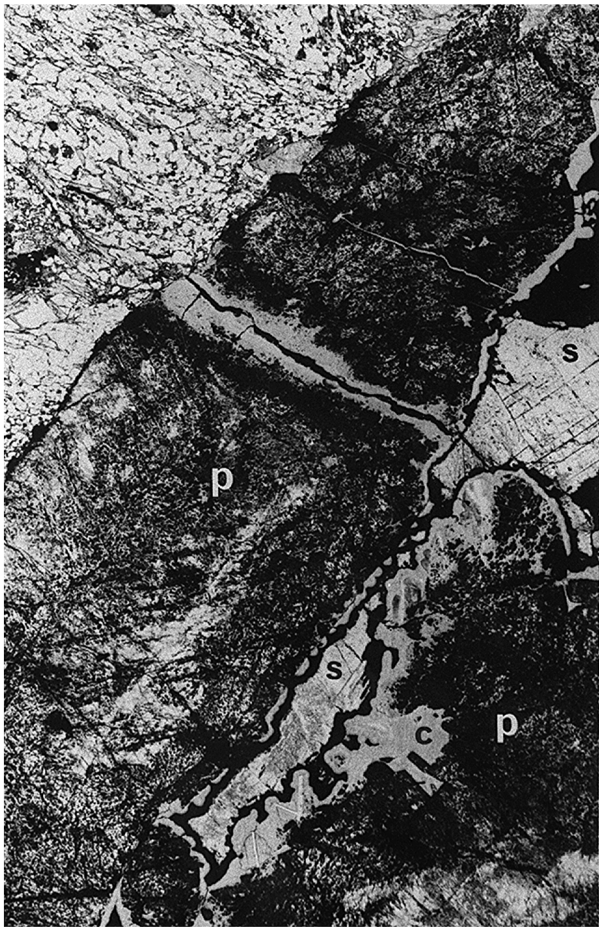
a



b



c



d

Figure 112. (preceding page). Iron rich chlorite microstructures.

(a) Garnet replaced by Fe rich chlorite. This rock consists of garnets in a quartz-Fe poor chlorite matrix with a chalcopyrite-pyrrhotite vein at left. The vein contains a lath of Fe poor chlorite (c). Some garnets are unaltered and others, closer to the vein, are partly (lower centre) or completely (top left) altered. The garnets furthest from the vein are unaltered. [PPL. Sample No. 517-024. Photo width is 1.3mm]

(b) Irregular fracture (arrowed) filled with Fe rich chlorite (c). Some of the garnets adjacent to the fracture are partially replaced by Fe rich chlorite, leaving the pseudomorphic shape of the former idiomorphic garnet. [PPL. Sample No. 517-024. Photo width is 2.9mm]

(c) Zone of intensely kinked biotite and shattered garnet. The latter is partially replaced by Fe rich chlorite (c) but the biotite is not. [PPL. Sample No. 517-069. Photo width is 1.3mm]

(d) Contact between quartz rich lode schist (top left) and a vein consisting of a post-peak metamorphism assemblage of cloudy plagioclase (p), siderite (s), Fe rich chlorite (c) and chalcopyrite. [PPL. Sample No. 517-200. Photo width is 9.0mm]

All of the three associations appear to be related to a post-S_2, brittle deformation event that also caused local kinking of biotite. It is likely that they are related to the large fractures in the area and that Fe-rich chlorite in the mine represents the effects of a regional, relatively late stage metasomatic event.

6.10 Discussion and conclusions

6.10.1 The genetical relationship between S_1 and S_2

The issue to be considered here is whether S_1 and S_2 represent two stages of one deformation or two separate deformations. It was shown that in some samples where S_1 and S_2 are discordant they could be related most simply by a process whereby S_2 develops from a version of S_1 following bulk rotation and grain growth (section 6.3.5 and Figure 5.7). Although S_1 and S_2 in GAB(1) schist, GAB(2) schist, GAB(3) schist and quartz rich Lode schists are typically discordant there are rare examples where they are continuous (e.g. Figure 5.1b) which demonstrates that S_2 was derived from S_1, in some cases at least.

Lindqvist (1969) concluded that S_1 and S_2 represent different stages of a single deformation. However, several authors later concluded that they represent two deformations and that S_2 was produced from S_1 by a crenulation cleavage mechanism (Spry, 1976; Schiller, 1978; Mancktelow, 1979). Mancktelow (1979) correlated S_1 with his regional S_1 and further considered the development of S_2 in the Kanmantoo area to be one of the best in the Mount Lofty Ranges.

Crenulation cleavages are zones of mineral differentiation coincident with the limbs of microfolds in crenulated rock fabrics (Gray, 1977). Summaries of crenulation cleavage characteristics can be found in Hobbs et al., (1976) and Passchier and Trouw (1996). Cleavage development is essentially considered to be a process involving microfolding and accompanying solution-transfer and regrowth of minerals (Marlow and Etheridge, 1977; Gray, 1979). Two important characteristics of many crenulation cleavages in pelitic schists, that are pertinent to schists of the Kanmantoo Mine area, are the development of a domainal matrix comprising two domain types, and different overall orientations of the micas within the domains. In crenulated pelitic schists one domain typically is relatively mica rich and quartz poor, and the other domain is relatively quartz rich and mica poor. In many crenulated schists the mica rich domains have mica grains with preferred orientations parallel to, or slightly

oblique to, the domains, whereas in quartz rich domains the micas tend to be at a high overall angle to the domains. A continuous, crenulated fabric is evident in all but the most intensely crenulated rocks, and in these cases all micas tend to be parallel to the domains (Marlow and Etheridge, 1977). Bell and Rubenach (1983) described six successive stages in crenulation cleavage development that can be preserved as inclusion trails in porphyroblasts. The stages range from the original unfolded foliation (Stage 1), through the development of folding and domains (Stages 2 to 5), to a new, homogenised and undifferentiated foliation (Stage 6) in which all micas are subparallel. Passchier and Trouw (1996) elaborated on the effect of temperature on Bell and Rubenach's stages but they did not include stage 6 in their sequence.

In the Kanmantoo Mine area, GAB(1) schists are domainal, with most micas preferentially oriented parallel to the domains and no evidence of prior crenulation, except perhaps straight inclusion trails, some of which are oblique to S_2. Morphologically, they are closest to Bell and Rubenach's Stage 5. In domainal schists, like GAB(1) schist especially, the Q domains have porphyroblasts in which S_1 is discordant to S_2 and can be interpreted as the hinges or the short limbs of a crenulated fabric. However, schists in the Kanmantoo Mine area have features that are difficult to explain by a crenulation process, as follow:

(a) Only porphyroblastic rocks are domainal. Even non-porphyroblastic rocks adjacent to porphyroblastic rocks are not domainal, for example QMF schist beside GAB(1) schist or non-andalusite interbeds in GAB(1) schists.

(b) In the Q domains of GAB(1) schist the andalusite porphyroblasts rarely preserve a curved S_1, such as one might expect in the zones of greatest curvature in crenulated fabrics. Instead, S_1 appears to be planar, with very few exceptions.

If the microfabric of GAB(1) schist is a result of a crenulation cleavage mechanism then to account for the two observations above the following sequence of events is indicated. Firstly, most andalusite porphyroblasts must have grown before S_1 was buckled, or at least in the early stages of buckling, to account for the preservation of straight trails. Then, to account for the coincidence of andalusite and Q domains, the crenulations presumably nucleated on the pre-existing porphyroblasts and so the crenulation fold pattern was determined by the distribution pattern of andalusite porphyroblasts. In particular, the pattern of andalusite porphyroblasts determined the positions of either crenulation hinges, if the folding was symmetrical, or crenulation short limbs, if the folding was asymmetrical, because these are the zones of crenulated fabrics which become Q domains during later mineral differentiation (Hobbs et al., 1976). Such a process would explain why only porphyroblastic rocks are domainal. Alternatively, the crenulation cleavage fabric of non-porphyroblastic rocks may have homogenised, as ascribed by Bell and Rubenach (1983) to their stage 6, but not in porphyroblastic rocks.

The mineral differentiation process is not exclusive to crenulation cleavages. In low to medium grade metamorphic rocks mineral differentiation is generally thought to be related to pressure solution. According to Kerrich and Allison (1978, p111), "pressure solution is a deformation mechanism involving intercrystalline diffusive mass transport in the response to applied stress". In metapelites, pressure solution involves the effective migration of "more mobile" minerals like quartz to relatively low stress regions leaving zones depleted in quartz and enriched in "less mobile" minerals like micas and oxides. The production of stress gradients in deforming rocks appears to involve heterogeneities that were either present before deformation or developed during it. An example of the latter alternative is crenulation cleavage, in which mineral differentiation is thought to follow initial buckling of a planar fabric because it is promoted by strain inhomogeneities developed in the buckled fabric (Cosgrove, 1976). Many authors (see Kerrich, 1977, page 524, for a review; Hobbs et al., 1976; Passchier and Trouw, 1996) have attributed the formation of domains in crenulation

cleavages to pressure solution driven by stress gradients developed during folding. Cosgrove (1976) suggested that in zones where the folded planar fabric is at a low angle to the maximum principal stress, quartz experiences relatively lower stress compared to neighbouring zones, and migrates from the latter to the former.

However, there are other rigid structures in deforming rocks besides buckled fabrics, for example rigid particles. Pressure solution can be initiated at the boundaries of rigid particles that are large with respect to matrix minerals, such as sedimentary clasts or porphyroblasts. Rigid particles like porphyroblasts affect the stress pattern in the surrounding matrix (Stromgard, 1973) and control the partitioning of deformation around them because of their coarse size and greater strength compared to matrix minerals (Etheridge and Vernon, 1981; Bell et al, 1986; Bell, 1985). In metapelites rigid particles can promote pressure solution in their vicinity producing mica rich domains at their margins that propagate in a direction normal to the maximum principal stress (Kerrich and Allison, 1978, page 111). When these structures are of limited extent laterally and are positioned on the rigid particle they are referred to as strain caps (Passchier and Trouw, 1996).

It was argued above that if a crenulation cleavage mechanism was widespread in GAB(1) schists the andalusite must have grown in its very early stages. Therefore, a rigid particle would have been present anyway and the need to invoke crenulation cleavages to explain the domains is unnecessary. Pressure solution associated with rigid particles also explains more easily than a crenulation cleavage process, why only porphyroblastic rocks are domainal. It is suggested that domains were not developed in some porphyroblastic rocks, namely GAB(2) and GAB(3) schists, because in these the differential stress was reduced by high fluid contents, and was too low for pressure solution to be an important process.

Although the formation of S_2 in the Kanmantoo Mine area seems unlikely to have involved crenulations generally, there are rare examples of clearly crenulated S_1 which are anomalous in this area and presumably have an anomalous history. The example shown in Figure 87 is in a probable high strain zone and may have had a more complex history than adjacent schists. In other cases S_1 is only gently buckled and appears to be preserving Bell and Rubenach's stage 2 of crenulation development. It is inferred that in these cases S_1 was at a high angle to the early S_2 plane, leading to buckling rather than bulk rotation and subsequent crenulation. A planar fabric that is at a low angle to the maximum principal stress will tend to buckle, whereas one at a high angle will tend to rotate without buckling. The latter case seems to have been prevalent for the deformation of S_1 in the Kanmantoo Mine area, and is consistent with Mancktelow's observation that, regionally, (his) S_1 and S_2 are only slightly discordant. However, if S_1 had local irregularities in orientation then, locally, crenulations could develop.

In most rocks of the Kanmantoo Mine area, S_2 appears to have developed from S_1 but it is uncertain whether one or two deformations were involved. The evidence described in this chapter (together with the lack of mesoscopic overprinting structures) is equally consistent with one deformation during which the principal stress components rotated, as it is with two events recognised in the region. Certainly, if the precursor to S_1 is a bedding fabric, then only one deformation is indicated. The relatively rapid growth of porphyroblasts during a progressive, non-coaxial deformation will record *stages* of the history whose timing may be more relevant to thermal progress than tectonic events.

6.10.2 Growth relationships between andalusite and staurolite

Several authors have discussed the relative timing of andalusite and staurolite development in the Mount Lofty Ranges. In the Springton area, Mills (1964) reported that the first appearance of staurolite was downgrade of andalusite. To the north, near Angaston, Fleming (1965, 1971) found the opposite sequence, that andalusite formed prior to staurolite. Mancktelow (1979) considered that staurolite and andalusite generally formed simultaneously, but conceded that separate times of formation were possible in some areas. Offler and Fleming (1968) and Fleming (1971) postulated a pressure gradient between the Angaston and Springton areas to explain the variations. In particular, andalusite preceded staurolite in relatively aluminous rocks metamorphosed at lower pressures.

In the Kanmantoo Mine area staurolite is interpreted to have formed at two stages: syn- and post- andalusite. The only rocks in which andalusite and staurolite appear to have grown simultaneously are GAB(3) schists in which both minerals form composite porphyroblasts. In all other rocks where an age difference can be inferred staurolite appears to post-date andalusite and this applies to some GAB(3) schists also.

6.10.3 Chlorite and sulphide minerals

In the Kanmantoo Mine area, a close spatial relationship between sulphide mineralisation and chlorite bearing rocks has been demonstrated in previous chapters. Furthermore, it was shown that both chloritic rocks and sulphide mineralisation are grossly discordant to bedding in GAB schist and so indicate a common hydrothermal origin. Constraining the timing of this hydrothermal event (or events) is vital in understanding the origin of the mineralisation. The temporal relationship between chlorite and sulphide minerals, as indicated from microfabrics, is now considered.

Three key observations relevant to the timing of formation of chlorite follow.

(a) Chlorite, unlike sulphide minerals, does not occur within andalusite or staurolite porphyroblasts.

(b) Most chlorite is parallel to S_2 in a non-domainal, non-crenulated fabric that shows no evidence of earlier deformational events.

(c) Some chlorite appears to be associated with a metasomatic event during S_2.

With respect to (a), only in one sample from the mine was chlorite observed within andalusite and this single occurrence could be explained as a fortuitous section of a matrix chlorite grain growing within an irregular portion of the andalusite surface. It cannot be assumed from one grain that chlorite was present prior to andalusite growth. On the other hand, its absence in porphyroblasts does not demonstrate that no chlorite was present, for it may have been completely consumed at the reaction site during porphyroblast growth, leaving chlorite only in the matrix, to later define S_2.

Next, the evidence for a metasomatic event during S_2 development is that of chlorite rimming andalusite and also occurring within micro-boudinaged biotite porphyroblasts. In the first case the chlorite in the coronas is typically parallel to S_2 (Figure 111), and in the second case chlorite wedges in biotite porphyroblasts (Figure 99b) appear to be filling gaps formed in biotite by rupture on (001) planes during extension. However, although a chlorite producing metasomatic event during S_2 formation is indicated, it cannot be assumed that all chlorite was produced at this time.

One interpretation of the three observations discussed above is that all chlorite in the Kanmantoo Mine area was produced by a metasomatic event during the formation of S_2. Alternatively, Lindqvist (1969) suggested that all chlorite formed during a metasomatic event post-dating S_2, by mimetic replacement of biotite principally. However, neither of these interpretations explains the following features of the Kanmantoo deposit.

Firstly, it does not explain the spatial coincidence of sulphide mineralisation and chlorite, unless all the sulphide is also post- S_2, or there are two separate but spatially coincident events responsible for each. The occurrence of chalcopyrite and pyrrhotite parallel to S_1 within andalusite porphyroblasts indicates that at least some sulphide minerals were present in the schists during the development of S_1 and perhaps before. Spatially coincident events are considered unlikely because the sulphide minerals and chlorite are too intimately associated.

Secondly, evidence of replacement by chlorite is limited to andalusite mainly and rare biotite grains. Biotite porphyroblasts in chloritic rocks do not appear to be replaced, rather the chlorite exists in stable intergrowths with biotite, typically sharing (001) planes as boundaries between the minerals. In particular, biotite porphyroblasts are not rimmed in these rocks (e.g. Figures 99a,b,d; 111), so it is difficult to explain why Lindqvist's proposed late stage chlorite should so completely replace the matrix biotite laths (to form S_2) but leave biotite porphyroblasts untouched. Furthermore, in Lindqvists's proposal the chlorite must replace biotite mimetically so that both the schistosity and mineral lineation are preserved. When reviewing Lindqvist's data it is important also to remember that two temporally distinct chlorite varieties occur. Chloritization of garnet and staurolite is associated with a late stage, post- S_2 event and a distinctive variety of chlorite (the Fe rich variety), but this chlorite is a very small proportion of the total chlorite associated with the deposit. Nor does the association of chlorite with the sulphide mineralisation imply necessarily alteration as a retrogressive event.

Therefore, chlorite microstructures are not definitive in tying down the time of development of the chloritic halo associated with mineralisation because the earliest demonstrable growth of chlorite is syn-S_2 but the earlier presence of chlorite is not negated. Unlike chlorite an earlier syn-S_1 presence of sulphide minerals is established and because the two minerals are so closely associated it seems likely that chlorite was present at this stage as well. Chlorite was probably a widespread mineral in the Kanmantoo rocks at an earlier stage of low metamorphic grade and was lost from most rocks by normal prograde reactions near the amphibolite facies boundary. But chlorite formed in an early alteration zone can persist beyond this boundary under certain circumstances, as discussed in the next two chapters. If early alteration occurred, say associated with a sea floor feeder system as suggested by Seccombe et al, (1985), then the sulphide minerals and alteration products would have experienced the same metamorphic history as the surrounding sediments. It is assumed that both chlorite and sulphides developed a fabric parallel to S_1 but during subsequent porphyroblast growth all chlorite was consumed at the reaction site leaving only sulphides and quartz as inclusions and chlorite in the matrix. Then further deformation and recrystallisation would have formed S_2, but at this stage another metasomatic event led to the production of more chlorite (as coronas on andalusite etc) in the same site.

In conclusion, the microstuctural evidence is consistent with the presence of sulphide minerals and probably chlorite at the time of the earliest tectonic fabric. Unfortunately, the important question of whether there was more than one metasomatic event has not been answered, nor was any microstructural support found for or against a syn-sedimentary alteration event.

6.10.4 Conclusions

1. Unlike many regional rocks S_2 developed from S_1 generally not by a crenulation cleavage mechanism, but by rotation and recrystallisation during flattening.

2. Not all porphyroblasts developed at the same time, a series of porphyroblast producing reactions is indicated in most rock types.

3. Sulphide minerals and chlorite (or the assemblage needed for the subsequent formation of chlorite) were introduced to the metasediments together by a hydrothermal event during or before S_1 formation.

4. Many microfabric differences amongst the metasediment and the lode schists (e.g. biotite shape and size) are attributed to high fluid contents near the sulphide deposit. In particular, the fluid possibly caused significant local reductions in the differential stress during deformation.

7. METAMORPHISM

7.1 Introduction

Studies of the Mount Lofty Ranges have shown that the regional metamorphism accompanying the Delamerian Orogeny was of the low pressure-high temperature type (Offler and Fleming, 1968; Mancktelow, 1979, 1990; Dymoke and Sandiford, 1992; Sandiford et al., 1995). Offler and Fleming recognised five metamorphic zones defined by the first appearance of index minerals. The zones were (from the western side to the eastern side): chlorite, biotite, andalusite-staurolite, sillimanite and migmatite zones. The Kanmantoo Mine area is located within Offler and Fleming's andalusite-staurolite zone. Later, Mancktelow (1979) showed that the chlorite zone contained biotite, and he also effectively separated the andalusite-staurolite zone into two sub-zones, which he called the andalusite-staurolite zone (lower grade) and the fibrolite zone (higher grade). In the Callington area he also recognised a locally developed biotite zone, indicating relatively short distances between zone boundaries in this district. The Kanmantoo Mine occurs in Mancktelow's andalusite-staurolite zone (as inferred from his Figure 5.2), but is only about one kilometre from the boundaries of both the fibrolite zone (to the northwest) and the biotite zone (to the southeast).

In this study, rare fibrolite was observed in andalusite and staurolite bearing rocks in the Kanmantoo Mine, indicating that the positioning of Mancktelow's zone boundaries need to be adjusted. Andalusite and staurolite are inferred to have formed with biotite at the expense of the lower grade assemblage of muscovite and chlorite. In the fibrolite zone, fibrolite increases in abundance towards the higher grade regions until coarse, prismatic sillimanite occurs, marking the lower boundary of the sillimanite zone (Mancktelow, 1979). Andalusite and, less commonly, kyanite occur with sillimanite in the sillimanite zone.

In this chapter the mineral assemblages are described, including the unusual chlorite rich assemblages from the lode schists. Next mineral compositions as derived from electron microprobe analyses for the common minerals are discussed. Finally, evidence of chemical equilibrium and estimates of metamorphic conditions are presented. Where necessary, abbreviations for minerals and oxygen fugacity buffers are used in this chapter according to the following key.

alm	almandine	her	hercynite
als	aluminosilicate	ilm	ilmenite
and	andalusite	ksp	potash feldspar
bio	biotite	kya	kyanite
chd	chloritoid	mt	magnetite
cht	chlorite	mus	muscovite
cor	corundum	phl	phlogopite
crd	cordierite	sta	staurolite
cum	cummingtonite	sil	sillimanite
gar	garnet	tlc	talc
ged	gedrite	ulv	ulvospinel
hem	hematite		
FMQ	fayalite-magnetite-quartz oxygen fugacity buffer		
NNO	nickel-bunsenite oxygen fugacity buffer		

7.2 Mineral assemblages

The term mineral *assemblage* is taken here to mean a group of co-existing minerals constituting a single rock type with no apparent disequilibrium, as seen in thin section. It is

recognised that all minerals within a thin section may not be in chemical equilibrium even though no obvious disequilibrium microfabrics are observed. However this means of determining a mineral assemblage is objective.

Table 19. Mineral assemblages of the Kanmantoo Mine area.

	Qtz	Plg	Mus	And	Sil	Bio	Gar	Sta	Crd	Cht	Cum	Ilm	Mt
QMF schist	x	x	x			x	x					x	
	x	x	x			x						x	
QMA schist	x	x	x	x		x	x					x	
	x	x	x	x		x	x	x				x	
GB schist	x					x	x	x				x	
	x			x		x	x	x				x	
GAB(1) schist	x		x	x		x	x	x				x	
	x		x	x		x	x	x	x			x	
	x		r	x	x	x	x					x	
	x		x	x		x	x			r		x	
	x		x	x		x	x		x	r		x	
	x			x	x	x	x	x				x	
	x			x		x	x	x	x			x	
	x		r	x		x	x		x			x	
	x			x		x	x					x	
	x			x		x		x	x	x		x	
	x	x	x	x		x	x	x				x	
GAB(2) schist	x			x		x	x			x		x	
	x			x		x	x	x		x		x	
	x		r	x		x	x	x				x	x
GAB(3) schist	x			x		x	x	x				x	
	x		x	x		x	x	x				x	
	x			x		x	x	x		x		x	x
	x		r	x		x	x	x	x	x		x	x
Lode schist	x						x			x		x	x
	x					x	x	x		x		x	x
	x			x		x	x	x		x		x	x
	x		x			x	x	x				x	x
	x		x			x	x					x	x
	x					x	x	x				x	x
	x			x		x	x	x	x	x		x	
	x					x	x		x			x	
	x					x	x					x	x
	x					x	x			x		x	x
	x					x	x				x	x	x
	x						x			x	x	x	x
						x	x	x		x		x	x
						x	x			x		x	x
						x	x			x	x	x	x
							x			x		x	x
							x			x	x	x	x
							x	x		x		x	x
							x			x		x	x
			x			x	x	x		x		x	x

x = primary r = retrograde

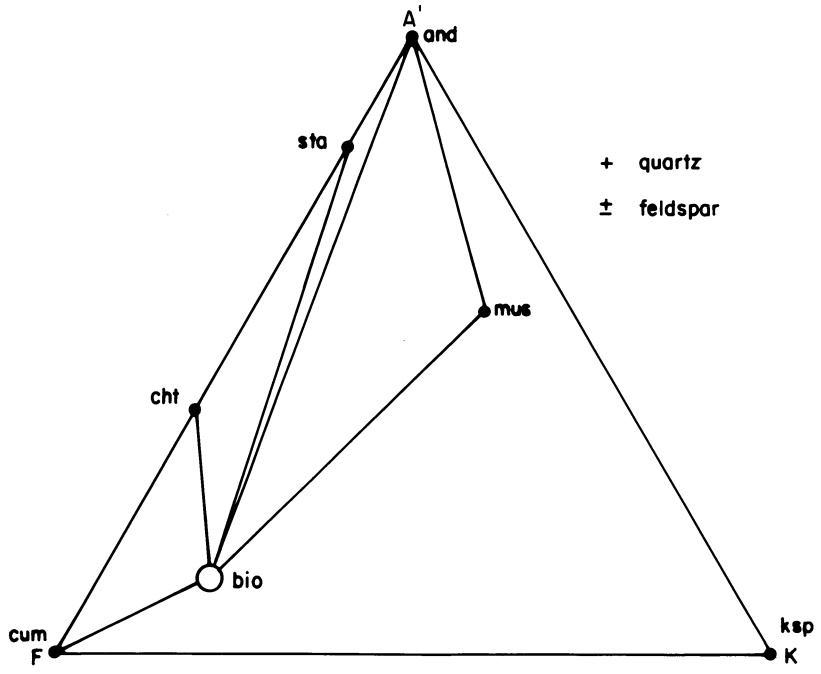
A group of minerals in chemical equilibrium forms a mineral *paragenesis*. Compared to a mineral assemblage, the commonly accepted criteria for recognition of a paragenesis are more rigorous and more subjective (Zen, 1963; Vernon, 1976). Included in such criteria are that

minerals forming a paragenesis must be in mutual contact, must have a similar composition for the edges of different grains of the same phase and must have a similar distribution of components between pairs of phases throughout the chosen rock volume.

In this study mineral assemblages have been determined generally, but experience has shown that, in most cases these appear to be parageneses as well. Cases where this is not thought to be so will be discussed in a subsequent section. Mineral assemblages that have been observed in the Kanmantoo Mine area are shown in Table 19, also shown are the lithologies which contain the various assemblages. Note that all lithologies contain more than one assemblage and that certain assemblages occur in more than one lithology. In the latter case the proportions of minerals vary considerably such that the rocks are recognisably different.

The assemblages of QMF schist and QMA schist are typical of metasediments of amphibolite grade, however GAB(1) schist is, in many cases, atypical in that two minerals, muscovite and plagioclase, which are common in the former lithologies are generally not present. Also occurring in some samples of GAB schist is cordierite, a mineral which has not been previously reported from the Kanmantoo Mine area. An unusual aspect of the lode schist assemblages, compared to the metasediments, is the lack of quartz in many samples.

In order to better understand the mineral assemblages of the Kanmantoo Mine area, an attempt has been made to represent them on ternary diagrams. The first of these is Figure 113, a standard A'FK diagram (see Winkler, 1976, p42):



$A' = Al_2O_3 - K_2O - Na_2O$

$K = K_2O + Na_2O$

$F = FeO + MgO + MnO$

Figure 113. A'FK Diagram

This diagram is useful in helping to visualise the relationship between muscovite and biotite.

K-feldspar has not been observed but could be present in QMF schists with low ferromagnesia contents. In Figure 113, QMF and QMA schists are represented by the andalusite-muscovite-biotite triangle. GAB(1) schist is represented by the andalusite-biotite- staurolite triangle but note that muscovite may be present too. Lode schists are represented by the biotite-chlorite-staurolite and biotite-chlorite-cummingtonite triangles.

Figure 113 illustrates the relationship between K_2O bearing minerals but does not help with ferromagnesian minerals such as garnet, staurolite and chlorite, all of which plot on the A'F axis. This problem can be overcome to some extent by considering FeO and MgO separately, as on Thompson's (1957) AFM diagram. Thompson proposed that the chemistry of typical pelitic rocks may be represented by the following six components: K_2O, Al_2O_3, MgO, FeO, SiO_2 and H_2O (the "ideal" pelitic system). For comparison purposes these six components can be reduced to the first four in rocks that contain quartz (so that SiO_2 is "in excess"), and similarly, the amount of H_2O relative to other components can be ignored, either because H_2O is "in excess" or is controlled externally to the rock volume being considered.

Thus, pelitic rocks can be represented within a K_2O -FeO-MgO- Al_2O_3 tetrahedron and, because most meta-pelites contain muscovite, rock and mineral compositions can be projected onto the FeO - MgO - Al_2O_3 plane from muscovite (Thompson, 1957). In the case of the Kanmantoo Mine area, rocks containing quartz and muscovite are restricted to QMF and QMA schists, and to some GAB schists. The topologies of observed assemblages are shown on the A'FM diagram in Figure 114. The positions of the minerals shown in this diagram are not accurate, as there is little information on the mineral chemistries of suitable assemblages. In particular, the change of biotite composition with various assemblages has not been demonstrated.

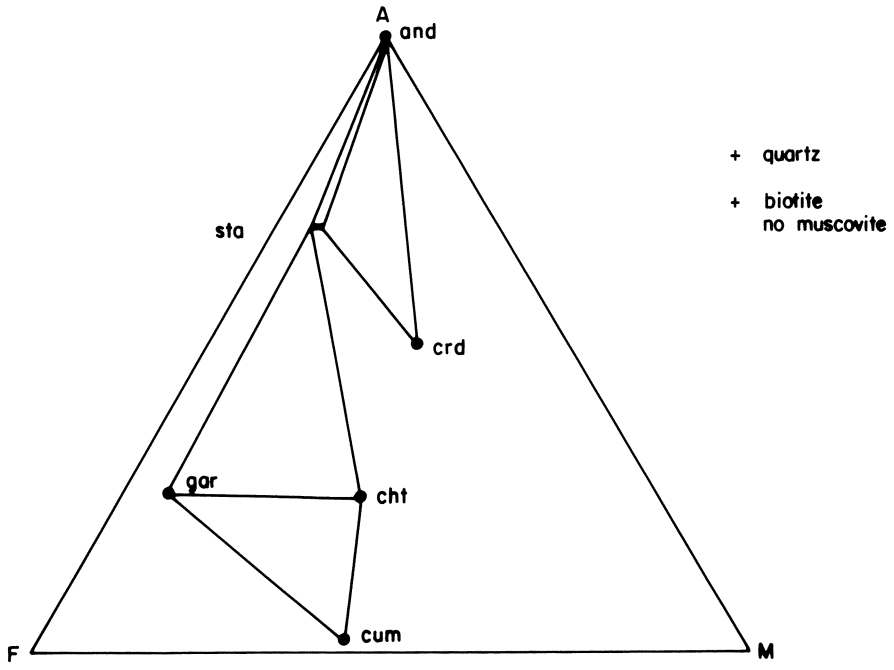


Figure 114. AFM diagram

Garnet was omitted from consideration in Figure 114 because it occurs in all assemblages shown on the diagram and, in fact, in all assemblages except one in the Kanmantoo Mine area (see Table 6). The presence of garnet may be influenced by a component not represented by

an AFM diagram, such as MnO or CaO which are commonly concentrated preferentially in garnet in comparison to co-existing minerals (Chinner, 1965).
The schists in the Kanmantoo Mine area without muscovite (or K-feldspar) cannot be represented on a Thompson AFM projection. These rocks, in which biotite is the only K_2O bearing major phase, can be plotted on the AFM plane of the tetrahedron, as shown in Figure 115, with the understanding that all phases have tie lines extending to biotite. Quartz, biotite and garnet are present in all these assemblages, and garnet has been included in the plot because it does not complicate the diagram. Electron microprobe data (discussed later) indicate little change in the compositions of garnets of different assemblages. Similarly, the compositions of chlorite and cummingtonite do not vary much. Only one cordierite bearing assemblage was analysed by electron microprobe. The composition of staurolite, however, varied slightly; those co-existing with cordierite had slightly higher MgO/FeO ratios than those with chlorite. No assemblages plotting in the staurolite-chlorite-corderite field were observed, it is possible that rocks whose bulk chemistries plotted in this field would have staurolite-chlorite bearing assemblages with the MgO/FeO ratios of these two minerals increasing as the bulk ratio increased, until the staurolite-chlorite tie line was reached and at that point chlorite would not be present.

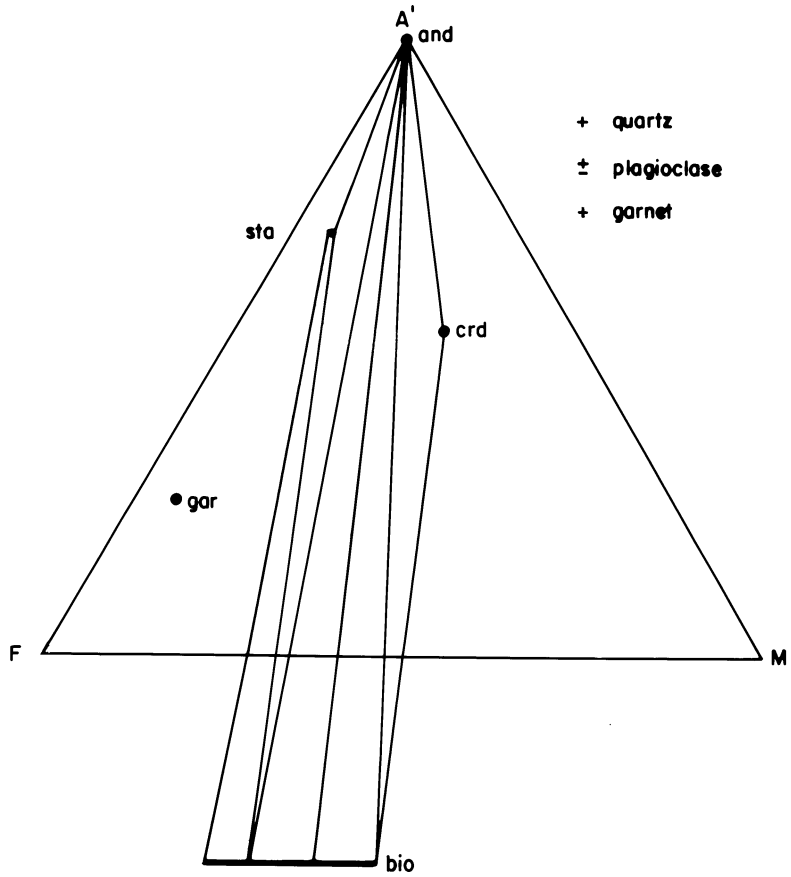


Figure 115. A'FM Diagram (Thompson projection)

The three diagrams discussed so far apply to quartz bearing assemblages. The relationship between quartz bearing and quartz free assemblages can be appreciated on a SiO_2- Al_2O_3-(*FeO+MgO) plot, as shown in Figure 116. On this diagram GAB(1) schist is represented by the quartz-andulasite-staurolite triangle. Quartz bearing lode schists are represented by the quartz-staurolite-chlorite-cummingtonite triangles. Quartz free lode schists are represented by the staurolite-chlorite-cummingtonite-magnetite triangles.

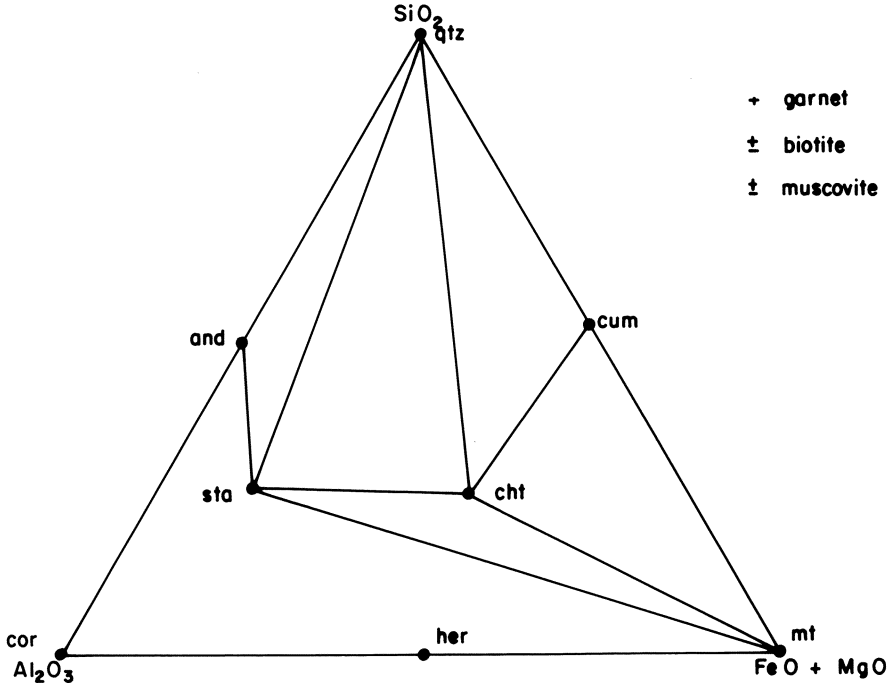


Figure 116. SiO_2-Al_2O_3-FeO-MgO diagram

Whilst representing many observed assemblages, Figure 116 has several deficiencies, some of which will now be discussed. Firstly, magnetite and quartz co-exist, apparently stably, and this is probably related to Fe_2O_3 contents, especially in rocks where this component is too high to be accommodated in biotite and other silicate minerals. Although a staurolite-chlorite-magnetite-(garnet) assemblage has been observed in this study, Lindqvist (1969, Fig. 5.10) reported a corundum-chlorite assemblage from the Kanmantoo deposit which requires crossing tie lines on Figure 116. This topological problem may be related to the inadequacies of the plot, in particular to a component like Fe_2O_3 not represented on it. Alternatively, the chlorite and corundum may not be in equilibrium for Lindqvist's sketch (his Figure 5.10) appears to involve the late stage iron rich chlorite variety. Finally, assemblages with garnet and cordierite cannot be properly represented in Figure 116. To do this requires considering FeO and MgO separately, thus introducing the FeO-MgO- SiO_2- Al_2O_3 tetrahedron shown on Figure 117.

When considered in terms of a FeO-MgO- SiO_2- Al_2O_3 plot, many of the problems met in attempting to represent observed assemblages in the (FeO+MgO)- SiO_2- Al_2O_3 plot are overcome. However, it is difficult to represent and appreciate the three dimensional properties of the plot in a two dimensional diagram. Figure 117 is drawn from a model, constructed in order to see the relationships clearly in three dimensions. Unlike the diagrams discussed previously, garnet cannot be ignored in Figure 117 without introducing problems in representing assemblages and this indicates that garnet is not simply stabilised in all cases to accommodate components such as MnO or CaO.

Observed assemblages that can be represented in Figure 117 occupy two portions, but the zone between them is a little problematical. Firstly, GAB(1) schists are represented by the quartz-andalusite-staurolite-cordierite tetrahedron (see Figure 118 for an enlargement of part of Figure 117). Secondly, lode schists are represented by the three tetrahedrons within the quartz-cummingtonite-garnet-chlorite-magnetite volume. The problem with this plot is that garnet is common to all assemblages but obviously cannot be connected by tie lines to all other phases. Nor can it be omitted from the plot as was done on other diagrams because this

would enable a tie line between cummingtonite and staurolite to be drawn.

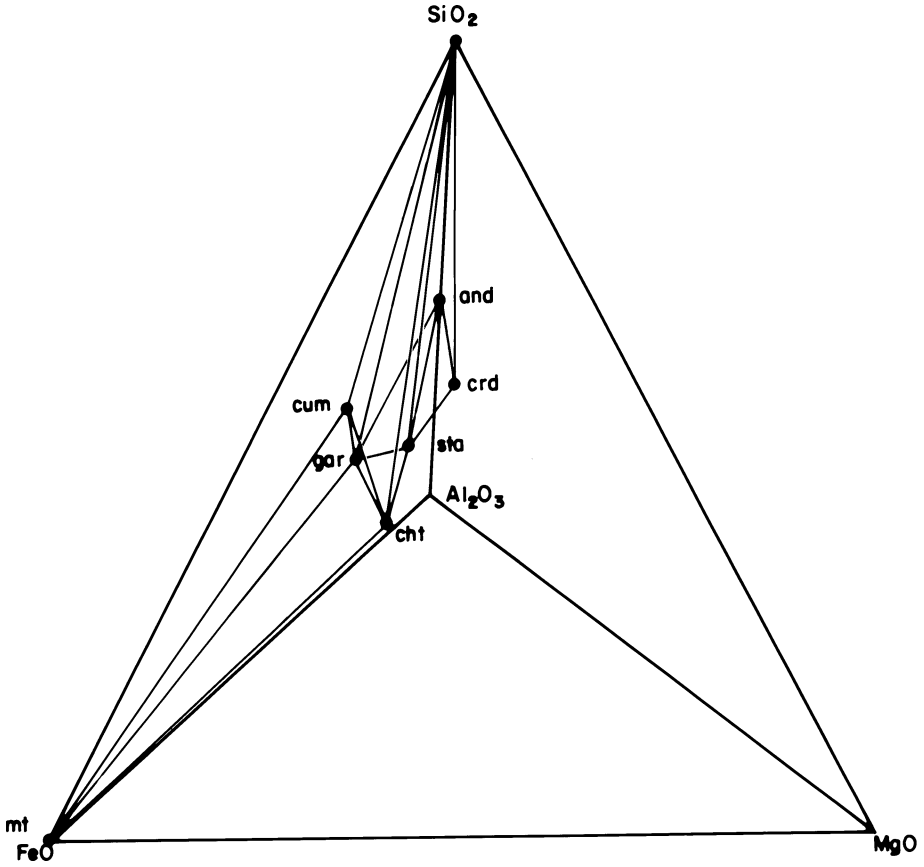


Figure 117. SiO_2-FeO-MgO-Al_2O_3 tetrahedron

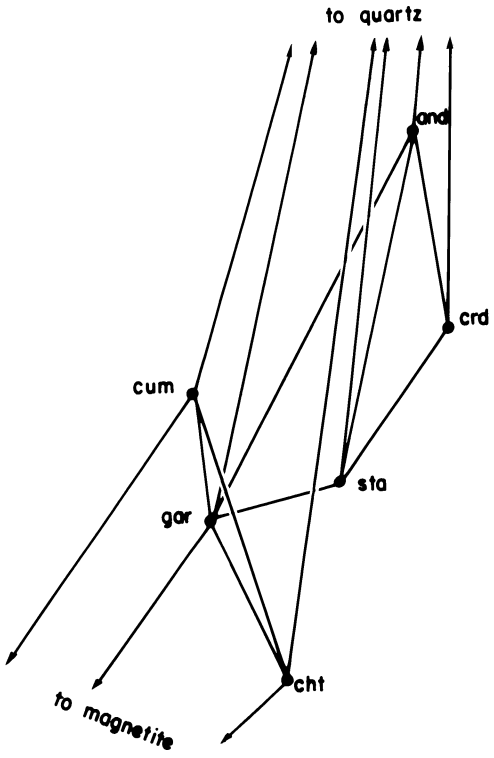


Figure 118. SiO_2-FeO-MgO-Al_2O_3 tetrahedron enlargement

Although occurring in many lode schists, cummingtonite and staurolite have not been observed together and it is assumed that they do not form a paragenesis. They can be effectively separated on Figure 118 by the quartz-garnet-chlorite plane. These relationships suggest that whereas garnet may be stabilised in many assemblages by their MnO or CaO contents, it is not the case in quart-chlorite-garnet assemblages containing either staurolite or cummingtonite.

7.3 Mineral chemistry

A total of 374 chemical analyses of minerals was made by electron microprobe from 24 rocks. Twelve different minerals were studied: garnet (121 analyses), biotite (70 analyses), staurolite (66 analyses), chlorite (36 analyses), cummingtonite (22 analyses), cordierite (22 analyses), magnetite (13 analyses), ilmenite (10 analyses), muscovite (8 analyses), plagioclase (3 analyses), andalusite (1 analysis), tourmaline (1 analysis) and hematite (1 analysis). Most of the analyses were carried out on the electron microprobe at Melbourne University and a lesser number at Macquarie University. All results are tabulated in Appendix 5. An expression used commonly in this section is X_{Fe}, which refers to the molar proportion in a rock or mineral of total iron relative to iron and magnesium. It is defined as:

$$X_{Fe} = Fe/(Fe+Mg)$$

7.3.1 Andalusite

Only one andalusite grain was analysed, from a lode schists (Sample No. 517-055). It contains a significant iron content of 0.90%, presumably mostly present as ferric iron. The total iron contents of andalusites from eight rocks analysed by Fleming (1971, Table 9) correlate negatively with the total iron content of the rocks containing them and the single specimen analysed here is consistent with Fleming's trend.

7.3.2 Staurolite

Despite considerable study, many aspects of the chemical composition and crystal chemistry of staurolites remain enigmatic. Studies by Smith (1968) and Griffen and Ribbe (1973) indicated that the structural formula of staurolite could be represented by $Fe_4Al_{18}Si_8O_{44}(OH)_4$ and this was used to calculate formulae for staurolites analysed in this study. However, it is known that staurolites do not conform to this idealised formula, for example Holdaway et al. (1986) showed that H contents vary for staurolites in different assemblages and quoted ranges from 2.7 to 4.16 H ions per 48-oxygen formula unit. Griffen et al (1982) suggested a generalised formula of:

$$(Fe,Mg,Zn)_{25.6-1.25\,x}\,Al_{1.52-8.2}\,Si_{16.2-0.5\,x}\,O_{48}H_4 \qquad \text{where } 16.58 < x < 18.61$$

Staurolites from the Kanmantoo Mine have similar compositions to other published analyses of staurolite but tend to be at the high end of the X_{Fe} range. X_{Fe} of Kanmantoo staurolites varies between 0.81 and 0.89, in comparison the range of X_{Fe} for staurolites studies by Griffen and Ribbe (1973) was 0.56-0.91. The high X_{Fe} values probably reflect the high iron contents of the rocks in the Kanmantoo Mine area, however a comparison between the X_{Fe} values of staurolite grains and their host rocks does not indicate a strong mutual relationship (Figure 119a).

In all rocks analysed, staurolite grains contain much more zinc than co-existing silicate or

oxide minerals, with a range from 0.08 to 1.32% ZnO. Relatively high zinc contents in staurolite have been reported from many metamorphic belts, and Ashworth (1975) concluded that staurolite could be stabilised at abnormally high metamorphic grade if it had high zinc contents. Guidotti (1970) observed an increase in zinc content with decreasing modal staurolite, and suggested that staurolite accommodates most of the zinc available in its host rocks, if sulphide minerals are absent. Preferential concentration of zinc in staurolite has been reported by many authors, including Nemec (1978) who quoted a natural range of 0.01 to 7.5% ZnO. Subsequently, Spry and Scott (1986) reported staurolite with 8.77% ZnO from the Bleikvassli massive sulphide deposit, and Spry (2000) refers to examples with "up to 9 wt percent ZnO". Huston and Patterson (1995) reported staurolite from the Dry River massive sulphide deposit in Queensland with ZnO contents up to 6.8%. In the Mount Lofty Ranges, zinc contents in staurolite up to 6.3% were reported by McElhinney (1994) from the Angas massive sulphide deposit. From a drillhole located adjacent to base metal sulphide rock at the Angas Prospect, Toteff records staurolite with 5.01% ZnO from an assemblage that included sphalerite, gahnite and staurolite. Closer to the Kanmantoo Mine, the author measured ZnO contents up to 6.48% (Appendix 4) in staurolite from staurolite- and gahnite-bearing quartz vein material obtained from the old St. Ives workings south of Kanmantoo.

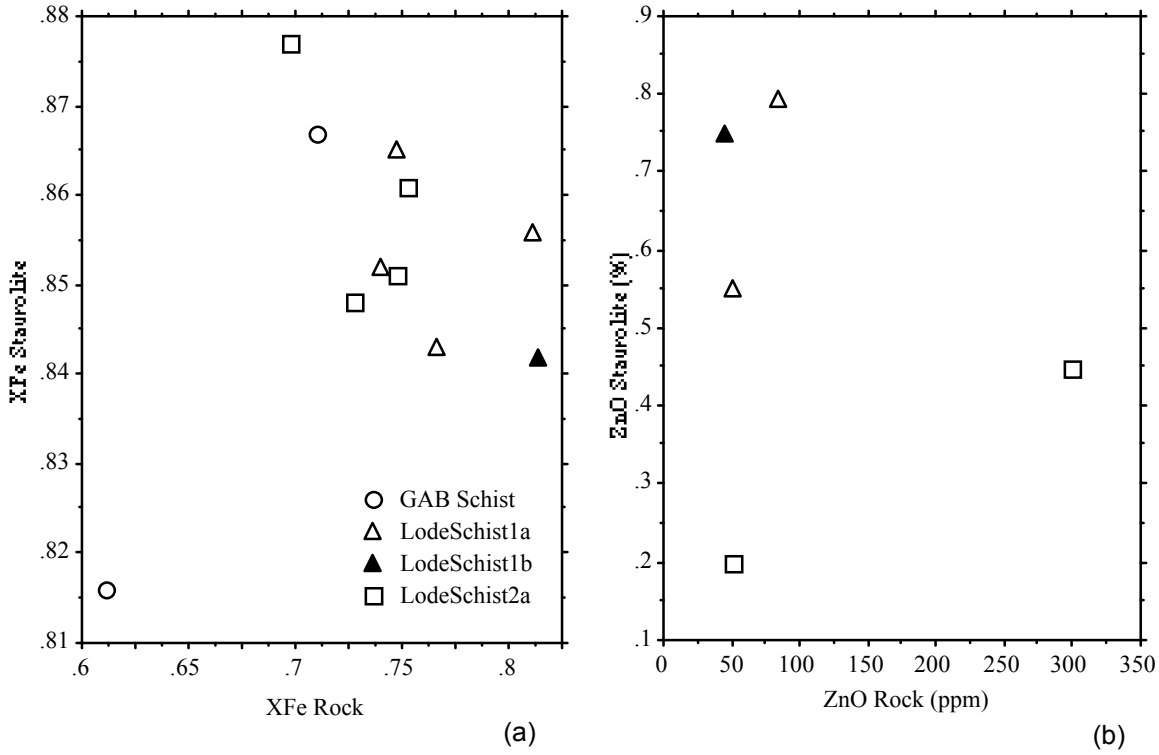


Figure 119. Graphs of staurolite composition. Lode schist 1a and 1b refer to Group 1 (quartz rich) lode schists with and without andalusite respectively. Lode schist 2a is Group 2 (quartz poor/absent) lode schist.

In the Kanmantoo area the range of ZnO contents of staurolite within one rock is variable, as shown in Figure 119b. No measurements of modal proportions of staurolite were done here but visual estimates indicate that the most staurolite rich rocks tend to have the most zinc poor staurolites. There is no apparent relationship between the zinc content of staurolite and its host rock (Figure 119b). Hence, the zinc content of staurolite appears to be inversely related to modal staurolite, as suggested by Guidotti (1970).

Several staurolite grains were analysed in detail to detect any zoning present. In all grains, these analyses revealed considerable inhomogeneity but in no case could regular or consistent

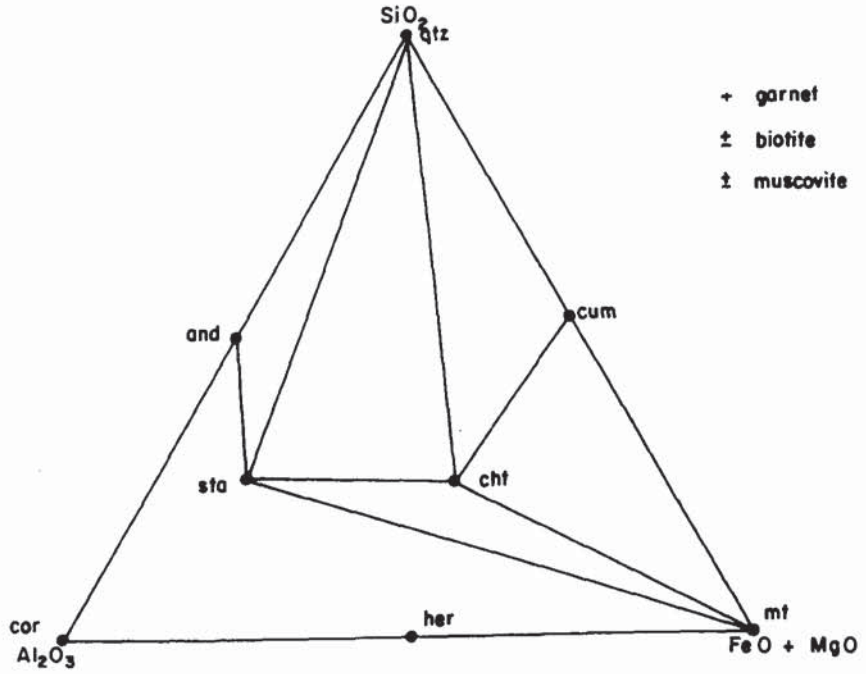


Figure 116. SiO_2-Al_2O_3-FeO-MgO diagram

Whilst representing many observed assemblages, Figure 116 has several deficiencies, some of which will now be discussed. Firstly, magnetite and quartz co-exist, apparently stably, and this is probably related to Fe_2O_3 contents, especially in rocks where this component is too high to be accommodated in biotite and other silicate minerals. Although a staurolite-chlorite-magnetite-(garnet) assemblage has been observed in this study, Lindqvist (1969, Fig. 5.10) reported a corundum-chlorite assemblage from the Kanmantoo deposit which requires crossing tie lines on Figure 116. This topological problem may be related to the inadequacies of the plot, in particular to a component like Fe_2O_3 not represented on it. Alternatively, the chlorite and corundum may not be in equilibrium for Lindqvist's sketch (his Figure 5.10) appears to involve the late stage iron rich chlorite variety. Finally, assemblages with garnet and cordierite cannot be properly represented in Figure 116. To do this requires considering FeO and MgO separately, thus introducing the FeO-MgO- SiO_2- Al_2O_3 tetrahedron shown on Figure 117.

When considered in terms of a FeO-MgO- SiO_2- Al_2O_3 plot, many of the problems met in attempting to represent observed assemblages in the (FeO+MgO)- SiO_2- Al_2O_3 plot are overcome. However, it is difficult to represent and appreciate the three dimensional properties of the plot in a two dimensional diagram. Figure 117 is drawn from a model, constructed in order to see the relationships clearly in three dimensions. Unlike the diagrams discussed previously, garnet cannot be ignored in Figure 117 without introducing problems in representing assemblages and this indicates that garnet is not simply stabilised in all cases to accommodate components such as MnO or CaO.

Observed assemblages that can be represented in Figure 117 occupy two portions, but the zone between them is a little problematical. Firstly, GAB(1) schists are represented by the quartz-andalusite-staurolite-cordierite tetrahedron (see Figure 118 for an enlargement of part of Figure 117). Secondly, lode schists are represented by the three tetrahedrons within the quartz-cummingtonite-garnet-chlorite-magnetite volume. The problem with this plot is that garnet is common to all assemblages but obviously cannot be connected by tie lines to all other phases. Nor can it be omitted from the plot as was done on other diagrams because this would enable a tie line between cummingtonite and staurolite to be drawn.

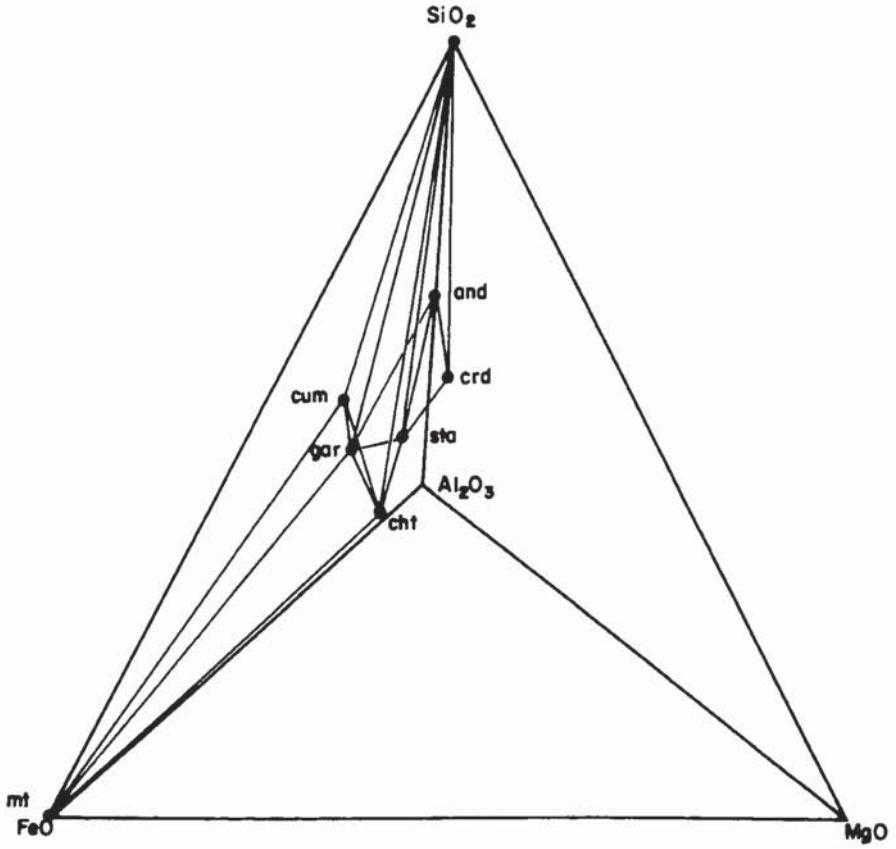


Figure 117. SiO_2-FeO-MgO-Al_2O_3 tetrahedron

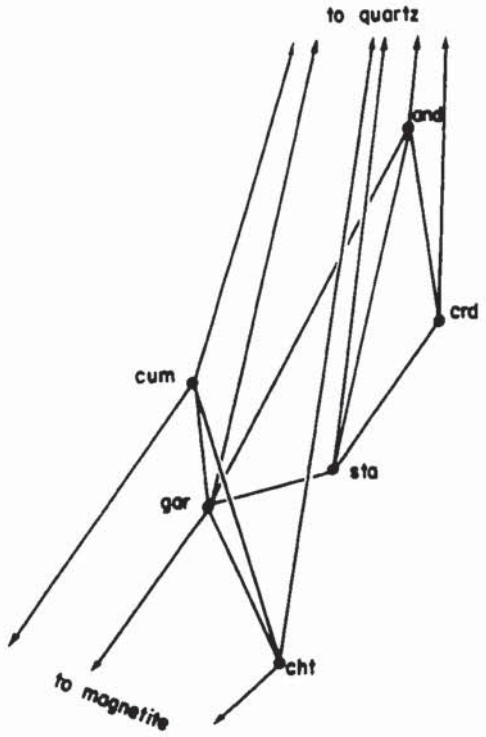


Figure 118. SiO_2-FeO-MgO-Al_2O_3 tetrahedron enlargement

patterns be detected. Figure 120 illustrates one example. In this case the chemical inhomogeneity suggests a fairly complex growth pattern, at odds with the simple shape of the crystal. Note that the rim compositions vary, indicating that the rim has not equilibrated with the matrix, even against similar minerals.

7.3.3 Garnet

Most garnets in metamorphic rocks (Kretz, 1994) are solid solutions between almandine ($Fe_3Al_2Si_3O_{12}$), pyrope ($Mg_3Al_2Si_3O_{12}$), spessartine ($Mn_3Al_2Si_3O_{12}$) and grossular ($Ca_3Al_2Si_3O_{12}$), and they have the general formula $(Fe,Mg,Mn,Ca)_3Al_2Si_3O_{12}$. All garnets analysed from various rocks of the Kanmantoo Mine area were similar and most were almandine rich. This is shown clearly in Figure 121. The exceptions were garnets from the only QMF schist sample analysed, which have relatively higher Mn and Ca than all other garnets (Figure 121b). In general, like

In the examples analysed, these components are present in the following molar proportions (excepting the QMF schist sample which is relatively spessartine rich):

Almandine	73.7 - 94.2 %
Pyrope	4.8 - 11.2 %
Spessartine	1.5 - 15.7 %
Grossular	0.2 - 7.5 %

Typically, the pyrope component exceeds both spessartine and grossular, the latter rarely exceeding 1%. As such the garnets are principally of the pyralspite series of Deer et al. (1976), as are most garnets in metasediments.

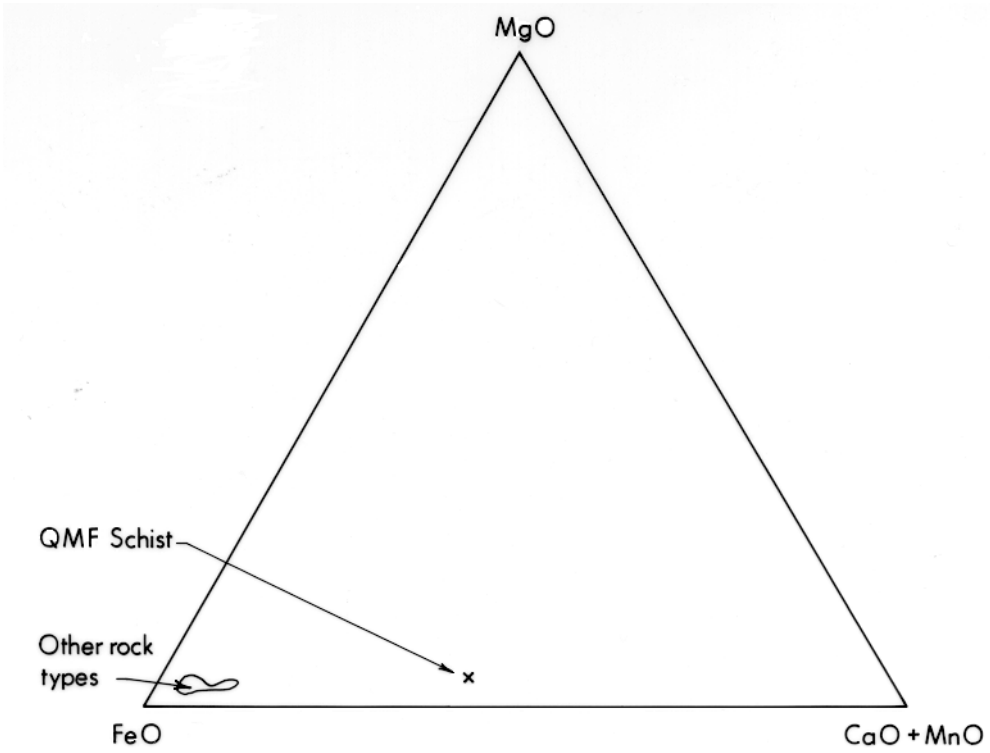


Figure 121a. Garnet composition ternary diagram showing rim compositions by weight. For detail of FeO corner refer to Figure 121b.

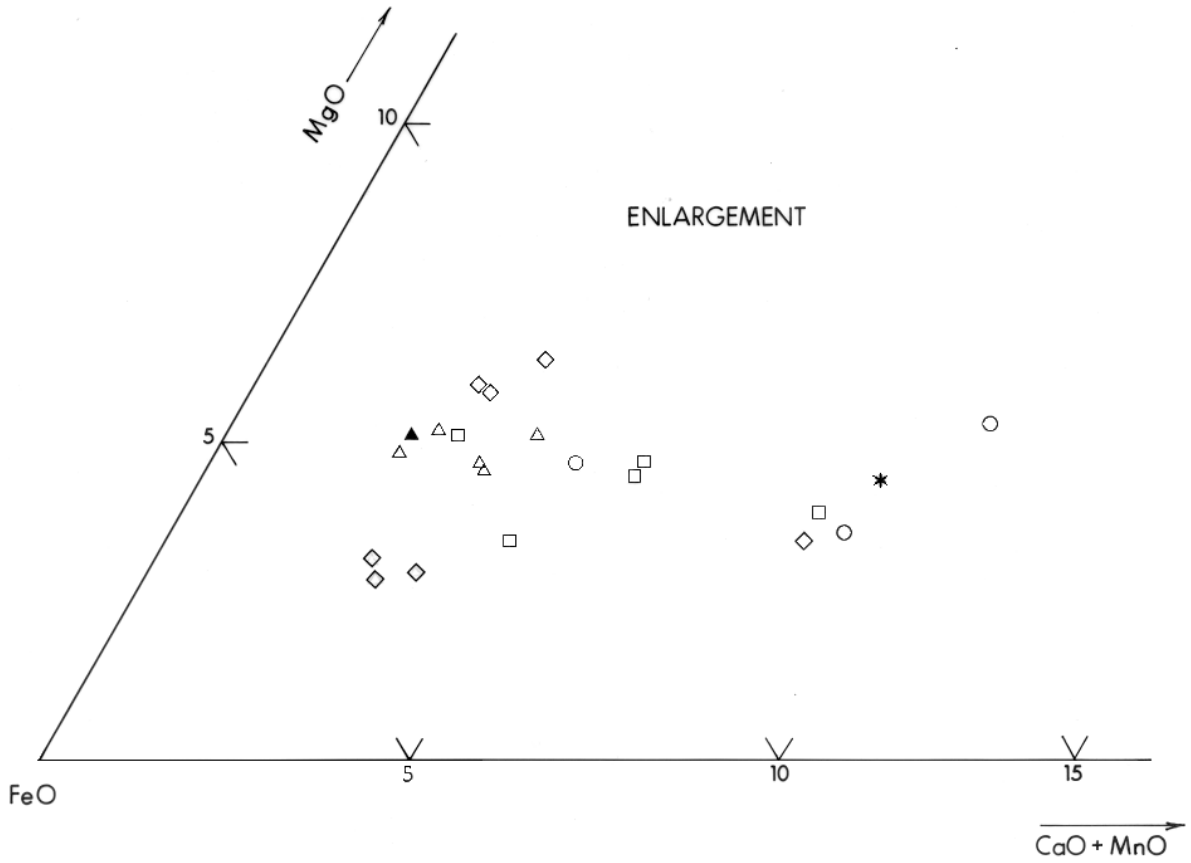


Figure 121b. Garnet composition ternary diagram showing rim compositions by weight (detail). Symbols represent: * QMA schist, ● QMF schist, ○ GAB(1) schist, Δ lode schist (1a), ▲ lode schist (1b), □ lode schist (2a), ◊ lode schist (3).

The variations in garnet rim compositions, both between different rock types and within the same rock type, are shown in Figure 121. Most rock types have compositions plotting over the entire field of scatter of the group, however quartz rich lode schists have a limited range. Garnets from GAB(1) schist tend to be less iron rich than those from lode schists, and the garnet enclosed in pyrrhotite and chalcopyrite (Figure 109b) has a lower iron content than those in lode schists. MnO and CaO were grouped together in the plots on Figure 121 because they are typically lower in abundance than FeO and MgO, however there appears to be no relationship between CaO and MnO, as shown by Figure 122a. A possible relationship between garnet rim compositions and host rock chemistry is demonstrated in Figures 122b and 123. These show no overall correlations but within certain rock types relationships are suggested. For example, the contents of FeO and MnO in garnets from GAB(1) schists appear to increase as these components increase in the host rocks. This is also the case for FeO and MgO in quartz rich lode schists. The CaO contents of garnets and their host rocks appear to be independent.

Compared to co-existing minerals, garnets are enriched in Ca and Mn, with the exception of plagioclase in the case of Ca, but plagioclase is rare except in QMF schists. It appears that most Ca present in GAB schists and lode schists is accommodated in garnet. As one would expect, whole rock chemistries (presented later) reveal only small quantities of CaO present in all rocks except QMF schists. The preferential enrichment of Ca and Mn in garnet is not unusual and has been reported by many other authors. As with Zn in staurolite, high bulk contents of Mn or Ca are thought to stabilise garnet in metamorphic conditions in which it would otherwise be unstable (Atherton, 1965).

The possibility of internal compositional zoning in garnets was investigated by analysing the cores and rims of many garnets and also by traversing across several garnets. Many studies have been done on zoning in garnets in metapelites. The typical pattern is a decrease in the spessartime component from core to rim due to the strong partitioning of MnO into garnet compared to other phases and the fractionation effect as the matrix MnO content is depleted (Hollister, 1966; Atherton, 1968). The affinity of garnet for MnO is believed to lead to the early crystallisation of garnet during prograde metamorphism. In fact, Symmes and Ferry (1991) argue, on the basis of modelling thermodynamic data, that MnO-free systems do not produce garnet bearing mineral assemblages over the 400^{o}-600^{o}C range considered. Natural bulk compositions are not MnO free. As MnO increases in a rock, its effect is to lower the temperature at which garnet first appears. Most garnets analysed at the Kanmantoo Mine were found to be zoned, but the specific changes in composition vary considerably. By far the most common factor is a tendency for Fe, or the almandine component, to increase from the core towards the rim. This is usually at the expense of Mn, Mg and Ca, but in many cases both Fe and Mn increased towards the rim. These findings of variable zoning trends contrast with data by Lindqvist, who proposed consistently Fe rich rims and Mn rich cores for garnets from "wall and country rocks" (his Figure 6-1). Lindqvist studied zoning in 9 garnets by X ray diffraction and in one of these also by semi quantitative electron microprobe.

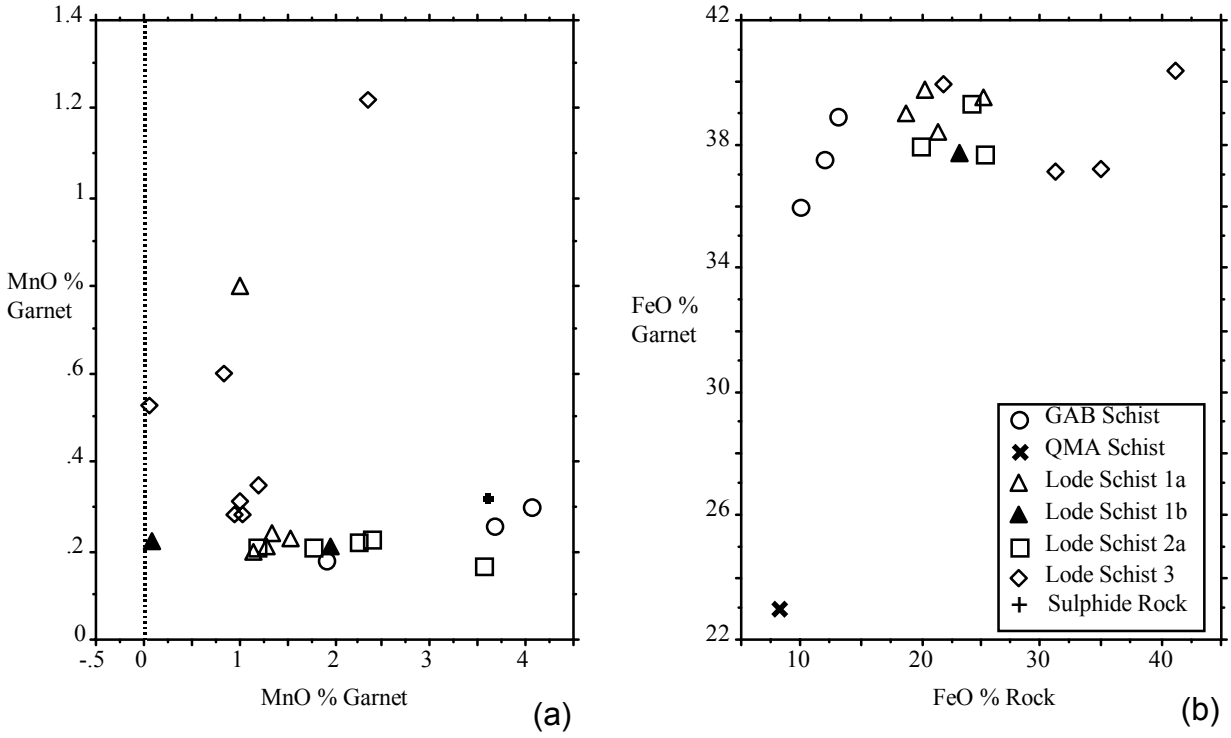


Figure 122. Graphs of garnet composition for all rock types analysed. Lode schist 3 refers to Group 3 (amphibole bearing) Lode Schist, for the other lode schists refer to Figure 119.

The various types of zoning observed in garnets are shown in Table 20. Note that the type of zoning varies even within a single thin section of a sample. Unzoned garnets were found in only two samples. Reversals of the tendency for Fe to increase towards the rim were also observed in two samples - in the first case, a lode schist, the zoning was essentially between Fe and Mg whereas in the other case the zoning was between Fe and Mn.

In two samples several analyses were made within a garnet grain to study the regularity of composition changes. Figure 124 illustrates a coarse grained garnet from a garnet rich zone in

an amphibole bearing lode schist sample. At one side the garnet has many quartz inclusions. The rest of the grain is interpreted to have grown in a quartz poor environment by replacing biotite principally, leaving residual bunches of ilmenite grains as a reaction product. The graphs in Figure 124 show that in this example no regular variation in composition exists across the garnet, and so an irregular growth history is indicated, as was the case for some staurolite grains. Mg and Mn have antipathetic patterns yet neither has a significant change across the boundary between garnet with many quartz inclusions and that with few. On the other hand, Fe and Ca appear to have abrupt changes at this boundary.

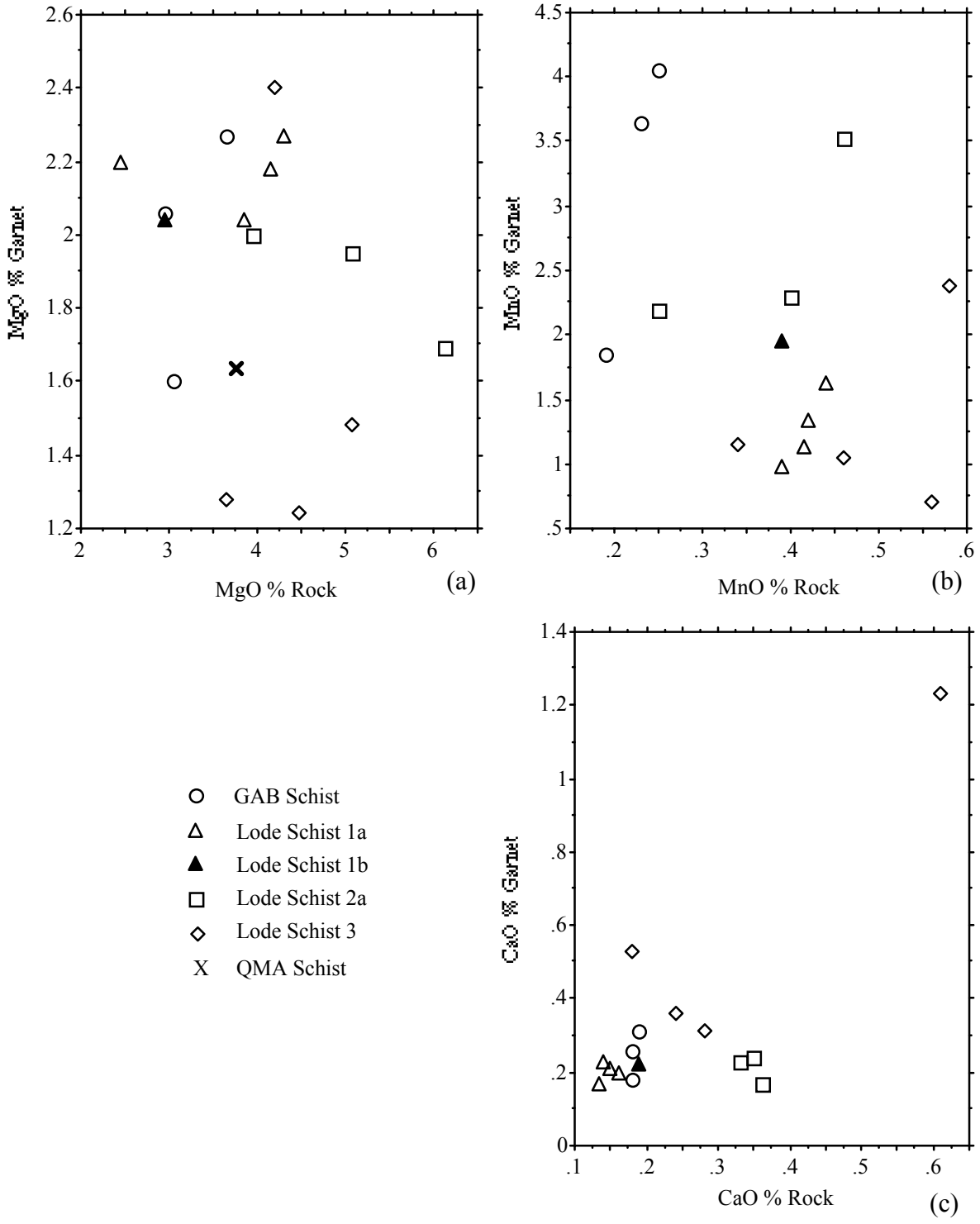


Figure 123. Graphs of Garnet Composition. Lode schist descriptions used in this figure are explained in Figures 119 and 122.

patterns be detected. Figure 120 illustrates one example. In this case the chemical inhomogeneity suggests a fairly complex growth pattern, at odds with the simple shape of the crystal. Note that the rim compositions vary, indicating that the rim has not equilibrated with the matrix, even against similar minerals.

7.3.3 Garnet

Most garnets in metamorphic rocks (Kretz, 1994) are solid solutions between almandine ($Fe_3Al_2Si_3O_{12}$), pyrope ($Mg_3Al_2Si_3O_{12}$), spessartine ($Mn_3Al_2Si_3O_{12}$) and grossular ($Ca_3Al_2Si_3O_{12}$), and they have the general formula $(Fe,Mg,Mn,Ca)_3Al_2Si_3O_{12}$. All garnets analysed from various rocks of the Kanmantoo Mine area were similar and most were almandine rich. This is shown clearly in Figure 121. The exceptions were garnets from the only QMF schist sample analysed, which have relatively higher Mn and Ca than all other garnets (Figure 121b). In general, like

In the examples analysed, these components are present in the following molar proportions (excepting the QMF schist sample which is relatively spessartine rich):

Almandine	73.7 - 94.2 %
Pyrope	4.8 - 11.2 %
Spessartine	1.5 - 15.7 %
Grossular	0.2 - 7.5 %

Typically, the pyrope component exceeds both spessartine and grossular, the latter rarely exceeding 1%. As such the garnets are principally of the pyralspite series of Deer et al. (1976), as are most garnets in metasediments.

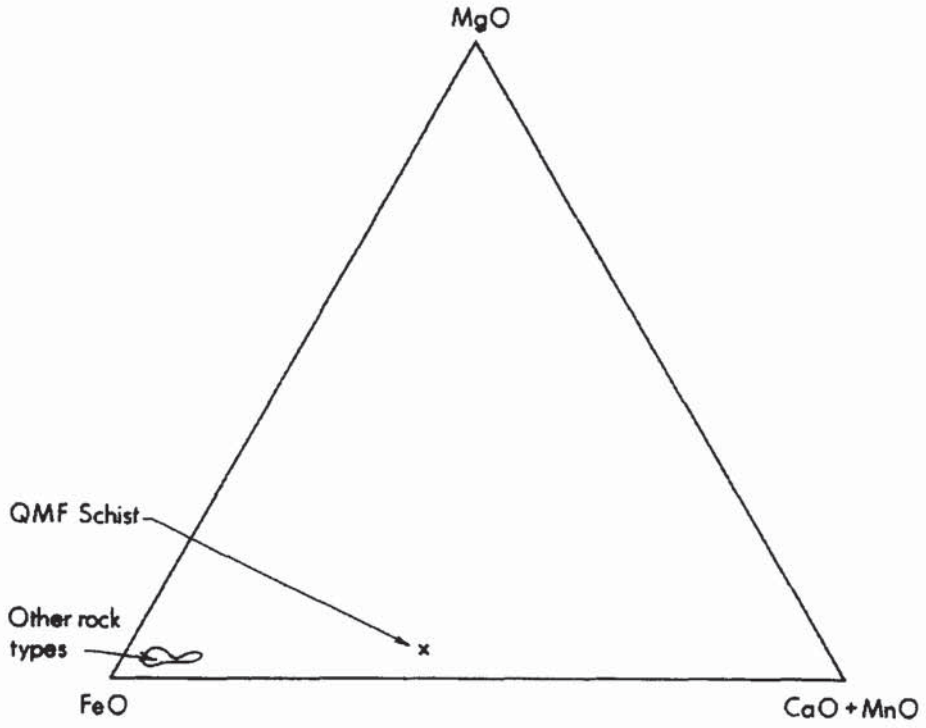


Figure 121a. Garnet composition ternary diagram showing rim compositions by weight. For detail of FeO corner refer to Figure 121b.

A second garnet, also in an amphibole bearing lode schist sample, was studied with four analysis points. In this case, the analyses produced poor totals and so have not been graphed as above. However, the results indicate that Fe and Mg both have antipathetic patterns to Mn and Ca. Unlike the garnet discussed above, the Fe content is greatest in the portion with abundant quartz inclusions, and the Ca content is lowest. With respect to their microfabrics, the relatively coarse grained garnets in the samples of amphibole bearing lode schist samples studied are atypical and so their rather irregular chemical zoning patterns may not be representative of garnets in other rock types. The latter were not investigated with more than two points, at core and rim positions.

Table 20. Observed types of chemical zoning in Kanmantoo Mine garnets.

Lithology group	Characteristics	Sample number	Zoning types (see code at base)
Lode schist (1a)	Quartz rich, andalusite bearing	517-004	2, 5, 6
Lode schist (1a)	Quartz rich, andalusite bearing	517-055	0, 2, 3, 6, 6, R1
Lode schist (1a)	Quartz rich, andalusite bearing	517-057	5, 6, 6
Lode schist (1c)	Quartz & biotite rich, no andalusite	517-060nam	5
Lode schist (2a)	Quartz absent	517-076B	0, 0
Lode schist (2c)	chlorite-magnetite rock, quartz absent	517-101	6
Lode schist (2b)	chlorite-muscovite rock, quartz absent	517-163	5
Lode schist (2a)	biotite-staurolite rock, quartz absent	517-177	5
Lode schist (3)	Amphibole bearing	517-059	3, 3*
Lode schist (3)	Amphibole bearing	517-077S	6, 6
Lode schist (3)	Amphibole bearing	517-077	4
Sulphide rock	Massive cp-po-magnetite-(ilm-gar-bio)	517-220	6
GAB(1) schist		517-133	5
GAB(1) schist		517-148	5, 6
GAB(1) schist		517-149	6
QM schist		517-2870	R7

Code (changes from core to rim)

0	Unzoned
1	Fe increase, Mg decrease
2	Fe increase, Mg+Ca decrease
3	Fe increase, Mg+Mn decrease (* but Ca increases)
4	Fe increase, Ca+Mn decrease
5	Fe increase, Mg+Ca+Mn decrease
6	Fe+Mn increase, Mg+Ca decrease
7	Fe increase, Mn decrease
R	Fe decreases, extra number indicates reverse of same number above

7.3.4 Cordierite

Cordierite has been observed in several rocks of which one, a lode schist, was extensively analysed by microprobe. During this study cordierite was also observed in a sample from the Brukunga Mine (see Appendix 5, Sample No. 517-N203 for composition) which together with the Kanmantoo cordierite and Spry's (1976) reporting of cordierite at Wheal Ellen, indicate that this mineral may be more common in the staurolite-andalusite and fibrolite zones than previously supposed. Cordierite has been reported previously from the Kanmantoo Mine by Nero (1993) and Oliver et al. (1998).

In a cordierite bearing sample from the Kanmantoo Mine (Sample No. 517-055) cordierite is in contact only with biotite, garnet, quartz and andalusite, in the latter case as an inclusion in

andalusite. Three grains were analysed by microprobe for a total of 21 points. Although much of the cordierite rims had been pinitised some contiguous biotite-cordierite and garnet-cordierite rim compositions were obtained.

In the cordierite microprobe results, FeO content ranges from 9.18 to 9.80% by weight and MgO content from 6.97 to 7.37%. The molecular ratio Fe/Fe+Mg ranged between 0.41 to 0.44 and so these grains are somewhat more iron rich than most of the 62 cordierite analyses compiled by Leake (1960). Of the three grains analysed by microprobe all had similar Fe and Mg contents. There are variations within each grain indicating chemical disequilibrium, however no regular zoning pattern was found.

7.3.5 Amphiboles

Twenty two microprobe analyses of amphiboles were made from seven lode schist samples. All had Ca+Na contents of less than 0.1 per standard formula unit of 23 oxygen equivalents, and so, with Ca+Na being less than 1.34, they are within the amphibole group called Fe-Mg-Mn amphiboles by Leake (1978). Like most, and possibly all, amphiboles in lode schists, those analysed by microprobe were monoclinic and so they are part of the cummingtonite-grunerite series. Within this series, amphiboles with X_{Fe} greater than 0.7 are termed grunerite, the rest are either cummingtonite or magnesio-cummingtonite (Leake, 1978). No ortho-amphiboles were observed in this study, nor were they reported by Lindqvist (1969). However, Mancktelow (1979) shows a photograph of an assemblage from the Kanmantoo Mine comprising quartz-garnet-plagioclase-anthophyllite-cummingtonite-opaques-chlorite-biotite. In this photograph the coarser amphiboles are described as being anthophyllite generally, whereas the cummingtonite is usually more fibrous and twinned. Apart from the anthophyllite, the occurrence of plagioclase in this assemblage is very unusual and has not been seen by the author.

Amphiboles have not been observed in assemblages with cordierite at Kanmantoo, indicating that the following reaction did not occur, and that chlorite and quartz was a stable assemblage at peak metamorphism :

chlorite + quartz = cordierite + orthoamphibole

Nor has evidence been seen of the K_2O depleting metasomatic reactions reported by Arnold and Sandiford (1990) in which andalusite and biotite, or staurolite and biotite, produced gedrite and cordierite.

The range of X_{Fe} in the amphiboles analysed in this study is 0.54 to 0.70, and hence they are all cummingtonite, although many are at, or close to, the grunerite boundary. The X_{Fe} ratios of the cummingtonites show no consistent relationship with the X_{Fe} ratios of the host rocks, in the cases where data allowed comparison (Figure 125). The Mn contents of all amphiboles analysed were very low, with the ratios 100Mn/Mn+Fe+Mg in the range of 0.2 to 0.4. A1 contents were also low, relative to many other amphibole varieties, with the molecular proportion of A1 to the total cations (excluding H) ranging between 0.8% and 3.7%.

Basal sections in three samples were analysed by microprobe at core and rim sites to determine any chemical zoning present. The only consistent pattern in each of the three grains was a decrease in A1 content of the cores relative to adjacent rims, usually substituted by combinations of Si, Fe and Mg. No consistent changes of X_{Fe} between cores and rims were found.

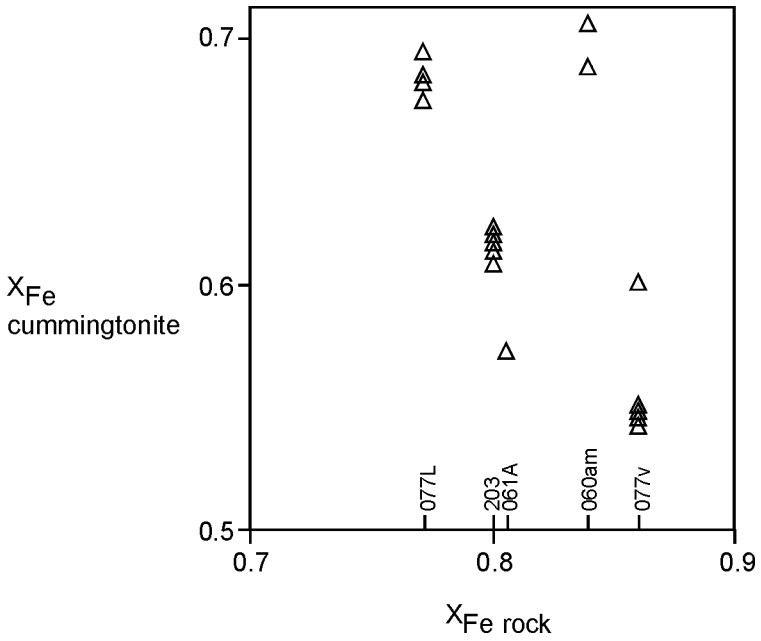


Figure 125. Graphs of cummingtonite compositions.

7.3.6 Chlorite

In Section 5.8, the two most common types of chlorite were distinguished on the basis of microstructure, however each type can also be distinguished by their Fe and Mg proportions. In addition, the compositions of some uncommon chlorite types were analysed.

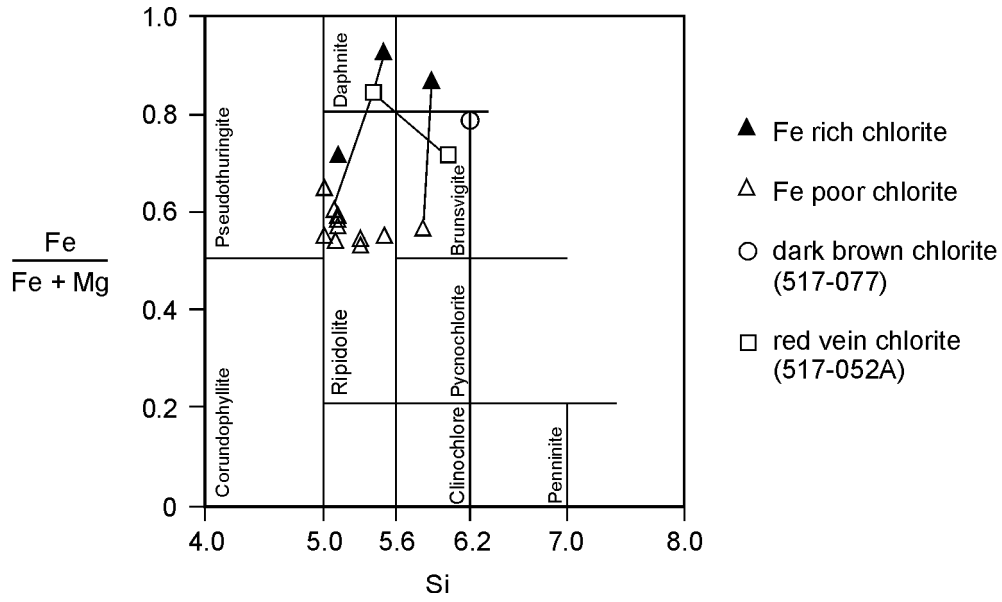


Figure 126. Graphs of chlorite composition.

The most common chlorite type, Fe-poor chlorites, have X_{Fe} ratios between 0.52 and 0.64, whereas Fe-rich chlorites vary between 0.71 and 0.92, as shown by the ordinate axis of Figure 126a. Also shown on this figure are the high X_{Fe} ratios of the rare chlorite types; those represented by triangles are intergrown pink and clear grains in a chlorite-albite-tourmaline vein and that represented by a square is a dark brown chlorite in a chlorite-garnet-cummingtonite rock (Figure 107d).

The measured FeO (total Fe) contents of Fe-rich chlorites was as high as 48.38 weight % in a chlorite-muscovite rock sample (Sample No. 517-163). The X_{Fe} ratios of chlorites are much more variable than the X_{Fe} ratios of the host rocks and Figure 126a suggests a possible weak antipathetic relationship between the chlorite and rock X_{Fe} ratios. Note that whereas the iron poor chlorites are believed to be part of a metamorphic paragenesis, the iron rich chlorites are not - they appear to represent metasomatism and disequilibrium.

The Al contents of chlorites are variable, even within different chlorite types, with a range for Fe-rich chlorites of 3.9 to 5.9 Al cations per standard formula unit (based on 28 oxygen equivalents) and a range of 4.3 to 6.0 for Fe-poor chlorites. The Si content is also variable but less so than Al, with a range of 5.0 to 6.0 Si cations per formula unit.

Using the nomenclature scheme of Hey (1954), based on the XFe and Si contents of chlorites, most of the Fe-poor chlorites belong to the ripidolite variety (Figure 126b). Fe-rich chlorites plot in the ripidolite and daphnite fields and also in an un-named field. The unusual chlorite types are either daphnite of brunsvigite.

7.3.7 Biotite

Most biotite compositions deviate substantially from trioctahedral stoichiometry with the total number of ions in octahedral sites as low as 5.52, compared to a possible 6 per formula unit. However, in some biotites this figure exceeds 5.95, but does not seem to depend on rock type. Between 8 and 16 per cent of the octahedral sites are occupied by Al. Of the tetrahedral sites, Al occupies a relatively minor range of 2.4 to 2.7 of the possible 8 sites (the rest being occupied by Si). Quartz poor or quartz free lode schists have slightly higher Si/Al ratios in tetrahedral sites, possibly due to a buffering effect on Si by free quartz.

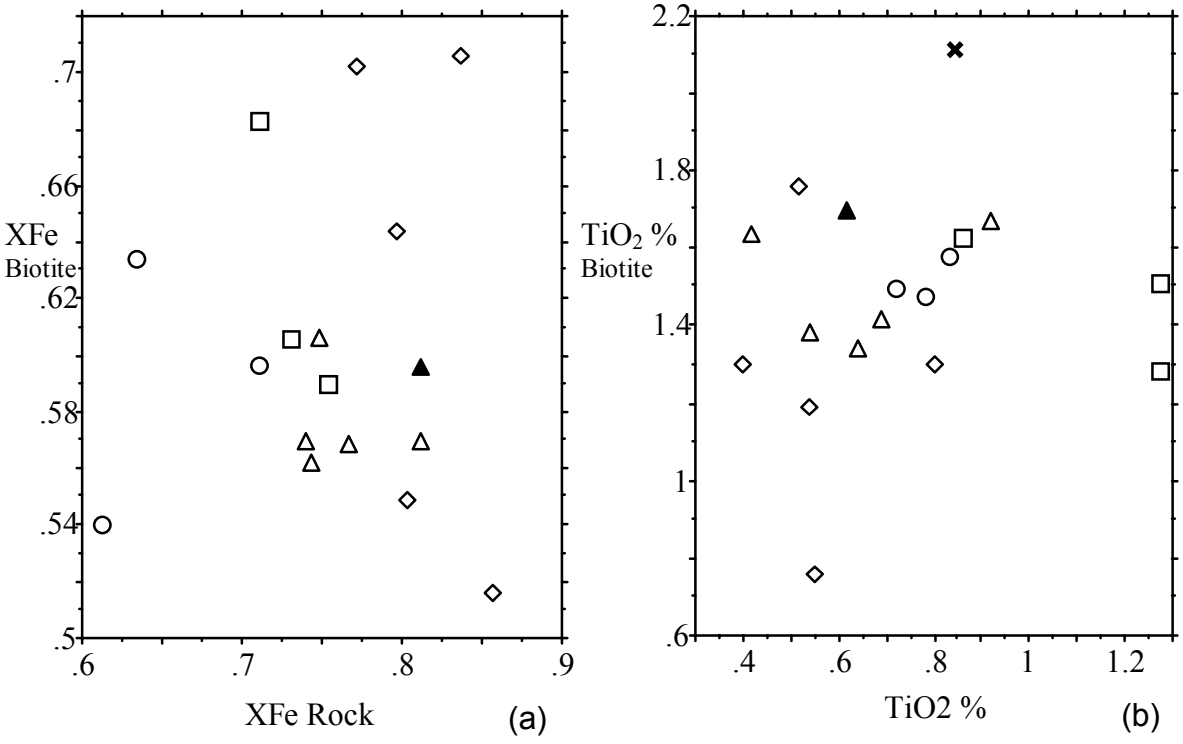


Figure 127. Graphs of Biotite Composition. (Symbols as for Figure 122)

Biotite X_{Fe} ratios vary between 0.52 and 0.72 and show no dependence on the X_{Fe} ratio of the host rocks (Figure 127a). The amphibole bearing lode schists have the highest and lowest values of X_{Fe} for biotite, although the latter is shared with a QM schist specimen.

Biotite is the most TiO_2 rich mineral after ilmenite, with which it typically co-exists, and the buffering effect of ilmenite may account for the relatively constant TiO_2 content measured of biotite from a range of rock types. TiO_2 contents of biotite vary between 0.76% and 2.13% but most are between 1.2% and 1.6%. The TiO_2 contents of biotites and their host rocks show no relationship (Figure 127b).

When biotite analyses are recalculated to 24 (O, OH) the total of K and Na and Ca is invariably less than 2, possibly due to vacancies in this site or analytical errors.

7.3.8 Muscovite

Muscovite was analysed from only three specimens: a quartz poor lode schist, a QMF schist and also a GAB(1) schist in which it may be a late stage mineral. In all rocks the compositions deviate only slightly from the ideal composition $K_2Al_4(Si_6Al_2)(OH)_4$. Paragonite components vary between 5% and 8.5% and the amount of phengite substitution is also small with a maximum of 6.24 Si cations per formula unit. Fe+Mg cations vary between 0.24 and 0.46, per formula unit.

7.3.9 Plagioclase

Plagioclase was analysed from only two rocks: a QMF schist, and from within a chlorite-plagioclase-tourmaline vein. In the former case, the plagioclase has measured Ca:Na:K ratios of 0.70:0.27:0.03 and so is classified on the boundary between labradorite and bytownite varieties. The same ratio from the vein plagioclase is 0.05:0.95:0.01 and so this is albite. Ba in this plagioclase was found to be 0.01% or less.

7.3.10 Oxide Minerals

Magnetite and ilmenite are by far the most common oxide minerals. Six rocks were analysed by microprobe for magnetite compositions and in four of these ilmenite was also analysed. Both magnetite and ilmenite conform closely to ideal compositions of Fe_3O_4 and $FeTiO_3$, respectively.

Al substitutes for up to 0.6% of total cation sites in magnetite and for much less in co-existing ilmenite. Ti contents in magnetite do not exceed 0.2% of total cation sites. Si, Mn, Mg and Ca are all below 0.1% of total cation sites. In one sample analysed for both core and rim compositions of magnetite (Sample No. 517-101), no chemical zoning was indicated.

7.4 Evidence of chemical equilibrium

Minerals co-existing in chemical equilibrium, or more specifically *frozen equilibrium* (Kretz 1994), should fulfil the following two conditions (Vernon, 1976):

1. similar edge compositions of different grains of the same mineral, and
2. similar distribution of components between a given mineral pair.

These two points will now be considered, with particular reference to Fe and Mg contents.

Table 21 lists a selection of different rock types from which, for a given mineral, more than one rim analysis was made. The results show that the X_{Fe} ratios of garnet, biotite and staurolite are not precisely the same within any rock sample, however they generally have variations of less than 4% of the value of the maxima (refer to the last column). An exception is sample number 517-055, the cordierite bearing specimen, which has considerable variation of X_{Fe} in biotite, and in the same rock cordierite has a variation in X_{Fe} of 4.59%. X_{Fe} values of chlorite and cummingtonite rims could be compared in only one specimen in each case and both showed relatively high variations (4.77% and 10.2% respectively).

Ratios of Al/Al+Si for the rims of co-existing biotite and chlorite grains were also calculated and are shown on Table 22. This comparison shows that, generally, this ratio varies by less than 5%, except in the case of sample number 517-055 again, in which it is much higher. As with the X_{Fe} ratios, the Al/Al+Si ratio has least variation in the GAB(1) schist specimen.

A second method of investigating chemical equilibrium is to compare the variations in partitioning of elements between the same minerals in various rocks. In this case the distribution of Fe and Mg between several minerals, in particular garnet and biotite, will be investigated. The Fe-Mg distribution between co-existing garnet and biotite can be represented by the following reaction:

Fe garnet + Mg biotite = Mg garnet + Fe biotite

Table 21. X_{Fe} ratios of grain edges for various minerals.

Rock type	Sample number	Mineral	XFe	% (max-min) max
GAB(1) schist	517-148	gar	0.914, 0.920	0.65
		bio	0.597, 0.598	0.17
		sta	0.866, 0.870	0.46
Lode schist (1a)	517-004	gar	0.916, 0.919, 0.907, 0.909	0.98
		bio	0.605, 0.594	1.82
		sta	0.866, 0.842	2.77
Lode schist (1a)	517-049	cht	0.548,0.566, 0.539	4.77
Lode schist (1a)	517-055	gar	0.918, 0.904, 0.898, 0.909, 0.916, 0.912, 0.904, 0.903, 0.909, 0.907, 0.908	2.18
		bio	0.597, 0.589, 0.576, 0.533, 0.554, 0.562, 0.533	10.7
		sta	0.850, 0.844	
		crd	0.421, 0.416, 0.432, 0.424, 0.426, 0.436	4.59
Lode schist (1b)	517-112	gar	0.912, 0.884	3.07
Lode schist (2a)	517-076B	gar	0.918, 0.912, 0.914	0.65
		bio	0.592, 0.605	2.14
Lode schist (2b)	517-163	gar	0.926, 0.914, 0.934	2.14
		bio	0.686, 0.690	0.58
		sta	0.878, 0.880	0.23
Lode schist (3)	517-059	gar	0.896, 0.905, 0.908, 0.904	1.32
		bio	0.551, 0.554, 0.547	1.26
		cum	0.606, 0.544	10.2

If garnet and biotite behave as ideal solid solutions then the equilibrium constant, K, of this reaction is (Goldman and Albee, 1977),

$$K = K_{D(Fe)}^{gar\text{-}bio} = (X_{Fe}^{gar}).(1- X_{Fe}^{gar})^{-1}.(1- X_{Fe}^{bio}).(X_{Fe}^{bio})^{-1}$$

where X_{Fe}^{bio} refers to the molecular ratio Fe/Fe+Mg in biotite and $1-X_{Fe} = X_{Mg}$. In future the term K_D will be used for the above expression. K_D has been found to depend on temperature but not on pressure, so providing garnet and biotite behave as ideal solid solutions and equilibrate under uniform P-T conditions, then a plot of $X_{Fe_{bio}}$ and $X_{Fe_{gar}}$ should be regular. Such a plot for co-existing garnet and biotite rim compositions for Kanmantoo rocks is shown in Figure 128a. The 34 data points form a well defined line with a correlation coefficient of 0.92. Linear regression analysis provides the following relationship.

$$X_{Fe\ bio} = 3.24\ X_{Fe\ gar} - 2.37$$

Clearly, this line does not pass through zero on both axes. The reason for this is that the data should conform to a curved line (Kretz, 1964) because $X_{Fe_{gar}}$ is greater than $X_{Fe_{bio}}$, and Figure 128b shows a suitable curve conforming to the data, in which the solid part of the curve represents the data shown in Figure 128a. Comparative plots of X_{Fe} between chlorite-garnet, staurolite-garnet and staurolite-biotite are shown in Figure 128c,d,e, however there are fewer data than for garnet-biotite pairs. Linear relationships are indicated for garnet-chlorite and possibly garnet-staurolite but not so clearly for staurolite-biotite although in this latter case a single point could be misleading.

Table 22. Al and Si ratios of biotite and chlorite grain edges.

Rock type	Sample number	Mineral	% max-min / max	Al/Al+Si
GAB(1) schist	517-148	biotite	0.50	0.398, 0.396
Quartz rich lode schist (with andalusite)	517-004	biotite	2.04	0.385, 0.393
	517-049	chlorite	0.74	0.539, 0.537, 0.543
	517-055	biotite	20.4	0.397, 0.392, 0.397, 0.3940.399, 0.316, 0.396
Quartz poor lode schist	517-076B	biotite	0.52	0.388, 0.386
	517-163	biotite	4.42	0.367, 0.384
Muscovite bearing lode schist	517-059	biotite	1.13	0.349, 0.347

A further indication of chemical equilibrium can be obtained by the relative values of X_{Fe} of co-existing Fe-Mg silicates. Empirically, X_{Fe} has been found to decrease in the following order (for example Thompson 1976): garnet, staurolite, biotite, chlorite and cordierite. This order applies to metamorphism at low to medium pressure - at higher pressures of eclogite pressures Bellevue et al (1989) reported staurolites more iron rich than co-existing garnets. The order can also be affected by bulk composition - in extremely magnesium rich compositions the X_{Fe} ratios of biotite and chlorite can be the reverse of the normal order above (Guidotti et al, 1975; Tewhey and Hess, 1975). The normal order is consistently found in all samples analysed from the Kanmantoo Mine area (refer Table 21) and is typically the case in assemblages of the Mount Lofty Ranges (Dymoke and Sandiford, 1992). In addition, X_{Fe} of cummingtonite is intermediate between garnet and biotite; its relationship to staurolite is unknown because these two minerals do not co-exist, but the range of X_{Fe} of cummingtonite is below that of staurolite.

In summary, the relatively close agreement between rim compositions of given minerals in most rocks, plus the regular X_{Fe} plots and the relative X_{Fe} values for different minerals indicate a close approach to chemical equilibrium within rocks from Kanmantoo Mine.

7.5 Physical conditions of metamorphism

7.5.1 Comparison with experimental data

The stability of metamorphic assemblages depends on many physical conditions, including temperature, total pressure, water pressure, oxygen fugacity and bulk composition. The results of experiments on geologically relevant reactions can be applied to estimate the conditions of formation of natural assemblages, providing allowance is made for the possible errors involved which arise from the experimental conditions. Problems include the short reaction times involved compared to geological systems and the uncertainty of equilibrium being attained.

Figure 129 shows published experimental determinations of the pressure-temperature dependence of several reactions relevant to the Kanmantoo Mine area. The most important equilibria considered here are Al_2SiO_5 stability and reactions involving chlorite.

For many years the P-T conditions of the invariant (triple) point of the Al_2SiO_5 polymorphs, andalusite, sillimanite and kyanite, were obscured from metamorphic petrologists by conflicting experimental determination. Two of the key early studies were published by Richardson et al. (1969) and Holdaway (1971). While there was reasonable agreement in many studies on the sillimanite-kyanite transition and the andalusite transition, the transition between andalusite and sillimanite remained controversial. Several subsequent studies, both thermodynamic (Anderson et al., 1977; Day and Kumin, 1980; Robie and Hemingway, (1984), and field-based (Hodges and Spear, 1982; Ganguly and Saxena, 1984; Grambling, 1984) supported Holdaway's results which placed the invariant point at 500 C and 3.8kbar

Part of the problem with experimentally establishing the andalusite-sillimanite transition appears to be that in nature sillimanite occurs in two forms, fine grained fibrolite and coarser grained sillimanite. Salje (1986) pointed out that the energetic variations between the two forms are likely to result in a range of triple point positions. Kerrick (1987,1990) suggested that fibrolite and sillimanite are likely to behave in a similar manner. A new triple point position at 520 ± 20ºC and 4.2 ± 0.3 kb was proposed by Bohlen et al (1989). These authors report new data on andalusite-kyanite and sillimanite-kyanite transitions which conform to Holdaway's triple point. Bohlen et al's triple point seems to be constrained mostly by the andalusite-sillimanite transition derived from data quoted from Heninger (1984). As the authors state, their triple point agrees with petrological studies discussed by Kerrick (1987), and careful work on the Ballachulish aureole by Pattison (1992). They state also that their triple point applies to coarse sillimanite. Syntheses of experimental and thermodynamic data by Hemingway et al. (1991) and Holdaway and Mukhopadhyay (1993) also produced similar triple point estimates of 511 ± 20ºC and 3.9 ± 0.3 kbar, and 504 ± 20ºC and 3.75 ± 0.25 kbar, respectively.

In the Kanmantoo Mine area, andalusite is the dominant Al_2SiO_5 polymorph but rare samples have additional fibrolite, suggesting that peak conditions slightly exceeded the andalusite-sillimanite transition. Complete conversion of andalusite to sillimanite may have been affected by the sluggish reaction rate, which partly accounts for the controversy in its experimental location (Holdaway, 1971). Mancktelow's (1979) regional study outlined a small area of andalusite (no fibrolite) around Callington, surrounded by an area, including Kanmantoo, containing andalusite and fibrolite. Thus, his observations are consistent with this study. Kyanite has not been observed near the Kanmantoo Mine, but occurs at Brukunga with fibrolite and andalusite (Sample No. 517-N203), and so, on a regional scale, the grade appears to lie close to the Al_2SiO_5 invariant point.

Biotite X_{Fe} ratios vary between 0.52 and 0.72 and show no dependence on the X_{Fe} ratio of the host rocks (Figure 127a). The amphibole bearing lode schists have the highest and lowest values of X_{Fe} for biotite, although the latter is shared with a QM schist specimen.

Biotite is the most TiO_2 rich mineral after ilmenite, with which it typically co-exists, and the buffering effect of ilmenite may account for the relatively constant TiO_2 content measured of biotite from a range of rock types. TiO_2 contents of biotite vary between 0.76% and 2.13% but most are between 1.2% and 1.6%. The TiO_2 contents of biotites and their host rocks show no relationship (Figure 127b).

When biotite analyses are recalculated to 24 (O, OH) the total of K and Na and Ca is invariably less than 2, possibly due to vacancies in this site or analytical errors.

7.3.8 Muscovite

Muscovite was analysed from only three specimens: a quartz poor lode schist, a QMF schist and also a GAB(1) schist in which it may be a late stage mineral. In all rocks the compositions deviate only slightly from the ideal composition $K_2Al_4(Si_6Al_2)(OH)_4$. Paragonite components vary between 5% and 8.5% and the amount of phengite substitution is also small with a maximum of 6.24 Si cations per formula unit. Fe+Mg cations vary between 0.24 and 0.46, per formula unit.

7.3.9 Plagioclase

Plagioclase was analysed from only two rocks: a QMF schist, and from within a chlorite-plagioclase-tourmaline vein. In the former case, the plagioclase has measured Ca:Na:K ratios of 0.70:0.27:0.03 and so is classified on the boundary between labradorite and bytownite varieties. The same ratio from the vein plagioclase is 0.05:0.95:0.01 and so this is albite. Ba in this plagioclase was found to be 0.01% or less.

7.3.10 Oxide Minerals

Magnetite and ilmenite are by far the most common oxide minerals. Six rocks were analysed by microprobe for magnetite compositions and in four of these ilmenite was also analysed. Both magnetite and ilmenite conform closely to ideal compositions of Fe_3O_4 and $FeTiO_3$, respectively.

Al substitutes for up to 0.6% of total cation sites in magnetite and for much less in co-existing ilmenite. Ti contents in magnetite do not exceed 0.2% of total cation sites. Si, Mn, Mg and Ca are all below 0.1% of total cation sites. In one sample analysed for both core and rim compositions of magnetite (Sample No. 517-101), no chemical zoning was indicated.

7.4 Evidence of chemical equilibrium

Minerals co-existing in chemical equilibrium, or more specifically *frozen equilibrium* (Kretz 1994), should fulfil the following two conditions (Vernon, 1976):

1. similar edge compositions of different grains of the same mineral, and
2. similar distribution of components between a given mineral pair.

These two points will now be considered, with particular reference to Fe and Mg contents.

The lower boundary of the andalusite (kyanite)-staurolite zone in the Mount Lofty Ranges was defined by Mancktelow (1979) by the first appearance of biotite with andalusite and/or staurolite at the expense of chlorite and muscovite (and quartz). In the Kanmantoo Mine area, prograde chlorite in the metasediments surrounding the mine has not been observed and the assemblage chlorite + quartz + muscovite is inferred to have reacted to form biotite with andalusite and staurolite or cordierite. In the lode schists however, chlorite is common, but the assemblage chlorite + quartz + muscovite has been observed only in one sample, a quartz vein, which appears to represent a rare retrograde assemblage. The assemblages of quartz + chlorite, quartz + muscovite and, in one case, chlorite + muscovite, occur in lode schists and it appears that metamorphic conditions were sufficiently high for the three phases to react, but once any one of the reactants was consumed the remaining two were stable.

Several experimental determinations of reactions involving chlorite + muscovite ± quartz are shown on Figure 129, in most cases involving the system MgO-K_2O-SiO_2-Al_2O_3-H_2O but also included are reactions for FeO instead of MgO (reaction 3), and for mixtures of FeO and MgO (reactions 4, 5, 6). The reactions display an apparent tendency for bulk X_{Fe} ratios to affect the physical conditions of reaction, especially temperature. For example, compare the equivalent reactions 4 and 8 in which X_{Fe} = 0.6 and 0.0 respectively; or reactions 3 (extended), 5 and 10 at 2kb in which X_{Fe} = 1.0, 0.44 and 0.0 respectively. This tendency was supported by experiments on the prograde breakdown of chlorite at 2kb (McOnie et al., 1975, Fig. 7) in which the Mg-Fe chlorites break down at increasingly lower temperatures as X_{Fe} increases, but was not supported for the breakdown of chlorite + quartz at 2kb in the experiments of Fleming and Fawcett (1976, Fig. 9), who found a maximum stability temperature of approximately 590°C for X_{Fe} = 0.0 to 0.75 (refer reaction 12 on Figure 129). In an experimental study of the stability of Fe-chlorite, James et al. (1976) obtained a reversal for the reaction

Fe-chlorite = Fe-cordierite + magnetite ss + quartz + fluid

at 530°C and 2kb P P_{H_2O} and concluded that Fe-chlorite, persisting to approximately 600°C in their other experiments, was metastable.

Hence, most experimental data indicate that the breakdown equilibria of chlorite, chlorite + quartz or chlorite + muscovite + quartz are dependent on X_{Fe} and so the curves shown on Figure 129 represent the trace of divariant surfaces for fixed X_{Fe}.

In applying Figure 129 to the metasediments surrounding the Kanmantoo Mine, the occurrences of the assemblages andalusite + staurolite + biotite and andalusite + cordierite + biotite in GAB schist, and the general absence of prograde chlorite are significant. X_{Fe} ratios in GAB(1) schists studied here have the range 0.49 - 0.70 and a mean of 0.66, so reactions 4 and 6 can be applied generally and clearly the higher temperature assemblages were formed. As an upper limit, reaction 11 represents the upper stability of staurolite in the assemblage muscovite + biotite + quartz + Al_2SiO_5 (Hoschek, 1969).

In the lode schists, the assemblage quartz + chlorite (without muscovite) is common in rocks with bulk X_{Fe} ratios ranging between 0.74 and 0.81. Garnet, biotite and magnetite are usually present and, in some cases, staurolite too. Cummingtonite may be present (without staurolite) but neither orthoamphibole nor cordierite has been observed. The maximum temperature for this assemblage would lie between reactions 3 and 10 on Figure 129, and presumably closer to reaction 3 because of the high X_{Fe}. It should also lie on the low temperature side of the extension of reaction 5, so a maximum temperature of approximately 565°C is indicated. The occurrence of staurolite + biotite + quartz indicates that reaction 4 may provide the minimum

temperature, although the higher X_{Fe} may require a lower temperature than that shown.

Low K_2O assemblages, like cordierite-orthoamphibole or chlorite-quartz bearing assemblages, in the Kanmantoo Group were described by Mills (1964, for the Cambrai area), Spry (1976, for sulphide deposits in the Kanmantoo-Strathalbyn district), Mancktelow (1979, for the whole eastern Mount Lofty Ranges) and Arnold and Sandiford (1990, for the Springton area).

Cordierite-orthoamphibole bearing assemblages have been reported in association with sulphide deposits in the Kanmantoo Group including Kanappa Mine in the upper sillimanite zone (Mancktelow, 1979), and the Wheal Ellen Mine (Spry, 1976) in the fibrolite zone. The Wheal Ellen sulphide deposits occur in schists of a similar metamorphic grade to the Kanmantoo deposit yet the prograde reaction,

chlorite + quartz = cordierite + orthoamphibole.

appears to have proceeded at Wheal Ellen but not at Kanmantoo. Similarly, Mills (1964) reported the first appearance of cordierite and orthoamphibole just below the first appearance of fibrolitic sillimanite, again in contrast to the Kanmantoo area. Additional data is needed to resolve the reasons for the differences, but bulk X_{Fe} of rocks in each area are expected to be important. The cordierite-orthoamphibole bearing assemblages at Springton were not produced by the above reaction according to Arnold and Sandiford (1990), but by metasomatic reactions at sillimanite grade in which andalusite and biotite, or staurolite and biotite, were the reactants.

Chlorite + muscovite (no quartz) was observed in only one sample of lode schist (Sample No. 517-163), which had the assemblage muscovite + chlorite + staurolite + biotite + garnet + ilmenite + magnetite. Quartz was present in trace amounts as small inclusions in staurolite but not in contact with other minerals and may be a remnant from a staurolite forming reaction involving quartz. Muscovite and chlorite, apparently in microstructural equilibrium, comprise about 90% of the rock and it has a X_{Fe} ratio of 0.70. This sample represents conditions on the low temperature side of reaction 4, and so is at odds with assemblages found in GAB(1) schist, as discussed previously.

On the basis of the experimental data discussed above, the most likely P-T conditions indicated for the rocks of the Kanmantoo Mine area are within the stippled area in Figure 29.

7.5.2 Garnet-biotite geothermometry

Many studies have shown that the distribution of Fe and Mg between co-existing garnet and biotite is dependent on temperature (Kretz, 1964; Hietanen, 1969; Saxena, 1969; Thompson, 1976). The exchange reaction is:

$$\underset{\text{pyrope}}{Mg_3Al_2Si_3O_{12}} + \underset{\text{annite}}{KFe_3AlSi_3O_{10}(OH)_2} = \underset{\text{almandine}}{Fe_3Al_2Si_3O_{12}} + \underset{\text{phlogopite}}{KMg_3AlSi_3O_310(OH)_2}$$

and the distribution coefficient is $K_D = (Mg/Fe)_{gar}/(Mg/Fe)_{bio}$. The natural logarithm of K_D has been calibrated relative to temperature by three methods, by comparison with experimental phase equilibria (Saxena, 1969; Thompson, 1976; Perchuk, 1977), by laboratory experiments (Ferry and Spear, 1978) and by comparison with oxygen isotope geothermometry (Goldman and Albee, 1977).

Table 23. Cation ratios of garnet and biotite rims.

Rock Type	Sample No.	Mg/Fe bio	Mg/Fe gar	XMn gar	XCa gar	XFe bio	XTi bio	XAl bio
GAB(1) schist	517-133	0.5773	0.0764	0.082	0.008	0.634	0.032	0.150
GAB(1) schist	517-148	0.6732	0.0873	0.042	0.007	0.5977	0.030	0.155
GAB(1) schist	517-149	0.8449	0.1130	0.091	0.009	0.5420	0.046	0.219
QMF schist	517-2870	0.8994	0.1266	0.318	0.089	0.5264	0.044	0.134
Lode schist (1a)	517-004	0.6528	0.0887	0.030	0.006	0.6050	0.028	0.136
Lode schist (1a)	517-024	0.7581	0.1006	0.035	0.007	0.5688	0.032	0.146
Lode schist (1a)	517-049	0.6929	0.0894	0.031	0.007	0.5907	0.031	0.133
Lode schist (1a)	517-055	0.6763	0.1087	0.023	0.006	0.5966	0.029	0.138
Lode schist (1a)	517-055	0.6981	0.0912	0.023	0.006	0.5889	0.027	0.154
Lode schist (1a)	517-055	0.7368	0.0969	0.024	0.007	0.5758	0.029	0.159
Lode schist (1a)	517-055	0.8023	0.1075	0.022	0.004	0.5548	0.028	0.119
Lode schist (1a)	517-055	0.7726	0.0999	0.023	0.006	0.5624	-	0.174
Lode schist (1a)	517-057	0.7836	0.1168	0.022	0.006	0.5607	0.028	0.129
Lode schist (1a)	517-057	0.7833	0.1094	0.021	0.005	0.5607	0.009	0.176
Lode schist (1a)	517-057	0.7513	0.0983	0.025	0.006	0.5710	0.030	0.136
Lode schist (1a)	517-057	0.7867	0.0916	0.024	0.006	0.5596	0.030	0.134
Lode schist (1b)	517-112	0.6749	0.0963	0.045	0.006	0.5970	0.032	0.163
Lode schist (2)	517-163	0.4634	0.0933	0.056	0.006	0.6833	0.026	0.094
Lode schist (2)	517-163	0.4483	0.0702	0.082	0.006	0.6904	0.022	0.100
Lode schist (2)	517-177	0.6906	0.0939	0.051	0.007	0.5915	0.032	0.147
Lode schist (3)	517-059	0.8135	0.1048	0.024	0.006	0.5514	0.028	0.084
Lode schist (3)	517-059	0.7870	0.1061	0.022	0.021	0.5596	0.027	0.092
Lode schist (3)	517-060am	0.9399	0.1130	0.023	0.010	0.5154	0.026	0.084
Lode schist (3)	517-061A	0.8219	0.1039	0.016	0.027	0.5489	0.024	0.087
Lode schist (3)	517-076B	0.6878	0.0893	0.052	0.007	0.5924	0.029	0.137
Lode schist (3)	517-077s	0.4541	0.0612	0.022	0.008	0.6877	0.025	0.099
Lode schist (3)	517-077s	0.4387	0.0619	0.023	0.010	0.7123	0.013	0.109
Lode schist (3)	517-077l	0.4265	0.0576	0.026	0.011	0.7010	0.037	0.090
Lode schist (3)	517-077v	0.4015	0.0553	0.023	0.009	0.7134	0.013	0.098
Lode schist (3)	517-077v	0.4371	0.0513	0.024	0.009	0.6958	0.014	0.141
Lode schist (3)	517-077v	0.4138	0.0545	0.024	0.009	0.7073	0.016	0.104
Lode schist (3)	517-203	0.5532	0.0736	0.025	0.007	0.6438	0.026	0.105
Lode schist (3)	517-203	0.5994	0.0592	0.029	0.030	0.6252	0.033	0.114
Lode schist (3)	517-203	0.5125	0.0614	0.027	0.039	0.6611	0.024	0.084

(1a) refers to lode schist variety: quartz rich with andalusite (group 1). (1b) refers to lode schist variety: quartz rich without andalusite (group 1). (2) refers to lode schist variety: quartz poor/absent (group 2). (3) refers to lode schist with amphibole (group 3).

Although the distribution coefficient K_D is primarily dependent on temperature it is also dependent to a lesser extent on pressure (Ferry and Spear, 1978), but the effect of pressure is considered to be small compared to the effect of temperature (Kretz,1994). Another factor influencing K_D is the departure from ideal Fe-Mg phases due to additional components, like Ca, Mn in garnet and Ti in biotite (Goldman and Albee, 1977). This subject was reviewed by Kretz (1994) who concluded that only Ca in garnet has a significant effect. To avoid the uncertain effects of additional components, their contents should be low in garnet and biotite used for thermometry and fortunately, they are generally low in the minerals of the Kanmantoo Mine area (Table 23), except the sample of QM schist (No. 517-2870) which has relatively high Mn and Ca in garnet.

The garnet-biotite calibrations used here are those of Thompson (1976), Goldman and Albee (1977), Ferry and Spear (1978) and Kretz (1994). The results for 34 garnet-biotite pairs from 20 different rock samples, including lode schists, GAB schist and QMF schist, are shown in Table 24. Thompson's calibration is semiquantitive, whereas Goldman and Albee's is more

specific and includes a correction for Mn and Ca in garnet and Ti and octahedrally co-ordinated Al in biotite. Ferry and Spear's calibration is based on experiments in the binary Fe-Mg system, and so has no allowance for other elements in solid solution, but has a pressure correction. As the pressure is not known accurately for the Kanmantoo Mine samples, two sets of calculations were made with estimates of 3.5kb and 4.0kb, but the calculated difference in temperature was found to be only 2ºC.

Table 24. Garnet-biotite geothermometry. K_D = (Mg/Fe)bio / (Mg/Fe)gar, refer to Table 23 for data and rock types. Calibrations are from: 1. Thompson (1976); 2. Goldman and Albee (1977); 3. Ferry and Spear (1978) using assumed P = 3.5kb (column 3A) and P = 4.0kb (column 3B); 4. Ferry and Spear using corrections of Pigage and Greenwood (1982). 5. Kretz (1994).

		Temperature estimates (ºC)					
Sample No.	K_D	1	2	3A	3B	4	5
Metasediments							
517-133	7.556	493	413	484	486	528	530
517-148	7.711	489	412	478	480	503	523
517-149	9.678	444	412	423	424	468	482
517-2870	7.104	507	550	501	503	706	640
Lode schists							
517-004	7.360	499	410	491	493	510	532
517-024	7.536	494	418	485	486	507	528
517-049	7.751	488	404	477	479	497	522
517-055	6.222	537	440	540	542	558	571
517-055	7.654	491	411	480	482	496	523
517-055	7.604	492	417	482	484	499	526
517-055	7.463	496	413	487	489	502	525
517-055	7.734	488	405	478	479	492	521
517-057	6.709	519	433	517	519	533	553
517-057	7.160	505	438	499	500	514	536
517-057	7.643	491	411	481	483	496	523
517-057	8.588	467	394	451	453	465	499
517-112	7.008	510	430	505	507	532	543
517-163	4.967	594	455	617	619	654	629
517-163	6.386	531	416	532	534	578	564
517-177	7.354	499	420	491	493	520	534
517-059	7.762	488	400	477	478	493	520
517-059	7.418	497	412	489	491	512	556
517-060am	8.318	473	398	459	460	476	513
517-061A	7.910	484	404	472	473	495	552
517-076B	7.702	489	411	479	480	508	524
517-077S	7.420	497	382	489	491	505	534
517-077S	7.087	507	392	502	503	518	547
517-077l	7.404	498	378	489	491	510	540
517-077v	7.262	502	382	495	497	515	540
517-077v	8.520	469	373	453	454	472	507
517-077v	7.593	492	378	483	484	503	531
517-203	7.516	494	391	485	487	503	529
517-203	7.781	487	386	476	478	493	560
517-203	8.347	473	378	458	460	494	559
mean		**497**	**411**	**488**	**490**	**516**	**539**

Ferry and Spear's calibration has been modified by Pigage and Greenwood (1982, p947) to include a correction for Mn and Ca in garnet, using data from Ganguly (1979). Estimates using this modified calibration are also included in Table 24; note that for the Mn rich garnet in sample no. 517-2870, the modified temperature is unrealistically high, suggesting that the correction used is too severe. Temperature estimates 1 to 4 shown in Table 24 were published in Spry et al. (1988). The final column of estimates (labelled 5 in Table 24) is based on a

calibration proposed by Kretz (1994). Kretz used the experimental data of Ferry and Spear (1978) and Perchuk and Lavrent'eva (1983), and incorporated a correction for Ca in garnet using field-based data from Kretz (1990) for sillimanite-Kfeldspar zone rocks, and Phinney (1963) for staurolite zone rocks. A possible source of error for the temperature estimates shown in Table 24 is the ferric iron content of garnet and, especially, biotite. Ferric iron contents were not analysed in this study and all iron is assumed to be ferrous generally. Because higher temperatures of equilibration result in a smaller difference in X_{Fe} and garnet is richer in iron than biotite, then ignoring ferric iron contents tends to give lower temperature estimates (Schumacher, 1991).

The temperature estimates according to the calibrations of Thompson (1976) and Ferry and Spear (1978) agree quite well and both are much higher than the estimates from Goldman and Albee's (1977) calibration. This agrees with the observation of Hodges and Spear (1982), who claimed that at conditions comparable to the Al_2SiO_5 invariant point, the Thompson and Ferry-Spear calibrations usually produce virtually indistinguishable results. In this case, the two calibrations indicate temperatures between 480 –510ºC and this agrees closely with Holdaway's position of the invariant point (Figure 129). However, the experimental results of phase equilibria, discussed in the previous section, indicate higher temperatures, in the range 530 –580 C. The lower end of this bracket is consistent with the estimates obtained using the Kretz calibration, which produced the highest average estimates.

Of particular importance with regard to the history of the mineralised rocks is the similarity between the temperature estimates obtained from the lode schists and the surrounding metasediments. This similarity is relevant regardless of the exact values obtained. It supports the microstructural evidence that the host rocks of the copper mineralisation were present during peak metamorphism.

7.5.3 Garnet-cordierite geothermometry

The partitioning of Fe and Mg between co-existing garnet and cordierite has been calibrated as a geothermometer by Thompson (1976), by comparison of natural assemblages with experimental phase equilibria studies. In one sample of lode schist (No. 517-055), five garnet-cordierite rims were analysed. Temperature estimates according to Thompson's (1976) calibration are shown in Table 25 in which the distribution coefficient

$$K_D = (Mg/Fe)_{crd} / (Mg/Fe)_{gar}$$

The results have quite a large range (45ºC) for one sample but, like the garnet-biotite pairs, indicate a temperature around 500ºC. Temperature estimates for garnet-biotite pairs at the same site and also according to Thompson's calibration are in reasonably good agreement.

Table 25. Garnet-cordierite thermometry. Metamorphic temperature estimates derived from rim compositions in Sample No. 517-055, using Thompson's (1976) calibration.

$X_{Mg\ crd}$	$X_{Mg\ gar}$	K_D	T (^oC)
0.5790	0.0953	13.063	513
0.5678	0.0980	12.088	531
0.5761	0.0939	13.118	512
0.5741	0.0836	14.781	486
0.5641	0.0908	12.953	515

7.5.4 Garnet-cordierite-quartz- Al_2SiO_5 equilibrium

Fe-Mg partitioning between garnet and cordierite in the assemblage above has been recognised as a potential geothermometer and geobarometer, and several conflicting calibrations have been proposed (Currie, 1971; Hensen and Green, 1973; Weisbrod, 1973; Hensen 1977; Holdaway and Lee, 1977; Newton and Wood, 1979; Lonker, 1981; and Martingole and Sisi, 1981).

The end member reactions are, at low temperatures and high temperatures respectively:

Fe cordierite = almandine + sillimanite + quartz
Mg cordierite = pyrope + sillimanite + quartz

Between the end member reactions, the four phase divariant assemblage, with intermediate Fe/Mg ratios, is stable. Because the reactions involve a large volume change the equilibrium slope on a P-T grid is small, such that Fe/Mg ratios are more sensitive to pressure variation than temperature variation. Thus, the assemblage is a potentially useful geobarometer, however many aspects of the equilibria are poorly understood, particularly the importance of P_{H_2O} and the position and slope of the reactions. The uncertainties associated with this geobarometer and geothermometer were reviewed by Lonker, 1981; Martingole and Sisi, 1981; and Newton, 1985.

Table 26. P-T estimates from gar+crd+qtz+and bearing assemblages. For all calibrations shown, estimates were obtained by projecting published calibration curves. Calibration numbers refer to the studies of: 1. Martingole and Sisi (1981); 2. Lonker (1981); 3. Newton and Wood (1979); 4. Holdaway and Lee (1977); 5. Thompson (1976).

Calibration No.	P-T slope	Using the intersection of isopleths (where possible)			Separate isopleths assuming T=500°C	
		Assumption	P (Kb)	T (°C)	Pgar	Pcrd
1	positive	nH20=0.8	2.7	450	3.5	3.5
		nH20=0.5	2.3	490		
2	negative	P_{H2O}=1.0	7.4	430	6.7	6.3
		P_{H2O}=0.5	6.2	460		
3	positive	-	-	very low	5.1	4.3
4	negative	P=3.5	-	very high		
		T=500	6.7	-	6.7	-
		T=550	6.5	-		
5	negative	-	6.3	390	6.0	5.6

To use the various calibrations, Mg/Fe for garnet and cordierite must be known as well as the number of moles of water in cordierite (which is related to P_{H_2O}). In the one sample analysed from the Kanmantoo Mine (No. 517-055) the assemblage contains andalusite rather than sillimanite which is awkward because the calibrations are for the sillimanite field. Hence, the Mg/Fe isopleths for garnet and cordierite must be projected to lower temperatures than calibrated. Pressure and temperature results obtained using five different calibrations are shown in Table 26. The number of moles of water in cordierite is not known, so various values are assumed in part (a) of Table 26. Using the intersection of the garnet and cordierite

isopleths, none of the calibrations gives what seem to be realistic results. Lonker (1981) proposes corrections for the Mn content of garnet which amount to a decrease in the pressure estimate of approximately 1 kb for each 5% increase in X_{Mn}, for a given temperature, and the activity of water equal to unity. As the X_{Mn} in the garnets of the sample analysed here is only approximately 2%, the effect is not significant.

As an alternative, the five calibrations were used to estimate pressure, assuming a temperature of 500 C and using Mg/Fe ratios typical of garnet and cordierite. Because separate isopleths for both garnet and cordierite are involved, two pressure estimates were obtained. They are shown in part (b) of Table 26. In most cases cordierite indicates a higher pressure than garnet, but only the two calibrations with positive P/T slopes give apparently realistic results, namely those of Newton and Wood (1979), and Martingole and Sisi (1981). The latter, in particular, gives approximately the same pressure for both minerals, 3.5 kb, which is consistent with the application of Holdaway's (1971) Al_2SiO_5 invariant point to the Kanmantoo Mine assemblages.

7.5.5 Magnetite-ilmenite equilibrium

In rocks with co-existing ilmenite and magnetite, experimental results on the proportions of hematite (Fe_2O_3) in ilmenite ($FeTiO_3$) and ulvospinel (Fe_2TiO_4) in magnetite (Fe_3O_4) enable an estimation of the temperature of equilibrium to be made (Buddington and Lindsley, 1964). Although normally used for higher grade rocks, revised calibrations by Spencer and Lindsley (1981) and Anderson and Lindsley (1988) using additional experimental data and improved thermodynamic models, allow estimates to be made at temperatures as low as 500ºC.

Co-existing magnetite and ilmenite occur in many lode schists and GAB(3) schists. Table 27 lists oxide proportions for three magnetite-ilmenite pairs from three different lode schists. In one of these, the ilmenite has a much higher hematite component than others analysed and may be an erroneous analysis. According to Spencer and Lindsley's T-fO_2 calibration, the most reliable data in Table 27 indicate temperatures around 490-500ºC for lode schists from Kanmantoo Mine, and so agree with the garnet-biotite geothermometric estimates. However, this estimate must be regarded as approximate, because Buddington and Lindsley (1964) place a 30ºC error on temperature estimates using their calibration and Oliver (1978) suggested that Fe-Ti oxides of amphibolite grade rocks re-equilibrate during cooling. The data by Anderson and Lindsley (1988) cannot be used because the Kanmantoo data plot outside their area of calibration. However, by projection beyond the calibrated area, temperatures somewhere around 500ºC are indicated for the first sample in Table 27, and well below 500ºC for the other two.

Table 27. Results of Fe-Ti oxide thermometry estimates. Estimates were derived using the calibration of Spencer and Lindsley (1981), fO_2=oxygen fugacity, T = temperature.

Sample Number	Mt:Ulv	Ilm:Hem	T(ºC)	Log fO_2
517-049	99.8 : 0.2	88.6 : 11.4	?	?
517-112	99.6 : 0.4	96.8 : 3.2	495	-24
517-163	99.7 : 0.3	96.8 : 3.2	495	-24

7.5.6 Conclusions

The peak metamorphic temperature and pressure are similar for both lode schists and surrounding metasediments. Pressure is estimated at 3-4 kb and temperature estimates differ depending on whether experimental phase equilibria studies or mineralogical geothermometers are used. The former provide a temperature range of 530-565ºC, the latter 480-510ºC, but with a few higher values overlapping the former range.

8. GEOCHEMISTRY

8.1 Introduction

In preceding chapters it was shown that the Kanmantoo copper mineralisation is associated with rocks of anomalous chemistry compared to others in the district. In particular, the mineralisation is associated with iron rich lithologies, both with respect to the mineralised lode schists and also the host metasedimentary unit of GAB(1) schist. This chapter has two main sections. Firstly, aspects of the geochemistry of the metasediments are described with the aim of placing the GAB(1) schists of the Paringa Andalusite Member within their local geochemical context. This issue has developed extra significance recently with the discovery of probable exhalites within the Paringa Andalusite Member close the Kanmantoo mineralisation (Toteff, 1999). An important question is whether GAB(1) schists are anomalous in elements other than iron, especially copper, thus providing substantial support for a syn-sedimentary origin for the mineralisation. This issue is studied here by comparing the geochemistry of GAB(1) schist with other lithologies in the Kanmantoo district using data from this study and others.

The second approach in this chapter is to describe the chemical composition of the copper mineralised lithologies, that is GAB(2) schist, GAB(3) schist and the lode schists. The objects here are to describe the differences between the varieties of both GAB schist and lode schist, and look for a link that may tie all lithologies into a mineralising process. This includes examining the possibility that the mineralised rocks were derived by alteration of GAB(1) schist and studying whether any alteration was accompanied by volume changes.

For this study 21 samples of GAB schist and 24 samples of lode schist were analysed for a total of 23 elements. Individual analytical results are compiled in Appendix 2.

When studying the geochemistry of metamorphic terrains, and especially when trying to determine original sedimentary rock types from their chemical composition, the degree of change during regional metamorphism due to loss and gain of elements must be considered. This is an old problem that is still being debated. Some authors have argued that, with the exception of some volatile components like H_2O and CO_2, significant transport of material over large distances does not occur during metamorphism (for example, Winkler, 1976, p16; Vernon, 1976, p22). Ronov et al (1977) concluded that regional metamorphism conserves all elements except CO_2, H_2O, S, Cl, B, Hg, U, Cd and heavy rare earths. The degree of change depends on many factors, of which an important one from the point of view of possible leaching of base metals from sediments during metamorphism is whether the elements are present in percentage levels or trace amounts (like copper for example). For example, Haack et al (1984) argued that during regional metamorphism the concentration of the major elements is not appreciably changed but the trace elements are, because the ratio of released volatiles to trace elements is many orders of magnitude higher. In particular, these authors, as well as Shaw (1954) and Engel and Engel (1958), showed that Cu content decreases by up to 60% with increasing metamorphism and so Cu (and other trace metals) are released into the metamorphogenic fluids which are then potentially ore forming.

Despite the conclusions of some authors that major element change is minimal during regional metamorphism, the issue is still unclear. In particular, major element metasomatism on the microscale during cleavage and foliation development is well documented. The scale of chemical mobility during cleavage development appears to vary. For example, Cox and Etheridge (1989) argued that in low grade volcanic rocks deformed by plane strain, material removed from cleavage films was deposited in adjacent inter-film zones, thus locally conserving volume and material. In contrast, the data of Marlow and Etheridge (1977)

indicated bulk chemical change during crenulation cleavage formation in Kanmantoo Group rocks. Similarly, Wall and Ceplecha (1976), Stephens et al. (1979) and Etheridge et al. (1984) argued for bulk chemical losses during low grade deformation. The losses were mostly of SiO_2 and were far greater than could be accounted for by local quartz veins.

Etheridge et al. (1983, p.207) contend that the volume lost from sites of dissolution during foliation development can rarely be accounted for by material added to adjacent sinks, and that substantial volume loss, on the scale of metres to kilometres, may be characteristic of low grade foliated rocks. Bulk volume losses may vary from a few percent to 50%. Wright and Henderson (1992) estimated that up to 50% of the total volume of metasediments was lost as a result of pressure solution processes associated with cleavage development during low grade metamorphism. It is unlikely that the material lost will be of precisely the same chemical composition, as the original rock and so one must conclude that large scale chemical changes may attend regional metamorphism. The mechanism in which this material is transported through the metamorphic pile is another complex issue and was reviewed by Oliver (1996). The fluids may move in a pervasive manner or be channelised and these processes can occur at different scales. Important controls include physical features such as bedding and deformation structures and metamorphic conditions such as P_{H2O} changes.

In comparing the chemistries of various rock types in the Kanmantoo Mine area no adjustments are needed for possible changes resulting from different metamorphic grades. However, in this chapter the chemistries of the rocks in the Kanmantoo Mine area will be compared with other metasediments from the Kanmantoo Group and also with unmetamorphosed typical sediments. Problems occur when comparing rocks of various metamorphic grades, using weight percentages of elements, because of the corresponding variation in volatile contents. The weight percentages of elements like Si, Al and so on in most unmetamorphosed sediments are lower than in equivalent rocks of high metamorphic grade that have lost much of their volatiles. To overcome this, it is useful in many cases to compare element ratios, especially Niggli ratios (Niggli, 1954).

To determine Niggli ratios for a rock, the oxide weight percentages are converted to molecular proportions by dividing by the appropriate molecular weights, in the same way that mineral formulae are calculated from oxide analyses. The results are used to calculate various ratios, of particular interest here are the Niggli ratios termed *al*, *fm*, *c*, *alk* and *fe*. For this study,

al = molecular Al_2O_3 / T,
fm = molecular FeO(total)+MgO+MnO / T,
c = molecular CaO / T,
alk = molecular K_2O+Na_2O / T,
T = total molecular $Al_2O_3+FeO+MgO+MnO+CaO+Na_2O+K_2O$.
fe = molecular FeO(total) / FeO+MgO+MnO.

Note that most of the major elements are included in these ratios but not SiO_2 (although it is part of another Niggli ratio) and this omission is useful in comparing metasediments where significant proportions of silica were contributed to the original sediments by variable amounts of detrital quartz. The ratios *al*, *fm*, *c* and *alk* relate to minerals other than quartz and, in addition, are not influenced by variable volatile contents between samples being compared. A valuable parameter is the difference between *al* and *alk* (*al-alk,* Senior and Leake, 1978). Its value lies in the possibility of distinguishing the Al contributed to sediments by minerals other than alkali feldspars. Note that *al-alk* for alkali feldspars is zero (Table 28) and so rocks with positive *al-alk* values are likely to have had at least some of their Al contributed by other minerals. For example, typical shales have higher *al-alk* values than typical feldspathic sediments (Table 29).

Table 28. Examples of Niggli *al-alk* ratios for common aluminous minerals in sediments. Calculated from ideal compositions and analyses published in Deer, Howie and Zussman (1976).

Mineral group	Mineral	Niggli *al-alk*
Feldspars	K feldspar	0 when pure
	Albite	0 when pure
	Anorthite	50 when pure
Clays	Kaolinite	90 - 100
	Illite	25 - 75
	Smectite	60 - 85
	Vermiculite	15 - 20
Chlorites	Penninite/amesite	8 - 33
Micas	Muscovite	30 - 50
	Glauconite	low to negative
	Biotite	0 - 20

Table 29. Chemical compositions and Niggli ratios of some common sedimentary rock types.

	Shale*		Shale**		Greywacke**		Arkosic sandstone	
		R		R		R		R
SiO2	50.9	61.5	60.64	65.44	73.04	76.17	75.57	77.44
Al_2O_3	15.1	18.3	17.32	18.69	10.17	10.61	11.38	11.66
FeO(tot)	6.0	7.3	5.68	6.13	4.65	4.85	2.37	2.43
MnO	0.11	0.13	tr	tr	0.18	0.19	0.05	0.05
MgO	2.22	2.68	2.60	2.81	1.43	1.49	0.72	0.74
CaO	3.5	4.2	1.54	1.66	1.49	1.55	1.69	1.73
Na_2O	0.89	1.07	1.19	1.28	3.56	3.71	2.45	2.51
K_2O	2.77	3.35	3.69	3.98	1.37	1.43	3.35	3.43
TiO_2	0.75	0.91	-	-	-	-	-	-
P_2O_5	0.18	0.22	-	-	-	-	-	-
Total	82.42	100.00	92.66	100.00	95.89	100.00	97.58	100.00
al	37.24		42.55		33.13		41.59	
fm	35.81		35.96		34.13		19.21	
c	15.84		6.88		8.83		11.23	
alk	11.11		14.62		23.91		27.98	
al-alk	26.13		27.93		9.22		13.61	
fe	0.60		0.55		0,63		0.64	
mg	0.39		0.45		0.36		0.35	

R = recalculated to 100% total; * = from Krauskopf (1967), a compilation from various sources; ** = from Pettijohn (1957); tr = trace; FeO(tot) = total iron expressed as FeO.

8.2 Geochemistry of the metasediments

8.2.1 Introduction

The most common lithologies in the Kanmantoo Group are metasediments derived from the range between pelites to psammites (Daily & Milnes, 1973; Mancktelow, 1979). Whole rock chemical analyses for these rocks in the southern part of the Kanmantoo Group are available from George (1967), Fleming (1971), Spry (1976), Mancktelow (1979), and Oliver et al. (1998). Together with the analyses from this study, these results have been compiled in

Table 30. The Kanmantoo group results are consistent with published average compositions for pelites and psammites, as shown in Table 29, and this point will be discussed more fully elsewhere.

Table 30. Mean chemical compositions and Niggli ratios for some common Kanmantoo Group metasediments. All units are percentages.

	GAB schist[1]	QMA schist[2]	GB schist[3]	QMF schist[4]	Meta-clastics[5]	Pyritic schists[6]
SiO_2	62.47	60.82	65.79	62.76	59.33	51.94
Al_2O_3	16.28	18.78	13.04	15.98	18.02	12.69
FeO	11.47	6.84	12.28	6.68	6.58	19.47
MnO	0.25	0.07	0.15	0.16	0.09	0.23
MgO	3.30	3.32	1.58	3.16	3.44	3.28
CaO	0.19	0.93	0.12	1.87	1.52	4.66
Na_2O	0.13	1.61	0.16	1.44	1.72	1.22
K_2O	3.26	4.06	3.24	4.22	4.28	1.77
TiO_2	0.74	0.81	0.62	0.75	0.77	0.51
P_2O_5	0.15	0.17	0.11	0.13	0.15	0.25
Total	98.24	97.41	97.09	97.15	95.90	96.02
S	0.14	0.002	0.002	0.02	-	12.14
C	*	<0.01	-	*	-	0.27
CO_2	*	<0.01	-	*	-	0.03
al	35.9	41.1	33.7	36.3	38.8	20.7
fm	55.1	39.8	56.0	40.2	39.2	59.1
c	0.8	3.7	0.6	7.7	5.9	13.8
alk	8.3	15.4	9.8	15.8	16.1	6.4
al-alk	27.6	25.7	23.9	20.5	22.7	14.3
fe	0.65	0.53	0.81	0.54	0.51	0.76

Notes.

1. Mean of 14 GAB(1) schist samples from the Paringa Andalusite Member and the unit just east of the Kanmantoo Mine. Analysed by the author. Sample No.s 517-093, 121, 133-138, 146-149, 178, 185.
2. QMA schist sample analysed by the author. Sample No. 517-186.
3. Mean of two GB schist samples collected 400m east of the Kanmantoo Mine and analysed by the author. Sample No.s 517-179, 180.
4. Mean of five QMF schist samples collected near the Kanmantoo Mine and analysed by the author. Sample No. 517-181, 2870, 3070, 3370, 3810.
5. Mean of 31 Kanmantoo Group rocks analysed by N. Mancktelow (1979), described as phyllites, schists, greywackes and siltstones. Sample No. 474-291, 403, SC50A, SC58, K25, 390, 333B, 321, 526, 87, 318, 288, 404, 405, CN1, 263C, 380, 384, K26, 81, 289, K27, 354, K40, K44, 283, K30, K37, 247S, 293, K34.
6. Mean of 27 pyritic schist samples from the Brukunga Mine, collected by R. George and analysed by the author. Significant base metal contents are present in many samples.
7. Total iron calculated as FeO (although present in the analysed sample predominantly or completely as Fe_2O_3.

* C and CO_2 measurements on five GAB(1) schist and one QMF schist were < 0.01%, the limit of detection.

Three of the less common metasediments in the Kanmantoo Group are iron rich. The most iron rich metasediments known to the author are the small, banded iron formation units occurring a couple of kilometres north of the Kanmantoo Mine in which the iron is present mainly as an oxide mineral. Three analyses of these banded iron formations reported by Smith (1998) had total iron (as Fe_2O_3) contents of 74.56%, 26.06% and 25.4%. The second most iron rich group of metasediment is pyritic schist in which the iron occurs predominantly in sulphide minerals, and the third iron rich metasediment is GAB(1) schist in which iron occurs predominantly in silicates. In a general way the iron sulphide rich and iron silicate rich metasediments appear to correspond to the sulphide and silicate facies of James (1954) classification of iron formations. However, James' definition of an iron formation requires at

least 15% Fe and this limit is exceeded in only 6.9% of the 695 analyses of pyritic schists from the Talisker Calc-Silicate in the Brukunga area published by Mason (1968), and is never exceeded in samples of GAB(1) schist to the author's knowledge. Thus, both groups would be classified as iron rich metasediments rather than iron formations.

All three types of iron rich metasediment are important from the point of view of regional base metal mineralisation. The banded iron formations are thought to be a minor component of one of several proposed exhalite horizons in the Kanmantoo to Strathalbyn region that are directly associated with base metal mineralisation, of which the best examples are the Angas and Aclare Pb-Zn deposits (Smith, 1998; Toteff, 2000). The pyritic schists have consistently high base metal contents and sub-economic resources such as the Mt Torrens deposit in the Talisker Calc-Siltstone are known. Both of these preceding two metasediments are known to have anomalous base metal contents and the case for a syn-sedimentary or syn-diagenetic origin of the base metals is compelling. This has not been demonstrated for GAB schist and unfortunately no comprehensive geochemical survey of this important lithology has been done to the author's knowledge. In this study only rocks from the Kanmantoo Mine were analysed. However, some valuable regional data are available from studies by Drexel (1978) and Spry (1976) and are discussed in the next section. For example, Drexel (1978) in a study of exposures of the Kanmantoo Group metasediments along the South Eastern Freeway analysed all exposed types of metasediments including metapelites, metapsammite, varieties of pyritic schist and garnet-andalusite rich rocks equivalent to GAB schists representing the inferred southern extension of the Paringa Andalusite Member. The data provide a useful background of trace element contents for various lithologies within the Kanmantoo district and selected parts of the data are shown in Table 31**.** These data are discussed in a subsequent section, and support the idea that GAB schists and similar rocks represent metal enriched sediments.

Table 31. Metal contents of Kanmantoo Group metasediments from road cuts along the South-Eastern Freeway (after Drexel, 1978).

Lithological description		No.		Concentration (ppm)				
Drexel	This study	Samples		Cu	Pb	Mn	Co	Ni
Andalusite-garnet-mica-quartz schist	QMA schist or GAB schist	8	mean	85	35	700	75	95
			max.	*200*	*100*	*800*	*80*	*100*
Metasandstone	QMF schist	29	mean	15	5	60	5	15
			max.	*50*	*20*	*100*	*30*	*100*
Laminated metasandstone	QF schist	13	mean	35	10	200	30	80
			max.	*100*	*10*	*500*	*50*	*150*
Micaceous metasandstone (<10% mica)	QF schist	17	mean	25	10	250	35	65
			max.	*80*	*50*	*500*	*50*	*80*
Mica-feldspar-quartz schist (10-25% mica)	QMF schist	284	mean	45	35	300	30	70
			max.	*250*	*200*	*800*	*100*	*200*
Biotite schist (>25% mica)	QM schist	28	mean	60	20	200	35	80
			max.	*150*	*70*	*300*	*80*	*150*
Andalusite-mica-feldspar-quartz schist	QMA schist	16	mean	65	30	350	40	110
			max.	*150*	*70*	*700*	*70*	*300*
Laminated pyrite-andalusite-muscovite-quartz schist	Pyritic schist	55	mean	90	60	65	55	55
			max.	*250*	*1000*	*300*	*500*	*250*
Muscovite schist	Pyritic schist	63	mean	150	200	90	15	30
			max.	*2000*	*1000*	*500*	*250*	*200*
Feldspathic metasandstone	Pyritic schist	31	mean	300	130	160	60	50
			max.	*3000*	*700*	*500*	*700*	*200*

In following sections, the chemistry, especially the major elements, of GAB(1) schist is

described and compared to other metasediments of the Kanmantoo Mine area, then to regional metasediments of the Kanmantoo Group and finally to pyritic schists from the Brukunga Mine.

8.2.2 QMF schists

QMF schists of the Kanmantoo Mine area are similar to the common metapelites and feldspathic metapsammites that make up the bulk of the exposed Kanmantoo Group. The mean values of the analyses of five QMF Schist samples from the Kanmantoo Mine area are shown in Table 30, together with the means of thirty-two Kanmantoo Group metapelites and metapsammites collected throughout the southern Mount Lofty Ranges by Mancktelow (1979). This mean will be used here as an approximation of a typical Kanmantoo Group metasediment.

As described in a previous section, field and mineralogical studies indicate that most Kanmantoo Group metasediments were pelites and immature psammites prior to metamorphism. The means of the QMF schists and Mancktelow's meta-clastic rocks (Table 30) compare most closely with mean shale compositions, rather than those of greywacke or arkosic sandstone (Table 29), in particular the lower silica contents, higher alumina contents, low Niggli *alk* values and high *al-alk* values suggest a shale. The Kanmantoo Group rocks tend to have higher K_2O, MgO and FeO (total) contents than the published means of shales. Comparing the mean compositions of the five QMF schist samples from the Kanmantoo Mine area with Mancktelow's larger meta-clastic suite, it is clear that both means are generally similar. Although some differences are apparent, the variations do not appear significant (with the possible exception of MnO) given that only five QMF schist samples were used.

8.2.3. GAB(1) schist

The mean composition of fourteen samples of GAB(1) schist analysed by the author are shown in Table 30. Eleven of the samples are unweathered and were collected from the Kanmantoo Mine, the remaining three are surface samples collected from within 3 km of the mine. Of the published analyses of detrital sediments shown in Table 29, the lithology most closely comparable to GAB(1) schist is shale. However, the GAB(1) schist mean differs from the means of shales in having higher contents of FeO, MnO and MgO, and lower contents of CaO, Na_2O and, to a lesser extent, Al_2O_3.

Similar differences are observed when GAB(1) schist is compared to the mean of the Kanmantoo Group meta-clastic rocks shown (Table 30). GAB(1) schist is relatively enriched in FeO and MnO and depleted in CaO, Na_2O, K_2O and Al_2O_3. Further evidence of the higher iron content of GAB(1) schist relative to adjacent QMF schists at the Kanmantoo Mine can be obtained from analyses by Kanmantoo Mine Limited of diamond drill-hole KS 31. Means of these analyses are shown in Table 32. The mean value of 10.0% FeO in Table 32 is lower than the mean value of 11.40% FeO obtained from the author's fourteen GAB(1) schist samples and the reason may be because the former mean includes samples of lower iron content from,

- QMF schist collected near the interbedded contact between the two units, and
- lithologies that would be classified as QMA schist in this study.

Table 32. FeO contents of GAB(1) schist and QMF schist in drill hole KS 31

Rock Type	No. of analyses	Aggregate core length (m)	Mean FeO (%)
GAB(1) schist	13	214.6	10.0
QMF schist	31	468.8	5.7

The possibility that GAB(1) schists are simply iron rich varieties of typical Kanmantoo Group meta-clastics seems unlikely because the former have much lower contents of calcium and sodium than the latter. This is shown in Figure 130, in which iron free chemistries are represented. In this plot GAB(1) schist and meta-clastics plot in separate fields, largely as a result of differing Al_2O_3 : $CaO+Na_2O+K_2O$ proportions.

The copper content of fresh GAB(1) schist samples analysed in this study varies from 3 ppm to 307 ppm. The higher values were obtained from relatively pyrrhotitic samples near West Limb mineralisation and the lowest value was obtained from a sample collected only 30m from high grade East Limb mineralisation.

Because no rigorous regional study of background copper contents in GAB schist has been done, it is uncertain whether GAB(1) schist is an anomalously copper rich metasediment. Available data includes studies by Spry (1976) and Drexel (1978). In fresh rocks from South Hill, Spry found that GAB(1) schist contained lower Cu contents than adjacent metasediments (28 ppm vs 88 ppm), but he found higher Cu contents in GAB(1) schist at Wheal Ellen (83 ppm vs 31 ppm). Moderately weathered GAB(1) schist seems to have higher Cu contents than adjacent metasediments excepting pyritic schist. This was found by Spry at South Hill and also by Drexel for the presumed southerly extension of the Paringa Andalusite Member.

Drexel (1978) in his study of exposures of the Kanmantoo Group metasediments along the South Eastern Freeway analysed all exposed types of metasediments including metapelites, metapsammite, varieties of pyritic schist and garnet-andalusite rich rocks equivalent to GAB schists. Selected parts of the data are shown in Table 31**.** Although there are only 8 samples from a total of 544 from this garnet-andalusite rich unit (a reflection of its relative abundance in the road cuts), Drexel's data shows that the unit is anomalously high in several elements and, significantly, in copper. This is an important result and it would be interesting to know if it applies throughout the Kanmantoo district. In Drexel's data only the pyritic schist lithologies have higher average copper contents than GAB Schists. With the exception of the pyritic schist lithologies, the garnet-andalusite rich unit has the highest contents of Cu, Ba, Co, Cr, V and is equal with the large psammo-pelite group in having the highest average Pb and Zn levels. In addition, the unit has the outright highest levels of Mn of any metasediment including pyritic schists. Second in abundance for many of these elements was the QMA schist group consistent with a link between the two lithologies.

These results support the idea that GAB schists and similar rocks represent metal enriched sediments, even though the concentrations are less than those in strongly metalliferous metasediments like the pyritic schists. By way of comparison, the average abundance of copper in the crust is quoted as 55ppm by Taylor (1965, p.177) but the element is unevenly distributed among different rock types. For shales, the average is quoted as 50ppm by Taylor (1965) and 45ppm by Turekian and Wedepohl (1961). For greywackes, the average for copper of 40ppm was quoted by Taylor (1965). Sandstones have lower levels of copper, with

average levels of 10-20ppm (Pettijohn, 1963) and 1-9ppm (Turekian and Wedepohl (1961). Black shales have a somewhat higher average of 70ppm (Vine and Tourtelot, 1970).

Table 33. Niggli ratios for GAB(1) schist samples.

Sample No.	093	121	133	134	135	136
Source	P	P	P	P	P	P
al	33.66	34.87	40.55	30.04	38.96	38.45
fm	57.62	55.28	49.81	58.80	54.84	52.51
c	0.80	0.56	0.67	0.89	0.94	0.69
alk	7.92	9.30	8.97	10.27	5.25	8.35
al-alk	25.74	25.57	31.59	19.77	33.71	30.10
fe	0.64	0.65	0.67	0.68	0.75	0.66

Sample No.	137	138	146	147	148	149
Source	P	P	P	P	P	P
al	35.11	35.73	33.00	35.97	32.66	39.01
fm	54.99	54.56	60.94	55.17	59.31	52.16
c	0.83	0.84	0.92	0.81	0.74	0.75
alk	9.06	8.86	5.14	8.04	7.28	8.07
al-alk	26.06	26.86	27.86	27.93	25.37	30.94
fe	0.59	0.58	0.74	0.66	0.70	0.60

Sample No.	178	182	183	185	Spry	Spry
Source	PE	O	O	P	SH	SH
al	35.52	41.02	36.91	36.62	33.59	35.66
fm	53.65	48.84	52.94	53.10	46.64	45.61
c	0.98	1.02	0.60	0.54	6.17	4.94
alk	9.86	9.11	9.54	9.74	13.61	13.79
al-alk	25.66	31.91	27.36	26.84	19.98	21.88
fe	0.57	0.54	0.58	0.60	0.62	0.62

Sample No.	715	232	233	234	235
Source	O	O	O	O	O
al	36.26	38.49	39.41	38.01	38.18
fm	51.71	43.09	41.47	46.89	44.42
c	1.48	4.11	5.05	2.06	4.03
alk	10.55	14.31	14.07	13.04	13.37
al-alk	25.71	24.18	25.35	24.97	24.81
fe	0.61	0.50	0.49	0.54	0.50

All samples were analysed by the author except as shown below. Samples were collected from: P, Paringa Andalusite Member; PE, GAB(1) schist unit 400m east of mine; SH, South Hill, analysed by Spry, 1976; O, Other GAB units, 232-235, 715 were analysed by Fleming, 1971.

To compare the chemistries of samples of GAB(1) schist from the Paringa Andalusite Member with those from other units, the Niggli ratios derived from various analyses are shown in Table 33. One sample (517-178) was collected from the GAB schist unit immediately east of the mine. A further two samples (517-182, 183) are included from a GAB schist unit 8km northwest of Kanmantoo and to the west of the Paringa Andalusite Member. Also included are ratios for two groups of inferred GAB(1) schist samples analysed in previous studies. Firstly, there are five samples collected by Fleming (1971) from a stratigraphic position that appears to be similar to that of the two samples mentioned above (ie 517-182,183), but 3.8 to 5.0 km further north. These samples are inferred from Fleming's mineralogical analyses to be GAB(1) schist. Secondly, ratios derived from two analyses by Spry (1976) of GAB(1) schist from South Hill, 3.5 km southeast of the Kanmantoo Mine, are included.

Data in Table 33 show that GAB(1) schists from the Paringa Andalusite Member and those from other units are similar yet have significant differences. Chiefly, the samples from other units tend to have lower Niggli *fm* and higher *alk* ratios, to have many higher *c* ratios and generally lower *fe* ratios. To further illustrate these relationships two ternary plots of *al* - *fm* - *alk* and *al* - *fm* - *c* are shown in Figure 131. These demonstrate a pronounced tendency to plot as separate groups.

8.2.4 QMA schist

The structural interpretation of the Kanmantoo district, described in Chapter 5, proposed that the Paringa Andalusite Member is stratigraphically associated with andalusite rich units containing abundant QMA schist. Although commonly similar in appearance to GAB(1) schist, QMA schist has visibly fewer mafic minerals and therefore would be expected to have lower iron and magnesium contents.

In this study only one sample of QMA schist was analysed, a sample with coarse andalusite, collected from a road cutting seven kilometres north-northwest of the mine. This analysis is very close to the mean composition of the Kanmantoo Group meta-clastics, differing most notably in having a higher calcium content. Despite the prominent andalusite crystals, the QMA schist sample has only slightly lower Al_2O_3 and Niggli *al* values. More data on this lithological group is needed.

8.2.5 GB schist

Two samples from a unit of interbedded GAB(1) schist and GB schist located 400m east of the mine were analysed. Both samples have similar chemistries and the mean composition and Niggli ratios are shown in Table 30.

The mean analysis of the GB schist samples is much closer to GAB(1) schist than other Kanmantoo Group metasediments shown and, like GAB(1) schist, it has relatively high iron and low calcium, sodium and potassium contents. Compared to GAB(1) schist, the GB schist samples differ in having lower alumina contents and higher FeO/MgO ratios. The Niggli *fe* ratio of 0.81 is the highest of any rock considered in this comparison.

8.2.6 Pyritic schists

Previous studies of the major element geochemistry have concentrated on samples from the Brukunga Mine (George, 1967), where the thickest sequence of pyritic schists occurs. A sample collected near the Wheal Ellen Mine was analysed by Spry (1976). George (1967) analysed seventeen samples of pyritic schist from the Brukunga Mine for major elements including sulphur, but did not analyse carbon, carbonate or base metal contents. To obtain this information a suite of twenty seven fresh samples from Georges' collection, held at Adelaide University, was analysed by the author. Results are summarised in Table 34.

The most important chemical characteristics of pyritic schists are their consistent enrichment in base metals (especially iron), sulphur and carbon compared to enclosing schists (Table 30). Measured contents of non-carbonate carbon (presumably metamorphosed organic material) varied between 0.1% and 0.72%. Unlike any other lithology analysed, small contents of carbonate were detected in most pyritic schist samples, with a maximum of 11.75% CO_2.

Table 34. Base metal and trace element contents of GAB(1) schist and pyritic schist.

	GAB(1) schist			Pyritic schist		
	mean	maximum	minimum	mean	maximum	minimum
Cu	76	307	3	111	224	32
Co	50	76	17	34	107	7
Zn	91	162	33	3970	1.59%	21
Ni	60	77	38	55	142	20
Pb	-	-	-	3520	1.78%	31
Ba	343	848	168	1210	3150	35
Sc	14	19.3	10.2	15.1	20	8
Sr	11	25.0	7.8	115	231	35
Rb	155	196	102	105	226	2
Y	31	37	23	50	133	11
Th	17	19	9.5	32	137	10
Zr	149	208	125	93	223	53
Nb	17	18.6	12.3	9.5	19	4

Note: All values are in parts per million except as shown otherwise. All samples were analysed by the author, totals are: 14 GAB schist samples, 27 pyritic schist samples. Unignited samples were analysed. Pyritic schist samples are from the Brukunga Mine.

The highest sulphur content measured was 24.2%. The highest recorded content is 25.7% (Mason, 1968) in a 0.43m (estimated true width) section of drill core, taken along strike from the rocks in the Brukunga Mine. This core also had the highest recorded iron content of 23.3% Fe. Lead and zinc contents are also high, up to 1.78% and 1.59% respectively. Copper on the other hand, while exceeding the general content of Kanmantoo Group meta-sediments (about 37ppm as deduced from the data of Drexel, 1978) is not as enriched as lead and zinc; the highest recorded Cu content is 800ppm (Mason, 1968). Mirams (1965 ,p.316) stated that "the sulphide beds contain at least 10 to 20 times the amount of lead, zinc and copper in the greywackes as well as appreciably more silver and vanadium".

Compared to the mean of the major elements of regional meta-clastic rocks shown in Table 30, the pyritic schists analysed have higher contents of iron and calcium and lower contents of other elements. In addition, they presumably would have higher contents of sulphur and non-carbonate carbon as well, but data from regional samples are not available. The analyses of individual samples indicate considerable variation in chemistry, even when considered on an iron free basis, as in Figure 130. In this figure the pyritic schists have a more scattered plot than any other group, including the regional meta-clastics. They overlap with the relatively calc-alkali rich members of the regional meta-clastics but do not overlap with the GAB(1) schists.

In contrast, George's (1967) analyses show a very restricted range of composition when considered on an iron free basis and he concluded that variable amounts of pyrite were originally added to a sediment of approximately constant composition. The samples analysed in this study indicate that pyrite was added to sediments of variable composition, all having relatively high calcium contents and some chemically similar to the calc-alkali rich members of regional meta-clastics.

8.2.7 Pre-metamorphic mineralogy of metasediments

In this section, whole rock chemistries of GAB(1) schist, QMF schist and pyritic schists will be used to estimate possible mineralogies and, in particular, to determine the source of iron in GAB(1) schist. Chemical compositions of metamorphic rocks can be used to indicate possible original mineral compositions, but the results will only be meaningful if no significant change occurred in bulk chemistry during metamorphism. Additional obstacles to

determining original mineralogy are, firstly, the chemical similarity of many common minerals in sediments (for example illite and potassium feldspar) making a unique choice unlikely, and secondly, the unknown effects of possible regional metasomatism, for example as proposed by Oliver et al. (1998).

The most common minerals in clastic sediments include quartz, feldspar, chlorite and various clays such as illite, montmorillonite and kaolin. Less common are biotite, muscovite, iron-titanium oxides, limonite, sulphides, carbonaceous material and carbonate. Some elements, such as silicon and aluminium, can be added to sediments by many detrital minerals, whereas other elements have more restricted sources. For example, in non-carbonate bearing clastics, the most common calcium and sodium bearing mineral is plagioclase. The principal sources of potassium are feldspar or illite. Chlorite is the principal magnesium bearing mineral (in the absence of carbonates) and also of some of the iron, although oxides and hydroxides may be significant iron contributors.

The iron contents of Kanmantoo Group meta-clastics and QMF schists plotted on Figure 132 (excluding the GAB Schist samples) are closely related to the magnesium contents. With the exception of three iron rich metasediments shown on Figure 132, the remaining 43 samples define a linear relationship with a correlation coefficient of +0.94. This trend is defined predominantly by Mancktelow's suite of Kanmantoo Group samples, derived from all metamorphic grades and formations. Also included are three non-sulphide bearing psammites from the Brukunga Mine area, analysed by George (1969) and selected schists from Fleming's (1973) study. This strong relationship suggests that iron and magnesium were contributed during sedimentation in approximately the same proportion to a variety of meta-clastic sediments throughout this part of the southern Mount Lofty Ranges.

In contrast, the GAB(1) schist samples from the Kanmantoo Mine area plotted on Figure 132 do not follow the iron-magnesium trend defined by most other meta-sediments. Instead, they form a scattered group on the iron rich side of the trend. A weak negative correlation is apparent in these samples but more samples are needed to determine whether it is a real trend. Fleming (1973) also included several samples (not included in Figure 132) that plot above the correlation line, in a similar field to the GAB schists from the Kanmantoo Mine. Fleming's iron rich samples were all collected from an area located 9km north of the mine. From his descriptions, these rocks are equivalent to GB schist and GAB schist as used in this study, and are characterised by high staurolite contents (0.4 –16% modal, mean 8.7%) and high biotite : muscovite ratios. By projecting southwards, Fleming's regional interpretation places them stratigraphically near, or on the western margin of, the Paringa Andalusite Member. Other rocks that plot above the trend in Figure 132 are Spry's (1976) analyses of GAB schist from South Hill and Lindqvist's analysis of GAB schist from the mine area. Only one of Mancktelow's regional suite does the same – it was described as a staurolite schist and was collected from Salt Creek, near Monarto.

Although the correlation is not as close as FeO vs. MgO, similar relationships are seen for FeO vs. K_2O and FeO vs. Al_2O_3. For example, Figure 133 shows that, for rocks other than GAB(1) schist, K_2O has a positive correlation with FeO that is stronger if samples with FeO contents less than 5% are ignored. However, no regular relationship is evident for GAB(1) schist, although a weak negative correlation is indicated again.

Clearly, GAB(1) schist differs chemically from other local rocks and possible reasons for the relationships between FeO, MgO, Al_2O_3 and K_2O will now be considered. The close relationship between iron and magnesium in meta-sediments other than GAB schist is most easily explained by assuming that the relationship was established during sedimentation, and that both elements were combined in the same detrital mineral rather than being in separate

iron rich and magnesium rich minerals. Common iron and magnesium rich minerals in sediments are chlorite and, to a lesser degree, biotite. Both of these are aluminous minerals and so a correlation of iron with aluminium is consistent and the observed weaker correlation of FeO vs. Al_2O_3 compared to FeO vs. MgO can be explained by the presence of variable amounts of additional aluminium in iron poor minerals such as feldspar or illite. The weak correlation between iron and potassium indicates that some, but not all, of the iron bearing minerals may have been potassic. Alternatively, if Fe-Al bearing minerals were uncommon, the potassic mineral must accompany the iron minerals in approximately similar proportions in many Kanmantoo Group sediments.

The slope of the line of best fit through the data points defining the iron-magnesium trend on Figure 132 indicates a mean FeO:MgO ratio by weight of 1.6:1 or a molar ratio of 0.9:1. In the case of biotite, any detrital biotite presumably would have been derived from the crystalline basement provenance of the Kanmantoo Trough. The molar FeO:MgO ratios of these biotites are not known but according to Winkler's (1976, Fig. 14-11a) range for high grade metapelites, should lie between 0.9:1 and 0.25:1, and this range just includes the inferred ratio above. For chlorite the FeO:MgO ratio of detrital grains is unknown.

The source of much of the iron in GAB(1) schist appears to differ to that of surrounding metasediments discussed above, and Figures 132 to 133 show that the iron content of GAB(1) schist exceeds that of other metasediments for given MgO or K_2O contents. This anomalism associated with GAB schist may have resulted from sedimentary, diagenetic or metamorphic processes. With respect to sedimentary processes, iron may have been contributed to the precursor sediment of GAB(1) schist in two ways. Firstly, the precursor sediment of GAB(1) schist may have been anomalous in the stratigraphic pile in having a significantly different provenance for its detrital minerals compared to surrounding sediments. Thus, it received detrital minerals that were chemically distinct from most other sediments, especially with respect to the iron and magnesium bearing minerals. Alternatively, the iron may have been added to the precursor sediment to GAB(1) schist in two components. One component may have been the same detrital mineral common to surrounding sediments, with its apparently regular Fe-Mg ratio. The second component must contain iron that is not related to MgO, Al_2O_3 or K_2O, and the lack of correlation of iron with other elements, except perhaps manganese, suggests that an iron oxide or hydroxide may have been the additional mineral.

Other potential indicators of sedimentary mineralogy are the contents of calcium and sodium. Commonly both elements are added in plagioclase and calcium can also be added as carbonate. In Kanmantoo Group meta-clastics, carbonate minerals appear to have been insignificant except in rare marble beds, minor pyritic schist beds and possibly calc-silicate schists in which the amphiboles may be the metamorphic products of carbonate-silicate reactions. Analyses for carbonate in one QMF schist sample and five GAB(1) schist samples produced results below the analytical detection limit (0.01%). These same rocks also have non-carbonate carbon contents below the detection limit, confirming the observation that carbonaceous material is not a significant constituent of meta-clastic rocks of the Kanmantoo district, with the exception of pyritic schists, although it may be widespread in trace amounts.

Because of the apparent widespread lack of carbonate minerals, the calcium and sodium contents of regional meta-clastic rocks are inferred to result principally from original plagioclase. In contrast, the analysed GAB(1) schist samples have very little calcium or sodium, and this is one of the most significant differences between GAB(1) schist and most other rocks considered here. If the low calcium and sodium in GAB schist was present during sedimentation it is likely that the precursor sediment had little or no detrital plagioclase. Alternatively, calcium and sodium may have been present in the precursor sediment to GAB Schist but were leached during diagenesis or regional metamorphism.

The cause of the anomalous geochemical compositions of GAB Schist within the Paringa Andalusite Member and of associated rocks has been contentious amongst previous workers. Toteff (2000) favoured early alteration to sub-sea floor hydrothermal alteration associated with exhalative activity. In contrast, Oliver et al. (1998) attributed it to alteration associated with regional fluid flow during peak metamorphism. Neither theory can be argued with any conviction and more work must be done on the broad scale characteristics of GAB schists. It is curious however, that the GAB schists with the lowest calcium and sodium contents occur in the Kanmantoo Mine where evidence of metasomatism is clear. This fact suggests a connection between metasomatism and the regional distribution of GAB schist. This subject will be considered further in the next chapter.

In conclusion, many possible original mineralogical combinations can explain the present chemistry of GAB(1) schist but the simplest explanation is that the precursor sediments consisted predominantly of quartz, illite, chlorite and iron oxide or iron hydroxide. An association with metasomatism is possible. Surrounding sediments appear to have differed principally in their relative abundance of plagioclase and lack of iron oxide, or hydroxide.

8.3 Geochemistry of the rocks closely associated with mineralisation

In Chapter 5 it was concluded that the Kanmantoo copper deposit was likely to have been of hydrothermal origin on the basis of its cross-cutting relationship to relict bedding and the distribution of lithologies associated with the deposit. In this section this conclusion is further studied with respect to the chemistry of the rocks associated with the deposit. In particular, two aspects are considered, firstly the chemistries of the various lithologies are compared with one another and also with GAB(1) schist. Secondly, an attempt will be made to determine any trends in chemical composition and volume changes.

The lithologies closely associated with the Kanmantoo deposit include GAB(2) schist, GAB(3) schist and the various lode schists that were described in Chapter 3. Because these lithologies are enclosed by GAB(1) schist and some have gradational contacts with it, the assumption will be made that if hydrothermal alteration occurred, then GAB(1) schists or precursor lithologies were the rocks that were altered to produce the precursors to GAB(2) schist, GAB(3) schist and some of the lode schists. It will be assumed further that the metasomatic effects of regional metamorphism were similar for both GAB(1) schist and rocks derived from it, and had no significant effect on non-volatile elements. It is admitted that the latter assumption may be tenuous but it allows a comparison to be made. Possible effects of metamorphism were described in Chapter 7.

8.3.1 Chemical compositions

Mean compositions for samples of the various lithologies associated with the Kanmantoo deposit are shown in Table 35 (for GAB schist varieties) and Table 36 (for lode schist varieties). The most consistent major element trend shown in these tables is the change in iron content. Just as the iron content of GAB(1) schist exceeds that of surrounding metasediments, so do the iron contents of lithologies associated with copper mineralisation exceed that of surrounding GAB(1) schist.

Of the lithologies associated with the Kanmantoo copper mineralisation two groups, GAB(2)/GAB(3) schist and lode schist (1), will be considered separately. Firstly, GAB(2) and GAB(3) schists, as a group, have no major elements other than Fe that exceed GAB(1) schist and they both tend to be lower in Al, Mn, Mg and K. The most abundant of the lode schists are the quartz rich varieties of Group 1 and these tend to be lower in Al, Mg, K and Ti than

GAB(1) schist, and have higher Mn in addition to Fe. K_2O contents are lowest in lode schist (1); the minimum content measured was as low as 0.11%. Mineralogically, this is expressed in their high chlorite:biotite ratios.

Table 35. Mean chemical composition of GAB schist varieties that occur in the Kanmantoo Mine area.

	GAB(1) schist	GAB(2) schist	GAB(3) schist
No. of samples	14	3	4
SiO_2	62.47	64.55	62.22
Al_2O_3	16.28	12.36	14.96
FeO(tot)	11.47	14.99	14.47
MnO	0.25	0.21	0.23
MgO	3.30	2.43	2.69
CaO	0.19	0.18	0.17
Na_2O	0.13	0.09	0.12
K_2O	3.26	2.53	2.54
TiO_2	0.74	0.61	0.65
P_2O_5	0.15	0.14	0.13
S	0.16	1.18	0.78
Cu	76	279	370
Co	44	130	221
Zn	91	59	46
Ni	60	43	57
Ba	343	247	266
Sc	14	10	13
Sr	11	8	8
Rb	155	132	131
Y	31	36	27
Th	17	12	13
Zr	149	162	125
Nb	17	13	14
g	2.892	2.935	2.990
N(g)	14	3	4

All abundances for SiO_2 to S are expressed as percentages, the remainder as parts per million; g = density; N(g) = the number of samples used to obtain the density mean.

The two lode schist (2) samples (that is the quartz poor/absent varieties) shown in Table 36 are unique in having the lowest SiO_2 contents and the highest Al, Mg, K, Ti and P contents of all lithologies analysed. The chemistry is consistent with the observed lack of matrix quartz, abundance of ilmenite, apatite and either biotite or muscovite and chlorite.

Lode schist (3), the amphibole bearing variety, has the highest iron content of the mineralised rocks, (excluding massive sulphide samples), with contents measured as high as 39.49% FeO (total Fe).

To further illustrate the chemical differences between the rocks considered here they were plotted onto a ternary diagram representing variations of Niggli *fm*, *al* and *alk*+*c* ratios, as shown in Figure 134. The diagram shows that most samples plot in a band with GAB(1) schist at one end, lode schist at the other, and GAB(2) and GAB(3) schists between. This chemical trend is consistent with the observed spatial trend within the Kanmantoo Mine of GAB(1) schist surrounding GAB(2) and GAB(3) schist, which in turn surround lode schist.

Table 36. Mean chemical compositions of lode schists from the Kanmantoo Mine.

Type	1a	1b	1c	2a	2b	3	4
No. of samples	9	3	3	2	1	5	1
SiO_2	62.25	58.43	56.92	30.55	33.02	35.63	61.69
Al_2O_3	11.96	12.10	12.08	34.07	27.04	14.09	14.68
FeO(tot)	18.82	21.29	20.81	22.09	24.32	37.69	13.07
MnO	0.29	0.45	0.32	0.32	0.46	0.64	0.25
MgO	3.24	3.53	3.68	4.53	6.10	4.19	2.55
CaO	0.16	0.18	0.19	0.34	0.36	0.35	0.22
Na_2O	0.05	0.13	0.12	0.15	0.29	0.10	0.26
K_2O	1.50	0.37	3.04	3.24	4.10	1.83	4.59
TiO_2	0.58	0.55	0.58	1.07	1.27	0.64	0.70
P_2O_5	0.11	0.12	0.09	0.28	0.30	0.15	0.14
S	0.81	0.38	0.24	0.79	0.92	2.84	0.38
Cu	1940	2200	59	670	109	1.29%	92
Co	85	88	77	70	134	68	57
Zn	41	54	104	140	65	160	91
Ni	71	33	35	74	109	47	43
Ba	148	823	-	-	459	-	328
Sc	9	8	-	-	25	-	16
Sr	6	5	-	-	26	-	21
Rb	78	20	-	-	122	-	268
Y	32	45	-	-	44	-	25
Th	11	14	-	-	17	-	14
Zr	122	143	-	-	268	-	149
Nb	12	12	-	-	22	15	
g	3.038	3.104	3.043	3.468	3.062	2.373	2.84
N(g)	8	3	2	1	1	2	1

All abundances for SiO_2 to S are expressed as percentages, the remainder as parts per million; g = density; N(g) = the number of samples used to obtain the density mean.

In Figure 134, the various lithological groups, which were initially distinguished according to their mineralogies and fabrics, mostly plot in separate fields along the trend and so are chemically distinctive also. QMF schist and QMA schist, however, do not form part of the trend and hence the chemical data supports the observed close spatial relationship between the mineralised lithologies and GAB(1) schist, rather than other metasediments. The amphibole bearing lithologies, lode schist (1c),(3) plot on the *alk+c* side of the trend defined by most common lithologies. Similarly, lode schist (2a),(4) do not plot on the main trend.

The geochemical trend described above defines a relative increase in Niggli *fm* at the expense of *al* principally and *alk+c* from GAB(1) schist to lode schist (1). This trend is consistent with the formation of a chlorite-quartz assemblage and it is interpreted as representing hydrothermal alteration accompanying mineralisation. This is considered further in Section 8.3.3.

8.3.2 Composition-volume relationships

The chemical changes involved when rock A is altered to rock B can be studied by comparing major and trace element contents of both rocks. Major elements in particular provide information on the major changes involved that in turn are related to the compositions of the mineral phases stable in the alteration environment. However, a direct comparison of analyses of A and B is only meaningful if no volume change occurred during hydrothermal

alteration. This is usually very difficult to establish. For example, an altered rock can contain a lower proportion of a given element after alteration, even though it has been added during alteration if, during a volume increase, the content of the element added is relatively less than the volume increase. In such a case, the balance of the volume change must be accounted for by other elements.

The problem of volume changes can be overcome in many cases by using calculations described by Gresens (1967), for which it is necessary to know the specific gravity of the rocks involved. This method was used by Appelyard (1980), Gibson et al (1983), Morton and Nebel (1984), and Binns and Appleyard (1986), and modified by Grant (1986). For the alteration of rock (or mineral) A to B, Gresens derived the following formula.

$$Xn = 100\ fv(gB/gA)CnB-CnA$$

where Xn = total amount of component n (e.g. SiO_2 etc) lost or gained (in grams).
fv = volume factor
g = specific gravity
CnA = weight fraction of component n in rock before metasomatic alteration
CnB = weight fraction of component n in rock after metasomatic alteration.

Of particular interest is the volume factor, fv. If fv=1, there has been no volume change; if it is less than one a volume reduction occurred during alteration; and if fv is greater than one a volume increase resulted. Only components that remained immobile during alteration will record the true fv and although it is usually not known what the immobile components were, they can be inferred using the above formula. To do this, each component in turn is assumed to have been immobile (that is, Xn = 0) and an apparent fv is calculated. Once this has been done for all components analysed the results are compared. Ideally, the fv values of immobile elements will be the same, usually between the elements lost and gained. Thus, one looks for a grouping of some of the fv values and if found this is inferred to represent the fv value of the alteration and can be used to calculate losses and gains of all components.

To apply Gresen's method to rocks of the Kanmantoo Mine several points need to be considered. Firstly, the original rock is not known for certain but is assumed to be GAB(1) schist (or its precursor). The effects of variations in the chemistry of GAB(1) schist are reduced by using a mean composition. Secondly, to obtain a fv estimate, at least two (and preferably more) elements must be immobile, so that a clustering of fv values is found. Thirdly, the accuracy of the calculated fv value depends on the abundance of the elements used, particularly when small contents are involved. For example, a difference of 1ppm makes a significant difference to the calculated fv value in cases where abundances of only 10 ppm are involved. In rocks from the Kanmantoo Mines, the elements most vulnerable to this error are Ca, Na, P, Sc, Sr, Th and Nb and so apparent fv values determined from their analyses are less reliable than other elements. Lastly, even in cases where fv cannot be confidently estimated it may be possible to determine whether a general volume loss or gain is involved in cases where elements which are commonly immobile during metasomatism have the same trend in fv values even though they do not have the same value.

The results of composition-volume calculations are presented in Appendix 4. Apparent fv values for the major elements are plotted on Figure 135 and are summarised in Table 37. The indicated changes tend to be similar for related rock types and in these cases they are considered together.

Table 37. Summary of indicated changes in element abundance and volume by alteration.

Rock type	No. of samples	fv	Elements gained*	Elements lost*	Immobile elememts
GAB(2) schist	1	1.12	Fe, S	Mg, Na	Ti, P, Y, Nb
GAB(3) schist	4	1.12	Fe, S	-	Ti, P, Y, Nb, Rb, Zr
Lode schist (1a)	8	1.31	Si, Fe, Mn, Mg, S, Cu	K, Na	Al, P, Nb
Lode schist (1b)	1	1.25	Si, Fe, Mn, Mg, S, Cu	K, Na	Al, Ti, P, Th, Zr, Nb
Lode schist (1c)	1	1.4	Si, Fe, Mn, Mg, Ca, K, S	Cu	Al, Ti, Sc, Nb
Lode schist (2a)	1	**	?Fe, Al, Mg	?	?
Lode schist (2b)	1	0.55	S	Si, K	Al, Mg, Mn, Ca, Ti, P, Ni, Sc, Zr
Lode schist (3)	1	0.75	Fe, Mn, Mg, S	Si, K	Al, Ti, P, Zn, Zr, Nb
Lode schist (4)	1	1.10	Fe, Ca, Na,K, S	-	Al, Ti, P, Nb

Refer to text for the methods and assumptions made in producing these figures.
* Only changes greater than 20% of original content are shown, refer to Appendix 4 for further data.
** Less than 1.0 is indicated by the least mobile elements.

GAB(2) schist and GAB(3) schist

The composition of one GAB(2) schist sample and the mean of four GAB(3) schist samples were compared with the mean of GAB(1) schist samples. Data are shown in Table A1 of Appendix 3 - in both cases a grouping of apparent fv values around 1.10 to 1.17 is suggested by the elements of Ti, P, Y and Nb, suggesting these elements were relatively immobile. The fv values suggest a 10% to 17% increase in volume during alteration. Using an arbitrary value of fv = 1.12, Xn and relative changes measured in percentages were calculated and are shown on Table A1.

The general changes in both GAB(2) and GAB(3) schists are similar. Of the major elements, Fe and to a lesser extent, Si are substantially increased. Of the minor elements large relative increases (greater than 20% of original contents say) are indicated in the GAB(2) schist sample only, for Mg and also Ca and Na, but because the latter two elements are in low concentrations the indicated changes may not be reliable, as mentioned previously. Furthermore, the absolute amounts of the changes (Xn) is insignificant compared to the substantial increases indicated for FeO and SiO_2. Therefore the change indicated is a modest volume increase accounted for by addition of FeO and SiO_2 essentially.

Lode schist (1a), (1b) and (1c)

Estimations of composition-volume changes are shown in Table A2 of Appendix 4 for eight samples of lode schist (1a) and in Table A3, one sample each of lode schists (1b) and (1c). In all three cases the calculations indicated substantial relative increases in both volume and most major elements. Furthermore, the least mobile elements indicated are Al and Nb but Ti, P, Ni and Sc seem relatively immobile in certain cases.

The indicated finite volume increases for lode schists (1a), (1b) and (1c) are, respectively, 30%, 25% and 40% approximately. All three lithologies appear to have had substantially increased relative contents of Si, Fe, Mn, Mg and S. Types 1a and 1b differ from type (1c) in that the former two show substantial gain of Cu in contrast to the others. The indicated absolute changes are similar for GAB(2) schist and GAB(3) schist in that significant increases

in FeO and SiO_2 are indicated. In addition, small absolute increases in MgO are indicated for lode schist (1a) and lode schist (1b). A calculation for the change between adjacent samples of GAB(2) schist and lode schist (1c) was also made (Table A3). The two samples (nos. 517-139,-140) were collected from within one metre of each other. As expected, a volume increase is indicated with Al, Ti, Sc, Nb the least mobile elements.

Lode schist (2a) and (2b)

Varieties of lode schists (2) differ most in their mineralogy and microstructure compared with other lithologies and many occur as veins and vein-like masses, so it is less easy to envisage that they were derived from GAB schist. Therefore, this process of calculating volume changes may be erroneous for this group.

The calculations of apparent fv for a sample of lode schist (2a), the biotite-staurolite rich lithology, are shown in Table A4. Because there is no tendency for grouping amongst the values, no estimate of the real fv can be made. However, because elements which appear to be the least mobile during the formation of other rocks considered here, such as Al, Ti, P, Y and Zr have apparent values less than one, a volume decrease could be inferred.

For the sample of lode schist (2b), a muscovite-chlorite rich rock, a volume change to approximately 55% of the original volume is indicated by Al, Mn, Mg, Ca, Ti, P, Ni, Sc and Zr. No major elements appear to have experienced large relative increases, although Fe increased approximately 18%. Large relative decreases are indicated for Si and K. Of the minor elements S increased and Cu decreased.

Lode schist (3) and (4)

Lode schist (3) is a varied lithological group with the common presence of minor amphibole. The results of a composition-volume calculation for one sample are shown in Table A5. A decrease to approximately 75% of the original volume is indicated by Al, Ti, P, Zn, Zr and Nb. Major relative losses are indicated for Si, Na and K whereas significant gains are indicated for Fe, Mn, Mg, S and Cu.

The sample of lode schist (4) selected is a quartz-muscovite-biotite schist. Clustering of some fv values can be interpreted as indicating a volume increase of approximately 1.02 or 1.10, but as the latter figure is indicated by elements like Al, Ti, P and Nb which tend to be immobile in other rock types, this is favoured. Using fv = 1.1 to calculate the changes in elements gives significant increases in many elements, including Fe again, but no significant losses of the major elements.

Summary of Indicated Changes

Assuming each of the rocks associated with copper mineralisation was derived from GAB(1) schist or its precursor lithology the following are indicated.

(a) The indicated changes tend to be similar for groups of lithologies that are mineralogically and texturally similar, for example GAB(2) and GAB(3) schist or the varieties of lode schist (1).

(b) Elements that appear to have been substantially immobile during alteration are similar in many of the lithologies considered and similar to those considered by other authors as immobile in many hydrothermal events, for example Al, P, Ti, Sc, Y, Zr and Nb (Pearce and Cann, 1973; Floyd and Winchester, 1978; Finlow-Bates and Stumpl, 1981).

(c) The most common rocks associated with copper mineralisation appear to have undergone volume increases during alteration. This includes GAB(2) schist, GAB(3) schist and lode schist (1). Less common lithologies, including the narrow sulphide rich, coarse grained silicate zones (that is lode schist (2)), mostly appear to have undergone a volume decrease.

(d) For all lithologies where an alteration trend can be deduced Fe and S were added during alteration. (The exception is the lode schist (2a) sample for which a trend is not clear.) Changes in other elements vary. The common lode schist (1) generally appears to have experienced addition of Si, Mn, Mg and Cu, but a depletion of the alkalis Na and K.

(e) For GAB(2) and GAB(3) schists the major element changes are increases in SiO_2, FeO and weak losses of Na_2O and K_2O. Lode schists (1a) and (1b) were similar but unlike the former rocks also gained significant MgO. In all cases the indicated gains are much higher than the losses. Of particular interest was the general lack of change in the major component Al_2O_3.

8.3.3 Discussion

The chemical composition of hydrothermally altered rocks reflects the minerals that are stable under the conditions prevailing during alteration. In order to demonstrate the main minerals produced during the apparent hydrothermal alteration associated with the Kanmantoo deposit refer to Figure 136 in which the fields for the lithological groups in Figure 134 are shown. As mentioned previously, this diagram illustrates a chemical trend from GAB(1) schist to lode schist (1), which is represented by a relative increase in Niggli *fm* at the expense of *al* and *alk* + *c*. Also plotted on this figure are the compositions of a typical chlorite from a lode schist (1) specimen, determined by microprobe, and the range of chlorites between amesite and penninite, accordingly to data published by Deer et al. (1976). All plot on the *fm* - *al* axis. Clearly, the inferred alteration trend is consistent with the production of a chlorite rich assemblage from GAB(1) schist. Although the chlorite microprobe analysis shown is from a metamorphic assemblage, apart from quartz, chlorite is the dominant mineral present and so its composition will not change significantly during isochemical metamorphism unless major new phases form by reactions involving chlorite. Hence, the present chlorite compositions are likely to be similar to any pre-metamorphic hydrothermal chlorite compositions.

For comparison with the chemical trend in the rocks of the Kanmantoo deposit, Figure 136 also includes four alteration trends plotted from published data on three other copper deposits. These are: chloritisation of andesite and rhyolite in the alteration pipe of the Millenbach volcanogenic massive sulphide deposit, Quebec (Riverin and Hodgson, 1980), sericitisation of dacite in the Copper Hill porphyry copper deposit, N.S.W. (Scott, 1978) and biotite-sericite alteration of quartz monzonite of the Bingham stock, Utah (Moore, 1978). Also plotted are the mean composition of 16 analyses of biotite from the Bingham stock (from Lanier et al, 1975) and the ideal compositions of muscovite and potassium feldspar.

Of the alteration trends plotted in Figure 136, only the Millenbach chloritisation trends are similar to the Kanmantoo trend, in particular the more altered (that is more chloritic) part of the trend which is almost identical to the Kanmantoo rocks. Note that the less altered part of the chloritisation trend links the field of QMF schist and GAB(1) schist, possibly reflecting a relationship by alteration between these two groups. This idea is considered further in the next chapter.

The muscovite rich lode schists (that is Group 3), which occur in some peripheral parts of the Kanmantoo deposit were not studied in sufficient detail to compare possible alteration trends as was done for other lode schists. The one sample analysed plots to the left of the GAB(1) schist field in Figure 134, that is towards the muscovite-biotite tie line, so is consistent with possible alteration of GAB(1) schist by sericitisation. More samples are needed to investigate this fully.

9. ORIGIN OF MINERALISATION

9.1 Introduction

Previous chapters showed that the rocks containing the Kanmantoo copper mineralisation have undergone a fairly complex structural and metamorphic history, and that at least some of the mineralisation has participated in much of this history. Like many deposits in metamorphic settings, previous views on the origin of mineralisation at Kanmantoo tended to lean towards either syn-sedimentary or syn-metamorphic origins, often with ambiguous support for both views. Much of this chapter is occupied with examining the possible roles of these two ideas. Unfortunately, tectonism at amphibolite grade is likely to have obscured possible early features, so that while it is clear that various parts of the mineralisation at Kanmantoo were involved in tectonic events, early events are uncertain and the story is not straightforward.

The aim of this chapter is firstly to describe the legacy of work done on, or pertaining directly to, the Kanmantoo deposit. Next, some constraints on any theory of the origin of mineralisation at Kanmantoo are discussed. This is followed by a discussion of many factors that may have played a role in mineralisation at Kanmantoo, and a comparison with similar deposits. Finally, some conclusions on the origin of copper mineralisation at Kanmantoo are presented.

9.2 Previous theories

In 1942 Dickinson, the Assistant Government Geologist, produced a report including a description of copper deposits in the Callington-Kanmantoo district. At that time the Callington lodes had the largest previous ore production and were considered the most important deposits in the field. At Kanmantoo the lodes available for inspection to Dickinson were limited to the shallow Kanmantoo workings, a north-south trending group of workings along the eastern side of Macfarlane Hill, the Paringa workings and the West Kanmantoo workings. The Main Lode was not known at the time and lay hidden beneath the ferricrete cap beside the Kanmantoo workings. The Kanmantoo workings inspected by Dickinson had exploited relatively high grade lodes. He noted that the lodes were pipe-like shoots of limited strike extent and width and they were persistent down plunge. For example, the Kangaroo lode was measured at 4.3m length, 3.7m width and 61m-91m plunge extent. Dickinson was the first to note that these steeply plunging lodes were pipe-like and discordant to the folds in bedding.

Regarding the origin of the copper deposits, Dickinson considered that all copper lodes in the district had similar origins and were “mesothermal”, quoting Lindgren’s (1933) classification based on temperature of formation. Dickinson considered that the various deposits were associated with zones of locally increased metamorphic grade represented in part by andalusite bearing schists, and that the source of the higher metamorphism and the copper was an unspecified igneous body underlying the area. Control on the localization of copper deposits was ascribed to a number of intersecting sets of fractures. At Kanmantoo, the intersecting fractures were considered to result in many pipe-like deposits whereas at other places, like the Bremer lodes at Callington, they produced tabular deposits. Dickinson’s ideas on copper origins held sway for many years. Kleeman and Skinner (1959) stated that the copper deposits of the Kanmantoo-Callington area were "localised by shearing or extreme contortion" within incompetent schists, and were the first of several workers to discount Dickinson's localised metamorphic high concept. Mirams (1962) also proposed the concentration of sulphides in intersecting shears and that the copper may have been derived from the host andalusite schists (or alternatively the pyritic schists) and concentrated during

metamorphism.

The next significant breakthrough in understanding the Kanmantoo deposits resulted from the discovery of the Main Lode beneath the ferricrete cap in 1962. Subsequent drilling provided excellent data on what was recognized as the biggest known copper deposit in the Kanmantoo Group. W.F. Lindqvist's PhD study between 1966 and 1969 (Lindqvist, 1969) produced much valuable data, particularly on silicate, sulphide and oxide relationships. His work was based on drill core from the mineralisation and its immediate host rocks and outcrop mapping of the surrounding area prior to any mining. Lindqvist recognised two types of mineralisation: disseminated, fine grained and concentrated, coarse grained. In addition, Lindqvist described two major rock types associated with the Kanmantoo mineralisation: (his) *lode schists* and *alteration zone* rocks. Both are contained within (his) andalusite-staurolite schist (called GAB schist here) and each has different styles of mineralisation and was attributed different origins.

Lindqvist (1969, p.19) considered that his *lode schists*, which contain disseminated chalcopyrite and pyrrhotite grains and abundant chlorite, were part of "a single metamorphic unit that most probably represents, within the pelitic rocks, a relatively iron-enriched subfacies of shale". Lindqvist (p.162-166) considered that disseminated mineralisation had been present in the schists from the earliest stages of metamorphism and was probably deposited syngenetically with the sediments. The disseminated sulphides were principally pyrrhotite with lesser chalcopyrite and sphalerite. Lindqvist's *alteration zones* form discrete bodies within the *lode schists*, and are characterised by the coarse grain size of their constituent minerals, principally biotite, muscovite, garnet, staurolite, minor grunerite and sulphide and oxide minerals. The *alteration zones* vary in width from one centimetre to one metre approximately. These zones account for most of the high grade mineralisation.

Lindqvist (pp. 158-159) proposed a two stage process for the formation of the *alteration zones*. Initially, disseminated sulphides diffused from the *lode schists* and the country rocks into low pressure dilational zones parallel to the previously formed schistosity, and so formed the early *alteration zones.* This was inferred to have produced pyrrhotite rich (and chalcopyrite poor) bodies. The proposed mechanism of transport was "by bulk migration of disseminated sulphides from surrounding schists" by "hydrous products of metamorphic dehydration reactions" (p.158). The proposed driving force was a "prolonged period of dilational movements" (p.162) following the major folding event. The late timing in the tectonic history is required by Lindqvist's observation that the *alteration zones* are parallel to the schistosity, but have no major shearing or displacement (p.53). Lindqvist's second stage (p. 158) involved the reaction of the pyrrhotite rich bodies in the *alteration zones* with cupriferous solutions, producing chalcopyrite from the pyrrhotite and releasing considerable amounts of iron that then formed the iron rich silicates now present in the zones. The proposed source of copper was again nearby rocks.

Chlorite was regarded by Lindqvist as an almost insignificant feature of the deposits and he described it as a late stage mineral resulting from the breakdown of previously formed silicates, principally biotite. Lindqvist stated that "chloritisation appears to be only incidental to ore development". Little or no chlorite was inferred to be present until a post mineralisation, metasomatic event caused chloritisation of silicates principally within the *alteration zones*. He considered that the reason chlorite was most abundant in the *alteration zones* was due to the abundance of biotite there, but he noted (p. 21) that "some *lode schists* are strongly chloritized". The strong alignment of chlorite parallel to the schistosity was ascribed to mimetic replacement of schistose biotite.

Lindqvist was unable to comment authoritatively on the structural setting of the deposit because of lack of data. His concept is summarized in his Figure 4.6 e-g and entails a

combination of stratiform and discordant copper distributions, depending on what copper concentration is being considered. At low copper concentration (he suggested a rather high 0.5%) Lindqvist believed the copper distribution to be stratiform with bedding. At higher copper concentration (say 1.5%) he believed that discordant bodies were oriented parallel to the schistosity.

The next major advance in understanding of the Kanmantoo mineralisation was provided by the information gained by initial mining and a little of this data was presented in a brief paper by Verwoerd and Cleghorn (1975), two of the early mine geologists. Regarding the genesis of the deposit, these authors followed Lindqvist. They favoured a sedimentary origin for sulphide mineralisation, followed by local remobilisation of sulphide minerals during, or directly after, the Delamerian Orogeny.

D. P. H. O'Connor (pers. comm. 1976), the chief geologist at Kanmantoo Mine between 1973 and 1976, contributed another version of Lindqvist's concept of concentration of locally dispersed sulphides. O'Connor was impressed by the coincidence of the gross northerly plunge of the deposit and the apparently parallel plunge that he interpreted for the northern end of the O'Neil zone. To explain the northern plunge O'Connor proposed a two stage process of sulphide migration. Firstly, during the major D_2 deformation, disseminated sulphide minerals within the andalusite schist migrated into tabular concentrations along S_2 fold axial planes that dip steeply to the east. O'Connor proposed a subsequent, less intense folding event with an approximately east-west strike and a steep northerly dipping axial plane, that refolded the schists and produced plunge reversals in the earlier F_2 folds. O'Connor proposed that during this later event the sulphides migrated again towards these second axial planes, producing new concentrations at the steeply north plunging intersections of both sets.

During the period of mining at Kanmantoo, between 1970 and 1976, and certainly when the present author was first employed there in 1975, a syn-sedimentary origin of the deposits was the preferred theory, and the degree of any subsequent structural modification was debated. However, pit face and underground mapping by the author at this time confirmed that the Main Lode was grossly discordant to bedding and no evidence could be found from mapping data to support any association of sulphide minerals with sedimentary structures.

New data and its implications for the genesis of the copper at Kanmantoo were presented by the author (Schiller, 1978) based on geological mapping and microstructural studies. The relationships between S_1 and S_2 in the Kanmantoo Mine area were described and correlated with the regional structural interpretation that had arisen from the then-current work of Mancktelow (1979). The origin of S_2 at the mine was attributed to a crenulation cleavage mechanism during D_2, and S_1 was considered to represent a separate, earlier event, D1. The discordant nature of the Main Lode and the two spatially associated styles of mineralisation were described. (At this time the East Limb style of mineralisation was called Emily style and GAB(3) schist was called poikiloblastic schist.) Regarding timing of mineralisation, it was noted that sulphide minerals helped define both S_1 and S_2. Regarding the alteration lithologies surrounding the mineralisation, it was noted that most of the chlorite was present during D_2, and that the characteristic poikiloblastic fabric of GAB(3) schist was developed in the period between D_1 and D_2. It was noted that there was no evidence for syn-sedimentary mineralisation at Kanmantoo. Thus, the mineralisation at Kanmantoo Mine was inferred to be metamorphogenic, and to have formed in two stages spanning the D_1 and D_2 events. In the first stage East Limb style mineralisation was interpreted to have been formed during the period spanning D1 and D2, and in the second stage the West Limb style formed during D_2.

The source of the sulphur within the Kanmantoo copper deposits, and other sulphide deposits in the Kanmantoo district, was addressed in a sulphur isotope study by Seccombe et al.

(1985). The isotope results, together with the knowledge that all the Kanmantoo lodes were discordant to bedding (except perhaps at very low copper contents), led to a variation on the syn-sedimentary theory that was able to accommodate the discordant nature of the Kanmantoo deposits. This theory suggested that the lodes were formed in feeder pipes close to the sea water-sediment interface. It was found that in the deposits studied there was a wide overall range of $\delta^{34}S$ values and overlap of the ranges from individual deposits with one another. The $\delta^{34}S$ values for Kanmantoo copper lodes were at the highest end of the overall range. Most of the Kanmantoo lodes have $\delta^{34}S$ between +3.5 to +12.4 per mil and have a mean of +8.0 per mil. The results from Kanmantoo were characterized by isotopic disequilibria among coexisting sulphide minerals and significant isotopic variation within and between individual lodes. In contrast to the Kanmantoo lodes, the sulphur isotopes for pyritic schists were depleted in ^{34}S, with $\delta^{34}S$ values from –19.9 to –11.9 per mil. It was argued that, assuming that the Kanmantoo deposits were derived partly from reduced Cambrian seawater sulphur, then the range of sulphur isotope ratios found for the Kanmantoo copper mineralisation cannot be explained by a single source of sulphur. Possible mixing candidates cited were fluids derived from igneous or biogenic processes. In view of the lack of igneous sources known in the region and the abundance of pyritic schists, Seccombe et al. proposed that the mineralising fluids were derived from convecting seawater that leached sulphur from pyritic schists to depths in the basin of at least 3 km to 4 km. These depths are sufficient to allow the fluids to make contact with numerous pyritic schists (they were pyritic black shales and sandstones at the time) in the Tapanappa Formation and perhaps the Talisker Calc-Siltstone, but the authors conceded that greater depths (~10km) were required to heat the fluids sufficiently to transport copper and sulphur in sufficient concentrations. Variation in the mixing proportions of both sulphur sources was proposed as the explanation for observed differences in sulphur isotope ratios between and within the lodes measured at Kanmantoo.

Spry et al. (1988) documented the structural and metamorphic histories of numerous Cu, Pb-Zn and Fe sulphide deposits in the Kanmantoo-Strathalbyn region, including the Kanmantoo deposit. They argued that in all cases the sulphide deposits were metamorphosed and could have been present from sedimentary times. They concurred with Seccombe et al.'s conclusion that the Kanmantoo copper deposits represent a series of closely spaced vents that were located just below the sea floor and were active during sedimentation. Further, the apparently conformable lead-zinc deposits in the region, such as Aclare and Wheal Margaret, were proposed as distal products from the same fluid after it had issued in to the water column. This latter conclusion relies heavily on a stratigraphic correlation of the various deposits.

In 1993 Nero completed an Honours project on structural and metamorphic aspects of the Kanmantoo mineralisation, with a particular focus on quartz veining, especially the suite of veins with selvages. Nero refers to previous oxygen isotope results by Miller (1992) that have not been sighted by this author. Nero commented that these results and the previous sulphur isotope results by Seccombe et al. (1985) could be interpreted to indicate a magmatic source for the Kanmantoo mineralisation.

No new data pertaining directly to the Kanmantoo copper mineralisation was published until Oliver et al. (1998). This paper presented data on bulk chemistry and oxygen isotopes from suites of rocks collected from within the Kanmantoo Mine and also from the surrounding district. Oxygen isotope data from the regional suite indicated a regular depletion in $\delta^{18}O$ in meta-pelites over a distance of 20km from lower to higher metamorphic grade rocks. The $\delta^{18}O$ ratios decreased from 13.5 per mil in the biotite zone to 8.3 per mil in the sillimanite zone. The results were similar to those reported for meta-pelites and marbles from the Karinya Syncline by Cartwright et al. (1995). The regional trend in $\delta^{18}O$ was attributed to lateral fluid flow during metamorphism in the direction of increasing temperature, accompanied by progressive equilibration between the fluids and rocks. The average $\delta^{18}O$ of

rocks from within and near the Kanmantoo Mine was 9.6 per mil and, importantly, the isotope ratios were found to be depleted with respect to the regional gradient. Oliver et al. (1998) argued that the best explanation for both the oxygen isotope results, and the sulphur isotope results of Seccombe et al. (1985), was that the fluids responsible for the Kanmantoo mineralisation included a magmatic component. On the basis of geochemical data and microstructural interpretations, it was concluded that copper mineralisation was emplaced late during the metamorphic cycle, associated with Fe metasomatism and Ca and Na depletion, from an externally derived fluid expelled from a crystallizing magma. A granitoid body was inferred to occur at depth below the deposit. Oliver et al. differ significantly from previous workers in the inferred timing of mineralisation. Like most modern workers, Oliver et al. correlated the regional dominant schistosity to S_2, but unlike others, the mesoscopic schistosity in the Kanmantoo area was ascribed to S_3. The reasons for this are not made clear, but a consequence is that it requires the peak of metamorphism at Kanmantoo to occur later (that is syn-D_3) than for the rest of the region (syn-D_2). Oliver et al. argue that this local thermal anomaly at Kanmantoo is related to the late arrival of a granitoid intrusion below. The conclusion is similar to that of Dickinson back in 1942. Regarding ore genesis, these authors argue against any syn-sedimentary contribution, though the dilemma posed by the apparent stratigraphic control on Kanmantoo and other deposits in the region is conceded. Instead, mineralisation at Kanmantoo is concluded to have occurred by the mixing of regional metamorphic fluids with channelised granite-derived fluids, but the oxygen and iron budgets were considered to be mainly granite related.

The discovery in the early 1990s of the Angas Pb-Zn deposit with its associated garnet rich rocks (Both et al., 1995) led to a regional search for similar rocks. Much of the regional mapping was completed by Steve Toteff, who traced inferred exhalites from Strathalbyn to near Kanmantoo, but his work was described initially only in unpublished company reports. Smith (1998) completed an Honours project on petrological and geochemical aspects of garnet-rich rocks associated with several base metal deposits in the Kanmantoo-Strathalbyn region. The study included data on inferred meta-exhalites (coticles and banded iron formations) located near the Kanmantoo Mine, but did not include data specifically on the Kanmantoo deposits. Toteff (1999), in a detailed report on the inferred exhalative base metal mineralisation, concluded that the Kanmantoo copper deposits represented a “feeder to overlying exhalative mineralisation” and, on the basis of geological mapping, also concluded that the known deposits “probably came to within 200m of the sea floor”.

Marshall and Spry (2000) suggested that the overall combination of evidence for the Kanmantoo deposit indicated that it represented “metamorphosed, pretectonic, sedimentary exhalative mineralisation”.

9.3 Some constraints on the origin

Several features of the copper mineralisation at Kanmantoo place constraints on any model proposed for its origin. They are listed below and not all of them are accommodated in the theories outlined in the previous section. The constraints are as follows:

(a) Copper mineralisation at Kanmantoo is stratabound in a meta-sedimentary unit that is of anomalous chemistry. Compared to most other meta-sediments in the Kanmantoo Group, the host unit has higher contents of Fe and Mn and lower Na and Ca. What is not clear is the time that this chemical distinction occurred. It may reflect the original unaltered sedimentary composition or it may represent alteration, perhaps at or soon after the time of sedimentation (such as sea floor alteration or diagenesis), or later during metamorphism.

(b) In the mine area, no evidence for a conformable relationship between bedding and

copper distribution was found, whether at the scale of the open cut mine or at micro-scale, or whether considered in terms of copper concentrations of 0.1% or 5%. So the mineralisation is stratabound but not stratiform.

(c) Mineralisation in the Main Lode is grossly transgressive to bedding and fold geometry in the host rock. Similarly, other smaller lenses near the Main Lode, such as C Lens, D Lens and O'Neil Lode are transgressive to bedding. As in (a), the time of origin of this feature is not satisfactorily constrained, even to the extent that the feature can be used to diagnose epigenetic mineralisation, because some of the mineralisation could have formed in cross features at the time of sedimentation.

(d) The two distinct styles of mineralisation (East Limb and West Limb styles) have a clear association with particular fold limbs. Almost all East Limb style mineralisation occurs in oblique lodes forming an en echelon pattern within the eastern limb of the Mine Synform. Most West Limb style mineralisation occurs on the western limb in numerous zones sub-parallel to S_2.

(e) Sulphide minerals occur in the following settings: as inclusions within poikiloblasts, as disseminated grains and composite grains in the matrix of lode schists, in sulphide veins, quartz-sulphide veins and in silicate veins and masses. Sulphide minerals have been metamorphosed.

(f) Sulphide mineralisation is parallel to the following structural features: S_1 on the micro-scale, S_2 on the micro-scale and meso-scale, and East Limb style lodes are parallel to oblique pre-S_2 quartz veins. The plunge of the Main Lode lies on, or close to, the average S_2 orientation but is not parallel to F_2 or L_2. It is parallel only to the steep fold axes of the pre-S_2 fold axes.

(g) Sulphide mineralisation is associated with Fe rich lode schists, and texturally and chemically distinct varieties of the host unit (i.e. GAB(2) and GAB(3) schist). All of these lithologies are transgressive to bedding, like the sulphide mineralisation. Characteristic of most lode schists are variable contents of chlorite, generally in inverse proportion to andalusite. Many lode schists have no andalusite and consist predominantly of quartz and chlorite, with minor garnet and ilmenite, and perhaps biotite and staurolite.

(h) The andalusite free lode schists and the higher grade copper zones are not strictly parallel to one another in either the East or West Limbs. Nor are they parallel to S_2.

(i) Higher grade mineralisation tends to be hosted by veins and irregular tabular bodies within the lode schists, that are parallel to S_2 and consist of relatively coarse-grained Fe rich silicate minerals and generally little or no quartz.

(j) Chlorite appears to have formed at several stages. Two types of chlorite are recognized, called Fe rich and Fe poor varieties. The latter is by far the most common. In quartz rich lode schists Fe poor chlorite was present during D_2, and a limited amount of Fe poor chlorite was produced as a syn-D_2 metasomatic product. Fe rich chlorite is associated with a late stage brittle event and though some chalcopyrite is associated with it, it is volumetrically insignificant.

9.4 Discussion

9.4.1 Evidence for hydrothermal activity

Clearly, the discordant mineralisation at Kanmantoo does not reflect a simple sedimentary origin in its present disposition at least. Rather, an epigenetic origin is indicated and, consequently, a hydrothermal origin. (Epigenetic is used here in the sense that it indicates deposition of the mineralisation later than that of the enclosing rocks.) Consistent with high levels of hydrothermal activity are the presence of abundant sulphides, the abundant quartz-chlorite rocks, abundant veining, chlorite coronas on andalusite, and evidence for high P_f during formation of some lode-related rocks like GAB(3) schist. The implications of S and O

isotope data as indicators of hydrothermal activity associated with the Kanmantoo deposit (Oliver et al., 1998) has been questioned by Marshall and Spry (2000), who concluded that "oxygen and sulphur isotope studies neither confirm nor rule out metamorphosed syngenetic and metamorphogenic models".

9.4.2 Timing of mineralisation

At its broadest scale, the age of the discordant, pipe-like envelope to mineralisation cannot be deduced directly from its gross shape and its relationship to enclosing structures. On this basis it could have formed at any time since sedimentation. Indeed, the discordant nature of the lodes has been used to support arguments for both a pre-metamorphic origin (Seccombe et al., 1985) and also a syn-metamorphic origin (Oliver et al., 1998). If the pipe-like structure was early, one might expect later overprinting, like folding of the whole pipe for example. But in this case the overall plunge of the package of both sulphide mineralisation and associated lithologies is so close to the plunge of the L_2 stretching direction that D_2 folding of the gross structures is unlikely. The plunge of the pipe is approximately perpendicular to the average F_2 fold axes, as would be expected if the pipe was originally sub-vertical and perpendicular to undeformed bedding. So the gross shape of the pipe is consistent with either a pre-metamorphic or a syn-metamorphic origin.

At a more detailed scale, evidence for the timing of hydrothermal activity and sulphide mineralisation with respect to metamorphism and deformation is available principally from internal features of the lodes, especially the microstructure of porphyroblasts. In the lode schists, garnet and andalusite have sulphide inclusions parallel to S_1. This key evidence establishes that disseminated sulphide minerals participated in the D_1 stage of deformation. The total volume of disseminated mineralisation present during D_1 is not known, but it may have included most or all of the disseminated sulphide minerals now parallel to S_2. The presence during D_1 of possible larger masses of non-disseminated sulphide minerals has not been established, nor can it be excluded. Most of these types of bodies formed during D_2 but some have evidence of multiple deformation, consistent with their formation before D_2. While there is clear evidence of the presence of sulphide minerals prior to porphyroblast growth, there is no unambiguous evidence that probable hydrothermal silicate minerals such as chlorite were also present at this stage. However, the lack of chlorite inclusions in porphyroblasts does not rule out the former presence of chlorite at this stage, because any chlorite participating in porphyroblast-forming reactions may have been entirely consumed during the reaction or, for other reasons, not included in the porphyroblasts.

Understanding the role of chlorite is important in understanding the origin of the deposit, and chlorite's role has been mis-interpreted in some previous work. For example, Lindqvist's (1969) conclusions that all chlorite is post-mineralisation and that most chlorite microstructures resulted from mimetic replacement of biotite do not agree with the observations of this study. A key argument against Lindqvist's conclusion is seen in the lode schists with unaltered biotite porphyroblasts enclosed in a schistose quartz-chlorite matrix. Why would the matrix biotite be thoroughly replaced but none of the biotite porphyroblasts? Most (Fe poor) chlorite occurs in quartz-chlorite-garnet schists, lesser amounts occur in veins with other silicate and sulphide minerals. Both have different microstructures. In quartz-chlorite-garnet schists the microstructure of chlorite is dominated by its parallelism to S_2. Compared to S_2 in surrounding GAB(1) schists and QM schists, S_2 is more weakly defined, but it is distinct nevertheless. Like biotite in nearby GAB(1) schists, the matrix chlorite in quartz-chlorite-garnet schists is deflected around porphyroblasts but, unlike GAB(1) schists, it does not define a domainal schistosity and only the weakest of strain caps. In quartz-chlorite-garnet schists, and in some very garnet rich lode schists, S_2 defined by chlorite is seen to be continuous with inclusion trails (presumed S_1) in porphyroblasts, suggesting its presence

during D1. Unequivocal evidence of the presence of chlorite at this stage has not been found but further work on particular lithologies may well establish this.

Many andalusite bearing lode schists have evidence of late D_2 metasomatism involving chlorite. This resulted in (Fe poor) chlorite replacement of the rims of andalusite porphyroblasts, but not of coexisting biotite, staurolite or garnet. Typically the andalusite porphyroblasts are not completely replaced, indicating a limited supply of this metasomatic fluid. Many of the chlorite grains in the coronas on andalusite are continuous with S_2 as defined by matrix chlorite grains, and both types have similar chemistries, suggesting that the metasomatism occurred prior to or during D_2.

Many quartz rich lode schists contain veins consisting of coarse-grained chlorite, biotite, garnet, staurolite and sulphide minerals. Quartz may be present in patches. These veins are approximately parallel to S_2 in the host rock. Typically, the minerals in the veins show little or no evidence of deformation, leading to the common conclusion by previous workers that they post-date tectonism. The present author considers that most of these veins are more likely to represent late-D_2 structures, because the chlorite in them has the same composition as the host rock chlorite, the veins are parallel to S_2 and are commonly associated with chlorite coronas on andalusite that appear to be syn-D_2. The apparent lack of deformation in most of the veins can be explained by their late D_2 timing and because they were zones of low to nil deviatoric stress as a result of high fluid pressures during crystal growth and subsequent deformation. Other similar quartz poor/absent lithologies to these discrete veins also occur within quartz rich lode schists and many contain microstructural evidence of multiphase deformation, as described in Chapter 6.

Therefore, conclusions by previous workers that the quartz poor lode schists, including those forming veins, post-date all deformation are not consistent with the observations of this study. Rather, their microstructures indicate participation in the deformation at least during late D_2 and earlier in some cases at least. It seems likely that there were multiple stages of development of these rocks during the deformational history, spanning from D1 (and perhaps before) to late D_2 (and perhaps after). As for the quartz rich lode schists (that host the quartz poor lode schists), they were present during D_2 and probably before.

Constraints on the time of formation of the bodies of GAB(2) schist and GAB(3) schists can also be obtained using their porphyroblasts. The envelope around these lithologies, like that around the lode schists, is transgressive to bedding and spatially these rocks are closely associated with mineralisation. They are characterised by their porphyroblast fabrics that were developed during metamorphism, and so they must have been distinctive lithological entities at least as early as the porphyroblast growth stage of metamorphism. Microstructural studies show their characteristic fabrics developed between D_1 and D_2. The reason for the characteristic fabrics is attributed here to locally high fluid pressures during this period that resulted in a temporary and local lowering of the deviatoric stress. The high fluid pressures are inferred to be related to hydrothermal activity focused in the sulphide mineralized lode schists nearby. In GAB(3) schist this period of presumed lower deviatoric stress post-dates D_1 because andalusite and staurolite preserve excellent S_1 trails. Unique to GAB(3) schist was the growth of biotite porphyroblasts, in the inferred absence of any deviatoric stress. Growth of the biotite porphyroblasts extended probably to the time of stress resumption associated with D_2, as indicated by some biotite porphyroblasts that have appendages parallel to S_2 in the matrix. Subsequently, biotite porphyroblasts were deformed during D_2 resulting in deflection of S_2 around the porphyroblasts and some pull-apart structures within biotite. However, the degree of deformation of the biotite porphyroblasts does not appear to be severe, probably due to continued high fluid pressures during D_2. In the case of GAB(2) schist the evidence for reduced deviatoric stress compared to surrounding GAB(1) schists is shown by the weaker

development of S_2.

When compared on the scale of the deposit, the non-parallelism between the orientations of andalusite free lode schists, copper distribution and S_2 is suggestive of multiple controls involved in the development of these features. It is likely that some of the copper lodes and lode schist bodies owe their orientations to pre-D_2 controls. In the West Limb, most mineralisation shows a pronounced mesoscopic control by S_2 whereas this is less obvious in the East Limb. In the West Limb mapping data show that the andalusite free lode schists are steeper than both the copper lodes and average S_2 orientation. Conversely, in the East Limb the lodes are steeper than S_2 and much of the andalusite free lode schists.

In conclusion, the timing of sulphide mineralisation is a complex issue. It seems that there were several phases of hydrothermal activity responsible for sulphide deposition. The earliest that sulphide minerals can be established is syn-D_1. There is no microstructural evidence to preclude an even earlier presence, but it is considered unlikely because there is broader scale evidence linking the East Limb style mineralisation with the development of the Mine Synform. This is discussed in the next section. Phases of metasomatism, accompanied in part by sulphide mineralisation, are indicated for the latter part of the period between D_1 and D_2, and for a late D_2 event. The relative impact of each metasomatic event is not clear. It is likely that the late D_2 event was not large. Most mineralisation is associated with the bulk of the chlorite bearing rocks and while the timing of their formation is ambiguous, the weight of evidence favours a pre-D_2 origin. Thus the biggest metasomatic event or events appear to pre-date D_2.

9.4.3 Structural controls of mineralisation.

Structural controls on sulphide mineralisation are seen on many scales. For example, microscopic sulphide grains are parallel to S_1 and S_2. On a mesoscopic scale many sulphide veins are parallel to S_2. On a larger scale, sulphide lodes, especially within the West Limb of the Main Lode, are also parallel to S_2. S_2 is clearly an important mesoscopic control but at larger scales its influence becomes less apparent. However, many important features of the lodes appear to be unrelated to D_2 geometry. For example, the plunge direction of the Main Lode is neither parallel to the fold axes (F_2) nor the mineral lineation (L_2), though it lies close to the S_2 plane. Also many of the quartz veins in the mine and most of the quartz veins immediately surrounding the mine are not parallel to S_2.

A key structural control on mineralisation in the mine is the Mine Synform. Each of its limbs has different styles of mineralisation. Mineralisation on the eastern limb occurs in a series of NNE trending lodes that are oblique to the axial plane and all other known D_2 elements. These lodes are associated with GAB(2) and GAB(3) schists. On the western limb, lodes tend to be sub-parallel to S_2 and are not associated with GAB(2) and GAB(3) schists. Other details of both styles were presented in a preceding chapter. Because of its association with GAB(2) and GAB(3) schists, the latest age of East Limb style mineralisation is considered to be in the D_1 to D_2 period. West Limb style mineralisation is considered to be D_2 in age because of its close association with S_2 structures. However, as discussed in the preceding paragraphs, the ages of mineralisation and metasomatism are not well understood, and both styles could be younger than these ages.

Given the close association of mineralisation with the Mine Synform it would be helpful to know the age of this structure. The axial plane of the Mine Synform, as measured over the vertical extent of several benches in the mine, appears to be very close to parallel to the overall orientation of S_2. But it is quite possible that the fold was initiated as a D_1 structure and subsequently tightened during D_2. This is consistent with the common observation that S_1

is close in orientation to S_2. So again, it is not possible to constrain absolutely the timing of mineralisation to D_1 or D_2. However, it is possible to say that the association of mineralisation with the Mine Synform rules out the likelihood of pre-tectonic mineralisation. The only alternatives to this conclusion are to infer that one or both of the two styles of mineralisation existed before deformation and that their physical presence influenced the shape and position of the Mine Synform as it developed, or that the association is a complete coincidence. Though possible, both seem unlikely.

Possible origins for the oblique lodes of the East Limb style of mineralisation will now be considered. The zone containing these lenses extends for at least 450m from Emily Lens in the north to the C and D Lenses in the South Eastern Mineralisation. The zone may continue for a similar distance to the south where very small but similar lodes occur. The biggest of the lodes, the East Limb itself, strikes between 020 and 035 and dips between 80˚ to 90˚ east. This orientation is shared only by some quartz veins found in the pit and surrounding rocks. These veins are usually folded and boudinaged. The East Limb lodes occur in a north-south trending zone bounded to the east and west by surfaces approximately parallel to S_2. The western surface is well defined and corresponds to the axial plane of the Mine Synform. The eastern surface is less well defined but is close to the axial plane of the small antiform on the eastern side of the pit. Possible origins for these lodes are:

- Large tension veins formed during D_1 or D_2 folding
- Dilational openings associated with locking up of folds
- Tensional veins formed during non-coaxial deformation.

1. Tension veins formed during folding will be more or less perpendicular to the axial plane foliation and the stretching lineation. The lodes are not perpendicular to S_2 or the L_2 stretching lineation, and so they are not typical tension gashes formed during D_2 compressive strain. The orientation of the principal strain axes during D_1 is not known but regional studies (Mancktelow, 1979) and local information suggests that they were not greatly different from the D_2 orientation. So it seems unlikely that tension veins in this orientation could have formed during D_1 either. Oliver and Zakowski's (1995) sub-horizontal extension described from gneisses near Palmer is more favourably oriented to produce the steep East Limb lodes, but it has not been recognized in the Kanmantoo area and would not have produced upright folds anyway.

2. During the development of folds in well-bedded sediments in low metamorphic grades, many folds tend to be kink-like, and after a certain amount of shortening they will tend to resist further tightening. At this point the fold can lock up and further strain will be accommodated by reverse faulting. The faults are parallel to bedding along one of the fold limbs and transgressive on the other. Continued strain can result in dilational zones along the faults that fill with mineralized material, especially quartz veins. The classic examples of this style of mineralisation are the gold deposits in Victoria, for example the Bendigo field (Sharp and MacGeehan, 1990, Cox et al., 1991) or the Wattle Gully field (Potter, 1990). The model is of interest for Kanmantoo because it provides a means of creating discordant veins only on one limb of a fold. When examples of some Victorian gold deposits are viewed in cross section they look remarkably like a plan view of the East Limb at Kanmantoo (for example Figure 10 in Cox et al., 1991). However, in the third dimension there is a critical difference. For the model to be applied strictly, the line of intersection of the transgressive vein/fault and the axial plane should be parallel to the fold axis. In the case of the East Limb lodes, the line of intersection between the lodes and the axial plane of the Mine Synform is steeply north, at a large angle to the fold axes. Therefore, the model does not apply strictly to the Kanmantoo lodes.

The Mine Synform has fairly planar limbs and is kink-like in profile. Its limbs are not symmetrically arranged across the axial plane. The eastern limb has an angular discordance of approximately 40˚-50˚ whereas the discordance of the western limb is only about 10˚. As tightening of the fold progressed during D_2 shortening, a point may have been reached when the significant difference in orientation of bedding with respect to the principal compressive stress direction resulted in different strengths for each limb. The eastern limb would have been stronger. Consequently, further strain may have been partitioned such that the weaker western limb was preferentially deformed by non-coaxial shearing and the eastern limb deformed predominantly by coaxial deformation. This concept is similar to that proposed at a much smaller scale for crenulation development (Bell, 1981). This concept of strain partitioning on each limb of the Mine Synform may account for several features:

- The distribution of shear zones in the mine. The western limb has a relative abundance of discrete shear zones and broader zones of shearing, both sub-parallel to S_2, whereas the eastern limb has few shears.
- The tendency for the mineralisation on the western limb to occur in zones that are parallel to S_2 and appear to be of ductile origin, whereas on the eastern limb the mineralisation occurs in cross-cutting, apparently semi-brittle structures.

Thus mineralisation in the western limb is considered to be associated with shear-generated dilational zones with the S_2 (or reactivated S_1) schistosity being exploited as an existing anisotropy during D_2 shearing. In contrast, deformation and mineralisation on the eastern limb has not exploited the existing schistosity to any great degree, and the lodes appear to be more in the character of dilation zones formed during semi-brittle deformation. Both of these differing styles of mineralisation could form at the same time because they rely on different local controls that develop during a single deformation event. The development of semi-brittle structures in a ductile regional metamorphic regime is explained by the observation that the lode schists in the structures pre-date D_2 and therefore also the peak metamorphic temperatures associated with this stage. Metamorphic conditions during the initiation of the cross-cutting structures may have been significantly lower. A second factor favouring local semi-brittle deformation is high fluid pressures, which increase the strength of rocks and promote more brittle behaviour, even in ductile regimes (Etheridge, 1983). Evidence of high fluid pressures in this zone has already been described to account for the biotite porphyroblasts in GAB(3) schists.

3. During non-coaxial shearing, tension veins form at an angle to the boundaries of the shear zone and rotate during progressive shearing. For the Kanmantoo Mine area this idea has some initial attraction as an explanation of the East Limb and West Limb lodes and perhaps the numerous oblique quartz veins in the mine area also. The West Limb lodes may have formed oblique to the shear zone and rotated into parallelism, whereas the East Limb lodes developed between zones of strong non-coaxial shearing. There are many shears parallel to S_2 on the margins of the bounding surfaces to the East Limb lodes including, as explained above, the whole of the western limb of the Mine Synform which can be regarded as a shear zone. In ideal shear zones the tension veins will form such that their line of intersection with the plane of shearing will be perpendicular to the stretching lineation. The East Limb lodes are sub-vertical, so if they formed this way then the stretching direction at the time of their formation must have been sub-horizontal. The NNE trend of the East Limb lodes would require dextral movement. No evidence for such a stretching direction has been seen in the Kanmantoo district. However, a stretching lineation may not have formed if the associated deformation was not sufficiently intense. Intense deformation is not required to create tensional failure and vein formation. Once failure has occurred, all that is then needed is a tendency for movement, provided it is sustained over a long enough period for sustained or repeated vein opening and deposition from fluids. Further strain will deform the veins. If there was sub-horizontal stretching the timing options are syn-D_1, or it may represent a later, perhaps short-lived period

of transcurrent shearing in which substantial dilation was created but few folds and no penetrative fabric resulted. The first alternative is unlikely because (as mentioned above) D_1 was a major deformation event and no studies in the Kanmantoo district have proposed a sub-horizontal stretching lineation for it. If the early sub-horizontal extensional event with a north-south stretching lineation that was described by Oliver and Zakowski (1995) was active in the Kanmantoo district, evidence of it appears to have been destroyed, except perhaps for the S_1 inclusion trails. Some detailed microstructural work may resolve this matter but in the absence of any support for the deformation it must be discounted in this study. Alternatively, a short-lived change in the stress regime at Kanmantoo is possible, associated either with local or regional stress field changes. The period of the stress field changes would have to last long enough for at least the East Limb style lodes to form. The indicated timing for these lodes is between D_1 and D_2, or perhaps during D_1.

Previous theories on the local structural controls of mineralisation at the Kanmantoo Mine will be considered now. The theories involved concentration of sulphide minerals in structurally prepared sites resulting from the following:

(a) intersecting fractures (Dickinson, 1942),
(b) dilation zones associated with deformation (Lindqvist, 1969),
(c) intersecting fold axial planes (O'Connor, pers. comm.. 1976)

Dickinson (1942) favoured the idea of intersecting fractures to explain the pipe-like nature of mineralisation, at Kanmantoo in particular. This study does not support a control by intersection of through-going fractures, but S_2 parallel and oblique fractures are considered to be involved in localizing sulphide mineralisation at Kanmantoo. This study is in accord with Dickinson's concept to the extent that the overall pipe-like character is controlled by oblique structures that are bounded by surfaces parallel to S_2, either shear zones or fold axial planes, or both. The line of intersection of these two planar elements is steeply north and because the structure persists down-plunge it has formed a steep pipe. Lindqvist's (1969) dilation zone concept is in accord with the observations of this study, but his proposed timing is not. O'Connor's concept of double migration of originally disseminated sulphide minerals is not accepted here. There is no evidence for a generation of post-D_2 folds with east-west axial planes. The only observations from this study that are comparable to this proposal are the plunge changes across surfaces trending approximately ENE in the pit. This feature is not well understood but it appears to have had no significant effect on copper distribution.

In summary, the Kanmantoo mineralisation has structural controls imposed. Most important are the mesoscopic and microscopic controls of S_2, and the mesoscopic and broader scale controls of the Mine Synform. Mineralisation and associated alteration is considered to have commenced during D_1 when East Limb style lodes developed on the eastern limb of the Mine Synform. The dilational mechanism associated with the East Limb lodes is not related to simple buckling during development of the Mine Synform and it probably developed from unusual circumstances like a change in the stress field after the fold was well established. West Limb style mineralisation probably developed later during D_2 as a result of shearing on the western limb.

9.4.4 Evidence for a syn-sedimentary origin

There is no unequivocal evidence supporting a sedimentary origin for copper mineralisation at Kanmantoo. Nor is there unequivocal evidence for syn-sedimentary epigenetic mineralisation. However, some features of the Kanmantoo mineralisation are consistent with a syn-sedimentary origin:

- Sulphide rich bedding.

- The Kanmantoo copper deposits are stratabound in a geochemically anomalous unit.
- Possible stratigraphic equivalence with stratiform Pb-Zn deposits.
- Association with possible exhalites.
- Sulphur isotopes.

1. Evidence for sulphide rich bedding in non-porphyroblastic rocks was presented by Lindqvist (1969) in figures of thin sections showing relict bedding with variable concentrations of disseminated sulphide minerals. While the present author does not dispute these data, such examples are very uncommon and their origin is open to debate. Lindqvists's examples may represent rare examples of genuine bedded sulphides as he proposed, or they may represent isolated examples of post-sedimentary metasomatic addition of sulphide minerals to some beds. Sufficient petrological and analytical work has been done to be confident that sulphide distribution is independent of bedding on all scales.

2. Kanmantoo copper mineralisation is stratabound within the Paringa Andalusite Member, a unit that is geochemically anomalous compared to other Kanmantoo Group metasediments. It is relatively Fe and Mn rich, and Ca and Na poor. It may also have relatively high Cu contents compared to other metasediments, according to data by Drexel (1978, compiled in Chapter 2) for the possible southern extension of the Paringa Andalusite Member on the South Eastern Freeway. There are three possible explanations for the major element geochemical anomalies: unusual sedimentary composition or metasomatic alteration of normal sediments, either during or soon after sedimentation, or later during metamorphism. Although possible, the latter explanation is considered the least likely because the Paringa Andalusite Member extends for 5km or more, no hydrothermal conduit of this size has been identified and its shape appears to be consistent with a sedimentary unit. Despite the lack of supporting data, this type of regional alteration cannot be discounted completely, especially in view of the results by Cartwright et al. (1995) and Oliver et al. (1998) that show substantial lateral movement of fluids during metamorphism in the Kanmantoo Group metasediments. Further support may lie in the qualitative observations during mapping of the Paringa Andalusite Member of an increase in the muscovite:biotite ratio with distance from the Kanmantoo Mine. Additional work must be done to confirm this.

If syn-metamorphic alteration is discounted, then the anomalous geochemistry must be attributed to either syn-sedimentary alteration or unusual sedimentary mineral composition. The pre-metamorphic precursor to GAB schist is inferred to have been relatively high in Fe-Mn oxides or hydroxides and low in plagioclase. Chemical alteration at or near the sea floor could have been effected by exhalative solutions, perhaps issuing from hydrothermal conduits in which the Kanmantoo lodes were developing as proposed by Seccombe et al. (1985). If the unaltered sediments were similar to the precursors to QMA schist or QMF schist, then plagioclase would probably have been a detrital mineral and if it was altered Ca and Na may have been lost from the sediment. In a preceding chapter it was suggested that Fe and Mn could have been added to the sediment as exhalative components, in a similar way to the exhalative Fe-Mn oxides deposited in the Atlantis II Deep of the Red Sea (Bischoff, 1972).

3. It is significant to the exhalative model that the stratiform Pb-Zn-Ag sulphide deposits at Aclare and Wheal Margaret are interpreted to occur at a similar or slightly higher stratigraphic level than the Kanmantoo Lodes. In the syn-sedimentary model of Seccombe et al. (1985) these are considered to be the distal sedimentary products of the exhalative solutions originating from the Kanmantoo lode area. The occurrences of laminated Pb-Zn-Ag sulphide mineralisation being deposited on the sea floor distally from an exhalative vent containing a pipe-like Cu rich body are well documented, (e.g. Plimer, 1978).

4. The fact that a probable exhalite horizon occurs within the Paringa Andalusite Member only hundreds of metres from the mine is compelling evidence in favour of the syn-sedimentary model. The exhalite horizons located by Toteff (1999) are also stratigraphically associated with the Aclare and Wheal Margaret Pb-Zn-Ag deposits, adding further weight to the syn-sedimentary model and perhaps Kanmantoo's association with it.

5. Sulphur isotope data were interpreted by Seccombe et al. to indicate a pre-metamorphic hydrothermal origin by convecting seawater. This interpretation was disputed by Oliver et al. (1998) who considered that alternative origins were consistent with the data, and in combination with their oxygen isotope data, favoured an origin from late metamorphic fluids that included a component derived from granite.

The strength of evidence in favour of syn-sedimentary mineralisation and the association of the Kanmantoo deposits with elements of the model create a dilemma because it is in apparent conflict with compelling evidence at Kanmantoo Mine of structural controls on mineralisation during metamorphism. The structural controls cannot be reconciled with possible pre-tectonic (and syn-depositional) hydrothermal processes unless:

- the limbs of the Mine Synform were located by regular, pre-existing lodes and the final location of much of the mineralisation was due to remobilization during metamorphism,
- all or most evidence of the sea floor feeder system was obscured by subsequent deformation and metamorphism.

9.4.5 Regional controls

Regional controls to be considered are stratigraphic and structural. The obvious stratigraphic control on the Kanmantoo mineralisation is the Paringa Andalusite Member although, as mentioned previously, the reasons are not understood. Also not known is the full extent of the Main Lode, for example whether the pipe persists below the base of the GAB schists.

No definite regional structural control on the location of the Kanmantoo deposits is known. The Mine Synform may be equivalent to the regional scale Kanmantoo Syncline but this has not been established, and its significance regarding sulphide mineralisation may be nil. No other copper deposits in the Kanmantoo region are specifically associated with major synclines. Other regional controls have been suggested in several studies. Thomson (1965) proposed the existence of a WNW trending structure near the Kanmantoo Mine that he speculated was important with respect to sulphide mineralisation. This proposed structure was also referred to by Parker (1986) in a review of the tectonic development and metallogeny of the Kanmantoo Trough. To the author's knowledge, the existence of this structure has not been confirmed.

The most commonly cited regional structure is the continental scale G2 lineament proposed originally by O'Driscoll (1973). This broad structure, or corridor, has a NNW trend and passes just to the east of Adelaide, past Brukunga and Kanmantoo and along the Padthaway Ridge. Authors who have promoted its significance within the Kanmantoo region, including its influence on mineralisation, are Mancktelow (1979), Preiss (1987, 1995) and Belperio et al. (1998). The structure is thought to be a deep crustal feature that has been active since Proterozoic times or before. Several copper deposits occur on or close to the G2 lineament in South Australia including Olympic Dam, Mount Gunson, Kapunda, Kanmantoo and Bremer deposits. The surface expression of the G2 lineament is subtle. In the Kanmantoo region the only geological features that may be an expression of it are the Woodside meta-dolerite dyke swarm and some faults near Dawesley and Brukunga (the Mount Beevor shear zone). The Woodside dykes generally trend NNW, like G2. They are now amphibolites that are one

group of many deformed mafic dykes that were intruded into the Kanmantoo Group at various stages of the deformation history, including as early as pre-D_1 (Liu and Fleming, 1990). Liu and Fleming point out that the intrusion of these dykes was part of an early thermal input into the Kanmantoo Trough that may have played a role in the circulation of basinal fluids as proposed in the model of Seccombe et al. (1985). An additional point not mentioned by these authors is that the mafic magmas themselves may have contributed metals directly.

9.4.6 Origin of the mineralising fluids

The mineralizing fluids may have been derived from one or more of the following sources:

- Formation waters and circulating seawater
- Metamorphic fluids
- Magmatic fluids.

1. Formation waters were proposed as the mineralizing fluids for the Kanmantoo Cu deposit and the regional stratiform Pb-Zn-Ag deposits by Seccombe et al. (1985), Spry et al. (1988), Both (1988), and Gum et al. (1994). Formation fluids are expelled from the sedimentary pile as a result of its dewatering by compaction. This process and the role of such fluids in ore genesis has been discussed by many authors including Jackson and Beales (1967), Sibson et al (1975), Hanor (1979), Badham (1981), Cathles (1981, a review) and Sawkins (1984, 1989). The fluids derived from the sediments are driven during compaction and porosity reduction into common escape routes from the sedimentary basin. In some cases fluid expulsion is believed to be episodic (Cathles and Smith, 1983) and may be caused by intermittent fault movements causing "seismic pumping" (Sibson et al, 1975).

Large volumes of formation waters must have been expelled from the rapidly deposited Kanmantoo Trough sediments. Escaping fluids are commonly focused into structural weaknesses in sedimentary piles (Hanor, 1979). Much of this fluid probably found its way up the large growth faults of the basin, but within intervening zones some water may have found alternative routes to the surface, perhaps in pipe-like systems of channelways at a high angle to the bedding. Once initiated as a fluid escape route, such systems could persist as a structural weakness and be exploited later by fluids released by early metamorphic devolatilisation reactions, perhaps even if deformation was occurring at the same time. Re-use of weaknesses as fluid pathways would explain how episodic mineralisation events can occur in the same site over a period of time and in different geological conditions.

The timing of the structural controls for the Kanmantoo copper mineralisation, especially the Mine Synform, indicates that formation waters were not the source of the mineralisation. It is likely that these fluids would have been expelled from the basin long before the Mine Synform developed.

2. Metamorphic fluids as a possible agent in the origin of the Kanmantoo copper deposit present similar uncertainties to syn-sedimentary fluids with respect to fluid and metal origin, fluid movement, mass transport, fluid focusing and metal deposition. But their timing is appropriate. Fluids are produced from the earliest stages of metamorphism as a result of prograde devolatilisation reactions (Walther and Orville, 1982). In addition, meteoric fluids (Wickham and Taylor, 1985; Jenkin et al., 1994) and magmatic fluids (Ferry, 1992, 1994) can augment metamorphic devolatilisation fluids. From any small rock volume the release of devolatilisation fluids will be episodic as conditions for successive reactions are reached, but production of metamorphic fluids from the whole pile would be expected to be continuous, if heating is uniform. The movement of fluids during regional metamorphism remains a contentious subject (Etheridge et al., 1983; Ferry, 1994; Rumble, 1994; Oliver, 1996). The

debate includes issues such as the creation of porosity and permeability, pervasive flow versus channelised flow, temperature and fluid pressure gradients, the effect of deformation, and the scale of movement being considered. Although large quantities of fluid are produced from all metamorphic reactions, many studies have shown that, on a single pass basis, the quantity is not sufficient to account for some common features of regional metamorphic belts (Rumble, 1994). This is particularly the case where deformation is involved. For example, rocks with domainal fabrics may have lost up to 50% of their volume (Wright and Platt, 1982; Wright and Henderson, 1992) during shortening. The known solubilities of the dissolved components, principally silica, require fluid:rock ratios in the order of 10^3:1 (Etheridge et al., 1983; Ferry,1994). To date, there is no widely accepted mechanism to account for the many passes of fluid needed to achieve such high fluid:rock ratios. Theories have included the multiple convection cell model, proposed by Etheridge et al. (1983), in which fluid movement is driven by heat input in the lower crust. According to this model, the fluid transports material from the mid and lower crust into the upper crust where it is deposited, thus renewing the fluid's capacity to dissolve more material when it returns to the deeper parts of the crust. The deposited material in the upper crust also helps to form a seal that allows the convection cells to operate in conditions with $P_f \sim P_{lithostatic}$. While this model provides a means for achieving high fluid:rock ratios, it cannot be applied generally. For example, studies have indicated substantial horizontal, up-temperature fluid movement over many kilometres during regional metamorphism in Vermont (Ferry, 1992; Stern et al., 1992; Leger and Ferry, 1993), and in the Kanmantoo Trough (Cartwright, Vry and Sandiford, 1995; Oliver et al., 1998).

Sulphide deposits that formed from metamorphic fluids require, amongst other factors, high fluid volumes channeled through discrete structures. High fluid volumes provide sufficient dissolved metal to the site of deposition within the structure, and precipitation of metals is effected usually by chemical controls that are particular to the site. For epigenetic deposits the channelising of fluids is a key requirement in providing high fluid fluxes. Channelised flow, in contrast to pervasive flow, is favoured by large permeability and rheology contrasts, relatively low intrinsic permeability, high strains and relatively low rates of fluid flow compared to the rate of deformation (Oliver, 1996; Ord and Oliver, 1997). The scale of channelisation appears to be equivalent to the scale of permeability or rheology contrast during deformation (Ord and Oliver, 1997). Evidence of channelised flow in Kanmantoo Group metasediments was presented by Arnold and Sandiford (1990) for sillimanite grade rocks near Springton. Pods containing orthoamphibole and cordierite are 2m to 100m in length and were interpreted to represent steep pipe-like networks. This hydrothermal system could represent a similar system to that containing the Kanmantoo copper mineralisation, even though it is a little smaller. At the time of their formation the structures presumably passed upwards into lower grade rocks equivalent to those hosting the Kanmantoo mineralisation. To the author's knowledge, similar structures have not been reported from lower grade rocks, with the possible exception of some sulphide bearing zones like the Kanmantoo deposits. The pods at Springton were not reported to contain any sulphide mineralisation. Microstructures within the pods were interpreted by Arnold and Sandiford (1990) to indicate high temperature metasomatism resulting in K_2O depletion, but there seems to be a question over whether the chemical entity that defines the pod was formed prior to these metamorphic reactions.

In the case of Kanmantoo region, many of the structures that must have acted as syn-metamorphic channels would have been reactivated faults, perhaps former growth faults. The most obvious candidate here would be the large Bremer Fault located 6km to the east of Kanmantoo Mine and perhaps the proposed Kanmantoo Fault (refer Chapter 2) located 2km east of the mine. No similar structure is known to occur very close to the Kanmantoo Mine. If the Kanmantoo deposit, in particular the East Limb lodes, occupy channelways then they must have been connected at depth to other channels that fed them with fluids. The Kanmantoo channels may have collected pervasive and channelised flow from a large volume

of rocks. The persistence with depth of the Mine Synform (and therefore the channeling control) is unknown. If it does not persist for more than a kilometre or two with depth then alternative systems of channels would be expected at depth.

The reason for ore bearing solutions to be focused into the Kanmantoo deposit area is not known. Perhaps there were many channels in the district but only in the area of the Kanmantoo deposits were the conditions suitable for metal deposition. Perhaps the GAB schists had unique rheological or chemical properties suitable for metal deposition. Perhaps the relatively iron rich GAB schists were the most reactive rocks along the various channelways and the metals were deposited by wall-rock reactions. Or perhaps metal deposition resulted from mixing of the channeled fluids with fluids peculiar to the Paringa Andalusite Member.

3. Magmatic fluids have not been proposed generally as agents of mineralisation at Kanmantoo because of lack of evidence of magmatic activity in the immediate district and lack of sulphide mineralisation genetically associated with known magmatic bodies in the region. No igneous dykes or volcanic rocks have been recognized near Kanmantoo Mine. The nearest known igneous rock to the Kanmantoo Mine is a granite body that outcrops 13km to the east. This granite is part of the Murray Bridge suite of generally I-type granites that were intruded during the Delamerian Orogeny (Mancktelow, 1979, 1990; Fleming and White, 1984; Foden, Turner and Michard, 1989; Sandiford et al., 1992; Foden, Turner and Sandiford, 1995). These intrusions and others like them are confined to a 70km long belt between Murray Bridge and Angaston that corresponds approximately to the areas of highest metamorphic grade in the Mount Lofty Ranges. The best known copper mineralisation associated with granite in the region are the Kitticoola Cu-Au veins hosted by the Palmer Granite, but the veins are clearly not contemporaneous with the granite. Studies of this mineralisation indicate that it formed in late stage, brittle structures within a foliated Delamerian granite (Thomson, 1975; Drexel, 1979; Both, 1990). The quartz-ankerite-chlorite-sericite gangue mineralogies in the veins indicate much lower temperatures of formation than the metamorphic temperatures of the surrounding sillimanite grade rocks. The very close proximity of the veins to the Palmer Fault suggests a possible genetic association.

Despite the lack of direct evidence for magmatic activity at the Kanmantoo Mine, it has been proposed as an agent of mineralisation by Dickinson (1942) to explain perceived higher metamorphic grades associated with mineralisation in the Kanmantoo district, and by Oliver (1996) and Oliver et al. (1998) to account again for an inferred local thermal anomaly and also oxygen isotope results. Dickinson's local thermal high is based on the inference that the coarse-grained andalusite rich rocks indicate higher metamorphic grades, a conclusion that is now known to be incorrect. The evidence for Oliver et al.'s (1998) local thermal anomaly relies on a correlation of the main schistosity in the mine being S_3. As explained in a preceding section, the S_3 correlation is not supported by this study and therefore neither is the conclusion regarding a thermal anomaly. Oliver et al. (1998) also argued that oxygen isotope data supported an externally derived fluid from a crystallizing magma. Marshall and Spry (2000) questioned this interpretation and pointed out that the oxygen isotope patterns could also have formed during syngenetic exhalation and then been preserved during amphibolite facies metamorphism.

If granitoid rocks played a role in mineralisation at Kanmantoo as proposed by Oliver et al. (1998), then the ages of granite intrusion in the Kanmantoo Group are important, especially their timing with respect to deformation. This subject, including a geochronological compilation, was reviewed by Farrand and Preiss (1995). Contributions to the subject have been made by many authors (Milnes et al., 1977; Mancktelow, 1979, 1990; Fleming and White, 1984; Foden et al., 1989, 1990, 1995; Sandiford et al., 1991, 1992, 1995; Oliver and

Zakowski, 1995; Foden et al., 1999). Absolute ages of the deformed granites as determined from measurements on zircons range from 514 – 490 Ma. Relative ages with respect to deformation phases have been proposed as early as pre-tectonic (Milnes et al., 1977), but the evidence for pre-tectonic age is not conclusive (Farrand and Preiss, 1995). The age of igneous crystallization of the oldest and most strongly deformed granite in the Adelaide Fold Belt, the Rathjen Gneiss, has been dated at 514±5 Ma by Foden et al. (1999). Field relations indicate that the Rathjen Gneiss pre-dates the earliest fabric (a sub-horizontal foliation) attributed to S_1. Most syn-tectonic granites, however, like the Palmer Granite and the Monarto Granite, appear to contain no evidence of D_1 deformation (Mancktelow, 1979; Sandiford et al., 1992).

The relative ages of Delamerian granites with respect to deformation was addressed by Sandiford et al. (1995). These authors suggested that regional deformation associated with peak metamorphism in the eastern Mount Lofty Ranges was associated with thermal weakening of crustal rocks as a result of advective heat transfer from intruding granites. That is, deformation was localized by magmatic activity. Amongst others, this concept explains neatly the confinement of D_2 structures to the highest grade rocks. A result of this process would be diachronous ages for the resultant peaks of metamorphism and deformation for different metamorphic grades as the thermal pulse moved through the region. Oliver and Zakowski (1995) accepted the concept that a propagating thermal pulse coupled deformation and metamorphism, but they disputed that the causative relationship proposed for these factors was exclusive. Instead, they suggested that the regional stress field for each deformation was geographically widespread, but local strain intensity depended on the relative timing of, and was enhanced by, the passage of the thermal pulse. Oliver and Zakowski (1995) also proposed an early extensional deformation (their D_1) that had associated granite intrusion (associated with the Rathjen Gneiss) and mid-crustal heat input prior to the compressional deformation normally associated with the Delamerian Orogeny.

A second group of magmatic rocks that may have played a role in the genesis of the Kanmantoo copper mineralisation are the numerous occurrences of meta-dolerite dykes in the eastern Mount Lofty Ranges. Aspects of their geology have been commented upon by many authors including Pain (1968), Mancktelow (1979), Fleming and White (1984), Liu and Fleming (1989,1990), Chen and Liu (1996) and they have been referred to in preceding sections. A key feature of this suite of rocks is their relatively early age; the proposed relative ages of some of the dykes are pre- to syn-D_1 Fleming and White (1984), Liu and Fleming (1989,1990). Geochemically, they have MORB-like affinities (Liu and Fleming, 1989,1990) suggesting thermal input from mantle heat sources before or early in the deformational history. Liu and Fleming (1990) point out that the lack of (known) intercalated mafic volcanic rocks in the Kanmantoo Group may mean that dyke intrusion did not commence until after sedimentation had finished. Even so the magmas responsible for the mafic dykes are clearly a better candidate as a magmatic source for heat and perhaps metals than the known granitoids, assuming that mineralisation was pre- or syn-D_1.

In conclusion, the intrusion of some felsic and mafic magmas are of suitable timing to provide fluids directly, or heat to generate fluid flow, for the Kanmantoo mineralisation.

9.5 Similar deposits

Although there are many sediment hosted copper-iron rich sulphide deposits in fold belt settings throughout the world, few appear to be similar to the Kanmantoo deposits. Two that are similar and will be discussed here are the Cobar deposits in New South Wales and the Ducktown deposit in Tennessee. Although the origin of these deposits has been contentious for years, current opinion favours a syn-metamorphic origin. Several other base metal deposits also have been reinterpreted as syn-metamorphic. For example, the Rosebery Cu-Pb-

Zn deposit in Tasmania is considered by many to be a strongly deformed, exhalative sulphide deposit (Brathwaite, 1972, 1974; Green et al., 1981; Lees et al., 1990). Work by Aerden (1991, 1994) was interpreted to show that the lodes are discordant to bedding and folding, and he proposed an origin based on structural control during lower greenschist facies metamorphism. However, Aerden's conclusions were challenged by Marshall and Spry (2000). Similarly, De Roo (1989) proposed a syn-metamorphic origin for the Elura Pb-Zn deposit in the Cobar region. Work by several authors over the past 15 years or so has shown that the huge copper deposit at Mount Isa was derived from metamorphic fluids associated with compressive deformation (Perkins, 1984; Swager, 1985; Bell et al., 1988; Heinrich et al., 1995).

9.5.1 Cobar copper deposits

Copper deposits in the Cobar district are similar to those at Kanmantoo in their turbiditic host sequence, their deposit scale structural setting, the apparent absence of magmatic influence and because they have been metamorphosed. They differ from Kanmantoo in containing higher concentrations of Zn and Au and the low metamorphic grade of the enclosing sequence. The Cobar mining district, contains many sulphide rich deposits within deformed Early Devonian turbidites. Deposits lie approximately along a linear trend that is discordant to regional bedding and extends for 60 km from the Elura Mine in the north to the Queen Bee Mine in the south. Deposits along this trend have the following historical and indicated reserves: 431,000t Cu, 2,5000,000t Zn, 1,600,300t Pb, 4,050t Ag and 56t Au (Glen, 1991). These reserves are from many deposits which are of three main types (Glen, 1987): copper + gold (e.g. The Peak, and Central deposits); copper + zinc + lead (CSA deposit); and lead + zinc + silver (Elura deposit). Only the copper rich deposits are discussed here. General descriptions of the Cobar district have been published by many authors including Andrews (1913), Russell and Lewis (1965), Rayner (1969), Brooke (1975); Glen (1987) and Suppel and Scheibner (1990). At present only one mine is operating, The Peak.

The Cobar Basin formed around the Silurian-Devonian boundary and was filled mainly with a relatively monotonous sequence of turbiditic sediments and a general absence of volcanic rocks (Glen, 1987). Recent seismic studies have indicated the presence of a mid-crustal detachment fault below the basin suggesting its origin as a cold ramp basin, rather than a classical extension basin (Drummond et al., 1992). Most of the copper rich deposits occur near the eastern margin of the basin within the Great Cobar Slate, or to a lesser degree within thin bedded turbidites of the underlying Chesney Formation or the overlying CSA Siltstone. The basement subsided by movement along faults developed in the upper plate during movement on the detachment fault. The basin was subsequently deformed and metamorphosed, probably during the late Early Devonian and Carboniferous (Glen, 1990).

Regional structures formed in the deformed Cobar Basin have been described most recently by Glen (1985, 1990, 1991), who recognised three zones on the basis of variations in geometry, overprinting relations and finite strain. Zone 1 occurs on the eastern side of the basin and is a D_1 relatively high strain zone, characterised by a regional subvertical S_1 cleavage, a down dip L_1 lineation and folds of varying tightness. Zone 1 is bounded to the east and west by faults. To the east it is bounded by the Rookery Fault, which is believed to have been active during basin formation, and to the west it is juxtaposed sharply against Zone 2 by the Myrt Fault system. Zone 2 occupies most of the rest of the Cobar Basin and exhibits lower strain. It contains 2 fold generations. F_1 folds, with rare S_1 cleavage, are folded by variably plunging, upright, open F_2 folds which have a variably developed S_2 cleavage. The regional S_1 cleavage characteristic of Zone 1 is not developed in Zone 2. Zone 3 is an incompletely understood, low strain zone occupying a relatively small portion of the basin.

All known copper rich deposits are in Zone 1. They have similar styles and occur as steeply north plunging lenses consisting of sulphide veins, quartz-sulphide veins and sulphidic silicified host rock (Glen, 1985). The lenses are contained in north-northwest trending zones of silicificiation and quartz veining, with some chloritization and carbonate veining. Primary ore consists of chalcopyrite + pyrite + pyrrhotite + native gold (Rayner, 1969). In the deposits south of Cobar galena + sphalterite are minor, but in the CSA deposit further north they form separate lenses. The degree of silicification of host rocks varies from moderately silicified (but still recognisable as slate or siltstone), to chert. The chert is locally known as elvan (Glen, 1985, Binns and Appleyard, 1986).

Glen (1985) noted that copper deposits in the Cobar area occur in three settings:
(a) Group 1 deposits lie on or immediately west of faulted contacts between the Chesney Formation and the Great Cobar Slate.
(b) Group 2 deposits occur on faults within the Great Cobar Slate.
(c) Group 3 deposits occur within the CSA siltstone, and this group mainly comprises the CSA deposit.

Features common to all the copper rich deposits are a marked vertical persistence and they are typically discordant to folded bedding and are discordant or concordant to S_1 cleavage (Rayner, 1969; O'Connor, 1980). With respect to these features they are similar to the Kanmantoo copper deposits. Other similarities are that in both areas the deposits plunge steeply north whereas the surrounding fold plunges are variable but predominantly shallowly south plunging. Thus, the structural setting and geometry of both areas are remarkably similar.

Early theories on the origin of the copper rich deposits at Cobar favoured epigenetic processes (Andrews, 1913; Thomson, 1953; Rayner, 1969; and others), on the basis of discordance to bedding and the relationship of deposits to structure and alteration. However, various syngenetic – exhalative related origins were proposed to better explain the elvan cherts and the association of copper rich versus lead-zinc rich lenses seen in the CSA mine. The discordancy with bedding was explained by remobilization during deformation of syngenetically deposited sulphide minerals (Robertson, 1974; Brooke, 1975; Sangster, 1979; Marshall et al., 1981; Suppel, 1984). The remobilized-syngenetic model was rejected by the work of O'Connor (1980), Kirk (1983), Binns and Appleyard (1986), Glen (1985), Scott and Phillips (1990); and Hinman and Scott (1990). Another theory advocated by Marshall and Sangameshwar (1982) and Marshal et al. (1983) held that both remobilized syngenetic and epigenetic origins occurred in different deposits throughout the Cobar district and that the "percentage contribution of differing processes" should be emphasized in these complex deposits.

The most recent theories on the origin of copper rich deposits at Cobar propose that metamorphically derived fluids were focused along major faults, and copper and gold were deposited in local trap sites in second and third order faults (Glen, 1985, 1987, 1991; Brill, 1988; Glen et al., 1990; Hinman and Scott, 1990). The inferred metal source was dispersed in the deforming sediments.

9.5.2 Ducktown Copper Deposits

The Ducktown mining district contains a number of Fe-Cu-Zn sulphide deposits hosted within multiply deformed meta-greywackes of lower amphibolite metamorphic grade. Ducktown is located in the extreme southeastern corner of Tennessee, in the southern part of the Blue Ridge Province of the Southern Appalachia. The deposits are contained within Precambrian rocks of the Copperhill Formation of the Great Smoky Group, within the Ocoee Series (Hall et

al., 1991). The Great Smoky Group occurs in a 65 km wide thrust sheet of the Blue Ridge – Inner Piedmont allochthon (Hatcher, 1978; Hall et al., 1991), bounded to the west by the Great Smoky Thrust (of Alleghanian age) and to the east by the Hayesville Thrust (of Taconic age).

The Great Smoky Group consists predominantly of meta-greywackes and schists that are rather uniform in their mineralogy. Both consist of different proportions of quartz, plagioclase, muscovite, biotite, K-feldspar, garnet, staurolite, clinozoisite, calcite and secondary chlorite (Nesbitt & Essene, 1982). Minor lithologies include meta-quartzite, metz-conglomertate and calc-silicate rocks. Several additional lithologies occur only near the sulphide deposits; chlorite schist, muscovite schist, biotite schist, plagioclase-rich rock and spessartine-rich rock (Hall et al., 1991).

The sulphide deposits and their host rocks have experienced multiphase deformation and regional metamorphism, extending from the Cambrian Taconic Orogeny to the Permo-Carboniferous Alleghanian Orogeny (Hatcher, 1978; Hall et al., 1991). The first recognized deformation, F_1, produced tight, isoclinal and transposed folds. The second deformation event, F_2, produced more open folds within the Ducktown area (the Burra Anticline and Coletown Syncline).

The metamorphic sequence is of the Barrovian style and peak thermal conditions are believed to correspond with F_2, representing the Taconic Orogeny. Addy and Ypma (1977) proposed five deformation events (F_1-F_5) and three metamorphic events (M1-M3). The M2 event corresponds to the thermal peak and it is possible that M1 and M2 represent a single prograde series (Hall et al., 1991). In the mine area the assemblage staurolite-kyanite is characteristic and the deposits are estimated to have experienced peak conditions of 540° ±40°C and 6 kb (Nesbitt and Essene, 1983).

The Ducktown deposits comprise eight major deposits totalling 182 million tonnes and ranging in size from 0.25 to 71.1 million tones. Sulphide mineralisation varies from massive to disseminated and the lodes are approximately 65% massive sulphide and 35% gangue minerals. Ore grades vary from 0.5% to 2% Cu and 1% to 3% Zn. The massive sulphide varies from pyrite-rich to pyrrhotite rich but, on average, consists of 60% pyrrhotite, 30% pyrite, 4% chalcophyrite, 4% sphalerite and 2% magnetite (Magee, 1968; Nesbitt, 1982). The sulphide deposits are more or less tabular in shape and generally conform to enclosing bedding. They are disposed around both limbs of the Burra Anticline, apparently in two or three stratigraphic positions. However, the lack of marker units in the area makes it difficult to define the fold structures precisely. The Burra Anticline has small doubly-plunging fold structures, 30m to 300m in length, which may control sulphide localization and shape (Magee, 1968). Many of the deposits conform to drag fold structures defined by bedding. Even though the deposits are generally conformable to bedding (unlike those at the Kanmantoo Mine), divergences of up to 15° have been noted. The overall plunge of the Burra Anticline is to the northeast, but the deposits generally plunge to the southwest as do minor folds in adjacent schists (Magee, 1968).

The origin of the Ducktown deposits is contentious and proposed theories include syngenetic-sedimentary, metamorphic and post-metamorphic hydrothermal origins. The work of Nesbitt (1982) and others appear to have established that the wall rocks and country rocks equilibrated at peak metamorphism, thus dating the ore as syn-metamorphic at least and perhaps pre-metamorphic. Epigenetic theories involved the replacement by sulphides of calcareous sediments (Emmons and Laney, 1926) or shear zones (Ross, 1935) or both (Magee, 1968). The latter author believed the replacement by sulphide minerals took place during a Devonian deformation and that further mineralization probably occurred in a later deformation.

Addy and Ypma (1977) carried out an isotope study to assess the various theories and concluded that the sulphides were pre-tectonic, probably syn-sedimentary, and partly of later stage hydrothermal origin. They suggested that bedded sulphide horizons became the preferred sites of shears during isoclinal folding. Subsequent metamorphic fluids leached trace sulphides from the sedimentary sequence and deposited more sulphide minerals in the shears.

The Ducktown deposits have many similarities to the Kanmantoo deposits but they appear to be even more complex. They are similar with respect to their sulphide mineralogy, host metasediments, metamorphic grade and some aspects of their structural setting. However, unlike the Kanmantoo deposits, most deposits at Ducktown are conformable or approximately conformable to relict bedding. Because of this and the uncertain origin of the Ducktown deposits, it is difficult to make useful inferences from them regarding the origin of the Kanmantoo deposits.

9.6 Conclusions

(a) Despite the growing weight of evidence over the last decade in favour of exhalative mineralisation in the Kanmantoo-Strathalbyn region, detailed mapping in the mine does not support its circumstantial link to the Kanmantoo copper deposit.

(b) The Kanmantoo copper deposit has no firm evidence for a pre-metamorphic and sedimentary exhalative origin. However, this possibility has not been excluded.

(c) A strong structural control is imposed on the distribution of copper and of certain lithologies associated with copper mineralisation. Most important are the broad scale control of the Mine Synform and the mesoscopic and microscopic controls of S_2. The inferred dilational mechanism associated with the East Limb lodes is not related to simple buckling during development of the Mine Synform and probably developed from unusual circumstances such as a change in the stress field after the fold was established. West Limb style mineralisation probably developed later during D_2 as a result of shearing on the western limb.

(d) The timing of sulphide mineralisation involved several phases of hydrothermal activity of which the earliest that can be established is syn-D1. There is no microstructural evidence to preclude an earlier presence. Phases of metasomatism, accompanied in part by sulphide mineralisation, are indicated for the latter part of the period between D_1 and D_2, and for a late-D_2 event. The relative effect of each metasomatic event is not clear. It is likely that the late-D_2 event was not large. The biggest metasomatic event or events appear to pre-date D_2.

(e) Ore fluids were probably derived from either metamorphic fluids or magmatic fluids, or some combination of both. Both felsic and mafic intrusions in the region have appropriate timing and may have contributed heat, metals and, for the felsic intrusions, fluids. Mafic magmatism is known to be associated with a proposed major lineament that passes through Kanmantoo. Sedimentary formation waters are considered unlikely to have been the mineralizing fluids because they predate the timing of the observed structural controls on mineralisation.

REFERENCES

ADDY, S.K. & YPMA, P.J.M., 1977. Origin of massive sulphide deposits at Ducktown, Tennessee: An oxygen, hydrogen and carbon isotope study. *Economic Geology*, 72:1245-1268.

AERDEN, D.G.A.M., 1991. Foliation-boudinage control of the formation of the Rosebery Pb-Zn orebody, Tasmania. *Journal of Structural Geology*, 13(7):759-775.

AERDEN, D.G.A.M., 1994. Microstructural timing of the Rosebery massive sulphides, Tasmania: Evidence for a metamorphic origin through mobilization of disseminated base metals. *Journal of Metamorphic Geology*, 12:505-522.

ANDERSEN, D.J. & LINDSLEY, D.H., 1988. Internally consistent solution models for Fe-Mg-Mn-Ti oxides; Fe-Ti oxides. *American Mineralogist,* 73:714-726.

ANDERSON, P.A.M., NEWTON, R.C. & KLEPPA, O.J., 1977. The enthalpy change of the andalusite-sillimanite reaction and the Al_2SiO_5 diagram. *American Journal of Science,* 277:585-593.

ANDREWS, E.C., 1913. Report on the Cobar copper and gold-field, Part 1, *Geological Survey of New South Wales Mineral Resources,* 17.

ALLEN, R., 1977. Metamorphic phase relationships in the Kanmantoo. B.Sc. (Hons.) thesis, University of Adelaide (unpublished).

APPELYARD, E.C., 1980. Mass balance computations in metsomatism: metagabbro/nepheline syenite pegmatite interaction in northern Norway. *Contributions to Mineralogy and Petrology*, 73:131-144.

ARNOLD, J & SANDIFORD, M. 1990. Petrogenesis of cordierite-orthoamphibole assemblages from the Springton region, South Australia. *Contributions to Mineralogy and Petrology,* 106:100-109.

ASKINS, P.W., 1968. Geochemical exploration around the Aclare mine and mineral deposits of the surrounding region. *B.Sc. (Hons.) thesis, University of Adelaide (unpublished)*.

ASHWORTH, J.R., 1975. Staurolite at anomalously high grade. *Contributions to Mineralogy and Petrology*, 53:281-291.

ATHERTON, M.P., 1965. The composition of garnet in regionally metamorphosed rocks. In *Controls of Metamorphism*, (ed. W.S. Pitcher and G.W. Flinn), New York: Wiley, 281-290.

BADHAM, J.P.N., 1981. Shale hosted Pb-Zn deposits. Products of exhalation of formation waters? *Institute of Mining and Metallurgy Transactions*, 90:B70-B76.

BARNES, I., 1970. Metamorphic waters from the Pacific tectonic belt of the west coast of the United States. *Science* 158:1973.

BELL, T.H., 1985. Deformation partitioning and porphyroblast rotation in metamorphic

rocks: a radical reinterpretation. *Journal of Metamorphic Petrologyi, 3:109-118.*

BELL, T.H. & DUNCAN, A.C., 1978. A rationalized and unified shorthand terminology for lineations and fold axes in tectonites. *Tectonophysics*, 47:T1-T5.

BELL, T.H. & RUBENACH, M.J., 1983. Sequential porphyroblast growth and crenulation cleavage development during progressive deformation. *Tectonophysics*, 92:171-194.

BELL, T.H., PERKINS, W.G. & SWAGER, C.P., 1988. Structural controls on development and localization of syntectonic copper mineralization at Mount Isa. *Economic Geology*, 83:69-85.

BELPERIO, A.P., PREISS, W.V., FAIRCLOUGH, M.C., GATEHOUSE, C.G., GUM, J., HOUGH, J. & BURTT, A., 1998. Tectonic and metallogenic framework of the Cambrian Stansbury Basin-Kanmantoo Trough. *AGSO Journal,* 17(3):183-200.

BINNS, R.A. 1964. Zones of progressive regional metamorphism in the Willyama Complex, Broken Hill district, N.S.W. *Journal of the Geological Society of Australia*, 11:283.

BINNS, R.A. & APPLEYARD, E.C., 1986. Wallrock alteration at the Western System of the C.S.A. Mine, Cobar, New South Wales, Australia, *Applied Geochemistry,*1:211-225.

BIRD, G.W., & FAWCETT, J.J., 1973. Stability relations of Mg-Chlorite, muscovite and quartz between 5 and 10 kb water pressure. *Journal of Petrology*, 14(3): 415-428.

BISCHOFF, J.L., 1972. Ferroan nontronite from the Red Sea geothermal system. *Clays and clay minerals*, 20:217-223.

BOHLEN, S.R., MONTANA, A., KERRICK, D.M., HUGGINS, C. & MANNING, C.E., 1989. The kyanite = sillimanite transition revisited. *EOS*, 70:153-169.

BOTH, R.A., 1990. Kanmantoo Trough – geology and mineral deposits. In: Hughes, F.E. (editor), Geology of the Mineral Deposits of Australia and Papua New Guinea. *Australasian Institute of Mining and Metallurgy,* Melbourne, 1195-1203.

BOTH, R. A., MCELHINNEY, R. and TOTEFF, S., 1995: The Angas Zn-Pb-Ag deposit in the Kanmantoo Group, South Australia: synsedimentary or metamorphic? in *The Mineral Deposits: From their Origin to their Environmental Impacts* (Eds. J. Pasava, B. Kríbek and K. Zák). A. A. Balkema, Rotterdam, p. 847-850.

BOWES, D.R. 1953. The metamorphic and igneous history of Rosetta Head, South Australia. *Transactions of the Royal Society of South Australia*, 77:181-216.

BRATHWAITE, R.L., 1972. The structure of the Rosebery ore deposit, Tasmania. *Proceedings of the Australasian Institute of Mining and Metallurgy*, 241:1-13.

BRATHWAITE, R.L., 1974. The geology and origin of the Rosebery ore deposit, Tasmania. *Economic Geology*, 69:1086-1101.

BRILL, B.A., 1988. Geochemistry and genesis of the CSA Cu-Pb-Zn deposit, Cobar, NSW, Australia. *Ph.D. thesis, University of Newcastle,* New South Wales.

BROOKE, W.J.L., 1975. Cobar mining field, in *Economic Geology of Australia and Papua New Guinea, Vol.* 1 Metals (Ed. C.L. Knight), pp 683-694 (The Australasian Institute of Mining and Metallurgy: Melbourne.)

BRYANT, B. & READ, J.C., 1969. Significance of lineations and minor folds near major thrust faults in the Southern Appalachians and the British and Norwegian Caledonides. *Geology Magazine,* 106:412-429.

BUDDINGTON, A.F. & LINDSLEY, D.H., 1964. Iron-titanium oxide minerals and synthetic equivalents. *Journal of Petrology,* 5:310-537.

CAMPANA, B., 1955. The structure of the eastern South Australian ranges: the Mt Lofty-Olary arc. *Journal of the Geological Society of Australia*, 2:47-62.

CARTWRIGHT, I., VRY, J., & SANDIFORD, M., Changes in stable isotope ratios of metapelites and marbles during regional metamorphism, Mount Lofty Ranges, South Australia: Implications for crustal scale fluid flow. *Contributions to Mineralogy and Petrology,* 120, 292-310.

CATHLES, L.M., 1981. Fluid flow and genesis of hydrothermal ore deposits. In *Economic Geology, Seventy-fifth Anniversary Volume*, B.J. Skinner (ed.), pp 424-457.

CATHLES, L.M., & SMITH, A.T., 1983. Thermal constraints on the formtion of Mississippi Valley-type lead-zinc deposits and their implications for episodic basin dewatering and deposit genesis. *Economic Geology*, 78:983:1002.

CHEN, Y.D., & LUI, S.F., 1996. Precise U-Pb zircon dating of a post-D2 meta-dolerite: constraints for rapid tectonic development of the southern Adelaide Fold Belt during the Cambrian. *Journal of the Geological Society of London*, 149:185-192.

CHILMAN, J.K., 1982. Silver and a trace of gold. South Australian Department of Mines and Energy, *Special publication No. 1.*

CHINNER, G.A., 1965. The kyanite isograd in Glen Clova, Angus, Scotland. *Mineralogical Magazine,* 34:132-143.

COOPER, J.A., JENKINS, R.J.F., COMPSTON, W., WILLIAMS, I.S., 1992. U-Pb zircon dating of a tuff in the South Australian Lower Cambrian. *Geological Society of London Journal,* 149:185-192.

COSGROVE, J.W., 1976. The formation of crenulation cleavage. *Journal of the Geological Society of London*, 132:155-178.

COX, S.F., ETHERIDGE, M.A. & WALL, V.J., 1987. The role of fluids in syntectonic mass transport, and the localization of metamorphic vein-type ore deposits. *Ore Geology Reviews,* 2:65-86.

COX, S.F. & ETHERIDGE, M.A., 1989. Coupled grain-scale dilatancy and mass transfer during deformation at high fluid pressures: examples from Mount Lyell, Tasmania. *Journal of Structural Geology*, 11:147-162.

COX, S.F., WALL, V.J., ETHERIDGE, M.A. & POTTER, T.F., 1991. Deformational and

metamorphic processes in the formation of mesothermal vein-hosted gold deposits – examples from the Lachlan Fold Belt in central Victoria, Australia. *Ore Geology Reviews,* 6:391-423.

CURRIE, L., 1971. The reaction 3 cordierite = 2 garnet + 4 sillimanite + 5 quartz as a geological thermometer in the Opinicon Lake region, Ontario. *Contributions to Mineralogy and Petrology,* 33:215:226.

DAILY, B., 1956. The Cambrian in South Australia. Ph.D. thesis, University of Adelaide (unpublished).

DAILY, B. & MILNES, A.R., 1971. Stratigraphic notes on Lower Cambrian fossiliferous metasediments between Campbell Creek and Tunkalilla Beach in the type section of the Kanmantoo Group, Fleirieu Peninsula, South Australia. *Transactions of the Royal Society of South Australia*, 95:199-214.

DAILY, B. & MILNES, A.R., 1972. Revision of the stratigraphic nomenclature of the Cambrian Kanmantoo Group, South Australia. *Journal of the Geological Society of Australia*, 19:197-202.

DAILY, B. & MILNES, A.R., 1973. Stratigraphy, structure and metamorphism of the Kanmantoo Group (Cambrian) in its type section east of Tunkalilla Beach, South Australia. *Transactions of the Royal Society of South Australia,* 97:13-242.

DALZIEL, I.W.D., 1991. Pacific margins of Laurentia and east Antarctica – Australia as a conjugate rift pair: Evidence and implications for an Eocambrian supercontinent. *Geology*, 19:598-601.

DAY, H.W. & KUMIN, H.J., 1980. Thermodynamic analysis of the aluminium silicate triple point. *American Journal of Science*, 280:265-287.

DE ROO, J.A., 1989. The Elura Ag-Pb-Zn mine in Australia – ore genesis in a slate belt by syndeformational metasomatism along hydrothermal fluid conduits. *Economic Geology*, 84:256-278.

DEER, W.A., HOWIE, R.A. & ZUSSMAN, J., 1976. *An introduction to the rock forming minerals*. 528 pp. Longman Group Ltd, London.

DICKINSON, S.B., 1942. The structural control of ore deposition in some South Australian copper fields. *Geological Survey of South Australia, Bulletin* 20:79-99.

DREXEL, J.F., 1978. Geology and geochemistry of the South-eastern Freeway - Mt Barker summit to Callington section. *South Australian Department of Mines and Energy Report no.* 78/91.

DREXEL, J.F., 1979. The geology of the Kitticoola Mine. *Mineral Resources Review South Australian Department of Mines and Energy,* 146:5-19.

DRUMMOND, B.J. GLEN, R.A., GOLEBY, B.R, WAKE-DYSTER, K.D., & PALMER, D., 1992. Deep seismic of the Cobar Basin-II a ramp basin controlled by a deep detachment. *Geological Society of Australia, Abstracts*, 32, 44.

DUNCAN, N., 1973. Exploration at the Bremer Mine, Callington, South Australia. *Northern Mining Proprietary Limited, unpublished report,* 28p.

DURNEY, D.W. 1972. Solution transfer, an important geological deformation mechanism. *Nature*, 235:315-317.

DYMOKE, P. & SANDIFORD, M., 1992. Phase relations of Buchan facies series pelitic assemblages: calculations and applications to the Mount Lofty Ranges, South Australia. *Contributions to Mineralogy and Petrology,* 110:121-132.

DYSON, I.A., GATEHOUSE, C.G., & JAGO, J.B., 1994. The significance of the sequence boundary at the base of the Early Cambrian Talisker Calc-siltstone and its relationship to mineralisation in the Kanmantoo Trough, *Geological Society of Australia, Abstracts* 37.

EMMONS, W.H. & LANEY, F.B., 1926. Geology and ore deposits of the Ducktown mining district, Tennessee. *U.S. Geological Survey Professional Paper,* 139, 114pp.

ENGEL, A.E.J. & ENGEL, C.G., 1958. Progressive metamorphism and granitization of the major paragneiss, Northwest Adirondack Mountains, New York, Part 1. *Bulletin of the Geological Society of America*, 71:1.

ETHERIDGE, M.A., 1973. Variation in length/thickness ratio of biotite crystals in metamorphic rocks: a discussion. *Journal of Geology*, 81(2):234-236.

ETHERIDGE, M.A., 1983. Differential stress magnitudes during regional deformation and metamorphism: upper bound imposed by tensile fracturing. *Geology*, 11:231-234.

ETHERIDGE, M.A., PATERSON, M.S. & HOBBS, B.E., 1974. Experimentally produced preferred orientation in synthetic mica aggregates, *Contributions to Mineralogy and Petrology*, 44:275-294.

ETHERIDGE, M.A., WALL, V.J. & VERNON, R.H., 1983. The role of the fluid phase during regional metamorphism and deformation. *Journal of Metamorphic Geology*, 1:519-522.

ETHERIDGE, M.A., WALL, V.J., COX, S.F. & VERNON, R.H., 1984. High fluid pressures during regional metamorphism and deformation: implications for mass transport and deformation mechanisms. *Journal of Geophysical Research*, 89:4344-4358.

FARRAND, M.G. & PREISS, W.V., 1995. Delamerian Orogeny. In: Drexel, J.F. & Preiss, W.V. (Editors), The Geology of South Australia. Vol 2. The Phanerozoic, South Australia. *Geological Survey Bulletin* 54(2):54-57.

FERGUSON, C.C. & HARTE, B., 1974. Textural patterns at porphyroblast margins and their use in determining the time relations of deformation and crystallisation. *Geological Magazine*, 112(5):467-480.

FERRY, J.M. & SPEAR, F.S., 1978. Experimental calibration of the partitioning of Fe & Mg between biotite and garnet. *Contributions to Mineralogy and Petrology,* 66:113-117.

FERRY, J.M., 1992. Regional metamorphism of the Waits River Formation, Eastern Vermont: delineation of a new type of giant hydrothermal system. *Journal of Petrology*, 33:45-94.

FERRY, J.M., 1994. A historical review of metamorphic fluid flow. *Journal of Geophysical Research*, 99:15487-15498.

FINLOW-BATES, T. & STUMPFL, E.F., 1981. The behaviour of so-called immobile elements in hydrothermally altered rocks associated with volcanogenic submarine-exhalative ore deposits. *Mineralium Deposita*, 16:319-328.

FLEMING, P.D., 1965. The geology of an area east of Angaston, South Australia. B.Sc(Hons.) thesis, University of Adelaide (unpublished).

FLEMING, P.D., 1971. Metamorphism and folding in the Mt. Lofty Ranges, South Australia, with particular reference to the Dawesley-Kanmantoo area. Ph.D. thesis, University of Adelaide (unpublished).

FLEMING, P.D., 1973. Mg-Fe distribution between coexisiting garnet and biotite, and the status of fibrolite in the andalusite-staurolite zone of the Mt Lofty Ranges, South Australia. *Geological Magazine*, 109:477-482.

FLEMING, P.D. & FAWCETT, J.J., 1976. Upper stability of chlorite + quartz in the system MgO-FeO-Al_20_3- SiO_2-H_2O at 2 kbar water pressure. *American Mineralogist*, 61:1175-1193.

FLEMING, P.D. & OFFLER, R., 1968. Pre-tectonic metamorphic crystallization in the Mt Lofty Ranges, South Australia. *Geological Magazine,* 105:356-359.

FLEMING, P.D. & WHITE, A.J.R., 1984. Relationships between deformation and partial melting in the Palmer migmatites, South Australia. *Australian Journal of Earth Sciences*, 31:351-360.

FLEUTY, M.J., 1964. The description of folds. *Geological Association Proceedings*, 75:461-492.

FLINN, D., 1965. Deformation in metamorphism: Pp 46-72 in *Controls of Metamorphism*, W.S. Pitcher and G.W. Flinn (eds). Oliter and Boyd, Edinburgh, 368pp.

FLINT, D.J. 1978. Deep sea fan sedimentation of the Kanmantoo Group, Kangaroo Island. *Transactions of the Royal Society of South Australia*, 102:203-222.

FLOTTMANN, T., JAMES, P.R., ROGERS, J. & JOHNSON, T., 1994. Early Palaeozoic foreland thrusting and basin reactivation at the southeastern Paleo-Pacific margin of the Australian Precambrian Craton: a reappraisal of the structural evolution of the Southern Adelaide Fold-Thrust Belt. *Tectonophysics,* 234: 95-116.

FLOTTMAN, T. & COCKSHELL, C.D., 1996. Palaeozoic basins of southern South Australia: new insight to their structural history from regional seismic data. *Australian Journal of Earth Sciences,* 43:45-55.

FLOTTMAN, T., HAINES, P.W., COCKSHELL, C.D. & PREISS, W.V, 1998. Reassessment of the seismic stratigraphy of the Early Palaeozoic Stansbury Basin, Gulf St Vincent, South Australia. *Australian Journal of Earth Sciences,* 45(4):547-558.

FLOYD, P.A. & WINCHESTER, J.A., 1978. Identification and discrimination of altered and metamorphosed volcanic rocks using immobile elements. *Chemical Geology*, 21:291-306.

FODEN, J.D., TURNER, S.P., and MICHARD, A., 1989. Chemical and isotopic characteristics of igneous activity in the Adelaide Fold Belt: implications for mechanisms of crustal growth. Clare Valley Conference, (South Australia), SGTSG, *Geological Society of Australia Abstracts*, 40:45-48.

FODEN, J.D., TURNER, S.P., and MORRISON, R.S., 1990. The tectonic implications of Delamerian magmatism in South Australia and western Victoria, In: J.B. Jago and P.S. Moore (Editors), The evolution of a late Precambrian-Early Palaeozoic Rift Complex: The Adelaide Geosyncline. *Geological Society of Australian Special Publication*, 16:465-482.

FODEN, J.D., TURNER, S.P., and SANDIFORD, M., 1995. Granite composition in the Delamerian Orogen: a response to orogenic crustal thickening and thinning. Australasian Tectonics Conference, (February, Kangaroo Island, South Australia), SGTSG, *Geological Society of Australia Abstracts*, 24:47-48.

FODEN, J.D., SANDIFORD, M., DOUGHERTY-PAGE, J. & WILLIAMS, I. 1999. Geochemistry and geochronology of the Rathjen Gneiss: implications for the early tectonic evolution of the Delamerian Orogen. *Australian Journal of Earth Sciences*, 46:377-389.

FORBES, B.G., 1957. Stratigraphic succession east of Grey Spur, South Australia. *Transactions of the Royal Society of South Australia*, 80:59-66.

FORBES, B.G., COATS, R.P. & DAILY, B., 1972. Truro Volcanics. *South Australia, Geological Survey, Quarterly Geological Notes*, 44:1-5.

FRENCH, B.M., 1968. Progressive contact metamorphism of the Biwabik iron formation, Mesabi Range. *Minnesota Geological Survey Bulletin*, 45, 103pp.

FYFE, W.S., 1976. Chemical aspects of rock deformation. *Philosophical Transactions of the Royal Society of London*, 283: 221-226.

GANGULY, J., 1979.Garnet and clinopyroxene solid solutions and geothermometry based on Fe-Mg distribution coefficient. *Geochimica et Cosmochimica Acta*, 43:1021-1029.

GANGULY, J. & SAXENA, S.K., 1984. Mixing properties of aluminosilicate garnets: constraints from natural and experimental data, and applications to geothermo-barometry. *American Mineralogist*, 69:88-97.

GATEHOUSE, C.G., JAGO, J.B., RANKING, L.R., CLOUGH, B.J., GRAVESTOCK, D.I. & McCULLOCH, A.J., 1992. The extent and significance of the early Cambrian Truro volcanics. Earth Sciences, computers and the environment, Eleventh Australian Geological Convention, January 1992. *Geological Society of Australia, Abstracts*, 32.

GIBSON, H.L., WATKINSON, D.H. & COBRA, C.D.A., 1983. Silicification: Hydrothermal alternation in an Archean geothermal system within the Amulet Rhyolite Formation, Noranda, Quebec. *Economic Geology,* 78:954-971.

GEORGE, R.J., 1967. Metamorphism of the Nairne pyrite deposit. Ph.D. thesis, University of Adelaide, (unpublished).

GEORGE, R.J., 1969a. Sulphide-silicate reactions during metamorphism of the Nairne Pyrite deposit. *Proceedings of the Australasian Institute of Mining and Metallurgy*, 230:1-7.

GEORGE, R.J., 1969b. Sulphide vein formation during metamorphism of the Nairne Pyrite deposit. *Proceedings of the Australasian Institute of Mining and Metallurgy,* 230:9-18.

GLEN, R.A., 1985. Basement control on the deformation of cover basins: an example from the Cobar district in the Lachlan Fold belt, Australia. *Journal of Structural Geology*, 7:301-315.

GLEN, R.A., 1987a. Copper and gold rich deposits in deformed turbidites at Cobar, Australia: their structural control and hydrothermal origin. *Economic Geology*, 82:124-140.

GLEN, R.A., 1990. Formation and inversion of transtensional basins in the western part of the Lachlan Fold Belt, Australia, with emphasis on the Cobar Basin. *Journal of Structural Geology,* 12:601-620.

GLEN, R.A., 1991. Inverted transtensional basin setting for gold and copper and base metal deposits at Cobar, New South Wales. BMR *Journal of Geology and Geophysics*, 12:13-24.

GOLDMAN, D.S. & ALBEE, A.L., 1977. Correlation of Mg/Fe partitioning between garnet and biotite with O^{18}/O^{16} partitioning between quartz and magnetite. *American Journal of Science*, 277:750-761.

GRAMBLING, J.A., 1984. Coexisting paragonite and quartz in sillimanitic rocks from New Mexico. *American Mineralogist*, 69:79-87.

GRANT, J.A., 1986. The Isocon diagram – simple solution to Gresen's equation for metasomatic alteration. *Economic Geology*, 81:1976-1982.

GRAVESTOCK, D.I. & GATEHOUSE, C.G., 1995. Stansbury Basin. In: Drexel J.F. & Preiss W.V. (editors) The Geology of South Australia, Volume II: The Phanerozoic. pp. 5-19. *Geological Survey of South Australia Bulletin* 54.

GRAY, D.R., 1977. Morphologic classification of crenulation cleavage. *Journal of Geology*, 85:229-235.

GRAY, D.R., 1978. Cleavages in deformed psammitic rocks from Southeastern Australia: their nature and origin. *Bulletin of the Geological Society of America,* 80:577-590.

GRAY, D.R., 1979. Microstructure of crenulation cleavages: an indicator of cleavage origin. American Journal of Science, 279:97-128.

GREEN, G.R., SOLOMON, M. & WALSHE, J.L., 1981. The formation of the volcanic-hosted massive sulphide ore deposit at Rosebery, Tasmania. *Economic Geology,* 76:304-338.

GRESENS, R.L., 1967. Composition-volume relationships of metasomatism. *Chemical Geology*, 2:47-55.

GRIFFEN, D.T., GOZNEY. T.C. PHILLIPS, W.R., 1982. The chemical formula of natural staurolite. *American Mineralogist*, 67:292-297.

GRIFFEN, D.T. & RIBBE, P.H., 1973. The crystal chemistry of staurolite. *American Journal of Science*, 273A:471-495.

GUIDOTTI, C.V., 1970. The mineralogy and petrology of the transition from the lower to upper sillimanite zone in the Oquossoc area, Maine. *Journal of Petrology*, 11:277-336.

GUIDOTTI, C.V., 1974. Transition from staurolite to sillimanite zone, Rangeley quadrangle, Maine. *Geological Society of America Bulletin*, 85:475-490.

GUIDOTTI, C.V., CHENEY, J.F. & CONATORE, P.D.,1975. Interrelationship between Mg/Fe ratio and octahedral Al content in biotite. *American Mineralogist,* 60:849-853.

GUM, J.C., 1998. The sedimentology, sequence stratigraphy and mineralisation of the Silverton Subgroup, South Australia. Ph.D. thesis (unpublished), Department of Applied Gelogy, University of South Australia.

GUM, J.C., JAGO, J.B., & GATEHOUSE, C.G., 1994. Sedimentological constraints on mineralisation in the Southern Kanmantoo Trough. *Proceedings of the Australian Research on Ore Genesis Symposium.* Australian Mineral Foundation.

HAACK, U., HEINRICHS, H., BONEF, M. & SCHNEIDER, A., 1984. Loss of metals from pelites during regional metamorphism. *Contributions to Mineralogy and Petrology*, 85:116-132.

HAINES, P.W. & FLOTTMAN, T., 1998. Delamerian Orogeny and potential foreland sedimentation: a review of age and stratigraphic constraints. *Australian Journal of Earth Sciences,* 45(4): 559-570.

HALL, D.L., BODNAR, R.J., & CRAIG, J.R., 1991. Fluid inclusion constraints on the uplift history of the metamorphosed massive sulphide deposits at Ducktown, Tennessee. *Journal of Metamorphic Geology*, 9:551-565.

HANMER, S. & PASSCHIER, C., 1991. Shear-sense Indicators: A Review. *Geological Survey of Canada Paper* 90-17.

HANOR, J.S., 1979. The sedimentary genesis of ore fluids. In Barnes, H.L. (ed). *Geochemistry of Hydrothermal ore deposits (2nd ed.).* New York, John Wiley and Sons, pp 137-172.

HARTE, B. & JOHNSON, M.R.W., 1969. Metamorphic history of Dalmation rocks in Glens Clova, Esk and Lethnot, Angot, Scotland. *Scottish Journal of Geology*, 5:54-80.

HATCHER, R.D. Jr., 1978. Tectonics of the western Piedmont and Blue Ridge, southern Appalachians. *American Journal of Science,* 278:276-304.

HAYWOOD, N., 1992. Controls of syntectonic replacement mineralization in parasitic antiforms, Haile Gold Mine, Carolina Slate Belt. *Economic Geology*, 87:91-112.

HEINRICH, C.A., 1995. Fluid and mass transfer during metabasalt alteration and copper mineralisation at Mount Isa, Australia. *Economic Geology*, 90(4):705-730.

HEITANEN, A., 1969. Distribution of Fe and Mg between garnet, staurolite and biotite in aluminium-rich schist in various metamorphic zones north of the Idaho batholith. *American Journal of Science*, 267:422-456.

HEMINGWAY, B.S., ROBIE, R.A., EVANS, H.T. Jr., & KERRICK, D.M., 1991. Heat capacities and entropies of sillimanite fibrolite, andalusite, kyanite and quartz and the Al_2SiO_5 phase diagram. *American Mineralogist,* 76:1597-1613.

HENSEN, B.J., 1977. Cordierite-garnet bearing assemblages as geothermometers and geobarometers in granulite facies terrains. *Tectonophysics*, 43:73-88.

HENSEN, B.J. & GREEN, D.J., 1973. Experimental study of the stability of cordierite and garnet in pelitic compositions at high pressures and temperatures, 111. Synthesis of experimental data and geological implications. *Contributions to Mineralogy and Petrology*, 38:151-166.

HINMAN, M.C. & SCOTT, A.K. 1990. The Peak gold deposit, Cobar. In: *Geology of the Mineral Deposits of Australia and Papua New Guinea* (Ed. F.E. Hughes), pp. 1345-1351. The Australasian Institute of Mining and Metallurgy, Melbourne.

HOBBS, B.E., MEANS, W.H. & WILLIAMS, P.F., 1976. *An outline of structural geology*. New York: John Wiley and Sons.

HODGES, K.V. & SPEAR, F.S., 1982. Geothermometry, geobarometry and the $A1_2Si0_5$ triple point at Mt. Moosilauke, New Hampshire. *American Mineralogist*, 67:1118-1134.

HOLDAWAY, M.J., 1971. Stability of andalusite and the aluminium silicate phase diagram. *American Journal of Science*, 271:97-131.

HOLDAWAY, M.J. & LEE, S.M., 1977. Fe-Mg cordierite stability in high grade pelitic rocks based on experimental, theoretical and natural observations. *Contributions to Mineralogy and Petrology*, 63:175-198.

HOLDAWAY, M.J. & MUKHOPADHYAY, B., 1993. A reevaluation of the stability relations of andalusite: thermochemical data and phase diagram for the aluminium silicates. *American Mineralogist*, 78:298-315.

HOLLISTER, L.S., 1966. Garnet zoning: an interpretation based on the Raleigh fractionation model. *Science,* 154:1647-1650.

HOSCHEK, G., 1969. The stability of staurolite and chloritoid and their significance in the metamorphism of pelitic rocks. *Contributions to Mineralogy and Petrology*, 22: 208-232.

HUSTON, D.L. & PATTERSON, D.J., 1995. Zincian staurolite in the Dry River South volcanic-hosted massive sulphide deposit, northern Queensland, Australia. *Applied Geochemistry,* 10:329-336.

JACKSON, S.A. & BEALES, F.W., 1967. An aspect of sedimentary basin evolution. The concentration of Mississippi Valley type ores during late stages of diagenesis. *Canadian Petroleum Geology Bulletin*, 15:383-433.

JAMES, H.L., 1954. Sedimentary facies of iron-formation. *Economic Geology,* 59:1313-1342.

JAMES, R.S., TURNOCK, A.C. & FAWCETT, J.J., 1976. Stability and phase relations or iron chlorite below 8.5 kb PH20. *Contributions to Mineralogy and Petrology*, 65:1-25.

JENKIN, G.R.T., CRAW, D. & FALLICK, A.E., 1994. Stable isotope and fluid inclusion evidence for meteoric fluid penetration into an active mountain belt; Alpine Schist, New Zealand. . *Journal of Metamorphic Geology*, 12:429-444.

JENKINS, R.J.F., 1990. The Adelaide Fold Belt: Tectonic reappraisal. In: J.B. Jago and P.S. Moore (Editors), The evolution of a late Precambrian-Early Palaeozoic Rift Complex: The Adelaide Geosyncline. *Geological Society of Australia Special Publication,* 16:396-420.

JENKINS, R.J.F. and SANDIFORD, M., 1992. Observations on the tectonic evolution of the southern Adelaide fold Belt. *Tectonophysics,* 214:27-36.

JENSON, M.L. & WHITTLE, A.W.G., 1969. Sulphur isotopes of the Nairne Pyrite deposit, South Australia. *Mineralium Deposita*, 4:241-247.

JONES, K.A. & GALWEY, A.K., 1972. Variation in the length: thickness ratio of biotite crystals in metamorphic rocks. *Journal of Geology*, 80:112-120.

KERRICH, R., 1977. An historical review and synthesis of research on pressure solution. *Zbl. Geol. Palaent. Tiel. I.,* H5/6:512-550.

KERRICH, R. & ALLISON, I., 1978. Flow mechanisms in rocks: microscopic and mesoscopic structures and their relation to physical conditions of deformation in the crust. *Geoscience Canada*, 5(3):109-118.

KERRICK, D.M., 1987. Fibrolite in contact aureoles of Donegal, Ireland. *American Mineralogist*, 72:240-254.

KERRICK, D.M., 1990. The Al_2SiO_5 polymorphs. *Reviews of Mineralogy*, 22:1-406.

KIRK, B.I., 1983. A review of the geology and ore genesis of the Cobar mining field, in *Broken Hill Conference, Melbourne. Autralasian Institute of Mining and Metallurgy.*

KLEEMAN, A.W. & SKINNER, B.J., 1959. The Kanmantoo Group in the Strathalbyn – Harrogate region, South Australia. *Transactions of the Royal Society of South Australia*, 82:61-71.

KLEEMAN, A.W. & WHITE, A.J.R., 1956. The structural geology of portion of the eastern Mt. Lofty Ranges. *Journal of the Geological Society of Australia*, 3:17-31.

KRETZ, R., 1964. Analysis of equilibrium in garnet-biotite-sillimanite gneisses from Quebec. *Journal of Petrology*, 5(1):1-20.

KRETZ, R., 1966. Interpretation of the shape of mineral grains in metamorphic rocks. *Journal of Petrology*, 7:68-94.

KRETZ, R., 1994. *Metamorphic Crystallization*. John Wiley and Sons, UK.

LANG, H.M. & DUNN, G.R., 1990. Sequential porphyroblast growth during deformation in a low-pressure metamorphic terrain, Orrs Island-Harpswell Neck, Maine. *Journal of Metamorphic Geology,* 8:199-216.

LANIER, G., FOLSON, R.B. & CONE, S., 1975. Alteration of equigranular quartz monzonite, Bingham district, Utah. *In Guidebook to the Bingham Mining District: Bingham Canyon, Utah, Society of Economic Geologists,* pp. 73-98.

LEAKE, B.E., 1960. Compilation of chemical analyses and physical constants of natural cordierites. *American Mineralogist*, 45:282-298.

LEAKE, B.E., 1978. Nomenclature of amphiboles. *Canadian Mineralogist*, 16:501-520.

LEGER, A. & FERRY, J.M., 1993. Fluid infiltration and regional metamorphism of the Waits River Formation, north-east Vermont, USA. *Journal of Metamorphic Geology*, 11:3-30.

LINDGREN, W., 1933. *Mineral Deposits*. Fourth edition. McGraw-Hill Book Company.

LINDQVIST, W.F.L., 1969. Geology and metamorphic history of the Kanmantoo copper deposit, South Australia. Ph.D. thesis (unpublished), Imperial College, London.

LIU, S.F. & FLEMING, P.D., 1989. Amphibolites/metadolerites and their tectonic implications from the Mouth Lofty Ranges metamorphic belt, South Australia. Australasian Tectonics Conference, (February, Kangaroo Island, South Australia), SGTSG, *Geological Society of Australia Abstracts*, 24:89-90.

LIU, S.F. & FLEMING, P.D., 1990. Mafic dykes and their tectonic setting in the southern Adelaide Foldbelt, South Australia. In: Parker, A.J., Rickwood, P.C. & Tucker, D.H. (editors), Mafic dykes and emplacement mechanisms. *Proceedings of the Second International Dyke Conference, Adelaide.* A.A. Balkema, Rotterdam, pp. 401-413.

LONKER, S.W., 1981. The P-T-X relations of the cordierite-garnet-sillimanite-quartz equilibrium. *American Journal of Science*, 281:1056-1090.

MAGEE, M., 1968. Geology and ore deposits of the Ducktown district, Tennessee. *In: Ore Deposits of the United States: 1933-1967* (ed. Ridge, J.D.), pp. 207-241. American Institute of Mining, Metallurgical and Petroleum Engineers.

MANCKTELOW, N.S., 1990. The structure of the southern Adelaide Fold belt, South Australia. In: J.B. Jago and P.S. Moore (Editors), The evolution of a late Precambrian-Early Palaeozoic Rift Complex: The Adelaide Geosyncline. *Geological Society of Australia Special Publication,* 16:215-229.

MARLOW, P.C., 1975. Structural investigations near Macclesfield, South Australia. M.Sc. thesis, University of Adelaide (unpublished).

MARLOW, P.C. & ETHERIDGE, M.A., 1977. Development of a layered crenulation cleavage in mica schists of the Kanmantoo Group near Macclesfield, South Australia. *Geological Society of America Bulletin*, 88:873-882.

MARSHALL, B. & GILLIGAN, L.B., 1993. Remobilization, syntectonic processes and massive sulfide deposits. *Ore Geology Reviews*, 8:39-64.

MARSHALL, B. & SANGAMESHWAR, S.R., 1982. Commonality and differences in ores of the Cobar Super Group, New South Wales (Abs). *Geological Society of Australia Abstracts*, 5:15-16.

MARSHALL, B. & SPRY, P.G., 2000. Discriminating between regional metamorphic remobilization and syntectonic emplacement in the genesis of massive sulfide ores. *Reviews in Economic Geology*, 11:163-202.

MARSHALL, B. & SANGAMESHWAR, S.R., O'CONNOR, D.P.H., SUN, S.S., & BOUFFLER, M., 1981. Genetic aspects of the C.S.A. and Q.T.S. mineralisations, Cobar, New South Wales.(abs.). *Geological Society of Australia Abstracts*, 3:4.

MARSHALL, B. & SANGAMESHWAR, S.R., PLIBERSEK, P.F., & KELSO, I.J., 1983. Cobar Supergroup deposits: Polymodal genesis during protracted tectonism (abs.). *Geological Society of Australia Abstracts*, 9:305-306.

MARTINGOLE, J. & SISI, J.C., 1981. Cordierite-garnet-H2O equilibrium: a geological thermometer, barometer and water fugacity indicator. *Contributions to Mineralogy and Petrology,* 77:38-46.

MASON, M.G., 1968. Report on Nairne Pyrite Deposit, Brukunga. Department of Mines, South Australia.

McELHINNEY, R., 1994. Style and genesis of base metal sulphide mineralisation ofAngas Prospect, Strathalbyn area, South Australia. *University of Adelaide, B.Sc(Hons) thesis* (unpublished).

McONIE, A.W., FAWCETT, J.J. & JAMES, R.S., 1975. The stability of intermediate chlorites and clinochlore – daphnite series at 2 kb PH20. *American Mineralogist,* 60:1047-1062.

MILLER, J., 1992. An examination of the relationship between metamorphism andtectonics as seen at Kanmantoo Mine, Mt. Lofty Ranges, South Australia. B.Sc. report, Monash University (unpublished).

MILLS, K.J., 1964. The structural petrology of an area east of Springton, South Australia. *University of Adelaide. Ph.D. thesis* (unpublished).

MILNES, A.R., 1973. The Encounter bay Granites, South Australia and their environment. *University of Adelaide, Ph.D thesis* (unpublished).

MILNES, A.R., COMPSTON, W., & DAILY, B., 1977. Pre- to syn-tectonic emplacement of early Palaeozoic granites in southeastern South Australia. *Transactions of the Royal Society of South Australia,* 24:87-106.

MILNES, A.R., BOURMAN, R.P. & NORTHCOTE, K.H., 1985. Field relationships of ferricretes and weathered zones in southern South Australia: a contribution to "laterite" studies in Australia. *Australian Journal of Soil Research*, 23:441-465.

MIRAMS, R.C., 1962. The geology of the Mount Barker-Callington area. *Mining Review South Australia Department of Mines*, 117:9-16.

MOORE, W.J., 1978. Chemical characteristics of hydrothermal alteration at Bingham, Utah. *Economic Geology*, 73 (7): 1260-1269.

MORTON, R.L. & NEBEL, M.L., 1984. Hydrothermal alternation of felsic volcanic rocks at the Helen siderite deposit, Waway, Ontario. *Economic Geology*, 79:1319-1333.

NERO, L., 1993. Structure and metamorphism of the Kanmantoo Mine and surrounding area, Kanmantoo Group, South Australia. Monash University BSc Honours thesis (unpublished) 122pp.

NEWTON, R.C. & WOOD, B.J., 1979. Thermodynamics of water in cordierite and some petrologic consequences of cordierite as a hydrous phase. *Contributions to Mineralogy and Petrology.* 68:391-405.

NEMEC, J. & VON, D., 1978. Zinc in staurolite. *Chem. Erde. Bd.,* 37S:307-314.

NESBITT, B.E., 1982. Metamorphic sulfide-silicate equilibria in the massive sulphide deposits at Ducktown, Tennessee. . *Economic Geology*, 77:364-378

NESBITT, B.E. & ESSENE, E.J., 1982. Metamorphic thermometry and barometry of a portion of the southern Blue Ridge Province. *American Journal of Science.* 282:701-729.

NEWTON, R.C., 1985. Geobarometry of high grade metamorphic rocks. *Adv. Phys. Geochemistry*, 5:36-59.

NICKELSEN, R.P., 1979. Sequence of structural changes of the Allegheny Orogeny, at the Bear Valley stripmine, Shamokin, Pennsylvania. *American Journal of Science,* 279:225-271.

NIGGLI, P., 1954. *Rocks and mineral deposits*. Freeman, San Francisco.

O'CONNOR, D.P.H., 1980. Evidence of an exhalative origin for deposits of the Cobar district, New South Wales: discussion. *BMR Journal of Australian Geology and Geophysics*, 5:70-72.

O'DRISCOLL, E.S.T., 1973. A structural syndrome for ore emplacement at Broken Hill, Australia. *Zeitschrift der Deutschen geologischen Gesellschaft*, 124:257-266.

O'DRISCOLL, E.S.T., 1981. Structural corridors in Landsat lineament interpretation. *Mineralium Deposita*, 16:85-101.

OFFLER, R., 1963. Structural geology of the Strathalbyn Anticline, South Australia. *Transactions of the Royal Society of South Australia* 87:199-208.

OLIVER, G.J.H., 1978. Ilmenite-magnetite geothermometry and oxygen barometry in granulite and amphibilite facies gneisses from Doubtful Sound, New Zealand. *Lithos*, 11:147-153.

OFFLER, R & FLEMING, P.D., 1968. A synthesis of folding and metamorphism in the Mount Lofty Ranges, South Australia. *Journal of the Geology Society of Australia,* 15:245-266.

OLIVER, G.J.H., 1978. Ilmenite-magnetite geothermometry and oxygen barometry in granulite and amphibolite facies gneisses from Doubtful Sound, New Zealand. *Lithos*, 11:147-153.

OLIVER, N.H.S., 1996. Review and classification of structural controls on fluid flow during regional metamorphism. *Journal of Metamorphic Geology*, 14:477-492.

OLIVER, N.H.S., & ZAKOWSKI, S., 1995. Timing and geometry of deformation, low-pressure metamorphism and anatexis in the eastern Mt Lofty Ranges: the possible role of extension. *Australian Journal of Earth Science,* 42:501-507.

OLIVER, N.H.S., DIPPLE, G.M., CARTWRIGHT, I. & SCHILLER, J. 1998. Fluid flow and metasomatism in the genesis of the amphibolite-facies, pelite-hosted Kanmantoo copper deposit, South Australia. *American Journal of Science*, 298:181-218. (Refer Appendix 7 of this thesis.)

ORD, A. & OLIVER, N.H.S., 1997. Mechanical controls on fluid flow during regional metamorphism: some numerical models. *Journal of Metamorphic Geology*, 15:345-360.

PAIN, A.M., 1968. A study of a metadolerite dyke swarm in the Woodside district, South Australia. B.Sc. (Hons.) thesis, University of Adelaide.

PARKER, A.J., 1986. Tectonic development and metallogeny of the Kanmantoo Trough in South Australia. *Ore Geology Reviews,* 1:203-212.

PASSCHIER, C.W. & TROUW, R.A.J., 1996. *Microtectonics*. Springer-Verlag.

PATERSON, M.S., 1969. The ductility of rocks: pp. 377-392 in *Physics of Strength and Plasticity, The Orowan 65th Anniversary Volume*, A.S. Argon (ed.). The M.I.T. Press.

PATTERSON, D.J., 1969. Micrometric analyses of Kanmantoo ore products. *Mines Exploration Proprietary Limited report No. 1969/28MP.*

PATTISON, D.R.M., 1992. Stability of andalusite and sillimanite and the Al2SiO5 triple point: constraints from the Ballachulish aureole, Scotland. *Journal of Geology*, 100:423-446.

PERCHUK, L.L., 1967. The biotite-garnet geothermometer. *Dokl. AN SSSR*, 177:131-134.

PERKINS, W.G., 1984. Mount Isa silica dolomite and copper orebodies: the result of a syntectonic hydrothermal alteration system, *Economic Geology*, 79: 601-637.

PHINNEY, W.C., 1963. Phase equilibria in the metamorphic rocks of St. Paul Island and Cape North, Nova Scotia. *Journal of Petrology,* 4:90-130.

PIGAGE, L.C. & GREENWOOD, H.J., 1982. Internally consistent estimates of pressure and temperature: the staurolite problem. *American Journal of Science*, 282:943-969.

POTTER, T.F., 1990. Wattle Gully gold deposits. In *Geology of the Mineral Deposits of Australia and Papua New Guinea* (Ed. F.E. Hughes), pp. 1281-1285 (The Australasian Institute of Mining and Metallurgy).

PREISS, W.V., 1987. The Adelaide Geosyncline – late Proterozoic stratigraphy, sedimentation, palaeontology and tectonics. *Geological Survey of South Australia, Bulletin,* 53:438pp.

PREISS, W.V., 1995. Delamerian Orogeny. In: Drexel, J.F. & Preiss, W.V. (Editors), The Geology of South Australia. Vol 2. The Phanerozoic, South Australia. *Geological Survey Bulletin* 54(2):45-60.

PEARCE, J.A. & CANN, J.R., 1973. Tectonic setting of basic volcanic rocks determined using trace element analyses. *Earth and Planetary Science Letters*, 19:290-300.

PERCHUK, L.C. & GREEWOOD, H.J., 1982. Internally consistent estimates of pressure and temperature: the staurolite problem. *American Journal of Science*, 282:943-969.

PERCHUK, L.L.&LAVRENT'EVA, I.D., 1983. Experimental investigation of exchange equilibria in the system cordierite-garnet-biotite. *Adv. Phys. Geochemistry*, 3:199-239.

PLIMER, I.R., 1978. Proximal and distal stratabound ore deposits. *Mineralium Deposita (Berl.).* 13:345-353.

POOLE, L.E., 1969. The structural geology of an area south of Kanmantoo, South Australia, B.Sc. (Hons.) thesis, University of Adelaide (unpublished).

POWELL, C.McA., Preiss, W.V., GATEHOUSE, C.G., KRAPEZ, B. & LI, Z.X., 1994. South Australian record of a Rodinian epicontinental basin and its mid-neo-proterozoic breakup (~700 Ma) to form the Palaeo-Pacific Ocean. *Tectonophysics*, 237:113-140.

RAMSAY, J.G., 1962. The geometry and mechanics of formation of "similar" type folds. *Journal of Geology*, 70:309-327.

RAMSAY, J.B., 1967. *Folding and fracturing or rocks*. McGraw-Hill, New York, 568p.

RANKIN, L.R., CLOUGH, B.J. & GATEHOUSE, C.G., 1991. Early Palaeozoic mafic suites of the western Tasman Fold Belt System. *South Australia, Department of Mines and Energy. Report Book* 91/113.

RAST, N., 1963. Structure and metamorphism of the Dalradian rocks of Scotland: pp 123-175 in *The British Caledonides,* M.R.W. Johnson and F.H. Stewart (eds.). Oliver and Boyd, London, 280pp.

RAYNER, E.O., 1969. The copper ore of the Cobar region, New South Wales. *Geological Survey of NSW, Memoir 10*.

RIDGE, K., 1975. Report on the geology of sheet K/262, Callington Mines Exploration Pty Ltd., unpublished company report.

RIVERIN, G. & HODGSON, C.J., 1980. Wall-rock alteration at the Millenbach Cu-Zn mine, Noranda, Quebec. *Economic Geology*, 75 (3):424-444.

RICHARDSON, S.W., BELL, P.M. & GILBERT, M.C., 1968. Kyanite-sillimanite equilibrium between 700 and 1500. *American Journal of Science*, 266: 515-541.

ROBERTS, J.L. & SANDERSON, D.J., 1973. Oblique fold axes in the Dalradian rocks of the Southwest Highlands. *Scottish Journal of Geology*, 9:281-296.

ROBERTSON, I.D.M., 1974. The environmental features and petrogenesis of the mineral zones of Cobar, New South Wales. Ph.D. thesis (unpublished), The University of New England.

ROBIE, R.A. & HEMINGWAY, B.S., 1984. Entropies of kyanite, andalusite and sillimanite: additional constraints on the pressure and temperature of the $A1_2Si0_5$ triple point. *American Mineralogist*, 69:298-306.

ROSE, W.J., 1973. Report on the geology of sheets K/243 & 244, Kanmantoo Mines Exploration Pty Ltd, unpublished report.

ROSENFELD, J.L., 1955. Inter-facial tensions and the measurement of stress differences in metamorphic rocks. *American Journal of Science*, 253:574-579.

ROSS, C.S., 1935. Origin of the copper deposits of the Ducktown type in the southern Appalachian region. *United States geological Survey Professional Paper 179,* 165p.

RUMBLE, D. III, 1994. Water circulation in metamorphism. *Journal of Geophysical Research*, 99:15499-15502.

RUOFF, A.L., 1972. *Introduction to Materials Science*. Prentice-Hall.

RUSSELL, R.T. & LEWIS, B.R., 1965. Gold and copper deposits of the Cobar district, in *Geology of Australian Ore Deposits* (ed. J. McAndrew), pp. 411-419 (8^{th} Commonwealth Mining and Metallurgical Congress: Melbourne and the Australasian Institute of Mining and Metallurgy: Melbourne).

SALJE, E., 1986. Heat capacities and entropies of andalusite and sillimanite: the influence of fibrolitization on the phase diagram of the Al_2SiO_5 polymorphs. *American Mineralogist*, 71:1366-1371.

SANDERSON, D.J., 1972. Oblique folding in South-West England. *Proc. Ussher Soc.*, 2:438-441.

SANDERSON, D.J., 1973. The development of fold-axes oblique to the regional trend. *Tectonophysics*, 16:55-70.

SANDIFORD, M, MARTIN, N., ZHOU, S., & FRASER, G., 1991. Mechanical consequences of granite emplacement during high-T, low-P metamorphism and the origin of "anticlockwise" PT paths. *Early Planeteray Science Letters,* 107:164-172.

SANDIFORD, M., FODEN J., ZHOU, S. & TURNER, S., 1992. Granite genesis and the mechanics of convergent orogenic belts with application to the southern Adelaide Fold Belt. *Transactions of the Royal Society of Edinburgh: Earth Sciences,* 83:83-93.

SANDIFORD, M., FRASER, G., ARNOLD, J., FODEN, J. & FARROW, T., 1995. Some causes and consequences of High-T, Low-P metamorphism, Mount Lofty Ranges. *Australian Journal of Earth Sciences,* 42:241-247.

SANGSTER, D.F., 1979. Evidence of an exhalative origin for deposits of the Cobar district: *BMR Journal of Australian Geology Geophysics*, 4:15-24.

SAWKINS, F.J., 1984. Ore genesis by episodic dewatering of sedimentary basins: Application to giant Proterozoic lead-zinc deposits. *Geology*, 12:451-454.

SAXENA, S.K., 1969. Silicate solid solutions and geothermometry. Distribution of Fe and Mg between co-existing garnet and biotite. *Contributions to Mineralogy and Petrology,* 22:259-267.

SCHILLER, J.C., 1974a. Report on the geology of sheet K/242, Kanmantoo. Mines Exploration Pty Ltd., unpublished company report.

SCHILLER, J.C., 1974b. Report on the geology of sheet K/261, Kanmantoo. Mines Exploration Pty Ltd., unpublished company report.

SCHILLER, J.C., 1974c. Monthly report for June 1974. Mines Exploration Pty Ltd., unpublished company report.

SCHILLER, J.C., 1978. Age relationships between deformation, porphyroblast growth and sulphide mineralisation at Kanmantoo Mine, South Australia (abstract), *Geological Society of Australia Specialist Group in Tectonics And Structural Geology Conference*, South Mission Beach, September 1978. (Refer Appendix 5 of this thesis.)

SCHWERTNER, W.M., 1970. Hornblende lineations in the Trout Lake area, Lac La Rouge map sheet, Saskatchewan. *Canadian Journal of Earth Sciences*, 7:884-889.

SCOTT, K.M., 1978. Geochemical aspects of the alteration – mineralisation at Copper Hill, New South Wales, Australia. *Economic Geology*, 73(5):966-976.

SCOTT, A.K. & PHILLIPS, K.G., 1990. C.S.A. copper-lead-zinc deposit, Cobar, in: *Geology of the Mineral Deposits of Australia and Papua New Guinea* (Ed. F.E. Hughes). Pp 1337-1343. The Australasian Institute of Mining and Metallurgy; Melbourne.

SECCOMBE, P.K., SPRY, P.G., BOTH, R.A., JONES, M.T. & SCHILLER, J.C., 1985. Base metal mineralization in the Kanmantoo Group, South Australia: A regional sulfur isotope study. *Economic Geology*, 80:1824-1841. (Refer Appendix 7 of this thesis.)

SENIOR, A. & LEAKE, B.E., 1978. Regional metasomatism and the geochemistry of the Dalradian metasediments of Connemarra, Western Ireland. *Journal of Petrology*, 19:585-625.

SHARPE, E.N. & MACGEEHAN, P.J., 1990. Bendigo Goldfield. In *Geology of the Mineral Deposits of Australia and Papua New Guinea* (Ed. F.E. Hughes), pp. 1287-1296 (The Australasian Institute of Mining and Metallurgy).

SHAW, D.M., 1954. Trace elements in pelitic rocks, I, II. *Geological Society of America Bulletin*, 65:151-1167.

SIBSON, R.J., MOORE, J.M. & RANKIN, A.H., 1975. Seismic pumping – A hydrothermal fluid transport mechanism. *Geological Society of London Journal*, 131:653-659.

SKINNER, B.J., 1958. The geology and metamorphism of the Nairne Pyrite Formation, A sedimentary sulphide deposit in South Australia. *Economic Geology,* 53:546-562.

SMITH, J.V., 1968. The crystal structure of staurolite. Amer. Mineralogist, 53:1139-1155.

SPENCER, K.J. & LINDSLEY, D.H. 1981. A solution model for coexisting iron-titanium oxides. *American Mineralogist,* 66:1189-1201.

SPRIGG, R.C. & CAMPANA, B., 1953. The age and facies of the Kanmantoo Group. *Australian Journal of Science*, 16:12-14.

SPRY, A.H., 1969. *Metamorphic textures*. Permagon, Oxford. 350p.

SPRY, P.G., 1976. Base metal mineralisation in the Kanmantoo Group, South Australia, the South Hill, Bremer, and Wheal Ellen areas. B.Sc. (Hons.) thesis, University of Adelaide (unpublished).

SPRY, P.G., 2000. Sulfidation and oxidation haloes as guides in the exploration for metamorphosed massive sulphide ores. *Reviews in Economic Geology*, 11:149-162.

SPRY, P.G. & SCOTT, S.D., 1986. Zincian spinel and staurolite as guides to ore in the Appalachians and Scandinavian Caledonides. *Canadian Mineralogist*, 24:147-163.

SPRY, P.G., SCHILLER, J.C. & BOTH, R.A., 1988. Structure and metamorphic setting of base metal mineralisation in the Kanmantoo Group, South Australia. *The Australian Institute of Mining and Metallurgy, Bulletin and Proceedings,* 293(1):57-65. (Refer Appendix 7 of this thesis.)

SPRY, P.G., PETER, J.M. & SLACK, J.F, 2000. Meta-exhalites as keys in the search for metamorphosed ore deposits. *Reviews in Economic Geology*, 11:163-202.

STANTON, R.L., 1972. *Ore Petrology*. McGraw-Hill, New York, 713pp.

STEINHARDT, C.C., 1991. The microstructural anatomy of a major thrust zone on Fleurieu Peninsula, South Australia. *Australian Journal of Earth Sciences*, 38:139-150.

STEPHENS, M.B., GLASSON, M.J. & KEAYS, R.K., 1979. Structural and chemical aspects of metamorphic layering development in metasediments from Clunes, Australia. *American Journal of Science*, 279:129-160.

STERN, L.A., CHAMBERLAIN, C.P., BARNETT, D.E., & FERRY, J.M., 1992. Stable isotope evidence for regional-scale fluid migration in a Barrovian metamorphic terrane, Vermont, USA*: Contributions to Mineralogy and Petrology,* 112:475-489.

STRINGER, P & LAJTAI, E.Z., 1979. Cleavage in Triassic rocks of southern New Brunswick. *Canadian Journal of Earth Sciences*, 16:2165-2180.

STROMGARD, K.E., 1973. Stress distribution during the formation of boudinage and pressure shadows. *Tectonophysics*, 16:215-248.

SUPPEL, D.W. & SCHEIBNER, E., 1990. Lachlan Fold Belt in New South Wales – regional geology and mineral deposits, in: *Geology of the Mineral Deposits of Australia and Papua New Guinea* (Ed. F.E. Highs), pp 1321-1327. The Australasian Institute of Mining and Metallurgy; Melbourne.

SUPPEL, D.W., 1984. A study of mineral deposits in the Cobar Supergroup, Cobar region, New South Wales, M.Sc. thesis (unpublished), The University of New South Wales.

SWAGER, C.P., 1985. Syndeformational carbonate-replacement model for the copper mineralization at Mount Isa, northwest Queensland: a microstructural study, *Economic Geology*, 80:107-125.

SYMMES, G.H. & FERRY, J.M., 1991. Evidence from mineral assemblages for infiltration of pelitic schists by aqueous fluids during metamorphism. *Contributions to Mineralogy and Petrology*, 108:419-438.

TALBOT, J.L., 1962. A study of the structural and metamorphic relationships between older and younger Precambrian rocks in the Mt. Lofty – Olary arc, South Australia. Ph.D. thesis, University of Adelaide (unpublished).

TALBOT, J.L. & HOBBS, B.E., 1968. The relationship of metamorphic differentiation of other structural features at three localities. *Journal of Geology,* 76:581-587.

TAYLOR, S.R. 1965. The application of trace element data to to problem in petrology. In *Physics and Chemistry of the Earth, Volume 6,* L.H.Ahrens (ed.), Pergamon, Oxford.

THOMPSON, J.B., 1957. The graphical analysis of mineral assemblages in pelitic schists. *American Mineralogist*, 42:842-859.

THOMPSON, A.B., 1976. Mineral reactions in pelitic rocks: II, Calculation of some P-T-X (Fe-Mg) phase relations. *American Journal of Science*, 276:425-454.

THOMSON, B.P., 1953. Geology and ore occurrences in the Cobar district. 5th *Empire Mining and metallurgical Congress, Australia and New Zealand,* 1:863-896.

THOMSON, B.P., 1964. Precambrian rock groups in the Adelaide Geosyncline; a new subdivision – general outline. *Geological Survey of South Australia, Quarterly Notes*, 9:1-3.

THOMSON, B.P., 1965. Source and distribution of heavy metals in Cambrian and Marinoan shelf sediments in South Australia. In: McAndrew, J. (editor), *Geology of Australian Ore Deposits*. Australian Institute of Mining and Metallurgy, Melbourne, pp. 270-284.

THOMSON, B.P. 1969a. The Kanmantoo Group and Early Palaeozoic tectonics. In: Parkin, L.W. (ed.), *Handbook of South Australian geology*, 97-108. Government Printer, Adelaide.

THOMSON, B.P., 1969b. Geological atlas of South Australia, Adelaide map sheet, 1:250,000 series, Geological Survey South Australia.

THOMSON, B.P., 1970. A review of the Precambrian and Lower Palaeozoic tectonics of South Australia. *Transactions of the Royal Society of South Australia*, 94:193-221.

THOMSON, B.P, 1975. Kanmantoo Trough – regional geology and comments on mineralisation. In: Knight, C.L. (ed.), *Economic geology of Australia and New Guinea, I, Metals*. Australian Institute of Mining Metallurgy, Monograph 5, pp. 555-560.

THOMSON, B.P. & HORWITZ, R.C., 1962. Geological atlas of South Australia, Barker map sheet, 1:250,000 series, Geological Survey South Australia.

TOTEFF, S., 1977. The geology of the Adelaidean-Kanmantoo sequences in the eastern Mount Lofty Ranges. Ph.D. thesis, University of Adelaide (unpublished).

TOTEFF, S., 1994. Synsedimentary mineralisation in the Kanmantoo Trough. Field Excursion Guide, September 1994. *South Australia, Department of Mines and Energy. Report Book* 95/43.

TOTEFF, S., 1999. Cambrian sediment-hosted exhalative base metal mineralisation, Kanmantoo Trough, South Australia. *Geological Survey of South Australia, Report of Investigations 57.*

TRELOAR, J.G., 1980. Copper ore mining at Kanmantoo Mines Ltd., Kanmantoo, South Australia. In *Mining and Metal. Practices in Australia*, J.T. Woolcock (ed.), Aust. I.M.M. Monograph Series No. 10.

TRUEMAN, N.A., 1972. Mineralogical and petrological analysis of Hole KS31, Kanmantoo. *Mines Exploration Proprietary Limited report No. 1972/25NP.*

TRUEMAN, N.A., 1974. Kanmantoo metallurgy: mineralogical analysis of flotation products from samples of the 'C' Lens, 'D' Lens and O'Neill Zone. *Mines Exploration Proprietary Limited report No. 1974/38MP & 45MP.*

TUREKIAN, K.K. & WEDEPOHL, K.H., 1961. Distribution of the elements in some major units of the earth's crust. *Geological Society of America Bulletin*, 72(2):175-191.

TURNER, S.P. & FODEN, J., 1990. The nature of mafic magmatism through the evolution of the Adelaide Fold Belt and subsequent Delamerian Orogeny, *Mafic dykes and emplacement Mechanisms,* Balkema, Rotterdam, 431-435.

TURNER, S.P., SANDIFORD, M., & FODEN, J., 1992. Some geodynamic and compositional constraints on "post-orogenic" magmatism, *Geology,* 20:931-934.

VERNON, R.H. 1968. Microstructures of high-grade metamorphic rocks at Broken Hill, Australia. *Journal of Petrology*, 9:1-22.

VERNON, R.H., 1976 *Metamorphic processes: reactions and microstructure development*. Murby, London, 247p.

VERNON, R.H., 1977. Relationship between microstructures and metamorphic assemblages. *Tectonophysics*, 39:439-452.

VERNON, R.H., 1978. Porphyroblast-matrix microstructural relationships in deformed metamorphic rocks. *Geologisches Rundschau*, 67:288-305.

VERNON, R.H. & FLOOD, R.H., 1979. Microstructural evidence of time-relationships between metamorphism and deformation in the metasedimentary sequence of the northern Hill End Trough, New South Wales, Australia. *Tectonophysics*, 58:127-138.

VERWOERD, P.J. & CLEGHORN, J.H., 1975. Kanmantoo copper ore body. In: Knight, C.L. (ed.), *Economic geology of Australia and New Guinea, I, Metals*. Australian Institute of Mining Metallurgy, Monograph 5, pp. 560-565.

VINE J.D. & TOURTELOT, E.B., 1970. Geochemistry of black shale deposits – a summary report. *Economic Geology*, 65:253-272.

VOKES, F.M., 1969. A review of the metamorphism of sulphide deposits. *Earth-Science Reviews*, 5:99-143.

VOKES, F.M., 2000. Ores and metamorphism: Introduction and historical perspectives. *Reviews in Economic Geology*, 10:1-18.

VOLL, G., 1960. New work on petro-fabrics. *Liverpool and Manchester Geological Journal*, 2:503-567.

VON DER BORCH, C.C., 1980. Evolution of Late Proterozoic to Early Palaeozoic Adelaide Foldbelt, Australia: comparisons with post-Permain rifts and passive margins. *Tectonophysics*, 70:115-134.

VON D. NEMEC, J., 1978. Zinc in staurolite. *Chem. Erde. Bd.* 37:307-314.

WALTHER, J.V. & ORVILLE, P.M. 1982. Volatile production and transport in regional metamorphism. *Contributions to Mineralogy and Petrology,* 79:252.

WEISBROD, A., 1973. Cordierite-garnet equilibrium in the system Fe-Mn-Al-Si-O-H. *Carnegie Institute of Washington Yearbook*, 72:515-523.

WICKHAM, S.M. & TAYLOR, H.P., 1987. Stable isotope constraints on the origin and depth of penetration of hydrothermal fluids associated with Hercynian regional metamorphism and crustal anatexis in the Pyrenees. *Contributions to Mineralogy and Petrology,* 95:255-268.

WINKLER, H.G.F., 1976. *Petrogenesis of metamorphic rocks.* 4th edition. Springer-Verlag, New York, 224p.

WHITTLE, A.W.G., 1968. Flotation test No. 9, Kanmantoo copper plant (carried out in the Nairne pyrite plant). *Mines Exploration Proprietary Limited report No. 1968/8MP.*

WRIGHT, T.O. & HENDERSON, J.R., 1992. Volume loss during cleavage formation in the Meguna Group, Nova Scotia, Canada. *Journal of Structural Geology*, 14(3):281-290

WRIGHT, T.O.& PLATT, L.B., 1982. Pressure dissolution and cleavage in the Martinsburg Shale. *American Journal of Science,* 282:122-135.

ZEN, E., 1963. Components, phases and criteria of chemical equilibrium in rocks. *American Journal of Science*, 261:929-942.

ZEN, E. 1963. Components, phases, and criteria of chemical equilibrium in rocks. *American Journal of Science,* 261:929-42.

APPENDIX 1

LITHOLOGICAL CODING SYSTEM

The rocks in the Kanmantoo mine were mapped by making reference to:

- The mineral constituents
- The fabric
- The appearance of the main porphyroblast (usually andalusite)
- The hardness of the rock.

The mineral constituents were always referred to as the basic lithology but the other three features were not always noted, though at least one of them usually was noted.

Mineral constituents.

Suggested code (column 1)	**As mapped**	**Minerals**
1	GAB schist	Garnet-andalusite-biotite schist
2	GAB(Cl) schist	Similar to above but with minor chlorite
3	GABCl schist	Similar to above but with more chlorite
4	G(A)BCl schist	Similar to above but with less andalusite
5	GBCl(A) schist	Similar to above but with minor andalusite
6	GBCl schist	Garnet- biotite chlorite schist, biotite>chlorite
7	GClB schist	Similar to above, but chlorite > biotite
8	GCl schist	Garnet-chlorite schist
9	GB schist	Garnet-biotite schist

Fabric and Porphyroblasts and Hardness.

Fabric (column 2)		**Porphyroblasts** (column 3)		**Hardness** (column 4)	
Code	As mapped	Code	As mapped	Code	As mapped
x	not specified	x	not specified	x	not specif.
m	massive	d	distinct andalusite	v	very hard
w	weakly schistose	i	indistinct andalusite	h	hard
s	schistose	o	round andalusite	s	soft
v	very schistose	e	elongate andalusite		
g	gneissic	p	poikilo./ragged andalusite		
k	speckled	u	euhedral andalusite		
y	clotty	y	yellow andalusite		
b	bedded	q	quartz rich andalusite		
l	layered	h	abundant andalusite		
c	country	l	rare andalusite		
t	transitional	a	coarse andalusite		
		g	coarse garnet		
		b	coarse, equant biotite		
		s	coarse staurolite		

Examples.

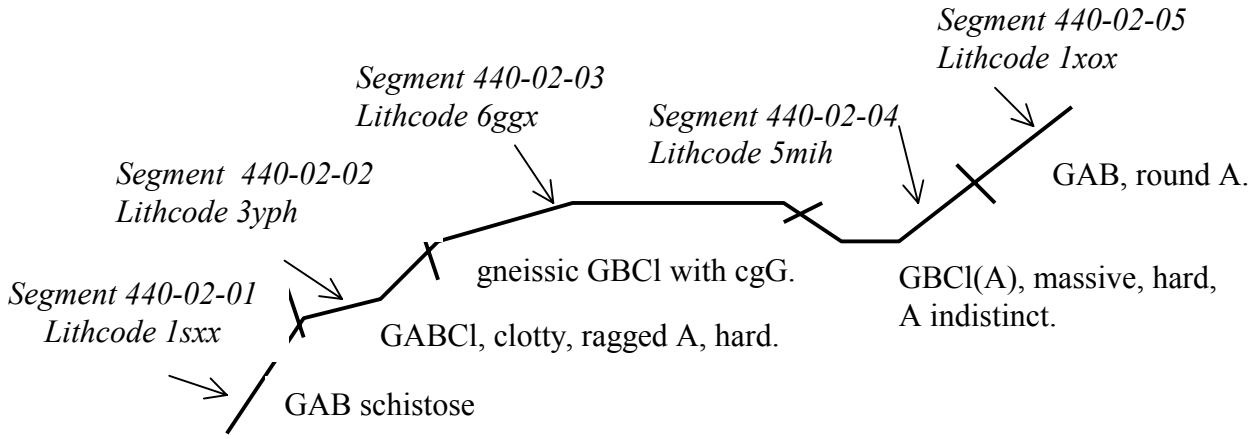
Code	Description as mapped
1sxx	GAB schistose
3srs	Soft, schistose GABCl schist with ragged andalusite
3yih	Hard GAB(3) schist, indistinct A
6ggx	gneissic GABCl schist with coarse grained garnets

Setting up database.

1. From original map sheets, each traverse was divided into segments, each representing one distinct mapped lithology. Each segment was assigned a number (called a *Segment No.*) and a code (called a *Lithcode*) for its lithology (see drawing).
2. An excel database with two columns was set up. The first column contains the id number for each segment and the second column contains the lithology code for that segment. The segment id number was used when the segments were digitised and is the link to the excel database.

Example of pit map sheet:

From Map Sheet No. 440-02:



Note. The line represents the mapped traverse along the face. The description below the line represents the rocks as they may have been mapped and is typical of real examples. The description above the line (in italics) represents the number assigned to the particular segment of the traverse (top) and also the suggested code for the lithology (bottom).

APPENDIX 2

SURVEYING AND GRIDS

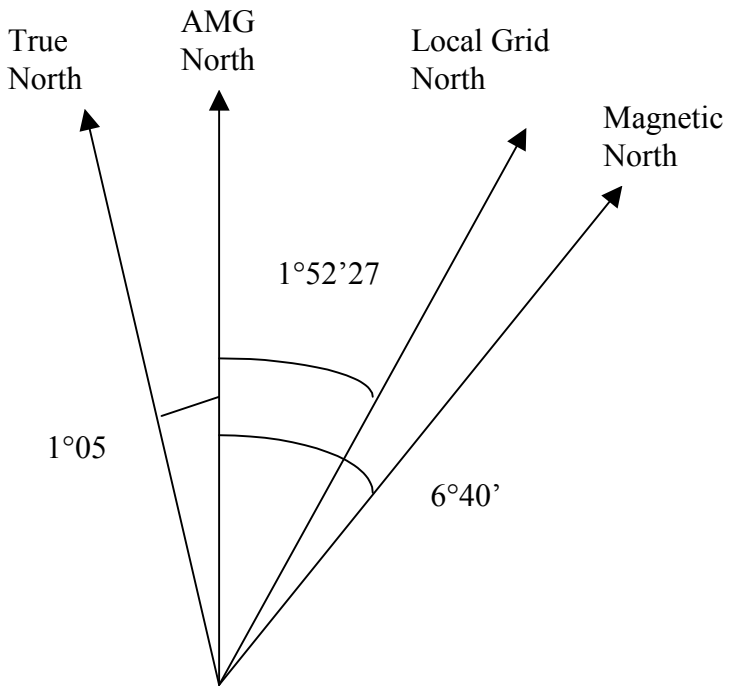
Regional grid

AMG Zone 54 (Australian Geodetic Datum, 1966). This metric grid was used for all regional mapping, for example the 1:5,000 scale mapping by Mines Exploration Proprietary Limited.

Local mine grid

The mining operations within the pit, underground and in the immediate mine surrounds used a local imperial grid, probably established ~1970. All records and mine data are referenced to this grid.

According to J. Ballinger (KML mine surveyor) grid N is 6° 57’ 27” east of true N.



Heights in the mine are referenced against mean sea level, thus RL 440’ is 440 feet above mean sea level.

APPENDIX 3

SAMPLE LOCATIONS

Sample No.	Northing	Easting	RL	Sample No.	Northing	Easting	RL
517-001	12100	4349	300	517-046	12169	4376	300
517-002	12022	4309	300	517-047	12164	4402	300
517-003	12025	4313	300	517-048	12135	4312	300
517-004	12092	4371	300	517-049	12100	4295	300
517-005	12093	4373	300	517-050	12196	4940	610
517-006	12097	4377	300	517-051	12196	4940	610
517-007	12122	4378	300	517-052	12287	4902	623
517-008	12128	4367	300	517-053	12270	4902	623
517-009	12132	4364	300	517-054	12553	3768	680
517-010	12130	4359	300	517-055	12003	4142	304
517-011	12127	4352	300	517-056	12035	4168	298
517-012	12125	4346	300	517-057	12031	4177	298
517-013	12122	4342	300	517-058	12033	4184	297
517-014	12122	4336	305	517-059	12037	4192	297
517-015	12119	4330	300	517-060	12041	4199	293
517-016	11900	4256	335	517-061	12041	4200	293
517-017	11896	4251	338	517-062	12031	4231	300
517-018	11890	4239	340	517-063	11985	4226	280
517-019	11936	4223	315	517-064	11978	4216	280
517-020	11940	4220	315	517-065	12715	4201	640
517-021	12170	4330	360	517-066	12064	4224	280
517-022	12178	4344	360	517-067	12055	4261	280
517-023	12172	4348	360	517-068	12043	4266	280
517-024	12161	4311	360	517-069	12037	4270	280
517-025	12172	4360	360	517-070	12037	4270	280
517-026	12172	4378	360	517-071	12293	3607	640
517-027	12180	4400	365	517-072	12293	3607	640
517-030	12448	4500	440	517-073	11817	3635	640
517-031	12440	4545	440	517-074	11817	3635	640
517-032	12440	4543	440	517-075	11878	4209	320
517-033	12430	4566	440	517-076	11882	4220	320
517-034	12402	4684	440	517-077	11976	3947	350
517-035	12322	4538	380	517-078	12521	4345	450
517-036	12321	4540	380	517-079	12549	4363	450
517-037	12318	4543	380	517-080	12560	4379	450
517-038	12314	4568	377	517-081	12562	4384	450
517-039	12314	4580	377	517-082	12563	4393	450
517-040	12255	4672	370	517-083	12564	4410	450
517-041	12189	4671	368	517-084	12563	4413	450
517-042	12107	4670	386	517-085	12057	4369	265
517-043	12149	4316	300	517-086	12060	4377	265
517-044	12154	4327	300	517-087	12124	4380	265
517-045	12168	4358	300	517-088	12126	4338	265

Sample No.	Northing	Easting	RL
517-089	11704	4421	440
517-090	11701	4464	440
517-091	12145	4200	300
517-092	12146	4267	300
517-093	12200	3785	445
517-094	12020	3780	440
517-095	11673	4190	355
517-096	11690	4205	355
517-101	11567	4590	603
517-102	11258	4544	450
517-103	11258	4521	450
517-104	11255	4541	455
517-105	11427	4672	455
517-106	11506	4726	455
517-107	11494	4742	349
517-108	11494	4742	349
517-109	11481	4760	349
517-110	12530	4380	440
517-111	12530	4380	440
517-112	12530	4380	440
517-114	13730	5790	720
517-115	12350	6690	720
517-116	13930	3290	720
517-117	13930	3290	720
517-118	13960	3080	720
517-119	13750	2820	720
517-120	11500	2500	720
517-121	11550	3300	720
517-122	10180	3260	720
517-123	10060	3730	720
517-124	11190	3250	720
517-125	11450	3390	720
517-126	11400	2600	720
517-128	11130	4653	385
517-133	12340	4760	440
517-134	12340	4760	440
517-135	12367	4707	440
517-136	12403	4650	440
517-137	12415	4597	440
517-138	12415	4596	440
517-139	12439	4541	440
517-140	12439	4539	440
517-141	12446	4526	440
517-142	12465	4477	440
517-143	12511	4412	440
517-144	12488	4344	440
517-145	12460	4312	440
517-146	12452	4167	440
517-147	12410	4065	440
517-148	12310	3918	440
517-149	12107	3772	440
517-160	12174	4347	400
517-178	12250	5920	720
517-179	12250	5900	720
517-180	12250	5900	720
517-181	9810	5230	720
517-182	9800	7030	720
517-183	9800	7030	720
517-184	9240	2750	720
517-185	7560	7830	720
517-186	11440	4080	720
517-187	10000	7900	720
517-212	10400	6390	720
517-214	10090	6090	720
517-215	10040	6140	720
517-216	9940	6110	720
517-217	9850	5110	720
517-218	9900	5110	720

APPENDIX 4

COMPOSITION-VOLUME ESTIMATIONS

Table A1. Estimates for GAB(2) schist and GAB(3) schist samples

	GAB(2) schist			GAB(3) schist		
	fv	Xn	% change	fv	Xn	% change
SiO_2	0.97	9.81	16	0.97	9.58	15
Al_2O_3	1.31	-0.69	-4	1.05	1.05	6
FeO	0.80	4.47	39	0.77	5.27	46
MnO	1.08	0.01	4	1.05	0.02	8
MgO	1.46	-0.76	-23	1.18	-0.18	-5
CaO	0.99	0.02	11	1.08	0.01	5
Na_2O	1.84	-0.06	43	1.09	-	-
K_2O	1.20	-0.21	-6	1.24	-0.31	-10
TiO_2	**1.11**	0.01	1	**1.10**	0.01	1
P_2O_5	**1.14**	-	-	**1.12**	-	-
S	0.22	6240	400	0.19	7460	478
Cu	5.38	-60	-79	0.20	352	463
Co	0.44	68	155	0.19	212	482
Zn	1.45	-21	-23	1.91	-38	-42
Ni	1.26	-7	-12	1.02	6	10
Ba	1.38	-64	-19	1.25	-35	-10
Sc	1.21	-1	-7	1.04	1	7
Sr	1.47	-3	-27	1.33	-2	-18
Rb	1.07	7	4	**1.14**	-3	-2
Y	**1.16**	-1	3	**1.11**	-	-
Th	1.31	-2	-12	0.61	-2	-12
Zr	0.86	44	30	**1.15**	-4	3
Nb	**1.17**	-1	-7	**1.17**	-1	-6

Notes.

1. GAB(2) schist : only one sample available, Sample No. 517-139. Xn was calculated using fv = 1.12.
2. GAB(2) schist : mean of 4 samples, Sample no.s 517-044, -067, -143, -145. Xn was calculated using fv = 1.12.
3. Both calculations assume that mean GAB(1) schist was the protolith.
4. The bold values of fv were used to obtain the assumed fv value.
5. Refer to text (Chapter 8.3.2) for explanations of fv and Xn.

Table A2. Composition-volume estimates for lode schist (1a).

	fv	Xn	% change
SiO_2	0.96	22.21	36
Al_2O_3	**1.31**	-	-
FeO	0.59	14.1	124
MnO	0.84	0.14	57
MgO	0.98	1.11	34
CaO	1.17	0.02	12
Na_2O	2.57	-0.07	-49
K_2O	2.08	-1.20	-37
TiO_2	1.24	0.04	6
P_2O_5	**1.30**	-	-
S	0.18	9570	610
Cu	0.04	2590	3400
Co	0.49	73	166
Zn	1.22	-35	-38
Ni	0.80	38	63
Ba	2.21	-139	-41
Sc	1.48	-2	-12
Sr	1.87	-3	-30
Rb	1.89	-48	-31
Y	0.92	13	42
Th	1.47	-2	-13
Zr	1.16	19	13
Nb	**1.33**	-	1

Notes.

1. Lode schist (1a) : mean of 8 samples, no.s 517-010, -012B, -024, -057, -066, -076A, -095, -112, -144.
2. Xn was calculated using fv = 1.31.
3. The calculation assumes that mean GAB(1) schist was the protolith.

Table A3. Composition-volume estimates for lode schist (1a), (1b) and GAB(2) schist.

Protolith:	Mean GAB(1) schist			Mean GAB(1) schist			GAB(2) schist
Final:	Lode schist (1b)			Lode schist (1c)			Lode schist (1c)
	fv	Xn	% change	fv	Xn	% change	fv
SiO_2	1.00	15.25	25	1.00	28.1	45	1.00
Al_2O_3	**1.25**	-0.03	0	**1.42**	0.51	3	**1.17**
FeO	0.46	19.25	169	0.67	13.45	118	0.80
MnO	0.55	0.32	128	0.96	0.13	52	0.86
MgO	0.88	1.38	42	1.21	0.69	21	0.80
CaO	1.17	0.01	7	1.06	0.07	40	1.03
Na_2O	6.27	-0.11	-80	1.23	0.02	14	0.62
K_2O	27	-3.09	-95	1.01	1.44	44	0.81
TiO_2	**1.26**	-0.01	-1	**1.35**	0.06	8	**1.17**
P_2O_5	**1.26**	-	-	1.50	0	-3	-1.26
S	0.27	-1560	-100	0.23	7784	499	1.04
Cu	0.02	4100	5400	2.93	-40	-52	0.54
Co	0.41	90	206	0.28	202	459	0.57
Zn	2.20	-39	-43	1.03	33	36	0.71
Ni	3.45	-38	-64	**1.34**	2.8	5	1.06
Ba	2.95	-198	-58	1.94	-96	-28	1.41
Sc	1.61	-3	-22	**1.38**	0.5	4	**1.14**
Sr	2.02	-4	-38	1.77	-2.3	-21	1.20
Rb	16	-143	-92	0.70	155	100	0.65
Y	0.53	42	137	1.49	-3.4	--11	1.29
Th	**1.20**	1	4	1.82	-3.9	-23	1.39
Zr	**1.24**	2	1	1.11	38	26	1.29
Nb	**1.30**	-1	-4	**1.31**	1.2	7	**1.12**

Notes.

1. Lode schist (1b) : Only one sample available, no. 517-045. Xn was calculated using fv = 1.25.
2. Lode schist (1c) : Only one sample available, no. 517-140. Xn was calculated using fv = 1.40.
3. The bold values of fv were used to obtain the assumed fv value.
4. Refer to text (Chapter 8.3.2) for explanations of fv and Xn.

Table A4. Estimates for lode schist (2a) and (2b) samples

	Lode schist (2a)			Lode schist (2b)		
	fv	Xn	% change	fv	Xn	% change
SiO_2	1.75			1.87	-43.9	-71
Al_2O_3	0.35			**0.60**	-1.26	-8
FeO	0.50			0.47	2.03	18
MnO	0.87			**0.54**	0.01	4
MgO	0.71			**0.54**	0.09	3
CaO	0.50			**0.53**	0.01	5
Na_2O	1.25			0.47	0.02	15
K_2O	1.14			0.79	-0.97	-30
TiO_2	0.75			**0.58**	-0.04	-5
P_2O_5	0.48			**0.51**	0.01	7
S	0.71			0.15	3815	245
Cu	0.39			0.66	-13	-17
Co	1.08			0.31	34	77
Zn	1.69			1.32	-53	-58
Ni	0.64			**0.52**	-22	-37
Ba	0.93			0.71	-76	-22
Sc	0.95			**0.54**	1	7
Sr	0.54			0.40	4	36
Rb	0.93			1.20	-84	-54
Y	0.63			0.67	-5	-16
Th	0.89			0.94	-7	-41
Zr	0.36			**0.53**	7	5
Nb	0.85			0.73	-4	-24

Notes.

1. Lode schist (2a) ; Only one sample available, no. 517-177.
2. Lode schist (2b) ; Only one sample available, no. 517-163. Xn was calculated using fv = 0.55.
3. Both calculations assume that mean GAB(1) schist was the protolith.
4. The bold values of fv were used to obtain the assumed fv value.
5. Refer to text (Chapter 8.3.2) for explanations of fv and Xn.

Table A5. Estimates for lode schist (3) and (4) samples

	Lode schist (3)			Lode schist (4)		
	fv	Xn	% change	fv	Xn	% change
SiO_2	1.56	-32.29	-52	1.04	3.64	6
Al_2O_3	**0.73**	-0.38	2	**1.14**	0.54	-3
FeO	0.23	26.49	232	0.90	2.53	22
MnO	0.20	0.68	272	1.02	0.02	8
MgO	0.56	1.10	34	1.33	-0.55	-17
CaO	0.38	0.18	1	1.16	0.05	25
Na_2O	2.11	-0.09	-65	0.53	0.15	108
K_2O	2.51	-2.27	-70	0.73	1.65	51
TiO_2	**0.80**	-0.05	-7	**1.09**	0.01	1
P_2O_5	**0.78**	-0.01	-4	**1.09**	-	-
S	0.03	38200	2450	0.42	2520	162
Cu	0.01	7500	9900	1.36	23	31
Co	0.32	60	136	0.79	18	41
Zn	**0.75**	-	-	1.02	7	8
Ni	1.58	56	96	1.42	-14	-23
Ba	3.05	-259	-76	1.06	11	3
Sc	1.04	-4	-29	0.89	3	22
Sr	3.70	-9	-82	0.53	12	105
Rb	1.59	-82	-53	0.59	134	87
Y	3.90	-25	-81	1.26	-4	-14
Th	0.28	28	165	1.27	-2	-14
Zr	**0.80**	-9	-6	1.02	12	8
Nb	**0.79**	-1	-6	**1.12**	-	-2

Notes.

1. Lode schist (3) : one sample available, no. 517-061. Xn was calculated using fv = 0.75.
2. Lode schist (4) : one sample available, no. 517-128. Xn was calculated using fv = 1.10.
3. Both calculations assume that mean GAB(1) schist was the protolith.
4. The bold values of fv were used to obtain the assumed fv value.
5. Refer to text (Chapter 8.3.2) for explanations of fv and Xn.

APPENDIX 5 (refer to CD)

ROCK GEOCHEMICAL ANALYSES

Notes:

1 **Sample numbers**
All sample numbers are prefixed by 517-

2 **Units**.
Results for SiO2 to CO2, Total and loss on ignition (LOI) are in per cent.
Results for Cu to V are in parts per million (ppm).
Density (D) is in grams per cubic centimetre.

3 **Type of samples used**.
SiO2 to P2O5 was measured on samples that were ignited at ~1,000 C.
The remaining results were measured on unignited samples.

4 **Abbreviations**. nd = not determined, bd = below detection limit, tr = trace.

5 **Iron**. Total iron in the sample is shown as ferrous (FeO) equivalent, except the sulphide rich samples 517-221 and 517-222 where it is shown as metallic (Fe) iron.

APPENDIX 6 (refer to CD)

ELECTRON MICROPROBE ANALYSES

APPENDIX 5
ROCK GEOCHEMICAL ANALYSES

Notes:

1 **Sample numbers**
All sample numbers are prefixed by 517-

2 **Units**.
Results for SiO2 to CO2, Total and loss on ignition (LOI) are in per cent.
Results for Cu to V are in parts per million (ppm).
Density (D) is in grams per cubic centimetre.

3 **Type of samples used**.
SiO2 to P2O5 was measured on samples that were ignited at ~1,000 C.
The remaining results were measured on unignited samples.

4 **Abbreviations**. nd = not determined, bd = below detection limit, tr = trace.

5 **Iron**. Total iron in the sample is shown as ferrous (FeO) equivalent, except the sulphide rich samples 517-221 and 517-222 where it is shown as metallic (Fe) iron.

Sample No 517-	001D	004	010	012	024	027	044	045
%								
SiO2	51.56	58.36	57.89	62.10	63.53	62.26	62.90	56.98
Al2O3	13.73	12.25	12.65	9.60	10.59	14.07	14.70	11.90
FeO	15.13	20.35	19.78	19.04	18.69	16.37	13.54	22.57
MnO	0.37	0.42	0.33	0.29	0.44	0.39	0.23	0.42
MgO	3.33	3.84	3.80	2.73	2.44	2.74	2.42	3.43
CaO	8.09	0.15	0.11	0.15	0.14	0.18	0.17	0.18
Na2O	1.49	0.03	0.04	0.01	0.05	0.09	0.11	0.02
K2O	0.36	0.47	2.06	0.45	0.38	1.46	2.70	0.11
TiO2	0.65	0.54	0.53	0.49	0.42	0.67	0.64	0.54
P2O5	0.41	0.10	0.08	0.10	0.10	0.16	0.11	0.11
S	0.041	0.328	0.314	1.713	0.906	0.080	0.776	0.523
C	nd	nd	nd	nd	nd	nd	nd	nd
CO2	0.01	nd	nd	nd	nd	nd	nd	nd
ppm								
Cu	0	1,710	620	9,300	1,180	61	410	3,080
Co	9	nd	115	139	82	93	444	99
Ni	25	nd	83	69	47	35	47	16
Pb	tr	nd	nd	nd	tr	tr	nd	nd
Zn	76	82	39	61	40	39	72	38
Ba	nd	63	180	51	nd	nd	252	107
Sc	nd	7.2	9.2	6.4	nd	nd	12.8	7.7
Sr	nd	3.8	3.3	6.4	nd	nd	8.7	4.7
Rb	nd	25	106	26	nd	nd	142	8.6
Y	nd	38	38	22	nd	nd	22	54
Th	nd	11.7	12.2	8.6	nd	nd	15.1	13
Zr	nd	124	78	149	nd	nd	117	111
Nb	nd	11.2	12.7	9.9	nd	nd	13.9	12
V	nd	nd	nd	nd	nd	nd	107	nd
Total %	95.18	97.05	97.71	97.66	97.82	98.49	98.46	97.14
LOI	0.56	0.63	0.53	0.09	0.09	0.09	0.76	0.62
D	nd	3.164	2.972	nd	nd	nd	2.967	3.142

Sample No 517-	053	055	057	060am	060nam	061B	066	067
%								
SiO2	60.87	42.91	54.31	34.84	51.10	30.82	64.72	59.18
Al2O3	17.01	20.46	15.23	13.39	14.13	16.65	11.73	15.43
FeO	13.62	25.12	21.44	34.16	23.55	38.85	15.62	16.04
MnO	0.30	0.42	0.39	0.85	0.64	0.35	0.20	0.24
MgO	2.53	4.31	4.18	3.28	4.65	4.05	3.50	3.08
CaO	0.09	0.16	0.13	0.30	0.14	0.39	0.16	0.14
Na2O	0.10	0.20	0.05	0.07	0.12	0.09	0.05	0.10
K2O	3.52	3.22	1.95	0.14	2.92	1.10	1.53	2.69
TiO2	0.69	0.92	0.64	0.40	0.68	0.68	0.58	0.63
P2O5	0.07	0.11	0.11	0.18	0.08	0.15	0.13	0.10
S	tr	0.007	0.009	5.834	0.046	5.155	0.022	0.958
C	nd	nd	nd	nd	nd	bd	nd	nd
CO2	0.01	nd	nd	nd	nd	bd	nd	nd
ppm								
Cu	416	22	78	46,180	145	10,890	147	833
Co	52	45	57	95	41	394	57	274
Ni	33	56	82	21	29	75	71	80
Pb	tr	tr	nd	tr	tr	nd	nd	nd
Zn	44	71	43	217	78	199	42	25
Ba	nd	nd	255	nd	nd	90	194	272
Sc	nd	nd	11.6	nd	nd	8	8.9	13.3
Sr	nd	nd	3.6	nd	nd	2.3	6	8.4
Rb	nd	nd	111	nd	nd	82	80	142
Y	nd	nd	43	nd	nd	5.4	20	37
Th	nd	nd	10.6	nd	nd	88	11.2	10.7
Zr	nd	nd	108	nd	nd	153	154	98
Nb	nd	nd	13.6	nd	nd	14.5	13.6	13.7
V	nd	nd	nd	nd	nd	148	nd	nd
Total %	98.86	97.86	98.52	98.10	98.09	99.50	98.32	98.77
LOI	0.66	-0.60	-0.42	1.33	-0.07	1.69	0.42	0.37
D	2.954	nd	3.22	nd	nd	nd	2.902	2.90

Sample No 517-	072	076A	076B	077L	077V	087	093	095
%								
SiO2	59.54	65.47	30.13	57.55	31.83	58.91	63.45	64.81
Al2O3	20.00	9.99	28.89	10.62	12.88	11.93	14.48	12.29
FeO	8.93	15.81	24.41	21.78	41.43	20.57	11.18	15.18
MnO	0.26	0.21	0.40	0.34	0.46	0.52	0.27	0.29
MgO	4.12	3.02	5.08	3.63	4.48	3.27	3.38	2.86
CaO	0.16	0.17	0.35	0.24	0.28	0.23	0.19	0.17
Na2O	0.14	0.05	0.21	0.13	0.18	0.35	0.11	0.04
K2O	3.54	1.49	4.00	3.00	3.32	0.54	2.98	0.96
TiO2	0.88	0.52	1.27	0.52	0.51	0.57	0.72	0.62
P2O5	0.15	0.13	0.29	0.10	0.13	0.16	0.15	0.12
S	0.011	2.001	1.394	0.023	0.636	0.552	0.430	0.606
C	nd	nd	nd	bd	bd	nd	nd	nd
CO2	nd	nd	nd	0.02	0.02	nd	nd	nd
ppm								
Cu	109	1,790	1,010	7	349	2,450	57	122
Co	32	114	108	20	27	77	54	48
Ni	77	65	68	34	41	50	77	73
Pb	nd	nd	nd	20	32	nd	nd	nd
Zn	155	41	239	149	210	43	86	26
Ba	399	137	nd	nd	nd	75	295	117
Sc	21	7.4	nd	nd	nd	9.4	13	9.3
Sr	6.4	7.3	nd	nd	nd	7.2	8.3	63
Rb	193	73	nd	nd	nd	27	156	45
Y	47	38	nd	nd	nd	44	26	35
Th	19.5	7.5	nd	nd	nd	15.9	14.5	11.3
Zr	152	12.2	nd	nd	nd	193	157	138
Nb	18.9	11.3	nd	nd	nd	12	16.8	12.8
V	nd	nd	nd	nd	nd	nd	nd	nd
Total %	97.85	99.09	96.57	97.98	96.22	97.90	97.44	98.02
LOI	1.58	1.58	1.42	-0.08	0.09	0.53	0.86	0.56
D	2.73	2.92	nd	3.085	nd	3.08	2.895	2.98

Sample No 517-	112	116	121	128	130	133	134	135
%								
SiO2	55.71	63.22	59.34	60.89	57.13	57.78	71.26	59.03
Al2O3	12.63	17.29	16.96	14.49	18.99	19.68	10.34	18.82
FeO	22.83	12.30	12.27	12.90	13.97	11.41	9.76	14.03
MnO	0.39	0.12	0.23	0.25	0.23	0.23	0.11	0.35
MgO	2.96	1.69	3.61	2.52	3.11	3.02	2.46	2.41
CaO	0.19	0.15	0.15	0.22	0.18	0.18	0.17	0.25
Na2O	0.07	0.12	0.21	0.26	0.16	0.13	0.13	0.09
K2O	1.35	2.32	3.86	4.53	2.38	3.82	3.07	2.21
TiO2	0.62	0.78	0.75	0.69	0.74	0.81	0.50	0.86
P2O5	0.13	0.15	0.15	0.14	0.13	0.14	0.12	0.15
S	0.666	0.005	0.004	0.378	0.893	0.001	0.008	0.015
C	nd	nd	nd	nd	nd	bd	bd	nd
CO2	nd	nd	nd	nd	nd	0.01	bd	nd
ppm								
Cu	2,860	23	nd	92	48	9	8	10
Co	84	7	nd	57	63	47	47	57
Ni	83	38	nd	43	125	62	38	61
Pb	nd	tr	nd	nd	nd	nd	nd	nd
Zn	39	25	nd	91	63	136	67	49
Ba	94	nd	482	328	308	363	300	241
Sc	9.3	nd	18.7	15.8	17.3	19	10.2	15.2
Sr	7	nd	10.7	21	11.9	11.7	8.7	11.1
Rb	73	nd	196	268	145	174	146	114
Y	42	nd	33	25	39	32	25	36
Th	16.6	nd	16.1	13.6	17.5	16.7	9.5	16.2
Zr	130	nd	125	149	112	141	131	171
Nb	12.8	nd	17.5	15.4	17	18.5	12.3	18.6
V	nd	nd	nd	nd	nd	143	nd	nd
Total %	97.89	98.15	97.62	97.38	98.01	97.33	98.01	98.30
LOI	0.34	0.51	1.00	1.30	0.95	0.97	0.68	0.08
D	3.15	nd	2.79	2.84	2.97	2.913	2.788	3.04

Sample No 517-	136	137	138	139	140	141	142	143
%								
SiO2	60.04	62.23	61.21	63.62	61.85	68.77	59.70	64.73
Al2O3	18.21	15.95	16.79	13.71	11.44	10.07	12.99	14.09
FeO	11.59	10.39	10.38	14.03	17.02	13.38	17.19	13.11
MnO	0.21	0.27	0.29	0.23	0.26	0.15	0.24	0.26
MgO	3.21	3.89	4.14	2.23	2.72	2.03	2.96	2.42
CaO	0.18	0.21	0.22	0.19	0.18	0.18	0.16	0.20
Na2O	0.11	0.11	0.10	0.07	0.11	0.08	0.11	0.13
K2O	3.49	3.64	3.69	2.68	3.21	2.04	2.81	2.36
TiO2	0.75	0.74	0.75	0.66	0.55	0.53	0.64	0.63
P2O5	0.13	0.15	0.18	0.13	0.10	0.14	0.14	0.15
S	0.037	0.001	0.001	0.690	0.643	1.828	1.010	0.623
C	nd	bd	nd	nd	nd	nd	bd	nd
CO2	nd	bf	nd	nd	nd	nd	bd	nd
ppm								
Cu	70	3	5	14	25	24	800	362
Co	48	30	31	99	169	181	109	87
Ni	52	54	55	47	43	42	40	42
Pb	nd	nd	nd	nd	nd	nd	nd	nd
Zn	105	161	162	62	85	52	64	29
Ba	342	383	407	247	170	213	281	287
Sc	16.7	16.9	16.9	11.5	9.6	8.7	10.7	12.7
Sr	8.8	8.6	10.5	7.4	5.9	7.8	7.7	80
Rb	162	175	180	143	213	104	150	122
Y	29	26	34	27	20	25	57	23
Th	16.1	16.2	17.7	12.9	9.2	11.8	12.6	12.2
Zr	130	158	174	171	129	170	145	147
Nb	17	15.4	17.1	14.4	12.5	12	13.9	13.8
V	nd	nd	nd	nd	89	nd	nd	nd
Total %	98.06	97.69	97.86	98.33	98.18	99.28	98.12	98.82
LOI	0.66	0.67	0.68	0.63	0.42	0.98	0.81	0.35
D	2.91	2.867	2.87	2.92	3.002	2.895	2.99	3.041

Sample No 517-	144	145	146	147	148	149	150	163
%								
SiO2	68.45	60.92	62.44	64.48	63.67	62.21	65.66	31.30
Al2O3	10.14	15.34	14.92	15.28	14.23	17.76	13.02	25.63
FeO	13.68	14.92	14.42	10.92	12.80	10.06	9.99	23.06
MnO	0.17	0.31	0.54	0.20	0.19	0.25	0.26	0.44
MgO	2.41	2.80	2.50	3.02	2.93	3.61	4.03	5.78
CaO	0.18	0.20	0.23	0.19	0.18	0.19	2.08	0.34
Na2O	0.09	0.13	0.10	0.12	0.12	0.17	1.08	0.27
K2O	2.07	2.36	2.00	2.97	2.75	3.14	3.72	3.89
TiO2	0.51	0.70	0.77	0.70	0.71	0.76	0.64	1.20
P2O5	0.10	0.14	0.15	0.15	0.13	0.16	0.17	0.28
S	1.141	0.757	0.531	0.103	0.682	0.158	0.004	0.923
C	nd	nd	nd	nd	bd	bd	nd	nd
CO2	nd	nd	nd	nd	bd	bd	nd	nd
ppm								
Cu	620	475	221	100	307	109	63	109
Co	76	91	76	42	43	35	36	134
Ni	39	57	44	48	44	52	61	109
Pb	nd	nd	nd	nd	nd	nd	nd	nd
Zn	37	42	33	70	36	88	252	65
Ba	159	251	168	375	304	294	190	459
Sc	7	12.7	12	13.8	12.9	15.2	13.6	25
Sr	5.1	7.2	9.9	12.1	7.8	7.8	74	26
Rb	113	116	102	148	143	155	222	122
Y	21	31	35	29	23	28	19.4	44
Th	7.3	14.2	13.2	16.1	14.8	17.7	136	17.3
Zr	97	139	162	136	145	147	171	268
Nb	10.8	15.2	13.9	15.9	17.6	17.2	15.8	22
V	nd	109	nd	114	nd	nd	nd	nd
Total %	99.06	98.71	98.69	98.24	98.50	98.56	100.78	93.25
LOI	0.50	0.34	0.24	0.52	0.68	0.65	1.00	5.20
D	2.998	3.053	3.024	2.887	2.934	2.896	nd	3.062

Sample No 517-	168	173	177	178	179	180	181	182
%								
SiO2	70.24	72.93	29.60	63.07	65.97	65.60	65.71	63.74
Al2O3	12.98	12.18	38.16	15.89	12.98	13.09	13.09	17.54
FeO	3.22	3.03	19.06	9.71	12.34	12.21	7.07	7.93
MnO	0.09	0.03	0.24	0.18	0.15	0.16	2.24	0.10
MgO	0.83	0.61	3.83	3.94	1.66	1.49	1.96	3.75
CaO	1.51	1.50	0.32	0.24	0.09	0.15	0.42	0.24
Na2O	0.12	3.69	0.09	0.22	0.15	0.18	0.54	0.25
K2O	6.34	3.63	2.38	3.74	3.00	3.48	5.50	3.22
TiO2	0.45	0.43	0.82	0.79	0.54	0.70	0.66	0.83
P2O5	0.09	0.09	0.26	0.17	0.08	0.15	0.10	0.19
S	0.157	0.009	0.181	0.002	0.002	0.003	0.001	0.005
C	nd	nd	nd	nd	nd	nd	nd	nd
CO2	2.19	0.38	nd	nd	nd	nd	nd	nd
ppm								
Cu	nd	nd	162	8	8	103	7	3
Co	nd	nd	34	24	16	11	11	9
Ni	nd	nd	67	80	54	58	42	74
Pb	nd	nd	nd	tr	tr	tr	22	tr
Zn	nd	nd	45	131	45	38	203	51
Ba	nd	nd	309	848	356	351	629	753
Sc	nd	nd	12.3	16.7	10.6	11.4	9.8	23
Sr	22	79	16.9	25	21	29	92	14
Rb	239	125	139	154	172	167	298	151
Y	46	33	41	37	20	23	22	38
Th	28	31	15.8	17	8	11	13	18
Zr	nd	nd	350	208	104	184	166	186
Nb	nd	nd	16.7	16.2	12.7	15.4	14.5	17.7
V	nd	nd	nd	nd	nd	nd	nd	nd
Total %	98.25	98.54	95.06	98.11	97.04	97.31	97.44	97.93
LOI	3.73	1.34	0.50	0.34	1.57	1.02	1.13	0.87
D	2.62	2.652	2.998	3.053	nd	nd	nd	nd

Sample No 517-	183	185	186	201	202	203	207	221
%								
SiO2	59.92	59.57	60.82	66.20	36.91	38.04	49.26	nd
Al2O3	17.77	17.36	18.78	11.04	28.16	11.69	17.87	nd
FeO	10.37	10.73	6.85	15.99	16.78	35.04	8.09	46.47
MnO	0.19	0.18	0.07	0.60	0.37	0.56	0.17	nd
MgO	4.15	3.83	3.32	2.37	5.76	5.03	6.59	nd
CaO	0.16	0.14	0.93	0.62	0.15	0.61	12.59	nd
Na2O	0.26	0.17	1.61	0.11	0.34	0.12	2.40	nd
K2O	3.85	4.01	4.06	0.95	6.55	0.60	0.40	nd
TiO2	0.80	0.75	0.81	0.69	1.53	0.76	1.04	nd
P2O5	0.15	0.15	0.17	0.24	0.15	0.30	0.13	nd
S	0.003	0.002	0.002	0.049	0.010	1.812	1.187	19.490
C	nd	nd	bd	nd	bd	nd	bd	bd
CO2	nd	nd	bd	nd	bd	nd	bd	bd
ppm								
Cu	11	82	3	92	93	1,798	nd	136,300
Co	11	17	13	42	28	57	nd	nd
Ni	82	58	74	28	44	26	nd	20
Pb	tr	tr	tr	tr	tr	tr	22	10
Zn	39	93	24	48	53	160	nd	241
Ba	662	55	1000	nd	nd	nd	nd	nd
Sc	21	19.3	23	nd	nd	nd	nd	nd
Sr	7	11	121	nd	nd	nd	nd	nd
Rb	184	171	186	nd	nd	nd	nd	nd
Y	32	28	29	nd	nd	nd	nd	nd
Th	16	19	19	nd	nd	nd	nd	nd
Zr	173	142	142	nd	nd	nd	nd	nd
Nb	17.8	16.5	17.6	nd	nd	nd	nd	nd
V	nd	nd	nd	nd	nd	nd	nd	nd
Total %	97.75	96.96	97.58	98.88	96.73	94.77	99.73	79.62
LOI	0.91	1.36	1063.00	0.03	1.48	-0.27	-0.27	nd
D	nd	2.814	nd	nd	nd	nd	nd	nd

Sample No 517-	222	227	2870	3070	3370	3810
%						
SiO2	nd	77.03	62.43	57.62	64.40	63.66
Al2O3	nd	1.71	14.97	19.38	15.35	16.52
FeO	44.88	2.96	7.95	6.63	5.79	5.97
MnO	nd	0.08	0.38	0.13	0.14	0.11
MgO	nd	0.24	3.74	3.57	3.29	3.22
CaO	nd	0.01	1.55	2.83	3.14	1.42
Na2O	nd	0.06	0.17	1.70	2.56	1.70
K2O	nd	0.70	4.73	4.04	2.57	4.28
TiO2	nd	0.07	0.84	0.70	0.77	0.79
P2O5	nd	0.01	0.11	0.14	0.16	0.15
S	29.060	5.530	0.004	0.045	0.066	0.003
C	bd	0.05	nd	nd	nd	nd
CO2	bd	bd	nd	nd	nd	nd
ppm						
Cu	144,300	293	nd	nd	nd	nd
Co	741	7	nd	nd	nd	nd
Ni	53	27	nd	nd	nd	nd
Pb	515	15560	bd	bd	nd	nd
Zn	632	84770	nd	nd	nd	nd
Ba	nd	nd	nd	nd	nd	nd
Sc	nd	nd	nd	nd	nd	nd
Sr	nd	4.5	nd	nd	nd	nd
Rb	nd	52	nd	nd	nd	nd
Y	nd	bd	nd	nd	nd	nd
Th	nd	94	nd	nd	nd	nd
Zr	nd	7.6	nd	nd	nd	nd
Nb	nd	0.3	nd	nd	nd	nd
V	nd	nd	nd	nd	nd	nd
Total %	88.56	98.53	96.87	96.79	98.24	97.82
LOI	nd	3.11	1.24	1.44	0.63	1.56
D	nd	nd	nd	nd	nd	nd

ELECTRON MICROPROBE ANALYSES

Information about the tables:

Mineral abbreviations are as used in the text.

Site	refers to the part of a grain probed, as shown below:
R	rim
C	core
S	same grain as immediately preceding analysis
RS	as above - rim
RSO	as above - opposite rim
CS	as above - core
AS	as above - adjacent site
SS	same site as previous analysis
I	inclusion in grain analysed immediately preceding
IC	as above - core
IR	as above - rim
X	different grain to immediately preceding analysis
RX	rim adjacent to immediately preceding analysis
RX001	rim adjacent to site of this number
T	part of traverse

Number		
	-	Refers to the order of points probed.
A	-	Analysed on probe at University of Melbourne, May 1978
B	-	Analysed on probe at University of Melbourne, February 19
C	-	Analysed on probe at Macquarie University, March 1979
1,2,3...		Refers to selected portions of a thin section chosen for microprobe study, usually less than 3mm diameter
-001	-	A sequential number given to an analysis by the microprobe computer.

H2Oc	Calculated from stoichiometric proportions
Al 1V	Calculated, tetrahedrally bounded Al
FeO +	Total Fe as FeO
O/OH	Shows the number of oxygens and hydroxyl groups used to calculate the formula. Where three figures are shown the first is the number of cations used, for ferr c iron estimates, shown in brackets in either the Al or Ba row.

SAMPLE NO.: 517-004

ROCK TYPE : Lode Schist (1a)

Mineral:	gar	gar	bio	gar	gar
Site	C	RS	RX	IC	RS
Number	Bl-183	Bl-184	Bl-185	Bl-186	Bl-186
SiO2	36.99	36.18	34.91	36.99	36.48
TiO2	0.00	0.07	1.38	0.00	0.04
Al2O3	20.63	20.78	18.55	20.95	20.74
FeO (tot)	37.88	39.23	22.52	37.09	39.19
MnO	1.53	1.31	0.12	1.37	1.33
MgO	2.60	2.03	8.25	2.44	1.95
CaO	0.33	0.21	0.00	1.09	0.20
Na2O	0.00	0.03	0.12	0.03	0.04
K2O	0.00	0.00	9.22	0.02	0.02
CoO	0.00	0.00	0.01	0.00	0.00
NiO	0.00	0.06	0.14	0.04	0.04
BaO	-	-	-	-	-
ZnO	0.04	0.05	0.18	0.29	0.81
Total	100.02	99.94	95.40	100.31	100.14
H2O c	- .	-	-	-	-
Cation Proportions					
basis O/OH	24/0	24/0	20/4	2410	24/0
Si	6.011	5.928	5.401	5.987	5.958
Al 1V	-		2.599	-	-
Al V1	3.951	4.013	0.785	3.996	3.993
Ti	0.000	0.008	0.161	0.000	0.005
Fe	5.147	5.376	2.915	5.020	5.354
Mn	0.210	0.182	0.016	0.188	0.185
Mg	0.631	0.496	1.903	0.588	0.475
Ca	0.058	0.036	0.000	0.189	0.034
Na	0.000	0.008	0.035	0.010	0.011
K	0.000	0.000	1.821	0.004	0.004
Co	0.000	0.000	0.001	0.000	0.000
Ni	0.000	0.007	0.017	0.006	0.006
Ba	-	-	-	-	-
Zn	0.005	0.007	0.020	0.035	0.026

SAMPLE NO.: 517-004
ROCK TYPE : Lode Schist (1a)

Mineral;	bio	bio	bio	gar	cht
Site	RX	-	-	R	RX
Number	Bl-188	Bl-189	Bl-190	B2-192	B2-193
SiO_2	35.05	34.61	34.90	37.23	23.97
TiO_2	1.32	1.44	1.52	0.05	0.04
Al_2O_3	18.86	18.74	18.47	21.03	22.70
FeO(tot)	21.72	22.13	21.33	38.52	27.63
MnO	0.07	0.07	O.02	1.30	0.05
MgO	8.34	8.49	1.96	2.22	12.35
CaO	0.00	0.00	0.00	0.26	0.03
Na_2O	0.25	0.20	0.06	0.04	0.02
K_2O	9.32	9.05	1.81	0.01	0.10
CoO	0.00	0.00	0.00	0.00	0.00
NiO	0.00	0.02	0.09	0.00	0.04
BaO	-	-	-	-	-
ZnO	0.21	0.00	0.00	0.00	0.04
Total	95.16	94.75	94.05	100.65	86.98
H_2O c	3.88	3.86	3.85	-	11.13

Cation Proportions

basis O/OH	20/4	20/4	20/4	24/0	20/16
Si	5.413	5.372	5.347	6.010	5.168
Al4	2.597	2.628	2.563	-	2.832
Al6	0.907	0.801	0.829	4.002	2.936
Ti	0.153	0.168	0.178	0.006	0.007
Fe	2.806	2.873	2.779	5.201	4.981
Mn	0.009	0.009	0.003	0.178	0.009
Mg	1.920	1.965	1.956	0.534	3.970
Ca	0.000	0.000	0.000	0.044	0.007
Na	0.075	0.061	0.059	0.012	0.010
K	1.837	1.792	1.808	0.003	0.027
Co	0.000	0.000	0.000	0.000	0.000
Ni	0.000	0.002	0.011	0.000	0.008
Ba	-	-	-	-	-
Zn	0.024	0.000	0.000	0.000	0.006

SAMPLE NO: 517-004
ROCK TYPE: Lode Schist

Mineral;	bio	sta	sta	cht	gar
Site	-	R	AS	-	R
Number	B3-195	B3-197	B3-199	B3-201	B7-203
SiO2	34.82	28.02	27.21	23.38	35.96
TiO2	1.69	0.37	0.44	0.08	0.04
Al2O3	18.87	53.89	54.02	22.74	21.01
FeO (tot)	21.35	14.59	14.43	27.42	39.44
MnO	0.05	0.06	0.10	0.05	1.35
Mgo	8.71	1.26	1.23	12.65	2.17
CaO	0.00	0.02	0.00	.0.01	0.17
Na2O	0.17	0.02	0.04	0.05	0.03
K2O	9.37	0.00	0.02	0.01	0.02
CoO	0.00	0.00	0.00	0.00	0.00
NiO	0.10	0.03	0.08	0.09	0.00
BaO	-	-	-	-	-
ZnO	0.13	1.08	0.82		0.05
Total	95.27	99.35	98.39	86.62	100.24
H2O c	3.89	2.18	2.16	11.07	-

Cation Proportions

basis O/OH	2014	2212	2212	20/16	24/0
Si	5.366	3.862	3.786	5.068	5.881
Al4	2.634	-	-	2.932	-
Al6	0.794	8.755	8.860	2.878	4.049
Ti	0.196	0.038	0.046	0.013	0.005
Fe	2.752	1.681	1.679	4.971	5.394
Mn	0.007	0.008	0.012	0.009	0.187
Mg	2.001	0.259	0.254	4.088	0.529
Ca	0.000	0.003	0.000	0.003	0.030
Na	0.050	0.005	0.010	0.020	0.011
K	1.842	0.000	0.003	0.004	0.004
Co	0.000	0.000	0.000	0.000	0.000
Ni	0.013	0.003	0.009	0.016	0.000
Ba	-	-	-	-	-
Zn	0.014	0.110	0.084	0.023	0.006

SAMPLE NO.: 517-004
ROCK TYPE : Lode Schist (1a)

Mineral:	gar	gar	sta	cht	cht
Site	AS	AS	RX	-	-
Number	B7-204	B7-205	B7-207	B7-209	B8-210
SiO2	36.62	36.35	27.49	23.28	23.53
TiO2	0.07	0.00	0.41	0.06	0.07
Al2O3	20.97	20.83	52.87	22.20	22.71
FeO (tot)	37.20	38.09	14.45	28.32	26.62
MnO	1.21	1.33	0.05	0.00	0.03
Mgo	2.14	2.13	1.52	11.52	12.33
CaO	0.20	0.16	0.02	0.00	0.03
Na2O	0.05	0.05	0.08	0.02	0.02
K2O	0.00	0.01	0.00	0.01	0.00
CoO	0.00	0.00	0.00	0.00	0.00
NiO	0.04	0.02	0.08	0.00	0.12
BaO	-	-	-	-	-
ZnO	0.02	0.10	1.07	0.12	0.05
Total	98.54	99.06	98.04	85.55	85.51
H2O c	-	-	2.14	10.87	10.98
Cation Proportions					
basis O/OH	24/0	24/0	22/2	20/16	20/16
si	6.017	5.975	3.846	5.136	5.140
Al 1V	-	-	-	2.864	2.860
Al V1	4.060	4.037	8.717	2.911	2.987
Ti	0.009	0.000	0.043	0.111	0.012
Fe	5.112	5.236	1.690	5.226	4.863
Mn	0.169	O.186	0.006	0.000	0.006
Mg	0.525	0.522	0.318	3.791	4.016
Ca	0.036	0.028	0.003	0.000	0.006
Na	0.015	0.014	0.023	0.009	0.007
K	0.000	0.001	0.000	0.003	0.000
Co	0.000	0.000	0.000	0.000	0.000
Ni	0.006	0.003	0.009	0.000	0,022
Ba	-	-	-	-	-
Zn	0.003	0.012	0.110	0.020	0.009

SAMPLE NO.: 517-004
ROCK TYPE : Lode Schist (1a)

Mineral:	gar	gar
Site	C	RS
Number	B8-211	B8-214
SiO2	37.17	36.60
TiO2	0.03	0.11
Al2O3	20.79	20.59
FeO (tot)	37.38	37.83
MnO	1.31	1.35
MgO	2.44	2.36
CaO	0.81	0.19
Na2O	0.04	0.06
K2O	0.00	0.01
CoO	0.00	0.00
NiO	0.06	0.02
BaO	-	-
ZnO	0.10	0.00
Total	100.14	99.12
H2Oc	-	-

Cation Proportions

basis O/OH		
si	6.020	6.002
Al 1V	-	-
Al V1	3.969	3.979
Ti	0.004	0.013
Fe	5.063	5.188
Mn	0.180	0.187
Mg	0.589	0.578
Ca	0.141	0.033
Na	0.013	0.019
K	0.000	0.002
Co	0.000	0.000
Ni	0.008	0.003
Ba	-	-
Zn	0.012	0.000

SAMPLE NO.: 517-024
ROCK TYPE: Lode Schist (1a)

Mineral:	gar	cht	cht	sta	cht
Site	-	-	-	-	-
Number	A7-379	A7-380	A7-381	A5-035	A5-037
SiO2	36.81	25.25	25.76	27.58	25.94
TiO2	0.03	0.05	0.03	0.39	0.23
Al2O3	20.60	15.95	15.92	52.96	16.09
FeO (tot)	37.95	41.79	43.31	14.79	43.14
MnO	1.59	0.29	0.32	0.10	0.37
MgO	2.75	3.78	2.44	1.39	2.32
CaO	0.32	0.00	0.02	0.02	0.02
Na2O	0.00	0.03	0.00	0.00	0.01
K2O	0.01	0.01	0.02	0.00	0.06
Cr2O3	0.06	0.00	0.07	0.03	0.00
NiO	0.00	0.00	0.00	0.04	0.11
BaO	0.02	0.06	0.00	0.12	0.07
ZnO	-	-	-	-	-
Total	100.15	87.21	87.88	97.42	88.35
H2O c	-	10.25	10.28	2.14	10.34

Cation proportions

basis O/OH	24/0	20/16	20/16	22/2	20/16
si	5.981	5.909	6.013	3.867	6.018
Al 1V	-	2.091	1.987	-	1.982
Al V1	3.945	2.307	2.392	8.753	2.417
Ti	0.004	0.008	0.005	0.041	0.040
Fe	5.157	8.178	8.456	1.735	8.370
Mn	0.219	0.057	0.063	0.012	0.072
Mg	0.666	1.319	0.851	0.290	0.802
Ca	0.055	0.000	0.005	0.002	0.004
Na	0.000	0.016	0.000	0.000	0.005
K	0.002	0.003	0.005	0.000	0.017
Cr	0.008	0.000	0.012	0.004	0.000
Ni	0.000	0.000	0.000	0.005	0.020
Ba	0.002	0.006	0.000	0.007	0.007
Zn	-	-	-	-	-

SAMPLE NO.: 517-024
ROCK TYPE: Lode Schist (1a)

Mineral:	cht	gar	cht	cht	cht
Site	-	-	-	-	-
Number	A5-038	A6-040	A6-042	A6-043	A6-044
SiO2	25.10	37.52	25.75	26.13	27.99
TiO2	0.02	0.06	0.04	0.00	0.15
Al2O3	17.51	20.58	16.49	15.76	21.47
FeO (tot)	42.10	38.42	41.86	43.10	26.68
MnO	0.15	1.47	0.19	0.27	0.09
MgO	3.76	2.55	3.65	2.77	12.23
CaO	0.01	0.21	0.02	0.00	0.02
Na2O	0.02	0.03	0.05	0.01	0.00
K2O	0.02	0.00	0.04	0.05	0.00
Cr2O3	0.05	0.01	0.06	0.02	0.01
NiO	0.09	0.00	0.01	0.06	0.02
BaO	0.00	0.08	0.06	0.01	0.00
ZnO	-	-	-	-	-
Total	88.83	100.93	88.21	88.19	88.65
H2O c	10.48	-	10.41	10.34	11.55

Cation proportions

basis O/OH	20/16	24/0	20/16	20/16	20/16
si	5.747	6.042	5.933	6.064	5.813
Al 1V	2.253	-	2.067	1.936	2.187
Al V1	2.471	3.907	2.412	2.375	3.068
Ti	0.004	0.008	0.007	0.001	0.023
Fe	8.060	5.176	8.066	8.365	4.634
Mn	0.030	0.200	0.037	0.054	0.016
Mg	1.282	0.613	1.254	0.957	3.786
Ca	0.002	0.036	0.004	0.000	0.005
Na	0.010	0.010	0.022	0.006	0.000
K	0.006	0.000	0.013	0.014	0.000
Cr	0.009	0.001	0.010	0.004	0.001
Ni	0.016	0.000	0.002	0.012	0.003
Ba	0.000	0.005	0.006	0.001	0.000
Zn	-	-	-	-	-

SAMPLE NO.: 517-024
ROCK TYPE: Lode schist (1a)

Mineral:	cht	bio	gar	gar
Site	I047	-	RX	S
Number	A2-045	A2-047	A2-048	A2-022
SiO2	23.64	36.00	37.81	37.85
TiO2	0.15	1.64	0.09	0.00
Al2O3	22.83	19.34	21.02	21.06
FeO (tot)	27.72	21.50	38.99	39.37
MnO	0.02	0.00	1.57	1.56
Mgo	12.65	9.14	2.20	2.23
CaO	0.01	0.00	0.23	0.20
Na2O	0.00	0.20	0.04	0.03
K2O	0.24	9.04	0.04	0.00
Cr2O3	0.00	0.01	0.00	0.00
NiO	0.02	0.05	0.07	0.06
BaO	0.00	0.04	0.00	0.05
ZnO	-	-	-	-
Total	87.29	96.95	102.06	102.40
H2O c	11.15	3.99	-	-

Cation proportions

basis O/OH	20/16	20/4	24/0	24/0
si	5.088	5.413	6.029	6.023
Al 1V	2.912	2.587	-	-
Al V1	2.878	0.842	3.951	3.950
Ti	0.025	0.185	0.010	0.000
Fe	4.988	2.704	5.200	5.240
Mn	0.003	0.000	0.212	0.211
Mg	4.058	2.050	0.523	0.529
Ca	0.002	0.000	0.040	0.035
Na	0.000	0.059	0.013	0.010
K	0.066	1.734	0.008	0.000
Cr	0.000	0.001	0.000	0.000
Ni	0.004	0.006	0.010	0.007
Ba	0.000	0.002	0.000	0.003
Zn	-	-	-	-

SAMPLE NO.: 517-049
ROCK TYPE : Lode schist

Mineral:	cht	cht	cht	bio	gar
Site	I307	X	X	-	RX
Number	Bl-303	Bl-304	Bl-305	Bl-307	Bl-308
SiO2	22.98	23.17	22.69	34.38	36.24
TiO2	0.10	0.09	0.05	1.54	0.00
Al2O3	22.76	22.78	22.90	18.70	201.78
FeO (tot)	27.79	27.77	26.95	22.01	38.64
MnO	0.02	0.07	0.04	0.04	1.33
MgO	12.47	11.96	12.60	8.56	1.94
CaO	0.00	0.00	0.03	0.00	0.24
Na2O	0.02	0.02	0.03	0.28	0.00
K2O	0.04	0.01	0.00	9.17	0.04
CoO	0.00	0.00	0.00	0.00	0.00
NiO	0.15	0.01	0.04	0.00	0.14
BaO	-	-	-	-	-
ZnO	0.00	0.04	0.02	0.07	0.11
Total	86.33	85.91	85.34	94.74	99.45
H2O c	11.03	10.96	10.94	-	-
Cation Proportions					
basis O/OH	20/16	20/16	20/16	20/4	24/0
Si	4.999	5.072	4.975	5.346	5.956
Al 1V	3.001	2.928	3.025	2.654	-
Al V1	2.834	2.950	2.893	0.772	4.025
Ti	0.016	0.014	0.009	0.180	0.000
Fe	4.902	5.083	4.814	2.862	5.311
Mn	0.004	0.012	0.007	0.005	0.185
Mg	4.042	3.901	4.118	1.983	0.476
Ca	0.000	0.001	0.007	0.000	0.042
Na	0.010	0.009	0.014	0.086	0.001
K	0.010	0.004	0.000	1.819	0.009
Co	0.000	0.000	0.000	0.000	0.000
Ni	0.026	0.002	0.007	0.000	0.018
Ba	(0.155)	(0.000)	(0.129)	-	-
Zn	0.000	0.006	0.003	0.008	0.013

SAMPLE NO.: 517-049
ROCK TYPE : Lode Schist (1a)

Mineral	mt	ilm
Site	C	I
Number	Bl-310	Bl-312
SiO2	0.04	0.08
TiO2	0.17	46.65
Al2O3	0.34	0.13
FeO (tot)	91.12	51.61
MnO	0.00	0.14
Mgo	0.00	0.31
CaO	0.05	0.03
Na2O	0.06	0.06
K2O	0.00	0.00
CoO	0.00	0.00
NiO	0.18	0.03
BaO	-	-
ZnO	0.06	0.08
Total	92.04	99.12
H2O c	-	-

Cation Proportions

basis O/OH	24/32/0	4/610
Si	0.013	0.004
Al 1V	(15.810)	(0.451
Al V1	0.126	0.008
Ti	0.039	1.770
Fe	7.896	1.727
Mn	0.000	0.006
Mg	0.000	0.023
Ca	0.017	0.002
Na	0.037	0.006
K	0.002	0.000
Co	0.000	0.000
Ni	0.046	0.001
Ba	-	-
Zn	0.014	0.003

SAMPLE NO.: 517-052A
ROCK TYPE : Late Stage Vein

Mineral:	tou	cht	cht	cht	plg
Site	C	-	S	-	-
Number	Al-422	Al-425	Al-426	A2-345	A3-347
SiO2	37.10	23.86	23.08	23.27	68.77
TiO2	0.04	0.04	0.00	0.00	0.05
Al2O3	32.36	18.69	20.30	21.17	20.14
FeO (tot)	9.90	26.10	29.64	37.08	0.02
MnO	0.01	0.04	0.08	0.32	0.00
MgO	4.30	5.83	6.82	3.99	0.01
CaO	0.12	0.04	0.03	0.04	1.00
Na2O	2.07	0.09	0.04	0.03	11.08
K2O	0.03	0.32	0.28	0.28	0.11
Cr2O3	0.06	0.10	0.03	0.00	0.01
NiO	0.00	0.36	0.21	0.01	0.00
BaO	0.00	0.10	0.05	0.09	0.01
ZnO	-	-	-	-	-
Total	85.99	75.57	80.55	86.28	101.21
H2O	-	9.61	10.07	10.41	-
Cation Proportions					
basis O/OH	18/4	20/16	20/15	20/16	32/0
Si	5.001	5.958	5.497	5.362	11.885
Al 1V	-	2.042	2.503	2.638	-
Al V1	5.142	3.457	3.203	3.113	4.102
Ti	0.004	0.007	0.000	0.000	0.007
Fe	1.116	5.450	5.905	7.147	0.002
Mn	0.001	0.009	0.015	0.062	0.000
Mg	0.864	2.169	2.423	l.372	0.003
Ca	0.017	0.012	0.007	0.009	0.185
Na	0.541	0.042	0.018	0.014	3.713
K	0.005	0.101	0.085	0.083	0.024
Cr	-	0.019	0.006	0.000	0.002
Ni	0.000	0.072	0.040	0.002	0.000
Ba	-	0.010	0.004	0.008	0.001
Zn	-	-	-	-	-

SAMPLE NO.: 517-052A
ROCK TYPE: Late Stage Vein

Mineral:	cht	plg	cht	sta
Site	-	-	-	-
Number	A2-352	A3-357	A4-360	A5-362
SiO2	22.22	67.50	22.48	27.39
TiO2	0.08	0.00	0.07	0.35
Al2O3	19.32	19.93	22.13	53.23
FeO (tot)	27.51	0.02	33.23	14.61
MnO	0.05	0.03	0.15	0.12
MgO	6.14	0.00	7.81	1.07
CaO	0.02	0.98	0.02	0.01
Na2O	0.04	11.14	0.00	0.03
K2O	0.19	0.10	0.07	0.01
Cr2O3	0.02	0.05	0.04	0.08
NiO	0.33	0.05	0.00	0.06
BaO	0.02	0.00	0.00	0.04
ZnO	-	-	-	-
Total	75.94	99.80	85.98	96.99
H2O c	9.55	-	10.61	2.13
Cation Proportions				
basis O/OH	20/16	32/0	20/16	22/2
Si	5.585	11.849	5.082	3.852
Al 1V	2.415	-	2.918	-
Al V1	3.309	4.123	2.979	8.824
Ti	0.016	0.000	0.012	0.038
Fe	5.782	0.002	6.284	1.719
Mn	0.010	0.005	0.029	0.014
Mg	2.300	0.000	2.631	0.224
Ca	0.006	O.185	0.004	0.002
Na	0.019	3.793	0.000	0.007
K	0.061	0.022	0.020	0.001
Cr	0.004	0.007	0.007	0.009
Ni	0.066	0.008	0.000	0.006
Ba	0.002	0.000	0.000	0.002
Zn	-	-	-	-

SAMPLE NO.: 517-055
ROCK TYPE : Lode Schist (1a)

Mineral:	gar	bio	gar	gar	bio
Site	C	R	RX078	C	-
Number	B2-078	B3-079	B3-081	B4-084	B4-085
SiO2	36.78	34.80	36.46	36.38	35.37
TiO2	0.11	1.33	0.06	0.03	1.66
Al2O3	21.26	19.43	21.00	21.27	19.53
FeO (tot)	38.78	19.38	39.46	38.92	21.10
MnO	0.92	0.06	1.11	1.02	0.06
Mgo	2.56	9.51	2.25	2.36	8.95
CaO	0.38	0.00	0.20	0.42	0.00
Na2O	0.01	0.33	0.00	0.02	0.30
K2O	0.01	8.63	0.01	0.00	9.11
Cr2O3	0.02	0.02	0.00	0.02	0.04
NiO	0.00	0.02	0.00	0.08	0.07
BaO	0.00	0.19	0.01	0.03	0.12
ZnO	-	-	-	-	-
Total	100.84	93.71	100.55	100.57	96.32
H2O c	-	3.88	-	-	-

Cation Proportions

basis O/OH	24/0	20/4	24/0	24/0	20/4
Si	5.932	5.378	5.927	5.902	5.365
Al 4	-	2.622	-	-	2.635
Al 6	4.042	0.918	4.023	4.068	0.855
Ti	0.013	0.155	0.007	0.003	0.190
Fe	5.232	2.505	5.364	5.281	2.676
Mn	0.126	0.007	0.153	0.141	0.008
Mg	0.617	2.192	0.544	0.571	2.023
Ca	0.066	0.000	0.036	0.073	0.000
Na	0.004	0.100	0.000	0.008	0.087
K	0.002	1.702	0.003	0.000	1.763
Cr	0.003	0.003	0.000	0.003	0.005
Ni	0.000	0.002	0.000	0,010	0.009
Ba	0.000	0.012	0.000	0.002	0.007
Zn	-	-	-	-	-

SAMPLE NO.: 517-055
ROCK TYPE: Lode Schist (1a)

Mineral:	crd	crd	crd	crd	gar
Site	-	S	-	RS	RX
Number	Bl-113	Bl-114	B6-117	B6-118	B6-122
SiO2	48.73	49.09	48.11	47.91	36.88
TiO2	0.00	0.00	0.00	0.03	0.05
Al2O3	31.02	30.97	30.81	30.79	21.57
FeO (tot)	9.43	9.49	9.18	9.34	38.70
MnO	0.10	0.05	0.09	0.09	0.88
MgO	7.37	7,2,0	7.32	7.20	1.93
CaO	0.04	0.03	0.01	0.03	0.22
Na2O	0.91	1.00	1.12	0.98	0.04
K2O	0.02	0.04	0.02	0.01	0.00
Cr2O3	0.00	0.07	0.02	0.00	0.00
NiO	0.07	0.00	0.00	0.02	0.08
BaO	0.11	0.02	0.06	0.00	0.13
ZnO	-	-	-	-	-
Total	97.79	97.96	96.75	96.40	100.49
H2O c	-	-	-	-	-

Cation Proportions

basis O/OH	18/0	18/0	18/0	18/0	24/0
Si	5.091	5.115	5.079	5.075	5.966
Al 4	0.909	0.885	0.921	0.925	-
Al 6	2.911	2.918	2.913	2.919	4.112
Ti	0.000	0.000	0.000	0.002	0.006
Fe	0.824	0.827	0.810	0.827	5.236
Mn	0.009	0.005	0.008	0.008	0.120
Mg	1.148	1.118	1.152	1.137	0.467
Ca	0.004	0.003	0.000	0.003	0.038
Na	0.184	0.202	0.229	0.202	0.013
K	0.002	0.005	0.003	0.001	0.000
Cr	0.000	0.006	0. 002	0.030	0.001
Ni	0.006	0.000	0. 000	0.002	0.011
Ba	0.004	0.001	0. 003	0.000	0.008
Zn	-	-	-	-	-

SAMPLE NO.: 517-055
ROCK TYPE : Lode Schist (1a)

Mineral	gar	gar	crd	crd
Site	C	RS	R	AS
Number	B6-124	B6-125	B6-131	B6-132
SiO2	36.73	36.75	48.35	48.07
TiO2	0.05	0.01	0.04	0.01
Al2O3	21.14	21.54	30.91	30.27
FeO (tot)	38.54	38.15	9.19	9.26
MnO	0.99	0.98	0.09	0.03
MgO	2.41	2.25	7.23	7.33
CaO	0.56	0.26	0.02	0.04
Na2O	0.04	0.10	1.11	1.27
K2O	0.00	0.01	0.03	0.02
Cr2O3	0.01	0.03	0.06	0.07
NiO	0.07	0.08	0.00	0.06
BaO	0.00	0.03	0.04	0.00
ZnO	-	-	-	-
Total	100.55	100.19	97.06	96.44
H2Oc	-	-	-	-

Cation Proportions

basis O/OH	24/0	24/0	18/0	18/0
Si	5.944	5.952	5.085	5.096
Al 4	-	-	0.915	0.904
Al 6	4.033	4.112	2.916	2.879
Ti	0.007	0.001	0.003	0.001
Fe	5.217	5.167	0.808	0.821
Mn	0.136	0.135	0.008	0.003
Mg	0.582	0.544	1.133	1.158
Ca	0.097	0.045	0.002	0.005
Na	0.012	0.032	0.227	0.261
K	0.000	0.003	0.004	0.002
Cr	0.002	0.004	0.005	0.006
Ni	0.009	0.010	0.000	0.005
Ba	0.000	0.002	0.001	0.000
Zn	-	-	-	-

SAMPLE NO.: 517-055
ROCK TYPE : Lode Schist

Mineral:	crd	crd	gar	gar	gar
Site	R	AS	RX	AS	CS
Number	B9-231	B9-232	B9-2.33	B9-234	B9-235
SiO2	47.91	47.35	36.13	36.72	36.46
TiO2	0.00	0.00	0.04	0.00	0.01
Al 2O3	30.69	30.53	20.79	20.68	20.76
FeO (tot)	9.70	9.70	38.52	37.57	38.35
MnO	0.04	0.11	0.93	1.000	1.07
MgO	7.15	7.13	2.47	2.29	2.56
CaO	0.03	0.02	0.25	0.22	0.28
Na2O	0.88	0.92	0.08	0.02	0.05
K2O	0.00	0.01	0.01	0.03	0.02
CoO	0.00	0.00	0.00	0.00	0.00
NiO	0.00	0.00	0.02	0.14	0.03
BaO	-	-	-	-	-
ZnO	0.13	0.01	0.00	0.09	0.15
Total	96.53	95.78	99.23	98.76	99.73
H2O c	-	-	-	-	-

Cation Proportions

basis O/OH	18/0	18/0	24/0	24/0	24/0
Si	5.077	5.060	5.934	6.030	5.955
Al 4	-	-	-	-	-
Al 6	3.833	3.846	4.024	4.003	3.998
Ti	0.000	0.000	0.005	0.000	0.001
Fe	0.859	0.867	5.291	5.160	5.239
Mn	0.003	0.010	0.130	0.139	0.149
Mg	1.129	1.135	0.604	0.561	0.623
Ca	0.004	0.002	0.044	0.038	0.048
Na	0.181	0.191	0.025	0.007	0.015
K	0.000	0.001	0.002	0.006	0.004
Co	0.000	0.000	0.000	0.000	0.000
Ni	0.000	0.000	0.002	0.018	0.004
Ba	-	-	-	-	-
Zn	0.010	0.000	0.000	0.011	0.018

SAMPLE NO.: 517-055
ROCK TYPE : Lode Schist (1a)

Mineral:	bio	gar	gar	gar	crd
Site	RX234	AS235	R	AS239	RX
Number	B9-236	B9-240	B9-239	B9-241	B9-243
SiO2	34.60	37.10	36.28	36.54	47.63
TiO2	1.46	0.00	0.00	0.04	0.00
Al2O3	18.89	21.05	20.78	20.72	30.75
FeO (tot)	22.13	38.78	39.08	38.55	9.25
MnO	0.06	0.91	1.01	0.95	0.09
MgO	8.40	2.41	2.20	2.24	7.06
CaO	0.00	0.20	0.23	0.21	0.00
Na2O	0.25	0.08	0.04	0.03	0.75
K2O	9.24	0.00	0.01	0.01	0.00
CoO	0.00	0.00	0.00	0.00	0.00
NiO	0.06	0.04	0.00	0.00	0.06
BaO	-	-	-	-	-
ZnO	0.18	0.00	0.16	0.14	0.00
Total	95.28	100.57	99.78	99.42	95.61
H2O c	3.88	-	-	-	-

Cation Proportions

basis O/OH	20/4	24/0	24/0	24/0	18/O
si	5.354	5.994	5.943	5.986	5.081
Al 4	2.646	-	-	-	-
Al 6	0.799	4.009	4.012	4.000	3.866
Ti	0.169	0.000	0.000	0.004	0.000
Fe	2.864	5.241	5.354	5.281	0.826
Mn	0.038	0.124	0.139	0.132	0.008
Mg	1.937	0.580	0.537	0.547	1.123
Ca	0.000	0.035	0.040	0.037	0.000
Na	0.075	0.025	0.011	0.009	0.155
K	1.825	0.000	0.001	0.002	0.000
Co	0.000	0.000	0.000	0.000	0.000
Ni	0.008	0.006	0.000	0.000	0.006
Ba	-	-	-	-	-
Zn	0.021	0.000	0.019	0.017	0.000

SAMPLE NO.: 517-055
ROCK TYPE : Lode Schist (1a)

Mineral	crd	bio	gar	crd	cht
Site	As	R	RX	RX	-
Number	B9-242	B9-244	B9-246	B9-247	B10-248
SiO2	47.49	34.27	36.33	48.54	23.58
TiO2	0.02	1.34	0.02	0.08	0.10
Al2O3	30.21	19.12	20.90	31.15	22.95
FeO (tot)	9.53	21.30	38.80	9.70	27.17
MnO	0.09	0.02	0.99	0.07	0.11
MgO	6.97	8.34	1.99	7.34	13.05
CaO	0.01	0.00	0.21	0.01	0.01
Na2O	1.09	0.26	0.04	0.91	0.00
K2O	0.02	8.82	0.02	0.01	0.00
CoO	0.00	0.00	0.00	0.00	0.00
NiO	0.00	0.00	0.00	0.00	0.13
BaO	-	-	-	-	-
ZnO	0.00	0.05	0.05	0.16	0.14
Total	95.43	93.53	99.34	97.98	87.35
H2O c	-	3.83	-	-	11.18

Cation Proportions

basis O/OH	18/0	20/4	24/0	18/0	20/16
Si	5.090	5.364	5.964	5.068	5.061
Al 4	-	2.636	-	-	2.969
Al 6	3.816	0.892	4.044	3.833	2.837
Ti	0.002	0.158	0.003	0.007	0.016
Fe	0.855	2.789	5.326	0.847	4.894
Mn	0.008	0.003	0.138	0.006	0.021
Mg	1.113	1.947	0.486	1.142	4.176
Ca	0.001	0.000	0.036	0.002	0.003
Na	0.226	0.078	0.1011	0.185	0.000
K	0.003	1.762	0.004	0.002	0.001
Co	0.000	0.000	0.000	0.000	0.000
Ni	0.000	0.000	0.000	0.000	0.022
Ba	-	-	-	-	-
Zn	0.000	0.006	0.006	0.013	0.023

SAMPLE NO.: 517.055
ROCK TYPE : Lode Schist (1a)

Mineral	crd	gar	gar	bio	crd
Site	-	C	RS	RX	c
Number	B1-250	B6-252	B6-253	B6~255	B6-257
SiO2	48.34	36.82	37.00	35.03	46.79
TiO2	0.02	0.05	0.06	1.41	0.02
Al2O3	30.39	21.06	20.94	19.33	30.12
FeO (tot)	9.67	38.18	39.00	20.73	9.44
MnO	0.00	0.94	1.04	0.00	0.06
MgO	7.17	2.54	2.12	8.57	7.10
CaO	0.04	0.66	0.25	0.00	0.02
Na2O	0.93	0.06	0.03	0.29	1.15
K2O	0.01	0.00	0.01	9.30	0.03
CoO	0.00	0.00	0.00	0.00	0.00
NiO	0.06	0.05	0.00	0.07	0.00
BaO	-	-	-	-	-
ZnO	0.17	0.00	0.07	0.00	0.00
Total	96.80	100.36	100.52	94.73	94.72
H2O c	-	-	-	-	3.89
Cation Proportions					
basis O/OH	18/0	24/0	24/0	20/4	18/0
Si	5.109	5.960	5.995	5.399	5.057
Al 4	-	-	-	2.601	-
Al 6	3.785	4.019	3.999	0.911	3.838
Ti	0.002	0.006	0.007	0.164	0.001
Fe	0.855	5.168	5.285	2.671	0.853
Mn	0.000	0.128	0.143	0.000	0.006
Mg	1.129	0.613	0.512	1.968	1.144
Ca	0.004	0.115	0.043	0.000	0.002
Na	0.190	0.017	0.010	0.087	0.240
K	0.002	0.000	0.002	1.829	0.004
Co	0.000	0.000	0.000	0.000	0.000
Ni	0.005	0.006	0.000	0.008	0.000
Ba	-	-	-	-	-
Zn	0.013	0.000	0.009	0.000	0.000

SAMPLE NO.: 517-055
ROCK TYPE : Lode Schist (1a)

Mineral	crd
Site	AS
Number	B6-258
Sio2	46.90
TiO2	0.05
Al 2O3	30.87
FeO (tot)	9.63
MnO	0.07
Mgo	7.12
CaO	0.02
Na2O	1.17
K2O	0.02
CoO	0.00
NiO	0.02
BaO	-
ZnO	0.09
Total	95.98
H2O c	-

Cation Proportions	
basis O/OH	18/0
Si	5.012
Al 1V	-
Al V1	3.888
Ti	0.004
Fe	0.861
Mn	0.007
Mg	1.134
Ca	0.003
Na	0.243
K	0.003
Co	0.000
Ni	0.001
Ba	-
Zn	0.007

SAMPLE NO.: 517-055
ROCK TYPE : Lode Schist (1a)

Mineral:	sta	sta	sta	and	crd
Site	R	CS	RS	-	-
Number	Cl-188	Cl-189	Cl-190	Cl-191	C2-193
SiO2	27.76	27.27	27.53	36.94	47.52
TiO2	0.35	0.37	0.41	-	-
Al2O3	54.01	53.10	53.31	61.10	30.29
FeO (tot)	13.56	14.36	14.40	0.90	9.60
MnO	-	-	-	-	-
MgO	1.34	1.61	1.49		7.07
CaO	-	-	-	-	-
Na2O	-	-	-	-	1.07
K2O	-	-	-	-	-
CoO	-	-	-	-	-
NiO	-	-	-	-	-
BaO	-	-	-	-	-
ZnO	1.05	0.67	0.80	-	-
Total	98.07	97.38	97.95	98.94	96.55
H2O c	-	-	-	-	-

Cation Proportions					
basis O/OH	46/0	46/0	46/0	5/0	18/0
Si	7.699	7.645	7.675	1.010	5.044
Al 4	-	--	-	-	
Al 6	17.689	17.579	17.551	1.973	3.861
Ti	0.074	0.078	0.087	-	-
Fe	3.148	3.371	3.361	0.205	0.839
Mn	-	-	-	-	-
Mg	0.557	0.675	0.622	1.168	
Ca	-	-	-	-	-
Na	-	-	-	-	0.229
K	-	-	-	-	-
Co	-	-	-	-	-
Ni	-	-	-	-	-
Ba	-	-	-	-	-
Zn	0.215	0.139	0.166	-	-

SAMPLE NO.: 517-055
ROCK TYPE : Lode Schist (1a)

Mineral:	crd	crd	gar	gar	gar
Site	AS	S	R	CS	T
Number	C2-194	C2-201	C2-202	C2-203	C2-204
SiO2	47.99	47.53	37.01	36.71	36.56
TiO2	-	-	-	-	-
Al2O3	30.95	31.00	21.21	20.82	21.09
FeO (tot)	9.63	9.50	38.38	37.88	37.92
MnO	-	-	0.90	0.91	0.92
MgO	7.22	7.28	2.20	2.58	2.54
CaO	-	-	0.21	0.39	0.30
Na2O	1.01	1.06	-	-	-
K2O	-	-	-	-	-
CoO	-	-	-	-	-
NiO	-	-	-	-	-
BaO	-	-	-	-	-
ZnO	-	-	-	-	-
Total	96.80	96.36	99.93	99.30	99.35
H2O c	-	-	-	-	-

Cation Proportions				
basis O/OH	18/0	24/0	24/0	24/0
si	5.038	6.002	5.992	5.964
Al 4	-	-	-	-
Al 6	3.880	4.061	4.011	4.061
Ti	-	-	-	-
Fe	0.843	5.211	5.177	5.179
Mn	-	0.124	0.126	0.127
Mg	1.152	0.532	0.628	0.620
Ca	-	0.036	0.069	0.524
Na	0.218	-	-	-
K	-	-	-	-
Co	-	-	-	-
Ni	-	-	-	-
Ba	-	-	-	-
Zn	-	-	-	-

SAMPLE NO.: 517-055
ROCK TYPE : Lode Schist (1a)

Mineral:	gar	bio	gar	bio	gar
Site	T	-	RX	R	RX
Number	C2-205	C2-212	C2-214	C3-216	C3-217
SiO2	36.57	34.52	36.70	35.58	36.64
TiO2	-	0.50	-	1.29	-
Al2O3	21.05	19.45	20.93	19.76	20.66
FeO (tot)	38.24	27.49	38.27	20.24	38.70
MnO	0.89	0.39	0.87	-	0.94
MgO	2.48	6.67	2.35	9.09	2.33
CaO	0.23	-	0.22	-	0.17
Na2O	-	0.23	-	0.33	-
K2O	-	4.96	-	8.50	-
CoO	-	-	-	-	-
NiO	-	-	-	-	-
BaO	-	-	-	-	-
ZnO	-	-	-	-	-
Total	99.47	94.21	99.40	94.79	99.44
H2O c	-	-	-	-	-
Cation Proportions					
basis O/OH	24/0	24/0	24/0	22/0	24/0
Si	5.965	5.879	5.946	5.91	5.99
Al 4	-	-	-	2.09	-
Al 6	4.053	3.911	4.083	0.65	3.99
Ti	-	0.063	-	0.15	-
Fe	5.222	3.919	5.253	2.58	5.30
Mn	0.124	0.056	0.134	-	0.13
Mg	0.603	1.697	0.558	2.07	0.57
Ca	0.402	0.038	-	-	0.03
Na	-	0.077	-	0.10	-
K	-	1.079	-	1.66	-

SAMPLE NO.: 517-055
ROCK TYPE : Lode Schist (1a)

Mineral:	gar	gar	crd	crd	crd
Site	AS204	C5217	-	S	AS
Number	C2-232	C3-235	C3-236	C3-237	C3-238
SiO2	36.61	36.87	47.86	47.35	47.06
TiO2	-	-	-	-	-
Al2O3	20.99	20.87	30.95	30.57	31.01
FeO (tot)	38.09	38.77	9.77	9.62	9.80
MnO	0.93	0.90	-	0.08	0.09
MgO	2.58	2.25	7.20	7.15	7.11
CaO	0.22	0.19	-	-	-
Na2O	-	-	1.03	1.05	0.45
K2O	-	-	-	-	-
CoO	-	-	-	-	-
NiO	-	-	-	-	-
BaO	-	-	-	-	-
ZnO	-	-	-	-	-
Total	99.42	99.87	96.84	95.87	95.56
H2O c	-	-	-	-	-
Cation Proportions					
basis O/OH	24/0	24/0	18/0	18/0	18/0
Si	5.971	5.999	5.053	5.054	5.031
Al 4	-	-	-	-	-
Al 6	4.042	4.010	3.858	3.852	3.914
Ti	-	-	-	-	-
Fe	5.200	5.281	0.863	0.859	0.877
Mn	0.128	0.124	-	0.007	0.008
Mg	0.629	0.547	1.136	1.139	1.135
Ca	0.038	0.336	-	-	-
Na	-	-	0.212	0.218	0.093
K	-	-	-	-	-
Co	-	-	-	-	-
Ni	-	-	-	-	-
Ba	-	-	-	-	-
Zn	-	-	-	-	-

SAMPLE NO.: 517-055
ROCK TYPE : Lode Schist (1a)

Mineral:	crd	gar	bio	bio	bio
Site	S	RX238	R	S	X
Number	C3-239	C3-240	C3-241	C3-243	C3-244
SiO2	47.95	36.45	35.17	35.82	35.88
TiO2	-	-	-	-	-
Al2O3	31.06	20.52	19.50	19.30	19.32
FeO (tot)	9.78	38.83	20.77	21.02	21.12
MnO	-	0.98	-	-	-
Mgo	7.06	2.18	9.06	9.10	9.03
CaO	-	0.19	-	-	-
Na2O	-	-	0.36	0.30	0.30
K2O	-	-	8.81	8.84	8.66
CoO	-	-	-	-	-
NiO	-	-	-	-	-
BaO	-	-	-	-	-
ZnO	-	-	-	-	-
Total	95.89	99.15	93.67	94.38	94.31
H 2 0 c	-	-	-	-	-
Cation Proportions					
basis O/OH	18/0	24/0	22/0	22/0	22/0
Si	5.088	5.990	5.458	5.511	5.521
Al 4	-	-	2.542	2.489	2.479
Al 6	3.890	3.982	1.030	1.018	1.031
Ti	-	-	-	-	-
Fe	0.869	5.343	2.944	2.709	2.721
Mn	-	0.137	-	-	-
Mg	1.119	0.534	2.290	2.093	2.076
Ca	-	0.034	-	-	-
Na	-	-	0.117	0.091	0.090
K	-	-	1.908	1.739	1.704
Co	-	-	-	-	-
Ni	-	-	-	-	-
Ba	-	-	-	-	-
Zn	-	-	-	-	-

SAMPLE NO.: 517-057
ROCK TYPE : Lode Schist (1a)

Mineral:	gar	gar	bio	bio	gar
Site	R	RSO	RX	AS	C
Number	Al-325	Al-326	Al-327	Al-328	A2-329
SiO2	37.19	36.97	35.42	35.04	36.99
TiO2	0.00	0.02	1.33	0.83	0.01
Al2O3	20.31	20.24	18.27	18.15	20.39
FeO (tot)	38.44	37.95	20.47	20.80	37.82
MnO	0.99	0.97	0.03	0.02	0.85
MgO	2.18	2.48	9.00	8.93	2.57
CaO	0.18	0.19	0.00	0.00	0.40
Na2O	0.03	0.01	0.26	0.32	0.02
K2O	0.04	0.00	9.37	9.17	0.00
CoO	0.00	0.02	0.00	0.07	0.03
NiO	0.03	0.00	0.07	0.01	0.00
BaO	0.01	0.07	0.00	0.06	0.07
ZnO	-	-	-	-	-
Total	99.40	98.93	94.21	93.40	99.15
H2O c	-	-	3.87	3.83	-
Cation Proportions					
basis O/OH	24/O	24/O	20/4	20/4	24/O
Si	6.079	6.055	5.488	5.492	6.050
Al 4	0.000	0.000	2.612	2.508	0.000
Al 6	3.914	3.914	0.725	0.845	3.931
Ti	0.000	0.003	0.155	0.098	0.001
Fe	5.255	5.207	2.653	2.727	5.173
Mn	0.137	0.134	0.004	0.003	0.117
Mg	0.532	0.608	2.079	2.086	0.625
Ca	0.032	0.034	0.000	0.000	0.071
Na	0.010	0.004	0.078	0.097	0.006
K	0.008	0.000	1.852	1.834	0.000
Co	0.000	0.003	-	-	0.004
Ni	0.004	0.000	0.009	0.001	0.000
Ba	0.000	0.005	-	-	0.004
Zn	-	-	-	-	-

SAMPLE NO.: 517-057
ROCK TYPE : Lode Schist (1a)

Mineral:	gar	bio	sta	bio	sta
Site	RS	RX	C	I	R
Number	A2-330	A2-331	A4-332	A4-333	A4-334
SiO2	37.55	35.46	27.67	35.62	26.88
TiO2	0.01	0.46	0.07	0.07	0.00
Al2O3	20.48	19.21	52.20	18.41	50.58
FeO (tot)	39.37	20.12	15.32	20.30	14.49
MnO	0.94	0.00	0.05	0.07	0.07
MgO	2.42	8.84	1.61	9.80	1.47
CaO	0.18	0.00	0.00	0.00	0.02
Na2O	0.00	0.30	0.00	0.31	0.02
K2O	0.00	9.49	0.01	9.55	0.15
CoO	0.00	0.02	0.00	0.02	0.00
NiO	0.00	0.04	0.00	0.02	0.03
BaO	0.00	0.00	0.00	0.12	0.01
ZnO	-	-	-	-	-
Total	100.95	93.94	96.92	94.30	93.73
H2O c	-	3.87	2.13	-	2.06

Cation Proportions

basis O/OH		24/0	20/4	22/2	24/022/2
Si	6.055	5.495	3.904	6.019	3.920
Al 1V	-	2.505	-	-	-
Al V1	3.892	1.004	8.682	-	8.694
Ti	0.001	0.054	0.007	0.009	0.00
Fe	5.310	2.607	1.808	2.869	1.767
Mn	0.128	0.000	0.006	0.010	0.009
Mg	0.581	2.042	0.339	2.468	0.320
Ca	0.031	0.000	0.000	0.000	0.003
Na	0.000	0.090	0.000	0.100	0.006
K	0.000	1.876	0.002	2.060	0.028
Co	0.000	-	-	0.002	-
Ni	0.000	0.005	0.000	0.002	0.004
Ba	0.000	-	-	0.008	-
Zn	-	-	-	-	-

SAMPLE NO.: 517-057
ROCK TYPE : Lode Schist (1a)

Mineral:	bio	cht	cht	sta	gar
Site	RX	RX334	-	-	c
Number	A4-336	A4-338	A3-376	A3-378	A5-380
SiO2	35.36	23.95	26.11	27.45	36.96
TiO2	0.16	0.04	0.07	0.50	0.06
Al2O3	18.17	22.54	22.74	51.46	20.34
FeO (tot)	20.45	26.73	25.88	14.48	37.07
MnO	0.00	0.02	0.05	0.03	1.51
MgO	9.07	15.27	12.31	1.43	2.52
CaO	0.00	0.02	0.02	0.03	0.30
Na2O	0.27	0.06	0.04	0.03	0.00
K2O	9.53	0.02	0.02	0.00	0.00
Cr2O3	0.00	0.00	0.00	0.00	0.01
NiO	0.00	0.06	0.09	0.04	0.05
BaO	0.00	0.08	0.00	0.06	0.03
ZnO	-	-	-	-	-
Total	93.01	86.80	87.33	95.50	98.86
H2O c	3.87	11.15	11.37	2.10	-

Cation Proportions

basis O/OH	20/4	20/16	20/16	22/2	24/0
Si	5.520	5.154	5.510	3.921	6.059
Al 4	2.480	3.846	2.490	-	-
Al 6	0.883	1.872	3.170	8.665	3.930
Ti	0.008	0.006	0.010	0.054	0.008
Fe	2.631	4.811	4.567	1.730	5.082
Mn	0.009	0.004	0.008	0.004	0.210
Mg	2.264	4.257	3.871	0.304	0.616
Ca	0.000	0.005	0.004	0.005	0.052
Na	0.093	0.025	0.018	0.009	0.000
K	1.888	0.005	0.006	0.000	0.000
Cr	-	-	0.000	0.000	0.002
Ni	0.002	0.010	0.016	0.004	0.006
Ba	-	-	0.000	0.003	0.002
Zn	-	-	-	-	-

SAMPLE NO.: 517-057
ROCK TYPE : Lode Schist (1a)

Mineral	gar	bio	cht	gar	gar
Site	RS	RX	RX	C	R
Number	AS-382	A5-385	AS-387	A6-388	A6-392
SiO2	37.26	35.24	23.71	37.41	36.83
TiO2	0.02	1.47	0.12	0.00	0.00
Al2O3	20.61	18.46	22.29	20.70	20.29
FeO (tot)	39.35	21.17	26.59	39.48	39.30
MnO	1.11	0.01	0.05	0.97	1.07
MgO	2.17	8.92	13.04	2.44	2.02
CaO	0.22	0.00	0.03	0.19	0.21
Na2O	0.04	0.32	0.00	0.07	0.00
K2O	0.00	9.56	0.02	0.01	0.01
Cr2O3	0.07	0.06	0.02	0.04	0.01
NiO	0.03	0.01	0.07	0.06	0.00
BaO	0.00	0.00	0.04	0.05	0.00
ZnO	-	-	-	-	-
Total	100.88	95.23	85.98	101.42	99.73
H 2 0 c	3.89	11.04	-	-	-

Cation Proportions

basis O/OH	24/0	20/4	20/16	24/0	24/0
Si	6.024	5.428	5.151	6.014	6.031
Al 4	-	2.572	2.849	-	-
Al 6	3.928	0.780	2.859	3.923	3.917
Ti	0.002	0.171	0.020	0.000	0.00
Fe	5.321	2.726	4.831	5.308	5.382
Mn	0.152	0.002	0.009	0.132	0.149
Mg	0.523	2.048	4.224	0.586	0.493
Ca	0.038	0.000	0.007	0.032	0.036
Na	0.012	0.095	0.000	0.022	0.001
K	0.000	1.879	0.005	0.003	0.001
Cr	0.009	0.008	0.004	0.005	0.001
Ni	0.003	0.001	0.011	0.008	0.000
Ba	0.000	0.000	0.003	0.003	0.000
Zn	-	-	-	-	-

SAMPLE NO.: 517-057
ROCK TYPE : Lode Schist (1a)

Mineral:	bio
Site	RX
Number	A6-394
SiO2	34.72
TiO2	1.48
Al2O3	18.28
FeO (tot)	20.58
MnO	0.04
MgO	9.08
CaO	0.00
Na2O	0.35
K2O	9.33
Cr2O3	0.07
NiO	0.00
BaO	0.03
ZnO	-
Total	93.96
H2O c	3.85

Cation Proportions	
basis O/OH	20/4
Si	5.411
Al 4	2.589
Al 6	0.770
Ti	0.173
Fe	2.682
Mn	0.006
Mg	2.110
Ca	0.000
Na	0.106
K	1.856
Cr	0.008
Ni	0.000
Ba	0.002
Zn	-

SAMPLE NO.: 517-057
ROCK TYPE : Lode Schist (1a)

Mineral:	sta	sta	sta	sta	sta
Site	T	SS	T	T	T
Number	Bl-141	Bl-142	Bl-143	Bl-144	Bl-145
SiO2	27.15	27.27	27.10	27.52	27.75
TiO2	0.53	0.48	0.44	0.45	0.40
Al2O3	53.30	53.35	52.77	53.07	53.07
FeO (tot)	15.00	15.08	15.12	15.11	14.66
MnO	0.10	0.08	0.08	0.09	0.03
MgO	1.60	1.51	1.44	1.67	1.69
CaO	O.OO	0.02	0.03	0.03	O.OO
Na2O	0.02	0.08	0.04	0.05	0.06
K2O	0.03	0.01	0.00	0.03	0.00
CoO	0.00	0.00	0.00	0.00	0.00
NiO	0.04	0.06	0.00	0.00	0.01
BaO	-	-	-	-	-
ZnO	0.85	0.68	0.74	0.66	0.77
Total	98.61	98.60	97.78	98.69	98.46
H2O c	2.15	2.15	2.13	2.16	2.16

Cation Proportions

basis O/OH	22/2	22/2	22/2	22/2	22/2
Si 3.784	3.798	3.809	3.829	3.859	
Al 4	-	-	-	-	-
Al	8.755	8.1757	8.741	8.701	8.699
Ti	0.055	0.051	0.047	0.047	0.042
Fe	1.748	1.756	1.777	1.758	1.706
Mn	0.012	0.009	0.009	0.011	0.003
Mg	0.332	0.312	0.302	0.346	0.351
Ca	0.000	0.003	0.005	0.005	0.000
Na	0.004	0.021	0.012	0.013	0.017
K	0.005	0.002	0.001	0.006	0.000
Co	0.000	0.000	0.000	0.000	0.000
Ni	0.004	0.007	0.000	0.000	0.002
Ba	-	-	-	-	-
Zn	0.088	0.069	0.076	0.067	0.079

SAMPLE NO.: 517-057
ROCK TYPE : Lode Schist (1a)

Mineral	sta	sta	sta	sta	sta
Site	T	RT	RS	T	T
Number	BI-146	Bl~147	Bl-148	Bl-149	Bl-150
SiO2	27.29	27.28	27.26	27.44	26.91
TiO2	0.53	0.49	0.50	0.50	0.39
Al2O3	52.47	51.97	53.00	53.24	52.19
FeO (tot)	15.00	14.35	14.69	14.63	14.69
MnO	0.05	0.08	0.02	0.07	0.05
MgO	1.60	1.65	1.43	1.55	1.60
CaO	0.03	0.01	0.02	0.02	0.04
Na2O	0.07	0.03	0.01	0.07	0.05
K2O	0.02	0.00	0.02	0.00	0.00
CoO	0.00	0.00	0.00	0.00	0.00
NiO	0.04	0.05	0.00	0.13	0.07
BaO	-	-	-	-	-
ZnO	0.65	0.74	0.55	0.46	-0.73
Total	97.72	96.63	97.50	97.20	96.73
H2O c	2.13	2.12	2.14	2.13	2.11
Cation Proportions					
basis O/OH	22/2	22/2	22/2	22/2	22/2
Si	3.834	3.865	3.826	3.865	3.819
Al 4	-	-	-	-	-
Al 6	8.689	8.680	8.786	8.689	8.728
Ti	0.056	0.053	0.053	0.053	0.042
Fe	1.763	1.700	1.725	1.732	1.743
Mn	0.006	0.009	0.002	0.009	0.006
Mg	0.336	0.348	0.299	0.325	0.339
Ca	0.000	0.001	0.003	0.003	0.006
Na	0.018	0.009	0.003	0.019	0.015
K	0.003	0.000	0.004	0.000	0.000
Co	0.000	0.000	0.000	0.000	0.000
Ni	0.005	0.005	0.000	0.014	0.008
Ba	-	-	-	-	-
Zn	0.067	0.078	0.057	0.047	0.076

SAMPLE NO.: 517-057
ROCK TYPE : Lode Schist (1a)

Mineral:	sta	sta	sta	sta	sta
Site	T	T	T	RT	T
Number	Bl-151	Bl-152	Bl-153	Bl-154	Bl-156
SiO2	27.34	27.39	27.21	27.13	27.18
TiO2	0.45	0.50	0.44	0.47	0.43
Al2O3	51.92	52.41	52.91	52.01	53.38
FeO (tot)	14.54	15.09	14.98	14.67	14.71
MnO	0.11	0.09	0.00	0.04	0.06
MgO	1.55	1.53	1.53	1.42	1.57
CaO	0.00	0.00	0.00	0.02	0.02
Na2O	0.04	0.04	0.05	0.05	0.01
K2O	0.02	0.00	0.00	0.02	0.01
CoO	0.00	0.00	0.00	0.00	0.00
NiO	0.01	0.00	0.08	0.01	0.00
BaO	-	-	-	-	-
ZnO	0.83	0.52	0.52	0.48	0.70
Total	96.80	97.56	97.72	96.32	97.07
H2O c	2.12	2.13	2.14	2.11	2.12
Cation Proportions					
basis O/OH	22/2	22/2	22/2	22/2	22/2
Si	3.873	3.852	3.817	3.857	3.838
Al 4	-	-	-	-	-
Al 6	8.668	8.635	8.750	8.714	8.719
Ti	0.048	0.053	0.016	0.051	0.046
Fe	1.722	1.775	1.758	1.744	1.738
Mn	0.013	0.010	0.000	0.005	0.007
Mg	0.327	0.320	0.320	0.301	0.331
Ca	0.000	0.030	0.000	0.002	0.002
Na	0.012	0.010	0.014	0.014	0.003
K	0.003	0.000	0.030	0.004	0.001
Co	0.000	0.000	0.000	0.000	0.000
Ni	0.001	0.030	0.039	0.001	0.000
Ba	-	-	-	-	-
Zn	0.087	0.054	0.053	0.051	0.073

SAMPLE NO.: 517-057
ROCK TYPE : Lode Schist (1a)

Mineral:	sta	sta	bio
Site	RT	T	RX154
Number	Bl-158	Bl-159	Bl-160
SiO2	26.97	27.31	35.20
TiO2	0.47	0.44	1.57
Al2O3	53.01	52.47	18.23
FeO (tot)	15.00	14.56	19.86
MnO	0.04	0.03	0.02
MgO	1.55	1.54	9.31
CaO	0.00	0.03	0.00
Na2O	0.05	0.10	0.24
K2O	0.00	0.00	8.91
CoO	0.00	0.00	0.00
NiO	0.05	0.00	0.04
BaO	-	-	-
ZnO	0.67	0.76	0.08
Total	97.81	97.23	93.46
H2O c	2.14	2.13	3.86

Cation Proportions

basis O/OH	22/2	22/2	20/4
Si	3.786	3.848	5.473
Al 4	-	-	2.527
Al 6	8.771	8.714	0.814
Ti	0.050	0.047	0.184
Fe	1.761	1.716	2.582
Mn	0.004	0.004	0.002
Mg	0.325	0.323	2.157
Ca	0.000	0.005	0.000
Na	0.013	0.026	0.071
K	0.000	0.000	1.768
Co	0.000	0.000	0.000
Ni	0.005	0.000	0.005
Ba	-	-	-
Zn	0.069	0.079	0.009

SAMPLE NO.: 517-059
ROCK TYPE : Lode Schist (3)

Mineral	gar	gar	gar	bio	cht
Site	C	RS	RSO	RX	RX367
Number	Al-365	Al-367	Al-369	Al-370	Al-372
SiO2	37.45	36.78	37.76	36.52	24.13
TiO2	0.04	0.05	0.00	1.43	0.05
Al2O3	20.77	20.75	21.12	16.58	20.91
FeO (tot)	39.03	36.69	38.98	22.63	26.75
MnO	0.85	0.92	1.05	0.00	0.04
MgO	2.88	2.57	2.29	10.33	13.40
CaO	0.20	0.60	0.34	0.00	0.02
Na2O	0.05	0.04	0.03	0.22	0.00
K2O	0.00	0.02	0.03	9.48	0.01
Cr203	0.00	0.06	0.04	0.03	0.03
NiO	0.00	0.00	0.00	0.00	0.00
BaO	0.03	0.00	0.06	0.08	0.04
ZnO	-	-	-	-	-
Total	101.30	101.48	101.70	97.31	85.38
H2O c	-	-	-	3.96	10.95

Cation Proportions

basis O/OH	24/0	24/0	24/0	20/4	20/16
Si	6.008	5.928	6.031	5.534	5.289
Al 4	-	-	-	2.466	2.711
Al 6	-	3.943	3.977	0.495	2.689
Ti	0.005	0.006	0.000	0.163	0.008
Fe	5.236	5.351	5.208	2.869	4.896
Mn	0.115	0.126	0.142	0.000	0.008
Mg	0.689	0.618	0.546	2.334	4.376
Ca	0.034	0.103	0.059	0.000	0.004
Na	0.015	0.014	0.008	0.066	0.001
K	0.000	0.003	0.006	1.833	0.003
Cr	0.000	0.007	0.005	0,004	0.006
Ni	0.000	0.000	0.000	0.000	0.000
Ba	0.002	0.000	0.004	0.005	0.003
Zn	-	-	-	-	-

SAMPLE NO.: 517-059
ROCK TYPE : Lode Schist (3)

Mineral	gru	bio	gru	gar	gar
Site	R	RX	R	RX	C
Number	A3-374	A3-376	A5-378	A5-379	A5-380
SiO2	51.25	35.80	52.93	36.40	36.90
TiO2	0.05	1.34	0.00	0.00	0.01
Al2O3	2.25	16.46	1.14	20.50	20.75
FeO (tot)	30.18	21.87	29.10	39.22	36.89
MnO	0.18	0.07	0.13	1.06	1.25
MgO	13.05	9.85	13.67	2.23	2.69
CaO	0.03	0.00	0.04	0.37	1.20
Na2O	0.21	0.23	0.03	0.03	0.02
K2O	0.02	9.28	0.00	0.00	0.00
Cr2O3	0.05	0.04	0.05	0.00	0.00
NiO	0.04	0.02	0.00	0.01	0.00
BaO	0.07	0.00	0.00	0.00	0.01
ZnO	-	-	-	-	-
Total	97.38	94.97	97.09	99.83	99.72
H2O c	1.98	3.87	1.99	-	-

Cation Proportions

basis O/OH	22/2	20/4	22/2	24/0	24/0
Si	7.737	5.548	7.966	5.963	5.994
Al 4	0.263	2.452	-	-	-
Al 6	0.138	0.554	0.202	3.958	3.974
Ti	0.006	0.156	0.000	0.001	0.001
Fe	0.383	2.835	3.662	5.372	5.012
Mn	0.024	0.010	0.017	0.147	0.173
Mg	0.247	2.277	3.067	0.546	0.650
Ca	0.005	0.000	0.006	0.055	0.209
Na	0.062	0.069	0.009	0.010	0.008
K	0.003	1.835	0.000	0.030	0.001
Cr	0.005	0.005	0.005	0.030	0.000
Ni	0.005	0.003	0.000	0.001	0.000
Ba	0.004	0.000	0.000	0.000	0.001
Zn	-	-	-	-	-

SAMPLE NO.: 517-059
ROCK TYPE : Lode Schist (3)

Mineral:	gar	gar	bio	bio
Site	S	RS	RX	AS
Number	A5-381	AS-382	AS-383	A5-384
SiO2	37.42	36.88	36.16	35.81
TiO2	0.05	0.08	1.21	1.35
A12O3	20.73	20.57	16.33	16.60
FeO (tot)	38.72	38.99	21.72	22.39
MnO	1.01	0.97	0.01	0.00
MgO	2.80	2.32	10.09	9.88
CaO	0.20	0.74	0.00	0.00
Na2O	0.06	0.00	0.15	0.14
K2O	0.01	0.01	9.37	9.42
Cr2O3	0.06	0.04	0.05	0.00
NiO	0.04	0.11	0.00	0.06
BaO	0.03	0.00	0.00	0.00
ZnO	-	-	-	-
Total	101.10	100.71	95.09	95.65
H2O c	-	-	3.88	3.89

Cation Proportions

basis O/OH	24/0	24/0	20/4	20/4
Si	6.013	5.977	5.587	5.522
Al 1V	-	-	2.413	2.478
Al V1	3.927	3.930	0.560	0.540
Ti	0.006	0.010	0.141	0.156
Fe	5.203	5.286	2.806	2.887
Mn	0.137	0.133	0.001	0.000
Mg	0.671	0.561	2.323	2.272
Ca	0.034	0.128	0.000	0.000
Na	0.018	0.000	0.045	0.043
K	0.002	0.002	1.848	1.854
Cr	0.007	0.005	0.006	0.000
Ni	0.005	0.014	0.000	0.007
Ba	0.002	0.000	0.000	0.000
Zn	-	-	-	-

SAMPLE NO.: 517-060nam
ROCK TYPE : Lode Schist (3)

Mineral	cht	bio	gar	gar
Site	I	R	RX	CS
Number	Bl-339	Bl-341	Bl-342	Bl-343
SiO2	23.48	-	36.33	36.41
TiO2	0.03	1.42	0.02	0.38
Al2O3	21.36	17.39	20.98	20.42
FeO (tot)	29.85	22.20	40.03	37.58
MnO	0.06	0.04	0.82	1.45
MgO	11.87	9.42	2.22	2.49
CaO	0.00	0.00	0.23	1.02
Na2O	0.05	0.23	0.00	0.02
K2O	0.00	9.03	0.02	0.02
CoO	0.00	0.00	0.00	0.00
NiO	0.00	0.15	0.11	0.00
BaO	-	-	-	-
ZnO	0.22	0.05	0.16	0.20
Total	86.92	95.37	100.93	100.00
H2O c	10.99	3.89	-	-
Cation Proportions				
basis O/OH	20/20/16	16/20/4	24/0	24/0
Si	5.124	5.470	5.902	5.938
Al 4	2.876	2.530	-	-
Al 6	2.618	0.634	4.018	3.927
Ti	0.005	0.164	0.002	0.046
Fe	5.180	2.866	5.430	5.126
Mn	0.012	0.005	0.113	0.200
Mg	3.861	2.167	0.538	0.606
Ca	0.000	0.000	0.040	0.179
Na	0.020	0.069	0.000	0.008
K	0.000	1.778	0.005	0.005
Co	0.000	0.000	0.000	0.000
Ni	0.000	0.018	0.014	0.000
Ba	(0.268)	(0.000)	-	-
Zn	0.036	0.006	0.019	0.024

SAMPLE NO.: 517-060am
ROCK TYPE : Lode Schist (3)

Mineral:	gru	gru	gru	bio	bio
Site	-	C	RS	-	AS
Number	Bl-315	Bl-316	Bl-318	B2-319	B2-320
SiO2	49.19	49.66	50.29	35.51	35.29
TiO2	0.03	0.10	0.03	1.30	1.30
Al2O3	3.17	3.43	2.50	16.44	16.34
FeO (tot)	30.50	29.78	30.26	20.89	20.82
MnO	0.19	0.13	0.19	0.00	0.03
MgO	12.70	12.81	13.08	10.98	10.98
CaO	0.04	0.02	0.00	0.00	0.00
Na2O	0.19	0.24	0.17	0.22	0.21
K2O	0.01	0.01	0.00	8.47	8.66
CoO	0.00	0.00	0.00	0.00	0.00
NiO	0.00	0.00	0.00	0.00	0.05
BaO	-	-	-	-	-
ZnO	0.38	0.17	0.00	0.00	0.21
Total	96.41	96.35	96.51	93.80	93.89
H2Oc	1.96	1.96	1.96	3.86	3.85

Cation Proportions

basis O/OH	25/22/2	15/22/2	22/2	16/20/4	16/20/4
Si	7.509	7.562	7.702	5.521	5.499
Al 1V	0.491	0.438	0.298	2.479	2.501
Al V1	0.080	0.177	0.154	0.535	0.502
Ti	0.003	0.012	0.004	0.152	0.152
Fe	3.429	3.481	3.876	2.717	2.714
Mn	0.025	0.016	0.024	0.000	0.004
Mg	2.889	2.907	2.985	2.544	2.551
Ca	0.006	0.003	0.001	0.000	0.000
Na	0.057	0.072	0.051	0.056	0.064
K	0.003	0.002	0.000	1.680	1.722
Co	0.000	0.000	0.000	0.000	0.000
Ni	0.000	0.000	0.000	0.030	0.007
Ba	(0.464)	(0.311)	-	(0.000)	(0.000)
Zn	0.043	0.019	0.000	0.000	0.024

SAMPLE NO.: 517-060am
ROCK TYPE : Lode Schist (3)

Mineral	gar	gru	gru
Site	RX	c	c
Number	Bl-324	B5-327	B5-328
SiO2	36.61	51.04	50.98
TiO2	0.04	0.04	0.09
Al2O3	20.58	0.89	0.81
FeO (tot)	38.66	29.33	29.80
MnO	1.02	0.18	0.22
MgO	2.45	13.92	13.79
CaO	0.37	0.03	0.04
Na2O	0.00	0.01	0.07
K2O	0.01	0.00	0.03
CoO	0.00	0.00	0.00
NiO	0.12	0.03	0.14
BaO	-	-	-
ZnO	0.21	0.14	0.00
Total	100.06	95.60	95.95
H2O c	-	1.95	1.96

Cation Proportions

basis O/OH	24/0	15/22/2	15/22/2
Si	5.970	7.834	7.805
Al 4	-	0.162	0.146
Al 6	3.956	0.000	0.000
Ti	0.004	0.005	0.010
Fe	5.273	3.602	3.565
Mn	0.141	0.024	0.028
Mg	0.596	3.186	3.147
Ca	0.064	0.004	0.007
Na	0.000	0.002	0.020
K	0.001	0.001	0.005
Co	0.000	0.000	0.000
Ni	0.016	0.003	0.017
Ba	-	(0.163)	(0.251)
Zn	0.025	0.015	0.000

SAMPLE NO.: 517-061A
ROCK TYPE : Lode Schist (3)

Mineral:	gru	bio	cht	bio	bio
Site	-	-	-	R	AS
Number	Al-382	Al-383	Al-384	A6-386	A6-387
SiO2	51.36	35.80	24.37	36.16	35.20
TiO2	0.09	1.38	0.09	1.19	1.24
Al2O3	3.20	16.48	21.11	16.74	16.83
FeO (tot)	30.46	21.89	26.62	21.88	22.19
MnO	0.14	0.00	0.09	0.02	0.06
MgO	12.85	10.00	13.83	10.17	10.23
CaO	0.05	0.00	0.00	0.00	0.00
Na2O	0.30	0.20	0.04	0.24	0.20
K2O	0.02	9.44	0.00	9.38	9.56
Cr2O3	0.04	0.05	0.03	0.03	0.03
NiO	0.00	0.01	0.00	0.09	0.08
BaO	0.08	0.08	0.12	0.00	0.00
ZnO	-	-	-	-	-
Total	98.61	95.34	86.30	95.89	95.61
H2O c	2.00	3.88	11.08	3.91	3.88

Cation Proportions

basis O/OH	22/2	20/4	20/16	20/4	20/4
Si	7.685	5.533	5.279	5.544	5.443
Al 4	-	2.467	2.721	2.456	2.557
Al 6	0.565	0.533	2.668	0.350	0.511
Ti	0.010	0.160	0.014	0.137	0.145
Fe	3.812	2.830	4.822	2.806	2.869
Mu	0.017	0.000	0.016	0.002	0.008
Mg	2.866	2.304	4.466	2.324	2.358
Ca	0.009	0.000	0.000	0.000	0.000
Na	0.088	0.051	0.018	0.072	0.061
K	0.004	1.862	0.000	1.834	1.886
Cr	0.005	0.006	0.006	0.033	0.003
Ni	0.000	0.002	0.000	0.011	0.010
Ba	0.005	0.005	0.010	0.000	0.000
Zn	-	-	-	-	-

SAMPLE NO.: 517-061A
ROCK TYPE : Lode Schist (3)

Mineral:	gar	gar	gar	bio	gar
Site	RX	RSO	AS	RX	T
Number	A6-388	A6-389	A6-390	A6-391	A6-393
SiO2	39.74	36.69	36.73	35.79	37.02
TiO2	0.03	0.03	0.06	1.42	0.00
Al2O3	19.77	20.21	20.72	16.66	20.45
FeO (tot)	37.07	38.02	38.96	21.80	39.50
MnO	0.70	0.68	0.68	0.00	0.82
MgO	2.40	2.22	2.55	10.22	2.34
CaO	0.54	0.95	0.61	0.00	0.20
Na2O	0.03	0.02	0.00	0.18	0.00
K2O	0.00	0.00	0.00	8.99	0.00
Cr2O3	0.06	0.05	0.06	0.05	0.05
NiO	0.00	0.09	0.00	0.00	0.01
BaO	0.00	0.00	0.05	0.00	0.05
ZnO	-	-	-	-	-
Total	100.35	98.95	100.42	95.10	100.44
H2O c	-	-	-	3.89	-

Cation Proportions

basis O/OH	24/0	24/0	24/0	20/4	24/0
Si		6.031	5.960	5.522	6.016
Al 4		-	-	2.478	-
Al 6		3.915	3.963	0.551	3.916
Ti		0.003	0.008	0.165	0.000
Fe		5.227	5.288	2.813	5.387
Mn		0.095	0.094	0.000	0.113
Mg		0.543	0.616	2.349	0.566
Ca		0.157	0.106	0.000	0.034
Na		0.006	0.000	0.053	0.000
K		0.000	0.000	1.769	0.000
Cr		0.006	0.008	0. 006	0.006
Ni		0.012	0.000	0.000	0.002
Ba		0.000	0.003	0.000	0.003
Zn					

SAMPLE NO.: 517-061A
ROCK TYPE : Lode Schist (3)

Mineral:	gar	gar	gar
Site	T	T	T
Number	A6-345	A6-346	A6-347
SiO2	36.63	36.61	36.44
TiO2	0.05	0.00	0.01
Al2O3	20.50	20.71	20.49
FeO (tot)	39.21	40.12	39.67
MnO	1.74	0.76	0.28
MgO	1.88	2.14	2.48
CaO	0.23	0.22	0.32
Na2O	0.01	0.04	0.00
K2O	0.00	0.00	0.00
Cr2O3	0.00	0.03	0.03
NiO	0.00	0.04	0.00
BaO	0.14	0.00	0.00
ZnO	-	-	-
Total	100.37	100.68	99.72
H2O c	-	-	-

Cation Proportions

basis O/OH	24/0	24/0	24/0
Si	5.982	5.954	5.966
Al 1V	-	-	-
Al V1	3.946	3.970	3.953
Ti	0.006	0.000	0.001
Fe	.5.356	5,456	5.431
Mn	0.240	0.105	0.039
Mg	0.459	0.520	0.606
Ca	0.039	0.038	0.056
Na	0.003	0.013	0.000
K	0.000	0.000	0.000
Cr	0.000	0.004	0.003
Ni	0.000	0.005	0.000
Ba	0.009	0.000	0.000
Zn	-	-	-

SAMPLE NO.: 517-061A
ROCK TYPE : Lode Schist (3)

Mineral:	mt	mt	mt	ilm
Site	R	AS	Igar	Igar
Number	Cl-262	Cl-263	C2-264	C2-266
SiO2	-	-	-	-
TiO2	0.29	0.30	0.30	49.99
Al2O3	0.34	0.30	0.41	0.08
FeO (tot)	92.64	91.92	90.61	48.25
MnO	-	-	-	0.13
MgO	-	-	-	-
CaO	-	-	-	-
Na2O	-	-	-	-
K2O	-	-	-	-
Cr2O3	-	-	0.72	-
NiO	-	-	-	-
BaO	-	-	-	-
ZnO	-	-	-	0.19
Total	93.27	92.72	92.08	98.69
H20c	-	-	-	-

Cation Proportions

basis O/OH	24/0	24/0	24/0	24/48/0
Si	-	-	-	-
Al 1V	-	-	-	(0.454)
Al V1	0.122	0.110	0.150	0.014
Ti	0.066	0.069	0.695	11.532
Fe	23.684	23.697	23.372	11.923
Mn	-	-	-	0.034
Mg	-	-	-	-
Ca	-	-	-	-
Na	-	-	-	-
K	-	-	-	-
Cr	-	-	0.176	-
Ni	-	-	-	-
Ba	-	-	-	-
Zn	-	-	-	0.043

SAMPLE NO.: 517-076A
ROCK TYPE : Lode Schist (2)

Mineral:	sta	sta	sta	sta
Site	R	T	T	T
Number	Bl-291	Bl~292	Bl-299	Bl-300
SiO2	27.25	26.45	26.08	25.46
TiO2	0.54	0.59	0.35	0.36
A2O3	52.82	52.97	52.99	53.55
FeO (tot)	15.94	16.47	15.85	16.50
MnO	0.21	0.11	0.12	0.09
MgO	1.56	1.57	1.52	1.47
CaO	0.00	0.00	0.00	0.00
Na2O	0.00	0.05	0-00	0.00
K2O	0.00	0.02	0.00	0.03
CoO	0.00	0.00	0.00	0.00
NiO	0.01	0.03	0.00	0.00
BaO	-	-	-	-
ZnO	0.19	0.08	0.19	0.15
Total	98.52	98.35	97.09	97.61
H2O c	2.15	2.14	2.11	2.12
Cation Proportions				
basis O/OH 22/2		22/2	22/2	22/2
Si	3.806	3.714	3.699	3.607
Al 1V	-	-	-	-
Al V1	8.695	8.766	8.860	8.943
Ti	0.056	0.62	0.037	0.038
Fe	1.862	1.935	1.880	1.956
Mn	0.025	0.013	0.014	0.011
Mg	0.325	0.329	0.322	0.310
Ca	0.000	0.000	0.000	0.000
Na	0.001	0.014	0.000	0.000
K	0.001	0.004	0.000	0.006
Co	0.000	0.000	0.000	0.000
Ni	0.001	0.004	0.000	0.000
Ba	-	-	-	-
Zn	0.020	0.008	0.019	0.016

SAMPLE NO.: 517-076B
ROCK TYPE : Lode Schist (2)

Mineral:	sta	bio	bio	gar	gar
Site	-	R	AS	IC	RS
Number	Al-397	Al-399	Al-401	Al-403	Al-404
SiO2	28.16	33.76	33.95	37.09	37.87
TiO2	0.27	1.47	1.42	0.00	0.10
Al2O3	51.76	18.07	18.24	20.59	20.71
FeO (tot)	14.87	21.84	21.41	38.52	39.31
MnO	0.12	0.02	0.04	2.19	2.33
MgO	1.56	8.21	8.26	2.14	1.96
CaO	0.00	0.00	0.00	0.21	0.24
Na2O	0.02	0.35	0.33	0.02	0.05
K2O	0.01	9.28	9.14	0.01	0.01
Cr2O3	0.07	0.03	0.05	0.06	0.00
NiO	0.03	0.05	0.06	0.04	0.07
BaO	0.00	0.07	0.00	0.00	0.07
ZnO	-	-	-	-	-
Total	96.85	93.12	92.90	100.87	102.73
H2O c	2.13	-	3.78	-	-

Cation Proportions

basis O/OH	22/2	20/4	24/0	24/0
Si	3.968	5.381	6.006	6.032
Al 1V	-	2.619	-	-
Al V1	8.597	0.788	3.931	3.838
Ti	0.029	0.109	0.000	0.0L2
Fe	1.752	2.838	5.218	5.237
Mn	0.015	0.006	0.300	0.314
Mg	0.327	1.952	0.516	0.465
Ca	0.000	0.000	0.036	0.041
Na	0.005	0.102	0.005	0.014
K	0.002	1.849	0.002	0.003
Cr	0.007	0.006	0.008	0.000
Ni	0.003	0.007	0.005	0.009
Ba	0.000	0.000	0.000	0.005
Zn	-	-	-	-

SAMPLE NO.: 517-076B
ROCK TYPE : Lode Schist (2)

Mineral	sta	gar	gar	gar	gar
Site	RX399	c	RS	AS	RSO
Number	Al-407	Al-409	Al-410	Al-411	Al-412
SiO2	27.14	36.80	37.85	37.45	37.48
TiO2	0.45	0.88	0.09	0.02	0.10
Al2O3	53.10	20.33	21.03	20.52	20.64
FeO (tot)	15.72	38.26	38.29	38.68	38.52
MnO	0.12	2.13	2.25	2.32	2.29
MgO	1.37	2.24	2.08	2.08	2.02
CaO	0.00	0.22	0.23	0.26	0.21
Na2O	0.04	0.01	0.08	0.04	0.01
K2O	0.00	0.00	0.11	0.00	0.02
Cr2O3	0.00	0.04	0.05	0.01	0.07
NiO	0.00	0.00	0.07	0.02	0.05
BaO	0.00	0.03	0.01	0.07	0.00
ZnO	-	-	-	-	-
Total	97.94	100.95	102.14	101.48	101.41
H2O c	2.14	-	-	-	-
Cation Proportions					
basis O/OH	22/2	24/0	24/0	24/0	24/0
Si	3.802	5.955	6.034	6.032	6.032
Al 1V	-	-	-	-	-
Al V1	8.768	3.877	3.952	3.896	3.915
Ti	0.047	0.107	0.01D	0.002	0.012
Fe	1.842	5.178	5.104	5.211	5.185
Mn	0.014	0.292	0.304	0.316	0.312
Mg	0.286	0.541	0.493	0.499	0.484
Ca	0.000	0.038	0.040	0.045	0.036
Na	0.012	0.004	0.025	0.012	0.004
K	0.000	0.000	0.022	0,000	0.004
Cr	0.000	0.005	0.007	0.002	0.008
Ni	0.000	0.001	0.009	0.003	0.006
Ba	0.000	0.002	0.001	0,004	0.000
Zn	-	-	-	-	-

SAMPLE NO.: 517-076B
ROCK TYPE : Lode schist (2)

Mineral	cht	bio	sta	sta
Site	-	-	C	AS
Number	A3-413	A3-415	A4-419	A4-421
SiO2	23.90	35.16	27.06	26.65
TiO2	0.07	1.52	0.50	0.42
Al2O3	22.78	18.79	53.27	52.70
FeO (tot)	28.70	22.23	15.63	15.92
MnO	0.09	0-01	0.09	0.10
MgO	12.49	8-13	1.53	1.31
CaO	0.02	0 00	0.00	0.01
Na2O	0.03	0 33	0.00	0.02
K2O	0.03	9.74	0.00	0.00
Cr2O3	0.02	0.00	0.05	0.08
NiO	0.00	0.08	0.02	0.08
BaO	0.04	0.00	0.03	0.00
ZnO	-	-	-	-
Total	88.15	95.99	98.16	97.30
H2O c	11.22	3.90	2.15	2.12
Cation Proportions				
basis O/OH	20/16	20/4	22/2	22/2
Si	5.109	5.404	3.782	3.768
Al 1V	2.891	2.596	-	-
Al V1	2.849	0.808	8.777	8.784
Ti	0.011	0.176	0.052	0.045
Fe	5.132	2.857	1.827	1.883
Mn	0.017	0.001	0.100	0.012
Mg	3.980	1.862	0.319	0.275
Ca	0.004	0.000	0.000	0.002
Na	0.010	0.098	0.000	0.007
K	0.009	1.910	0.000	0.001
Cr	0.003	0.000	0.005	0.008
Ni	0.000	0.009	0.002	0.009
Ba	0.003	0.000	0.001	0.000
Zn	-	-	-	-

SAMPLE NO.: 517-076B
ROCK TYPE : Lode Schist (2)

Mineral	
Site Number	BI-330
SiO2	26.97
TiO2	0.58
Al2O3	52.69
FeO (tot)	15.46
MnO	0.08
MgO	1.53
CaO	0.01
Na2O	0.00
K2O	0.01
CoO	0.00
NiO	0.15
BaO	-
ZnO	0.45
Total	97.94
H2O c	2.13

Cation Proportions	
basis O/OH	22/2
Si	3.789
Al 1V	-
Al V1	8.725
Ti	0.061
Fe	1.816
Mn	0.009
Mg	0.321
Ca	0.002
Na	0.001
K	0.002
Co	0.000
Ni	0.017
Ba	-
Zn	0.046

SAMPLE NO.: 517-077
ROCK TYPE : Lode Schist (3)

Mineral:	gar	gar	bio	bio	gru
Site	C	RS	RX	AS	C
Number	Al-354	Al-355	Al-357	Al-358	A2-360
SiO2	36.76	36.28	34.23	33.19	49.71
TiO2	0.00	0.05	1.25	1.25	0.03
Al2O3	20.46	20.89	16.66	16.35	1.20
FeO (tot)	38.90	40.01	26.82	27.36	36.17
MnO	1.73	0.93	0.07	0.00	0.15
MgO	1.63	1.37	6.83	6.55	9.20
CaO	0.37	0.28	0.00	0.00	0.03
NaO2O	0.00	0.00	0.28	0.28	0.03
KO2O	0.01	0.005	8.21	7.60	0.16
CrO2O3	0.00	0.001	0.01	0.00	0.00
NiO	0.03	0.000	0.01	0.00	0.01
BaO	0.04	0.000	0.00	0.02	0.00
ZnO	-	-	-	-	-
Total	99.93	99.87	94.37	92.60	96.69
H2O c	-	-	3.76	3.68	1.90

Cation Proportions

basis O/OH	24/0	24/0	20/4	20/4	22/2
si	6.019	5.956	5.458	5.411	7.840
Al 1V	-	-	2.542	2.589	-
Al V1	3.950	4.041	0.588	0.553	0.223
Ti	0.000	0.006	0.150	0.153	0.004
Fe	5.327	5.493	3.576	3.730	4.770
Mn	0.241	0.130	0.009	0.000	0.020
Mg	0.399	0.336	1.624	1.591	2.162
Ca	0.064	0.049	0.000	0.000	0.004
Na	0.000	0.000	0.086	0.038	0.010
K	0.002	0.010	1.670	1.531	0.032
Cr	0.000	0.001	0.001	0.000	0.000
Ni	0.004	0.000	0.001	0.000	0.002
Ba	0.003	0.000	0.000	0.001	0.000
Zn	-	-	-	-	-

SAMPLE NO.: 517-077
ROCK TYPE : Lode Schist (3)

Mineral:	gru	gru	cht	bio	gar
Site	ss	R	RX	-	R
Number	A2-361	A2-362	A2-363	A2-347	A2-348
SiO2	50.08	51.15	25.79	34.37	36.36
TiO2	0.06	0.08	0.27	0.63	0.03
Al2O3	1.60	0.61	12.71	16.78	20.68
FeO (tot)	35.96	36.65	39.71	27.52	40.38
MnO	0.18	0.12	0.03	0.06	0.98
MgO	9.10	9.49	5.73	6.67	1.40
CaO	0.04	0.04	0.10	0.00	0.36
Na2O	0.14	0.09	0.06	0.27	0.06
K2O	0.28	0.01	0.19	8.35	0.03
Cr2O3	0.03	0.05	0.03	0.03	0.03
NiO	0.01	0.05	0.10	0.06	0.04
BaO	0.14	0.00	0.00	0.05	0.17
ZnO	-	-	-	-	-
Total	97.62	98.32	84.72	94.80	100.51
H2O c	1.92	1.94	9.99	3.76	-

Cation Proportions

basis O/OH	22/2	22/2	20/16	20/4	24/0
Si	7.818	7.916	6.191	5.477	5.952
Al 1V	-	-	1.809	2.523	-
Al V1	0.295	0.112	1.786	0.628	3.990
Ti	0.007	0.009	0.049	0.075	0.003
Fe	4.695	4.743	7.965	3.668	5.528
MU	0.024	0.016	0.006	0.008	0.136
Mg	2.117	2.188	2.051	1.585	0.342
Ca	0.007	0.006	0.024	0.000	0.063
Na	0.043	0.027	0.030	0.084	0.019
K	0.055	0.001	0.057	1.698	0.006
Cr	0.003	0.006	0.006	0.004	0.004
Ni	0.002	0.006	0.020	0.008	0.005
Ba	0.009	0.000	0.000	0.003	0.011
Zn					

SAMPLE NO.: 517-077
ROCK TYPE : Lode Schist (3)

Mineral	bio	bio	gar	gar
Site	RX	S	C348	AS
Number	A2-349	A2-351	A2-352	A2-353
SiO2	32.93	34.06	37.25	36.37
TiO2	0.59	0.65	0.00	0.04
Al2O3	16.05	16.86	20.68	20.49
FeO (tot)	27.89	27.11	39.09	26.33
MnO	0.07	0.05	2.49	3.74
MgO	6.32	6.67	1.54	2.33
CaO	0.00	O.OD	0.47	0.42
Na2O	0.29	0.25	0.06	0.00
K2O	7.90	8.40	0.00	0.00
Cr2O3	0.01	0.01	0.03	0.00
NiO	0.05	0.04	0.08	0.07
BaO	0.04	0.00	0.06	0.00
ZnO	-	-	-	-
Total	92.15	94.10	101.75	99.81
H2O c	3.63	3.74	-	-

Cation Proportions

basis O/OH	20/4	20/4	24/0	24/0
Si	5.434	5.461	6.008	5.942
Al 1V	2.566	2.539	-	-
Al V1	0.555	0.647	3.931	3.935
Ti	0.073	0.078	0.000	0.004
Fe	3.850	3.636	5.273	5.415
Mn	0.010	0.007	0.340	0.328
Mg	1.555	1.595	0.370	0.387
Ca	0.000	0.000	0.081	0.065
Na	0.094	0.076	0.019	0.000
K	1.664	1.719	0.000	0.000
Cr	0.002	0.001	0.004	0.002
Ni	0.006	0.005	0.010	0.009
Ba	0.002	0.000	-	-
Zn	-	-	-	-

SAMPLE NO.: 517-077 lay
ROCK TYPE : Lode Schist (3)

Mineral	bio	gar	gar	gar	gru
Site	R	RX	CS	S	-
Number	Bl-397	Bl-398	Bl-399	Bl-405	B2-407
SiO2	33.52	35.56	36.66	36.37	48.77
TiO2	1.76	0.04	0.07	0.10	0.03
Al2O3	16.36	20.46	20.54	20.43	0.63
FeO (tot)	26.40	39.89	32.29	33.43	35.24
MnO	0.00	1.15	6.78	4.60	0.18
MgO	6.32	1.29	1.16	1.18	9.30
CaO	0.00	0.36	2.22	2.82	0.03
Na2O	0.29	0.03	0.06	0.06	0.02
K2O	8.75	0.01	0.00	0.01	0.00
coo	0.00	0.00	0.00	0.00	0.00
NiO	0.00	0.00	0.00	0.00	0.03
BaO	-	-	-	-	-
ZnO	0.34	0.07	0.00	0.21	0.13
Total	93.74	98.86	99.80	99.20	94.37
H2O c	3.71	-	-	-	1.86

Cation Proportions

basis O/OH	20/4	24/0	24/0	24/0	22/2
Si	5.413	5.923	5.999	5.984	7.897
Al 1V	2.587	-	-	-	0.103
Al V1	0.527	4.017	3.962	3.963	0.018
Ti	0.214	0.005	0.008	0.013	0.004
Fe	3.566	5.557	4.419	4.600	4.762
Mn	0.000	0.162	0.940	0.642	0.025
Mg	1.521	0.320	0.284	0.290	2.240
Ca	0.000	0.065	0.390	0.497	0.005
Na	0.091	0.008	0A20	0.018	0.006
K	1.803	0.002	0.000	0.002	0.000
Co	0.000	0.000	0.000	0.000	0.000
Ni	0.000	0.000	0.000	0.000	0.003
Ba	-	-	-	-	-
Zn	0.041	0.009	0.000	0.025	0.016

SAMPLE NO.: 517-077 Lay
ROCK TYPE : Lode Schist (3)

Mineral	gru	gru	gru
Site	AS	R	CS
Number	B2-410	B6-412	B6-413
SiO 2	49.92	49.91	50.20
TiO 2	0.07	0.08	0.02
A12 0 3	0.64	0.64	0.82
FeO (tot)	36.34	35.60	36.05
MnO	0.08	0.20	0. 15
Mgo	9.10	9.41	9.51
CaO	0,00	0.05	0.05
Na20	0.10	0.07	0.02
K 2 0	0.00	0.02	0.00
coo	0.00	0.00	0.00
NiO	0.00	0.08	0.03
BaO	-	-	-
ZnO	0.00	0.11	0.16
Total	96.26	96.15	97.01
H20 c	1.89	1.90	1.92
Cation Proportions			
basis O/OH	22/2	15/22/2	15/22/2
Si	7.907	7.877	7.854
Al 1V	0.093	0.118	0.146
Al V1	0.027	0.000	0.005
Ti	0.008	0.009	0.002
Fe	4.815	4.566	4.572
Mn	0.011	0.027	0.020
Mg	2.148	2.213	2.219
Ca	0.000	0.008	0.008
Na	0.031	0.020	0.007
K	0.000	0.005	0.000
Co	0,0C0	0.000	0.000
Ni	0,0C0	0.010	0.003
Ba	-	(0.133)	(0.145)
Zn	0.000	0.013	0.018

SAMPLE NO.: 517-077U
ROCK TYPE : Lode Schist (3)

Mineral:	bio	gar	bio	gar	gru
Site	R	RX	X349	RX	-
Number	BI-349	BI-351	Bl-358	Bl-360	Bl-364
SiO2	33.23	35.85	33.65	35.41	49.62
TiO2	0.65	0.01	0.69	0.02	0.01
Al2O3	16.76	20.44	18.37	20.27	0.74
FeO (tot)	28.26	40.35	25.98	40.46	36.76
MnO	0.05	1.01	0.09	1.09	0,19
MgO	6.37	1.25	6.37	1.17	9,00
CaO	0.00	0.31	0.00	0.30	0,04
Na2O	0.27	0.03	0.28	0.02	0,03
K2O	8.02	0.02	7.97	0.02	0.01
CoO	0.00	0.00	0.00	0.00	0.00
NiO	0.06	0.00	0.11	0.12	0.00
BaO	-	-	-	-	-
ZnO	0.11	0.20	0.10	0.06	0.26
Total	93.78	99.48	93.62	98.95	96.66
H2O c	-	-	3.75	-	1.90

Cation Proportions

basis O/OH	24/0	20/4	24/0	15/24/2
Si	5.940	5.378	5.915	7.825
Al 1V	-	2.622	-	0.138
Al V1	3.992	0.838	3.991	0.000
Ti	0.001	0.083	0.002	0.001
Fe	5.591	3.473	5.652	4.626
Mn	0.142	0.013	0.154	0.026
Mg	0.309	1.518	0.290	2.116
Ca	0.055	0.000	0.054	0.007
Na	0.011	0.087	0.006	0.008
K	0.005	1.626	0.005	0.002
Co	0.000	0.000	0.000	0.000
Ni	0.000	0.014	0.016	0.000
Ba	-	-	-	(0.221)
Zn	0.025	0.012	0.007	0.030

SAMPLE NO.: 517-077V
ROCK TYPE : Lode Schist (3)

Mineral:	mt	bio	gar	gru
Site	-	R	RX	-
Number	Bl-368	B2-370	B2-371	B4-372
SiO2	0.10	33.49	35.93	49.82
TiO2	0.24	0.76	0.03	0.05
Al2O3	0.32	17.28	20.79	0.74
FeO (tot)	91.65	27.45	41.23	37.30
MnO	0.00	0.04	1.08	0.19
MgO	0.00	6.37	1.26	8.79
CaO	0.00	0.00	0.31	0.04
Na2O	0.07	0.22	0.05	0.05
K2O	0.00	8.35	0.03	0.00
CoO	0.00	0.00	0.00	0.00
NiO	0.07	0.10	0.09	0.04
BaO	-	-	-	-
ZnO	0.00	0.44	0.11	0.00
Total	92.44	94.51	100.92	97.03
H2O c	-	3.74	-	-

Cation Proportions

basis O/OH	24/32/0	20/4	24/0	22/2
Si	0.030	5.374	5.886	7.869
Al Iv	(15.753)	2.626	-	0.131
Al V1	0.117	0.621	4.015	0.006
Ti	0.055	0.092	0.004	0.006
Fe	7.987	3.683	5.648	4.927
Mn	0.000	0.005	0.150	0.026
Mg	0.000	1.524	0.308	2.070
Ca	0.000	0.000	0.054	0.006
Na	0.039	0.069	0.015	0.016
K	0.000	1.710	0.006	0.000
Co	0.000	0.000	0.000	0.000
Ni	0.019	0.013	0.012	0.005
Ba	-	-	-	-
Zn	0.000	0.052	0.014	0.000

SAMPLE NO.: 517-101
ROCK TYPE : Lode Schist (2)

Mineral:	cht	sta	sta	hem	gar
Site	RX-349	R	AS	-	C
Number	Al-348	A5-345	A5-346	A6-351	Al-348
SiO2	22.95	26.93	26.99	1.33	36.52
TiO2	0.05	0.16	0.16	0.04	0.06
Al2O3	22.88	53.99	54.31	0.15	20.72
FeO (tot)	31.10	13.66	13.77	71.52	38.51
MnO	0.09	0.14	0.09	0.09	1.35
MgO	9.77	0.99	1.00	0.00	2.27
CaO	0.03	0.03	0.02	0.06	0.26
Na2O	0.00	0.06	0.06	0.07	0.06
K2O	0.03	0.00	0.00	0.00	0.00
Cr2O3	0.00	0.00	0.00	0.04	0.04
NiO	0.09	0.00	0.05	0.00	0.00
BaO	0.04	0.01	0.08	0.00	0.00
ZnO	-	-	-	-	-
Total	87.03	95.97	96.53	73.31	99.78
H 2 0 c	10.90	2.12	2.13	-	-

Cation Proportions

basis O/OH	20/16	22/2	22/2	24/0
Si	5.050	3.808	3.797	5.968
Al 1V	2.950	-	-	
Al V1	2.986	8.997	9.007	3.990
Ti	0.009	0.017	0.017	0.008
Fe	5.725	1.616	1.621	5.263
Mn	0.017	0.017	0.011	0.187
Mg	3.207	0.209	0.209	0.552
Ca	0.007	0.004	0.003	0.45
Na	0.000	0.016	0.015	0.017
K	0.007	0.000	0.000	0.000
Cr	0.000	0.000	0.000	0.005
Ni	0.016	0.000	0.006	0.000
Ba	0.000	0.001	0.004	0.000
Zn	-	-	-	-

SAMPLE NO.: 517-101
ROCK TYPE : Lode Schist (2)

Mineral	gar
Site	RS
Number	Al-349
SiO2	36.01
TiO2	0.00
Al2O3	20.81
FeO (tot)	39.63
MnO	1.75
MgO	1.53
CaO	0.21
Na2O	0.00
K2O	0.00
Cr2O3	0.01
NiO	0.00
BaO	0.09
ZnO	-
Total	100.05
H2O c	-

Cation Proportions

basis O/OH	24/0
Si	5.919
Al 1V	-
Al V1	4.032
Ti	0.000
Fe	5.448
Mn	0.244
Mg	0.376
Ca	0.037
Na	0.000
K	0.000
Cr	0.002
Ni	0.001
Ba	0.006
Zn	-

SAMPLE NO.: 517-101
ROCK TYPE : Lode Schist (2)

Mineral	sta	sta	cht	mt	mt
Site	C	RS	RX	C	RS
Number	B4-261	B4.264	B4-265	B6-266	B6-267
SiO2	27.49	27.64	23.04	0.11	0.16
TiO2	0.09	0.25	0.10	0.09	0.10
Al2O3	54.49	54.20	22.81	0.37	0.25
FeO (tot)	13.84	14.17	30.82	87.72	85.45
MnO	0.08	0.14	0.05	0.00	0.00
MgO	0.99	0.89	9.78	0.00	0.00
CaO	0.00	0.01	0.04	0.02	0.01
Na2O	0.06	0.09	0.00	0.06	0.04
K2O	0.00	0.01	0.01	0.00	0.00
CoO	0.00	0.00	0.00	0.00	0.00
NiO	0.10	0.00	0.05	0.08	0.11
BaO	-	-	-	-	-
ZnO	1.32	0.96	0.25	0.19	0.00
Total	98.47	98.36	86.95	88.64	86.14
H2O c	2.16	2.16	10.90	-	-
Cation Proportions					
basis O/OH	22/2	22/2	20/16	24/32/0	24/32/0
Si	3.816	3.839	5.070	0.035	0.054
Al 1V	-	-	2.930	(15.78)	(15.773)
Al V1	8.915	8.873	2.988	0.142	0.097
Ti	0.010	0.027	0.016	0.023	0.026
Fe	1.607	1.646	5.673	7.905	7.987
Mn	0.009	0.017	0.010	O.OOD	0.000
Mg	0.204	0.184	3.208	O.OOD	0.000
Ca	0.000	0.002	0.010	0.006	0.004
Na	0.016	0.023	0.000	0.039	0.029
K	0.000	0.001	0.002	0.001	0.000
Co	0.000	0.000	0.000	0.003	0.000
Ni	0.012	0.000	0.009	0.02D	0.031
Ba	-	-	-	-	-
Zn	0.136	0.098	0.040	0.046	0.000

SAMPLE NO.: 517-101
ROCK TYPE : Lode Schist (2)

Mineral	mt	mt
Site	AS	C
Number	B6-270	B6-271
SiO2	0.11	0.11
TiO2	0.13	0.14
Al2O3	0.34	0.35
FeO (tot)	88.94	89.76
MnO	0.08	0.00
MgO	0.00	0.00
CaO	0.01	0.02
Na2O	0.07	0.02
K2O	0.01	0.00
CoO	0.00	0.00
NiO	0.00	0.09
BaO	-	-
ZnO	0.00	0.13
Total	89.68	90.62
H2O c	-	-

Cation Proportions

basis O/OH	24/32/0	24/32/0
Si	0.034	0.036
Al 1V	(15.791)	(15.745)
Al V1	0.127	0.130
Ti	0.030	0.032
Fe	7.945	7.983
Mn	0.022	0.000
Mg	0.000	0.000
Ca	0.005	0.008
Na	0.041	0.012
K	0.005	0.000
Co	0.000	0.000
Ni	0.000	0.023
Ba	-	-
Zn	0.000	0.030

SAMPLE NO.: 517-112
ROCK TYPE : Lode Schist (1b)

Mineral	sta	bio	gar	bio	sta
Site	R	RX	RX	S	-
Number	Bl-162	Bl-163	Bl-164	Bl-166	Bl-167
SiO2	27.12	34.98	36.51	34.39	27.56
TiO2	0.44	1.57	0.01	1.69	0.51
Al2O3	53.23	19.51	20.79	19.36	52.37
FeO (tot)	14.89	21.28	37.61	21.09	14.96
MnO	0.10	0.09	1.96	0.13	0.15
MgO	1.56	8.06	2.03	8.01	1.58
CaO	0.00	0.00	0.22	0.00	0.00
Na2O	0.04	0.22	0.06	0.24	0.04
K2O	0.01	9.09	0.04	9.29	0.00
CoO	0.00	0.00	0.00	0.00	0.00
NiO	0.00	0.01	0.01	0.00	0.03
BaO	-	-	-	-	-
ZnO	0.75	0.00	0.00	0.27	0.46
Total	98.13	94.83	99.25	94.46	97.65
H2O c	2.14	3.89	-	3.86	2.14

Cation Proportions

basis O/OH	22/2	20/4	24/0	20/4	22/2
Si	3.792	5.391	5.990	5.344	3.869
Al 1V	-	2.609	-	2.656	-
Al V1	8.774	0.936	4.021	0.890	8.664
Ti	0.046	0.182	0.001	0.197	0.054
Fe	1.742	2.744	5.161	2.741	1.756
Mn	0.012	0.012	0.273	0.017	0.017
Mg	0.325	1.852	0.497	1.855	0.330
Ca	0.000	0.000	0.039	0.000	0.000
Na	0.010	0.067	0.019	0.071	0.012
K	0.003	1.788	0.008	1.842	0.000
Co	0.000	0.000	0.000	0.000	0.000
Ni	0.000	0.001	0.002	0.000	0.003
Ba	-	-	-	-	-
Zn	0.077	0.000	0.001	0.031	0.047

SAMPLE NO.: 517-112
ROCK TYPE : Lode Schist (1b)

Mineral:	bio	sta	sta	sta	sta
Site	AS166	-	-	S	S
Number	Bl-168	B2-169	B3-170	B3-172	B3-171
SiO2	34.02	27.08	27.45	27.66	27.14
TiO2	1.55	0.40	0.40	0.20	0.30
Al2O3	18.92	52.49	54.02	52.94	52.94
FeO (tot)	22.13	14.48	14.42	15.11	14 .67
MnO	0.06	0.14	0.11	0.08	0.12
MgO	7.57	1.38	1.42	1.56	l.42
CaO	0.00	0.01	0.00	0.02	0.02
Na2O	0.25	0.00	0.02	0.03	0.04
K2O	9.43	0.00	0.00	0.02	0.00
CoO	0.00	0.00	0.00	0.00	0.00
NiO	0.00	0.06	0.05	0.13	0.11
BaO	-	-	-	-	-
ZnO	0.19	0.68	0.88	0.65	0.68
Total	94.10	96.71	98.77	98.41	97.44
H2O c	3.82	2.12	2.16	2.15	2.13
Cation Proportions					
basis O/OH	20/4	22/2	22/2	22/2	22/2
Si	5.344	3.835	3.804	3.857	3.819
Al 1V	2.656	-	-	-	-
Al V1	0.847	8.762	8.823	8.703	8.779
Ti	0.183	0.042	0.042	0.021	0.032
Fe	2.907	1.715	1.671	1.763	1.726
Mn	0.008	0.016	0.013	0.009	0.015
Mg	1.773	0.292	0.292	0.325	0.297
Ca	0.000	0.000	0.000	0.003	0.003
Na	0.075	0.000	0.006	0.007	0.010
K	1.889	0.000	0.000	0.004	0.000
Co	0.000	0.000	0 000	0.000	0.000
Ni	0.000	0.007	0.006	0.015	0.012
Ba	-	-	-	-	-
Zn	0.021	0.071	0.091	0.067	0.071

SAMPLE NO.: 517-112
ROCK TYPE : Lode Schist (1b)

Mineral	sta	sta	cht	sta	sta
Site	S	SS	-		S173ss
Number	B3-173	B3-174	B3-175	B3-176	B3-177
SiO2	26.98	27.64	23.84	27.32	27.13
TiO2	0.33	0.27	0.13	0.11	0.10
Al2O3	52.58	53.12	22.74	52.74	53.14
FeO (tot)	13.90	14.77	27.33	14.44	15.26
MnO	0.09	0-11	0.04	0.14	0.15
MgO	1.61	1.57	12.46	1.52	1.48
CaO	0.01	0.01	O.OD	0.04	0.03
Na2O	0.06	0.00	0.05	0.04	0.03
K2O	0.01	0.03	0.02	0.02	0.00
coo	0.00	0.00	0.00	0.00	0.00
NiO	0.03	0.00	0.01	0.04	0.20
BaO	-	-	-	-	-
ZnO	0.46	0.70	0.25	0.61	0.83
Total	96.07	98.23	86.87	97.00	98.34
H2O c	2.11	2.15	11.12	2.13	2.14
Cation Proportions					
basis O/OH	22/2	22/2	20/16	22/2	22/2
Si	3.832	3.854	5.143	3.853	3.798
Al 1V	-	-	2.857	-	-
Al V1	8.801	8.731	2.926	8.768	8.769
Ti	0.035	0.029	0.022	0.012	0.011
Fe	1.651	1.722	4.930	1.703	1.787
Mn	0.011	0.013	0.007	0.016	0.018
Mg	0.340	0.327	4.006	0.320	0.308
Ca	0.002	0.001	0.000	0.006	0.004
Na	0.017	0.001	0.019	0.010	0.008
K	0.002	0.006	0.004	0.003	0.000
Co	0.000	0.000	0.000	0.000	0.000
Ni	0.003	0.000	0.002	0.004	0.022
Ba	-	-	-	-	-
Zn	0.049	0.072	0.041	0.063	0.086

SAMPLE NO.: 517-112
ROCK TYPE : Lode Schist (1b)

Mineral	ilm	mt	mt	sta
Site	-	-	AS	-
Number	B4-387	B4-390	B4-391	B4-394
SiO2	0.01	0.10	0.10	26.55
TiO2	50.39	0.34	0.23	0.11
Al2O3	0.04	0.32	0.32	53.06
FeO (tot)	45.67	88.34	88.53	15.59
MnO	1.07	0.00	0.05	0.14
MgO	0.00	0.00	0.00	1.55
CaO	0.02	0.01	0.01	0.02
Na2O	0.04	0.06	0.08	0.02
K2O	0.00	0.00	0.00	0.02
CoO	0.00	0.00	0.00	0.00
NiO	0.06	0.18	0.09	0.00
BaO	-	-	-	-
ZnO	0.08	0.05	0.04	0.59
Total	97.37	89.40	89.45	97.64
H2O c	-	-	-	2.13

Cation Proportions

basis O/OH	4/6/0	24/32/0	24/32/0	15/22/2
Si	0.000	0.033	0.032	3.746
Al 1V	(0.076)	(15.686)	(15.754)	(0.00)
Al V1	0.003	0.119	0.121	8.824
Ti	1.962	0.083	0.055	0.011
Fe	1.902	7.982	7.938	1.839
Mn	0.047	0.000	0.014	0.016
Mg	0.000	0.000	0.000	0.325
Ca	0.001	0.002	0.003	0.003
Na	0.004	0.036	0.050	0.005
K	0.000	0.000	0.000	0.003
Co	0.000	0.000	0.000	0.000
Ni	0.002	0.047	0.023	0.000
Ba	-	-	-	-
Zn	0.003	0.012	0.009	0.061

SAMPLE NO.: 517-112
ROCK TYPE : Lode Schist (1b)

Mineral	gar	gar	ilm	mt	ilm
Site	R	AS	I276	RX	Imt
Number	C4-269	C4-272	C3-275	C3-276	C2-277
SiO2	37.23	36.75	-	-	-
TiO2	-	-	50.12	0.40	49.70
Al2O3	21.05	21.16	-	0.47	-
FeO (tot)	38.90	38.54	48.45	91.83	47.66
MnO	0.67	1.83	0.90	-	0.83
MgO	2.86	2.31	0.12	0.06	0.06
CaO	0.34	0.25	-	-	-
Na2O	-	-	-	-	-
K2O	-	-	-	-	-
CoO	-	-	-	-	-
NiO	-	-	-	-	-
BaO	-	-	-	-	-
ZnO	-	-	-	0.16	-
Total	101.04	100.84	99.74	93.03	98.34
H2O c	-	-	-	-	-

Cation Proportions

basis O/OH	24/0	24/0	8/16/0	12/0
Si	5.976	5.939	-	-
Al 1V	-	-	(0.253)	-
Al V1	3.990	4.038	-	0.084
Ti	-	-	3.867	0.046
Fe	5.228	5.214	3.904	11.750
Mn	0.091	0.251	0.078	-
Mg	0.685	0.557	0.018	0.013
Ca	0.058	0.043	-	-
Na	-	-	-	-
K	-	-	-	-
Co	-	-	-	-
Ni	-	-	-	-
Ba	-	-	-	-
Zn	-	-	-	0.018

SAMPLE NO.: 517-133
ROCK TYPE : GAB(1) Schist

Mineral	gar	gar	bio	mus	gar
Site	C	RS	RX	-	-
Number	A2-370	A2-371	A2-372	A3-373	A2-375
SiO2	36.91	36.59	34.03	45.80	36.77
TiO2	0.03	0.05	1.58	0.35	0.05
Al2O3	20.29	20.49	19.22	34.78	20.63
FeO (tot)	35.92	37.49	22.56	1.24	36.71
MnO	3.67	3.61	0.05	0.03	3.77
MgO	1.72	1.60	7.27	0.49	1.76
CaO	-	0.26	0.00	0.00	0.58
Na2O	0.00	0.04	0.25	0.57	0.00
K2O	0.00	0.02	9.80	11.12	0.01
Cr2O3	0.00	0.06	0.07	0.07	0.05
NiO	0.04	0.00	0.08	0.00	0.11
BaO	0.04	0.08	0.09	0.21	0.02
ZnO	-	-	-	-	-
Total	99.68	100.29	95.00	94.65	100.46
H2O c	-	-	3.84	4.45	-
Cation Proportions					
basis O/OH	24/0	24/0	20/4	20/4	24/0
Si	6.041	5.985	5.316	6.174	5.987
Al 1V	-	-	2.684	1.826	-
Al V1	3.914	3.952	0.855	3.699	3.960
Ti	0.003	0.005	0.185	0.035	0.006
Fe	4.917	5.129	2.947	0.140	4.999
Mn	0.508	0.501	0.007	0.004	0.520
Mg	0.420	0.39D	1.694	0.098	0.428
Ca	0.186	0.045	0.000	0.000	0.101
Na	0.001	0.012	0.074	0.148	0.000
K	0.000	0.003	1.953	1.912	0.002
C r	0.000	0.008	0.009	0.007	0.006
Ni	0.005	0.003	0.010	0.000	0.015
Ba	0.003	0.005	0.005	0.011	0.001
Zn	-	-	-	-	-

SAMPLE NO.: 517-133
ROCK TYPE : GAB(1) Schist

Mineral	mus	bio	gar
Site			
Number	Al-3,77	AS-378	A6-379
SiO2	45.40	33.74	36.94
TiO2	0.43	1.43	0.03
Al2O3	34.72	19.46	20.81
FeO (tot)	1.15	22.03	36.59
MnO	0.01	0.06	3.55
MgO	0.55	7.20	1.42
CaO	0.00	0.00	0.87
Na2O	0.55	0.21	0.00
K2O	11.19	9.12	0.00
Cr2O3	0.02	0.09	0.05
NiO	0.00	0.03	0.05
BaO	0.30	0.07	0.02
ZnO	-	-	-
Total	94.30	93.45	100.34
H2O c	4.43	3.80	-

Cation Proportions

basis O/OH	20/4	20/4	24/0
Si	6.150	5.323	6.013
Al 1V	1.850	2.677	-
Al V1	3.693	0.942	3.992
Ti	0.044	0.170	0.004
Fe	0.130	2.907	4.980
Mn	0.001	0.008	0.489
Mg	0.110	1.694	0.344
Ca	0.000	0.000	0.152
Na	0.144	0.063	0.000
K	1.933	1.837	0.000
Cr	0.002	0.012	0.006
Ni	0.000	0.003	0.007
Ba	0.016	0.004	-
Zn	-	-	-

SAMPLE NO.: 517-148
ROCK TYPE : GAB(1) Schist

Mineral	gar	sta	bio	gar	sta
Site	C	R	-	R369	C
Number	A2-369	A2-370	A2-371	A2-373	A2-375
SiO2	37.18	26.74	35.04	36.61	26.47
TiO2	0.10	0.48	1.49	0.04	0.58
Al2O3	20.53	54.76	19.67	21.07	54.83
FeO (tot)	36.21	14.15	21.50	38.94	14.52
MnO	2.19	0.05	0.02	1.89	0.12
MgO	2.18	1.23	8.16	2.04	1.35
CaO	1.36	0.02	0.00	0.19	0.00
Na2O	0.00	0.01	0.25	0.02	0.03
K2O	0.00	0.00	9.17	0.01	0.00
Cr2O3	0.02	0.05	0.00	0.05	0.11
NiO	0.00	0.11	0.05	0.06	0.00
BaO	0.08	0.12	0.04	0.00	0.07
ZnO	-	-	-	-	-
Total	99.85	97.70	95.39	100.90	98.08
H2O c	-	2.15	3.91	-	2.15

Cation Proportions

basis O/OH	24/0	22/2	20/4	24/0	22/2
Si	6.041	3.728	5.376	5.934	3.685
Al 1V	-	-	2.624	-	-
Al V1	3.932	9.001	0.933	4.027	8.998
Ti	0.012	0.050	0.172	0.004	0.061
Fe	4.920	1.650	2.759	5.279	1.691
Mn	0.302	0.006	0.002	0.259	0.014
Mg	0.529	0.256	1.866	0.492	0.280
Ca	0.236	0.002	0.000	0.033	0.000
Na	0.000	0.003	0.074	0.005	0.007
K	0.001	0.000	1.794	0.002	0.001
Cr	0.002	0.005	0.000	0.006	0.012
Ni	0.000	0.012	0.006	0.007	0.000
Ba	0.005	0.007	0.002	0.000	0.004
Zn	-	-	-	-	-

SAMPLE NO.: 517-148
ROCK TYPE : GAB(1) Schist

Mineral	sta	sta	gar	gar	bio
Site	R	CS	RX273	C	RX277
Number	BI-273	Bl-274	Bl-277	Bl-278	Bl-280
SiO2	26.76	27.00	36.51	36.68	34.26
TiO2	0.48	0.55	0.04	0.04	1.44
Al2O3	53.62	53.35	20.80	20.61	19.01
FeO (tot)	14.86	14.79	38.36	38.33	21.30
MnO	0.10	0.06	1.86	1.75	0.03
MgO	1.25	1.33	1.88	2.12	8.05
CaO	0.00	0.00	0.26	0.43	0.00
Na2O	0.04	0.06	0.06	0.03	0.27
K2O	0.02	0.00	0.02	0.01	9.09
CoO	0.00	0.00	0.00	0.00	0.00
NiO	0.03	0.00	0.03	0.04	0.01
BaO	-	-	-	-	-
ZnO	0.83	0.80	0.20	0.07	0.06
Total	97.99	97.96	100.01	100.11	93.51
H2O c	2.14	2.14	-	-	3.82

Cation Proportions

basis O/OH	22/2	22/2	24/0	24/0	20/4
Si	3.750	3.782	5.967	5.983	5.374
Al 1V	-	-	-	-	2.626
Al V1	8.858	8.807	4.008	3.962	0.890
Ti	0.051	0.058	0.005	0.005	0.170
Fe	1.742	1.733	5.244	5.229	2.794
Mn	0.011	0.007	0.255	0.241	0.004
Mg	0.261	0.278	0.458	0.516	1.882
Ca	0.000	0.000	0.045	0.076	0.000
Na	0.010	0.016	0.019	0.010	0.082
K	0.003	0.001	0.004	0.001	1.820
Co	0.000	0.000	O.OOD	0.000	0.000
Ni	0.003	0.000	0.001	0.005	0.001
Ba	-	-	-	-	-
Zn	0.086	0.083	0.024	0.009	0.007

SAMPLE NO.: 517-149
ROCK TYPE : GAB (1) Schist

Mineral	sta	sta	gar	bio	gar
Site	R	c	R	RX	C364
Number	A2-360	A2-361	A2-364	A2-366	A2-368
SiO2	27.22	26.87	37.04	34.98	37.40
TiO2	0.56	0.48	0.00	1.48	0.00
Al2O3	53.40	53.87	20.82	19.24	20.88
FeO (tot)	12.49	13.83	36.03	20.86	34.80
MnO	0.18	0.20	4.01	0.07	3.55
MgO	1.57	1.37	2.28	9.89	2.46
CaO	0.02	0.02	0.31	0.00	1.15
Na2O	0.08	0.03	0.04	0.23	0.04
K2O	0.02	0.0.1	0.01	8.44	0.00
Cr2O3	0.04	0.00	0.01	0.05	0.00
NiO	0.00	0.00	0.00	0.07	0.11
BaO	0.12	0.00	0.12	0.00	0.00
ZnO	-	-	-	-	-
Total	95.70	96.69	100.67	95.31	100.40
H2O c	2.12	2.13	-	3.93	-

Cation Proportions

basis O/OH	22/2	22/2	24/0	20/4	24/0
Si	3.844	3.779	5.996	5.338	6.03
Al 1V	-	-	2.662	-	-
Al V1	8.890	8.930	3.973	0.798	3.967
Ti	0.060	0.051	0.000	0.169	0.001
Fe	1.475	1.626	4.878	2.662	4.692
Mn	0.022	0.024	0.550	0.009	0.485
Mg	0.331	0.288	0.551	2.249	0.592
Ca	0.004	0.003	0.054	0.000	0.199
Na	0.023	0.009	0.013	0.069	0.011
K	0.003	0.002	0.002	1.644	0.001
Cr	0.004	0.000	0.001	0.006	0.000
Ni	0.000	0.000	0.000	0.008	0.014
Ba	0.007	0.000	0.007	0.000	0.000
Zn	-	-	-	-	-

SAMPLE NO.: 517-163
ROCK TYPE : Lode Schist (2)

Mineral	gar	gar	cht	gar	cht
Site	c	RS	RX	-	-
Number	A4-354	A4-356	A4-357	AS-358	AS-359
SiO2	36.37	36.33	23.21	36.21	22.36
TiO2	0.04	0.05	0.07	0.09	0.10
Al2O3	2.0.49	20.43	22.43	20.67	13.44
FeO (tot)	36.33	37.62	30.17	37.58	48.38
MnO	3.74	3.53	0.11	3.83	0.24
MgO	2.33	1.69	10.94	1.57	2.50
CaO	0.42	0.17	0.03	0.45	0.03
Na2O	0.00	0.06	0.01	0.05	0.07
K2O	0.00	0.00	0.02	0.01	0.34
Cr2O3	0.00	0.04	0.04	0.00	0.04
NiO	0.07	0.00	0.01	0.00	0.03
BaO	0.00	0.04	0.08	0.01	0.09
ZnO	-	-	-	-	-
Total	99.81	99.96	87.13	100.45	87.63
H2O c	-	-	10.97	-	9.72

Cation Proportions

basis O/OH	24/0	24/0	20/16	24/0	20/16
Si		5.967	5.079	5.926	5.518
Al 1V		-	2.921	-	2.482
Al V1		3954	2865	3.987	1.429
Ti		0.007	0.012	0.011	0.019
Fe		5.167	5.521	5.144	9.986
m '		0.491	0.021	0.531	0.049
Mg		0.414	3.568	0.382	0.918
Ca		0.030	0.007	0.079	0.007
Na		0.019	0.002	0.015	0.034
K		0.000	0.005	0.001	0.108
Cr		0.005	0.007	0.000	0.008
Ni		0.001	0.003	0.000	0.007
Ba		0.002	0.007	0.001	0.009
Zn		-	-	-	-

SAMPLE NO.: 517-163
ROCK TYPE : Lode Schist (2)

Mineral	mus	mus	gar	bio	bio
Site	-	S	R	RX	S
Number	AS-361	A5-362	A3-363	A3-364	A3-365
SiO2	417.18	46.89	36.06	32.10	34.12
TiO2	0.25	0.29	0.02	1.27	1.28
Al2O3	35.95	35.33	20.71	15.82	16.64
FeO (tot)	2.13	2.51	38.75	25.59	26.36
MnO	0.00	0.00	2.49	0.05	0.13
MgO	0.56	0.61	2.03	6.58	6.85
CaO	0.00	0.00	0.21	0.00	0.00
Na2O	0.71	0.65	0.02	0.12	0.10
K2O	9.90	9.93	0.01	9.06	9.48
Cr2O3	0.06	0.03	0.05	0.01	0.01
NiO	0.11	0.00	0.01	0.00	0.09
BaO	0.08	0.00	0.00	2.33	0.16
ZnO	-	-	-	-	-
Total	96.95	96.25	100.36	92.93	95.21
H2O c	4.58	4.54	-	3.60	3.77

Cation Proportions

basis O/OH	20/4	20/4	24/0	20/4	20/4
Si	6.174	6.188	5.903	5.343	5.430
Al 1V	1.826	1.812	-	2.657	2.570
Al V1	3.719	3.684	3.995	0.447	0.551
Ti	0.025	0.029	0.002	0.159	0.153
Fe	0.233	0.276	5.305	3.563	3.509
Mn	0.000	0.000	0.345	0.007	0.018
Mg	0.110	0.121	0.495	1.633	1.626
Ca	0.000	0.000	0.037	0.000	0.000
Na	0.179	0.166	0.005	0.039	0.031
K	1.653	1.672	0.002	1.925	1.925
Cr	0.006	0.003	-	0.001	0.001
Ni	0.012	0.000	0.001	0.000	0.012
Ba	0.004	0.000	-	0.152	0.010
Zn	-	-	-	-	-

SAMPLE NO.: 517-163
ROCK TYPE : Lode Schist (2)

Mineral	sta	sta	sta	sta	mus
Site	R	R	AS	S	-
Number	A2-366	A2-348	A2-349	A2-351	A2-352
SiO2	27.07	26.59	27.41	27.20	45.52
TiO2	0.56	0.48	0.45	0.57	0.23
Al2O3	53.08	53.41	53.42	54.26	34.53
FeO (tot)	13.75	13.81	13.88	13.96	2.26
MnO	0.27	0.16	0.22	0.22	0.00
MgO	1.07	1.05	1.04	0.97	0.56
CaO	0.03	0.00	0.01	0.00	0.00
Na2O	0.04	0.05	0.01	0.02	0.73
K2O	0.02	0.00	0.00	0.00	10.01
Cr2O3	0.10	0.00	0.02	0.05	0.02
NiO	0.00	0.05	0.02	0.03	0.01
BaO	0.00	0.02	0.00	0.17	0.00
ZnO	-	-	-	-	-
Total	95.98	95.63	96.46	97.46	93.88
H2O c	2.12	2.11	2.13	2.15	4.42
Cation Proportions					
basis O/OH	22/2	22/2	22/2	22/2	20/4
Si	3.836	3.782	3.859	3.799	6.170
Al 1V	-	-	-	-	1.830
Al V1	8.863	8,956	8.866	8.933	3.688
Ti	0.060	0.051	0.048	0.060	0.024
Fe	1.629	1.643	1.635	1.630	0.256
Mn	0.033	0.020	0.024	0.026	0.000
Mg	0.227	0.223	0.218	0.202	0.113
Ca	0.004	0.000	0.002	0.000	0.000
Na	0.011	0.014	0.003	0.006	0.192
K	0.003	0.000	0.000	0.000	1.732
Cr	0.011	0.000	0.002	0.006	0.002
Ni	0.000	0.006	0.002	0.003	0.001
Ba	0.000	0.001	0.000	0.009	0.000
Zn	-	-	-	-	-

SAMPLE NO.: 517-163
ROCK TYPE : Lode Schist (2)

Mineral	cht	bio	cht
Site	-	-	-
Number	A2-354	A2-356	A4-358
SiO2	23.50	33.77	22.96
TiO2	0.10	0.84	0.08
Al2O3	22.67	17.91	22.60
FeO (tot)	29.78	24.87	31.08
MnO	0.07	0.10	0.19
MgO	11.68	7.31	10.76
CaO	0.01	0.00	0.01
Na2O	0.02	0.14	0.00
K20	0.01	9.31	0.00
Cr2O3	0.00	0.02	0.03
NiO	0.03	0.00	0.05
BaO	0.10	0.06	0.00
ZnO	-	-	-
Total	87.97	94.34	87.75
H2O c	11.11	3.77	10.99

Cation Proportions

basis O/OH	20/16	20/4	20/16
Si	5.073	5.369	5.014
Al 1V	2.927	2.631	2.986
Al V1	2.842	0.725	2.828
Ti	0.016	0.100	0.013
Fe	5.376	3.307	5.674
Mn	0.013	0.014	0.034
Mg	3.758	1.732	3.502
Ca	0.002	0.000	0.002
Na	0.008	0.045	0.000
K	0.003	1.888	0.000
Cr	0.000	0.003	0.005
Ni	0.004	0.000	0.008
Ba	0.009	0.004	0.008
Zn	-	-	-

SAMPLE NO.: 517-163
ROCK TYPE : Lode Schist (2)

Mineral	mus	bio	bio	gar	ilm
Site	-	-	AS	RX	-
Number	Bl-281	B1-282	Bl-283	Bl-285	B2-289
SiO2	44.74	32.3.8	32.63	35.77	0.02
TiO2	0.28	0.88	1.09	0.03	50.71
Al2O3	33.84	17.14	17.33	20.74	0.02
FeO (tot)	2.96	25.36	26.43	37.62	47.01
MnO	0.01	0.09	0.04	3.60	1.34
MgO	0.59	6.80	6.65	1.48	0.00
CaO	0.00	0.00	0.00	0.20	0.03
Na2O	0.62	0.04	0.11	0.02	0.03
K2O	10.32	9.60	9.66	0.02	0.00
CoO	0.00	0.00	0.00	0.00	0.00
NiO	0.00	0.03	0.03	0.00	0.00
BaO	-	-	-	-	-
ZnO	0.12	0.00	0.00	0.00	0.00
Total	93.48	92.31	93.97	99.47	99.15
H2O c	4.37	3.65	3.70	-	-

Cation Proportions

basis O/OH	20/4	20/4	20/4	24/0	4/6/0
Si	6.137	5.317	5.284	5.912	0.001
Al 1V	1.863	2.683	2.716	-	(0.124)
Al V1	3.609	0.634	0.591	4.040	0.001
Ti	0.029	0.108	0.132	0.004	1.938
Fe	0.340	3.483	3.578	5.200	1.873
Mn	0.001	0.012	0.006	0.503	0.058
Mg	0.12D	1.664	1.604	0.365	0.000
Ca	O.OOD	0.000	0.000	0.035	0.002
Na	0.166	0.014	0.035	0.005	0.003
K	1.805	2.011	1.995	0.004	0.000
Co	0.003	0.000	0.000	O.OOD	0.000
Ni	0.003	0.004	0.004	0.000	0.000
Ba	-	-	-	-	-
Zn	0.012	0.000	0.000	0.000	0.000

SAMPLE NO.: 517-163
ROCK TYPE : Lode Schist (2)

Mineral	mt
Site	R
Number	B2-290
SiO2	0.04
TiO2	0.27
Al2O3	0.23
FeO (tot)	91.10
MnO	0.00
MgO	0.00
CaO	0.02
Na2O	0-05
K2O	0.00
CoO	0.00
NiO	0.25
BaO	-
ZnO	0.00
Total	91.95
H2O c	-

Cation Proportions

basis O/OH 24/32/0	
Si	0.012
Al 1V	(15.793)
Al V1	0.083
Ti	0.064
Fe	7.949
Mn	0.000
Mg	0.000
Ca	0.006
Na	0.029
K	0.000
Co	0.000
Ni	0.063
Ba	-
Zn	0.000

SAMPLE NO.: 517-163
ROCK TYPE : Lode Schist (2)

mineral	ilm	ilm	ilm	ilm
Site	-	AS	S	AS
Number	C-281	C-282	C-283	C-284
SiO2	0.08	-	-	-
TiO2	47.76	48.05	48.08	48.08
Al2O3	-	0.13	0.09	-
FeO (.tot)	48.04	48.27	47.90	48.01
MnO	1.05	1.05	1.01	0.96
MgO	-	-	-	-
CaO	-	-	-	-
Na2O	-	-	-	-
K2O	-	-	-	-
CoO	-	-	-	-
NiO	-	-	-	-
BaO	-	-	-	-
ZnO	-	-	-	-
Total	97.08	98.17	97.08	97.05
H2O c	-	-	-	-

Cation Proportions

basis O/OH	24/48/0	24/48/0		
Si	0.025	-	-	-
Al 1V	(0.789)	(0.769)	(0.723)	(0.748)
Al V1	-	0.047	0.033	-
Ti	11.186	11.184	11.224	11.252
Fe	11.723	11.725	11.734	11.747
Mn	0.277	0.275	0.266	0.253
Mg	-	-	-	-
Ca	-	-	-	-
Na	-	-	-	-
K	-	-	-	-
Co	-	-	-	-
Ni	-	-	-	-
Ba	-	-	-	-
Zn	-	-	-	-

SAMPLE NO.: 517-177
ROCK TYPE : Lode Schist (2)

Mineral:	sta	sta	gar	gar	bio
Site	c	RS	c	RS	RX
Number	Al-025	Al-026	Al-028	Al-029	Al-031
SiO2	27.41	27.46	36.71	36.60	35.46
TiO2	0.34	0.50	0.07	0.00	
Al2O3	54.19	53.27	20.27	20.67	19.11
FeO (tot)	15.44	15.65	37.06	37.96	21.82
MnO	0.11	0.15	2.40	2.21	0.01
MgO	1.39	1.42	2.44	2.00	8.45
CaO	0.01	0.02	0.89	0.23	0.00
Na2O	0.03	0.02	0.02	0.05	0.42
K2O	0.01	0.01	0.03	0.02	8.98
Cr2O3	0.04	0.01	0.00	0.02	0.03
NiO	0.12	0.06	0.10	0.03	0.11
BaO	0.01	0.08	0.00	0.05	0.00
ZnO	-	-	-	-	-
Total	99.11	98.63	99.98	99.84	96.01
H2O c	2.17	2.16	-	-	3.93

Cation Proportions

basis O/OH	22/2	22/2	24/0	24/0	20/4
Si	3.788	3.820	5.989	5.986	5.407
Al 1V	-	-	-	-	2.593
Al V1	8.828	8.736	3.898	3.986	0.842
Ti	0.035	0.052	0.009	0.000	0.186
Fe	1.785	1.821	5.058	5.194	2.733
Mn	0.013	0.017	0.331	0.306	0.0D2
Mg	0.287	0.295	0.593	0.488	1.922
Ca	0.002	0.003	0.156	0.040	0.0D0
Na	0.008	0.005	0.007	0.015	0.124
K	0.001	0.002	0.006	0.005	1.748
Cr	0.004	0.001	0.000	0.002	0.003
Ni	0.013	0.007	0.013	0.003	0.013
Ba	0.001	0.004	0.000	0.003	0.030
Zn	-	-	-	-	-

SAMPLE NO.: 517-203
ROCK TYPE : Lode Schist (3)

Mineral	bio	gar	gar	gar	gar
Site	R	RXT	AS	T	T
Number	BI-087	B1-088	BI-090	Bl-091	Bl-092
SiO2	35.23	37.52	36.48	37.26	37.08
TiO2	1.31	0.08	0.07	0.08	0.04
Al2O3	16.41	20.93	21.10	21.09	20.69
FeO (tot)	25.06	37.08	40.16	39.36	39.37
MnO	0.01	2.38	1.12	1.29	1.44
MgO	7.78	1.48	1.66	1.47	1.57
CaO	0.00	1.23	0.23	0.39	0.45
Na2O	0.16	0.05	0.01	0.04	0.01
K2O	7.83	0.00	0.00	0.00	0.00
Cr2O3	0.02	0.00	0.00	0.00	0.06
NiO	0.00	0.03	0.09	0.04	0.01
BaO	0.18	0.00	0.06	0.10	0.00
ZnO	-	-	-	-	-
Total	93.99	100.78	100.97	101.11	100.72
H2O c	3.80	-	-	-	-

Cation Proportions

basis O/OH	20/4			24/0	24/0
Si	5.566			6.015	6.018
Al 1V	2.434			-	-
Al V1	0.622			4.014	3.958
Ti	0.156			0.009	0.005
Fe	3.310			5.314	5.344
Mn	0.001			0.177	0.198
Mg	1.831			0.354	0.380
Ca	0.000			0.067	0.078
Na	0.050			0.011	0.004
K	1.578			0.000	0.000
Cr,	0.002			0.000	0.008
Ni	0.000			0.006	0.001
Ba	0.011			0.006	0.000
Zn	-			-	-

SAMPLE NO.: 517-203
ROCK TYPE : Lode Schist (3)

Mineral:	gar	gar	gar	gar	gar
Site	T	T	T	SS	T
Number	B1-093	B1-094	B1-095	Bl-097	B1-099
SiO2	37.19	37.02,	37.35	36.64	37.12
TiO2	0.11	0.04	0.00	0.06	0.00
Al2O3	20.95	21.15	21.03	20.99	20.90
FeO (tot)	36.88	37.34	39.87	39.71	40.09
MnO	2.65	2.12	1.16	1.11	1.23
MgO	-	1.63	1.78	1.72	0.98
CaO	1.30	1.10	0.28	0.34	0.40
Na2O	0.01	0.03	0.10	0.05	0.03
K2O	0-01	0.02	0.00	0.01	0.04
Cr2O3	0.00	0.03	01.00	0.03	0.01
NiO	0.03	0.00	0.07	0.00	0.00
BaO	0.19	0.18	0.14	0.00	0.06
ZnO	-	-	-	-	-
Total	100.88	100.64	101.77	100.67	100.85
H2O c	-	-	-	-	-

Cation Proportions

basis O/OH	24/0	24/0	24/0	24/0	24/0
Si	6.010	5.992	6.002	5.955	6.030
Al 1V	-	-	-	-	-
Al V1	3.990	4.036	3.982	4.021	4.002
Ti	0.014	0.005	0.000	0.008	0.000
Fe	4.985	5.055	5.358	5.398	5.447
Mn	0.363	0.291	0.158	0.153	0.170
Mg	0.377	0.393	0.425	0.417	0.237
Ca	0.225	0.191	0.048	0.059	0.070
Na	0.003	0.009	0.030	0.015	0.009
K	0.002	0.004	0.000	0.003	0.007
Cr	0.000	0.003	0.000	0.004	0.001
Ni	0.003	0.000	0.009	0.000	0.000
Ba	0.012	0.011	0.009	0.000	0.004
Zn	-	-	-	-	-

SAMPLE NO.: 517-203
ROCK TYPE : Lode Schist (3)

Mineral	gar	gar	bio
Site	T	RT	RX
Number	B1-100	Bl-103	BI-110
SiO2	37.00	37.00	35.95
TiO 2	0.18	0.10	1.66
Al2O3	211.02	201.53	15.93
FeO (tot)	38.53	39.41	23.66
MnO	1.39	1.26	0.08
MgO	1.91	1.31	7.96
CaO	1.11	1.05	0.08
Na2O	0.07	0.00	0.16
K2O	0.02	0.03	6.29
Cr2O3	0.00	0.11	0.07
NiO	0.00	0.00	0.11
BaO	0.00	0.03	0.09
ZnO	-	-	-
Total	101.22	100.83	92.03
H2O c	-	3.78	-

Cation Proportions

basis O/OH	24/0	24/0	20/4
Si	5.961	6.001	5.701
Al 1V	-	-	2.299
Al V1	3.993	3.932	0.678
Ti	0.022	0.012	0.19B
Fe	5.192	5.355	3.138
Mn	0.189	0.173	0.010
Mg	0.459	0.317	1.881
Ca	0.192	0.182	0.013
Na	0.021	0.001	0.050
K	0.004	0.007	1.273
Cr	0.000	0.014	0.009
Ni	0.000	0.000	0.014
Ba	0.000	0.002	0.006
Zn	-	-	-

SAMPLE NO.: 517-203
ROCK TYPE : Lode Schist

Mineral	gru	gru	gru	gru	gru
Site	-	X	X	S	X
Number	B5-419	B2-420	B2-423	B2-424	B2-425
SiO2	50.78	50.82	50.14	49.78	49.97
TiO2	0.05	0.00	0.01	0.06	0.04
Al2O3	0.77	0.75	0.73	0.56	0.64
FeO (tot)	32.40	33.28	32.71	32.85	32.71
MnO	0.24	0.17	0.23	0.16	0.11
MgO	11.23	11.11	11.19	11.09	11.26
CaO	0.10	0.05	0.09	0.09	0.08
Na2O	0.07	0.11	0.05	0.00	0.03
K2O	0.05	0.02	0.02	0.01	0.01
CoO	0.00	0.00	0.00	0.00	0.00
NiO	0.00	0.12	0.01	0.00	0.08
BaO	-	-	-	-	-
ZnO	0.00	0.01	0.08	0.00	0.00
Total	95.68	96.43	95.27	94.60	94.95
H2O c	1.92	1.93	1.91	1.89	1.90

Cation Proportions

basis O/OH	15/22/2	15/22/2	15/22/2	15/22/2	15/22/2
Si	7.930	7.890	7.872	7.881	7.871
Al 1V	0.070	0.110	0.128	0.104	0.119
Al V1	0.071	0.027	0.008	0.000	0.000
Ti	0.006	0.000	0.002	0.007	0.005
Fe	4.215	4.201	4.156	4.228	4.168
Mn	0.032	0.023	0.031	0.021	0.014
Mg	2.614	2.572	2.619	2.618	2.645
Ca	0.016	0.008	0.015	0.015	0.014
Na	0.020	0.032	0.017	0.000	0.010
K	0.009	0.003	0.005	0.003	0.003
Co	0.000	0.000	0.000	0.000	0.000
Ni	0.000	0.015	0.002	0.000	0.011
Ba	(O.017)	(0.120)	(0.139)	(0.122)	(0.142)
Zn	0.000	0.001	0.009	0.000	0.000

SAMPLE NO.: 517-203
ROCK TYPE : Lode Schist (3)

Mineral	bio	gar
Site	R	RX
Number	Bl-427	B2-428
SiO2	33.52	36.09
TiO2	1.18	0.02
Al2O3	16.19	20.18
FeO (tot)	25.92	38.45
MnO	0.03	1.17
MgO	7.45	1.33
CaO	0.00	1.34
Na2O	0.24	0.02
K2O	8.70	0.01
CoO	0.00	0.00
NiO	0.03	0.07
BaO	-	-
ZnO	0.00	0.13
Total	93.26	98.81
H2O c	3.71	-

Cation Proportions

basis O/OH	20/4	24/0
Si	5.421	5.989
Al 1V	2.579	-
Al V1	0.506	3.948
Ti	0.144	0.002
Fe	3.504	5.337
Mn	0.004	0.164
Mg	1.796	0.328
Ca	0.000	0.238
Na	0.076	0.006
K	1.795	0.002
Co	0.000	0.000
Ni	0.004	0.010
Ba	-	-
Zn	0.000	0.015

SAMPLE NO.: 517-220/4
ROCK TYPE : Sulphide rock

Mineral	gar	gar	
Site	R	CS	
Number	Cl-296	Cl-297	
SiO2	36.60	36.61	This garnet surrounded
TiO2	-	-	by chalcopyrite and pyrrhotite
Al2O3	21.38	21.43	
FeO (tot)	36.95	35.96	
MnO	3.61	3.55	
MgO	1.87	1.94	
CaO	0.33	1.14	
Na2O	-	-	
K2O	-	-	
CoO	-	-	
NiO	-	-	
BaO	-	-	
ZnO	-	-	
Total	100.74	100.63	
H2O c	-	-	

Cation Proportions

basis O/OH	24/0	24/0
Si	5.927	5.920
Al 1V	-	-
Al V1	4.087	4.092
Ti	-	-
Fe	5.009	4.868
Mn	0.496	0.487
Mg	0-453	0.470
Ca	0.057	0.198
Na	-	-
K	-	-
Co	-	-
Ni	-	-
Ba	-	-
Zn	-	-

SAMPLE NO.: 517-2870
ROCK TYPE : QMF Schist

Mineral:	plq	gar	gar	bio	mus
Site	-	C	RS	RX	-
Number	B4-216	B6-217	B6-219	B6-220	B6-221
SiO2	49.96	36.47	37.03	35.38	46.60
TiO2	0.15	0.06	0.05	2.20	0.61
Al2O3	30.76	20.93	20.79	18.42	34.24
FeO (tot)	1.13	23.09	22.97	18.96	1.21
MnO	0.10	13.81	13.88	0.42	0.00
MgO	0.37	1.80	1.63	9.57	0.92
CaO	1.3.81	2.84	3.06	0.00	0.00
Na2O	2.94	0.08	0.00	0.09	0.45
K2O	0.55	0.00	0.03	9.44	10.64
CoO	0.12	0.00	0.00	0.00	0.00
NiO	0.00	0.00	0.00	0.00	0.11
BaO	-	-	-	-	-
ZnO	0.09	0.11	0.24	0.09	0.00
Total	99.97	99.19	99.68	94.58	94.79
H2Oc	-	-	-	3.19	4.48
Cation Proportions					
basis O/OH	32/0	24/0	24/0	20/4	20/4
si	9.175	5.957	6.014	5.432	6.237
Al 1V	-	-	-	2.568	1.763
Al V1	6-658	4.030	3.980	0.765	3.640
Ti	0.020	0.075	0.006	0.254	0.061
Fe	0-174	3.155	3.120	2.435	0.135
Mn	0.015	1.190	1.909	0.054	0.000
Mg	0.100	0.438	0.395	2.190	0.183
Ca	2.717	0.497	0.533	0.000	0.00
Na	1.046	0.026	0.000	0.027	0.116
K	0.129	0.000	0.007	1.849	1.822
Co	0.018	0.000	0.000	0.000	0.00
Ni	0.000	0.000	0.000	0.000	0.012
Ba	-	-	-	-	-
Zn	0.012	0.014	0.029	0.011	0.00

SAMPLE NO.: 517-2870
ROCK TYPE : QMF schist

Mineral	mus	bio	bio	gar
Site	AS	AS220	R	RX
Number	B6-222	B6-223	BS-224	B5-226
SiO2	46.59	34.70	35.11	36.67
TiO2	0.60	2.20	2.13	0.04
Al2O3	34.51	18.71	18.54	20.63
FeO (tot)	1.26	18.55	18.50	22.58
MnO	0.00	0.37	0.39	13.95
MgO	0.92	9.55	9.77	1.52
CaO	0.00	0.00	0.00	3.38
Na2O	0.38	0.14	0.13	0.02
K2O	10.75	9.46	9.36	0.07
CoO	0.00	0.00	0.00	0.00
NiO	0.13	0.04	0.05	0.06
BaO	-	-	-	-
ZnO	0.20	0.00	0.15	0.04
Total	95.34	93.73	94.15	98.96
H2O c	4.50	3.87	3.89	-

Cation Proportions

basis O/OH	20/4	20/4	20/4	24/0
Si	6.212	5.374	5.408	6.003
Al 1V	1.788	2.626	2.592	-
Al V1	3.636	0.788	0.774	3.981
Ti	0.060	0.057	0.247	0.005
Fe	0-140	2.403	2.383	3.091
Mn	0.019	0.049	0.051	1.934
Mg	0.184	2.205	2.244	0.370
Ca	0.000	0.000	0.000	0.593
Na	0.098	0.043	0.040	0.006
K	1.829	1.869	1.839	0.016
Co	0-000	0.000	0.000	0.000
Ni	0,000	0.005	0.006	0.008
Ba	-	-	-	-
Zn	0.014	0.000	0.017	0.005

SAMPLE NO.: 517-2870
ROCK TYPE : QM Schist

Mineral	gar	gar
Site	C	RS
Number	B6-380	B6-381
SiO2	35.92	36.37
TiO2	0.01	0.05
Al2O3	20.84	20.90
FeO (tot)	23.52	23.35
MnO	13.96	13.96
MgO	1.73	1.55
CaO	2.72	3.10
Na2O	0.05	0.00
K 2O	0.02	0.04
CoO	0.00	0.00
NiO	0.13	0.02
BaO	-	-
ZnO	0.14	0.29
Total	99.03	99.94
H2O c	-	-

Cation Proportions		
basis O/OH	24/0	24/0
Si	5.906	5.938
Al 1V	-	-
Al V1	4.040	4.022
Ti	0.002	0.006
Fe	3.235	3.188
Mn	1.944	1.930
Mg	0.423	0.377
Ca	0.478	0.542
Na	0.015	0.000
K	0.005	0.008
Co	0.000	0.000
Ni	0.018	0.003
Ba	-	-
Zn	0.017	0.035

SAMPLE NO.: 517-550
ROCK TYPE :

Mineral	sta	gahnite	sta	sta	gahnite
Site	-	X	C	RS	RX
Number	B1-134	B1-136	B3-138	B3-139	B3-140
SiO2	27.42	0.04	26.64	26.57	0.10
TiO2	0.48	0.01	0.45	0.46	0.01
Al2O3	53.45	57.19	53.56	54.75	57.76
FeO (tot)	9.54	9.93	9.44	9.34	9.60
MnO	0.38	0.14	0.39	0.38	0.19
MgO	1.50	1.951	1.48	1.05	1.56
CaO	0.02	-	0.00	0.00	0.03
Na2O	0.36	-	-	-	-
K2O	0.01	-	01.00	0.00	-
CoO	0.00	-	0.00	0.00	-
NiO	0.00	-	0.00	0.08	-
BaO	-	-	-	-	-
ZnO	5.92	30.58	5.37	6.48	30.76
Total	98.90	99.84	97.33	99.11	100.01
H2O c	2.15	-	2.13	2.16	-
Cation Proportions					
basis O/OH	22/2	12/0	22/2	22/2	12/0
Si	3.797	0.014	3.753	3.693	0.009
Al 1V	-	-	-	-	-
Al V1	8.783	5.987	8.893	8.969	6.027
Ti	0.050	0.002	0.048	0.048	0.001
Fe	1.112	0.737	1.112	1.086	0.710
Mn	0.044	0.010	0.046	0.044	0.015
Mg	0.311	0.258	0.310	0.218	0.205
Ca	0.003	-	0.000	0.000	0.006
Na	0.097	-	-	-	-
K	0.002	-	0.000	0.000	-
Co	0.000	-	0.000	0.000	-
Ni	0.000	-	0.000	0.009	-
Ba	-	-	-	-	-
Zn	0.609	2.005	0.558	0.665	2.011

SAMPLE NO.: 517-N203
ROCK TYPE : Brukunga Sulphidic Schist

Mineral	crd	bio
Site		
Number		
SiO 2	50.39	39.44
TiO 2	0.10	1.31
Al2O3	33.08	18.76
FeO (tot)	0.09	0.49
MnO	0.14	0.19
Mgo	13.14	22.25
CaO	0.01	0.00
Na2O	0.13	0.12
K2O	0.01	10.65
Cr2O3	0.03	0.11
NiO	0.07	0.05
BaO	0.13	0.31
ZnO	-	-
Total	97.31	93.69
H2Oc	-	4.22

Cation Proportions

basis O/OH	18/0	20/4
Si	5.054	5.600
Al 1V	-	2.400
Al V1	3.910	0.740
Ti	0.008	0.139
Fe	0.007	0.059
Mn	0.012	0.023
Mg	1.965	4.709
Ca	0.001	0.000
Na	0.024	0.032
K	0.002	1.928
Cr	0.002	0.013
Ni	0.005	0.005
Ba	0.005	0.017

APPENDIX 7

Publications resulting from this study

Copies of the following three reference papers are appended.

1. SECCOMBE, P.K., SPRY, P.G., BOTH, R.A., JONES, M.T. & SCHILLER, J.C., 1985. Base metal mineralization in the Kanmantoo Group, South Australia: A regional sulfur isotope study. *Economic Geology*, 80:1824-1841. (Refer Appendix 7 of this thesis.)

2. SPRY, P.G., SCHILLER, J.C. & BOTH, R.A., 1988. Structure and metamorphic setting of base metal mineralisation in the Kanmantoo Group, South Australia. *The Australian Institute of Mining and Metallurgy, Bulletin and Proceedings,* 293(1):57-65.

3. OLIVER, N.H.S., DIPPLE, G.M., CARTWRIGHT, I. & SCHILLER, J. 1998. Fluid flow and metasomatism in the genesis of the amphibolite-facies, pelite-hosted Kanmantoo copper deposit, South Australia. *American Journal of Science*, 298:181-218.

Seccombe, P. K., Spry, P. G., Both, R. A., Jones, M. T. & Schiller, J. C. (1985). Base metal mineralization in the Kanmantoo Group, South Australia; a regional sulfur isotope study. *Economic Geology*, *80*(7), 1824-1841.

NOTE:
This publication is included in the print copy
of the thesis held in the University of Adelaide Library.

It is also available online to authorised users at:
https://doi.org/10.2113/gsecongeo.80.7.1824

Spry, P. G., Schiller, J. C & Both, R. A. (1988). Structure and metamorphic setting of base metal mineralisation in the Kanmantoo Group, South Australia. *The Australian Institute of Mining and Metallurgy, Bulletin and Proceedings, 293* (1), 57-65.

NOTE:

This publication is included in the print copy
of the thesis held in the University of Adelaide Library.

Oliver, N. H. S., Dipple, G. M., Cartwright, I & Schiller, J. (1998). Fluid flow and metasomatism in the genesis of the amphibolites-facies, pelite-hosted Kanmantoo copper deposit, South Australia. *American Journal of Science, 298*(3), 181-218.

NOTE:
This publication is included in the print copy
of the thesis held in the University of Adelaide Library.

It is also available online to authorised users at:
https://doi.org/10.2475/ajs.298.3.181